2-1-1992

Validation of DIRSIG, an infrared synthetic scene generation model

Donna D. Rankin

Validation of DIRSIG
an Infrared Synthetic Scene Generation Model

Donna K. Rankin

Rochester Institute of Technology

A thesis submitted in partial fulfillment of the
requirements for the degree of Master of Science
in the Center for Imaging Science
in the College of Imaging Arts and Sciences
of the Rochester Institute of Technology

February 1992

Signature of the Author Donna K. Rankin

Accepted by Dana G. Marsh Feb. 9, 1993
Coordinator, M.S. Degree Program

COLLEGE OF IMAGING ARTS AND SCIENCES
ROCHESTER INSTITUTE OF TECHNOLOGY
ROCHESTER, NEW YORK

CERTIFICATE OF APPROVAL

M.S. DEGREE THESIS

The M.S. Degree Thesis of Donna K. Rankin
has been examined and approved by the
thesis committee as satisfactory for the
thesis requirement for the
Master of Science degree

Dr. John Schott, Thesis Advisor

Carl Salvaggio

Rolando Raqueño

2/9/93

Date

THESIS RELEASE PERMISSION FORM
ROCHESTER INSTITUTE OF TECHNOLOGY
COLLEGE OF IMAGING ARTS AND SCIENCES

Validation of DIRSIG
an Infrared Synthetic Scene Generation Model

I, Donna K. Rankin, hereby grant permission to the Wallace Memorial Library of R.I.T. to reproduce my thesis in whole or in part. Any reproduction will not be for commercial use or profit.

Date: 2/9/93

Validation of DIRSIG
an Infrared Synthetic Scene Generation Model

by
Donna K. Rankin

Submitted to the
Center for Imaging Science
in partial fulfillment of the requirements
for the Master of Science Degree
at the Rochester Institute of Technology

Abstract

A validation and sensitivity study was performed in which the accuracy of an infrared synthetic image generation model (DIRSIG) was examined. The majority of the error in the model is derived from two major programs: a temperature predictor and a radiative transfer model. A thermodynamic model computes kinetic temperatures of objects in a computer generated three-dimensional scene. These temperatures, atmospheric data, and sensor parameters are used as input to a ray_tracer which models the propagation of radiation in a source-target-sensor path within this scene. The output is a simulated infrared image which a sensor with the given input parameters would record. The accuracy of the model and the impact of uncertainties in individual input variables were determined by error propagation methods and comparison of the simulated imagery with actual imagery. The average theoretical error in radiance reaching the sensor was determined to be 1.58 W/m^2-sr, while the measured average error in radiance for an actual predicted scene was determined to be 2.98 W/m^2-sr (13.99%). Variables which had the greatest impact on the final predictive error of the model were identified and ranked accordingly. In addition, problem areas within the model were identified and suggestions for improvement were made.

Dedication

For my grandfather, Adolph S. Mager,
who always encouraged me in my education
and made me believe I could accomplish anything.

I love you Poppa.

CONTENTS

LIST OF FIGURES

LIST OF TABLES

Introduction

Many different areas such as computer animation, flight simulation, and optical sensor design have a need for synthetic images. Many computer models exist which simulate real-world scenes. They are commonly referred to as Synthetic Image Generation (SIG) models. These models can be used for a variety of applications such as training, mission planning and sensor evaluation. The advantages of these models include cost savings in research and development and more accurate performance expectations for various scenarios.

Many windows (bands) in the electromagnetic spectrum are modeled by SIG processes. One important band for airborne imaging and flight simulation is the long-wave infrared (LWIR) region between the wavelengths 8 to 14 microns. Within this bandpass, which is also known as thermal infrared (TIR), the signal (radiance) received by a sensor is dominated by thermal properties such as the kinetic temperatures and emissivities of objects within the scene. LWIR imagery is used in applications such as night imaging to provide information not available in images taken in the visible portion of the spectrum. The thermal signal measured by a sensor can also be used to assess the type and condition of the object emitting the signal. These specific set of signals for a given object is called the thermal signature (Lillesand, 1987).

One application of SIG models is in providing a means of determining optimum imaging times and conditions for airborne or spaceborne sensors. Instead of performing numerous flights to gather images of a specific area which contain the needed information, a SIG program can produce those images in potentially less time at substantially reduced cost. These images can then be analyzed to determine the optimal times to collect the actual imagery. For example, when imaging a desert scene, there are optimum times when the contrast between the sand and the objects of interest on the sand is greatest. A SIG model can be used to quickly determine these times. This process can save the users much time and money by eliminating unnecessary and possibly hazardous flight missions.

Another application involves testing sensor designs. Before an actual sensor is built, the design can be simulated on a computer to test for acceptable output image

quality and potential problems with any of the design specifications. The design can be modified by changing parameters in the computer model, again saving time and money.

In order for the use of SIG models to be practical and worthwhile, the accuracy of their performance must be known. They can be evaluated against a number of criteria such as radiometric accuracy, robustness to phenomenological variables, geometric fidelity, and speed of image generation. Radiometric accuracy of a SIG model is essential. The user must be certain that the final images produced by the model are valid representations of actual imagery. Although a number of TIR SIG models have been produced in recent years, very little in-depth validation of model accuracy has been performed. Model sensitivity is also important. The knowledge of which input variables have the most impact on the system's output is valuable when gathering data to run the model.

This project involved a validation and sensitivity study of the Digital Imaging and Remote Sensing Laboratory Image Generation (DIRSIG) model. DIRSIG's produced imagery were evaluated with respect to actual imagery and its sensitivity due to errors in the various input parameters was determined. The next section discusses validation studies performed on other SIG models and details the workings of the DIRSIG model.

Background

2.1) General Literature Review

Many SIG models exist which produce a variety of images for different applications. However, very little validation of the radiometric accuracy of these models has been performed. Some of the available literature discusses SIG validation with respect to how well the synthetic images represent real-world images. The focus of these projects usually involved automatic target recognition (ATR). For ATR, the goal is to have the computer segment out and identify objects in a scene for applications such as military reconnaissance. Object shape and grey level intensity are two parameters which the computer may use for segmentation and identification. Radiometric accuracy is important if the computer is to use the object's thermal signature in its decision process.

Other published studies include validation of separate components of SIG models, including model input parameters or temperature generators. Full scale radiometric validation and sensitivity testing such as proposed here have not been carried out on an entire SIG model.

In addition to the lack of validation, many models have classified components or are corporate confidential. Descriptions of the models and testing procedures are often very general and therefore difficult to evaluate. A few validation procedures found in the literature are discussed below, followed by a brief background of the research performed at RIT leading up to the development of DIRSIG.

Duncan (1990) discusses obtaining visible and thermal imagery of a scene to be simulated for ATR applications. The visible image is used as a reference for defining the boundaries of the objects in the thermal image. Once objects are defined, radiances are read from the IR imagery and converted to temperatures through Planck's equation (*cf.* Eq. 4.1). These temperatures are then assigned to target points in the synthetic model. The "quality" of the resulting simulated image can be tested against the original image, presumably by passing both through the ATR algorithm and comparing results.

This approach has some valuable aspects. Assigning object temperatures derived from actual imagery can aid when testing only the radiation propagation portion of a SIG model. However, this method gives no indication of how object temperatures will be

determined for scenes for which no true imagery is available. For a SIG model to perform well in the predictive mode (ie. predicting images for which no truth data are available) a temperature generation model is desirable. This method focuses on the success of the ATR algorithm in segmenting the synthetic scenes with minor regard to radiometric accuracy, but on the success of the ATR algorithm in segmenting the synthetic scenes. This is an acceptable premise for the scope of the ATR model tested. If, however, the ATR algorithm were to use spectral signatures in its decision process, the radiometric prediction must be validated. In addition, for other synthetic image applications such as training and sensor design, radiometric fidelity to actual imagery is essential.

Another validation of an ATR application is discussed by Lindahl et. al. (1990). They define validation as 'the quantitative measurement and evaluation of the "quality" of the synthetic representation attained with respect to real imagery'. This method involves defining a norm by which image quality is measured. A norm is a collection of specific features which characterize the image. The features are chosen based on their relevance to the ATR algorithm being tested. Possible features include grey level intensity, spatial and temporal information and object shape and texture. For this method, synthetic images are generated of scenes for which the actual imagery is available. Features are computed for subregions within both the real and simulated images. The defined norms for each subregion are then computed and compared. If differences between the norm values are small enough, the SIG process is considered valid.

Comparison of these norms is an interesting approach to SIG model validation. This approach provides flexibility in testing different ATR algorithms by allowing different norms to be defined for different applications. For validating any application, comparison with actual infrared images can give many insights into the abilities of the SIG model and illustrate areas which still need work. Again, this method is aimed at ATR applications and does not specifically concern itself with the radiometric fidelity of the output images. However, this method can be applied to radiometric validation by simply defining the norm to be the output digital count values in the actual and synthetic images.

Massie (1991) discussed future plans for validation of the radiometric accuracy of a SIG model. The approach was to use a radiometrically accurate system of cold and hot plates along with a plate at room temperature which has resolution test patterns machined

into it. Images taken by an IR system looking through the room temperature plate at the hot and cold plates can be compared to corresponding synthetic images from the SIG model. This simple set up is a good starting point for testing the model's accuracy and resolution. Again, comparison of the model's predicted imagery with actual images is a desirable approach. However, a more thorough test involving comparison with actual imagery of a complex scene is desirable. A more involved test such as this would better illustrate the SIG model's capabilities and shortcomings given different scenes and situations.

An infrared signature model, **PRISM**, was validated for its temperature predictions by Sullivan and Reynolds (1988). This thermal model computes facet temperatures based on heat transfer in the forms of conduction, convection and radiation for facet to facet and facet to background interactions. Two targets were used for the validation test. Temperatures of a simple structure composed of four aluminum plates connected by varying joint materials and insulation were recorded by thermocouples. In addition, an M2 Bradley IFV was imaged by an infrared system (8 - 14 μm) while thermocouples recorded temperatures of 62 facets on the vehicle. For the four aluminum plates, temperatures computed by **PRISM** were directly compared to the measured temperatures. The temperatures predicted for the M2 Bradley and digital counts from the thermal images were converted to blackbody equivalent temperatures. These derived temperatures and the temperatures recorded by the thermocouples were plotted as a function of time for comparison. The resulting thermal image and thermocouple temperatures were very similar. The model predictions did not peak as high as the actual temperatures at mid-day, but were close to the true temperatures at night. This model does not produce simulated imagery, but does give some insight into testing temperature generation models within a complete SIG process.

This background research illustrates the need for a complete radiometric validation and sensitivity testing of a SIG model. A good predictive model should incorporate radiometric propagation coupled with a temperature generation model. The radiometry model should include all influencing factors such as diurnal weather data, background effects, and atmospheric modeling. The temperature generator should provide accurate object temperature predictions without greatly increasing the computation time of the model. The entire model should be based as much as possible on first principles physics so that all input parameters can be easily defined and determined by the user.

The Digital Imaging and Remote Sensing Laboratory Image Generation model, DIRSIG, incorporates these capabilities with a main focus on radiometric accuracy. The following sections discuss the background research leading to the development of DIRSIG and give a complete description of the model.

2.2) Background Leading to the Development of DIRSIG

The Digital Imaging and Remote Sensing (DIRS) laboratory at RIT's Center for Imaging Science has had a long term interest in absolute radiometric calibration of thermal IR imagery with special interest in correction for atmospheric effects (*cf.* Schott and Schimminger, 1981; Schott and Volchok, 1985; and Byrnes and Schott, 1986). This interest has led to the development of methods and devices for measurement of normal and angular emissivity values for varying materials in the thermal IR region. These bandpass emissivity values along with bandpass atmospheric transmission and upwelled and downwelled radiance values have been used for estimating the effect of emissivity variation on imaging sensors (Schott, 1986). At that time, simple 2-D silhouettes with temperatures assigned to individual segments were used as the synthetic scenes to be imaged. This work demonstrated the necessity of including emissivity effects in IR SIG processes. Next, specular reflection of background surfaces and downwelled sky radiance were included by Schwartz et. al. (1985). All of this work was aimed at using SIG to help visualize target-to-background signatures as well as to visually evaluate the effect of improvements on radiometric propagation models.

The next step in DIRS research was to work toward producing realistic looking scenes. Schott and Salvaggio (1989) incorporated brightness variations within segments of the synthetic images by taking texture from images of laboratory physical models or actual thermal imagery. Schott and Salvaggio (1987) also simulated image degradation due to the MTF of the sensor by using asymmetric 3-D convolution kernels. The ability to add random and periodic detector noise was also added in the same study. In order to simulate more complex scenes, a 3-D scene generation capability was desired. Warnick et. al. (1990) developed a model incorporating CADCAM 3-D wire frame models and a ray-tracer.

At the same time, validation efforts were taking place in the areas of SIG modeling, radiation propagation modeling, and material parameter measurements. Schott et. al. (1990) extended emissivity measurements to encompass the 3-5 μm and 8-14 μm bands with greater accuracy. Feng (1990) demonstrated improved measurements of the

spectral bidirectional reflectance factors (BDRF) in the visible and shortwave infrared (SWIR) regions for future extension of SIG modeling into these shorter wavelength regions. Schott and Salvaggio (1989) studied the surface-leaving radiance portion of the model, validating the treatment of angular emissivity effects and the background and sky radiance equations used in the model. The radiometry and ray-tracing models used with the 3-D wire frames were preliminarily validated by Shor et. al. (1990).

Shor constructed a simple scene comprised of a pool of water, a mirror, and a wooden pyramid structure, all placed on a concrete surface. Temperatures of the objects were recorded by thermistors while thermal IR imagery (8-12 μm) of the scene was collected. The temperatures were assigned to facets in the computer generated scene. Radiosonde data from the day the scene was imaged were input to the model in order to model the atmosphere and synthetic imagery was generated. The resulting images were then compared to the actual thermal imagery.

These studies demonstrated the basic integrity of the SIG approach but also illustrated the need for various improvements. One critical need was for a thermal model to compute the temperature of each scene element. Spector et. al. (1991) had completed a SIG study which included initial validation of the temperature generation model Therm. It was determined that Therm could be accurate to within 1°C (average RMS error) when given the appropriate target parameters and full environmental data.

A second needed improvement was the inclusion of solar effects for modeling in the MWIR (3-5 μm) region. In the LWIR band, solar effects are negligible compared to the effects of self-emission. In the SWIR (short wave IR) and MWIR regions, solar reflection and scattering have a large impact on the radiance reaching the sensor and therefore must be included in the modeling process. Salvaggio et. al. (1991) had completed a study aimed at generating spectral atmospheric radiation propagation and energy-matter interaction terms needed for modeling both solar and thermal radiometric effects associated with horizontal surfaces (SVGM).

The model DIRSIG was formed, incorporating Therm and SVGM, for the purpose of developing an end-to-end image generation capability. The objectives of DIRSIG (Raqueño et. al., 1991) are to:

1.) function in the MWIR and LWIR regions,

2.) emphasize radiometry: in terms of dealing with as much radiometric phenomenology as necessary to achieve as much radiometric accuracy as is practical,

3.) be capable of dealing with scene elements which would be observed by high resolution airborne systems,

4.) use first principles physical models as much as possible, and

5.) use simple target and sensor models in initial versions and emphasize phenomenology.

This research has provided a model based largely on first principles physics, aimed at radiometric accuracy and incorporating a temperature generation program. The design of DIRSIG allows for output at many different stages of the model so that sources of error can be easily determined. The next section gives an overview of the function of each component of DIRSIG. For a complete technical description of the model, see Raqueño et. al. (1991).

2.3) DIRSIG Overview

The computer model DIRSIG consists of a number of submodels which perform specific tasks in the image generation process. These submodels are: scene geometry, a ray-tracer, the temperature generator Therm, radiometry, and the sensor submodel.

2.3.1) Scene Geometry Submodel

The scene geometry submodel consists of the 3-D geometry of the scene being modeled and the parameters associated with each facet in this scene. The scene is drawn with a computer aided drawing package, **AutoCAD** and custom software allowing the organization of a scene is shown in Figure 2.1. Each object is composed of parts which are made up of facets which are the basic building blocks of the system. The entire scene is tagged with a name, the date, and the latitude and longitude. The actual viewing conditions for the final image are defined within the sensor submodel. Each facet has assigned to it three nodes: attribute, geometry, and orientation (*cf.* Figure 2.2). These nodes contain information necessary for input to the other submodels.

The **geometry** node (*cf.* Figure 2.3) contains the coordinates of the points which define the plane of the facet, the number of points which define the plane, and the unit vector which specifies the normal to the facet. This geometry is used by the ray-tracer submodel in determination of the interaction of a ray with the facet.

The **orientation** node (*cf.* Figure 2.4) defines the exact orientation of the facet with respect to the earth and sun. Figure 2.5 illustrates the four angles which are defined. The **azimuth** is the number of degrees the facet is facing clockwise from North. The **slope** is the tilt of the facet with respect to the normal to the earth. The **sensor_facet** and **sun_facet angles** are defined from the **facet normal** to the sensor and sun respectively. The **slope** and **azimuth** angles are required by Therm for temperature computation. The **sensor_facet angle** is used for determination of angular emissivity of the facet. Finally, the **sun_facet angle** determines the amount of solar irradiance the facet receives.

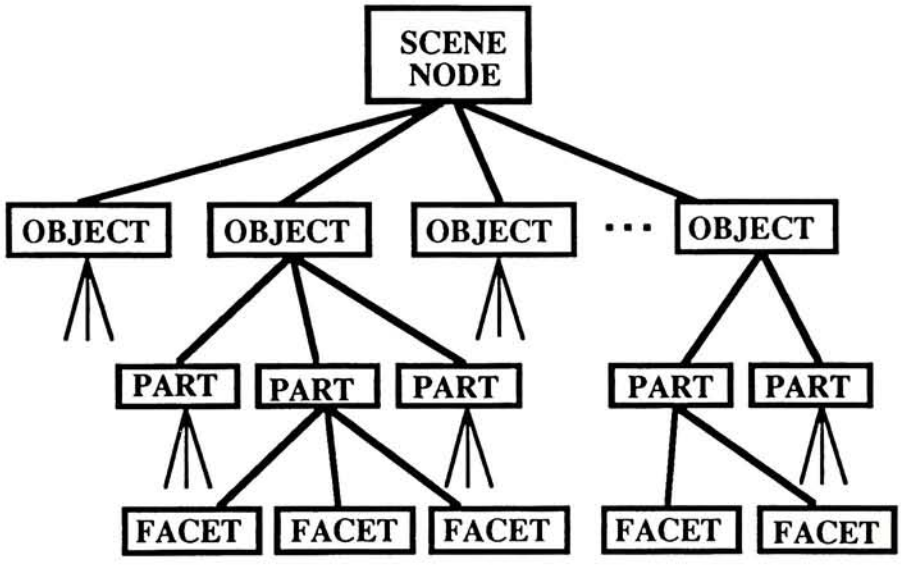

Figure 2.1 Scene Node Structure

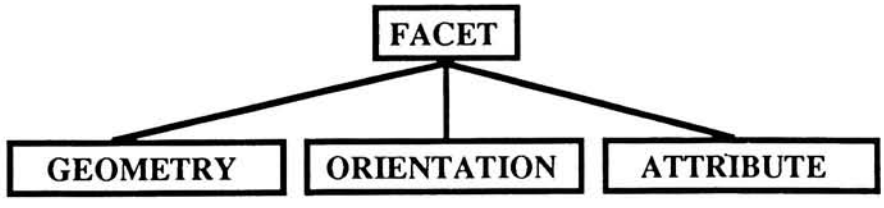

Figure 2.2 Nodes of the Scene Geometry Submodel

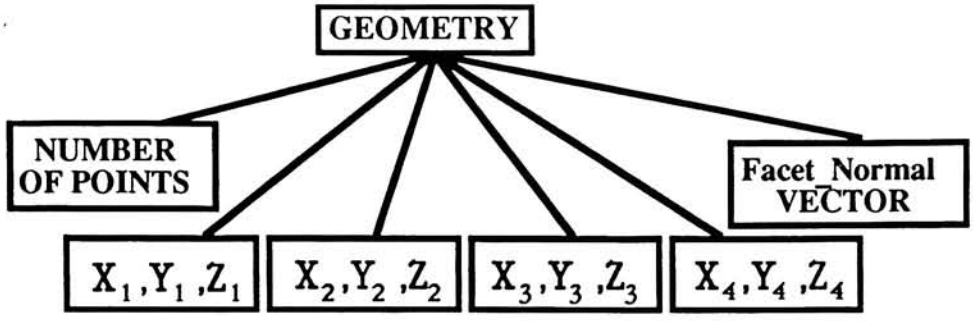

Figure 2.3 Geometry Node of the Scene Geometry Submodel

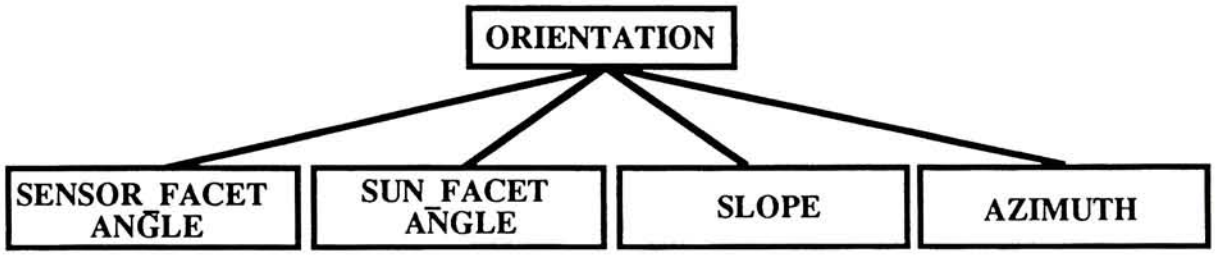

Figure 2.4 Orientation Node of the Scene Geometry Submodel

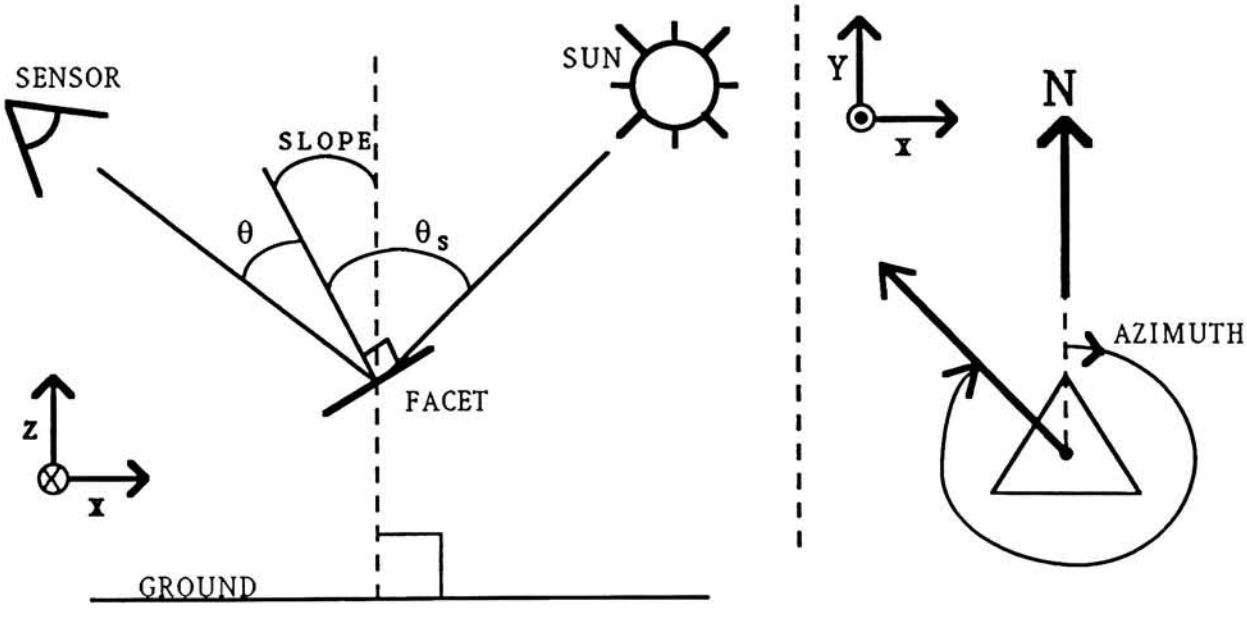

θ = Sensor to Facet Normal Angle
θ_S = Sun to Facet Normal Angle
Slope = Ground Normal to Facet Angle
Azimuth = North Direction to Facet Normal Ground Projection Angle

Figure 2.5 Orientation Angles

The **attribute** node (*cf.* Figure 2.6) contains the name and code of the material the facet is comprised of and the physical parameters associated with that material. Some of these parameters are contained in a **material** node within the **attribute** node. This **material** node holds parameters which are common to all facets comprised of the same material. These parameters are: heat capacity, thermal conductivity, visible and thermal broadband emissivities, specularity, exposed area, and an array of angular emissivities. Facet specific parameters are stored in the **attribute** node outside of the **material** node. Thickness, self-generated power, and shape factor are all facet specific parameters. The Therm submodel uses these parameters for computation of the kinetic temperature of the facet. The ray-tracer also makes use of the angular emissivity and specularity values for mapping photon interactions within the scene.

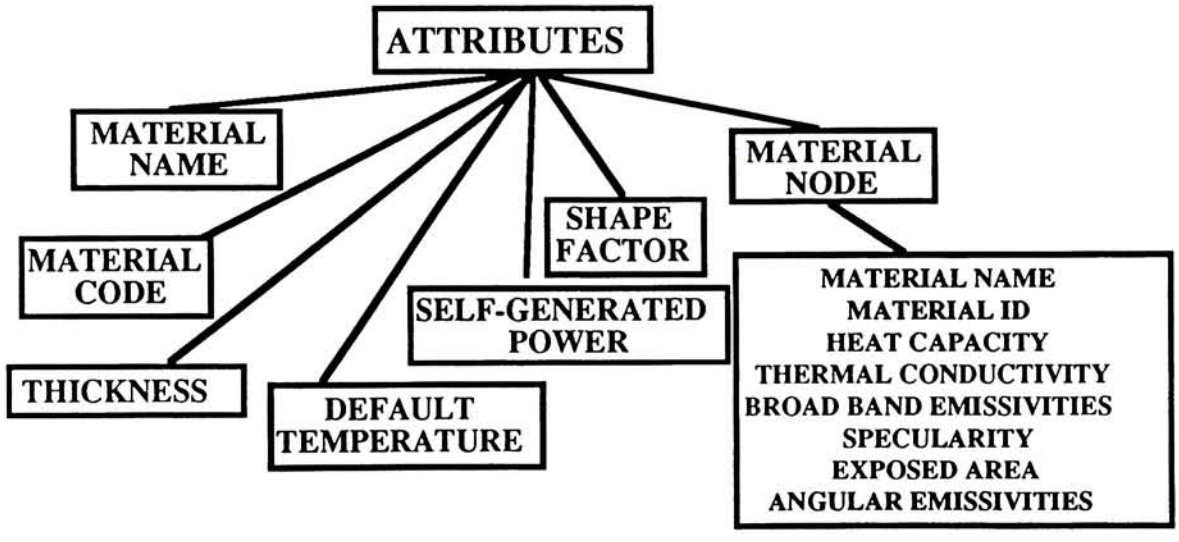

Figure 2.6 Attribute Node of the Scene Geometry Submodel

2.3.2) Ray-Tracer Submodel

The ray-tracer submodel integrates the information gathered from the other submodels to simulate the overall IR imaging system. Figure 2.7 illustrates the interaction of the ray-tracer with the other submodels and its resulting outputs.

The ray-tracer's primary function is the retracing of photon paths through the given optical system which is assumed to be of the pin-hole camera configuration (*cf.* Figure 2.8). This technique is similar to the ray-tracing calculations governed by Snell's Law and trigonometric formulas used in optics. Computer graphics ray-tracing extends

these calculations beyond the modeled optical system to include the scene objects being imaged. The path which each ray travels and its interactions along the way are determined. Energy losses due to material absorption and atmospheric attenuation and energy redistribution due to reflection and self-emission are factored into the process . In this way, the radiance incident on each pixel of the imaging system can be properly computed by the radiance submodel.

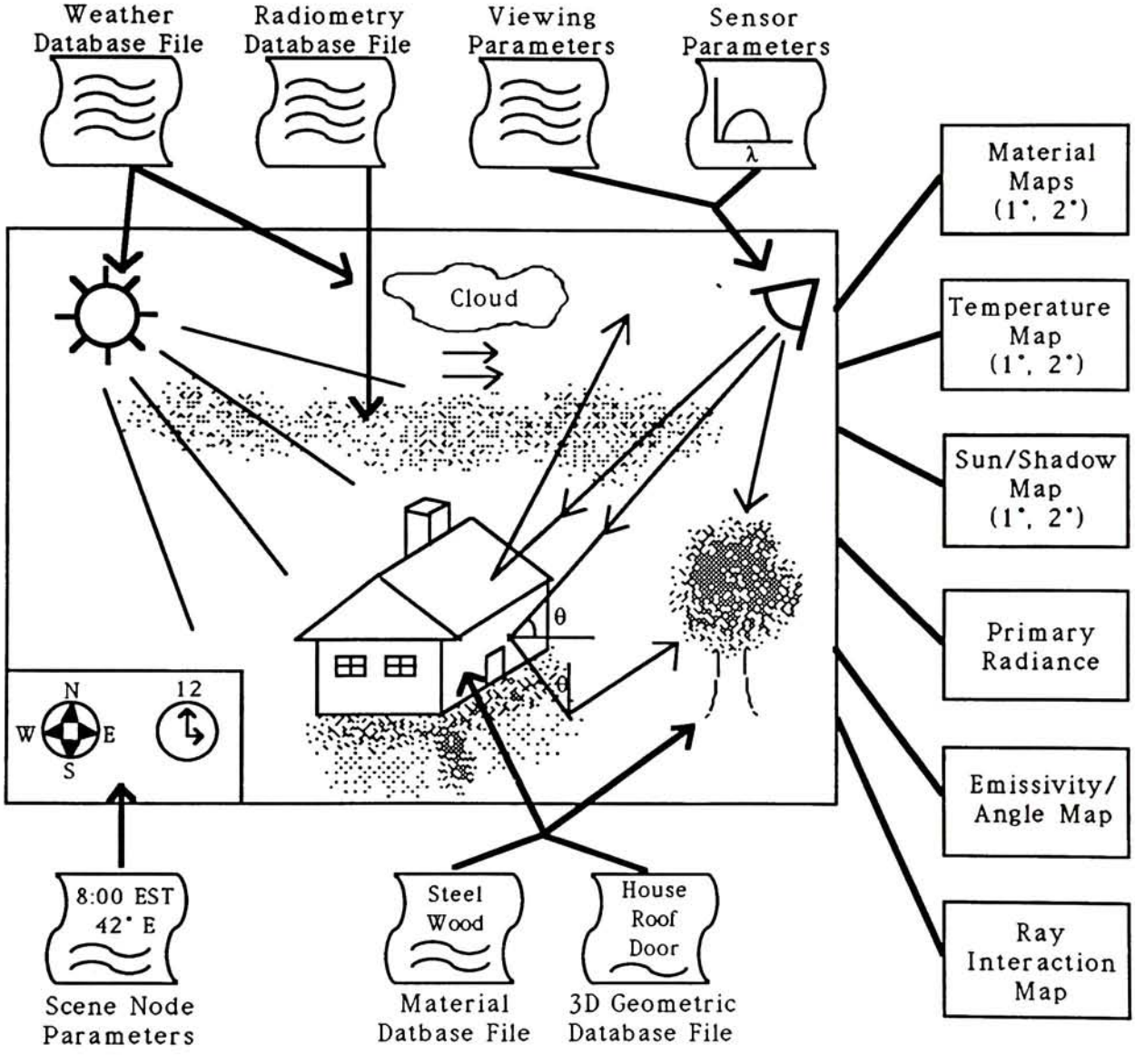

Figure 2.7 Ray-Tracer Interaction

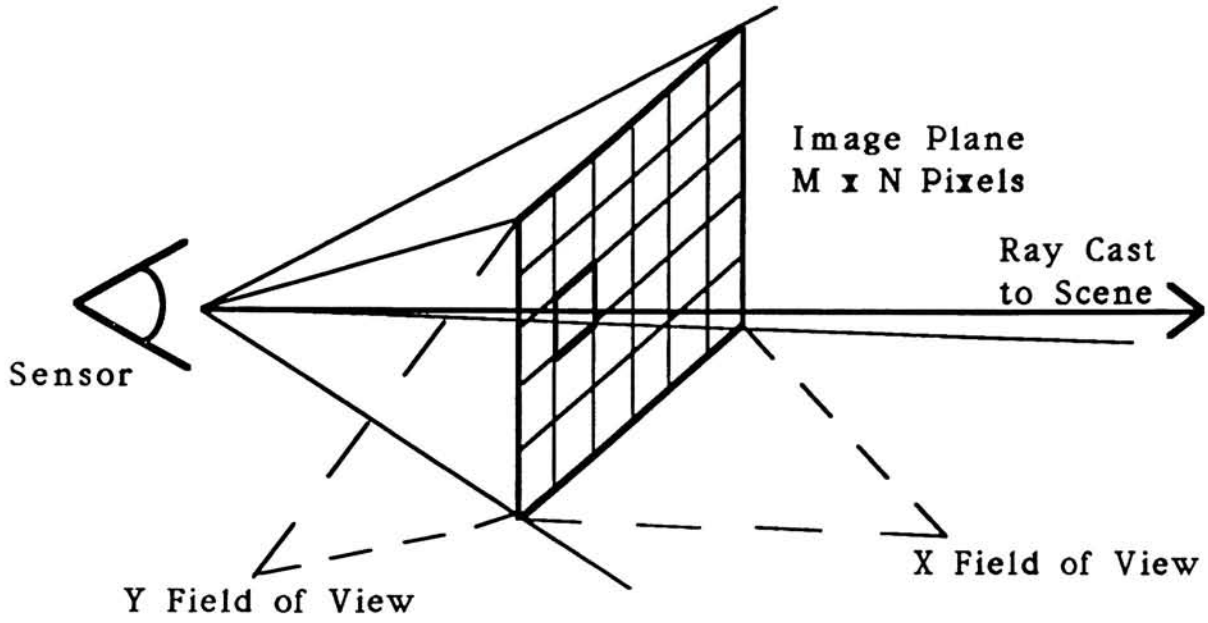

Figure 2.8 Pinhole Camera Ray-Tracing Schematic

Figure 2.9 shows the logic flow for the ray-tracer. The calculations begin by retracing the path a photon would take to reach a particular pixel in the focal plane. This is known as casting a ray from the sensor pixel. Once it is determined which facet is hit by the ray, its sun/shadow history is computed. The illumination of the facet (whether it was in the sun or shade) is determined as a function of time by this process. The result is stored as an array of 1's and 0's (*cf.* Figure 2.10). Because Therm only 'sees' one facet and is not aware of surrounding objects which may cause shadowing, this information is used to modify the input to Therm to increase the accuracy of its temperature computations. The direct insolation values (direct sunlight) in the weather file input to Therm are multiplied by the sun/shadow history. The result is a zero solar loading term (ie. direct insolation) when a facet is in shadow. When the facet is in the sun, the direct insolation value in the weather file is not changed.

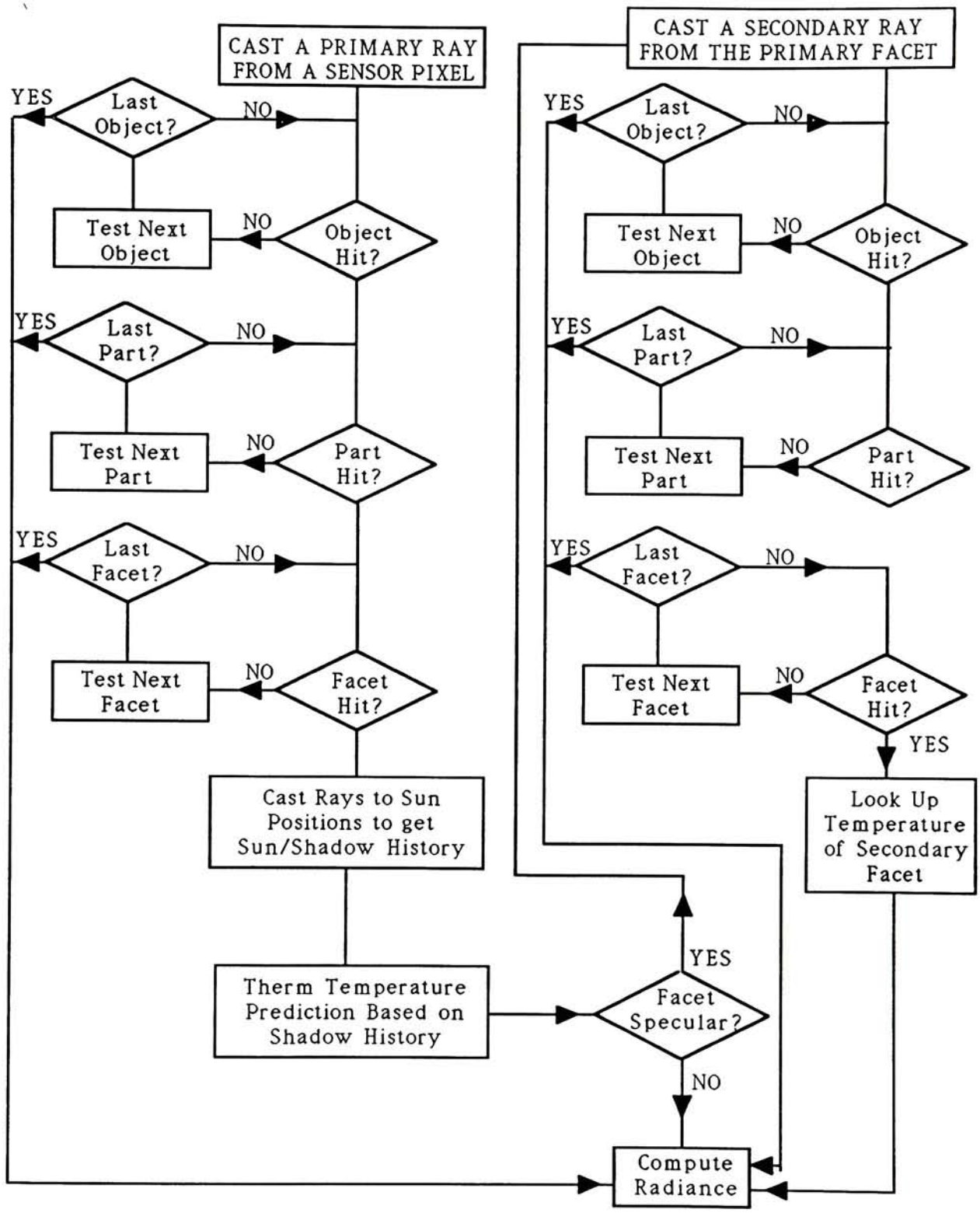

Figure 2.9 Ray-Tracer Flowchart

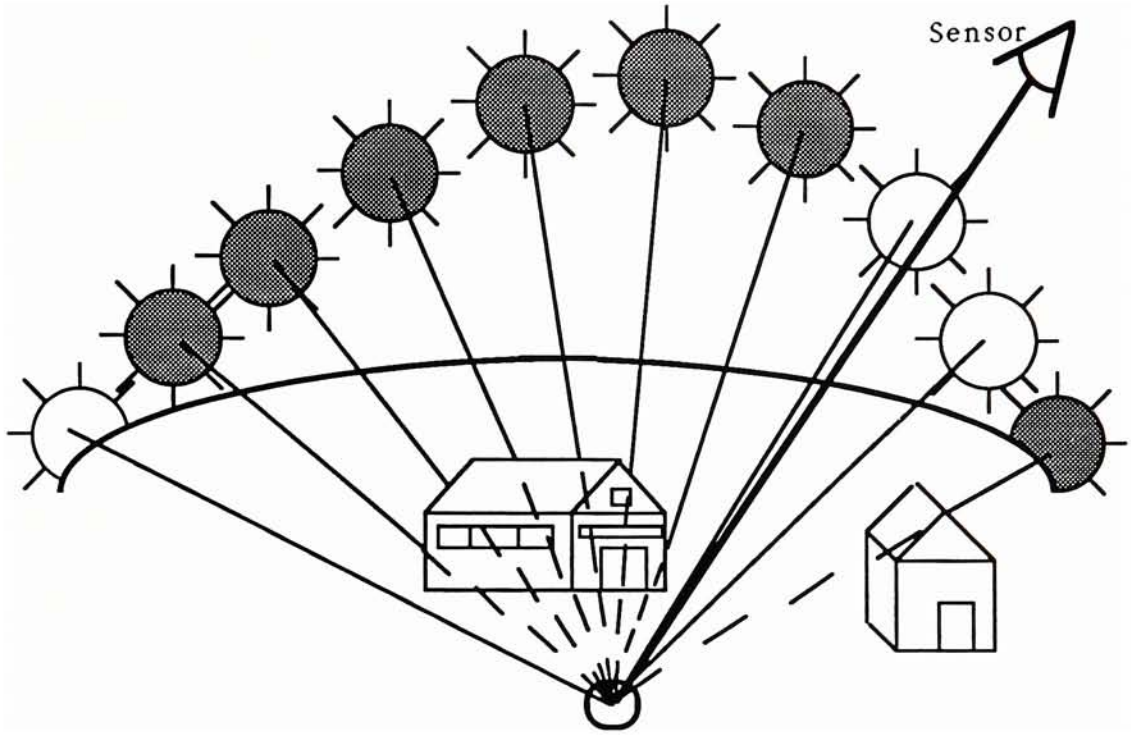

Sun/Shadow History	1	0	0	0	0	0	0	1	1	0

Figure 2.10 Example of Facet Sun/Shadow History

With sun/shadow history established, this and the material parameters of the facet are input to Therm which computes the facet temperature. The specularity of the facet is then checked. Specularity is currently a binary value in the model. A facet can either be perfectly specular or diffuse. If the facet is diffuse, the pixel radiance is computed by the radiometry submodel. If the pixel is specular, a secondary ray is cast from the facet intersection point using simple laws of reflection. This secondary ray is tested in the same manner as the primary ray to determine if a background facet is hit. If this is the case, the temperature of the background is factored into the radiance calculations. If no background facet is hit, the sky is assumed to be the background and the pixel radiance is computed based on the zenith angle of the ray cast to the sky. Shor (1990) determined that only two ray bounces are necessary to determine the final pixel radiance for the LWIR region. Additional computations of tertiary and quarternary ray-facet intersections result in insignificant contributions to the final radiance in the longwave regions. No

study has been performed to determine the minimum number of intersections necessary for accurate radiance computations in the MWIR region.

This ray-tracing process results in the output of a number of intermediate image maps including: material type, primary and secondary facet temperature, sun/shadow condition, emissivity, ray-interaction type, and angle maps, as illustrated in Figure 2.7.

2.3.3) Thermal Submodel

The purpose of Therm is to compute each facet's kinetic temperature which is dependent upon the material properties of the facet and the environmental conditions surrounding the facet.

Therm is a linear differential temperature generation model written by DCS Corporation (1990) and validated at RIT (Spector et. al., 1991). Object temperatures are computed as a function of time based on first principles models which determine the rate of heat transfer corresponding to a specific temperature difference between an object and its environment. The model assumes that a facet is thermally independent of the other facets and that each has an isothermal behavior across its entire surface.

Therm has been proven to accurately predict temperatures of real world objects within respectable error bounds. Figure 2.11 is an example of Therm's predictive capabilities plotted along with actual object temperatures as a function of time. As its assumptions imply, the model does not compute the conduction between adjacent facets and is therefore limited in its accuracy. A more complex model such as a finite element analysis model would require substantial amounts of computing time which would greatly increase the run-time of DIRSIG. Therm does allow for facets with self-generated power which can, when properly implemented, be used to overcome some of the limitations of non-conduction between facets. The addition of the sun/shadow history of each facet by the ray-tracer also greatly improves Therm's prediction capabilities within DIRSIG.

Beyond the inability to completely model the physical processes governing temperature generation, the largest source of error within the model is the prediction of accurate material parameters. Well-defined parameters are essential for accurate temperature prediction. This requirement is discussed in-depth in the results, Section 5.1.

These object parameters are stored within the attribute and orientation nodes of the scene geometry submodel and are listed in Table 2.1.

Weather Parameter	Object Parameter
Air Temperature (°C)	Heat Capacity (L/cm/°C)
Air Pressure (mbar)	Thermal Conductivity (L*cm/hr/°C)
Relative Humidity (%)	Thickness (cm)
Dew Point (°C)	Visible Emissivity (%)
Wind Speed (m/s)	Thermal Emissivity (%)
Direct Insolation (L/hr)	Exposed Area (%)
Diffuse Insolation (L/hr)	Self-Generated Power (L/hr)
Sky Exposure (%)	Slope (°)
Cloud Type (0-8)	Azimuth (°)
Precipitation Type (0/1)	
Precipitation Rate (cm/hr)	
Precipitation Temperature (°C)	

NOTE: 1 W/m2 = 0.086 L/hr	L = Langley

Table 2.1 Therm Weather and Object Inputs

Environmental parameters including location and meteorological data are also used as input to Therm. The location parameters include latitude and longitude, date, time and the time interval between temperature predictions,. The meteorological data (*cf.* Table 2.1) include air temperature and pressure, relative humidity, dew point, wind speed, direct and diffuse insolation (sunlight and skylight), sky exposure (percent of sky unobscured by clouds), cloud type (cirrus, cirrostratus, altocumulus, altostratus, stratocumulus, stratus, or fog), and precipitation type, rate, and temperature. These values are input as a function of time (usually in fifteen minute increments) over a twenty-four hour period.

Therm can also estimate these meteorological parameters given the location data and limited weather information such as sunrise and peak air temperatures, time of peak air temperature, and average cloud cover and cloud type. Figure 2.11 illustrates Therm's prediction of total insolation (direct + diffuse) versus actual conditions. Therm's final temperature predictions are more accurate when the complete weather history is given to

the model. In situations where needed parameters are unknown, eg. missing parameters or simulations of future dates, the weather prediction abilities of Therm must be used. For this project, both methods of temperature prediction (full environmental data and predicted weather data) were tested to illustrate the model's accuracy for both cases.

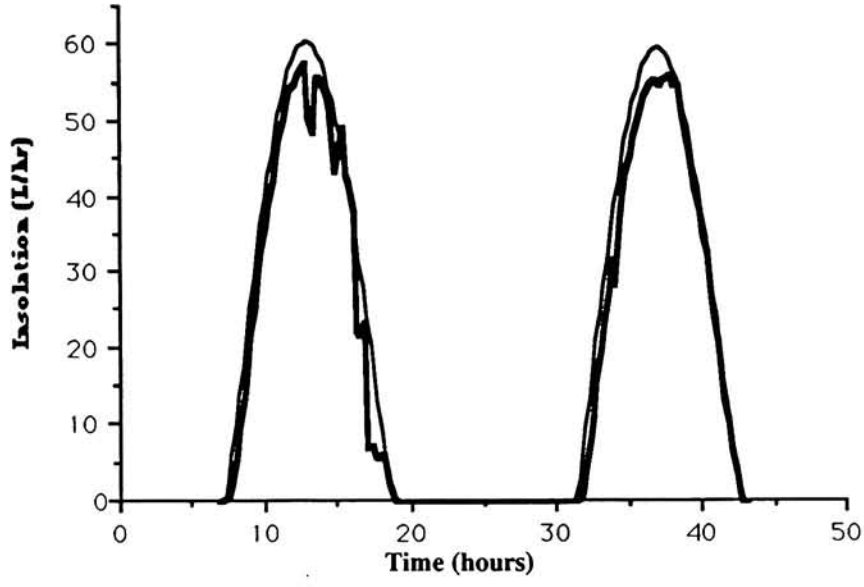

Figure 2.11 Therm Insolation Prediction vs. Truth (10/5-6/90)

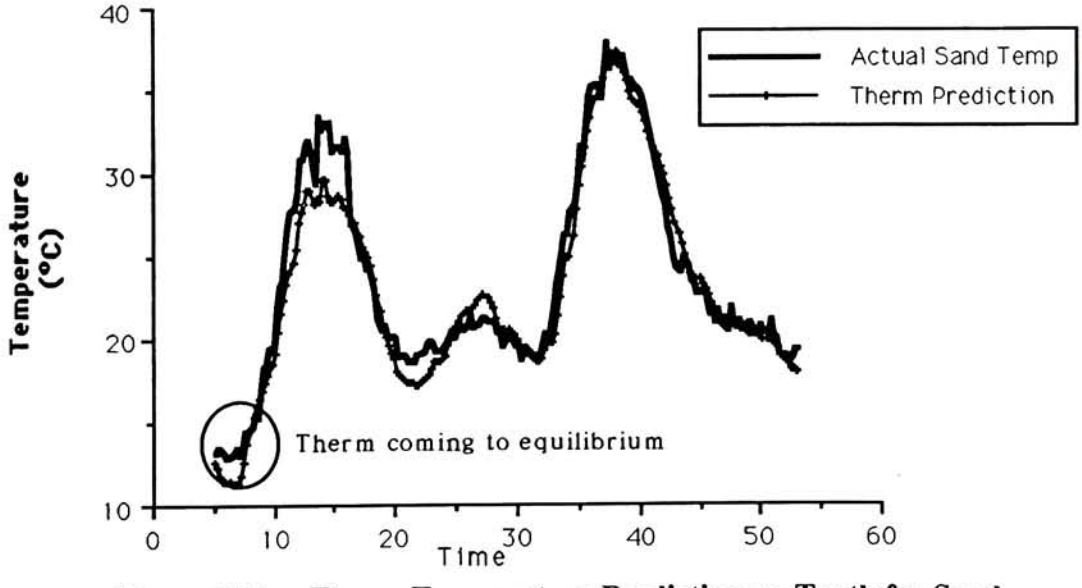

Figure 2.12 Therm Temperature Prediction vs. Truth for Sand (10/5-6/90)

Once the weather history is loaded into Therm, the model begins predicting object temperatures. At first, no temperatures are known and therefore the model assigns an initial value to all objects. It takes several computations for the initial predictions to come to equilibrium with the actual object temperatures. Therefore, Therm must be run starting several hours before the desired simulation time, as illustrated in Figure 2.12. Note in this figure that Therm's predictions are initially inaccurate and after approximately eight hours the model has come to equilibrium.

2.3.4) Radiometry Submodel

The radiometry submodel determines the radiance leaving each facet and arriving at the front end of the sensor based on the calculations of the ray-tracer and Therm. The intervening atmosphere must be modeled to accurately predict the propagation of the radiation from the facet to the sensor. The Spectral Vector Generation Model (SVGM) (Salvaggio et. al., 1991) is used for this purpose.

SVGM incorporates two atmospheric modeling routines, LOWTRAN 7 created by the Air Force Geophysics Laboratory (AFGL) (Kneizys et. al., 1988) and SCATRAN produced by the Eastman Kodak Corporation and the Air Weather Service (MAC). For the DIRSIG model, LOWTRAN 7 alone is used to compute all of the components necessary for modeling radiation propagation in a source-target-sensor path in both the MWIR and LWIR regions.

LOWTRAN 7 starts with a database created from experimental measurements of atmospheric composition taken on 'typical' days. For example, a typical data set contains variables describing altitude, temperature, water vapor density, ozone density, and vertical profiles for concentrations of the gases: H_2O, CO_2, O_2, O_3, N_2O, CH_4, NO, SO_2, NO_2, NH_3, and HNO_3. Presently, the user is allowed complete control of the atmospheric profiles in LOWTRAN 7. The model can simulate conditions for any given day when provided with an upper air weather observation record (radiosonde). If radiosonde data are not available, the model can use one of its 'typical' days to simulate the desired conditions. These stored atmosphere types include mid-latitude summer, maritime, and sub-arctic conditions.

The upper air atmospheric profiles used for the generation of meteorological conditions along the radiance propagation path are currently constant as a function of time. This approximation is adequate for the tropospheric, stratospheric, and upper

atmospheric layers. However, in the earth's boundary layer, conditions such as temperature and relative humidity change throughout the day and thus this approximation is inadequate (Salvaggio et. al., 1991). Hourly data which can be obtained from local airports or measured by the user can be used to make corrections for the boundary layer. Version 2.1 of DIRSIG incorporates this improvement.

Once the basic atmosphere is established, fundamental properties of scattering and absorption are applied to the data to model atmospheric conditions which would have occurred given user-specified parameters such as temperature, ground visibility, time of day, and sun-target-sensor geometry. The final outputs of the model are atmospheric transmission and radiance terms such as upwelled and downwelled radiance as a function of wavelength.

There are four possible interactions of a ray cast by the ray-tracer, illustrated in Figure 2.13. The four cases are:

(1) totally diffuse facet
(2) totally specular reflector from which the ray cast from the sensor to facet bounces to the sky
(3) totally specular reflector from which the ray cast from the sensor to facet bounces to a non-sky background
(4) the ray cast from the sensor misses the scene and hits the sky.

Computation of the radiance reaching the sensor is different for each case. The equations for each case are listed on the following page. The components for these equations are computed by LOWTRAN 7 or are provided by the other submodels. All are defined in Table 2.2. The origin of each component is listed in Table 2.3. Figure 2.14 illustrates the angles used in these equations.

Case 1:

$$L(\theta,\lambda) = \Big\{\varepsilon(0,\lambda)L_T + \Big[I_T \frac{E_S}{\pi}\tau_1 \cos(\theta_S) + F[L_{DE} + L_{DS}] + (1-F)[L_{TAB} + I_B \frac{E_S}{\pi}\tau_1 \cos(\theta_B)(1-\varepsilon_B(30^\circ,\lambda))]\Big](1-\varepsilon(0,\lambda))\Big\}\tau_2(\theta_E,\lambda) + L_{\mu E}(\theta_E,\lambda) + L_{\mu S}(\theta_E,\lambda)$$

Equation 4.1

Case 2:

$$L(\theta,\lambda) = \Big\{\varepsilon(\theta,\lambda)L_T + \Big[I_T \frac{E_S}{\pi}\tau_1 \cos(\theta_S) + L_{DE}(\theta_{SK},\lambda) + L_{DS}(\theta_{SK},\lambda)\Big](1-\varepsilon(\theta,\lambda))\Big\}\tau_2(\theta_E,\lambda) + L_{\mu E}(\theta_E,\lambda) + L_{\mu S}(\theta_E,\lambda)$$

Equation 4.2

Case 3:

$$L(\theta,\lambda) = \Big\{\varepsilon(\theta,\lambda)L_T + \Big[I_T \frac{E_S}{\pi}\tau_1 \cos(\theta_S) + \varepsilon_B(\theta_{BT},\lambda)L_{TB} + I_B \frac{E_S}{\pi}\tau_1 \cos(\theta_B)(1-\varepsilon_B(\theta_{BT},\lambda))]\Big](1-\varepsilon(\theta,\lambda))\Big\}\tau_2(\theta_E,\lambda) + L_{\mu E}(\theta_E,\lambda) + L_{\mu S}(\theta_E,\lambda)$$

Equation 4.3

Case 4:

$$L(\theta,\lambda) = L_{DE}(\theta_{SK},\lambda) + L_{DS}(\theta_{SK},\lambda)$$

Equation 4.4

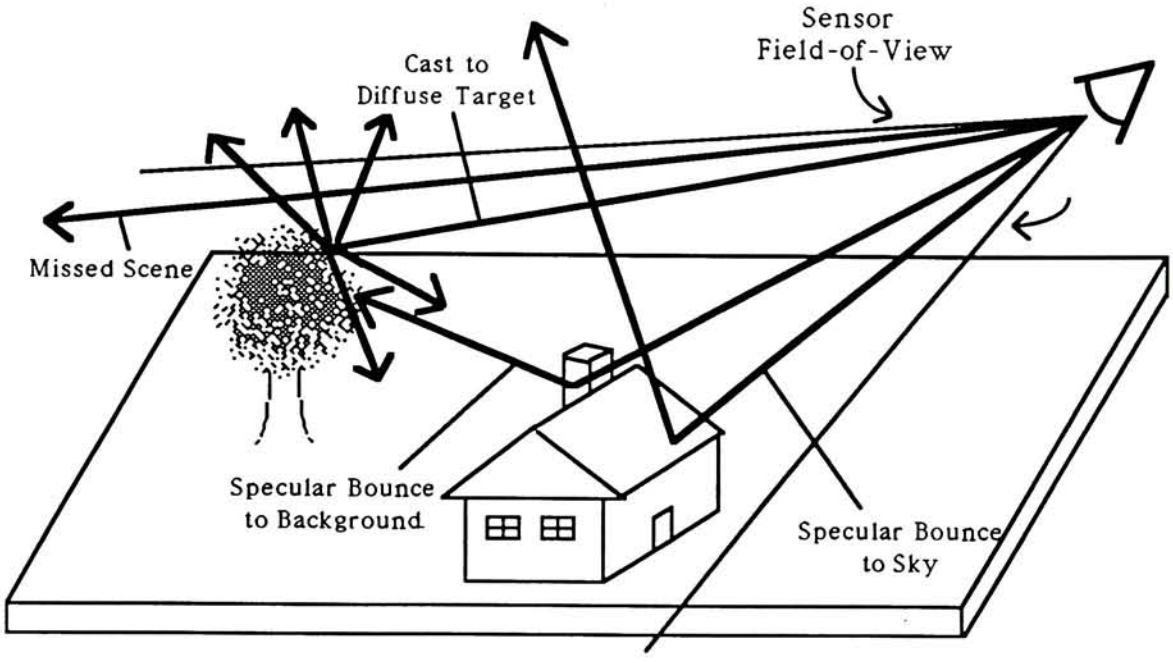

Figure 2.13 Illustration of the Four Ray Interaction Cases

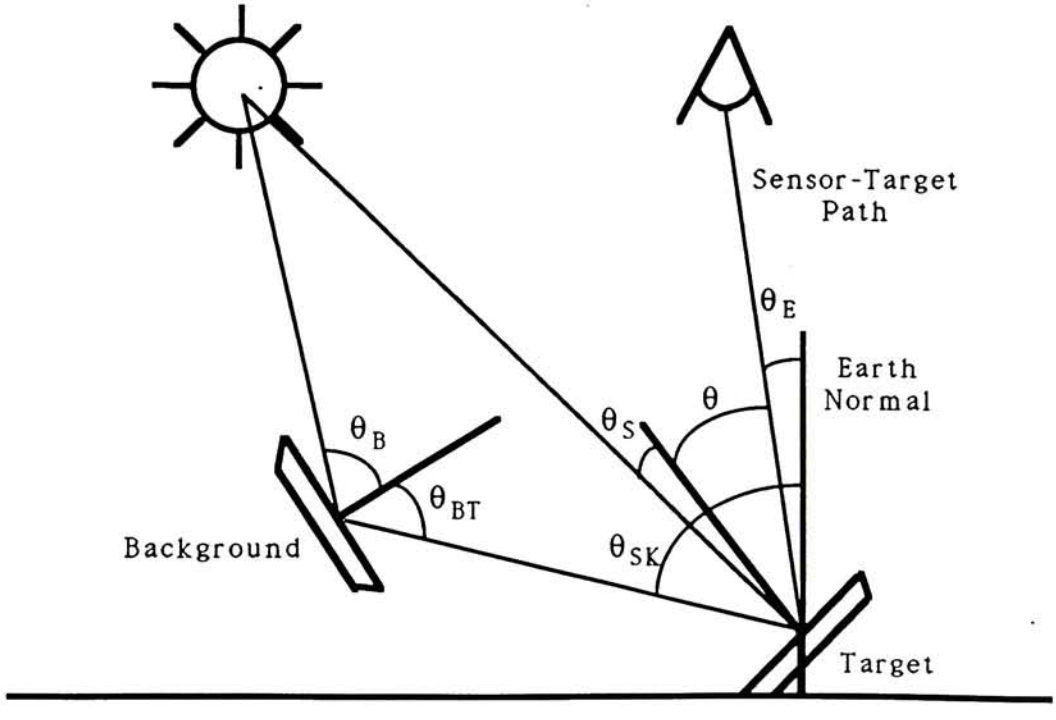

Figure 2.14 Angles Involved in Radiance Equations

Variable	Definition
$L(\theta,\lambda)$	Spectral radiance reaching the front end of the sensor
L_T	Self-emitted spectral radiance from a blackbody at temperature T (target)
L_{TB}	Self-emitted spectral radiance from a BBat temperature T (background)
L_{TAB}	Self-emitted spectral radiance from a BB at temperature T (ave. background)
E_S/π	Exoatmospheric solar spectral radiance
L_{DE}	Downwelled spectral radiance due to self-emission of the atmosphere, integrated over skydome
L_{DS}	Downwelled spectral radiance due to scattering, integrated over skydome
$L_{DE}(\theta_{SK},\lambda)$	Directional spectral downwelled radiance due to self-emission of the atmosphere
$L_{DS}(\theta_{SK},\lambda)$	Directional spectral downwelled radiance due to scattering
$L_{\mu E}(\theta,\lambda)$	Upwelled spectral radiance due to self-emission of the atmosphere along the target-sensor path
$L_{\mu S}(\theta,\lambda)$	Upwelled spectral radiance due to scattering along the target-sensor path
$\tau 1$	Atmospheric spectral transmission along the source-target path
$\tau 2(\theta_E,\lambda)$	Atmospheric spectral transmission along the target-sensor path
$\varepsilon(\theta,\lambda)$	Angular spectral emissivity for the target
$\varepsilon_B(\theta,\lambda)$	Angular spectral emissivity for the background
θ	Angle between the normal to the surface and the sensor-target path
θ_S	Angle between the normal to the surface and the sun-target path
θ_B	Angle between the normal to the surface and the sun-background path
θ_E	Angle between the normal to earth at target and the sensor-target path
θ_{SK}	Angle between the normal to the earth and the specularly reflected ray from the sensor to target cast
θ_{BT}	Angle between the normal to the background and the target hit point
F	Shape factor - Fraction of exposed skydome
I_T	Target sun/shadow flag (0/1) - Absence or presence of shadow
I_B	Background sun/shadow flag (0/1) - Absence or presence of shadow

Table 2.2 Definition of Radiance Equation Variables

Variable	Origin
$L(\theta,\lambda)$	Desired radiance vector
L_T	Temperature from Therm, Radiance from Planck's equation
L_{TB}	Temperature from Therm, Radiance from Planck's equation
L_{TAB}	Ave. Temperature from ray-tracer, Individual temperature from Therm, Radiance from Planck's equation
E_S/π	LOWTRAN7 (table look-up)
L_{DE}	SVGM (table look-up)
L_{DS}	SVGM (table look-up)
$L_{DE}(\theta_{SK},\lambda)$	SVGM (interpolated on θ_{SK},ϕ)
$L_{DS}(\theta_{SK},\lambda)$	SVGM (interpolated on θ_{SK},ϕ)
$L_{\mu E}(\theta,\lambda)$	LOWTRAN7 (interpolated on θ)
$L_{\mu S}(\theta,\lambda)$	LOWTRAN7 (interpolated on θ)
$\tau 1$	LOWTRAN7 (table look-up)
$\tau 2(\theta,\lambda)$	LOWTRAN7 (interpolated on θ_E)
$\varepsilon(\theta,\lambda)$	DIRS Database (table look-up to nearest degree)
$\varepsilon_B(\theta,\lambda)$	DIRS Database (table look-up to nearest degree)
$\theta, \theta_S, \theta_B, \theta_E, \theta_{SK}, \theta_{BT}$	Ray-tracer
F	Ray-tracer (not fully implemented)
I_T, I_B	Ray-tracer

Table 2.3 Origin of Radiance Equation Variables

2.3.5) Sensor Submodel

The sensor submodel uses the spectral radiance values computed by the radiometry submodel to create the final synthetic image.

The location of the sensor within the scene must be defined before any calculations can take place within the model. This is performed within AutoCAD using its CAMERA viewing function. This function provides the ability to simulate a camera view of the synthetic scene. This is also useful for visual verification of the given viewing parameters prior to a full-scale run of DIRSIG.

The camera format is defined by several parameters. First, the desired target point in world (scene) coordinates to which the sensor optical axis will point is defined. The sensor ground coordinates (x,y) and flying altitude (z) are specified relative to an origin placed in the center of the synthetic scene. Angles ω, Φ, κ are specified to describe the orientation of the sensor at this position. ω is the azimuthal angle of the sensor with respect to the x-axis of the world coordinates. Φ is the elevation angle of the sensor from the x-y plane of the scene. κ is the twist angle of the sensor above its optical axis. The camera's equivalent lens length is given to define the magnification and field of view of the sensor. Finally, the number of pixels per row and the number of rows in the sensor focal plane are given. All of these parameters are saved in a file with an **autocad_dview** tag. The ray-tracer accesses this file to establish the viewing angles it and the radiometry submodel need for their computations.

Once the spectral radiance values have been computed by the radiometry submodel, the sensor submodel converts them to final digital counts. First, the sensor's spectral response function is factored in. This function is defined on 100 cm-1 centers from 350 to 39850 cm-1 (0.25 to 28.57 μm) (*cf.* Figure 2.15). Defined between 0 and 1, it represents the sensor's relative response at each wavelength compared to the maximum spectral sensitivity of the sensor within the defined bandpass. The values of zero effectively limit the sensor's response to radiance values within the bandpass being simulated. The radiance values , $L(\theta,\lambda)$, computed by the radiometry submodel are multiplied by the spectral response function. This product is then integrated over the bandpass of interest as shown in Equation 2.5

$$L_w(\theta) = \sum_{\lambda=\lambda_{min}}^{\lambda_{max}} L(\theta,\lambda)\beta(\lambda)\, d\lambda$$

Equation 2.5

The resulting radiance, $L_w(\theta)$, which represents the radiance at zenith angle θ integrated over the given bandpass, is then converted to digital count (DC). The conversion is given by Equation 2.6

$$DC = \text{gain}\ L_w(\theta) + \text{offset}$$

Equation 2.6

Figure 2.15 shows a sample sensor parameter datafile which is input to the sensor submodel. This file contains the spectral response function, the minimum and maximum wavelengths of the bandpass of interest and the gain and offset of the sensor. Raqueño et. al. (1991) outline methods of determining appropriate gain and offset values for a given sensing system if the values are not known.

The resulting digital counts represent the final output of the sensing system and are displayed as the final synthetic image.

line 001	0.0000000	
line 002	0.0000000	
line 003	0.0000000	
line 004	0.0000000	
.	.	
.	.	
.	.	
line 382	0.0000000	
line 383	0.0000000	
line 384	0.0000000	
line 385	0.0000000	
line 386	0.0000000	
line 387	0.3000000	
line 388	0.9000000	sensor relative spectral response function data
line 389	1.0000000	defined on 100 cm-1 centers
line 390	0.9500000	
line 391	0.6000000	
line 392	0.2000000	
line 393	0.0000000	
line 394	0.0000000	
line 395	0.0000000	
line 396	0.0000000	
line 397	386	minimum wavelength index of the spectral bandpass (line number - 1)
line 398	391	maximum wavelength index of the spectral bandpass (line length - 1)
line 399	17.8751	sensor gain in units of DC/W/m^2 srμm
line 400	-221.0714	sensor offset in units of DC

Figure 2.15 Sample Sensor Parameters Datafile

2.3.6) DIRSIG Overview

The preceding has been an overview of each submodel within the DIRSIG model. Figure 2.16 illustrates the relationship between the submodels and datafiles included in the DIRSIG model. The scene geometry submodel allows the user to build the scene and assign physical parameters to each of the facets. The ray-tracer casts rays on a pixel-by-

pixel basis to determine their interaction with the objects within the scene. It also determines each facet's sun/shadow history for use in the thermal submodel. The thermal submodel Therm computes the temperature of each facet based on the object's material properties and input environmental data. The facet temperatures and ray interaction data are sent to the radiometry submodel which computes the spectral radiance reaching the front end of the sensor. The sensor submodel integrates these spectral radiance values over the bandpass of interest along with the sensor response function. The integrated radiance values are then converted to digital counts which are displayed in the final synthetic image.

There is a critical need to address what the total error is in the overall model and what each submodel contributes to the error. The main sources of error in the model are the governing equations of radiation propagation, temperature prediction and uncertainties in the input optical properties of the objects. Many variables input to both the thermal and radiometry submodels have uncertainties in their values which can be propagated through the model. These errors can result in uncertainties in the computed facet temperature, radiance reaching the sensor, or the final digital count in the synthetic image. Along with these uncertainties, the modeling processes have inherent limitations in their accuracy based on how well the physical principles of thermodynamics and radiometric propagation are known and modeled. The focus of this research was the investigation of these errors in order to determine where improvements should be made.

The follwing sections discuss the approach and results of the validation of the DIRSIG model. Again, the main focus of the testing was on the thermal and radiometry submodels. However, the scene geometry, ray-tracer, and sensor submodels were also inherently tested by comparison of the synthetic imagery with truth imagery.

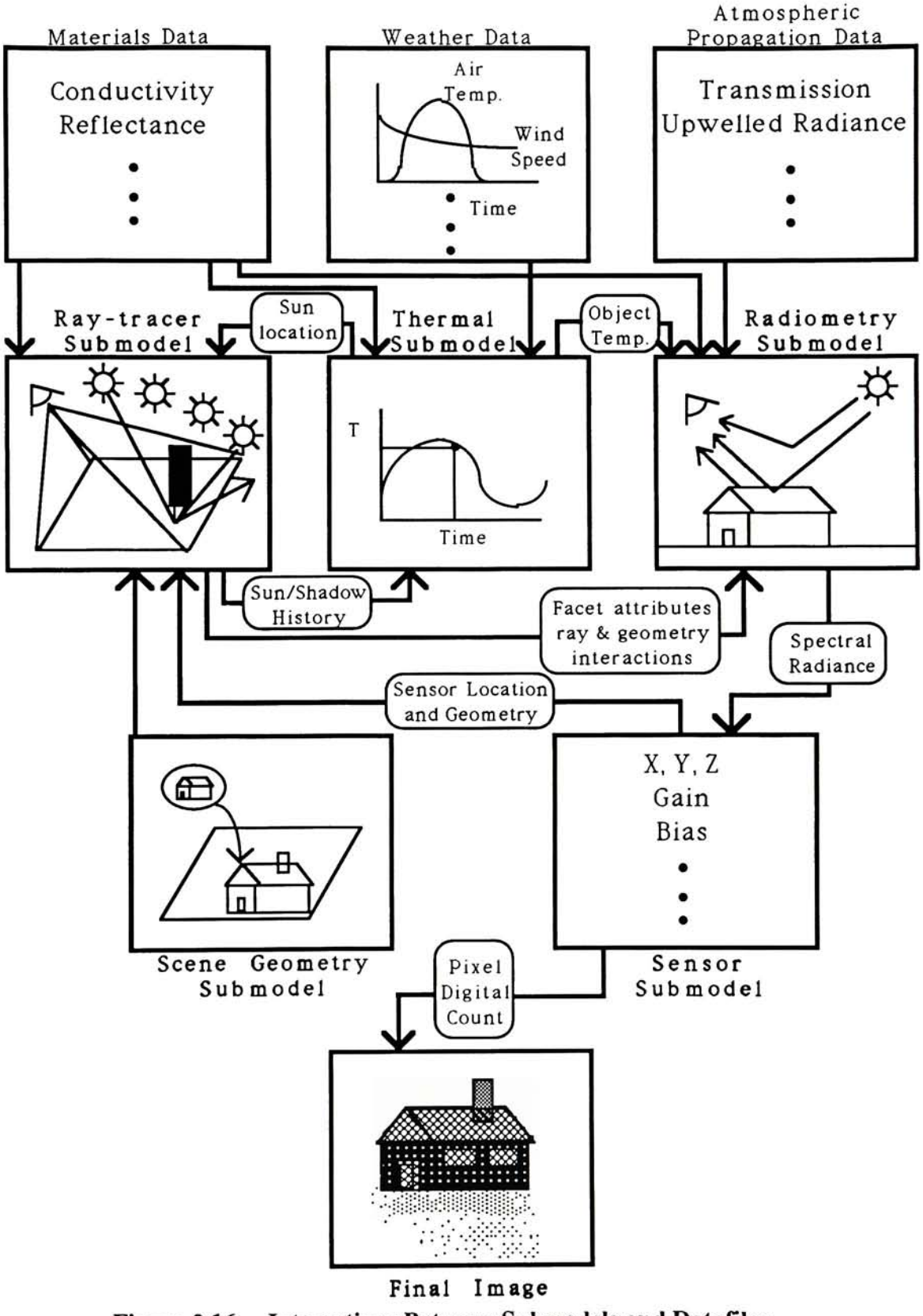

Figure 2.16 Interactions Between Submodels and Datafiles

Work Statement

3.1.) An experiment was set up and carried out in which all of the inputs necessary to run DIRSIG were collected. The data include all meteorological and atmospheric data surrounding a scene. Thermal imagery and actual temperatures of objects within the experimental scene were collected and used for comparison with model predictions.

3.2.) Optimum as well as general object parameters for input to the model Therm were determined for all of the objects within the experimental scene.

3.3.) The temperature generator Therm was run independently of the DIRSIG model to determine its sensitivity to variations in its input parameters. The model was run using both optimum parameters as well as standard inputs determined from available literature. The temperature prediction errors due to these different levels of knowledge of input parameters were determined

3.4.) The radiometric submodel of DIRSIG was tested for accuracy using error propagation techniques. This method also allowed for determination of the impact variations in individual radiometric variables have on the final radiance computed by Dirsig.

3.5.) Synthetic thermal images of the experimental scene were generated by DIRSIG and compared to the actual thermal imagery collected during the experiment. Discrepancies between the images were identified, thus giving insight into the limitations and potential of DIRSIG's modeling capabilities. Suggestions were made for future improvements to the model.

Approach

4.1) Task 1: Data Collection Experiment

Two data collection experiments were carried out in which all of the parameters necessary for input to DIRSIG were collected. The experiments ran for forty-eight hour periods on the dates of October 5, 6, and 7, 1990 and June 22 and 23, 1992.

The scene depicted in Figure 4.1 was imaged from the roof (four stories high, ground floor 0.218 km above sea level) of the RIT Center for Imaging Science building nearby. LWIR imagery was collected using an Inframetrics IR camera on half hour intervals. The camera contains a single Mercury/Cadmium/Telluride (HgCdTe) detector which was cooled by liquid nitrogen to a temperature of 77K within a cryogenic dewar. The image was scanned using electromechanical servos. During each time interval, five frames of the image were digitized using Werner Frei software on a PC containing an Image Technology board. These frames were then averaged to reduce noise within individual images.

Midwave infrared imagery was also gathered during the June 1992 collection. The MWIR camera was supplied by the ARMY Night Vision Laboratory and is a Platinum Silicide (PtSi) 2-D array video compatible IR imager. The MWIR imagery was also collected at half hour intervals during the entire collection.

Visible images were collected using a CCD camera for purposes of determining facet sun/shadow histories during the October 1990 collection. During the June 1992 collection, four separate images in different bands (red, green, blue, and SWIR) were collected by the CCD camera using different filters. These images are to be used for a validation study of DIRSIG's predictions in the visible region of the electromagnetic spectrum. All images were collected every half hour, stored on computer hard drive, and backed up on magnetic tape.

The thermal images were calibrated using a two-point blackbody (BB) measurement method. A blackbody of emissivity = 0.970 + 0.02 (CI Systems, 1989) was set at 0 °C and then 40 °C and imaged by the Inframetrics camera every half hour. It was assumed that these temperatures covered the dynamic range of the temperatures within the experimental scene. The BB was set at one temperature, imaged by the IR

camera, and then set at the other temperature. While the BB changed temperature, the camera imaged the scene on the ground. Once the scene imaging was complete, the second BB image was taken. The two BB images were then sampled within the Werner Frei software to determine an average digital count representing the BB temperature. The two temperatures were converted to radiance values using Planck's equation (*cf.* Equation 4.1). Radiance was plotted against the corresponding digital count to create the calibration curve.

$$L(\lambda) = \frac{2hc^2}{\lambda^5} \quad \frac{1}{\exp(hc/\lambda kT) - 1}$$

Equation 4.1

where: h = Planck's constant (6.6262×10^{-34} Js)
c = velocity of light (2.9979×10^{8} m/s)
k = Boltzmann's constant (1.3806×10^{-23} J/K)
T = absolute temperature (K)

Given the angular emissivity of the object, digital counts in the thermal images were converted to radiance values via the calibration curve generated for that time interval (*cf.* Figure 4.2). These radiance values were used for comparison with DIRSIG's computation of radiance reaching the sensor. The apparent target temperature was then calculated using the inverse of Planck's equation. These computed temperatures were used as a check against thermistor values. This method was used to double check the thermistor temperatures and DIRSIG's prediction of background object temperatures, such as grass which were not measured during the experiment. Figure 4.3 illustrates the resulting temperatures computed from the IR images plotted against the thermistor temperatures.

This method of temperature computation assumes that the radiance from the target is due solely to self-emission of the object. If the object's radiance is influenced by its background, this method will be inaccurate. For example, the car engine was turned on during the first night of the data collection. The radiances of all surrounding objects were greatly influenced by the heat of the nearby engine. In addition, upwelled radiance and reflected downwelled radiance values are not factored into the computation.

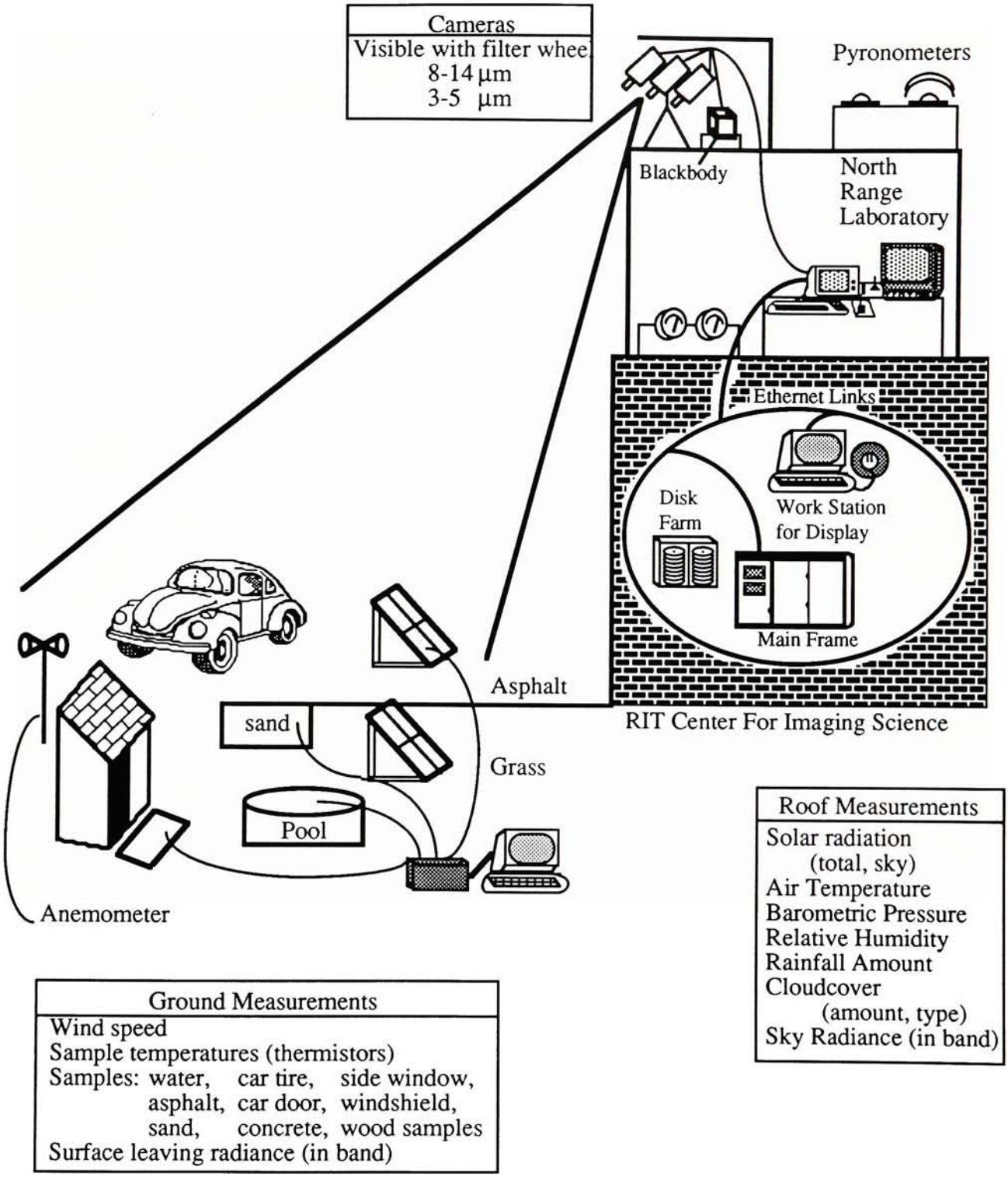

Figure 4.1 Experimental Scene Design

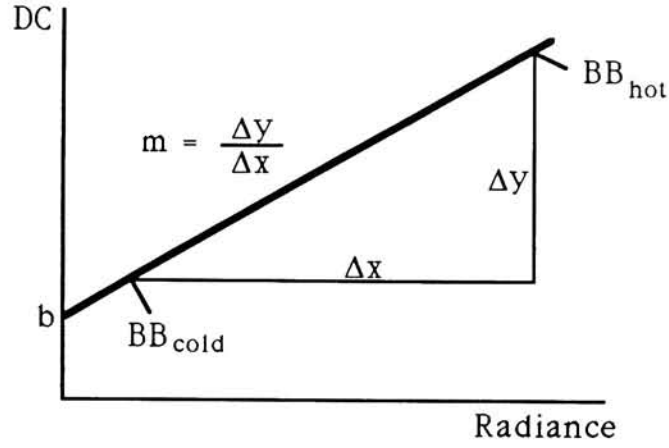

$$L_{target} = \frac{DC_{target} - b}{m\ \varepsilon_{target}} = \text{Target radiance}$$

$$T_{target} = \text{Planck}^{-1}(L_{target}) = \text{Target temperature}$$

Figure 4.2 DC-Radiance Conversion

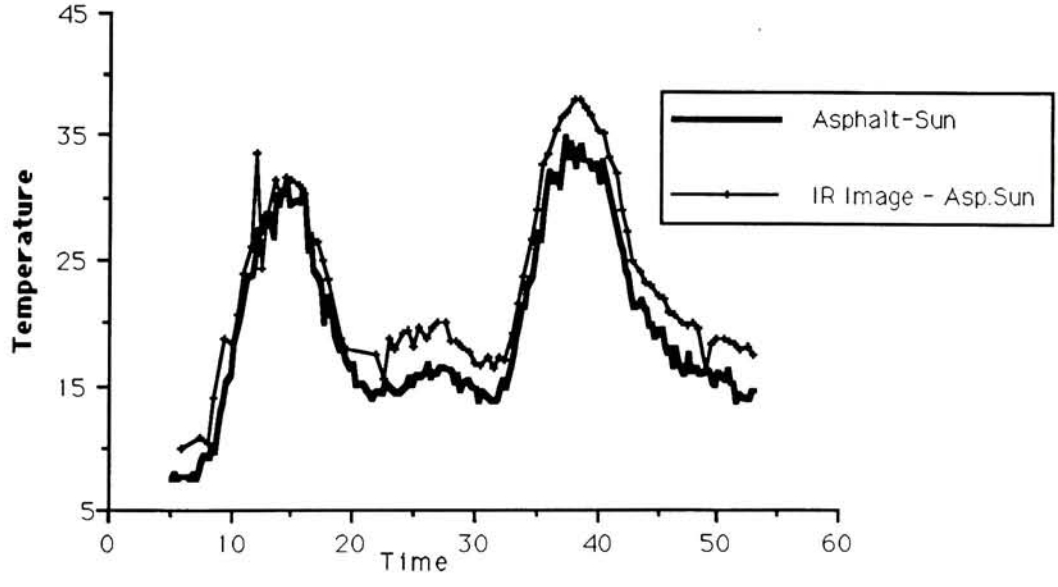

Figure 4.3 IR image derived temperatures vs. thermistor measurements Asphalt in the sun, 10/5-6/90

Exclusion of these variables adds a bias to the temperatures computed from the IR images. Because the background temperature and upwelled and downwelled radiance

effects are not included in this calculation, it is only used as a sanity check of thermistor temperatures.

Meteorological data for input to the temperature generator Therm were collected by various means listed in Table 4.1. Radiosonde data for input to the atmospheric models were ordered from the Buffalo Airport (*cf.* Appendix F).

Required Data	Collection Method
Air Temperature (°C)	Thermometer
Air Pressure (mbar)	Barometer
Relative Humidity (%)	Hygrometer
Wind Speed (m/s)	Anemometer
Direct Insolation (L/hr)	Pyronometer
Diffuse Insolation (L/hr)	Pyronometer
Sky Exposure (%)	Experimental Estimate
Cloud Type (0-8)	Experimental Estimate
Precipitation Type (0/1)	Experimental Observation
Precipitation Rate (cm/hr)	Rain Gauge
Precipitation Temperature (°C)	Thermometer
Kinetic Object Temperature (°C)	Thermistor
Radiance at Sensor (W/m2 sr)	Thermal Imagery
Orientation Angles	Experimental Measurement
Object Dimensions	Experimental Measurement

Table 4.1 Experimental Data and Collection Methods

Temperatures of objects in the scene were recorded by thermistors on fifteen minute intervals. The thermistors are simple devices which change their resistance as a function of temperature. By applying a voltage across the thermistor circuit, the change in resistance can be recorded. The output signal of the circuit was converted to a digital count which was then converted to a temperature value through a calibration curve. The calibration curve was generated by taking thermistor readings of known temperatures within a water bath. The thermistor readings were averaged for each temperature and then plotted against temperature for the calibration curve. The thermistors are calibrated to read the same temperature to within 0.1 °C of each other. The resulting temperatures

measured in the scene were used for testing the accuracy of Therm and validating Therm's input object parameters.

Object dimensions, angles, and locations in the scene were measured for the purpose of reconstructing the scene in AutoCAD. Object thicknesses and angles were entered in the attribute and orientation nodes of the scene geometry submodel.

The resulting data gathered from these experiments includes forty-eight hours of: thermal and visible images recorded every half hour for October 1990; LWIR, MWIR, and visible images recorded every half hour for June 1992; meteorological data and object temperatures recorded at fifteen minute intervals, object dimensions, angles and locations within the scene for both collections; and radiosonde data recorded at the Buffalo Airport on October 4, 5, 6, and 7, 1990 and June 22, 23, and 24, 1992.

4.2) Task 2: Object Parameter Derivation

As stated earlier, accurate object parameters are essential for Therm's generation of accurate temperatures. These parameters were determined before DIRSIG was run to generate synthetic images of the experimental scene.

Each of the object parameters has an effect on the behavior of an object's temperature as a function of time. All of the parameters are defined on a sound first principles physical basis for use in the thermodynamic equations. Therefore, the goal of this task was to define as many parameters of objects in the scene as possible on a physical basis.

The thermal emissivity, slope and azimuth can remain constant once the basic values are determined because they are generally known to sufficient accuracy beforehand. The objects in the experimental scenes had no self-generated power except for the car's engine which was turned on for two hours at midnight of October 5, 1990. The engine's heat affected many of the neighboring facets such as the car hood, side, tire, and windshield, and the surrounding asphalt. Therm does not account for neighboring facets and thus there is no straightforward method of indicating to Therm that there were heat sources in the vicinity of the above facets. Therefore, the self-generated power of these facets must be manipulated to make Therm's output best fit the actual object temperatures for the period of time which the engine's heat had an effect. A limited effort

to accurately model these active facets was expended here. Since this is a known limit, the passive facets were dealt with in more detail.

Visible emissivity and exposed area have similar effects on an object's thermal signature, but for different physical reasons. Visible emissivity represents the fraction of visible insolation that is absorbed by a material. Exposed area represents the fraction of an object's area which is exposed to environmental effects such as sun, sky, wind and rain. The exposed area can be adjusted based on the shadowing of a facet due to nearby objects. Both the exposed area and visible emissivity terms were adjusted while determining optimum object parameters.

Therm aggregates the heat capacity (defined as the product of the material's specific heat and density) and thickness parameters into one variable, thermal mass, for its temperature calculations. Thermal mass is defined as the product of the heat capacity and thickness. It is a measure of the resistance of a material to thermal changes (ie. kinetic temperature). For example, a thermally massive object takes longer to respond to thermal changes and retains its 'memory' of past thermal influences longer.

A second lumped parameter which Therm computes is the Biot number. This value is defined as the product of thickness and the calculated heat transfer rate, divided by the object's thermal conductivity. It is a measure of the insulating properties of a material.

When deriving object parameters, the thickness was usually varied while the heat capacity was held constant to adjust an object's thermal mass. A byproduct of this procedure was a change in the Biot number. If this change produced higher temperature prediction error, the thermal conductivity was varied to adjust the Biot number to a more appropriate value resulting in lower error in temperature prediction.

Therefore, when deriving optimum object parameters for the experimental scene, four parameters were varied to fine-tune Therm's output temperatures. These parameters were exposed area, visible emissivity, thickness and thermal conductivity. Once the other parameters were appropriately defined based on physical characteristics of the material, these four variables were adjusted individually and in combination for fine-tuning. The final combinations which resulted in the smallest RMS error (between computed temperatures and actual temperatures recorded by thermistors) were used as inputs to the

DIRSIG model. The facets requiring self-generated power were treated as a special case. This process of deriving optimum object parameters was used in order to correct text book material values for the specific targets observed in the experimental scenes. The resulting optimized parameters minimize Therm's RMS temperature prediction error for the targets in the scene.

4.3) Task 3: Testing Therm

Therm can be run as a stand alone model outside of DIRSIG. Testing the sensitivity of Therm involved determining the errors in the input variables and the amount of impact each variable has on output temperatures. Due to the fact that the model employs numerical solutions to differential equations for its computations, general error propagation methods were difficult to implement. The following is a description of the technique used for error propagation testing of Therm.

A specific error bound was defined for each variable input to Therm. The variation in output temperature due to this error was determined by multiple runs of Therm. Therm outputs the object temperature as a function of time. The program was first run with the original object and weather parameters to establish 'truth' temperatures for various objects. Then, one input was varied over its range of error while the remaining variables remained the same to produce a new temperature output for each object. An RMS error was computed between this new temperature output and the 'truth' temperatures. In this manner Therm's sensitivity to variations in individual parameters was determined.

Table 4.2 lists all variables computed by the thermal model and the sources of the truth values used to test each variable. The errors associated with each variable input to Therm were determined and are discussed at length in the next section. Each of the weather and object parameters were varied individually according to its error bound to determine its impact on the computation of final object temperature. Input variables which have the largest impact on the output temperature were identified. Also, Therm's prediction of meteorological data was compared to the actual data collected during the experiment. Final temperatures computed by Therm in both the weather prediction mode and full input environmental data mode with both generic and optimized object parameters were compared to thermistor measurements to determine temperature error values.

Inputs to Thermal Model Environmental Prediction		Environmental Model Output Validation		Inputs to Thermal Model Temperature Prediction		Temperature Model Output Validation	
Value	Source	Value	Source	Value	Source	Value	Source
Sunrise Time	Longitude, Latitude, Day of Year from Ephemeris	Air Temp(t)	Thermometer (t)	Density	Available Literature	Kinetic Tempera-ture(t)	Thermistor Measure-ment(t)†
Sunset Time		Air Pressure	Barometer (t)	Specific Heat	Available Literature		
Sunrise Air Temperature	Weather Service Report	Relative Humidity	Hygrometer (t)	Thermal Conductivity	Available Literature		
Peak Air Temperature		Dew Point(t)	* (t)	Exposed Area	Experiment Estimate		
Time of Peak Air Temp.		Wind Speed	Anemometer (t)	Visible Emissivity	Available Literature		
Air Pressure		Direct Insolation(t)	Pyronometer (t)**	Thermal Emissivity	Emissometer Measurement		
Humidity		Diffuse Insolation(t)	Pyronometer (t)**	Self-Generated Power	Available Literature		
Dew Point		Sky Exposure	Experimental Estimate (t)	Thickness	Measurement		
Wind Speed		Cloud Type	Experimental Estimate (t)	Slope	Measurement		
Sky Exposure		Rain Type	Experimental Estimate (t)	Azimuth	Measurement		
Cloud Type		Rain Rate	Rain Gauge (t)	Sun/Shadow History	Visible Imagery		
Rain Type		Rain Temperature	Experimental Estimate (t)	Plus all of the environmental model outputs and their corresponding experimental values as a function of time			
Rain Rate							
Rain Temperature	Engineering Estimate						

* Thermal model computes dew point based on air temperature and relative humidity
** Eppley Precision Pyronometers
† YSI Thermistors

Table 4.2 Thermal Submodel Variables: Truth and Prediction Sources

4.4) Task 4: Testing DIRSIG

The method of error propagation defined by Yardley Beers (1957) was used for the sensitivity study of DIRSIG. Beer's method states that given a quantity, V, which is a function of other variables, x and y, the error in V, dV, can be derived from the errors associated with x and y, dx and dy, and the deviations of individual measurements from the average values of x and y, δx and δy.

4.4.1) Error Definitions

There are three types of errors: independent, nonindependent, and correlated. When the error in one variable has no relation to the errors in the other variables, it is said to be an independent error. When errors in the input variables are due to a common cause, such as an inaccurate measuring instrument, they are said to be nonindependent. Correlated errors are ones for which the deviations of individual measurements from the means of two variables are systematically related. Beers uses the following example to illustrate the three types.

The area of a rectangle is to be determined by measurement of its width and length. One method is to take ten quick measurements of both variables under the same conditions using the same measuring tape. A second method is to take one measurement a day for ten days using the same measuring tape but now under different conditions.

Looking at the product of the deviations of the measurements from the average values for the first case, $\Sigma\delta x\delta y$, a logical pairing of deviations would be random. On average, this sum will then be zero. In this case, the errors are independent. There may also be some nonindependent error which could be due to thermal expansion of the measuring tape. This error affects all measured values equally and can be accounted for if it is known to exist. It cannot be detected by inspecting the deviations.

In the second case, without correction for expansion of the tape due to the different temperatures on different days, the only logical pairing of deviations is by measurements taken on the same day. The result is that on hotter days, the deviations of both variables are positive, larger than average. On cooler days, both deviations are negative, smaller than average. The product of these deviation pairs will always be positive. Therefore, the sum of the products ($\Sigma\delta x\delta y$) will not be zero. These errors are said to be correlated.

4.4.2) Propagation of Independent and Correlated Errors

For correlated errors, the average value of the sum $\Sigma\delta x\delta y$, ρ_{xy}, must be computed. This term is called the correlation coefficient. A value of 0 for ρ_{xy} indicates purely independent error, while a value of +1 indicates completely correlated error. The standard deviation, s, for each variable must also be either computed or estimated to predict the error in the output.

$$\rho_{xy} = \frac{1}{(k-1)\, s_x\, s_y} \sum_{n=1}^{k} (\delta x_n\, \delta y_n)$$

Equation 4.2

$$s = \sqrt{\frac{\sum_{n=1}^{k} (\delta x_n)^2}{k-1}}$$

Equation 4.3

The error in the output, V, due to correlated and independent error in the inputs can be expressed as a standard deviation, s_V:

$$s_V = \sqrt{\left(\frac{\delta V}{\delta x}\right)^2 s_x^2 + \left(\frac{\delta V}{\delta y}\right)^2 s_y^2 + 2\rho_{xy}\left(\frac{\delta V}{\delta x}\right)\left(\frac{\delta V}{\delta y}\right) s_x\, s_y}$$

Equation 4.4

Addition of errors in added input variables is straightforward. For example, addition of a third variable, w, would result in the following terms added under the square root in Equation 4.3.

$$\left(\frac{\delta V}{\delta w}\right)^2 s_w^2 + 2\rho_{wx}\left(\frac{\delta V}{\delta w}\right)\left(\frac{\delta V}{\delta x}\right) s_w\, s_x + 2\rho_{wy}\left(\frac{\delta V}{\delta w}\right)\left(\frac{\delta V}{\delta y}\right) s_w\, s_y$$

Equation 4.5

If only independent errors are present, the correlation coefficient is 0, and Equation 4.4 becomes:

$$s_V = \sqrt{\left(\frac{\delta V}{\delta x}\right)^2 s_x^2 + \left(\frac{\delta V}{\delta y}\right)^2 s_y^2}$$

Equation 4.6

4.4.3) Propagation of Nonindependent Errors

When the errors present in the inputs are nonindependent, the output error can be expressed as:

$$dV = \frac{\delta V}{\delta x} dx + \frac{\delta V}{\delta y} dy$$

Equation 4.7

4.4.4) Total Output Error

If both nonindependent and correlated and/or independent errors are present, the final error in the output value can be computed as:

$$\text{Total Error in V} = \sqrt{dV^2 + s_v^2}$$

Equation 4.8

These methods were applied to the four equations of radiation propagation in the radiometry model of DIRSIG. First, the type and amount of error associated with each variable were determined. Then, the above equations were applied to compute the error in the final radiance values. The radiometry variables tested are listed in Table 4.3 along with how truth values were determined and where the modeled values were computed.

4.5) Task 5: Evaluation of Synthetic Imagery

Final images computed by DIRSIG were compared to the thermal imagery gathered during the data collection experiments. Radiance values were derived from the truth images as described in section 4.1. These true radiance values were then compared to predicted radiance values from DIRSIG. The sensor submodel was also tested by comparison of the imagery. Table 4.4 lists the parameters of the sensor submodel tested and sources of variable validation. Discrepancies between the images will be discussed and explained in following sections. The potentials and limitations of the model will be addressed along with suggestions for further improvement of the model.

Inputs to Radiometry Submodel		Validation	Model Output	Validation
Value	Source	Source	Value	Source
ε -Target Emissivity	DIRS Database	Emissometer Measurement	Radiance Reaching the Sensor	Calibrated Radiance Imagery
LT - Target Radiance due to Temp.	Thermal Submodel (Planck)	Thermistor Measurement		
IT & IB Sun/Shadow Histories	Ray_tracer Submodel	Visible Imagery		
Es/p*t1	LOWTRAN	Pyronometer*		
θs - Target Slope	Geometry Submodel	Experimentor Measurement		
F - Shape Factor	Geometry Submodel	Experimentor Estimate		
LD - Downwelled Radiance	LOWTRAN	Spectro-radiometer**		
LTAB - Ave. Background Radiance due to Temp.	Thermal Submodel	Thermistor Measurement		
θB - Background Slope	Geometry Submodel	Experimentor Measurement		
εB - Background Emissivity	DIRS Database	Emissometer Measurement		
τ2 - Target-Sensor Transmission	LOWTRAN	Radiometric Ground Truth		
Lu - Upwelled Radiance	LOWTRAN	Radiometric Ground Truth		
LD^ -Directional LD	LOWTRAN	Spectro-Radiometer**		
Lu^ -Directional Lu	LOWTRAN	Radiometric Ground Truth		
LTB - Background Radiance due to Temp.	Thermal Submodel	Thermistor Measurement		

* Eppley Precision Pyranometer
** Infrared Systems Spectroradiometer

Table 4.3 Radiometry Submodel Variables: Truth and Prediction Sources

Inputs to Sensor Submodel		Validation	Model Output	Validation
Value	Source	Source	Value	Source
Sensor Response Function	Manufacturer Specifications	NA	Digital Count	Thermal Imagery
Sensor Gain	BB Calibration Data	BB Imagery		
Sensor Bias	BB Calibration Data	BB Imagery		
Field of View X	User Defined	Visual Inspection of Imagery		
Field of View Y	User Defined			
# of Pixels X	User Defined			
# of Pixels Y	User Defined			

Table 4.4 Sensor Submodel Variables: Truth and Prediction Sources

Results

5.1) Therm Test Results

Tables 5.1 and 5.2 list the errors associated with the weather and object variables input to Therm. Also listed are the RMS errors in output temperature resulting from these input errors. Two different types of error, prediction and measurement, are listed.

Therm can run in a predictive mode in which diurnal weather data is computed based on input averages of the weather variables. 'Predicted' RMS errors in the weather variables are computed between Therm's prediction of weather data and the actual measured diurnal weather.

When an object is being modeled and is not available for measurement, its objects parameters must be estimated. Lists of parameters for many different objects have been compiled (DCS Corp., 1990) for this situation. Many similar objects on these lists have varying parameters. The 'predicted' object parameter errors are the variabilities of each parameter within each group of materials.

'Measurement' errors of weather and object variables are those associated with the accuracy and precision to which a variable can be measured in an experiment. The measurement error of the weather variables is the error associated with the measuring equipment used during the October 1990 and June 1992 data collections. For example, the measurement error of the air temperature was 0.2°C. Some object parameters such as thickness and orientation can be measured very precisely by the user. Other variables are more easily determined by consulting manufacturer specifications or general material property tables found in thermodynamic and heat transfer literature. However, these references rarely list the variability associated with the given parameter value. For those easily measureable parameters, the actual measurement accuracy and precision are listed in the error table. For the other variables, a conservative estimate of 10% error in the given value was used for the sensitivity testing.

For the weather testing, complete diurnal weather data from six days: June 23 and 24, 1987; October 6 and 7, 1987; and October 5 and 6, 1990, was used. This weather information was used to generate all truth (output object temperatures) and served as a basis for the sensitivity tests.

Variable	Prediction Error	Resulting Temp. Error	Measurement Error	Resulting Temp. Error
Air Temperature	RMS: 1.57 Bias: 0.63	1.0947	0.2 °C	0.1027
Air Pressure	RMS: 1.87 Bias: -0.05	0.0017	0.2 mbar	0.0017
Humidity	RMS: 0.14 Bias: 0.05	0.1754	0.2 %	0.0069
Dew Point	RMS: 3.57 Bias: 1.46	0.2650	NA	NA
Wind Speed	RMS: 1.311 Bias: -0.021	0.3143	1.111 m/sec	0.2978
Direct Insolation	RMS: 10.20 Bias: -4.47	0.9146	Precision: .043 Accuracy: 0.2%	.0061
Diffuse Insolation	RMS: 8.06 Bias: -3.16	1.6752	Precision: .043 Accuracy: 2.0%	.0046
Sky Exposure	RMS: 0.21 Bias: 0.00	0.3637	0.05	0.0728
Cloud Type	RMS: 1 Bias: 0	0.1421	0 if CT=0,1,7,8 1 otherwise	0.0518
Precipitation Type	None	NA	None	NA
Precipitation Rate	RMS: 0.055 Bias: 0.00	0.1001	.0127 cm/hr	.0086
Precipitation Temperature	RMS: 7.14 Bias: -5.35	0.1617	2 °C	.0145
Total Error (no Rain)	----------	2.2721	----------	0.3276
Total Error (rain)	----------	2.2801	----------	0.3280

Table 5.1 Weather Parameter Errors and Resulting Temperature Errors

Variable	Prediction Error	Resulting Temp. Error	Measurement Error	Resulting Temp. Error
Specific Heat	Varies for each object	0.0188	10% of value	0.0718
Density	Varies for each object	0.0865	10% of value	0.072
Thermal Conductivity	Varies for each object	0.4362	10% of value	0.0477
Thickness	20%	0.1023	0.1 cm	0.0363
Visible Emissivity	Varies for each object	0.7774	10% of value	0.3934
Thermal Emissivity	Varies for each object	0.1983	0.025 (~5%)	0.0624
Self-Generated Power	Varies for each object	0.2488	10% of value	0.0236
Exposed Area	20%	0.5634	10% of value	0.2809
Slope	7.5°	0.1219	3°	0.0456
Azimuth	7.5°	0.2905	3°	0.1012
Total Error (passive)	----------	1.1265	----------	0.5137
Total Error (active)	----------	1.1536	----------	0.5142

Table 5.2 Object Parameter Errors and Resulting Temperature Errors

5.1.1) Weather parameter tests:

The truth data for the weather parameter tests were the temperatures of 11 objects (*cf.* Table 5.3) as computed by Therm using the original diurnal weather files. These objects were chosen because they were all used for the data collection experiment on October 5-7, 1990 and they cover a wide range of materials with differing thermal properties. The RMS error associated with one weather variable was added or subtracted randomly to the time dependent variable in the weather file while all other variables were left alone. Appendix A gives a listing of the computer program used to perform this task.

Next, the 11 object temperatures were computed using the revised weather file, and RMS errors between these output temperatures and the original truth temperatures were computed. The resulting temperature errors listed in Table 5.1 are averages over the RMS errors computed for each of the 11 objects.

Note that for the prediction errors, both a bias value and an RMS error are listed for each variable. For some variables, Therm tends to make optimistic or pessimistic predictions, resulting in a bias when compared to the actual data . For these cases, the bias was added to or subtracted from the true weather variable, depending upon its sign, and then the RMS error was randomly added.

The most important variables, ie. those that have the greatest impact on the error in output temperature, are air temperature, wind speed, and direct and diffuse insolation. Respectively, the errors in temperature due to errors in these variables are (*cf.* Table 5.1): (predicted) 1.09 °C, 0.31 °C, 0.91 °C and 1.68 °C, and (measured) 0.10 °C, 0.30 °C, 0.01 °C, and 0.00 °C.

Name	Density	Specific Heat	Thermal Conduct.	Thick-ness	Visible Emiss.	Thermal Emiss.	Exposed Area	Power	Slope	Azi-muth
Steel	7.833	0.1111	464.4	0.30	0.64	0.90	0.50	0	0	0
Aluminum	2.390	0.2198	1754.4	1.0	0.10	0.04	0.50	0	0	0
Asphalt	2.110	0.2200	6.36	3.0	0.86	0.98	0.70	0	0	0
Concrete	1.600	0.1600	0	12.0	0.70	0.95	0.60	-1.4	0	0
Brick	0.768	0.2098	8.17	0.5	0.75	0.93	0.50	0	0	0
Wood	0.600	0.6700	0.86	2.4	0.72	0.85	0.50	0	0	0
Plastic	1.400	0.0400	64.5	1.0	0.07	0.72	0.50	0	0	0
Window	2.707	0.1911	6.54	0.3	0.05	0.95	0.50	0	0	0
Tire	1.198	0.2986	1.30	0.3	0.95	0.99	0.50	0	0	0
Grass	1.000	1.0000	0	0.0	0.91	0.88	0.50	-4.5	85	180
Water	1.000	1.0000	5.0	16.6	0.50	0.96	0.50	0	0	0

Table 5.3 Objects used for weather sensitivity testing

Clearly, the errors resulting from Therm's prediction of the weather are greater than those errors resulting from variability in the measured data. One way to improve upon the prediction errors is to edit Therm's output weather. If the user has some idea of the weather patterns for the day being modeled, he can adjust the data predicted by Therm. For example, if it is known that the day was mostly sunny with a cloudy period

during the afternoon, the cloud type, sky exposure, and direct and diffuse insolations can be altered to better model that cloudy period. Also, some of Therm's weather predictions contain a bias which is more tolerable than an RMS error. Bias errors can be corrected by simply adding or subtracting the bias amount from the predicted data before running Therm to predict object temperatures.

It must be noted that Therm predicts the weather well when modeling stable days such as a typical sunny day with few clouds. Therm cannot predict rapidly changing weather conditions because it only works from values averaged over a 24 hour period. Depending upon the application of DIRSIG, this limitation may or may not be problematic. For training use and prediction of optimum imaging times, Therm's limitation is not critical. Many different scenarios can be defined with acceptable results from DIRSIG. However, modeling of actual imagery collected under unknown or unmeasured conditions may be limited.

For running Therm in the predictive mode, the critical weather parameters listed earlier (ambient temperature, sky cover, and solar loading) should be paid particular attention. Also note that for either method of weather generation, wind speed should be carefully watched. Even relatively small changes in wind speed (which Therm cannot predict) or errors in measured wind speed can have large effects on resulting object temperatures due to the convective cooling (or warming) nature of the wind.

When predicting object temperatures from measured weather data, errors in the object parameters have a much greater effect on the final temperature than do errors in the weather variables. In general, if the weather is very well known, the user should concentrate on determining correct object parameters. The impact of object parameter errors are discussed below.

5.1.2) Object parameter testing:

The truth data for the object parameter sensitivity tests are the temperatures of the 12 objects listed in Table 5.4. These objects were chosen from the lists provided by DCS Corporation so that materials with various thermal properties were represented. Each of these materials had at least five different listings of objects parameters from which the predicted parameter variability was computed. The tests were run in the same manner as the weather sensitivity tests: error was added to one parameter at a time, object temperatures were computed by Therm, then RMS errors between these output

temperatures and the truth temperatures were calculated. The average error due to each variable over all objects is listed in Table 5.2.

Name	Asphalt			Brick		
Variable	Value	Prediction Error	Measure Error	Value	Prediction Error	Measure Error
Density	1.841	.406	.184	1.259	.694	.126
Specific Heat	.2133	.0100	.0213	.2199	.0143	.0220
Conductivity	6.23	.25	.62	6.02	3.04	.60
Thickness	5.0	1	.1	5.0	1	.1
Vis.ible Emiss.	.91	.04	.091	.79	.06	.079
Thermal Emiss.	.96	.03	.025	.93	0	.025
ExposedArea	-.50*	.1	.05	-.50*	.1	.05
Power	0	0	0	0	0	0
Slope	0	7.5	3	90	7.5	3
Azimuth	0	7.5	3	0	7.5	3
Name	Concrete			Glass		
Density	1.893	.337	.189	2.643	.059	.264
Specific Heat	.1600	.0001	.0160	.1964	.0049	.0196
Conductivity	15.48	0	1.55	9.84	3.01	.98
Thickness	5.0	1	.1	3.0	.6	.1
Vis.ible Emiss.	.68	.24	.068	.13	.07	.013
Thermal Emiss.	.95	.04	.025	.85	.09	.025
ExposedArea	-.50*	.1	.05	.50	.1	.05
Power	0	0	0	0	0	0
Slope	0	7.5	3	0	7.5	3
Azimuth	0	7.5	3	0	7.5	3
Name	Grass			Gravel		
Density	1	0	.1	1.686	.225	.169
Specific Heat	1	0	.1	.1967	.0055	.0197
Conductivity	5	0	.5	9.37	7.86	.94
Thickness	.05	.01	.1	5	1	.1
Visible Emiss.	.79	.12	.079	.68	.27	.068
Thermal Emiss.	.94	.05	.025	.72	.30	.025
ExposedArea	.15	.03	.015	-.50*	.1	.05
Power	-1.18	1.50	.12	0	0	0
Slope	0	7.5	3	0	7.5	3
Azimuth	0	7.5	3	0	7.5	3

* Negative exposed area indicates that Therm should compute the temperature of the inner surface of the object

Table 5.4 Objects used for object parameter sensitivity tests

Name	Sand			Soil		
Variable	Value	Prediction Error	Measure Error	Value	Prediction Error	Measure Error
Density	1.606	.220	.161	1.478	.297	.148
Specific Heat	.1962	.0052	.0196	.2017	.0057	.0202
Conductivity	3.03	.72	.30	1.56	1.98	.16
Thickness	10	2	.1	12.0	2.4	.1
Visible Emiss.	.65	.07	.065	.83	.09	.083
Thermal Emiss.	.91	.02	.025	.94	.02	.025
Exposed Area	-.50*	.1	.05	-.50*	.1	.05
Power	0	0	0	-1.0	1	.1
Slope	0	7.5	3	0	7.5	3
Azimuth	0	7.5	3	0	7.5	3
Name	Steel			Water		
Density	7.772	.172	.777	1	0	.10
Specific Heat	.1107	.0006	.0111	1	0	.10
Conductivity	495.9	48.85	49.59	5.03	.06	.50
Thickness	2	.4	.1	20	4	.10
Visible Emiss.	.68	.18	.068	.75	.23	.075
Thermal Emiss.	.30	.28	.025	.96	0	.025
Exposed Area	.50	.10	.05	-.50*	-.50*	.05
Power	0	0	0	0	0	0
Slope	90	7.5	3	0	7.5	3
Azimuth	0	7.5	3	0	7.5	3
Name	Wood (Building)			Wood (Tree)		
Density	.600	.115	.06	.893	.149	.089
Specific Heat	.6532	.0407	.0653	.8413	.2035	.0841
Conductivity	.94	.12	.09	3.34	2.10	.33
Thickness	3.0	.6	.1	.25	.05	.1
Visible Emiss.	.74	.03	.074	.92	.07	.092
Thermal Emiss.	.83	.06	.025	.94	.02	.025
Exposed Area	-.50*	.1	.05	.15	.03	.015
Power	0	0	0	-1.14	1.10	.11
Slope	90	7.5	3	90	7.5	3
Azimuth	0	7.5	3	0	7.5	3

* Negative exposed area indicates that Therm should compute the temperature of the inner surface of the object

Table 5.4 Objects used for object parameter sensitivity tests

The object parameters whose errors have the greatest impact on output temperatures computed by Therm are: visible emissivity, exposed area, azimuth angle, and self-generated power. Respectively, the errors due to errors in these variables are (*cf.* Table 5.2) : (predicted) 0.78 °C, 0.56 °C, 0.29 °C, and 0.25 °C, and (measured) 0.39 °C, 0.28 °C, 0.10 °C, and 0.02 °C.

The error associated with self-generated power is misleading. Having acknowledged that Therm works poorly with active facets, only passive facets were fully tested during this study. The variability listed for self-generated power is that associated with facets that naturally have a low amount of power, such as growing grass and trees. Therefore, this output temperature error is not a true representation of Therm's ability to predict temperatures of active facets. If active facets were included in this study, the temperature error would most likely be much higher.

The high error due to prediction variability in thermal conductivity is due to one or two materials having a wide range of thermal conductivities listed in the literature. This large variability inflated the resulting temperature error. Comparing the error due to measurement variability of thermal conductivity to the error due to measurement variability in the other object parameters shows that the error due to thermal conductivity is not as critical as the errors in the variables listed above.

Error due to azimuth angle variability is easily understood. The azimuth of a facet determines the amount of solar loading the facet receives throughout the day. Relatively small errors can significantly increase or decrease the amount of solar energy the facet receives, thus affecting the facet's temperature.

Exposed area is a difficult parameter to quantify. It is used as a 'fudge factor' to give Therm a proportion of the facet area exposed to the environment. This parameter is not measured in a straightforward manner, but is estimated by the user. Again, small changes in the exposed area can have a significant effect on the facet's temperature.

Note that the magnitudes of the errors due to measured errors in object parameters are greater than those of the errors due to measured weather parameter variabilities. This reinforces the statement that the object parameters should be primarily focused on when running Therm with measured meteorological data.

Overall, Therm's combined sensitivity to variations in weather and objects parameters for passive facets is: 2.54 °C (prediction) or 0.61°C (measurement). It is important to keep in mind that when the goal is to predict true object temperatures, the definition of accurate object parameters is very important. The past two sections have

focused on Therm's sensitivity to errors in its input variables. The next section will discuss Therm's accuracy in predicting actual object temperatures.

5.1.3) Therm accuracy

Tables 5.5 and 5.6 list the optimum and generic object parameters determined for the facets in the scenes imaged during the October 1990 and June 1992 data collections. Optimum parameters are those which have been optimized for Therm's computations. These parameters yield the highest temperature prediction accuracy. Generic parameters are those which have been chosen from lists of object parameters with no optimization. Generic parameters represent the case in which there is no information available on the objects to be modeled and therefore the parameters must be estimated. Where applicable, parameters for similar objects from both collections were matched. Table 5.7 lists the RMS errors computed between Therm's prediction of object temperatures (using either optimum parameters or generic parameters taken directly from available literature) and the actual object temperatures measured by thermistors. Temperatures were computed using both full meteorological data and average weather values for Therm's weather prediction mode.

Clearly, Therm predicts object temperatures quite accurately when the total weather history is known and the object parameters have been fine tuned to fit the objects. However, it is a rare situation in which all weather and object information is known. More realistically, the user will have generic object profiles and perhaps an outline of the weather conditions for the day being modeled. In this case, Therm can generally predict object temperatures to within 3.5°C. It can be seen by comparison of the errors in Table 5.7 that it is very important to have a good profile of the object parameters.

The combination of full environmental data and optimum object parameters was used to create output images from DIRSIG. These images will help to illustrate how well the model can predict actual images. They will be presented in a later section along with corresponding truth images to illustrate the resulting errors. The next section details the sensitivity study performed on the radiometry submodel of DIRSIG. This section includes the effects errors in temperature have on the radiometry submodel's computation of radiance reaching the sensor.

Name	Density	Specific Heat	Thermal Conduct.	Thick-ness	Visible Emiss.	Thermal Emiss.	Exposed Area	Self. Power	Slope	Azi-muth
Aluminum	2.700	.2198	2064	0.0	.15	.10	-1.0	0	45	60
Asphalt	2.114	.2200	5.93	2.4	.93	.93	.40	2.2	0	0
Brick	0.768	.2098	8.17	5.0	.79	.93	-.34	0	45	60
Car Side	7.833	.1111	464.4	.21	.74	.44	1.0	1.45	90	90
Car Roof	7.833	.1111	464.4	.13	.74	.44	.53	0	0	0
Concrete	1.600	.1600	15.48	1.13	.90	.99	-.44	0	42.5	60
Grass	0.160	1.000	0.0	0.0	1.0	.98	.08	1.1	85	180
Gravel	1.000	.3400	17.2	.60	.90	.90	-.375	0	32	60
Sand	1.520	.1911	2.84	1.3	.76	.90	.39	0	0	0
Tire	1.198	.2986	1.3	.15	.93	.90	-.82	0	90	90
Water	1.000	1.000	11.0	14.0	.07	1.0	-.46	0	0	0
Window	1.000	.5200	12.04	.31	.61	.61	.95	.80	67	90
Windshield	1.000	.5200	12.04	.11	.61	.61	.52	0	17	180
Wood	0.400	.6689	1.1	2.15	.78	.90	.27	0	32	60

5.5a. Field Optimized Values

Name	Density	Specific Heat	Thermal Conduct.	Thick-ness	Visible Emiss.	Thermal Emiss.	Exposed Area	Self. Power	Slope	Azi-muth
Aluminum	2.700	.2198	2064	0.50	.74	.90	-.40	0	45	60
Asphalt	2.114	.2200	5.93	3.0	.93	.93	-.50	0	0	0
Brick	0.768	.2098	8.17	5.0	.75	.93	-.40	0	45	60
Car Side	7.833	.1111	464.4	0.5	.74	.44	.30	0	90	90
Car Roof	7.833	.1111	464.4	0.5	.74	.44	.50	0	0	0
Concrete	1.600	.1600	15.48	3.0	.90	.99	-.40	0	42.5	60
Grass	1.000	1.000	0.0	0.2	.91	.88	.16	-3.5	85	180
Gravel	1.700	.2000	17.20	3.0	.90	.90	-.40	0	32	60
Sand	1.510	.1900	2.67	5.0	.60	.90	-.40	0	0	0
Tire	1.198	.2986	1.30	2.0	.95	.99	-.30	0	90	90
Water	1.000	1.000	5.13	30.0	.50	.96	-.40	0	0	0
Window	2.600	.2000	12.04	2.0	.18	.79	.25	0	70	90
Windshield	2.600	.2000	12.04	2.0	.18	.79	.40	0	32	180
Wood	0.400	.6689	1.10	2.0	.78	.90	-.40	0	32	60

5.5b. Generic ("Textbook") Values

Table 5.5 October 1990 Object Parameters

Name	Density	Specific Heat	Thermal Conduct.	Thick-ness	Visible Emiss.	Thermal Emiss.	Exposed Area	Self. Power	Slope	Azi-muth
Asphalt	2.114	.22	5.93	2.4	.93	.93	.40	2.2	0	0
Blue Wood	.60	.67	.86	2.4	.60	.78	-.77	0	69	90
Bumper	7.833	.1111	464.4	.12	.88	.44	.69	0	90	90
Car Roof	7.833	.1111	464.4	.09	.88	.44	.53	0	0	0
Car Side	7.833	.1111	464.4	.01	.88	.44	1.0	1.8	90	90
Concrete	2.28	.1601	15.48	4.5	.73	.94	.39	0	0	0
Front Black	.60	.67	.86	2.4	.90	.78	-.77	0	90	90
Front White	.60	.67	.86	2.4	.20	.78	-.77	0	90	90
Green Wood	.60	.67	.86	2.4	.55	.78	-.77	0	69	90
Grey 1	.60	.67	.86	2.4	.50	.78	-.77	0	69	90
Grey 2	.60	.67	.86	2.4	.60	.78	-.77	0	69	90
Grey 3	.60	.67	.86	2.4	.70	.78	-.77	0	69	90
Grey 4	.60	.67	.86	2.4	.80	.78	-.77	0	69	90
Grey 5	.60	.67	.86	6.0	.72	.87	-.55	0	69	90
Red	.60	.67	.86	2.4	.65	.78	-.77	0	69	90
Sand	1.52	.1911	2.84	1.3	.76	.90	.39	0	0	0
Windshield	1.0	.52	12.04	.11	.61	.61	.52	0	17	180
Shingles	1.3	.35	6.36	.05	.74	.91	-.66	0	29	90
Specular	.60	.67	.86	3.0	.72	.87	-.45	0	0	0
Tire	1.198	.2986	1.3	.15	.93	.90	-.82	0	90	90
Water	1.0	1.0	11.0	47.0	.09	000	-.57	0	0	0
Window	1.0	.52	12.04	.31	.61	.61	.95	.80	67	90

5.6a. Field Optimized Values

Name	Density	Specific Heat	Thermal Conduct.	Thick-ness	Visible Emiss.	Thermal Emiss.	Exposed Area	Self. Power	Slope	Azi-muth
Asphalt	2.114	.22	5.93	3.0	.93	.93	-.50	0	0	0
Blue Wood	.40	.6689	1.10	1.0	.60	.90	-.40	0	69	90
Bumper	7.833	.1111	464.4	2.0	.94	.90	.40	0	90	90
Car Roof	7.833	.1111	464.4	.25	.60	.90	.50	0	0	0
Car Side	7.833	.1111	464.4	.25	.60	.90	.30	0	90	90
Concrete	1.600	.1600	15.48	5.0	.60	.88	-.40	0	0	0
Front Black	.40	.6689	1.10	1.0	.94	.90	-.30	0	90	90
Front White	.40	.6689	1.10	1.0	.16	.90	-.30	0	90	90
GreenWood	.40	.6689	1.10	1.0	.5	.90	-.40	0	69	90
Grey 1	.40	.6689	1.10	1.0	.30	.90	-.40	0	69	90
Grey 2	.40	.6689	1.10	1.0	.50	.90	-.40	0	69	90
Grey 3	.40	.6689	1.10	1.0	.75	.90	-.40	0	69	90
Grey 4	.40	.6689	1.10	1.0	.90	.90	-.40	0	69	90
Grey 5	.40	.6689	1.10	1.0	.70	.90	-.40	0	69	90
Red	.40	.6689	1.10	1.0	.65	.90	-.40	0	69	90
Sand	1.51	.19	2.67	2.5	.60	.90	-.40	0	0	0
Windshield	2.6	.20	12.04	2.0	.18	.79	.40	0	27	180
Shingles	1.3	.35	6.36	.30	.86	.91	-.40	0	29	90
Specular	.40	.6689	1.10	1.0	.50	.90	-.30	0	0	0
Tire	1.198	.2986	1.3	2.0	.95	.99	-.30	0	90	90
Water	1.0	1.0	5.13	30.0	.50	.96	-.40	0	0	0
Window	2.6	.20	12.04	2.0	.18	.79	.25	0	67	90

5.6b. Textbook ("Generic") Values

Table 5.6 June 1992 Object Parameters

Object	Observed Meteorological Data		Predicted Meteorological Data	
	Optimized	Generic	Optimized	Generic
Aluminum[1]	1.23	1.52	1.67	5.06
Asphalt[2]	2.31	4.33	5.05	8.14
Brick[1]	1.78	1.90	2.06	5.00
Car Roof (white)[1]	1.63	2.09	2.93	5.94
Car Side (white)[1]	2.91	4.59	2.52	4.15
Car Window[2]	2.49	8.44	7.78	10.58
Concrete Panel[1]	1.04	1.13	1.70	5.25
Roof Gravel[1]	1.36	1.59	1.35	5.30
Sand[2]	1.14	1.45	4.90	5.21
Tire[2]	3.36	6.22	9.49	7.28
Water [1]	1.05	3.45	1.62	7.24
Windshield[2]	2.27	7.24	5.03	9.39
Wood Panel[1]	1.23	1.77	1.54	7.13
Average Error	1.83	3.52	3.66	6.59

* 24 hours of data included on 15 minute centers

[1] 10/6/90 only (cloudy, low dynamic range)

[2] Parameters optimized for 6/23/92 (partly cloudy, high dynamic range), results include RMS errors for targets on both days

Table 5.7 RMS errors between thermistor truth and Therm prediction values for October 6, 1990 and June 23, 1992*

5.2.1) Radiometry submodel sensitivity

The same approach utilized for the thermal submodel tests was applied to the radiometry submodel testing. Errors due to measurement (ideal) and prediction situations were determined for all of the variables in the radiometry equations. The error in target radiance reaching the sensor due to the individual variable errors was computed using Beers' method of error propagation. Final prediction errors in radiance reaching the sensor were determined. This section details the methods by which each individual variable error was determined and is followed by the error propagation results.

$\varepsilon_S \varepsilon_B$:

The emissivities of many objects measured by Schott et. al. (1990) were used for targets in the ray_traced scenes. Emissivities of the painted panels and the roof shingles in the June 1992 scene were measured using the normal and angular emissometers described by Schott et. al (1990). The resulting values are listed in Appendix B. The error in these measured angular emissivities is listed as 0.025 emissivity units.

For targets for which no emissivity data were available, angular emissivity was approximated by using values from similar objects which had been measured. The resulting prediction error is estimated to be 0.05 emissivity units.

The target emissivities were measured in the wavelength band of 8-14μm. However, the Inframetrics camera used to gather the truth imagery is sensitive in the 8-12μm band. Data available in the literature (ref) indicate that for many targets the emissivity is well-behaved in the 8-14μm spectral region. Therefore, it is assumed that the emissivity in the subset 8-12μm region is equal to the emissivity measured in the 8-14μm band, within approximately 1% error.

L_T, L_B, L_{TAB}:

The error in radiance due to target temperature was determined from the error due to the model's temperature prediction. There are three different possible errors in temperature depending on the method used to determine target temperature. The ideal method for obtaining object temperatures is measurement by thermistor. If no thermistor data are available, the thermal submodel can be run using either full meteorological data and optimum object parameters or predicted environmental variables and object parameters as described in the thermal submodel testing section. Propagation of these

temperature errors through Planck's equation yields the errors in radiance due to temperature listed in Table 5.9.

Error Type	Thermistor (Ideal)	Therm Measurement	Therm Prediction
Temperature (°C)	0.14	0.95	2.55
Radiance (W/m2 sr)	0.09	0.63	1.73

Table 5.8 Radiance Error Resulting from Error in Object Temperature for an object at 300K

F:

The shape factor is a geometric variable which can be estimated to with 5-10% of its true value by use of a simple ray-tracing program. This program would cast rays from the facet to determine an approximate percentage of the sky the facet 'sees'. A conservative estimate for this ideal case was set at 10%.

The version of DIRSIG used for this project did not contain the program described above (Version 2.2.1 does incorporate this shape factor computation). A conservative estimate of 20% for user estimation of shape factor was used for the prediction error.

$E_S/\pi*\tau 1*\cos(\theta)$:

In the thermal region of the electromagnetic spectrum, the exoatmospheric solar radiance (E_S)is essentially zero. Therefore, the error in the direct solar insolation term (grouped as $E_S/\pi*\tau 1*\cos(\theta)$)was also set at zero.

An estimate of the error of Lowtran's prediction of solar insolation for other passbands such as the 3-5μm and visible regions was determined by comparison with the pyronometer data taken during the data collections. The direct solar insolation reaching a sensor which is sensitive in the 0.285-2.8μm region, mimicking the pyronometer sensitivity, was predicted by LOWTRAN7 (*cf.* Figures 5.1 and 5.2). The RMS error between the pyronometer data and these predicted values was then computed. A percent error was determined by dividing the RMS error by the range in insolation values. It is assumed that the prediction error in other passbands is proportional to this percent error.

Lowtran predicts well on well-behaved, cloud-free days, with an average percent error of 17.7%. However, errors as high as 50% arise for cloudy day predictions as shown in Figure 5.2. One factor in this problem is that the cloud definitions in the Lowtran program are not easily referenced to typical meteorological cloud types recorded during the data collections. A future improvement to the model would include a correlation between recorded cloud type and coverage and Lowtran cloud definitions.

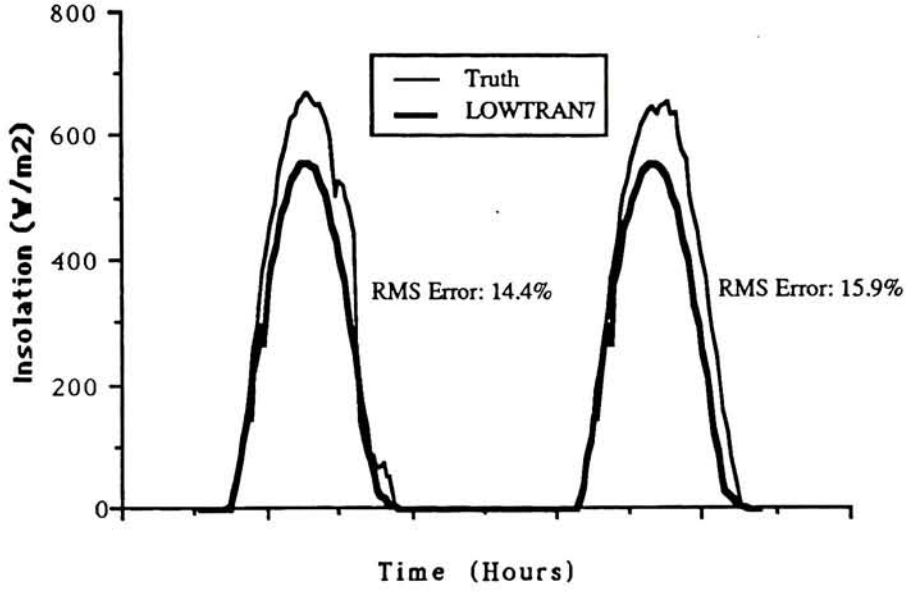

Figure 5.1 LOWTRAN Prediction of Total Insolation vs. Pyronometer Truth October 5&6, 1990

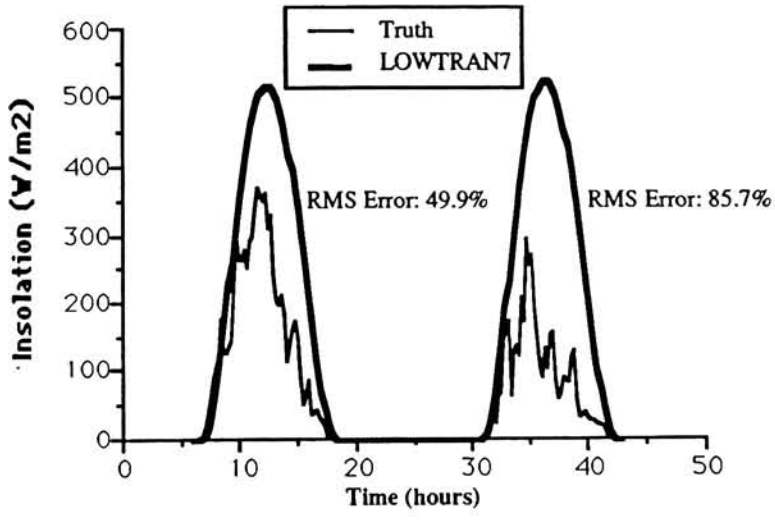

Figure 5.2 LOWTRAN Prediction of Total Insolation vs. Pyronometer Truth October 6&7 1987

L_D, L_{Dhat}:

Directional downwelled radiance measurements were made on a wavelength by wavelength basis with an Infrared Systems Spectroradiometer during the June 1992 data collection. Measurements were made at zenith angles of 8, 30, 45, 60, and 90 degrees, at each azimuth angle of 0, 90, 180, and 270 degrees. The data recorded in the thermal region is included in Appendix C. Figure 5.3 contains plots of the actual spectroradiometer measurements (integrated over 8-12μm) and Lowtran's predictions of directional downwelled radiance. Measurement (ideal) error was determined to be 2% from the available spectroradiometer documentation.

Measurements were made at four different times during the collection: 4:00pm and 10:00pm on June 22, and 8:00am and 4:00pm on June 23. June 22 was a relatively cloud-free day as evidenced by the low errors in L_D^ in Figures 5.3a and 5.3b. As with the direct insolation, Lowtran has problems predicting downwelled radiance when clouds are present. In Figures 5.3c and 5.3d, note the biased truth values due to the warm clouds present on June 23 which Lowtran did not accurately model.

The average prediction error for directional downwelled radiance was computed to be 2.64 W/m^2 sr when no clouds are present. Prediction error of downwelled radiance is assumed to be proportional to the errors in directional downwelled radiance over all zenith and azimuth angles. The percent error for both L_D and L_D^ is 18.8% (for cloud-free prediction), and for cloudy days this error is as high as 60%.

L_U, L_{Uhat}, τ_2:

Surface radiance and truth imagery measurements were performed on July 28, 1992. The same scene used during the June 1992 collection was imaged by the Inframetrics camera to collect truth imagery. Every hour from 9:30am to 4:30pm, the radiance leaving the surface of five targets in the scene was measured on the ground using a hand-held field radiometer sensitive in the 8-14μm region. At the same time, the scene was imaged from the Center for Imaging Science roof by the Inframetrics camera. Digital counts of the targets measured on the ground were extracted from the images. The radiance reaching the sensor was computed from the digital counts using blackbody calibration data as described in section 4.1 and as follows:

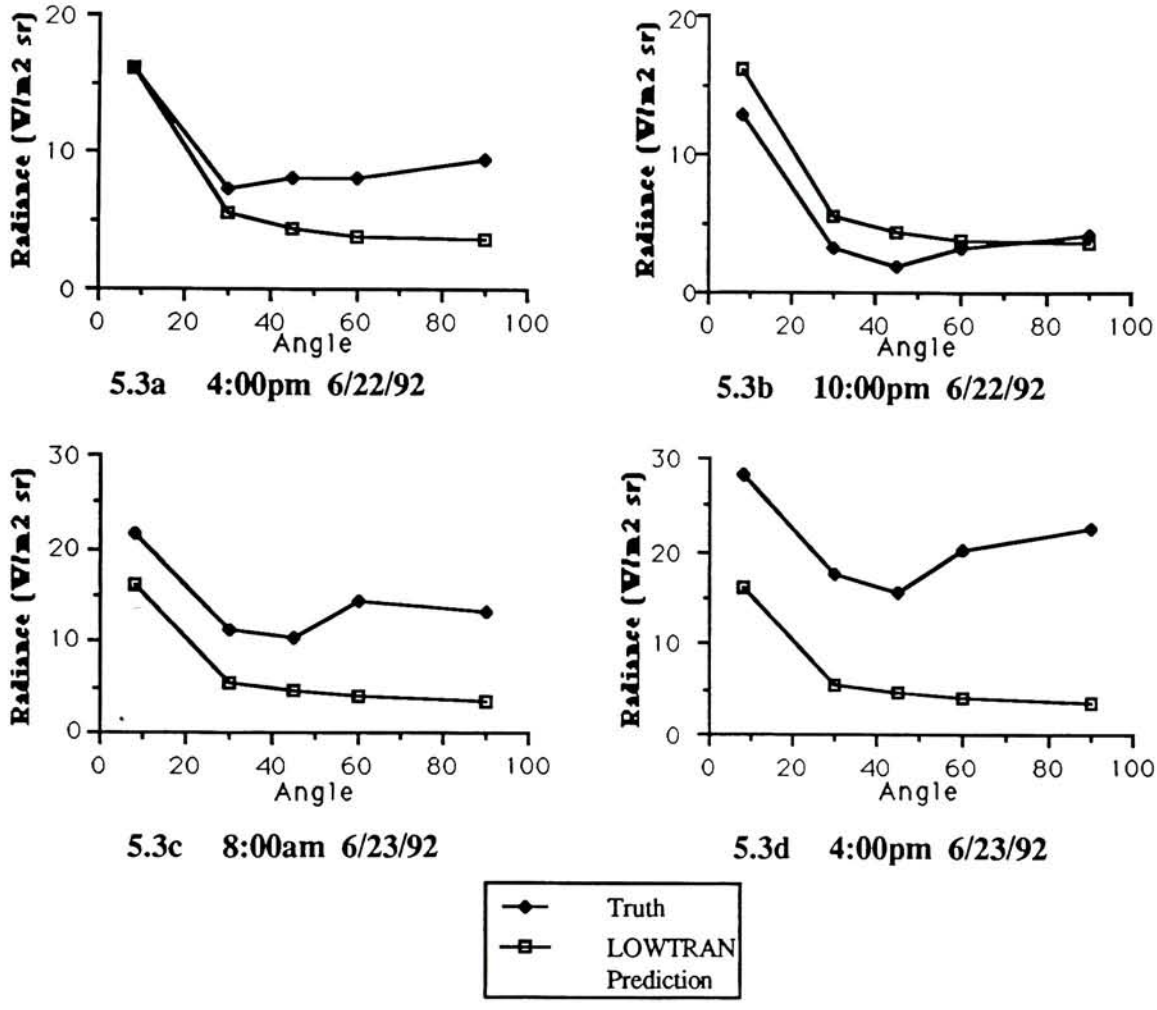

Figure 5.3 8-12μm Directional Downwelled Radiance June 22-23, 1992 Spectroradiometer Truth vs. LOWTRAN7 Prediction as functions of elevation angle

$$DC = mL_{sensor} + b$$

Equation 5.1

Where:

$$m = \frac{DC_{high} - DC_{low}}{L_{high} - L_{low}}$$

$b = DC_{hi} - mL_{low}$

DC_{high} = DC of blackbody at high temperature of 50°C

DC_{low} = DC of blackbody at low temperature of 10°C

L_{high} = Radiance in 8-12μm band corresponding to high temperature

L_{low} = Radiance in 8-12μm band corresponding to low temperature

Target-sensor transmission and upwelled radiance values were computed for each hour based on the relations in Equations 5.2 and 5.3.

$$L_{ground} = \varepsilon L_T + rL_D$$

Equation 5.2

$$L_{sensor} = L_{ground}\tau_2 + L_U$$

Equation 5.3

Where: L_{ground} = Radiance leaving the target at the ground (measured at ground)
L_{sensor} = Radiance reaching the sensor (extracted from imagery)
ε = Emissivity of the target
L_T = Radiance due to the target's temperature
r = Reflectance of the target
L_D = Downwelled radiance
τ_2 = Target-Sensor transmission
L_U = Upwelled radiance

The ground and sensor radiance values for all targets were plotted against each other as shown in Figures 5.4a - 5.4c. The slope of the resulting line is τ_2 and the y-intercept is L_U.

Variations in the surface leaving radiance due to wind, changing cloud cover, and the angle at which the radiometer was held during target radiance measurement resulted in a large margin of error in the ground radiance values. These errors caused slight variations in the slope (τ_2) of the resulting plots. Because the y-intercept is very close to zero, these slope variations resulted in high variability in the y-intercept value. Therefore, although the τ_2 errors were tolerable, the computed L_U values were unacceptable. The error between Lowtran's prediction of τ_2 and the measured τ_2 values is 0.03. The measurement (ideal) error in τ_2 was estimated at 0.03 due to the measurement variability described above.

Due to the similarity of the physics involved in modeling upwelled and downwelled radiance, it is assumed that the errors in Lowtran's prediction of upwelled and directional upwelled radiance are proportional to the prediction errors of downwelled and directional downwelled radiance. The available literature (Schott et. al., 1990) indicate that this assumption holds true in many scenarios.

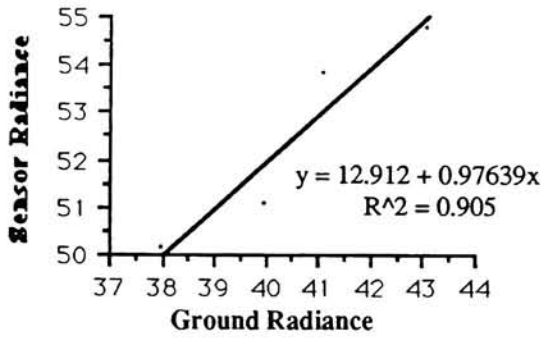

5.4a 10:30am July 28, 1992

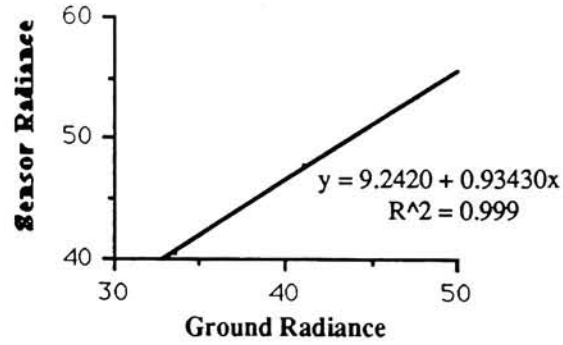

5.4b 2:30pm July 28, 1992

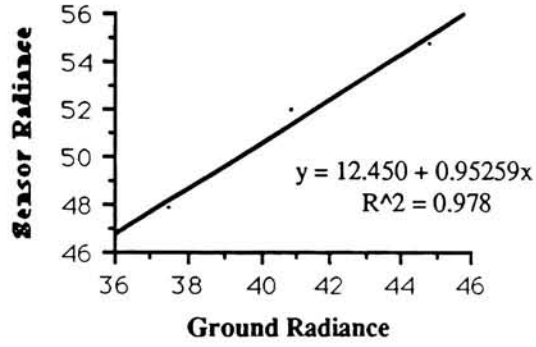

5.4c 4:30pm July 28, 1992

Figure 5.4 Experimental Measurement of $\tau 2$ and L_U

θ_S, θ_B:

As in the thermal submodel testing, measurement errors of the target-sun path angles for both primary and background targets were estimated at $\pm 3°$, while prediction errors (for unmeasured or simulated targets) were estimated to be $\pm 7.5°$.

I_T, I_B:

Investigation of the shadows in the visible images taken during the data collections and the ray-traced shadows in DIRSIG output images indicate that the ray-tracer correctly predicts the placement of sun shadows over time. Therefore, the error in the sun/shadow history terms was set to zero.

The following section describes the radiometry error propagation and contains a complete summary of the values of the errors determined above.

5.2.2) Radiometry Error Propagation Results

The following are the results from the sensitivity testing of the radiometry submodel, using Beers' method of error analysis as described in section 4.4.1. A detailed listing of the error propagation for all scenarios described below can be found in Appendix D.

For each scenario, four error types were defined: ideal (I), Therm measurement (M), Therm prediction (P), and clouds (C). Ideal errors (I) are the errors which would result if all of the radiometry variables were measured by the experimentor. They illustrate the best case scenario possible. However, these errors do not represent a realistic case for running DIRSIG and therefore serve only as a reference base for the other cases.

Therm measurement errors (M) include all prediction errors for the radiometry equation terms, except for terms involving object temperature. In this case, the error in radiance due to target temperature is equivalent to the error in object temperature when Therm predicts the temperatures using full environmental data and optimal object parameters.

Therm prediction errors (P) include predicted errors for all variables including the temperature error resulting from Therm's use of predicted weather data and generic object parameters. The only difference between the M and P errors used here is the error associated with object temperature prediction. The measurement error (M) includes optimized Therm temperature predictions, while the prediction errors (P) include Therm predictions using generic input variables as discussed in section 5.1. Both cases include the prediction errors determined for all other radiometry variables as described in the previous section. These two cases involving Therm predictions represent the most realistic situations DIRSIG would be used in. That is, a scene is to be simulated in which Therm will be used in its optimal or generic temperature prediction mode and the atmosphere is to be modeled by LOWTRAN7.

The final error set, clouds (C), includes errors induced in the radiometric variables by LOWTRAN7 when clouds were present in the actual scene. As discussed earlier, LOWTRAN7 has great difficulty making accurate predictions when clouds are present. Table 5.9 below is a summary of the error values assigned to each variable in the four cases described above.

Error Type	ε_s, ε_B	L_T,L_B, L_{TAB}	F	$E_s\tau_1$ cos(θ)	L_D, L_D^	L_U, L_U^	τ_2	θ_S, θ_B	I_T, I_B
Ideal	0.025	0.09	10%	0.20%	2.0%	2.0%	0.03	3.0°	0
Measured	0.05	0.63	20%	17.7%	18.8%	18.8%	0.03	7.5°	0
Predicted	0.05	1.73	20%	17.7%	18.8%	18.8%	0.03	7.5°	0
Cloud	0.05	1.73	20%	50%	60%	60%	0.03	7.5°	0

Table 5.9 Individual Variable Error Contribution

A representative situation was used to test each ray-interation case. For case 1, a ray hitting a diffuse target, grass was used as the target. Water was the object for case 2, a specular bounce to sky. For a specular bounce to background, case 3, a ray bouncing from asphalt to a car door background was used. For case 4, a missed scene (ray cast to sky), there is only one term in the radiance equation, L_D^ (*cf.* Eq. 2.4). Therefore, the resulting radiance error is simply equal to the error in directional downwelled radiance.

Two scenarios were used for the error testing, each having the representative cases for each ray-interaction type. The first scenario was a simulation of the rooftop scene used during the experimental data collections. The second scenario was a simulation of an airborne sensor flying at 3,000 feet. Figure 5.5 illustrates the ray-interaction cases and test scenarios. Table 5.10 contains the resulting error in radiance reaching the sensor (equivalent apparent temperature is listed in parentheses) for each ray-interaction case and test scenario. The values used for the individual variables and error terms in all of the different ray-interaction cases and scenarios can be found in Appendix D.

	Case 1				Case 2				Case 3			
Scenario	I	M	P	C	I	M	P	C	I	M	P	C
Rooftop	1.28 (1.92)	1.95 (2.93)	2.38 (3.57)	2.43 (3.65)	.95 (1.43)	1.46 (2.24)	1.90 (2.85)	2.32 (3.48)	1.26 (1.89)	1.45 (2.18)	2.04 (3.06)	2.01 (3.02)
Air-borne	1.22 (1.83)	1.80 (2.70)	2.18 (3.27)	2.80 (4.20)	.90 (1.35)	1.46 (2.24)	1.76 (2.64)	2.77 (4.16)	1.23 (1.85)	1.36 (2.04)	1.88 (2.82)	2.47 (3.71)

Table 5.10 Radiometry Submodel Error Propagation: Total Error in Radiance Reaching the Sensor (Equivalent Temperature Error in Parentheses)

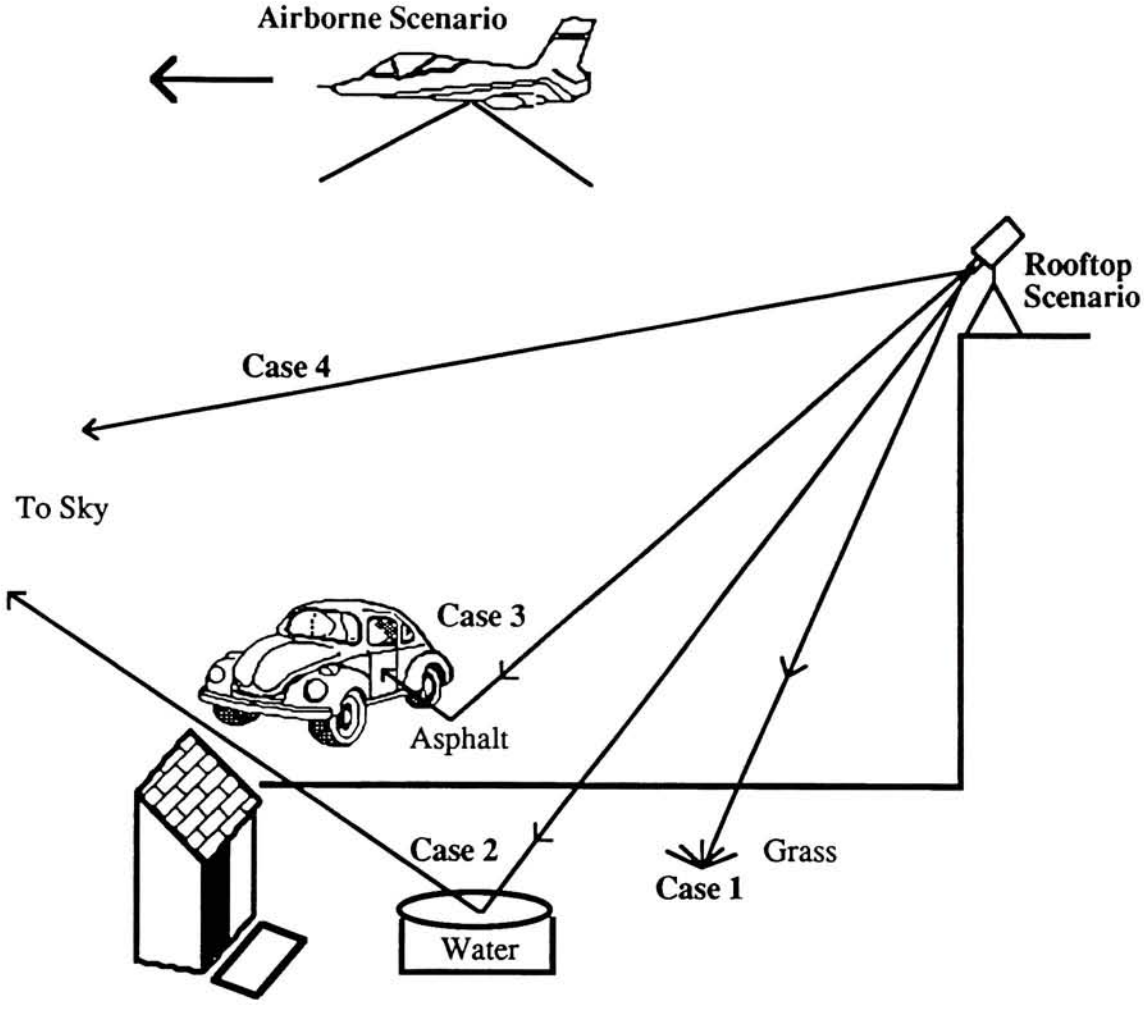

Figure 5.5 Ray-Interaction Cases and Test Scenarios for Radiometry Submodel Testing

All errors were assumed independent except for $\tau 2$ and L_U, which are inversely correlated. The correlation coefficient between these two terms was determined to be -0.8381 (*cf.* Eq. 4.2). The cross-term shown in Equation 5.4 was added to the error propagation equations as described in section 4.4 and as illustrated in Equation 4.4.

$$\text{Crossterm} = \rho\tau 2LU * \frac{\delta L}{\delta \tau 2} * \frac{\delta L}{\delta LU} * s\tau 2 * sLU$$

Equation 5.4

When LOWTRAN7 predicts the atmospheric terms for the radiometry equations, if $\tau 2$ is predicted above its true value, the predicted L_U value will be smaller than its true

value, and vice versa. Therefore, as the error in one term increases, so does the error in the other term. Although these errors offset each other in the computation of radiance reaching the sensor, Beers' method of uncorrelated error propagation does not acknowledge it. Instead, the errors become additive, resulting in an exaggerated error in the radiance reaching the sensor. The negative correlation coefficient (and thus negative cross-term) helps to reduce this inflation of the error in radiance.

As expected, the error in radiance reaching the sensor is lowest when computed from the ideal errors and increases to its highest value when cloud errors are used. Note that the errors in output radiance are lower for the airborne sensor simulation than for the rooftop simulation for all error types except clouds (C). This is due to the larger L_U term for the airborne sensor. The upwelled radiance term is larger because of the longer target to sensor path length, and thus the L_U error term (computed as a percentage of the L_U term) is larger. This larger L_U error results in a larger cross-term which is subtracted from the other errors, resulting in a lower final radiance error for the airborne simulation.

For cloud errors, the resulting radiance errors are lower for the rooftop simulation than for the airborne sensor. In this case, the downwelled radiance term and error value are much larger for the airborne simulation, resulting in larger final radiance error.

5.2.3) Individual Variable Sensitivity

The discussion in this section includes the radiometry submodel's sensitivity to errors in the individual input variables. The focus will be on the two error cases involving Therm optimal and generic temperature prediction with no clouds present. As stated earlier, these two cases represent the most common usage of DIRSIG and are therefore of the most interest for error propagation studies.

Tables 5.11a and 5.11b list the individual radiance error contributions of each variable for all of the cases and error types (equivalent temperature errors are listed in parentheses). Tables 5.12a and 5.12b list the percent error contribution for all ray-interaction types for the two cases of interest: Therm's two methods of temperature prediction. Note that a combined percent error contribution is listed for the correlated variables upwelled radiance and target-sensor transmission. In addition, Tables 5.13a and 5.13b list the ranking for each variable's contribution to the total error for all ray-interaction types for the two cases of interest.

Rooftop Scenario												
	Case 1				Case 2				Case 3			
Variable	I	M	P	C	I	M	P	C	I	M	P	C
ε	.70 (1.05)	1.40 (2.10)	1.40 (2.10)	1.40 (2.10)	.57 (.86)	1.15 (1.73)	1.15 (1.73)	1.15 (1.73)	.31 (.47)	.62 (.93)	.62 (.93)	.62 (.93)
L_T	.08 (.12)	.53 (.80)	1.47 (2.21)	1.47 (2.21)	.06 (.09)	.43 (.65)	1.18 (1.77)	1.18 (1.77)	.08 (.12)	.56 (.84)	1.54 (2.31)	1.54 (2.31)
F	.38 (.57)	.75 (1.13)	.75 (1.13)	.75 (1.13)	---	---	---	---	---	---	---	---
L_D,L_D^	.03 (.05)	.28 (.42)	.28 (.42)	.63 (.95)	.07 (.11)	.65 (.98)	.65 (.98)	1.47 (2.21)	---	---	---	---
τ_2	1.0 (1.50)	1.0 (1.50)	1.0 (1.50)	1.0 (1.50)	.75 (1.13)	.75 (1.13)	.75 (1.13)	.75 (1.13)	1.22 (1.83)	1.22 (1.83)	1.22 (1.83)	1.22 (1.83)
L_U,L_U^	.02 (.03)	.16 (.24)	.16 (.24)	.54 (.81)	.02 (.03)	.16 (.24)	.16 (.24)	.54 (.81)	.02 (.03)	.16 (.24)	.16 (.24)	.16 (.24)
ε_B	---	---	---	---	---	---	---	---	.11 (.17)	.23 (.35)	.23 (.35)	.23 (.35)
L_{TB}	---	---	---	---	---	---	---	---	.01 (.02)	.05 (.08)	.13 (.20)	.13 (.20)
L	1.28 (1.92)	1.95 (2.93)	2.38 (3.57)	2.43 (3.65)	.95 (1.43)	1.46 (2.24)	1.90 (2.85)	2.32 (3.48)	1.26 (1.89)	1.45 (2.18)	2.04 (3.06)	2.01 (3.02)

Table 5.11a

Airborne Scenario												
	Case 1				Case 2				Case 3			
Variable	I	M	P	C	I	M	P	C	I	M	P	C
ε	.629 (2)	1.259 (1)	1.259 (2)	1.259 (3)	.516 (2)	1.032 (1)	1.032 (1)	1.032 (4)	.280 (2)	.560 (3)	.560 (4)	.560 (4)
L_T	.069 (5)	.480 (5)	1.318 (1)	1.318 (2)	.055 (4)	.386 (5)	1.060 (1)	1.060 (3)	.072 (4)	.504 (4)	1.383 (1)	1.383 (1)
F	.338 (3)	.676 (3)	.676 (4)	.676 (5)	---	---	---	---	---	---	---	---
L_D,L_D^	.031 (6)	.278 (6)	.278 (6)	.628 (6)	.065 (3)	.588 (4)	.588 (5)	1.327 (2)	---	---	---	---
τ_2	1.01 (1)	1.01 (2)	1.01 (3)	1.01 (4)	.753 (1)	.753 (2)	.753 (3)	.753 (5)	1.216 (1)	1.216 (1)	1.216 (2)	1.216 (3)
L_U,L_U^	.071 (4)	.636 (4)	.636 (5)	2.12 (1)	.070 (5)	.636 (3)	.636 (4)	2.120 (1)	.020 (5)	.636 (2)	.636 (3)	2.120 (1)
ε_B	---	---	---	---	---	---	---	---	.102 (3)	.204 (5)	.204 (5)	.204 (5)
L_{TB}	---	---	---	---	---	---	---	---	.006 (6)	.043 (6)	.119 (6)	.119 (6)
L	1.22 (1.83)	1.80 (2.70)	2.18 (3.27)	2.80 (4.20)	.90 (1.35)	1.46 (2.19)	1.76 (2.64)	2.77 (4.16)	1.23 (1.85)	1.36 (2.04)	1.88 (2.82)	2.47 (3.71)

Table 5.11b

Table 5.11 Error Contributions and Rankings for Radiometry Variables

Rooftop Scenario								
	Case 1		Case 2		Case 3		Average	
Variable	M	P	M	P	M	P	M	P
ε	51.6	34.6	54.4	36.3	18.4	9.3	41.5	26.7
L_T	7.5	39.0	7.6	38.3	15.0	56.8	10.0	44.7
F	14.9	10.0	--	--	--	--	14.9	10.0
L_D,L_D^	2.0	7.0	17.6	11.8	--	--	9.8	9.4
τ_2,L_U(^)	24.0	9.4	20.4	13.6	64.0	32.3	36.1	18.4
ε_B	--	--	--	--	2.5	1.2	2.5	1.2
L_{TB}	--	--	--	--	0.1	0.4	0.1	0.4

Table 5.12a

Airborne Scenario								
	Case 1		Case 2		Case 3		Average	
Variable	M	P	M	P	M	P	M	P
ε	49.2	33.5	49.9	34.3	17.0	8.9	38.7	25.6
L_T	7.2	36.7	6.9	36.2	13.8	54.4	9.3	42.4
F	14.2	9.7	--	--	--	--	14.0	29.7
L_D,L_D^	2.0	1.3	16.2	11.1	--	--	9.1	6.2
τ_2,L_U(^)	27.4	18.8	27.0	18.4	66.8	35.1	40.4	24.1
ε_B	--	--	--	--	2.3	1.2	2.3	1.2
L_{TB}	--	--	--	--	0.1	0.4	0.2	0.4

Table 5.12b

Table 5.12 Percent Error Contributions for Radiometry Variables

Rooftop Scenario								
	Case 1		Case 2		Case 3		Average	
Variable	M	P	M	P	M	P	M	P
ε	1	2	1	2	2	3	1.33	2.33
L_T	4	1	4	1	3	1	3.67	1.00
F	3	4	--	--	--	--	3.00	4.00
L_D,L_D^	5	5	3	4	--	--	4.00	4.50
τ_2	2	3	2	3	1	2	1.67	2.67
L_U,L_U^	6	6	5	5	5	5	5.33	5.33
ε_B	--	--	--	--	4	4	4.00	4.00
L_{TB}	--	--	--	--	6	6	6.00	6.00

Table 5.13a

Airborne Scenario								
	Case 1		Case 2		Case 3		Average	
Variable	M	P	M	P	M	P	M	P
ε	1	2	1	2	3	4	1.67	2.67
L_T	5	1	5	1	4	1	4.67	1.00
F	3	4	--	--	--	--	3.00	4.00
L_D,L_D^	6	6	4	5	--	--	5.00	5.50
τ_2	2	3	2	3	1	2	1.67	2.67
L_U,L_U^	4	5	3	4	2	3	3.00	4.00
ε_B	--	--	--	--	5	5	5.00	5.00
L_{TB}	--	--	--	--	6	6	6.00	6.00

Table 5.13b

Table 5.13 Error Contribution Rankings for Radiometry Variables

For the Therm prediction method (P), in all cases, the error in target radiance due to temperature is the largest contributor to the error in final radiance (43.6% average over the three ray-interaction cases). This result emphasizes the need for accurate temperature prediction. When the error in this term is lowered, as in the Therm measurement error case (M), the primary error contributors become the error in target emissivity (40.1%) and the combined L_U, $\tau 2$ term (38.3%). The majority of error in the combined term is due to error in $\tau 2$. A distant third contributor is the error in shape factor (14.6%).

The emissivity error can be reduced by expanding the database of existing measured emissivities. Recall that the measurement error of emissivity is half the prediction error. Reduction of this error results in approximately a 50% reduction in the emissivity error contribution to final radiance error (*cf.* Tables 5.11a and 5.11b, ideal error results). As a result, the error in final radiance would be reduced by 20% when measured emissivity values are used.

To reduce the error in $\tau 2$, LOWTRAN7's prediction of atmospheric variables must be optimized. The intervening atmosphere can be well defined by using radiosonde data either from the location and day being predicted or data characteristic of the day being modeled. The inversion layers near the earth's surface can be corrected by using air temperature, air pressure, and dew point values measured on the ground, as described in section 2.3.4. Predictions made for clear, cloud-free days should also have reduced error

in not only $\tau 2$, but the upwelled and downwelled radiance terms as well when compared to predictions for cloudy days.

The error in shape factor can be greatly improved. At the moment, the shape factor of a facet is set to one unless changed by the user. A search routine could be devised which would cast out rays from the target at different angles and directions. This routine could determine any neighboring occluding objects and compute an estimate of the percentage of sky the facet 'sees', thus eliminating any guesswork on the user's part.

Overall, the most important consideration for final radiance error reduction is accurate temperature prediction. Primarily, object parameters must be well defined. When at all possible, measured data should be used. Suggestions for improvement include a more advanced thermal model which would include temperature effects from adjacent objects, shadowing effects, and still be based on first principle physics for ease of object parameter determination. Another improvement would be automatic computation of shape factor by a routine within DIRSIG as discussed earlier. Increasing the available database of not only emissivity values, but all object parameters would also aid in error reduction by eliminating the guesswork in assigning facet parameters.

Now that the theoretical error contributions have been determined, the next section will discuss actual radiance errors determined from comparison of truth and DIRSIG prediction images.

5.3.1) DIRSIG Image Evaluation

This section will discuss true radiance errors determined from DIRSIG images with reference to the theoretical radiance errors discussed earlier. In addition, image contrast and flaws in the prediction images will be discussed.

Table 5.14 lists the RMS and percent radiance errors as well as equivalent temperature errors determined for nine targets in the DIRSIG predicted images for June 1992. Percent error was calculated as the RMS error divided by the range of radiance values over time. The plots in Figure 5.6 are illustrations of DIRSIG predicted and truth radiances as a function of time for selected objects. As noted in Table 5.14, the average predicted radiance error for the June images is 2.98 W/m^2-sr (4.47 °C).

Target	Radiance RMS Error (W/m2-sr)	Equivalent Temp. RMS Error (°C)	% Radiance Error
Asphalt	2.29	3.44	9.12
White House Side	2.92	4.38	13.46
Black House Side	3.43	5.15	11.75
House Roof	3.03	4.55	8.54
Car Window	3.74	5.61	22.26
Car Door	4.53	6.80	16.78
Car Tire	3.78	5.67	13.26
Car Roof	2.07	3.11	7.26
Water	1.00	1.50	13.33
Grass	3.14	4.71	24.15
Average	2.98	4.47	13.99
Specular Bounce to Background	3.68	5.52	15.50
Specular Bounce to Sky	2.10	3.15	9.56

Table 5.14 Temperature and Radiance RMS & Percent Errors for DIRSIG Prediction Imagery June 1992

Note that errors are only listed for facets with two ray interaction types: specular bounce to background and specular bounce to sky. The sky is not present in any images, thus eliminating any missed scene cases. The only diffuse object in the scene is grass. In this case, the resulting radiance error is high, (*cf.* Figure 5.7) due to inaccurate temperature prediction . Grass temperatures coud not be easily recorded during the data collections and therefore the objects parameters input to Therm could not be optimized. The result is a high error in temperature and thus a high predicted radiance error.

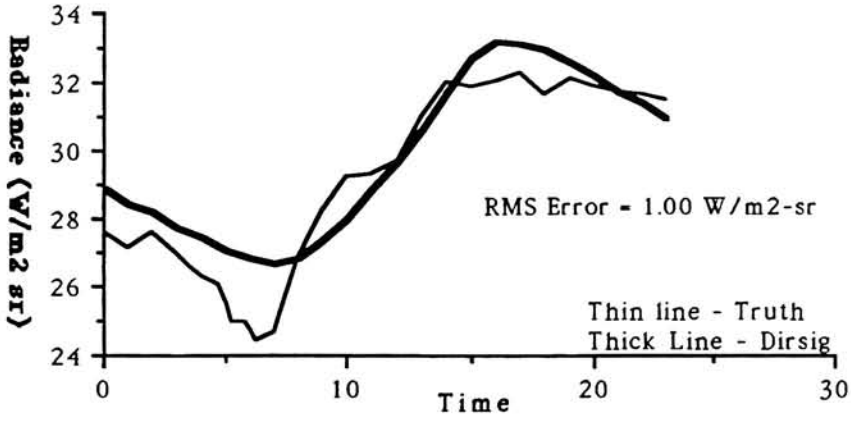

Figure 5.6a Water Radiance June 1992

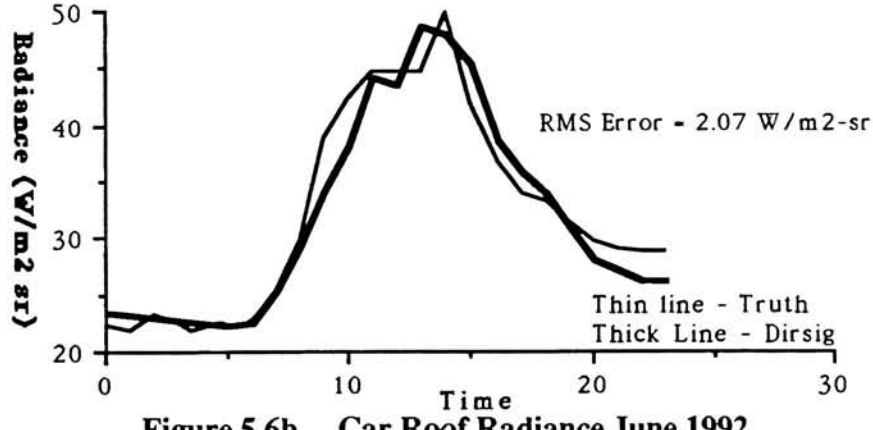

Figure 5.6b Car Roof Radiance June 1992

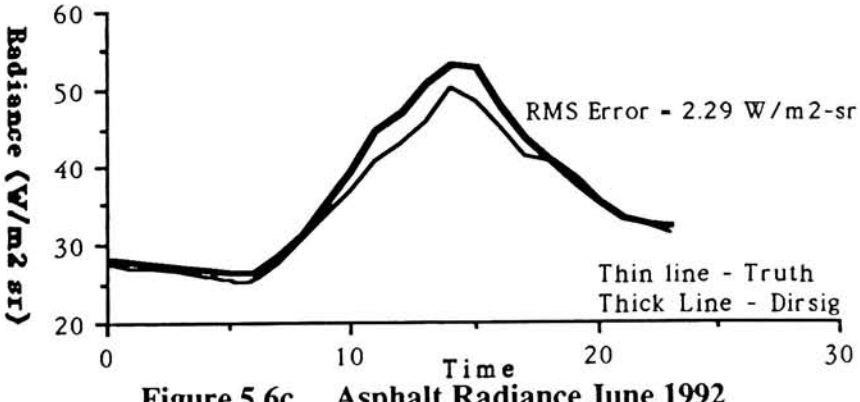

Figure 5.6c Asphalt Radiance June 1992

Figure 5.6 DIRSIG Prediction vs. Truth Radiance June 1992

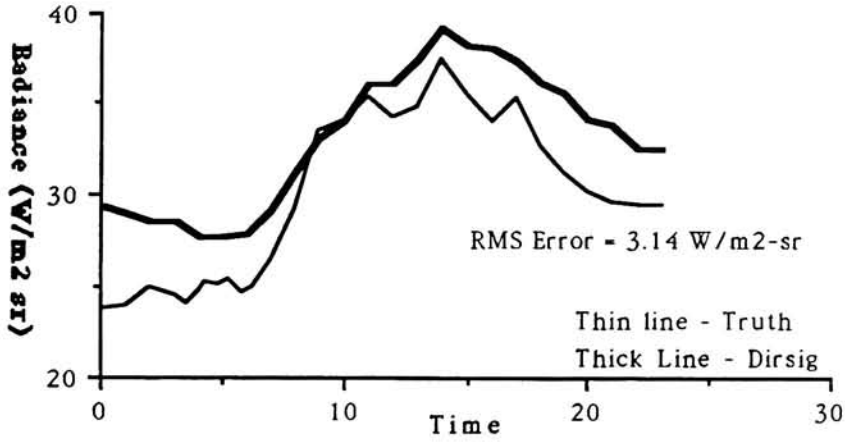

Figure 5.7 Grass Radiance June 1992

Also note that the radiance errors listed in Table 5.14 are only for the June data collection. The results of the predictions for the October collection are a case in point for the problems encountered with LOWTRAN7's cloud predictions. Figures 5.8a and 5.8b are, respectively, the target temperature and radiance reaching the sensor plots for DIRSIG prediction and truth for the asphalt in the October collection. As can be seen from Figure 5.8a, Therm's temperature predictions are very accurate (RMS error = 0.85°C). However, the predicted radiance values for the asphalt have a large added bias. The ray-interaction type for this facet is a specular bounce to the sky. If the target temperature prediction is not the major source of radiance error, two possibilities remain: downwelled and upwelled radiance. Upwelled radiance is a relatively small term based on the short target to sensor path length, leaving downwelled radiance as the only major source of error.

As discussed in section 5.2.1, LOWTRAN7 predicts very poorly when clouds are present, as was the case on October 6, 1990. This was a cloud covered day and LOWTRAN7 was told that clouds were present in order to reduce the total visible insolation prediction error (*cf.* Figure 5.1). The bias in predicted radiance observed in Figure 5.8b is characteristic of errors caused by overprediction of clouds (and therefore higher downwelled radiance). To double check that this was indeed the problem, LOWTRAN7 was then told that no clouds were present, and DIRSIG was rerun resulting in the predictions shown in Figure 5.8c. In this case, the predicted radiance is too small. This is the expected result: the predicted downwelled radiance term is reduced by the absence of clouds and thus the final radiance for a specular bounce to sky is lower. In

reality, the amount of downwelled radiance the facets received is somewhere between the two prediction cases illustrated here. Without better knowledge of LOWTRAN7's

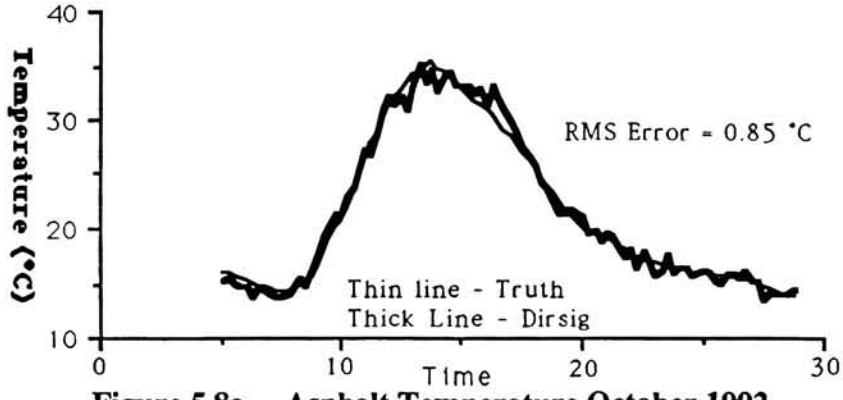

Figure 5.8a Asphalt Temperature October 1992

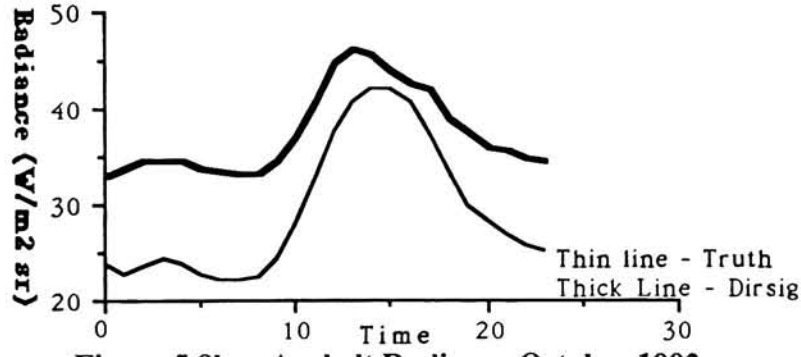

Figure 5.8b Asphalt Radiance October 1992

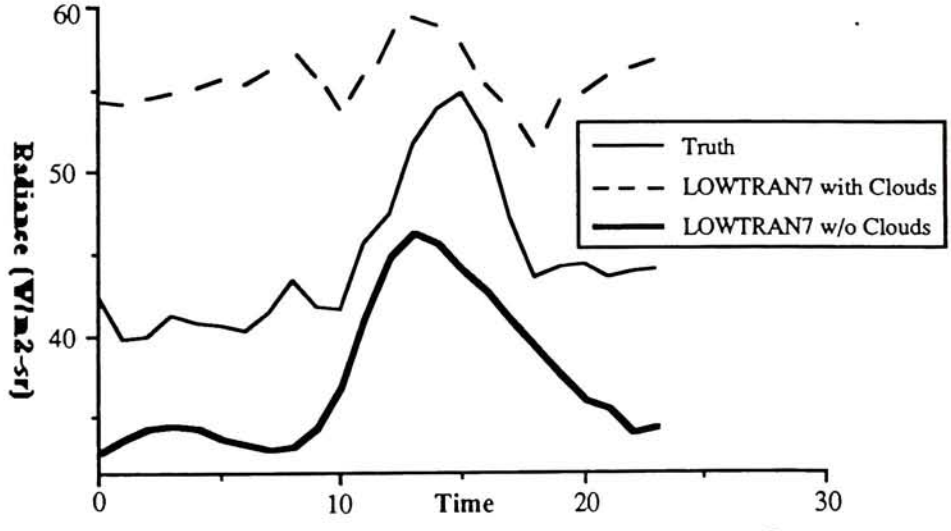

Figure 5.8c October 1990 Radiance Truth & LOWTRAN7 Cloud Predictions

Figure 5.8 Asphalt Temperature and Radiance Predicted vs. Truth for Lowtran Cloud Prediction Tests, October 1990

treatment of clouds, the correct downwelled radiance term can only be determined by trial and error. This case reinforces the need to better understand LOWTRAN7's use of clouds in order to improve upon DIRSIG's predictions when clouds are present.

In theory, the errors listed in Table 5.14 should be comparable to those predicted for the Therm measurement mode (M) in the radiometry error propagation section. However, June 23 was a partly cloudy day with cloud amounts increasing during the afternoon. Therefore, the results listed in Table 5.14 are more comparable to a combination of the M and C propagation methods. It must be notes that the theoretical error propagation serves more as a sensitivity indicator than as a predictor of absolute radiance error. Recall that representative situations were chosen for the error propagation for each ray-interaction type. One target at one time of day was chosen for each ray-interaction case. The error values listed for the theoretical propagation are then dependent on the objects chosen and the time of day simulated. The errors determined for the DIRSIG predicted images are RMS errors: averages over time and over many objects. The RMS errors give a measure of the model's prediction accuracy while the theoretical propagation gives an indication of the model's sensitivity to individual input parameters. Therefore, it is not appropriate to make direct comparisons between these RMS errors and the theoretical errors.

In order to make direct comparisons, the error propagation should be run with a variety of objects representing each case and different times of day. For now, the predicted and truth radiances for the specific cases and times used during the theoretical propagation can be compared to the propagation results. Table 5.15 is a listing of the radiance values and errors determined from the actual imagery and the theoretical propagation for the two specular ray_interaction cases.

Ray_interaction Type	Truth Radiance (W/m2-sr)	DIRSIG Radiance (W/m2-sr)	Observed Radiance Difference	Theoretical Radiance Error
Case 2: Water (11:45 am)	29.61	29.47	0.14	1.56
Case 3: Asphalt to Car(10:00 am)	36.77	39.70	2.93	1.45

Table 5.15 Radiance Values and Errors: Actual and Theoretical

For Case 2, the theoretical error is much higher than the observed error. This may be due to the choice of the target: water. The object parameters were very well known for water, resulting in a low temperature error of 1.05°C (*cf.* Table 5.7). In fact, for 11:45 am (the time used for the theoretical propagation) the water temperature prediction was almost exactly the same as the true water temperature. Therefore, the resulting radiance error was also very low.

For Case 3, the actual error is much greater than the theoretical error. This is mainly due to the binary specularity problem discussed below. Overall, a much more robust study including a variety of targets and imaging times is necessary before comparisons can be made between the theoretical and actual radiance errors.

The errors determined from the predicted images are higher than expected: Case 2 error (specular bounce to sky) is 2.10 W/m^2-sr (3.15 °C) and Case 3 error (specular bounce to background) is 3.68 W/m^2-sr (5.52 °C). There are several factors which contribute to this unexpected additional error in DIRSIG radiance predictions: DIRSIG definition of specularity, temperature prediction errors due to inaccurate object parameters and geometry errors resulting in incorrect facet azimuth, and the presence of clouds on the afternoon of June 23, 1992.

A large source of prediction error is caused by binary specularity values assigned to each facet. At present, a facet can only be defined as being perfectly specular or diffuse. Few real objects truly exhibit this type of behavior. In many cases, an object is partly diffuse with a specular component as illustrated in Figure 5.9.

This binary specularity leads to overprediction of radiance reaching the sensor for specular facets with reflection to a background. For example, the asphalt in the car's shadow is considered by DIRSIG to be specular, with the car acting as the background. The result of a completely specular solution for the radiance reaching the sensor is a distinct 'halo' of the car on the asphalt. Observe the afternoon DIRSIG prediction images for June 23, 1992 (2:00-5:00pm) at the end of this chapter. These figures illustrate this halo effect.

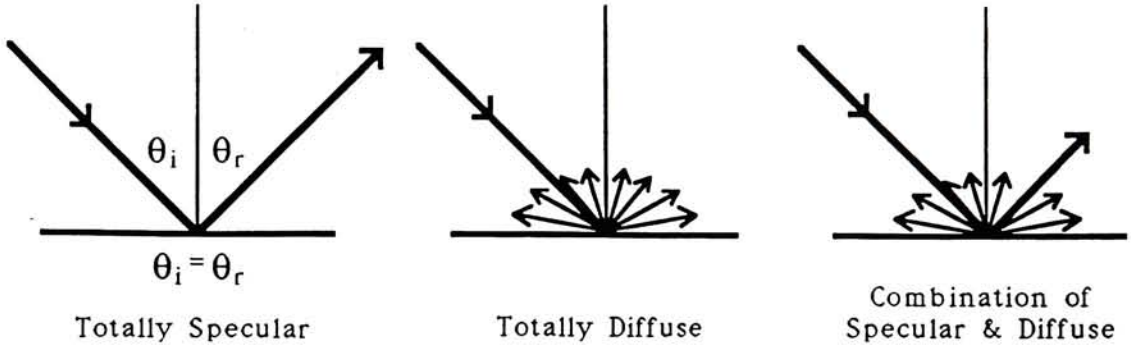

Figure 5.9 Illustration of Specularity Types

This is not to say that the specularity phenomenon does not occur in real life. Included in the images at the end of the chapter are the truth images taken during the June 1992 data collection. Although the halo effect in the truth afternoon images is not as profound, it is still present. Figure 5.10a is a graph of truth and predicted radiances reaching the sensor vs. distance from the car's rear tire. The radiance values were determined from the 2:00pm images. As can be seen in this graph, the predicted halo is a distinct, overemphasized step function. The truth halo is a more subtle, gradual change.

Note that the drop in predicted radiance occurs earlier than the drop in truth radiance. This is not an error in DIRSIG, but a geometry error. The car in the AutoCAD scene is facing due north, whereas the car in the experimental scene was turned slightly from north. The resulting effect is an error in the position of the car's projected shadow on the asphalt. In this case, the shadow stretches farther in the predicted images than in the truth images.

A solution to this binary specularity problem is to make specularity a fraction. In this case, both the diffuse and specular solutions would be computed for a facet and then combined proportionally, based on the specularity value. For example, the diffuse and specular solutions were computed for asphalt in and out of the halo for 2:00pm. These two solutions were averaged (ie. specularity = 0.5), resulting in a new, combined radiance value . Figure 5.10b illustrates the radiance computed from this combination along with a correction for the geometric azimuth error. In this figure it can be seen that the halo radiance value was lowered while the value of the asphalt radiance outside of the halo was raised. The result is a reduction in the contrast between the asphalt and the halo, which more accurately models the true halo phenomenon.

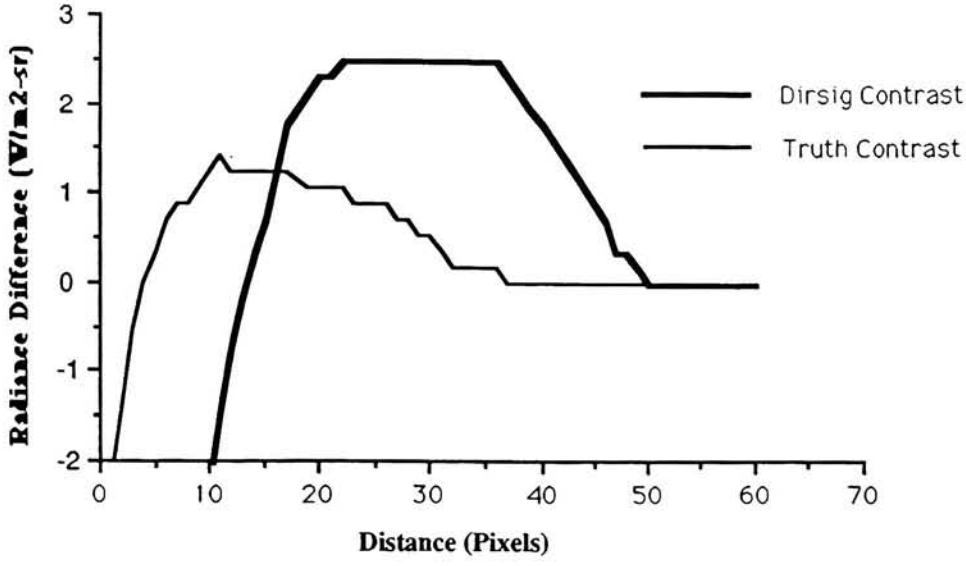

Figure 5.10a Predicted and Truth Halo Contrast

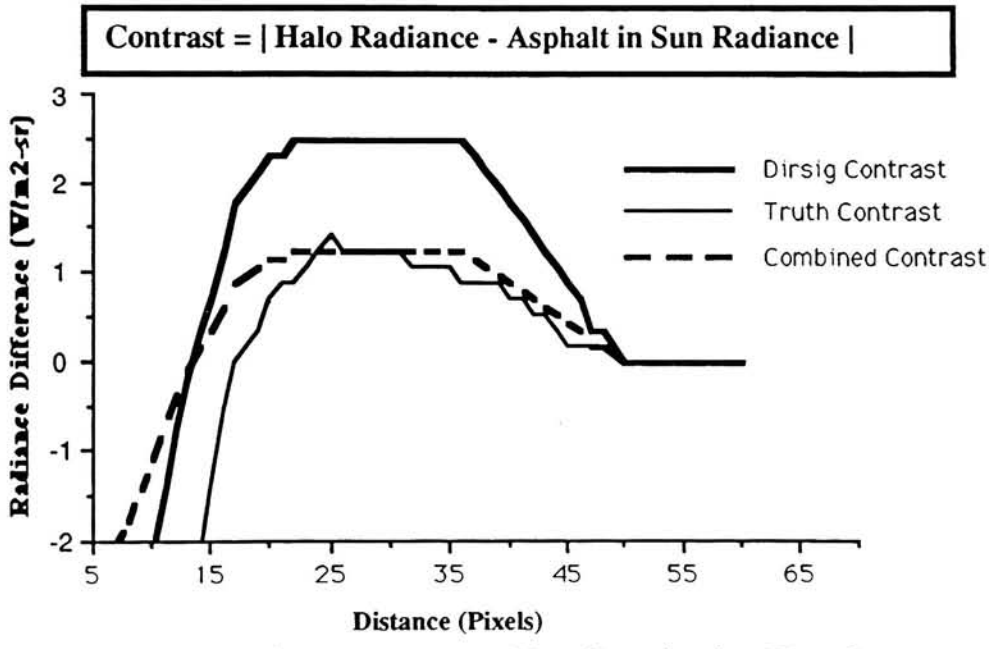

Figure 5.10b Predicted, Truth, and New Combination Halo Contrast

Returning to the errors listed in Table 5.14, it can be seen that the facets which are modeled as specular bounces to background have higher errors than the facets which are specular bounces to sky. Therefore, it can be assumed that if a solution for the binary specularity problem is implemented, the overall predicted radiance error will be reduced.

The temperature prediction error for the June 1992 scene targets is 1.83°C. This is the RMS error between the thermistor measured temperatures and Therm's optimized temperature predictions. Note that this number was not used for the theoretical error propagation (*cf.* Table 5.8). This is due to the fact that the error propagation was performed prior to completion of data testing for the June collection. This number is an approximate average of the values used for the M and P error propagation cases. As such, it can be inferred that the error contribution of this temperature error is an average of the contributions for the M and P cases. From Table 5.12a, the average percent error contribution for an error in L_T of 1.83°C is approximately 27% (M error: 10.0%, P error: 44.7%). This error is mostly due to incorrect object parameters defining the targets in the scene.

In addition, the geometry error mentioned earlier which resulted in error in the car's azimuth increases the the error in the final radiance values for the car and surrounding objects. As discussed in section 5.1.2, azimuth error is a major contributor to predicted temperature error. Again, temperature accuracy has a large impact on predicted radiance accuracy. Care should be taken when laying out the scene for the geometric database. Mistakes in the size and placement of targets can have an impact on the final model accuracy due to shadowing and shape factor influences.

Note the rise in predicted radiance in the afternoon which does not model the truth radiance for the car door in Figure 5.11a. This phenomenon is observed for all east facing perpendicular facets in the June scene. The error can be traced back to Therm's temperature predictions for these facets. When reporting the type and percentage of clouds present for a given time of day, no direction or location of those clouds is required by Therm. Therefore, the program assumes that all facets (regardless of the direction they are facing) 'see' the clouds.

This was not the case on June 23. During the afternoon (at approximately 1:00pm), clouds began to move into the area from the west. The east facing facets did not 'see' the clouds until approximately 5:00pm, when the entire sky was covered. Therm bases its temperature predictions partially on the amount of sky radiance a facet receives. Clouds are warmer than open sky, and therefore a facet receives more radiance from a cloudy sky than from a clear sky. Therm assumed that the east facing facets were receiving more radiance from the sky (from the clouds which were located in the west) than they actually were. Thus, the temperatures and radiances of the east facing facets

were overpredicted during those afternoon hours, as illustrated in Figure 5.11. This error can be improved by the addition of clouds in the DIRSIG scenes. A future improvement is planned in which clouds will be included in the predicted scenes. The clouds will be given thickness and opacity values which will allow the program to 'look' through clouds and model the radiance a facet receives from a cloudy sky.

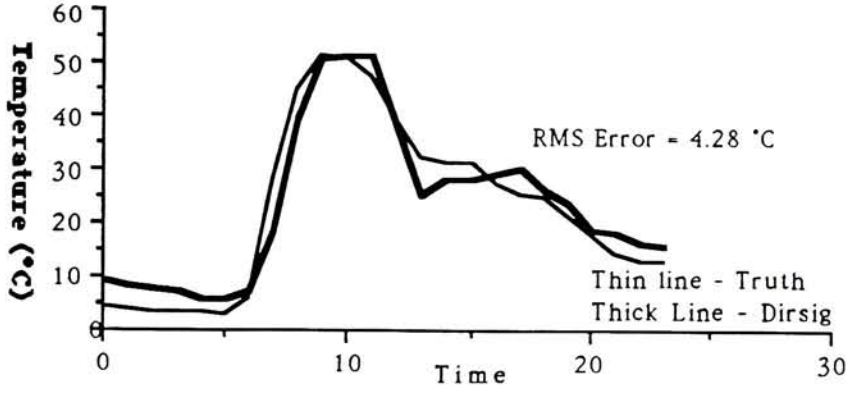

Figure 5.11a Car Door Temperature June 1992

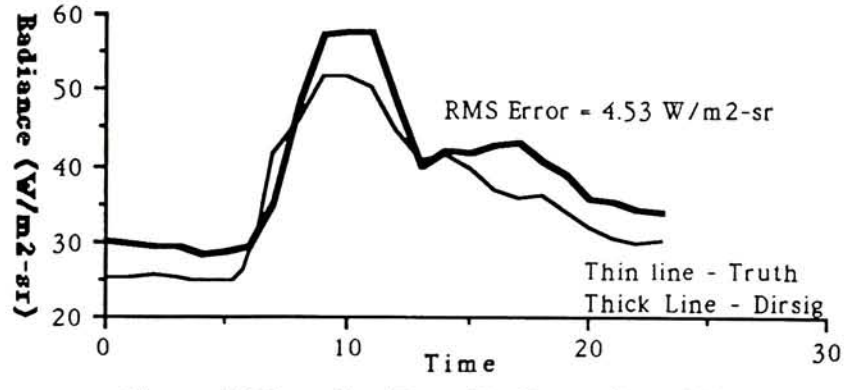

Figure 5.11b Car Door Radiance June 1992

Figure 5.11 Car Door Temperature and Radiance Predicted vs. Truth June 1992

As a final note, the constant shape factor value will also increase the error in predicted radiance. As stated earlier, shape factor is one for all facets, unless changed by the user. Obviously, the proximity of the building reduces the shape factors of all targets in the scene. Facets with slopes greater than zero, or adjacent to the car have even smaller shape factors. The perpendicular facets facing the building and the facets near the car have the highest error in shape factor. As indicated in the discussion in section 5.2.3 and Table 5.13, error in shape factor is a major contributor to the final radiance error.

Inspection of the radiometry equations 4.1 - 4.4 indicates that shape factor is not a variable for specular facets. However, the binary specularity solution of combining diffuse and specular radiance calculations to compute the final target radiance will incorporate shape factor errors. Version 2.2.1 of DIRSIG contains a shape factor calculation which should minimize this error. Therefore, although shape factor errors do not influence the radiance errors determined here, they will have an effect on future predictions once the specularity solution is implemented.

Overall, a large portion of the error observed in this simulation can be remedied by the specularity solution discussed earlier and careful attention paid to target object parameters, scene geometry, and cloud positions. The next section will discuss image quality in terms of contrast, ie. with all of the error in predicted radiance, how well does DIRSIG predict the contrast between objects in the scenes?

5.3.2) Image Contrast

The contrast of an image defines how well objects can be differentiated from one another. In many cases, the accuracy of the radiance values doesn't matter as much to the user as the accuracy of the contrast between objects. High radiance errors may be acceptable to the user if the program is still representing the image contrast correctly. In this section, contrast will be represented in three manners: contrast rankings, RMS contrast error and percent contrast error, and pictorially.

Figures 5.12 - 5.15 are contrast rank plots for the specular targets from the June collection for three different times of day: 8am, noon, and 4pm. The predicted radiance was plotted against the true radiance in Figures 5.12, 5.14, and 5.15. Figure 5.13 is a contrast plot for equivalent temperatures for the same objects in Figure 5.12. Ideally, the points should fall in a straight line if the predicted radiance (temperature) matches the true target radiance (temperature).

With all eight targets included, DIRSIG correctly predicts the high and low ends, but has some errors in the mid-range radiance values. Figures 5.14a-c are plots of those mid-range radiance values with the theoretical error bars (determined in section 5.2) included. Note the overlap of the error bars which indicates that the predicted contrast between the targets is within the theoretical predicted limits.

Part of the error in contrast is due to the bias error induced by the specularity problem with ray-interaction types of specular bounces to background. Note the lines indicating correct contrast drawn in Figures 5.12a-c. The four targets which are specular bounces to background fall above this line. If only the targets which are specular bounces to sky are considered (*cf.* Figures 5.15a-c), the predicted contrast is correct, with slight overlap for the mid-range radiances at noon. This result indicates that DIRSIG does correctly predict target contrast for some objects. When the specularity problem is fixed, DIRSIG's predictions should improve.

Percent contrast can be defined as follows:

$$\%\ \text{Contrast Error} = \frac{\text{RMS Contrast Error}}{\text{Scene Dynamic Range}}$$

where:

$$\text{RMS Contrast Error} = \sqrt{\frac{\sum \left\{ (L_1 - L_2) - (L\hat{}_1 L\hat{}_2) \right\}^2}{N}}$$

where: L_1 and L_2 are truth radiance values for object 1 and object 2

L_1^ and L_2^ are predicted radiance values for object 1 and object 2.

Table 5.16 is a listing of RMS contrast error, dynamic range, and percent contrast error values computed between the truth and DIRSIG images for the June collection. Total percent contrast is the sum over all difference pair combinations of the targets in the scene at one point in time. Case 2 percent contrast only includes target combinations with ray_interaction type of specular bounce to sky. Case 3 includes only specular bounce to background target combinations.

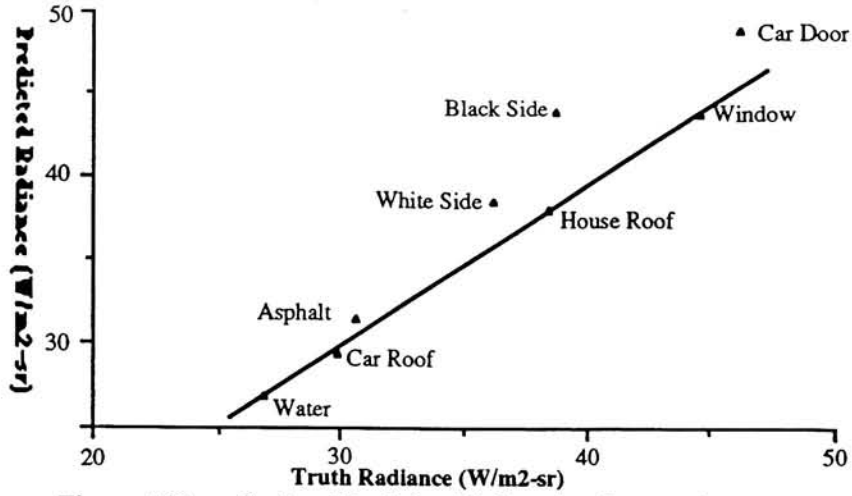

Figure 5.12a Contrast Rank for All Specular Targets: 8am

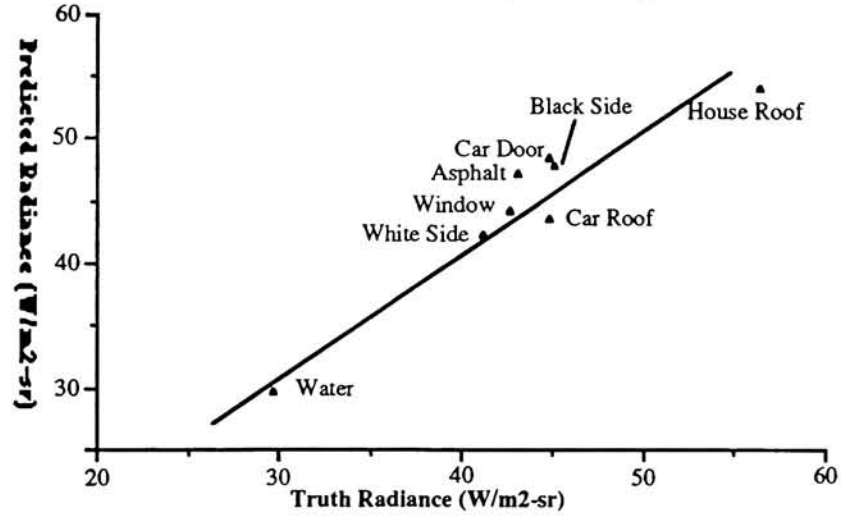

Figure 5.12b Contrast Rank for All Specular Targets: noon

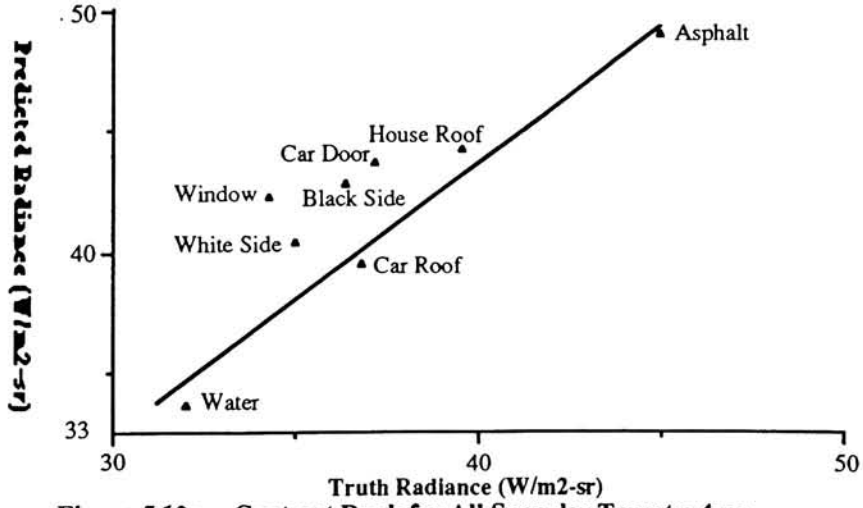

Figure 5.12c Contrast Rank for All Specular Targets: 4pm

Figure 5.12a-c Contrast Rankings for Eight Specular Targets June1992

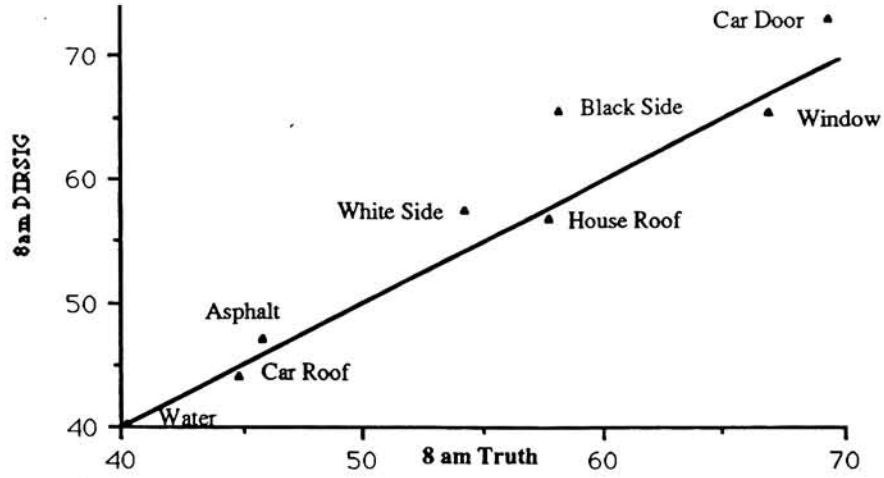

Figure 5.13a Contrast Rank for All Specular Targets: 8am Apparent Temperature

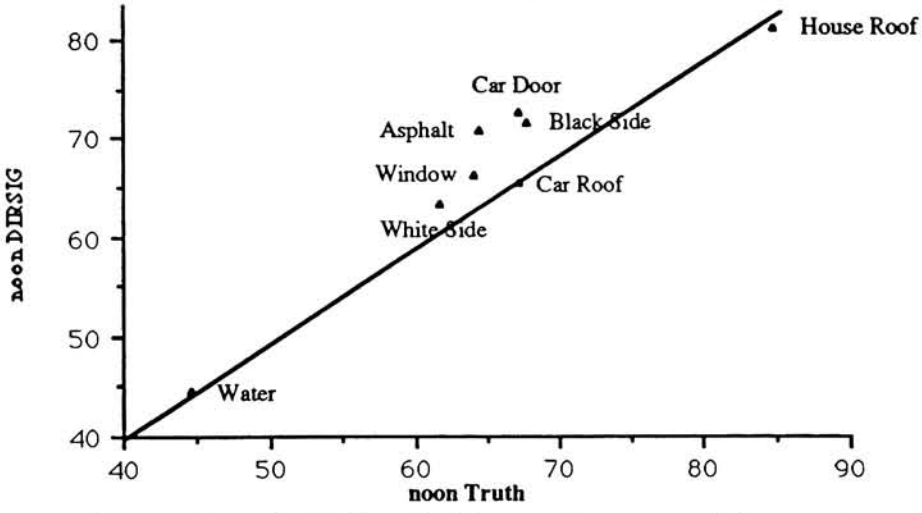

Figure 5.13b Contrast Rank for All Specular Targets: Noon Apparent Temperature

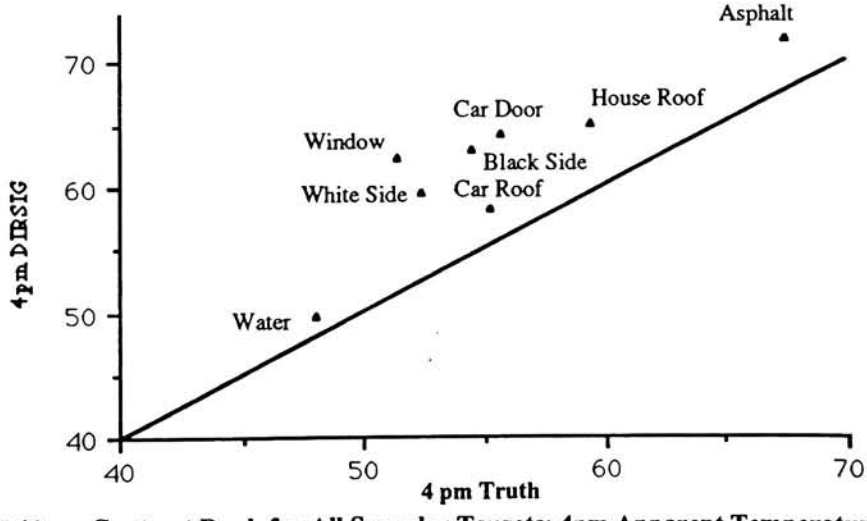

Figure 5.13c Contrast Rank for All Specular Targets: 4pm Apparent Temperature

Figure 5.13a-c Contrast Rankings for Eight Specular Targets Apparent Temperature

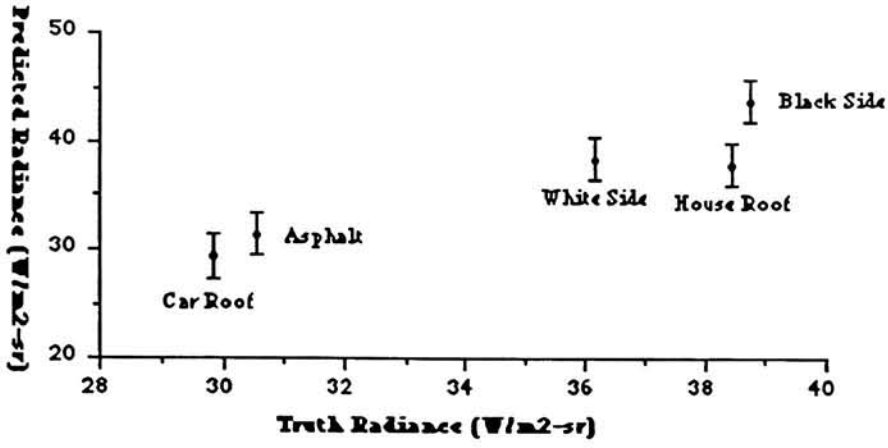

Figure 5.14a Mid-Range Radiance Values: 8am

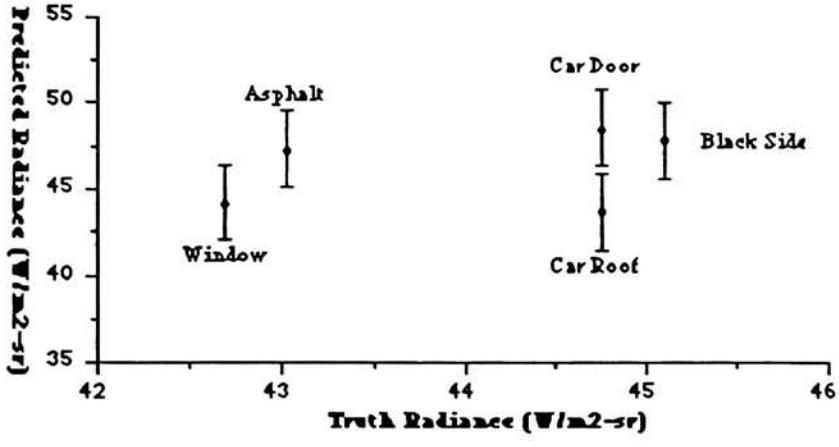

Figure 5.14b Mid-Range Radiance Values: Noon

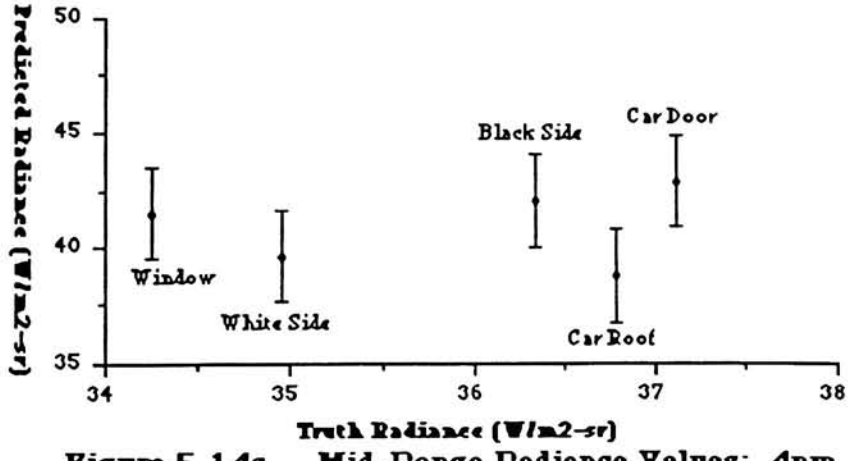

Figure 5.14c Mid-Range Radiance Values: 4pm

Figure 5.14a-c Contrast Rankings for Mid-Range Radiance Targets
June 1992

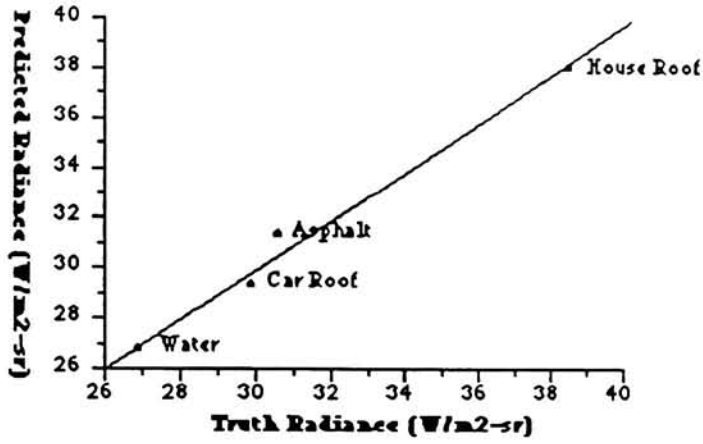

Figure 5.15a Contrast Rank Specular Bounce to Sky: 8am

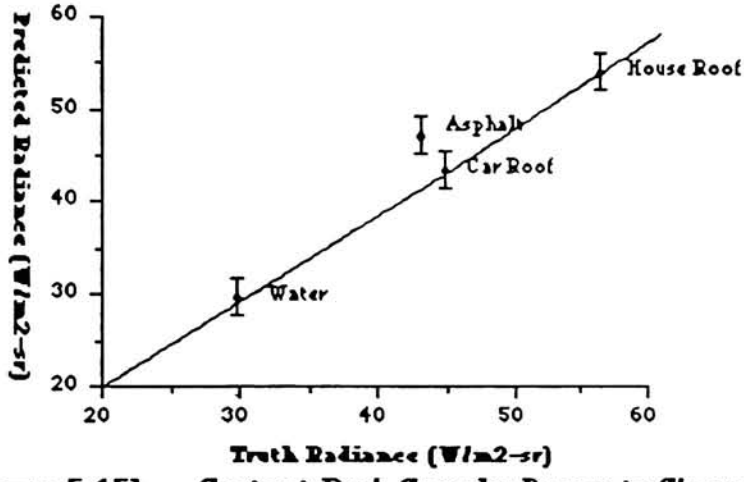

Figure 5.15b Contrast Rank Specular Bounce to Sky: noon

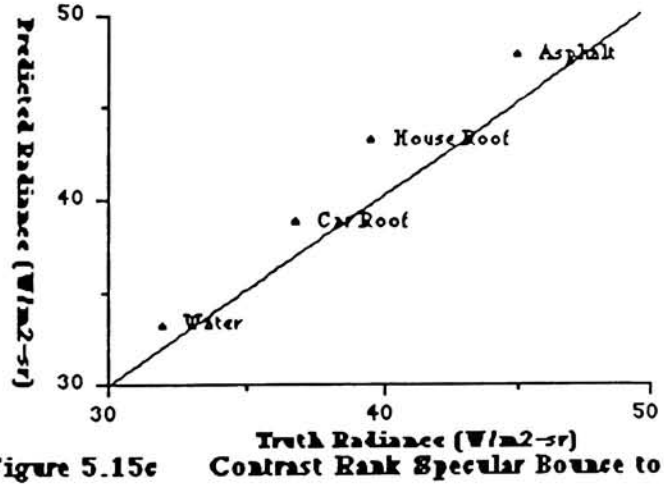

Figure 5.15c Contrast Rank Specular Bounce to Sky: 4pm

Figure 5.15a-c Contrast Rankings for Specular Bounce to Sky Type Targets
June 1992

		All Targets		Case 2 Targets		Case 3 Targets	
Time	Dynamic Range	RMS C. Error	% C. Error	RMS C. Error	% C. Error	RMS C. Error	% C. Error
0	5.364	2.005	.374	1.529	.285	1.276	.238
1	5.408	1.588	.294	.609	.113	1.275	.236
2	4.276	1.606	.376	.776	.181	1.516	.355
3	4.411	1.584	.359	.639	.145	1.412	.320
4	4.200	1.234	.294	.669	.159	1.039	.247
5	3.040	1.390	.457	1.051	.346	1.435	.472
6	5.840	1.522	.261	1.378	.236	.830	.142
7	16.799	4.911	.292	1.321	.079	5.069	.302
8	19.394	3.593	.185	.862	.044	3.217	.166
9	23.704	5.170	.218	4.500	.211	5.632	.238
10	26.086	5.192	.190	4.927	.189	5.473	.210
11	29.239	4.845	.166	3.4950	.120	5.860	.200
noon	26.848	3.338	.124	4.052	.151	2.074	.077
1	23.000	4.877	.212	3.355	.146	2.963	.129
2	24.330	4.178	.172	4.268	.175	1.698	.070
3	15.357	2.599	.169	3.363	.219	1.255	.082
4	13.016	2.664	.205	1.661	.128	1.464	.112
5	9.017	3.716	.412	3.064	.340	1.556	.173
6	8.888	2.852	.321	2.251	.2531	1.374	.155
7	6.100	3.259	.534	3.113	.510	1.403	.230
8	5.429	2.853	.526	2.665	.491	.990	.182
9	4.179	3.109	.744	3.245	.776	1.339	.320
10	3.291	2.835	.861	3.126	.950	1.080	.328
11	2.547	2.808	1.103	3.185	1.250	1.036	.407

Table 5.16 RMS Contrast Error and Percent Contrast Error

Figures 5.16a and b are plots of the RMS contrast error and percent contrast error asa a function of time. Note the rise in the total and Case 2 errors in the evening hours. The percent contrast error is greater than one because the RMS contrast error is greater than the dynamic range at those times. These high errors are due to the presence of

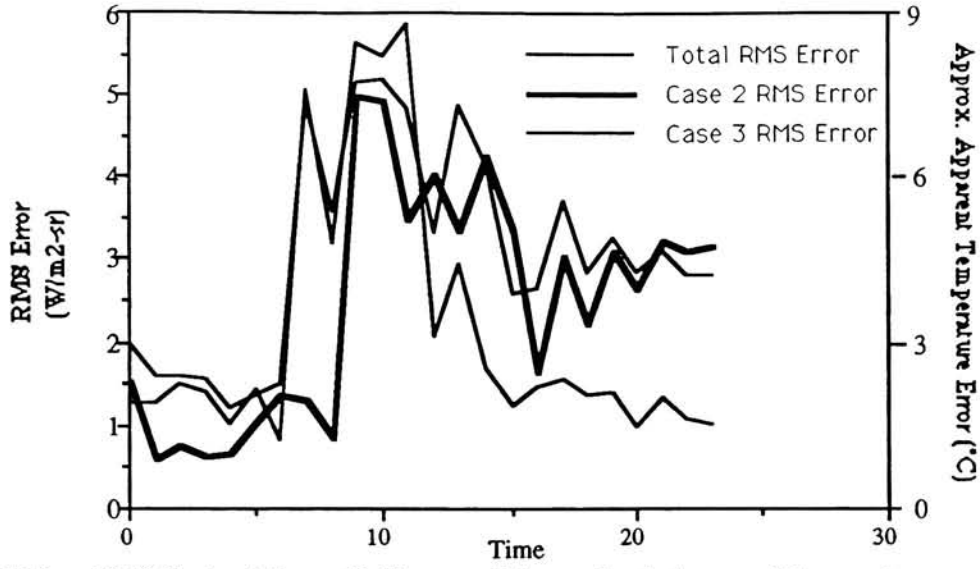

Figure 5.16a RMS Contrast Error: Radiance and Approximate Apparent Temperature

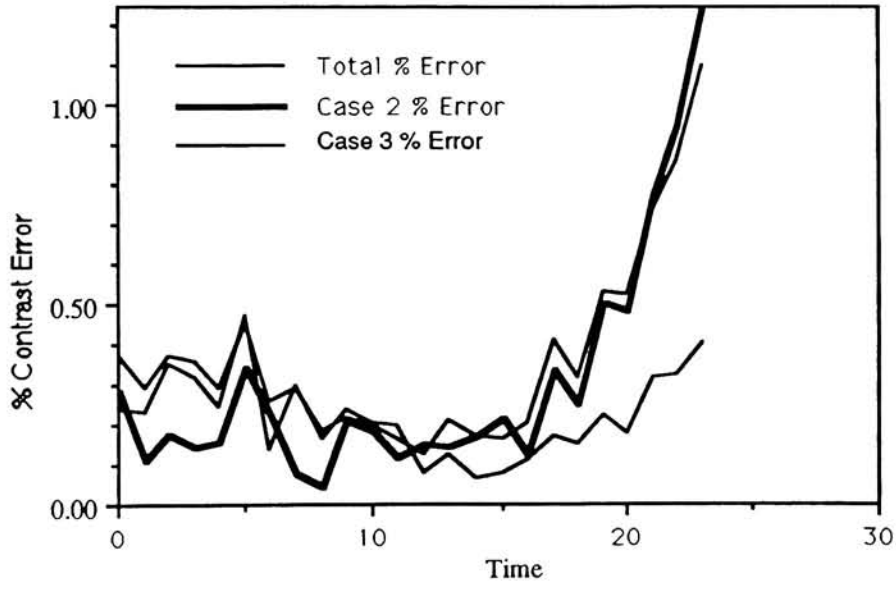

Figure 5.16b Percent Contrast Error

Figure 5.16 RMS Error and % Contrast Error: June 1992 Images

clouds and low dynamic range of the scenes. The specular bounce to sky targets have high predicted radiance errors because LOWTRAN7 did not model the sky radiance correctly at those times. The presence of clouds during the evening increases LOWTRAN7's prediction error. In addition, the dynamic range of the actual scene decreases into the night. The combination of increased radiance error (Figure 5.16a) and decreasing dynamic range elevates the percent contrast error (Figure 5.16b).

Overall, the percent contrast error is low for specular bounce to sky targets until clouds appeared in the scene. The percent contrast error for the specular bounce to background targets is high, but would improve if the binary specularity problem discussed earlier was solved.

The following is a discussion of DIRSIG's prediction of image contrast with reference to the truth images recorded during the June collection The figures at the end of this chapter are an hourly time series of the truth and prediction images. Keep in mind when referring to these images that a dark object is cold while a bright object is hot.

The early morning images (midnight through 3:00am) have some discrepancies to be addressed. Several of the obvious differences are due mainly to the binary specularity of the targets: the bright halos of the car side and painted panel on the asphalt, higher predicted radiance for the car side, very cold rear bumper and edge of the specular board in front of the house (due to specular bounce to cold sky), inner tire rims hotter than the tire in the prediction images, and contrast difference between water with specular bounce to sky and to background (pool edge).

Two limitations of Therm are also evident. In the truth images, the water level is clearly apparent from the outside of the pool and the asphalt under the car is warm even though it was shaded from the sun the entire day. In both cases, the objects were warmed by neighboring objects, a phenomenon which Therm cannot account for in its calculations. A final error, perhaps due to incorrect temperature prediction is that DIRSIG predicts that the sand and concrete have equal radiance, whereas in reality the concrete is hotter than the sand. At 4:00am, the concrete and sand true radiances became equal.

Note that from midnight to 5:00am DIRSIG did correctly predict the contrasts of the car roof and hood with the asphalt and car side, as well as the house roof with the grass and house front. Also notice the correct lack of contrast between the different squares of the grey level and colored panels.

At 6:00am, all of the targets in the real scene began heating up as morning was beginning to break. The 6:00am predicted image shows no heating, perhaps because the

sun did not actually rise until after 6:00. Therm does not anticipate the approach of sunrise as a possible source of heating.

At 7:00am, the targets in the predicted image have begun heating from the sunrise. The house and car sides, tires, and painted panels are facing east, directly into the sun, and are therefore heating up rapidly. The one major discrepancy at this time is the water. The water is barely visible in the true image; the water, pool, and grass all have similar radiance values. However, DIRSIG predicts a higher contrast between these objects.

Aside from the water, the predicted contrast is true to reality. Note the correct contrast between the different squares of the painted panels and the barely visible difference between the black and white sides of the house reflected in the specular board. Also, the car side is hotter than the windows which are hotter than the roof and hood of the car.

Throughout the rest of the morning the predicted contrast is generally correct. At 9:00am note that the car door is hotter than the rear car side. Again, Therm does not know that the materials behind the sides of the car are different, thus impacting their temperatures. Since the surface material is the same, Therm computes the same temperature for both targets. Also at 9:00am note that the predicted shadow of the house on the grass is in the correct position.

In the afternoon, the predicted tire radiance is less than the predicted car side radiance. The reverse is true in the truth imagery. Other discrepancies include a predicted pool shadow on the grass which does not really exist and shadows of the painted panel and house extending farther than they should. The missing pool shadow may be due to the error in grass radiance which resulted in a higher predicted contrast between the pool and the grass. This higher contrast would emphasize any shadow which may exist in the grass by the pool. The other shadow errors may be due in part to a discrepancy in target azimuth angles between the predicted and truth scenes. In general, the predicted contrast follows the true contrast through the early afternoon.

Recall that clouds moved into the scene in the afternoon, but DIRSIG did not know about them. This may explain some of the errors in the late afternoon images. At 4:00pm, the truth images are beginning to lose their contrast. Note that the different grey

levels on the painted panel on the asphalt are barely discernable. The predicted contrast in this panel is much higher, as is the predicted contrast for the entire scene. For much of the evening the predicted contrast is greater than the true scene contrast.

In general, DIRSIG predicts the scene contrast correctly. Many of the discrepancies noted above are due to inaccurate temperature prediction, errors caused by the target binary specularity, and cloud errors. These results indicate the need to improve upon the present temperature prediction model, DIRSIG's modeling of clouds, and to replace the binary specularity with a fraction. The next section offers recommendations to improve the prediction accuracy of DIRSIG.

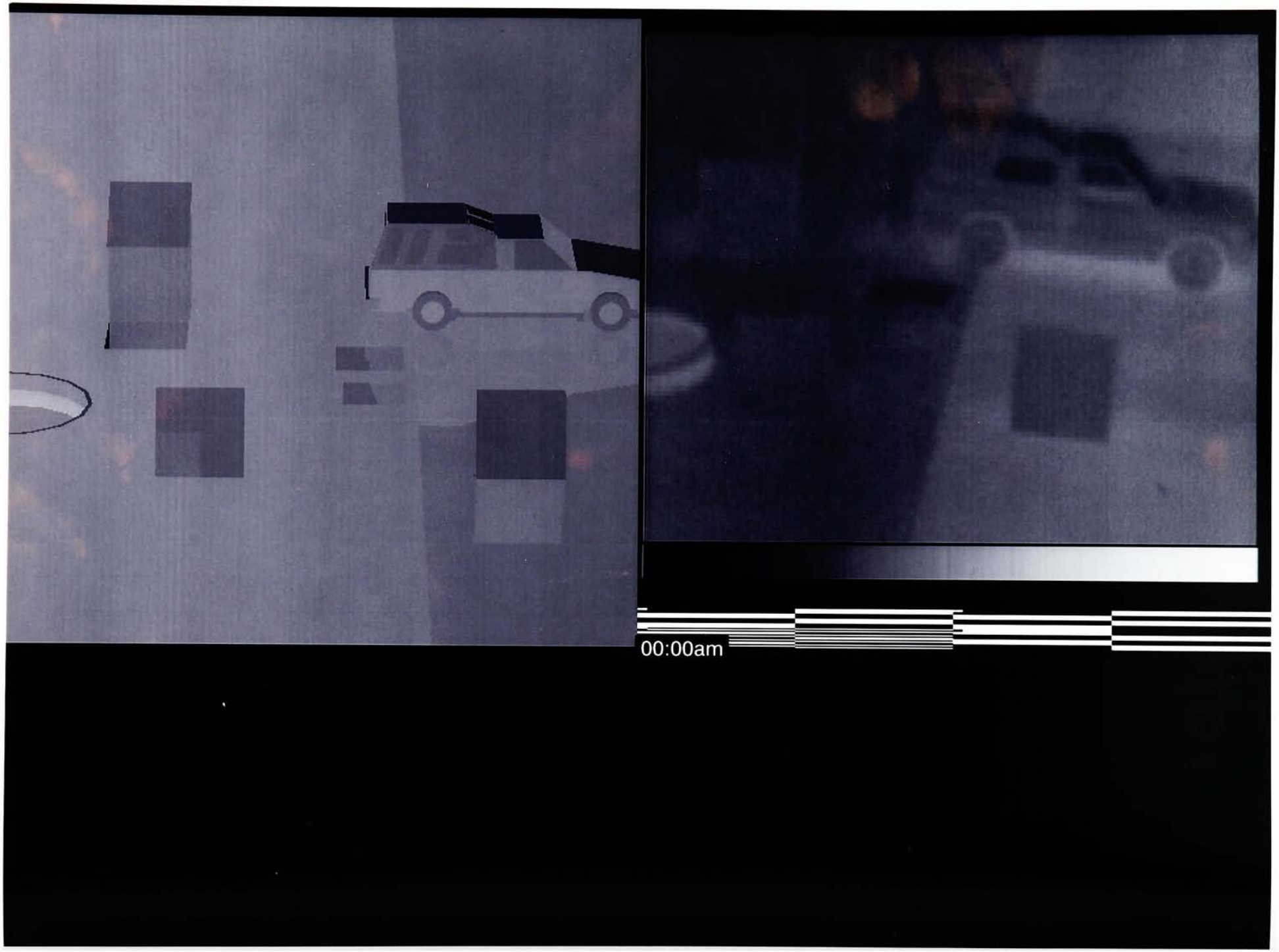
00:00am

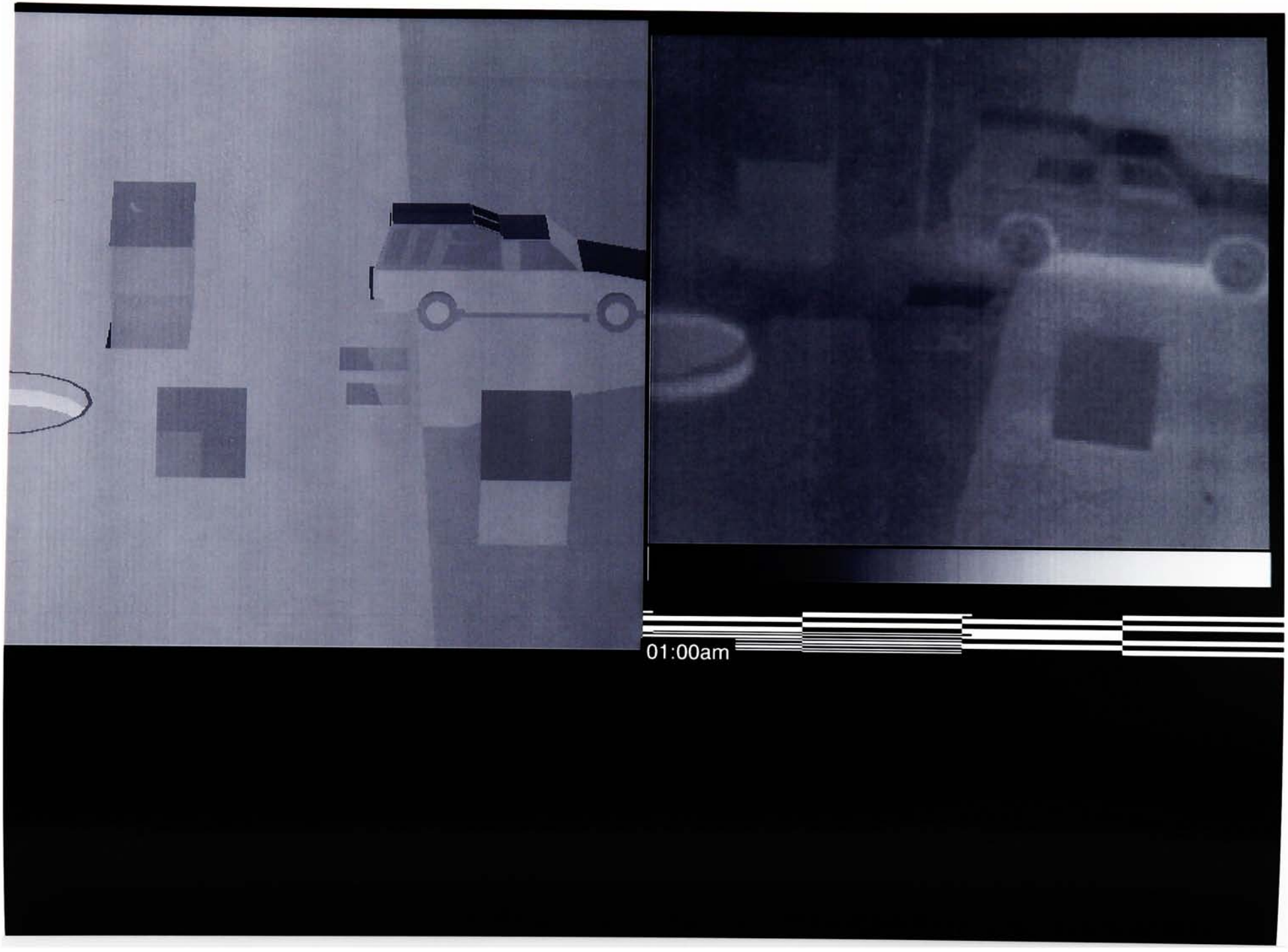
01:00am

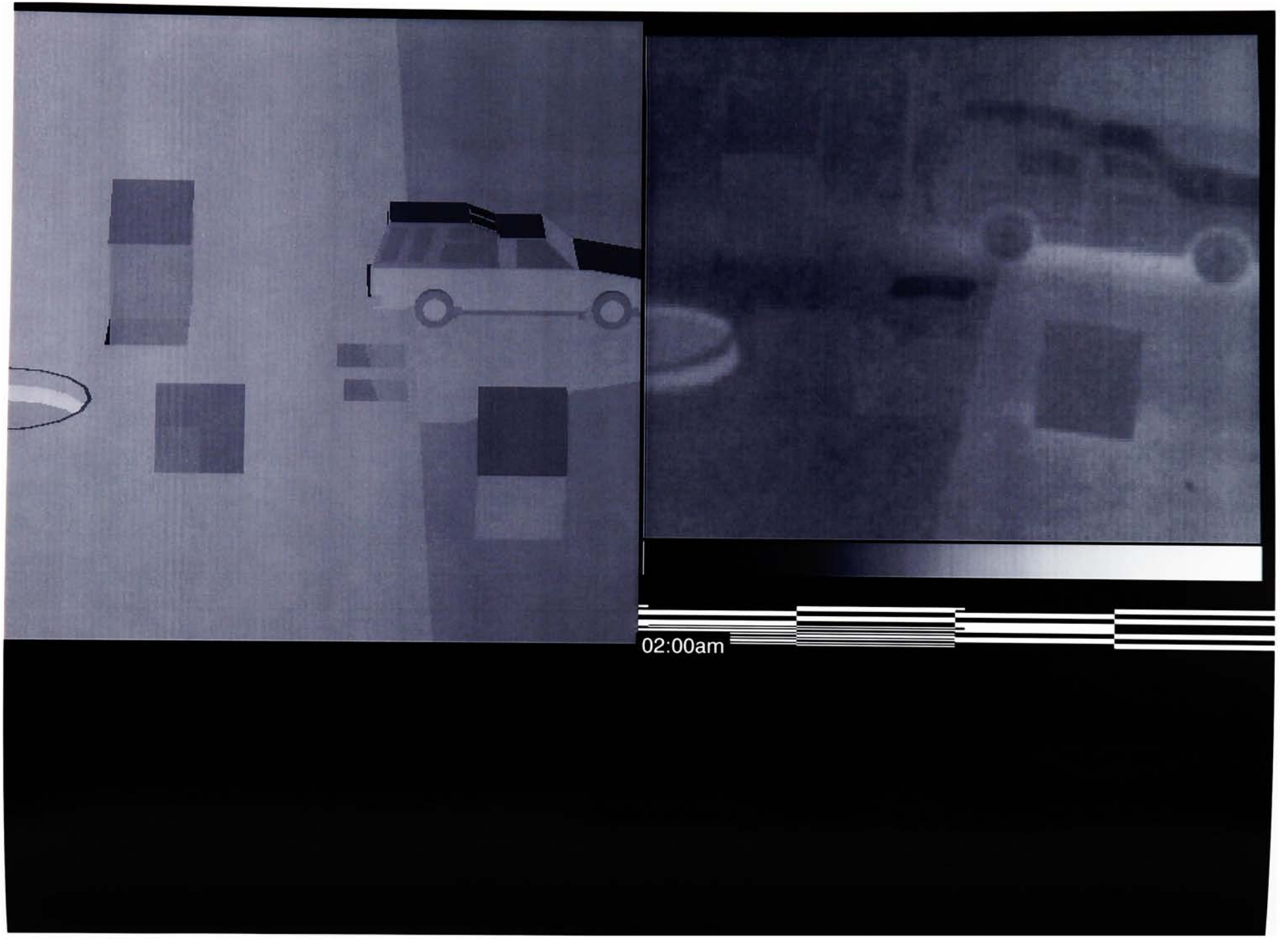
02:00am

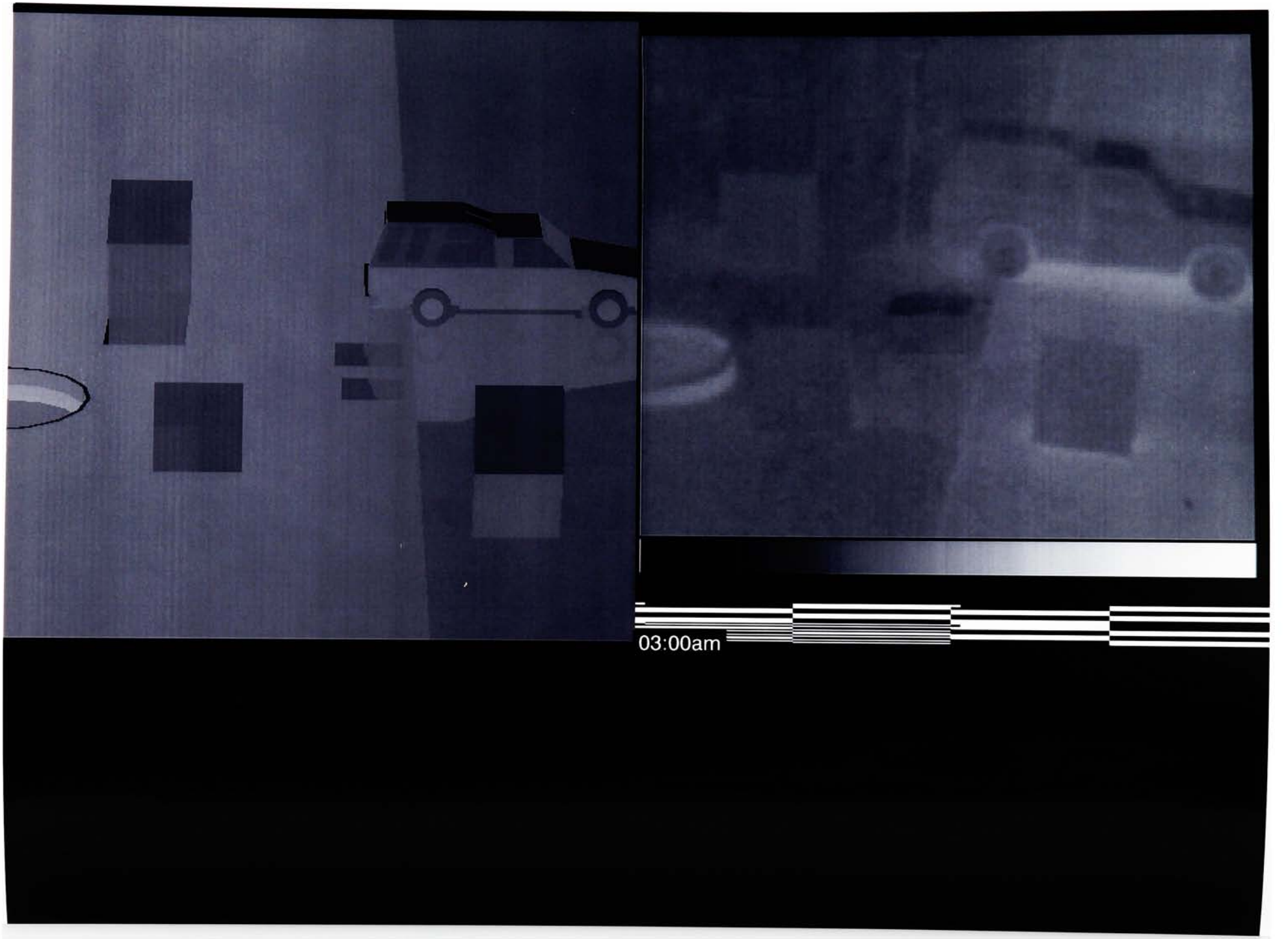
03:00am

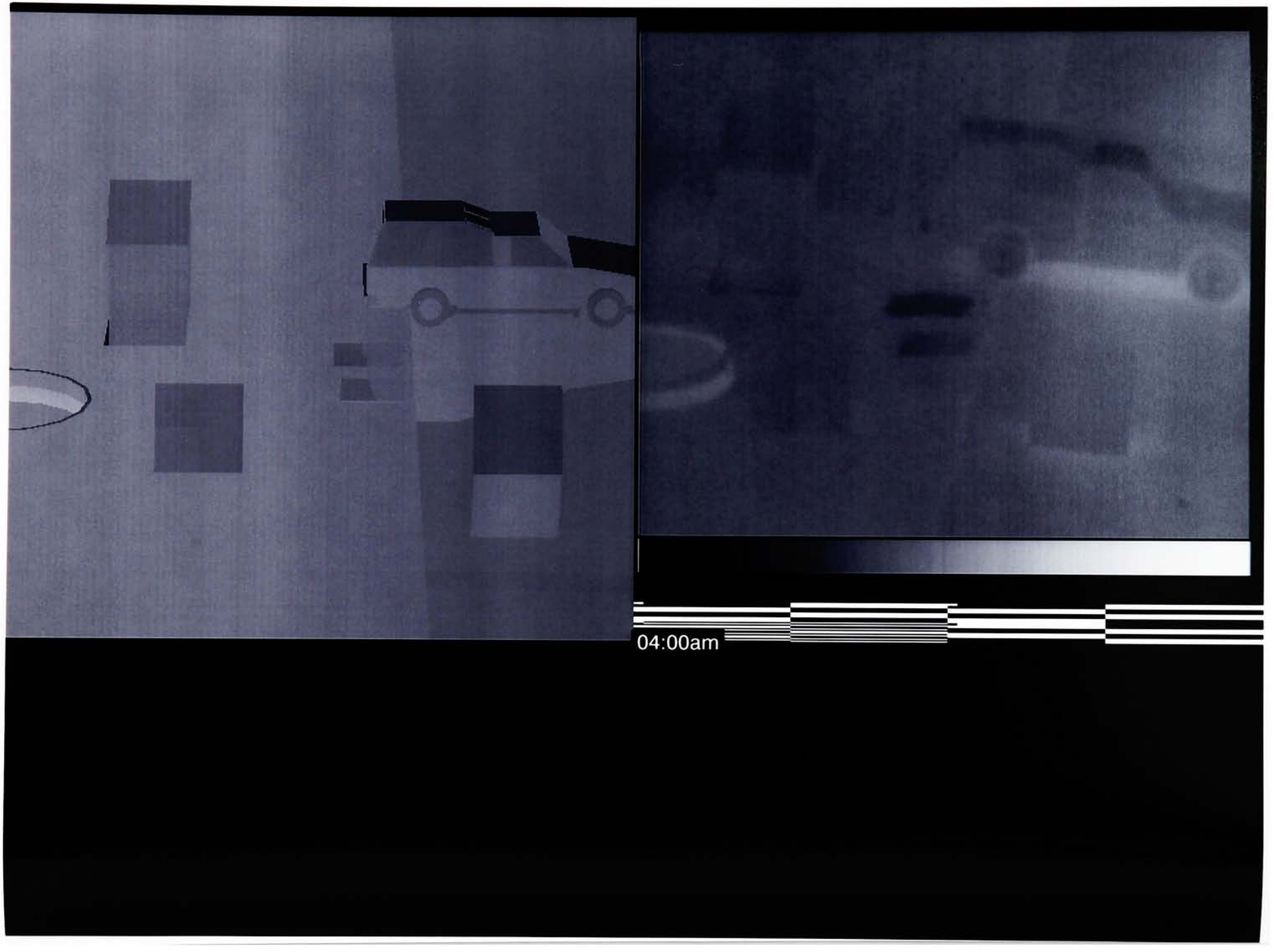
04:00am

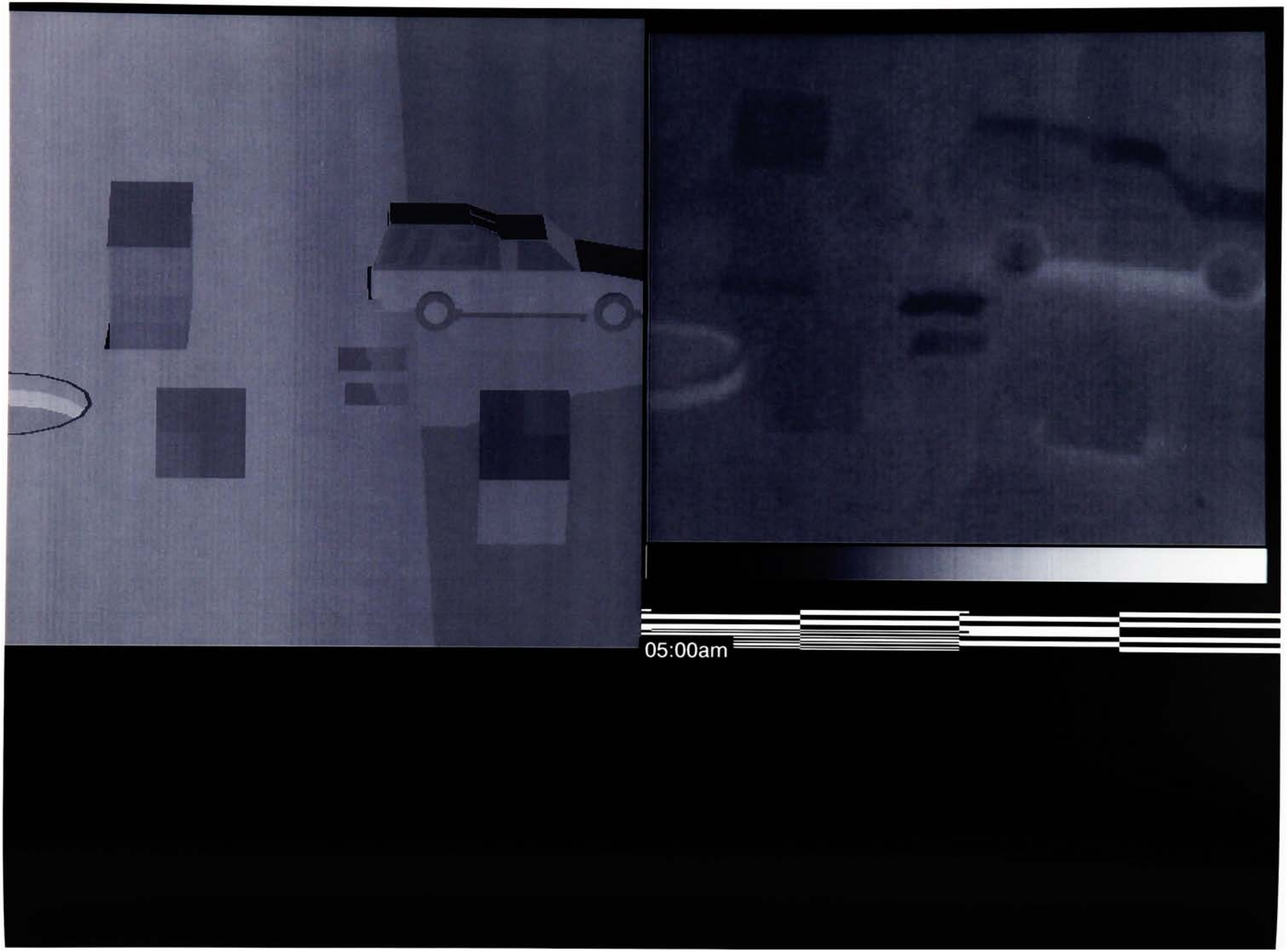
05:00am

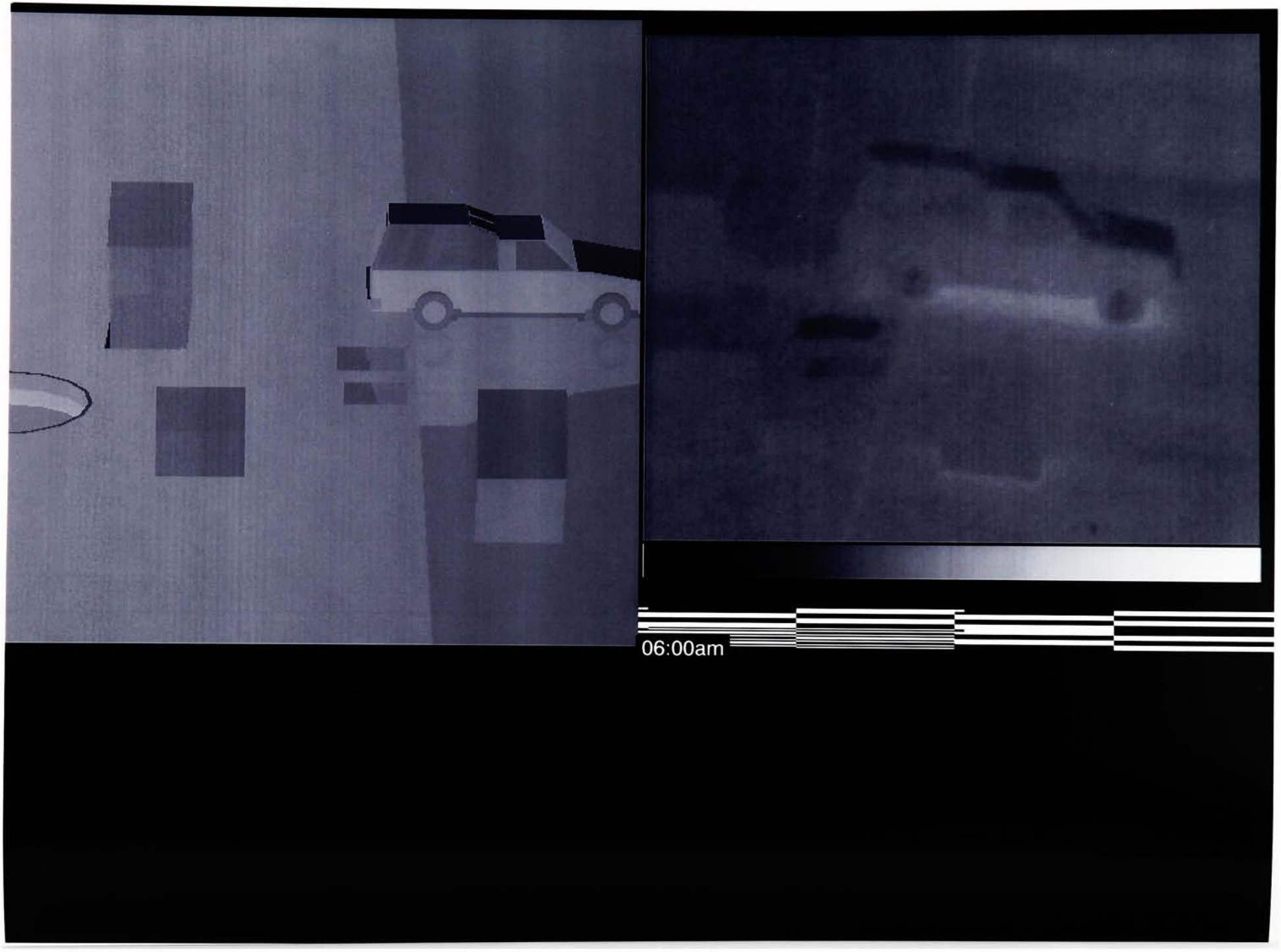
06:00am

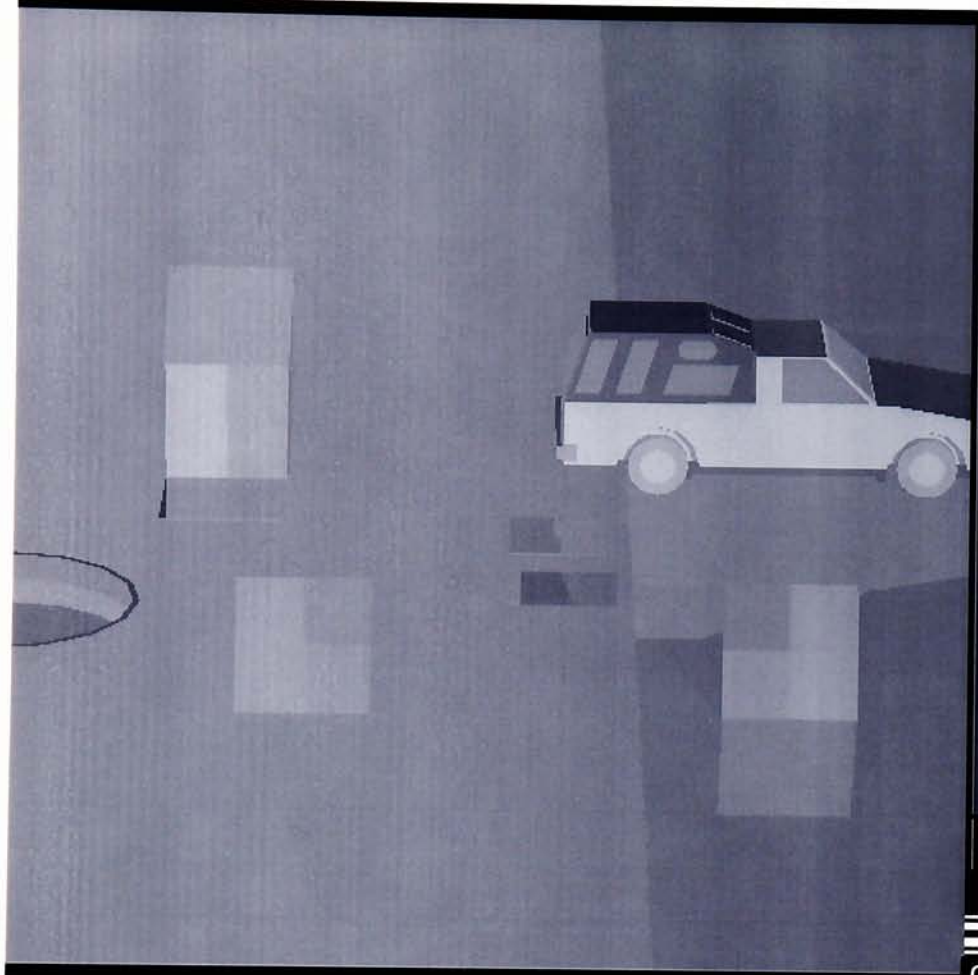

07:00am

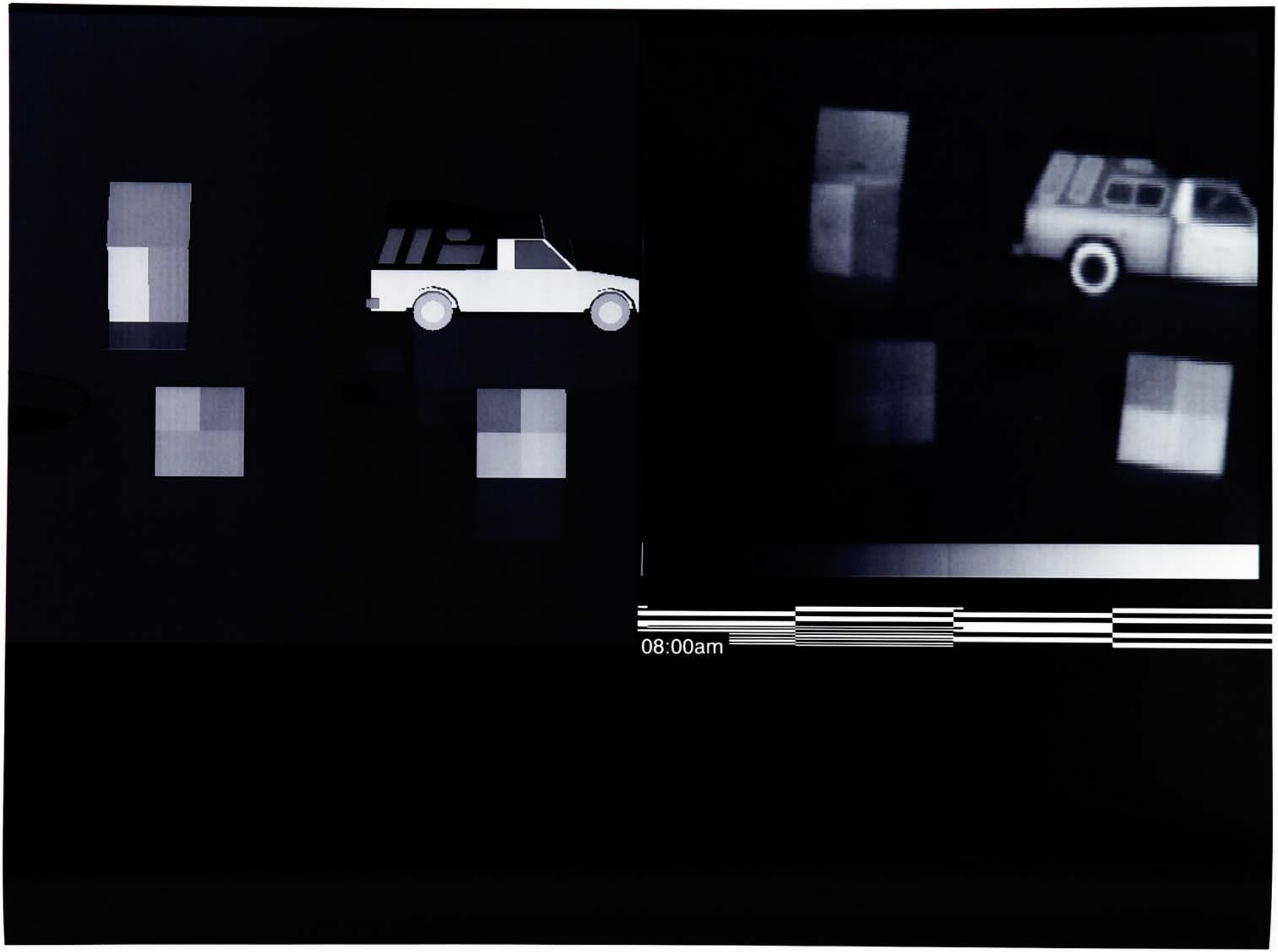
08:00am

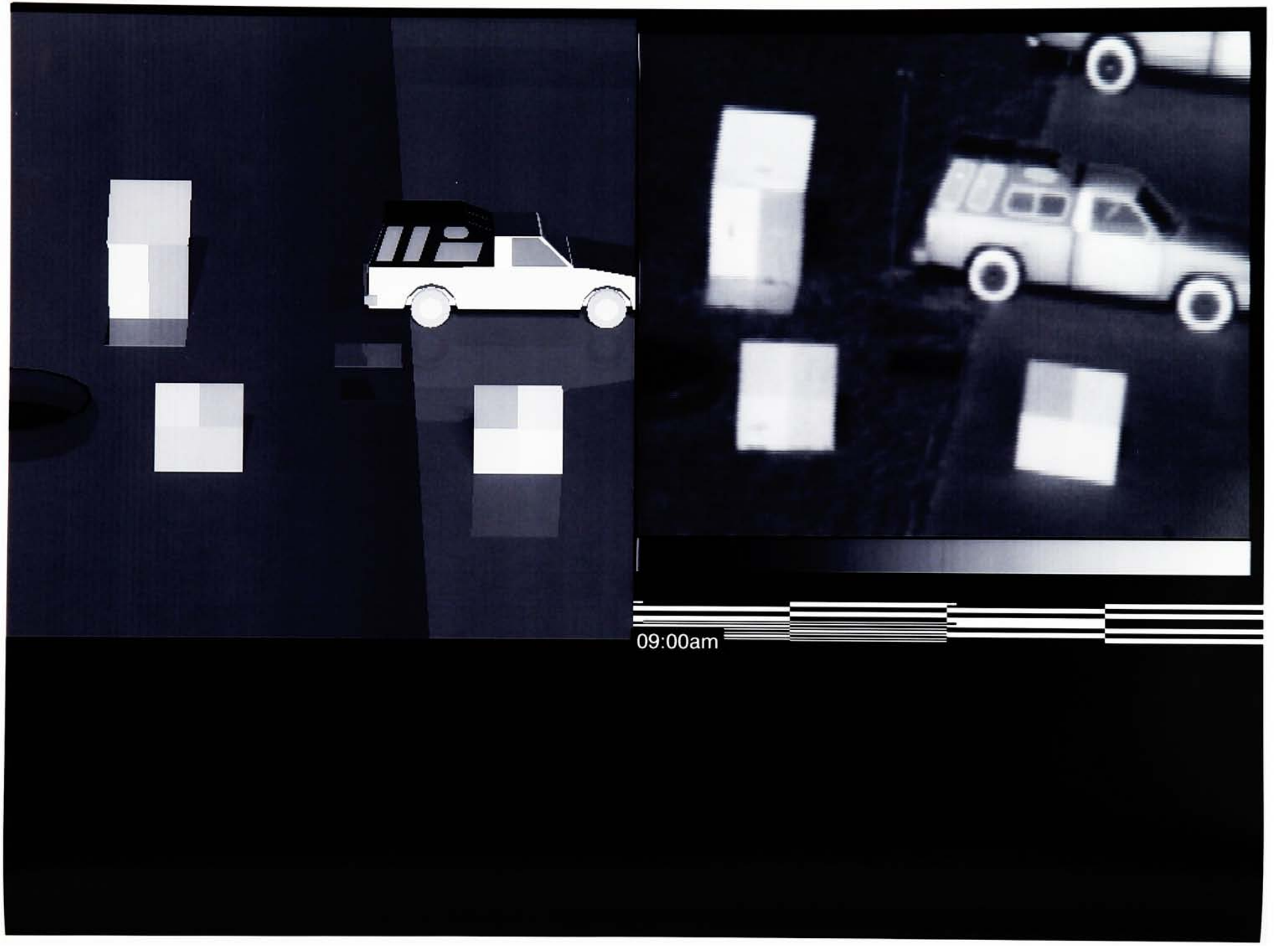
09:00am

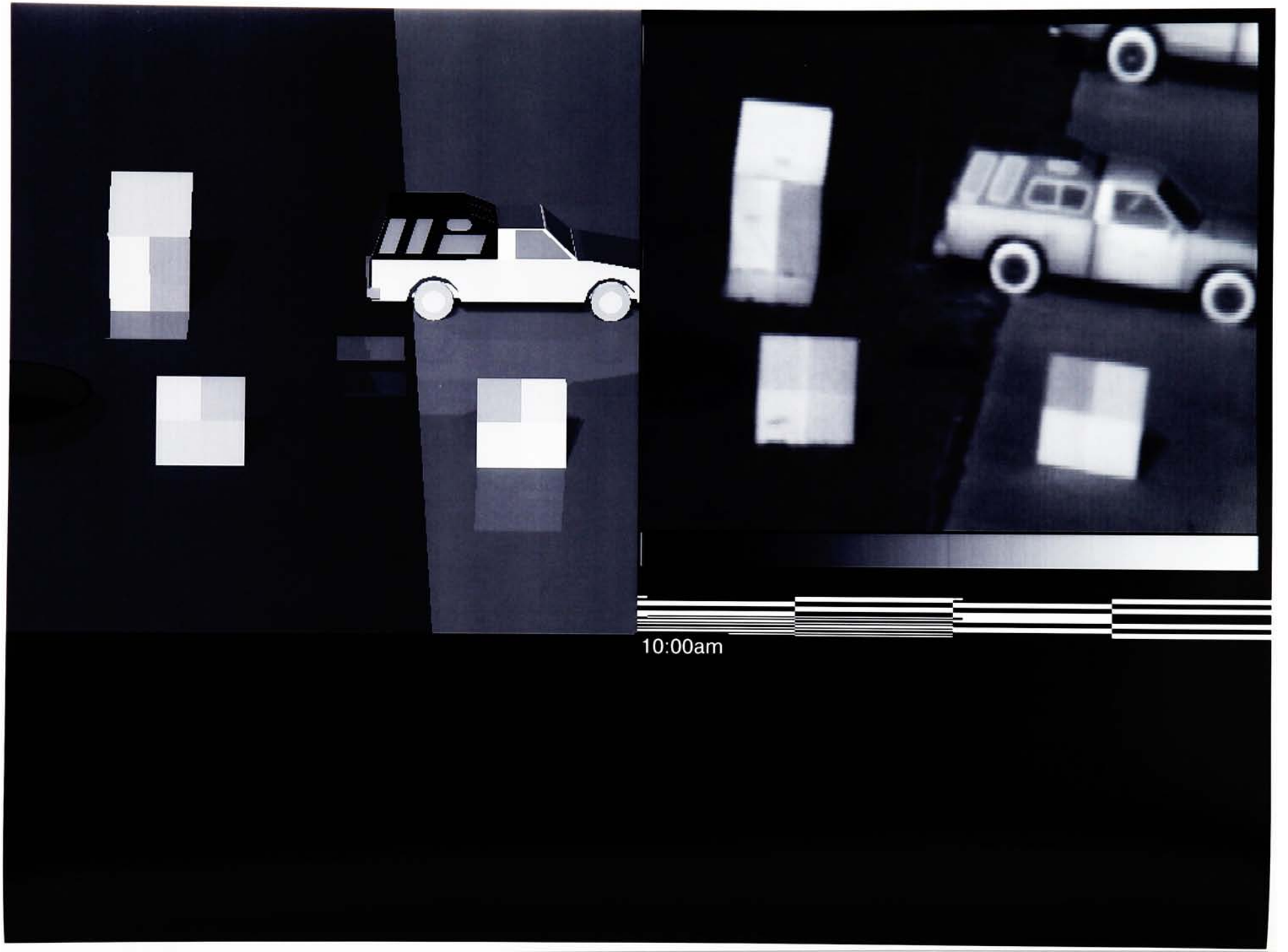
10:00am

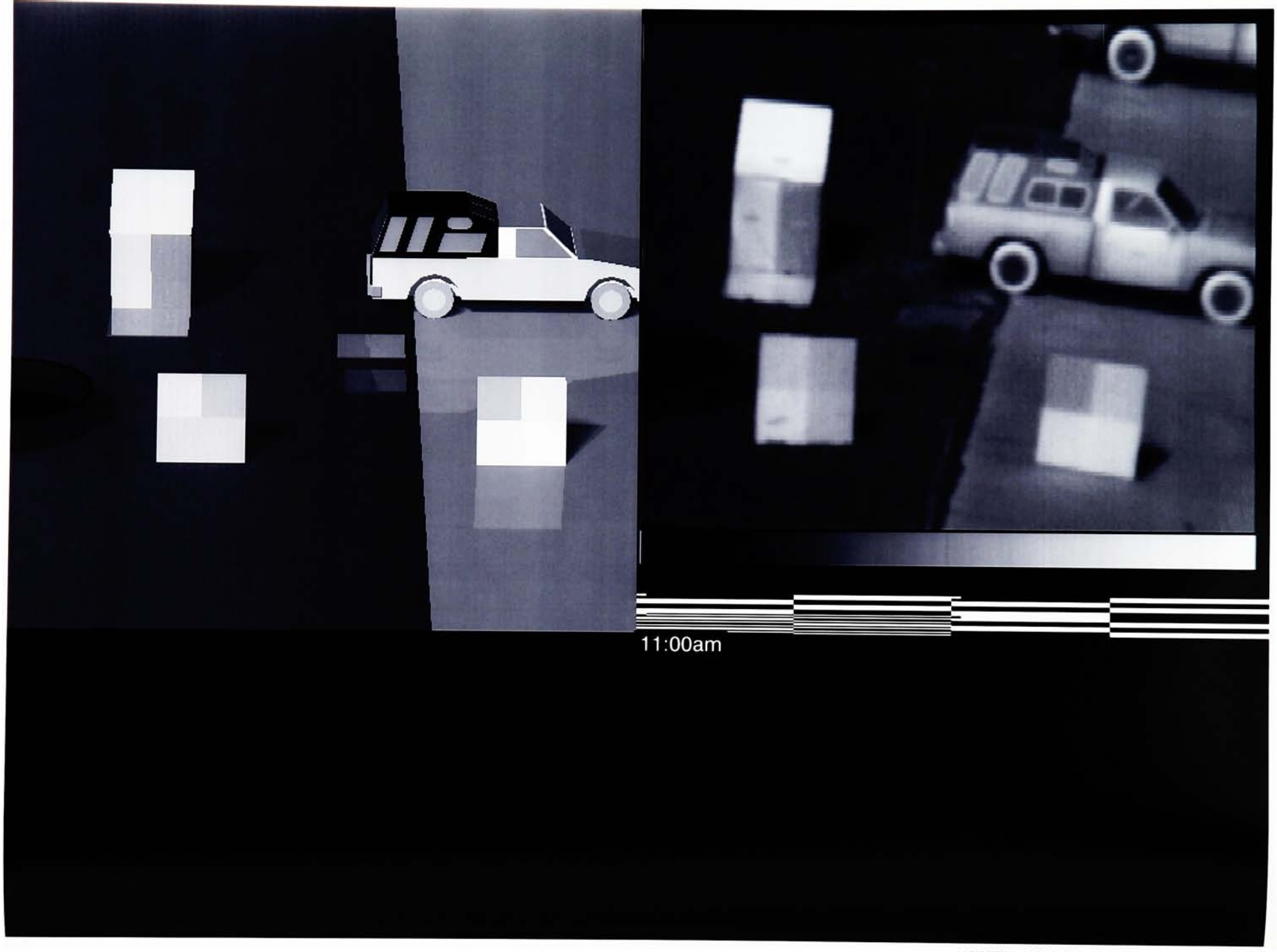
11:00am

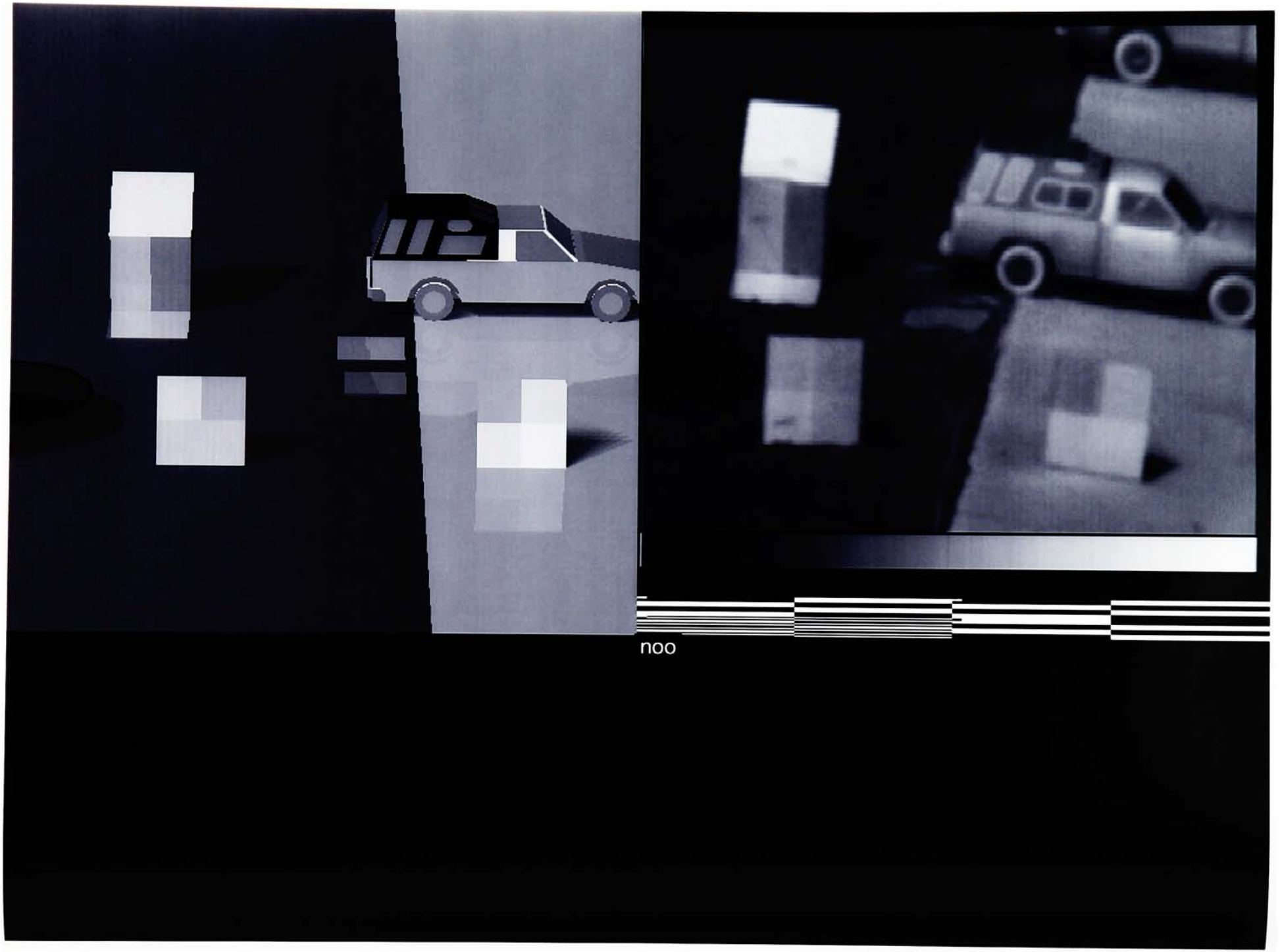

noo

13:00pm

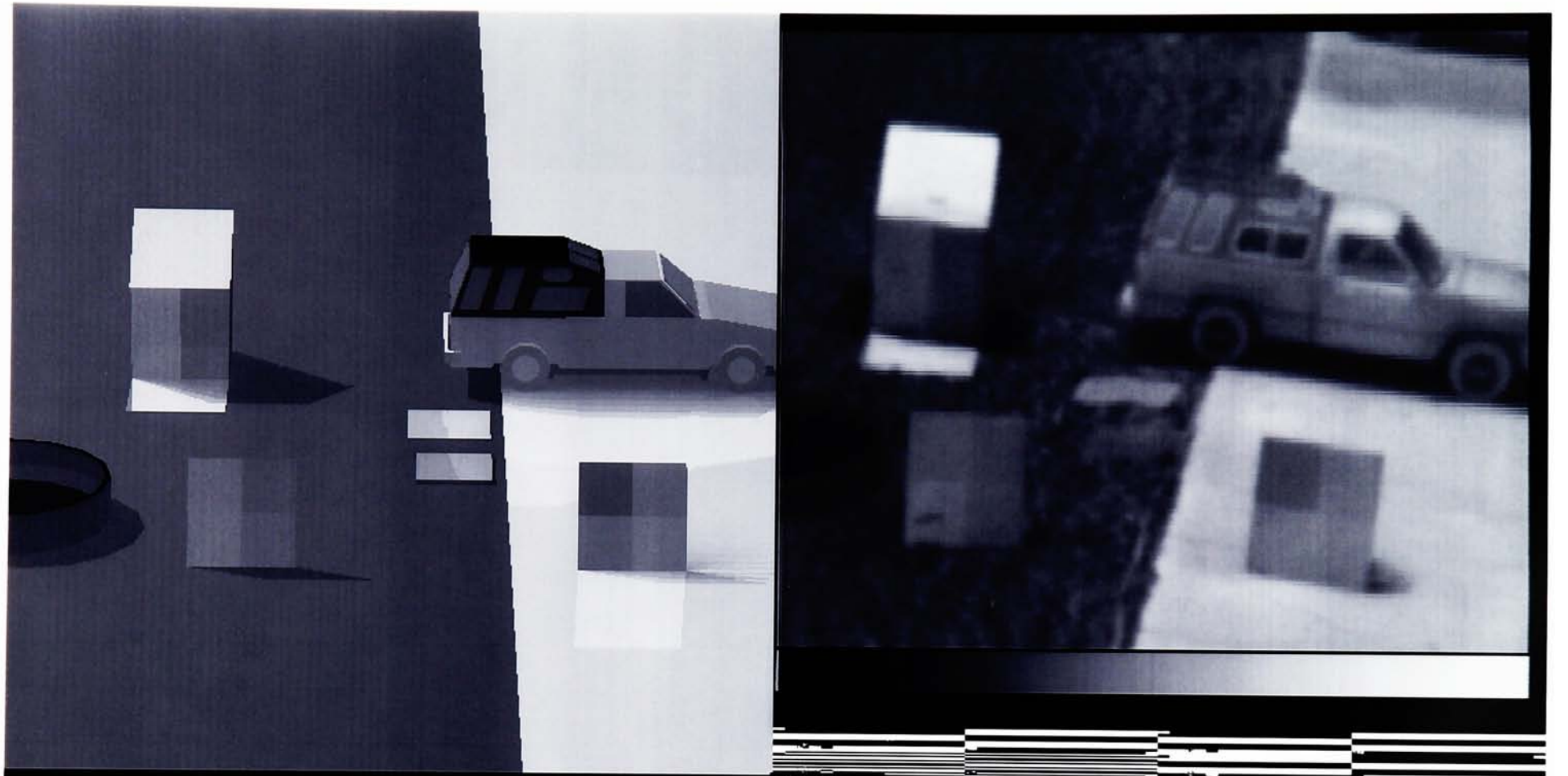

14:00pm

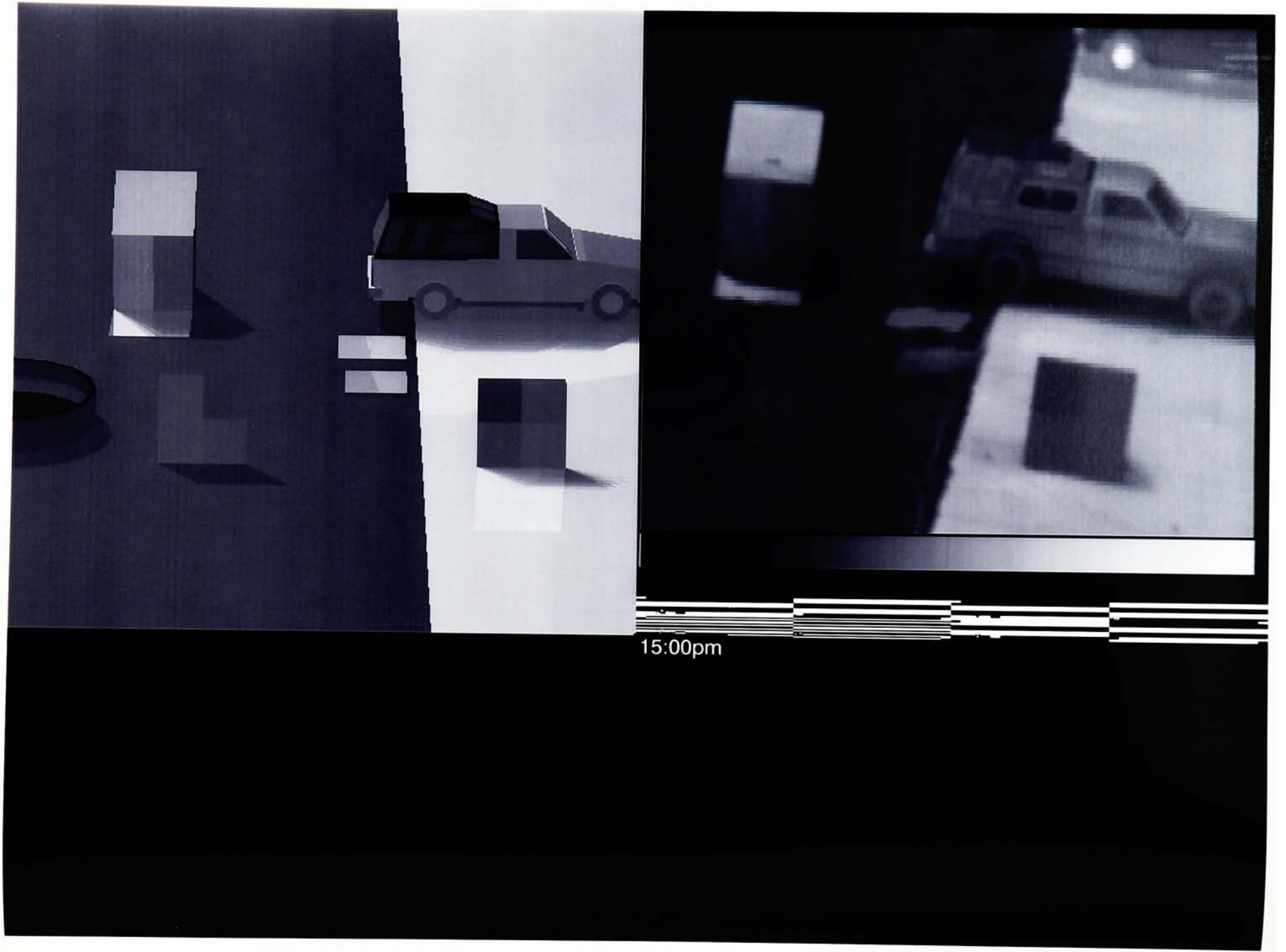

15:00pm

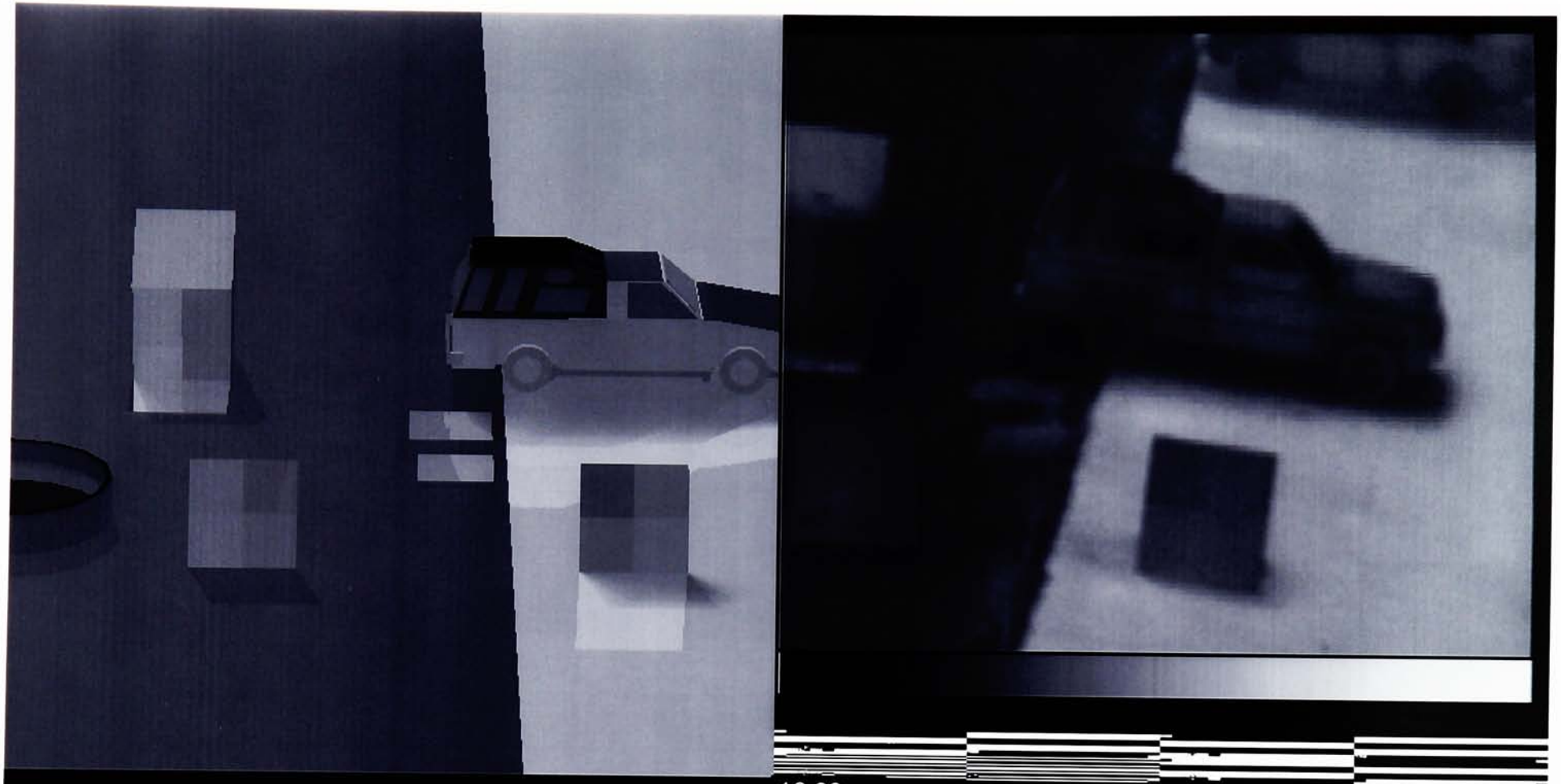

16:00pm

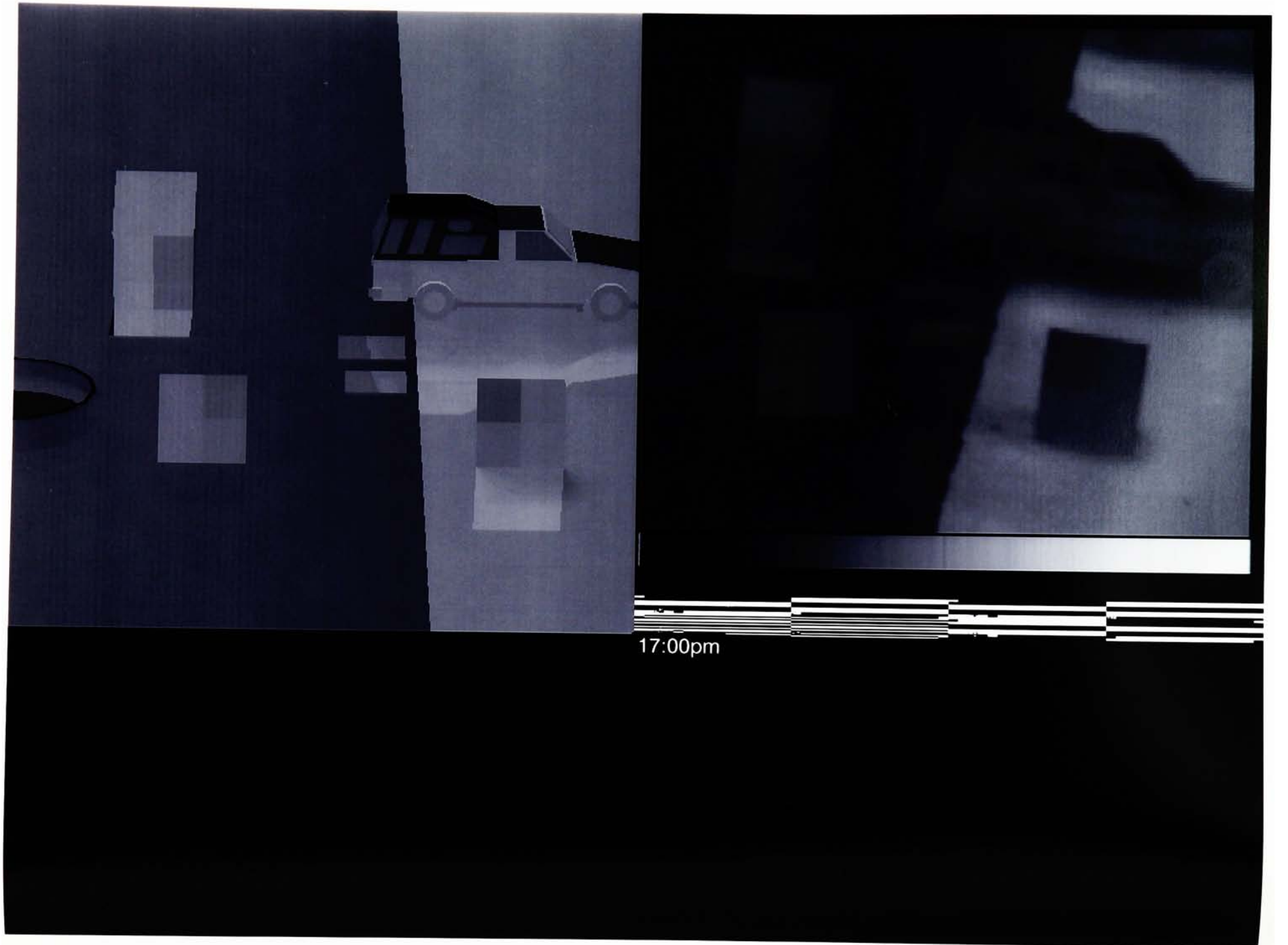

17:00pm

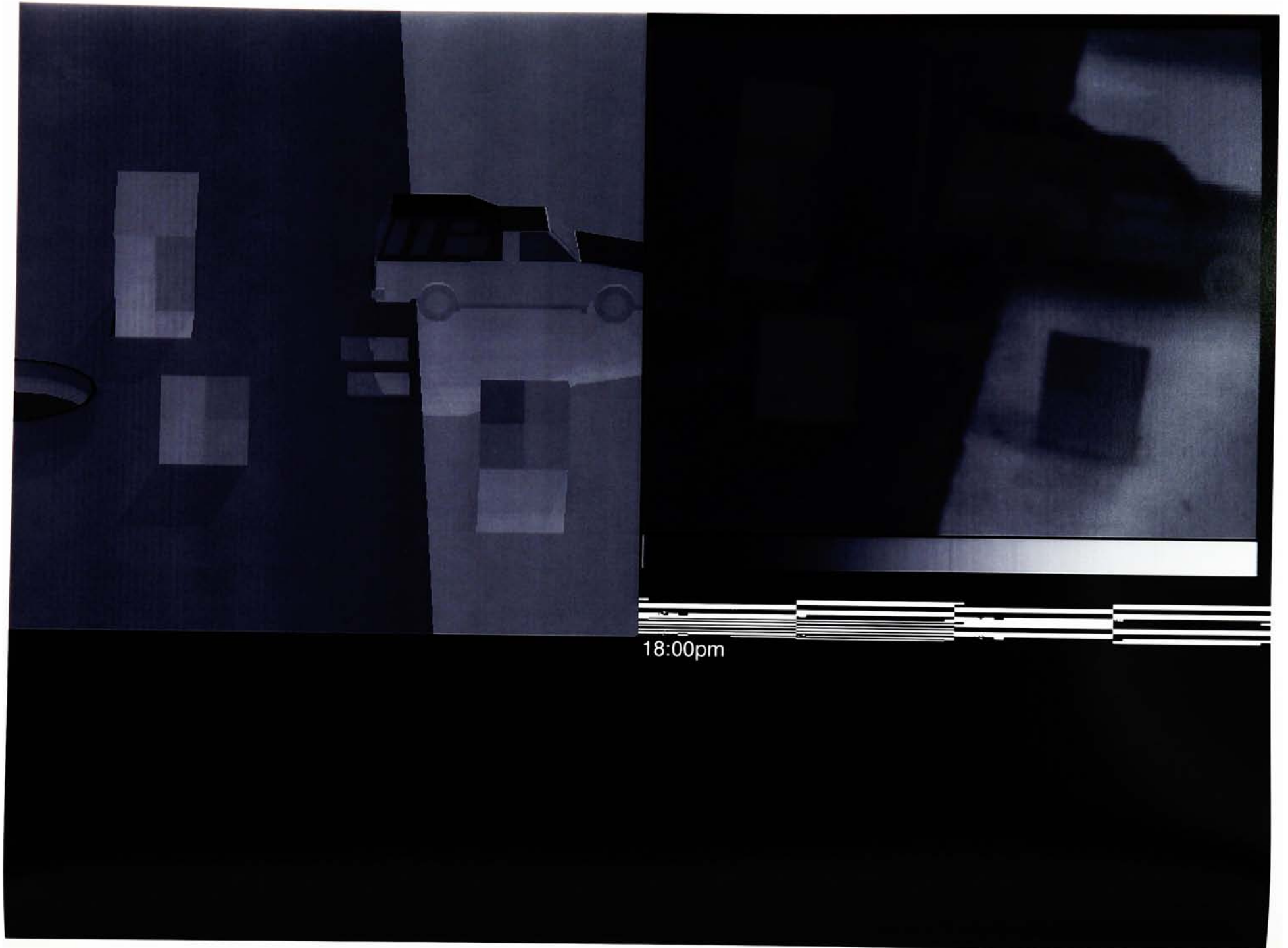
18:00pm

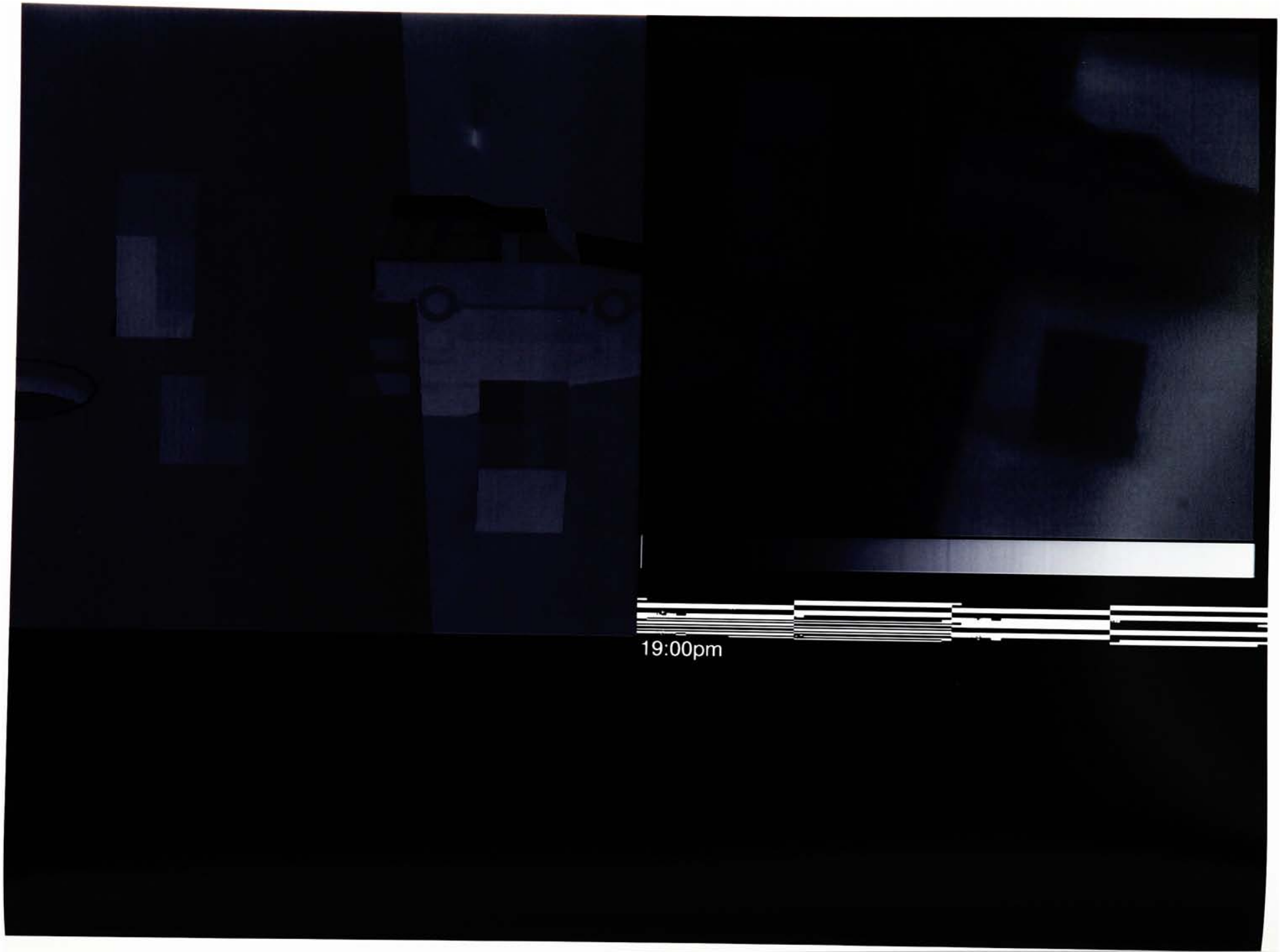
19:00pm

20:00pm

21:00pm

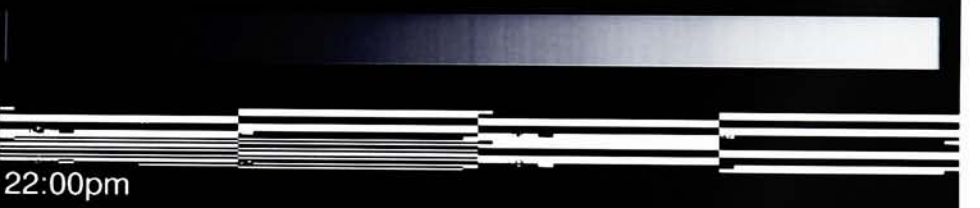
22:00pm

23:00pm

Conclusions and Recommendations

As indicated by the contrast results and inspection of the truth and prediction imagery, DIRSIG performs acceptably when clouds are not present in the scene. Although the observed radiance errors are high, the image contrast is generally correct. The absolute radiance errors can be improved by the following solutions (ranked in decreasing order of expected benefit and ease of implementation):

1.) Change from binary to fractional specularity,
2.) Shape factor computation,
3.) Increased database of material parameters,
4.) Modeling of clouds within scenes,
5.) Better understanding of LOWTRAN7's treatment of clouds, and
6.) Improved thermal model.

The following is a discussion of these solutions as well as minor suggestions for improvements to each submodel.

Geometric Submodel:

A better interface to the geometric subroutine is required so that individual object parameters can be changed easily. At present, in order to change some parameters such as thickness and self-generated power, either the entire scene must be rebuilt on AutoCAD or the huge geometric database file must be weeded through to find the correct facet to adjust.

When designing a scene, the size and positioning of targets must be dealt with carefully. Exact locations of objects must be taken into consideration to avoid shadowing errors such as those encountered in the halo of the car in the June scenes.

Ray tracer Submodel:

Addition of clouds into the actual AutoCAD scenes would allow for better modeling of downwelled radiance reaching the target. The ray_tracer submodel would include any ray interactions with clouds in its computations. Also, object shadowing by clouds will be taken into consideration when the sun/shadow history is computed.

Temperature Submodel:

In order to increase the accuracy of target temperature prediction, a better thermal model is required. As it stands, Therm cannot account for thermal effects between adjacent facets, wind direction effects, and cloud locations relative to facet directions. A better temperature generation model should include adjacency effects, good environmental modeling (wind speed and direction, cloud locations, etc.) and well-defined object parameters without a significant increase in program run time.

To improve Therm's predictions a large database of object parameters is desirable. Better definition of object parameters reduces predicted temperature errors, a large source of error in the prediction of radiance reaching the sensor. Increasing the database would also improve the error in the emissivyt term in the radiometry equations.

Radiometry Submodel:

The binary specularity problem should be resolved. One approach is to define specularity as a fraction between zero and one, where zero is totally diffuse and one is totally specular. In this manner, both the diffuse and specular solutions for each facet will be computed and the final target radiance will be a weighted combination of the two, according to the value of the specularity.

Along with the change in specularity should be a new computation for shape factor. The shape factor assigned to each facet should be a fraction. A program could be written to test the area around a facet for surrounding objects which may occlude its exposure to sky radiance. This program would eliminate any guesswork required of the user.

Cloud definitions within the LOWTRAN7 atmospheric modeling routine should be researched. As it stands, Dirsig's worst predictions occur when cloudy weather conditions exist. Correlation between the thermal submodel's defintion of clouds and LOWTRAN7's definitions of clouds should eliminate some of the guess work and errors encountered during this project.

Sensor Submodel:

The sensor submodel was minimally tested during this project. The sensor gain and bias were added after the images were created in order to be able to modify those values if necessary without having to rerun the entire program. Simple MTF blurring effects were also added outside of the program so that varying degrees of blurring could be

added and removed at will. The sensor spectral response function was the only variable utilized during this project. In this case, the spectral response was set to one from eight to fourteen microns, and was zero everywhere else. This definition produced acceptable results without any major problems encountered.

References

Beers, Y., Introduction to the Theory of Error, Addison-Wesley Publishing Company, Inc., Reading Mass., 1957.

Byrnes, A.E., and J.R. Schott, "Correction of thermal imagery for atmospheric effects using aircraft measurement and atmospheric modeling techniques," Applied Optics, Vol. 25, No. 15, August 1986.

DCS Corporation, "AIRSIM thermal signature and prediction analysis tool definition and analysis of object parameter inputs," DCS Technical Note 9090-002-004, December 1990.

Duncan, D., "Unified target modeling, validation, and ATR performance evaluation," Proceedings of the SPIE, Signal and Image Processing Systems Performance Evaluation, Vol. 1310, 1990.

Feng, X., "Comparison of methods for generation of absolute reflectance factor measurements for BRDF studies," M.S. Thesis, Rochester Institute of Technology, Center for Imaging Science, December 1990.

Kneizys, F.X., E.P. Shettle, L.W. Abreu, J.H. Chetwynd, G.P. Anderson, W.O. Gallery, J.E.A. Selby, and S.A. Clough, Users Guide to LOWTRAN 7, AFGL-TR-88-0177, Environmental Research Papers, No. 1010, Air Force Geophysics Laboratory, Optical/Infrared Technology Division, Hanscomb AFB, Maryland, August 1988.

Lillesand, T.M., R.W. Kiefer, Remote Sensing and Image Interpretation, 2nd ed., John Wiley and Sons, Inc., New York, 1987.

Lindahl, C., A. Cockcroft, T. Derryberry, J. Sigler, M. Yablonski, "Synthetic, multisensor database generation and validation," Proceedings of the SPIE, Signal and Image Processing Systems Performance Evaluation, 1990.

Massie, M., "CAD system evaluates focal-plane imagers," Laser Focus World, Vol. 27, No. 7, July 1991.

Raqueño, R., C. Salvaggio, J.S. Warnick, E. Kraus, J.R. Schott, "A thermal infrared synthetic image generation model," Final Report RIT/DIRS 90/91-63-142, prepared for Central Intelligence Agency, Office of Development and Engineering, April 1991.

Salvaggio, C., and J.R. Schott, "Laboratory techniques for assessment of longwave infrared models for synthetic scene generation," Proceedings of the SPIE, Infrared Technology XV, Vol. 1157, San Diego, CA, August 1989.

Salvaggio, C., G. Braun, J.R. Schott, "SVGM: a spectral vector generating model using the LOWTRAN 7 and SCATRAN atmospheric propagation codes," RIT/DIRS 90/91-63-141, prepared for Eastman Kodak Company, Federal Systems Division, January 1991.

Schott, J.R., E.W. Schimminger, "Data use investigations for applications explorer mission A (Heat Capacity Mapping Mission)," Calspan Report No. 6175-M-1, NASA Accession #E81-10079, January 1981.

Schott, J.R., and W.J. Volchok, "Thematic Mapper thermal infrared calibration," Photogrammetric Engineering and Remote Sensing, Vol. 51, No. 9, September 1985.

Schott, J.R., "Incorporation of angular emissivity effects in longwave infrared image models," Proceedings of the SPIE Symposium, Infrared Technology XII, Vol. 685, San Diego, CA, August 1986.

Schott, J.R., and C. Salvaggio, "LWIR radiometric modeling for use with synthetic scene generation," Final report prepared for Contract RD-86-6843 (Task 3), Report No. RIT/DIRS 86/87-51-114, February 1987.

Schott, J.R., and C. Salvaggio, "Inclusion of sensor noise in radiometric models for generation of synthetic longwave infrared images," Proceedings of the SPIE, Three-Dimensional Imaging and Remote Sensing, San Diego, CA, August 1987.

Schott, J.R., and C. Salvaggio, "LWIR radiometric modeling for use with synthetic scene generation 1987/88 results," Final Report RIT/DIRS 87/88-51-122, prepared for Contract RD-86-6843 (Task 3), Office of Development and Engineering, Central Intelligence Agancy, January 1989.

Schott, J.R., M. Fairchild, X. Feng, R. Raqueño, B. Brower, T. Gallagher, "Techniques for measurement of the optical properties of materials," Final Report RIT/DIRS 89/90-51-134, prepared for United States Department of Energy, January 1990.

Schwartz, I.B., K.A. Snail, J.R. Schott, "Infrared halo effects around ships," Naval Research Laboratory Memorandum 5529, 1985.

Shor, E.H., "3-D longwave infrared synthetic scene simulation," M.S. Thesis, Rochester Institute of Technology, Center for Imaging Science, May 1990.

Shor, E.H., C. Salvaggio, J.R. Schott, "Three-dimensional longwave infrared (LWIR) synthetic image generation incorporating angular emissivity effects using raytracing techniques," presented at the SPIE 35th Annual International Symposium on Optical and Optoelectronic Applied Science and Engineering, San Diego, CA, August 1990.

Spector, D.N., P.F. Lambeck, S.L. Sheller, S.C. Sawtelle, D.K. Rankin, J.R. Schott, "Air Force infrared simulated image models," Proceedings of the Infrared Information Symposia, Vol. 35, No. 2, January 1991.

Sullivan, S.P., W.R. Reynolds, "Validation of the physically reasonable infrared signature model (PRISM)," Proceedings of the SPIE, Infrared Systems and Components II, Vol. 890, 1988.

Warnick, J.S., E.H. Shor, J.R. Schott, "Thermal infrared scene simulation," Final Report RIT/DIRS 89/90-51-133, prepared for United States Department of Energy, January 1990.

APPENDIX A

Random Error Addition Program

```
*****************************************************************
*                                                               *
*       This program adds a bias and randomly assigns           *
*       input RMS error to a column of data in an input         *
*       Therm weather file.                                     *
*                                                               *
*                          Donna Rankin                         *
*                          2/19/92                              *
*                                                               *
*****************************************************************
*                                                               *
      REAL*4            BIAS1, RMS1, RAND, RMS2, BIAS2
      REAL*4            TIME,A,P,D,H,W,Dr,Df,SE,PR,PTmp
      REAL*4            H1, D1, PR1, PTMP1, JUNK
      INTEGER           X,CT,PT
      INTEGER*4         SEED,FLAG
      CHARACTER*80      F_IN,F_OUT,F_OUT2
*                                                               *
*****************************************************************
*                                                               *
      PRINT*,'PLEASE INPUT THE NAME OF THE TRUTH FILE'
      READ(*,'(a80)') F_IN
      OPEN(UNIT=1, FILE=F_IN, STATUS='OLD')
      PRINT*,'PLEASE INPUT THE NAME OF THE OUTPUT FILE'
      READ(*,'(a80)') F_OUT
      OPEN(UNIT=2, FILE=F_OUT, STATUS='NEW')
*     PRINT*,'INPUT THE BIAS VALUES TO BE ADDED TO THE DATA'
*     READ*,BIAS1
*     PRINT*,'BIAS VALUES ARE: ',BIAS1
*     PRINT*,'INPUT THE RMS VALUES TO BE RANDOMLY ADDED'
*     READ*,RMS1
*     PRINT*,'RMS VALUES ARE: ',RMS1
      PRINT*,'PLEASE INPUT A SEED VALUE FOR THE RANDOM FUNCTION CALL'
      READ*,SEED
5     X= X + 1.0
      READ(1,*, END = 15) TIME,A,P,H,D,W,Dr,Df,SE,CT,PT,PR,PTmp
      RAND = RANFUN(SEED)
      IF( DF .EQ. 0.0) GOTO 7
*     IF( RAND .LE. (0.33333333) ) THEN
*        DR = DR + BIAS1
*        FLAG = 0
*     ENDIF
      IF( (RAND .GT. (0.33333333)) .AND. (RAND .LE. (0.666666667)) ) THEN
         DF = DF + SQRT( (DF * .002)**2 + (.043**2) )
         FLAG = 1
      ENDIF
      IF( RAND .GT. (0.666666667) ) THEN
         DF = DF - SQRT( (DF * .002)**2 + (.043**2) )
         FLAG = 2
      ENDIF

      IF( DF .LT. 0.0 ) DF = ABS(DF)
 7    WRITE(2,10) TIME,A,P,H,D,W,Dr,Df,SE,CT,PT,PR,PTmp
10    FORMAT(1X,2F7.2,F7.2,1X,F6.3,1X,F6.2,3F7.3,F6.2,2I3,2F6.2)

      GOTO 5
15    CLOSE(1)
      CLOSE(2)
      STOP
      END
```

APPENDIX B

Emissivity Measurement Results

Emissivity

	Angle	Blue1	Blue2	Red	Green	Grey1	Grey2
1	0.000	0.970	0.970	0.971	0.968	0.966	0.978
2	10.000	0.970	0.970	0.971	0.956	0.960	0.978
3	20.000	0.979	0.970	0.966	0.950	0.955	0.978
4	30.000	0.970	0.975	0.945	0.938	0.955	0.968
5	40.000	0.956	0.948	0.918	0.914	0.960	0.958
6	50.000	0.916	0.894	0.928	0.902	0.943	0.953
7	60.000	0.921	0.899	0.912	0.938	0.926	0.978
8	70.000	0.980	0.986	1.014	1.045	1.001	1.039
9	80.000	0.523	0.521	0.668	0.827	0.279	0.303

	Grey3-1	Grey3-2	Grey4	Grey5-1	Grey5-2	Shingles-1	Shingles-2
1	0.980	0.980	0.965	0.969	0.969	0.965	0.965
2	0.946	0.946	0.965	0.963	0.969	0.958	0.951
3	0.925	0.929	0.965	0.956	0.969	0.958	0.986
4	0.914	0.901	0.971	0.963	0.962	1.006	1.014
5	0.892	0.871	0.959	0.963	0.923	0.999	0.993
6	0.934	0.898	0.965	0.943	0.916	0.965	0.965
7	0.911	0.892	0.930	0.969	0.943	0.944	0.951
8	0.831	0.822	0.941	1.034	1.027	1.062	1.071
9	0.200	0.222	0.057	0.460	0.441	0.777	0.743

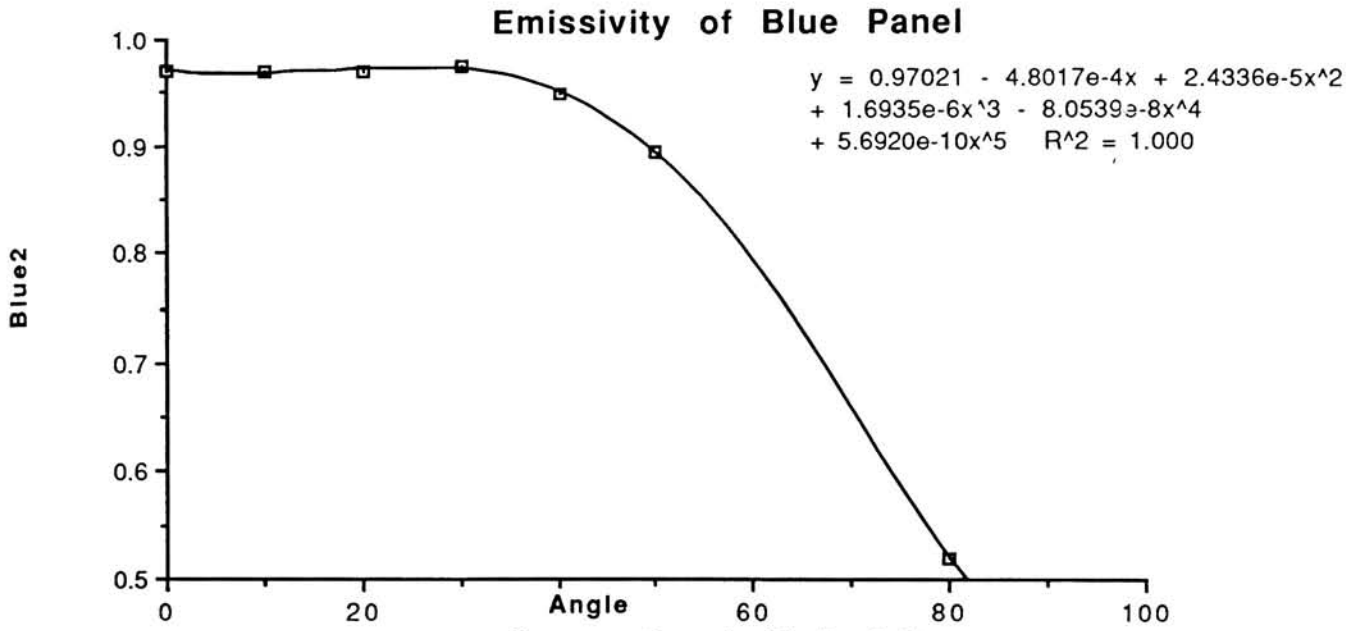
Emissivity of Blue Panel
y = 0.97021 - 4.8017e-4x + 2.4336e-5x^2
+ 1.6935e-6x^3 - 8.0539e-8x^4
+ 5.6920e-10x^5 R^2 = 1.000
Blue2
Angle
1.0
0.9
0.8
0.7
0.6
0.5
0
20
60
80
100

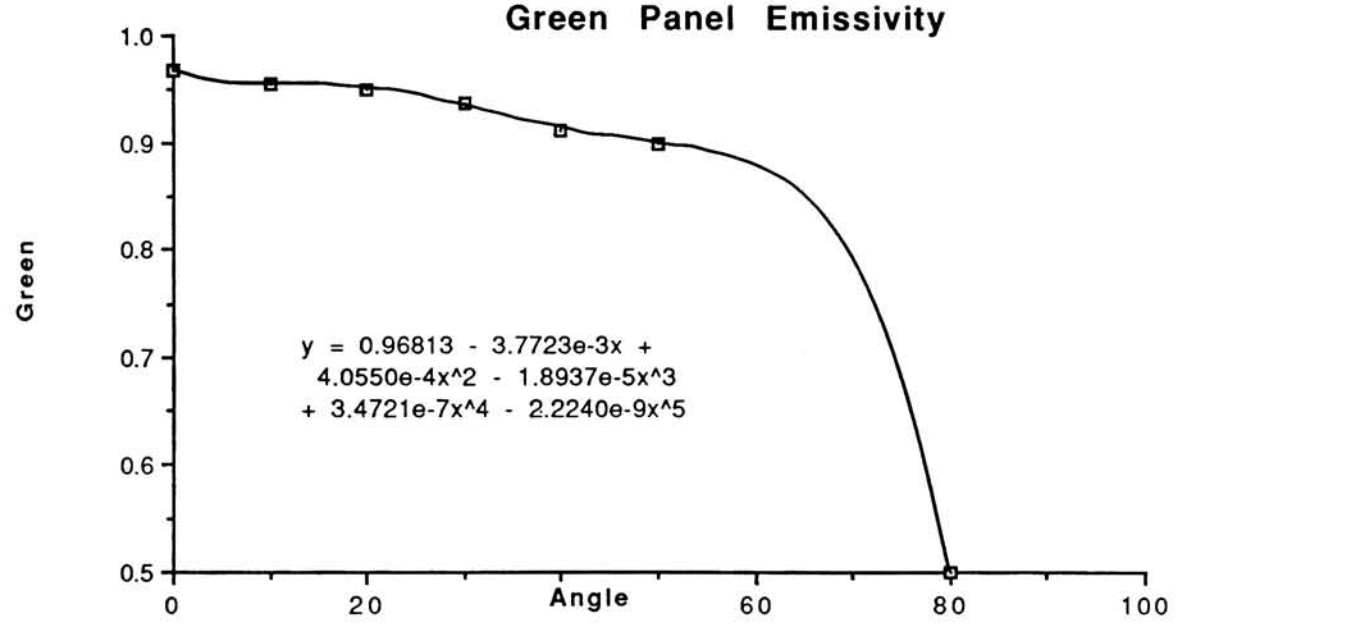
Green Panel Emissivity
y = 0.96813 - 3.7723e-3x +
4.0550e-4x^2 - 1.8937e-5x^3
+ 3.4721e-7x^4 - 2.2240e-9x^5
Green
Angle
1.0
0.9
0.8
0.7
0.6
0.5
0
20
60
80
100

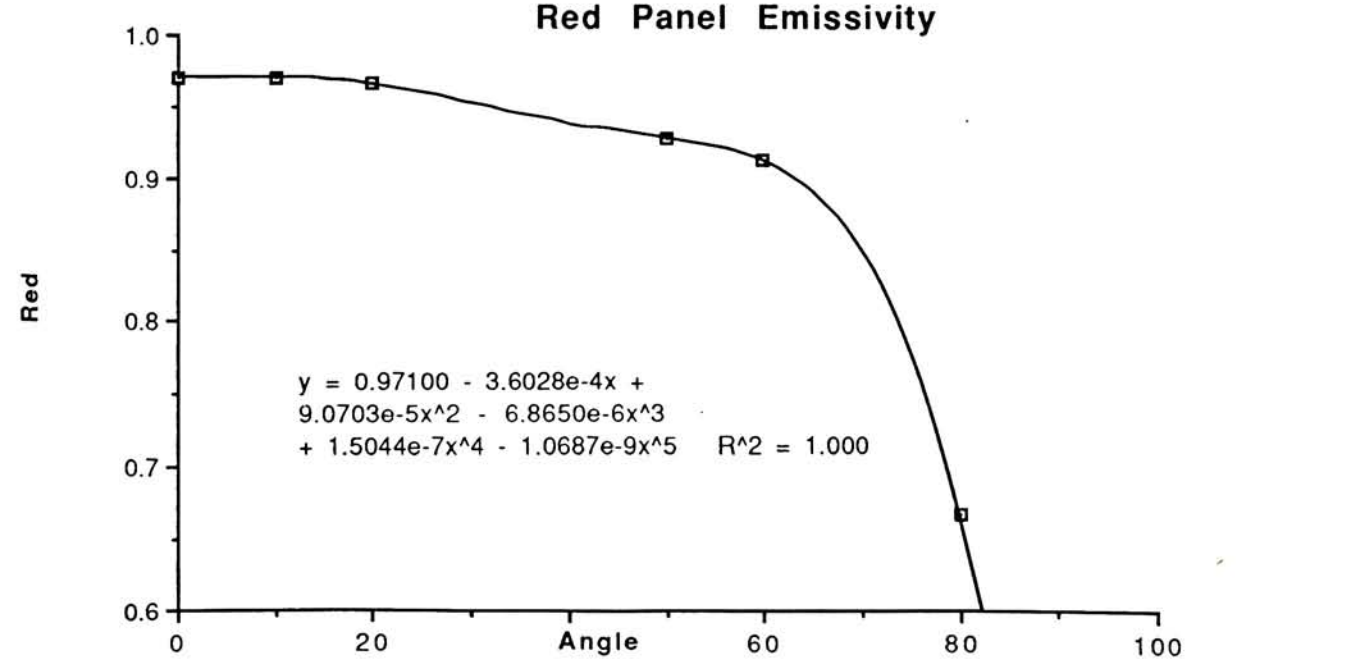
Red Panel Emissivity
y = 0.97100 - 3.6028e-4x +
9.0703e-5x^2 - 6.8650e-6x^3
+ 1.5044e-7x^4 - 1.0687e-9x^5 R^2 = 1.000
Red
Angle
1.0
0.9
0.8
0.7
0.6
0
20
60
80
100

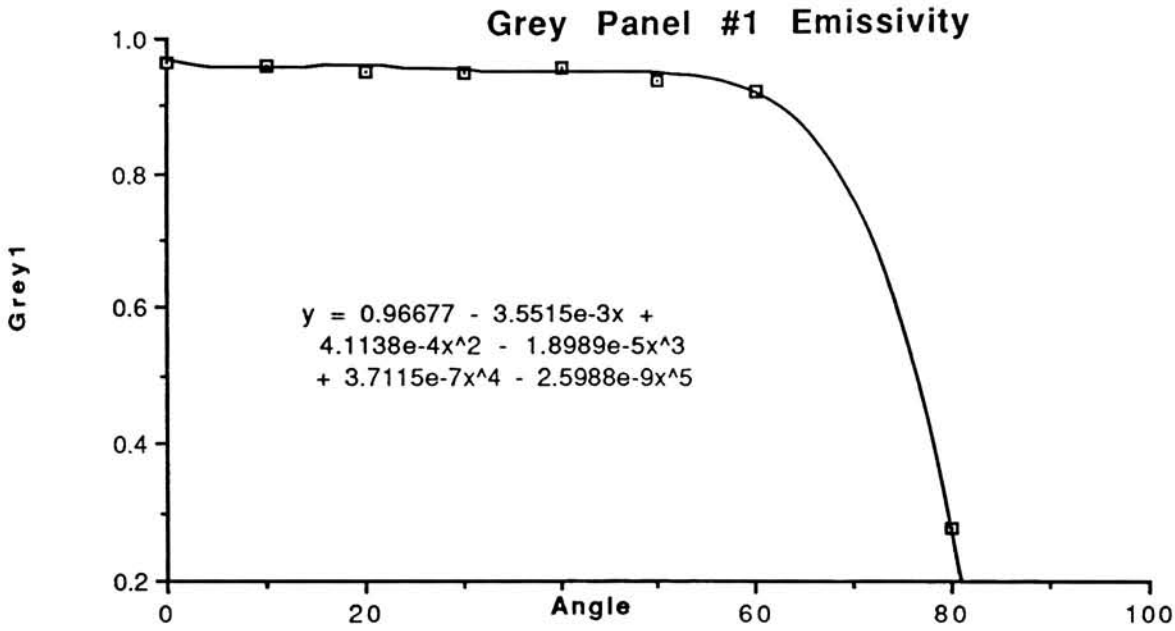
Grey Panel #1 Emissivity
Grey1
Angle
y = 0.96677 - 3.5515e-3x +
4.1138e-4x^2 - 1.8989e-5x^3
+ 3.7115e-7x^4 - 2.5988e-9x^5

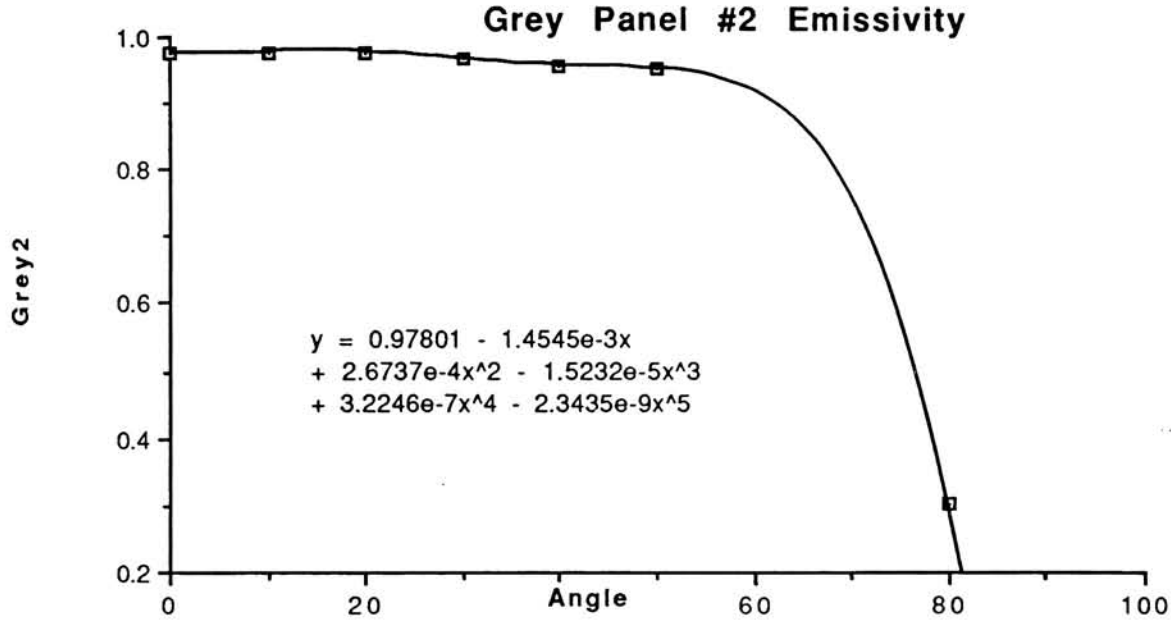
Grey Panel #2 Emissivity
Grey2
Angle
y = 0.97801 - 1.4545e-3x
+ 2.6737e-4x^2 - 1.5232e-5x^3
+ 3.2246e-7x^4 - 2.3435e-9x^5

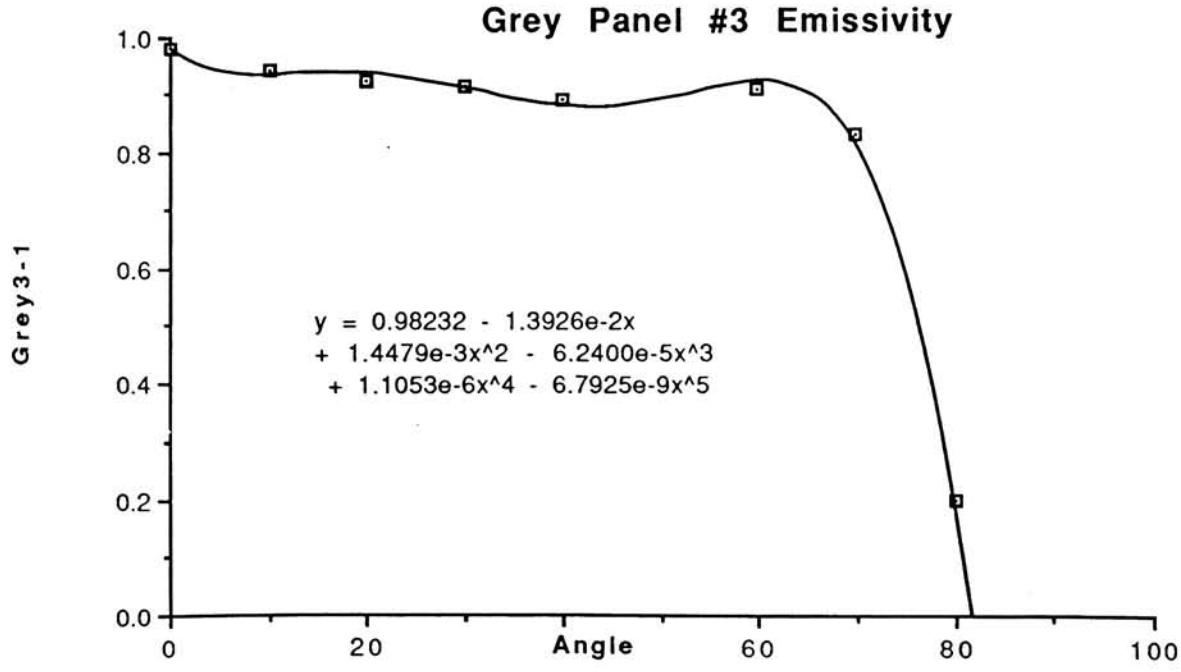
Grey Panel #3 Emissivity
Grey3-1
Angle
y = 0.98232 - 1.3926e-2x
+ 1.4479e-3x^2 - 6.2400e-5x^3
+ 1.1053e-6x^4 - 6.7925e-9x^5

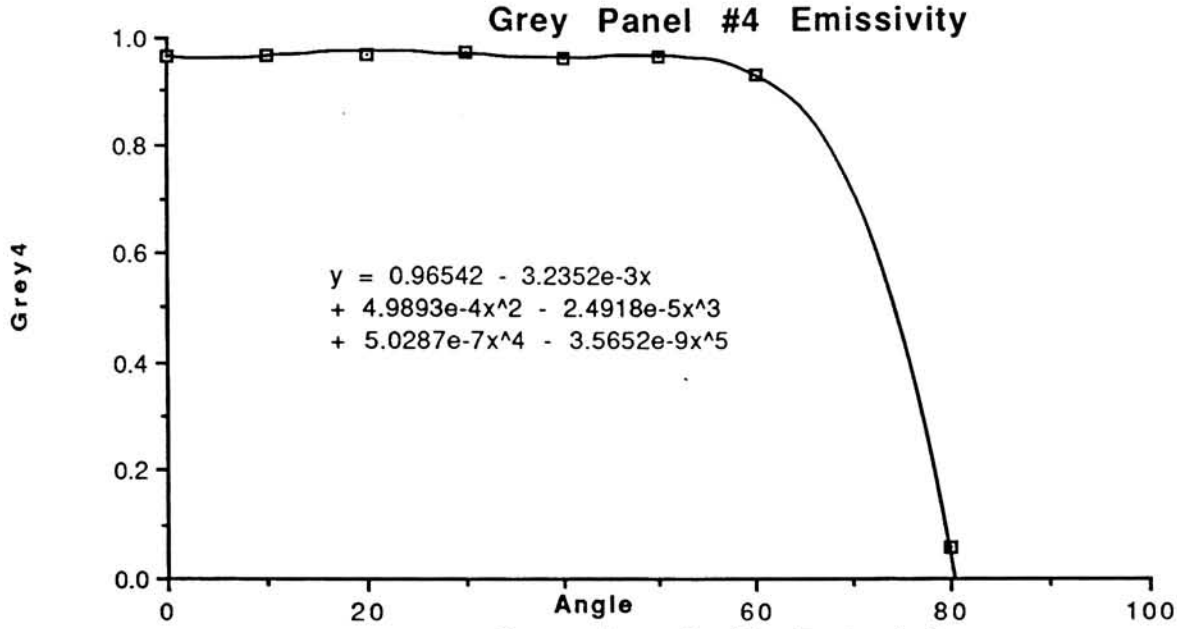
Grey Panel #4 Emissivity
Grey4
1.0
0.8
0.6
0.4
0.2
0.0
y = 0.96542 - 3.2352e-3x
+ 4.9893e-4x^2 - 2.4918e-5x^3
+ 5.0287e-7x^4 - 3.5652e-9x^5
0
20
Angle
60
80
100

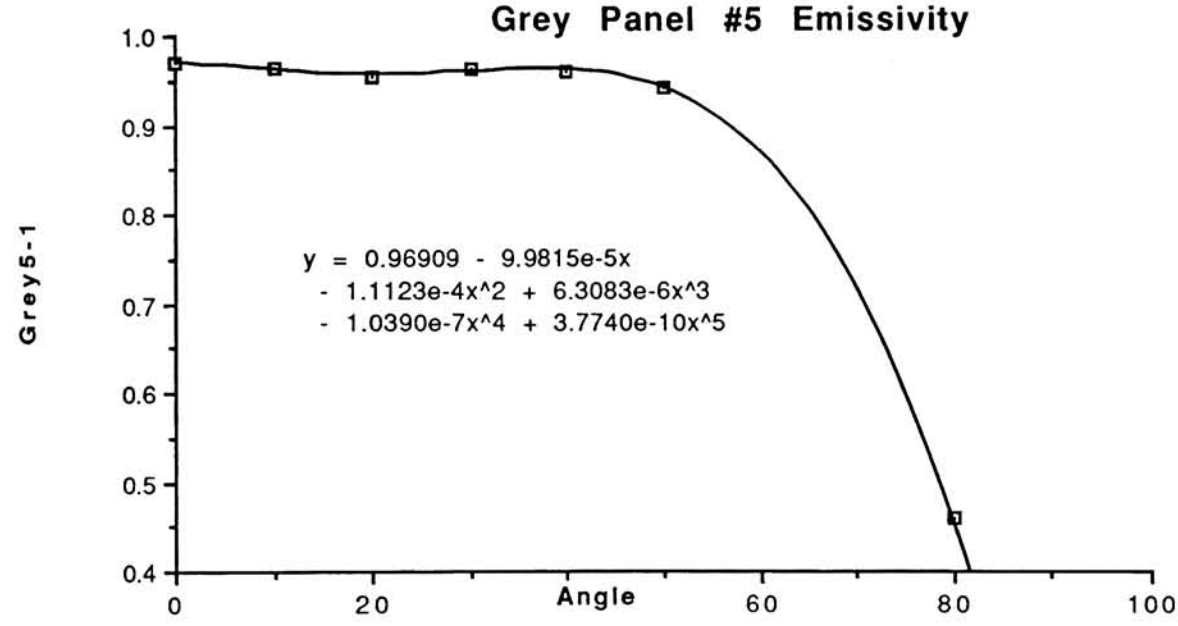
Grey Panel #5 Emissivity
Grey5-1
1.0
0.9
0.8
0.7
0.6
0.5
0.4
y = 0.96909 - 9.9815e-5x
- 1.1123e-4x^2 + 6.3083e-6x^3
- 1.0390e-7x^4 + 3.7740e-10x^5
0
20
Angle
60
80
100

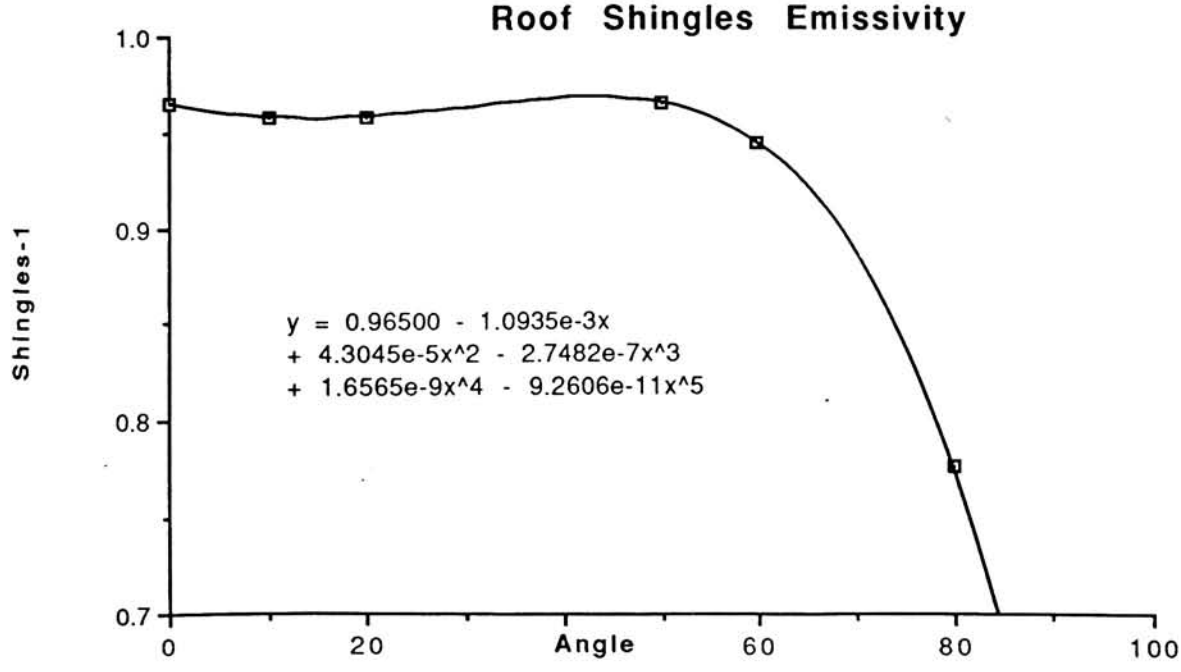
Roof Shingles Emissivity
Shingles-1
1.0
0.9
0.8
0.7
y = 0.96500 - 1.0935e-3x
+ 4.3045e-5x^2 - 2.7482e-7x^3
+ 1.6565e-9x^4 - 9.2606e-11x^5
0
20
Angle
60
80
100

APPENDIX C

Directional Downwelled Radiance Data
Surface Radiance ($\tau 2$ & L_U) Measurements

Directional Downwelled Radiance --> 8-14μm integrated

Code: direction_day_day_time_time_p_angle_angle

June 22, 1992 --> 4:00pm

e2204p08
total radiance=25.653257 W/m.m

s2204p08
total radiance=29.401123 W/m.m

w2204p08
total radiance=22.232285 W/m.m

n2204p08
total radiance=22.453043 W/m.m

e2204p30
total radiance=11.715730 W/m.m

s2204p30
total radiance=19.442553 W/m.m

w2204p30
total radiance=20.903988 W/m.m

n2204p30
total radiance=12.282344 W/m.m

e2205p45
total radiance=11.779091 W/m.m/Sr

s2205p45
total radiance=11.957067 W/m.m/Sr

w2205p45
total radiance=15.020347 W/m.m/Sr

n2205p45
total radiance=12.527041 W/m.m/Sr

e2205p60
total radiance=12.732491 W/m.m/Sr

s2205p60
total radiance=12.460793 W/m.m/Sr

w2205p60
total radiance=12.222880 W/m.m/Sr

n2205p60
total radiance=20.539314 W/m.m/Sr

c2205p90
total radiance=14.574777 W/m.m/Sr

June 22, 1992 --> 10:00pm

e2210p08
total radiance=19.394938 W/m.m/Sr

s2210p08
total radiance=24.578690 W/m.m/Sr

w2210p08
total radiance=18.951279 W/m.m/Sr

n2210p08
total radiance=17.036860 W/m.m/Sr

e2210p30
total radiance=5.230303 W/m.m/Sr

s2210p30
total radiance=7.812209 W/m.m/Sr

w2210p30
total radiance=5.798036 W/m.m/Sr

n2210p30
total radiance=5.051121 W/m.m/Sr

e2210p45
total radiance=3.616984 W/m.m/Sr

s2210p45
total radiance=4.429647 W/m.m/Sr

w2210p45
total radiance=4.168972 W/m.m/Sr

n2210p45
total radiance=3.438252 W/m.m/Sr

e2211p60
total radiance=4.638465 W/m.m/Sr

s2211p60
total radiance=6.220935 W/m.m/Sr

w2211p60
total radiance=6.234463 W/m.m/Sr

n2211p60
total radiance=5.036307 W/m.m/Sr

c2210p90
total radiance=6.587240 W/m.m/Sr

Directional Downwelled Radiance --> 8-14μm integrated

June 23, 1992 --> 8:00am

e2308a08
total radiance=28.737307 W/m.m/Sr

s2308a08
total radiance=36.186989 W/m.m/Sr

w2308a08
total radiance=37.170811 W/m.m/Sr

n2308a08
total radiance=26.534788 W/m.m/Sr

e2309a30
total radiance=17.976385 W/m.m/Sr

s2309a30
total radiance=17.093891 W/m.m/Sr

w2309a30
total radiance=17.988373 W/m.m/Sr

n2308a30
total radiance=15.551792 W/m.m/Sr

e2309a45
total radiance=14.802161 W/m.m/Sr

s2309a45
total radiance=18.657864 W/m.m/Sr

w2309a45
total radiance=15.785484 W/m.m/Sr

n2309a45
total radiance=13.701310 W/m.m/Sr

e2309a60
total radiance=27.136286 W/m.m/Sr

s2309a60
total radiance=22.370007 W/m.m/Sr

w2309a60
total radiance=22.050158 W/m.m/Sr

n2309a60
total radiance=20.494839 W/m.m/Sr

c2309a90
total radiance=19.789354 W/m.m/Sr

June 23, 1992 --> 4:00pm

e2304p08
total radiance=43.180706 W/m.m/Sr

s2304p08
total radiance=44.160851 W/m.m/Sr

w2304p08
total radiance=42.134850 W/m.m/Sr

n2304p08
total radiance=37.346626 W/m.m/Sr

e2304p30
total radiance=28.869549 W/m.m/Sr

s2304p30
total radiance=26.945642 W/m.m/Sr

w2304p30
total radiance=28.601021 W/m.m/Sr

n2304p30
total radiance=23.009699 W/m.m/Sr

e2304p45
total radiance=18.850622 W/m.m/Sr

s2304p45
total radiance=28.727957 W/m.m/Sr

w2304p45
total radiance=26.183432 W/m.m/Sr

n2304p45
total radiance=20.653997 W/m.m/Sr

e2304p60
total radiance=24.737181 W/m.m/Sr

s2304p60
total radiance=30.076376 W/m.m/Sr

w2304p60
total radiance=33.564980 W/m.m/Sr

n2304p60
total radiance=31.013168 W/m.m/Sr

c2304p90
total radiance=33.717075 W/m.m/Sr

Directional Downwelled Radiance --> 8-12μm integrated

JUNE 22, 1992 4:00 PM

e2204p08
total radiance=16.873964 W/m.m

s2204p08
total radiance=19.454010 W/m.m

w2204p08
total radiance=14.118902 W/m.m

n2204p08
total radiance=14.445287 W/m.m

e2204p30
total radiance=7.219686 W/m.m

s2204p30
total radiance=12.337778 W/m.m

w2204p30
total radiance=14.167905 W/m.m

n2204p30
total radiance=7.526423 W/m.m

e2205p45
total radiance=7.299139 W/m.m

s2205p45
total radiance=7.404237 W/m.m

w2205p45
total radiance=9.483997 W/m.m

n2205p45
total radiance=7.790837 W/m.m

e2205p60
total radiance=8.363483 W/m.m

s2205p60
total radiance=8.116655 W/m.m

w2205p60
total radiance=8.009930 W/m.m

n2205p60
total radiance=13.535789 W/m.m

c2205p90
total radiance=9.446352 W/m.m

JUNE 22, 1992 10:00 pm

e2210p08
total radiance=12.441139 W/m.m

s2210p08
total radiance=15.995576 W/m.m

w2210p08
total radiance=12.111075 W/m.m

n2210p08
total radiance=10.773189 W/m.m

e2210p30
total radiance=2.754607 W/m.m

s2210p30
total radiance=4.323673 W/m.m

w2210p30
total radiance=3.173949 W/m.m

n2210p30
total radiance=2.653605 W/m.m

e2210p45
total radiance=1.828374 W/m.m

s2210p45
total radiance=2.283284 W/m.m

w2210p45
total radiance=2.151051 W/m.m

n2210p45
total radiance=1.710547 W/m.m

e2211p60
total radiance=2.756899 W/m.m

s2211p60
total radiance=3.933718 W/m.m

w2211p60
total radiance=3.827646 W/m.m

n2211p60
total radiance=2.926000 W/m.m

c2210p90
total radiance=4.213174 W/m.m

Directional Downwelled Radiance --> 8-12μm integrated

JUNE 23, 1992 8:00am

e2308a08
total radiance=19.100262 W/m.m

s2308a08
total radiance=24.474653 W/m.m

w2308a08
total radiance=25.485411 W/m.m

n2308a08
total radiance=17.676954 W/m.m

e2309a30
total radiance=11.768017 W/m.m

s2309a30
total radiance=11.029357 W/m.m

w2309a30
total radiance=11.655375 W/m.m

n2308a30
total radiance=10.077591 W/m.m

e2309a45
total radiance=9.814184 W/m.m

s2309a45
total radiance=12.228863 W/m.m

w2309a45
total radiance=10.308121 W/m.m

n2309a45
total radiance=9.388185 W/m.m

e2309a60
total radiance=18.364521 W/m.m

s2309a60
total radiance=14.944476 W/m.m

w2309a60
total radiance=14.580288 W/m.m

n2309a60
total radiance=13.474545 W/m.m

c2309a90
total radiance=13.403801 W/m.m

JUNE 23, 1992 4:30 pm

e2304p08
total radiance=29.226480 W/m.m

s2304p08
total radiance=29.861403 W/m.m

w2304p08
total radiance=28.697969 W/m.m

n2304p08
total radiance=25.037270 W/m.m

e2304p30
total radiance=18.961964 W/m.m

s2304p30
total radiance=17.554424 W/m.m

w2304p30
total radiance=18.805878 W/m.m

n2304p30
total radiance=14.940652 W/m.m

e2304p45
total radiance=12.266003 W/m.m

s2304p45
total radiance=18.848848 W/m.m

w2304p45
total radiance=17.114798 W/m.m

n2304p45
total radiance=13.521529 W/m.m

e2304p60
total radiance=17.051464 W/m.m

s2304p60
total radiance=20.134298 W/m.m

w2304p60
total radiance=23.013903 W/m.m

n2304p60
total radiance=20.813843 W/m.m

c2304p90
total radiance=22.557602 W/m.m

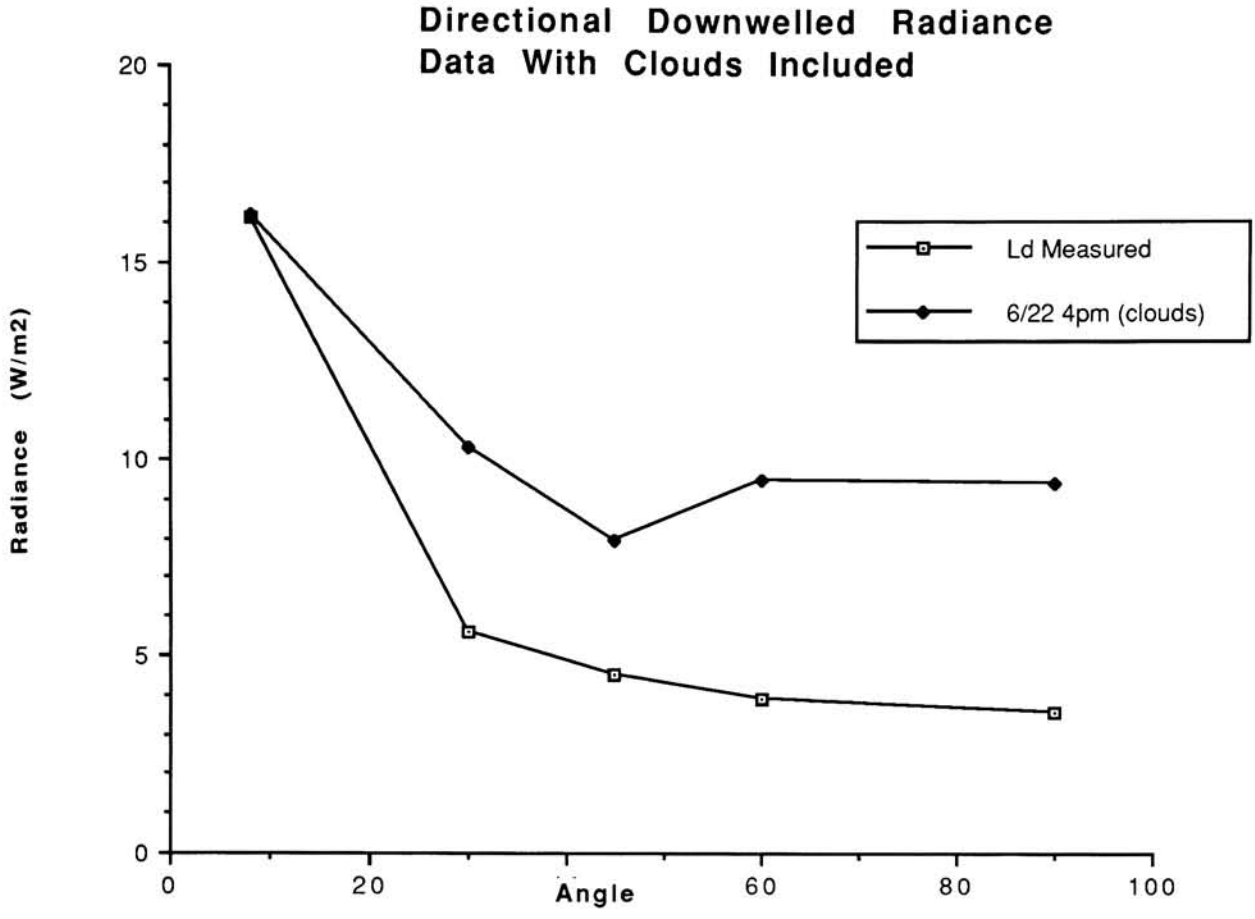
Directional Downwelled Radiance
Data With Clouds Included
Radiance (W/m2)
Angle
Ld Measured
6/22 4pm (clouds)
0
5
10
15
20
0
20
60
80
100

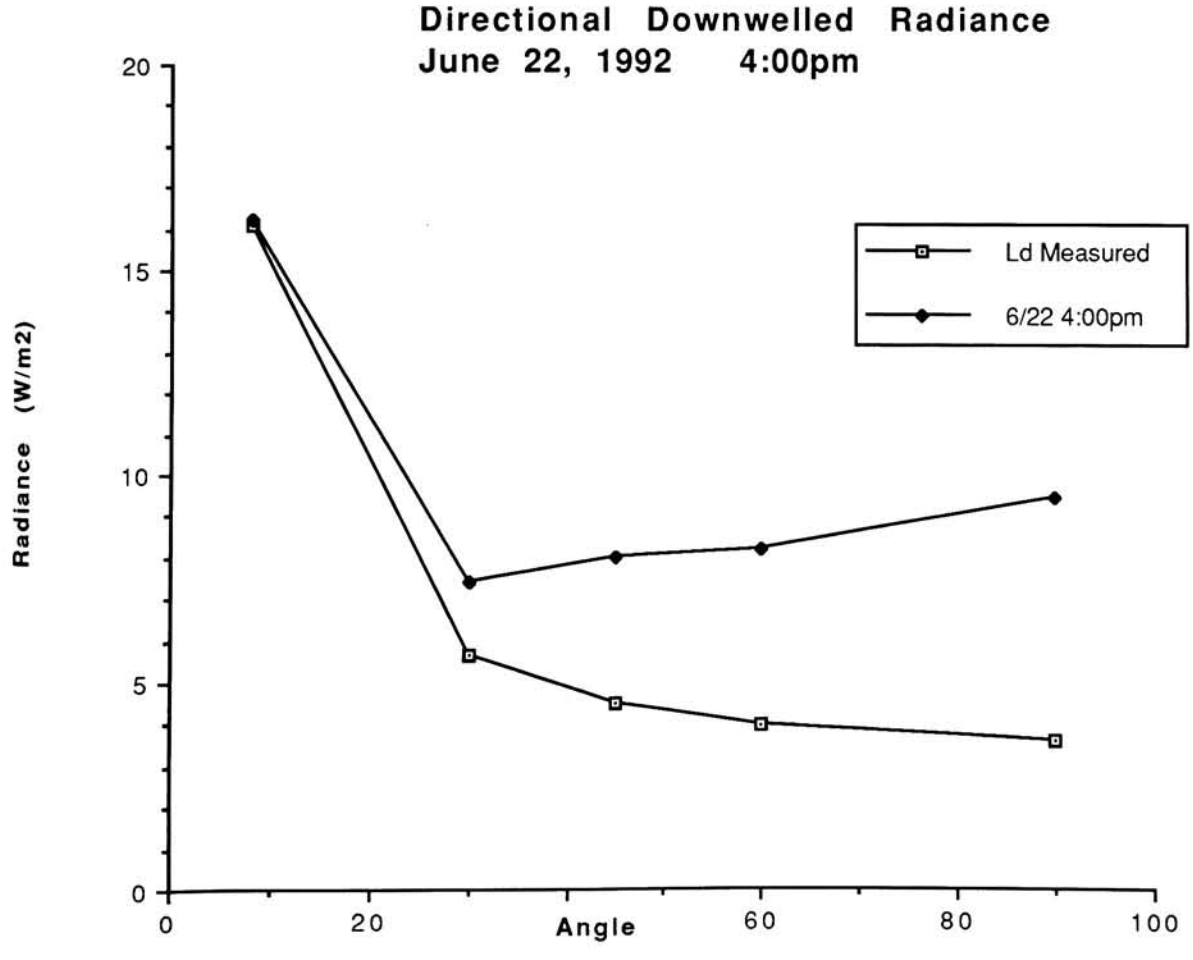
Directional Downwelled Radiance
June 22, 1992 4:00pm
Radiance (W/m2)
Angle
Ld Measured
6/22 4:00pm
0
5
10
15
20
0
20
60
80
100

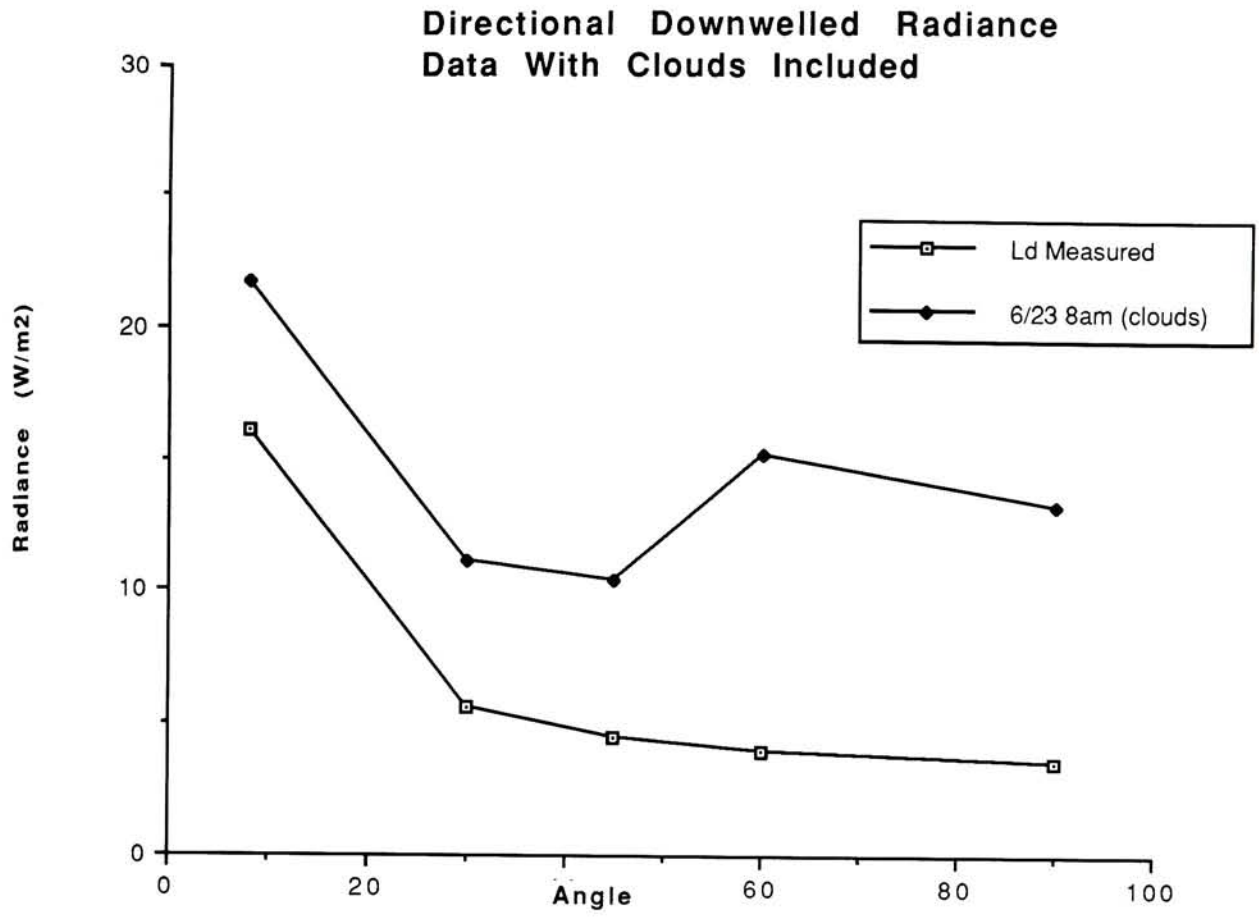
Directional Downwelled Radiance
Data With Clouds Included
Radiance (W/m2)
Angle
Ld Measured
6/23 8am (clouds)
0
10
20
30
0
20
60
80
100

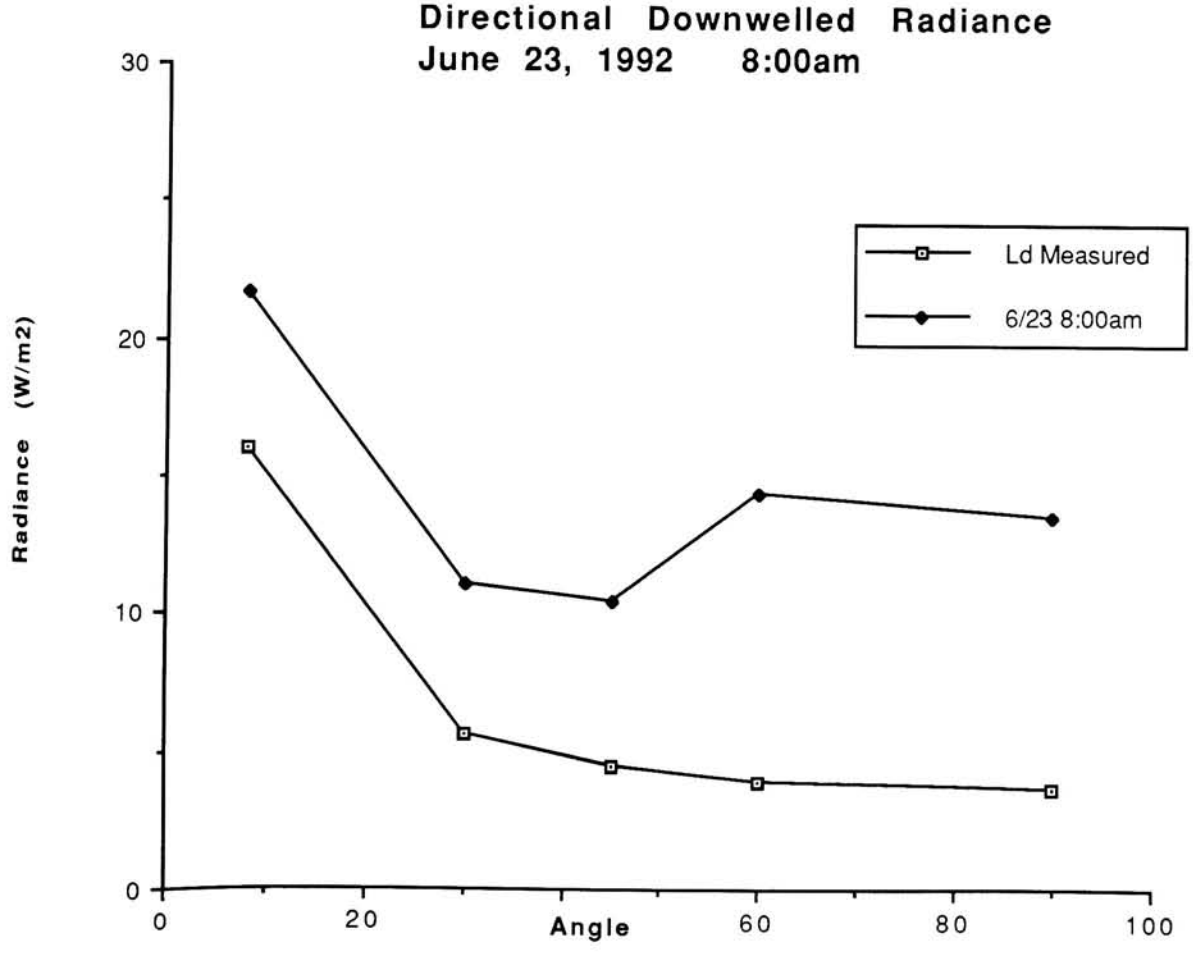
Directional Downwelled Radiance
June 23, 1992 8:00am
Radiance (W/m2)
Angle
Ld Measured
6/23 8:00am
0
10
20
30
0
20
60
80
100

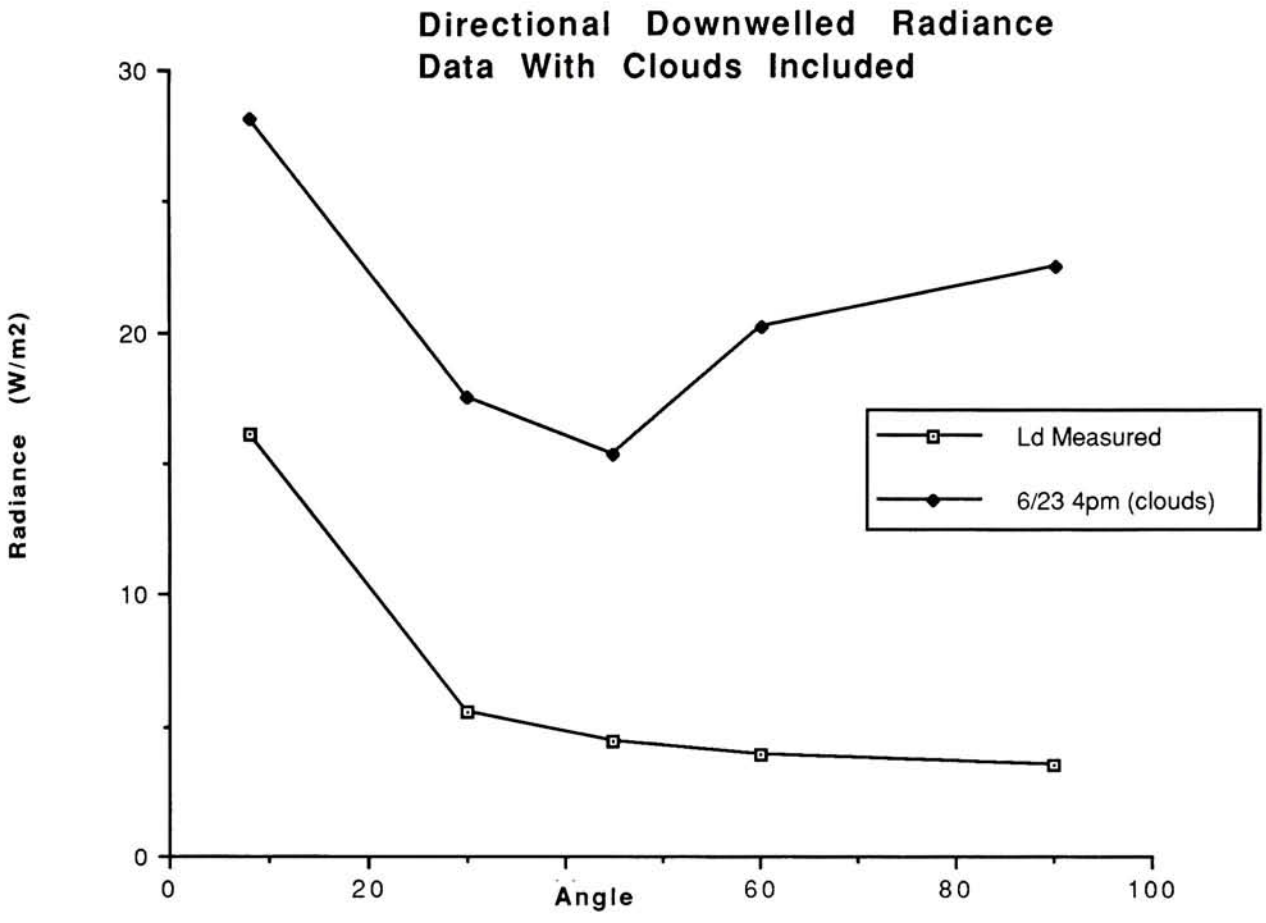
Directional Downwelled Radiance
Data With Clouds Included
Radiance (W/m2)
30
20
10
0
0
20
60
80
100
Angle
Ld Measured
6/23 4pm (clouds)

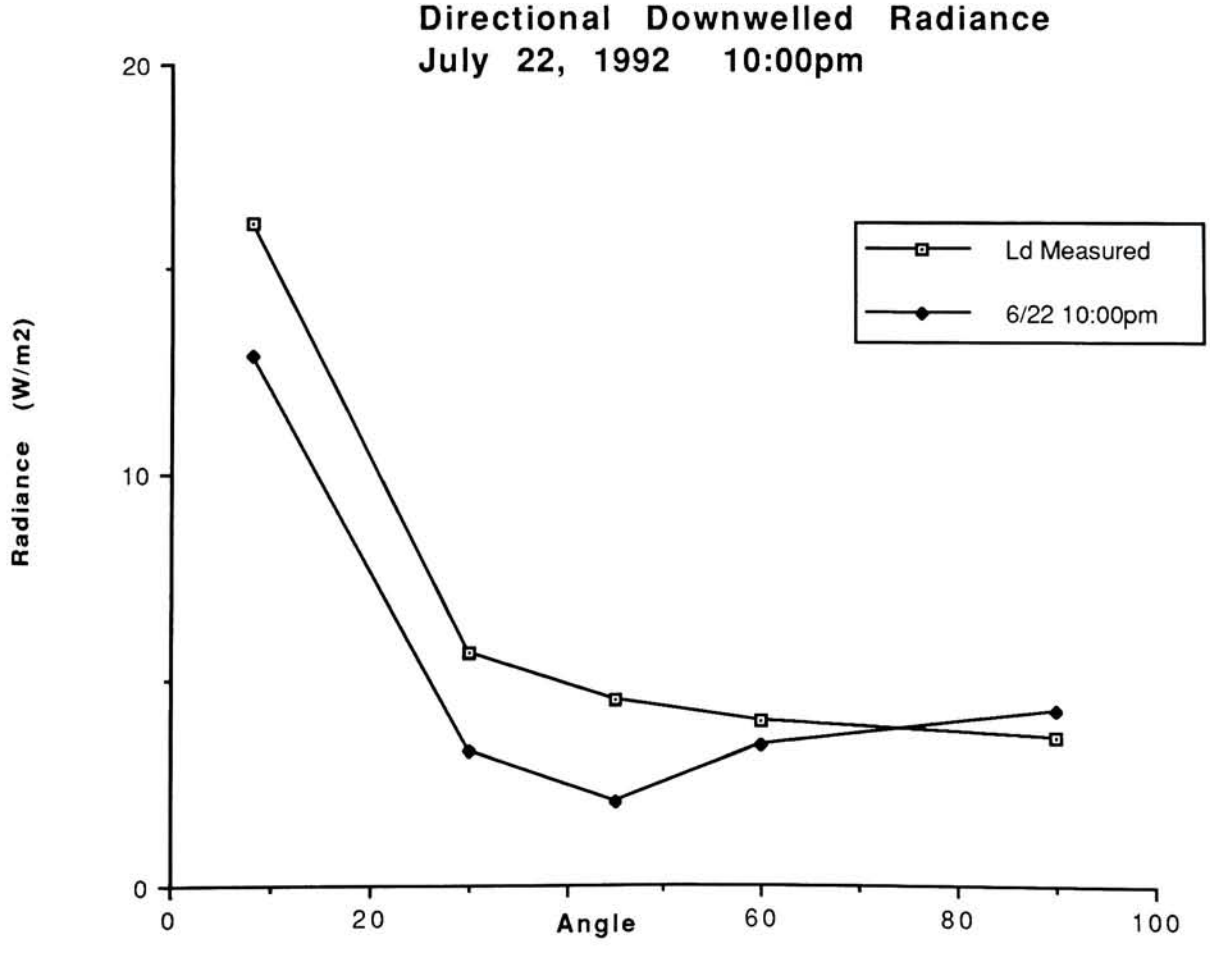
Directional Downwelled Radiance
July 22, 1992 10:00pm
Radiance (W/m2)
20
10
0
0
20
60
80
100
Angle
Ld Measured
6/22 10:00pm

Surface Radiance Measurements
July 28, 1992

Time	Object	Vave (Barnes)	L-ground	DC	L-sensor
9:30am	House Roof	0.566	37.12151	186.42	47.60672
	Car Side	0.505	36.23092	174.21	45.63025
	Asphalt	0.399	34.45305	155.78	42.64694
	Grass	0.293	32.32869	136.36	39.50338
	Grey 4	0.457	35.46475	171.52	45.19482
10:30am	House Roof	1.134	43.08368	230.65	54.79477
	Tire	0.909	40.95015	214.98	52.11915
	Car Side	0.820	40.08622	225.08	53.84370
	Grass	0.297	32.41589	154.71	41.82820
	Asphalt	0.632	37.99328	203.64	50.18287
11:30am	Hubcap	0.475	35.75924	73.55	35.31463
	House Roof	1.629	50.06690	228.28	54.51094
	Grey 1	0.791	39.79190	110.27	39.87023
	Grey 4	0.932	41.16698	132.38	42.61327
	Grass	0.410	34.65259	54.41	32.94005
1:30pm	Asphalt	1.171	43.45761	211.10	52.26400
	House Roof	1.292	44.79065	218.55	53.22699
	Grass	0.507	36.26155	133.62	42.24888
	White Front	0.692	38.71547	146.50	43.91376
	Water	0.375	34.00467	101.90	38.14873
2:30pm	Water	0.401	34.48960	119.36	40.42844
	Car Side	0.825	40.13620	179.24	33.49174
	Asphalt	1.437	46.71346	222.19	53.69854
	Black Front	0.873	40.60645	177.02	47.86940
	Hubcap	0.454	35.41480	118.62	40.33295
3:30pm	Concrete	0.651	38.22863	146.75	43.84406
	House Roof	1.125	42.99449	285.16	61.90924
	Water	0.447	35.29727	120.27	32.16902
	Asphalt	1.424	46.52275	227.00	54.31824
	Car Side	0.834	40.22565	171.11	47.02351
4:30pm	Grey 1	0.623	37.87949	174.17	46.42255
	Water	0.471	35.69456	160.90	30.02401
	House Roof	0.906	40.88379	211.78	51.98698
	Asphalt	1.290	44.76691	230.93	54.82024
	Concrete	0.675	38.51694	183.95	47.86951

Blackbody Calibration Data for Surface Radiance Measurements

Time	BB hi (50°C)	BB lo (10°C)
9:30am	230.75	70.07
10:30am	230.58	78.25
11:30am	230.47	20.82
1:30pm	230.58	29.36
2:30pm	230.59	29.04
3:30pm	230.56	31.28
4:30pm	230.67	54.87

Radiosonde Data From Buffalo Airport July 28, 1992 (Decoded)

Height-m	Pressure-mbar	Temperature-°C	Dew Point-°C
218	988	13.2	2.8
245	985	13.6	3.6
1472	850	5.2	0.7
1771	822	10.6	12
1952	805	10.2	18
2080	793	9.4	12
2486	755	7.0	14
2635	741	6.4	30
3073	700	4.8	30
4412	593	0.0	30
4812	561	-4.3	30
5575	500	-9.1	30
7743	400	-23.7	30
9836	305	-39.9	30
9946	300	-40.7	--
10068	250	-50.1	--
10839	232	-53.5	--
11697	212	-55.1	--
12211	200	-52.1	--
12779	187	-50.3	--
14398	150	-53.3	--
16655	100	-58.3	--

LOWTRAN7 $\tau 2$ L_U Predictions

Time	$\tau 2$	L_U
10:30am	.9758	.7881
11:30am	.9758	.8296
1:30pm	.9758	.8794
2:30pm	.9758	.8835
3:30pm	.9758	.8730
4:30pm	.9758	.8488

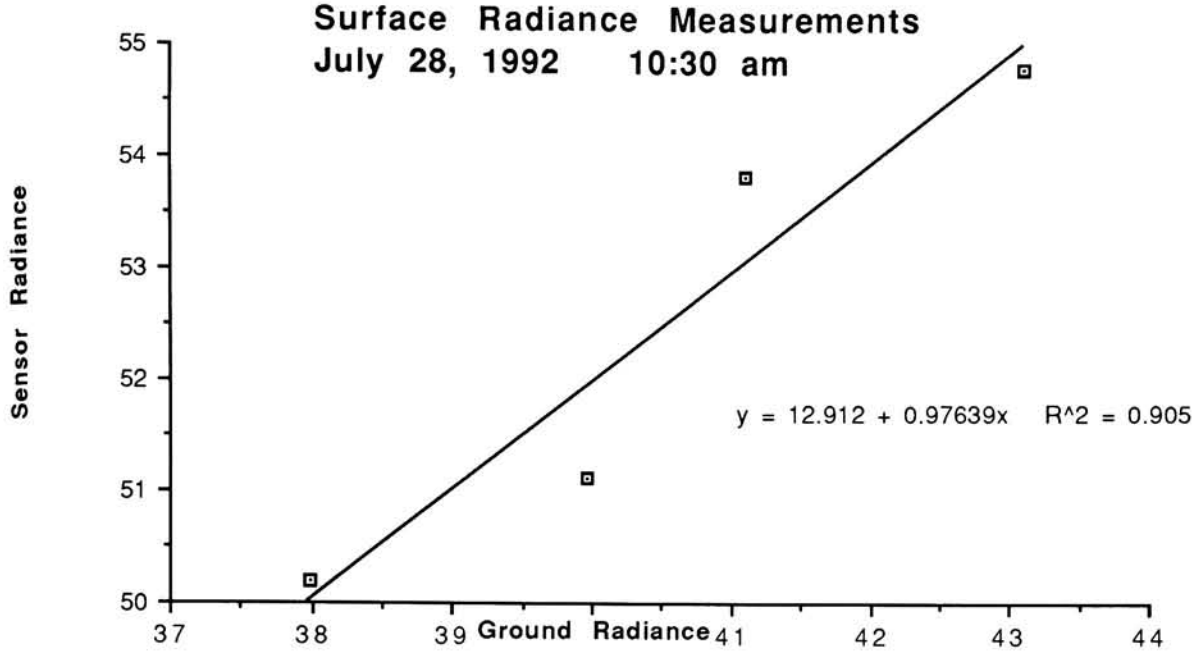
Surface Radiance Measurements
July 28, 1992 10:30 am
Sensor Radiance
Ground Radiance
y = 12.912 + 0.97639x R^2 = 0.905
55
54
53
52
51
50
37
38
39
41
42
43
44

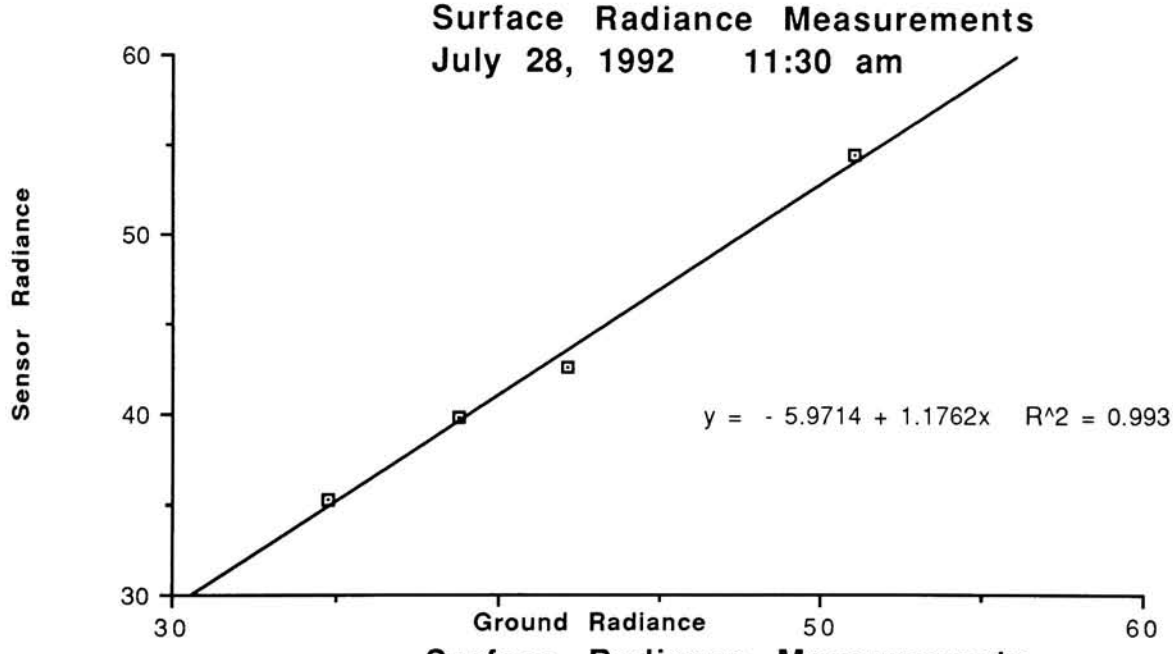
Surface Radiance Measurements
July 28, 1992 11:30 am
Sensor Radiance
Ground Radiance
y = - 5.9714 + 1.1762x R^2 = 0.993
60
50
40
30
30
50
60

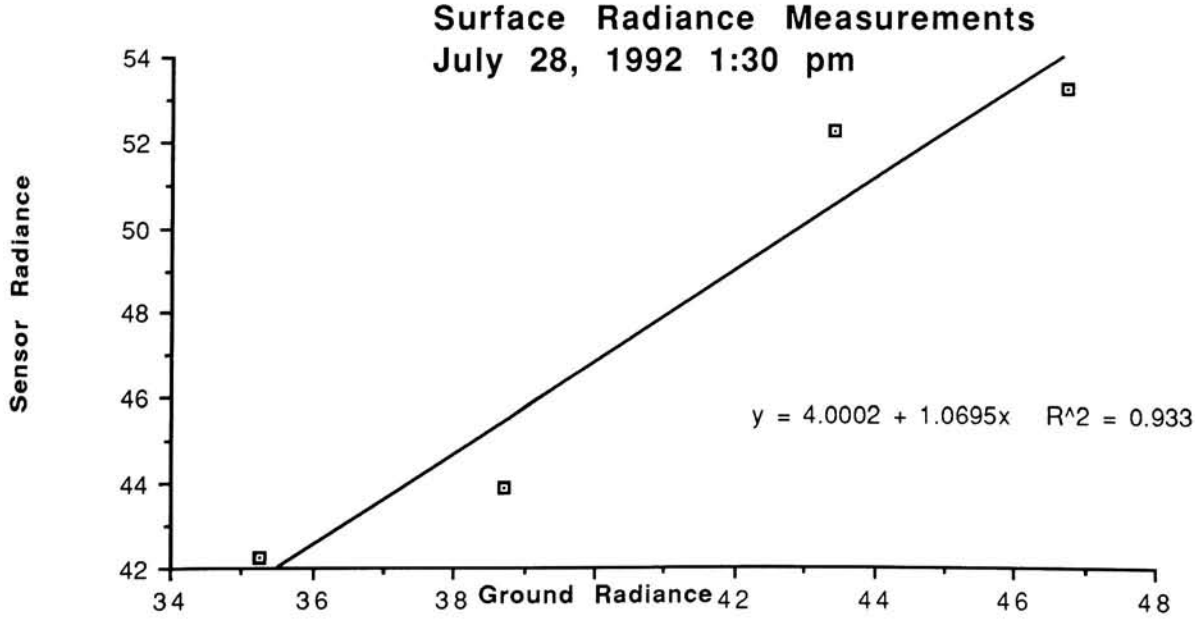
Surface Radiance Measurements
July 28, 1992 1:30 pm
Sensor Radiance
Ground Radiance
y = 4.0002 + 1.0695x R^2 = 0.933
54
52
50
48
46
44
42
34
36
38
42
44
46
48

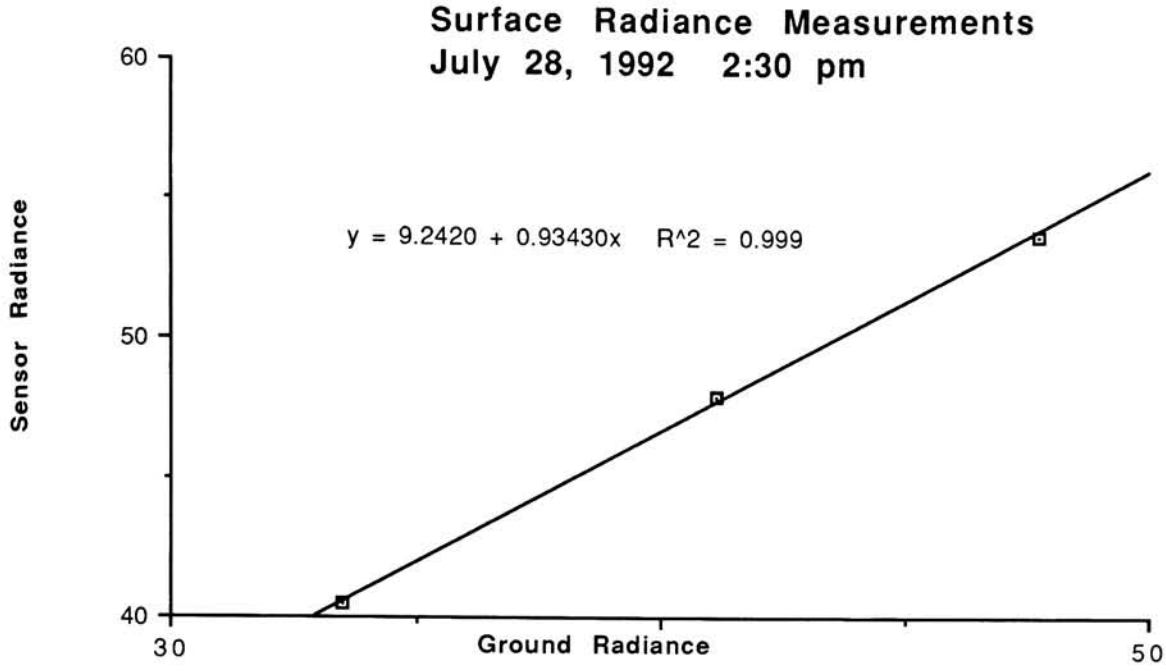
Surface Radiance Measurements
July 28, 1992 2:30 pm
y = 9.2420 + 0.93430x R^2 = 0.999
Sensor Radiance
Ground Radiance
60
50
40
30
50

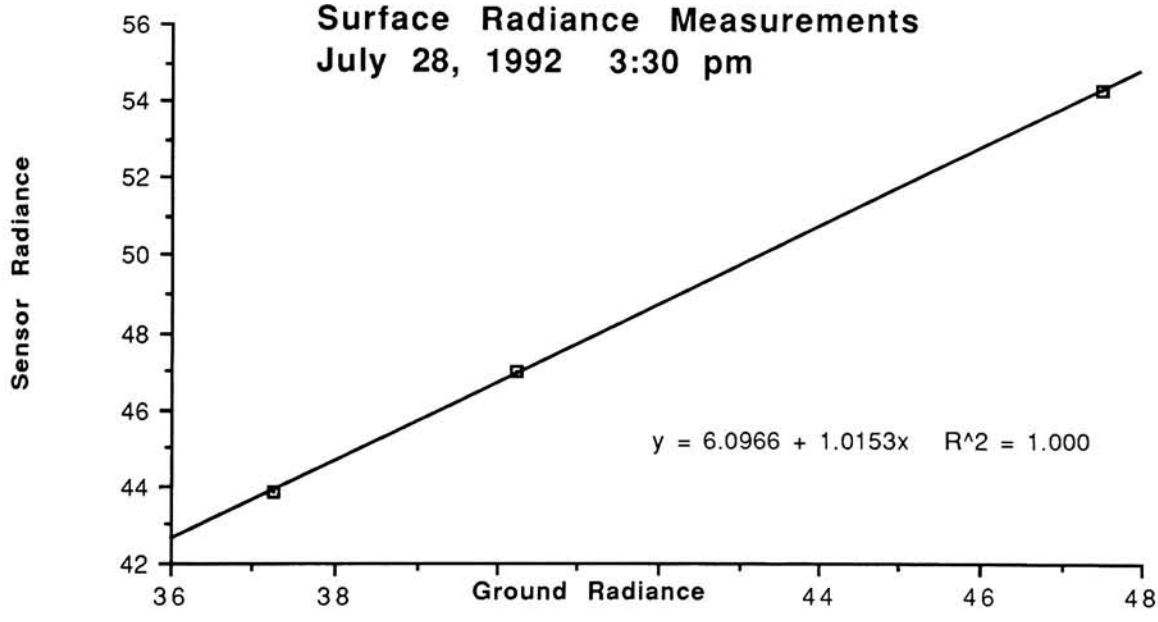
Surface Radiance Measurements
July 28, 1992 3:30 pm
y = 6.0966 + 1.0153x R^2 = 1.000
Sensor Radiance
Ground Radiance
56
54
52
50
48
46
44
42
36
38
44
46
48

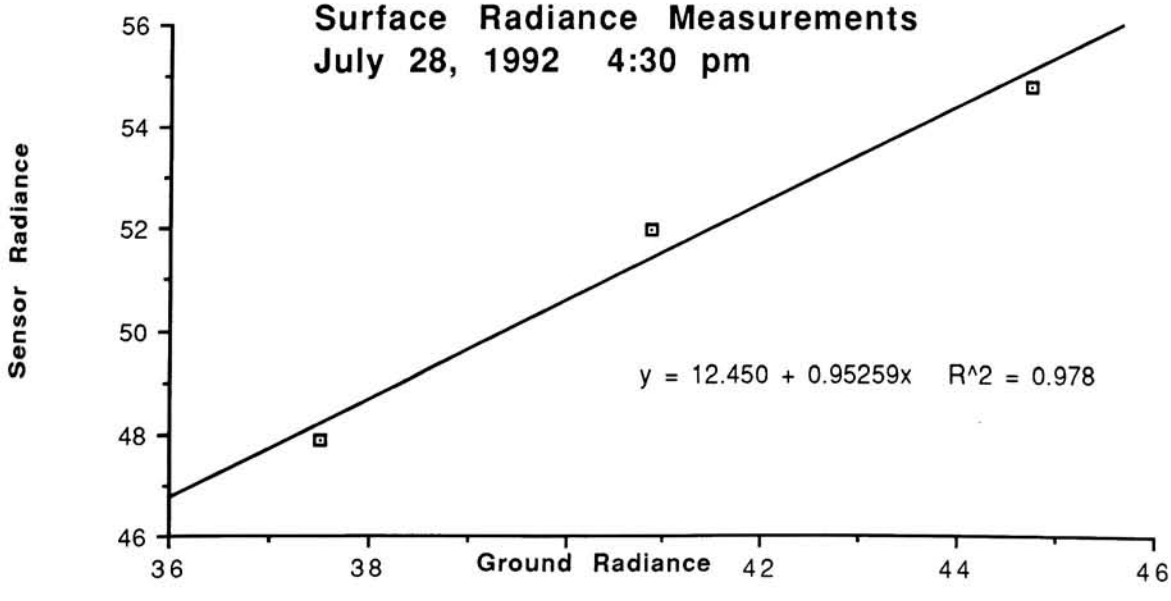
Surface Radiance Measurements
July 28, 1992 4:30 pm
y = 12.450 + 0.95259x R^2 = 0.978
Sensor Radiance
Ground Radiance
56
54
52
50
48
46
36
38
42
44
46

APPENDIX D

Radiometry Error Propagation

Ray_Interaction Type 1: Diffuse Target (Grass)

Rooftop Simulation
Error Type: I

The starting values for the equation are as follows:

$\varepsilon := .873$	$\varepsilon b := .900$	$Ld := 8.50$	$Lu := 0.90$
$Lt := 37.34$	$Ltab := 39.00$	$\tau 2 := 0.97$	
$\theta s := .523599$	$\theta b := .523599$	$Es := 0.00$	
$It := 1$	$Ib := 1$	$F := 1$	

Case 1: Diffuse target hit

$$L1 := (\varepsilon \cdot Lt + (It \cdot Es \cdot \cos(\theta s) + F \cdot (Ld) + (1 - F) \cdot (Ltab + Ib \cdot Es \cdot \cos(\theta b) \cdot (1 - \varepsilon b))) \cdot (1 - \varepsilon)) \cdot \tau 2 + Lu$$

$$L1 = 33.567$$

The MAPLE symbolic processor in MathCad was used to calculate the following derivatives:

$$dL1_{d\varepsilon} := (Lt - It \cdot Es \cdot \cos(\theta s) - F \cdot Ld - (1 - F) \cdot (Ltab + Ib \cdot Es \cdot \cos(\theta b) \cdot (1 - \varepsilon b))) \cdot \tau 2$$

$$dL1_{dLt} := \varepsilon \cdot \tau 2$$

$$dL1_{dIt} := Es \cdot \cos(\theta s) \cdot (1 - \varepsilon) \cdot \tau 2$$

$$dL1_{dEs} := (It \cdot \cos(\theta s) + (1 - F) \cdot Ib \cdot \cos(\theta b) \cdot (1 - \varepsilon b)) \cdot (1 - \varepsilon) \cdot \tau 2$$

$$dL1_{d\theta s} := -It \cdot Es \cdot \sin(\theta s) \cdot (1 - \varepsilon) \cdot \tau 2$$

$$dL1_{dF} := (Ld - Ltab - Ib \cdot Es \cdot \cos(\theta b) \cdot (1 - \varepsilon b)) \cdot (1 - \varepsilon) \cdot \tau 2$$

$$dL1_{dLd} := F \cdot (1 - \varepsilon) \cdot \tau 2$$

$$dL1_{dLtab} := (1 - F) \cdot (1 - \varepsilon) \cdot \tau 2$$

$$dL1_{dIb} := (1 - F) \cdot Es \cdot \cos(\theta b) \cdot (1 - \varepsilon b) \cdot (1 - \varepsilon) \cdot \tau 2$$

$$dL1_{d\theta b} := -(1 - F) \cdot Ib \cdot Es \cdot \sin(\theta b) \cdot (1 - \varepsilon b) \cdot (1 - \varepsilon) \cdot \tau 2$$

$$dL1_{d\varepsilon b} := -(1 - F) \cdot Ib \cdot Es \cdot \cos(\theta b) \cdot (1 - \varepsilon) \cdot \tau 2$$

$$dL1_{d\tau 2} := \varepsilon \cdot Lt + (It \cdot Es \cdot \cos(\theta s) + F \cdot Ld + (1 - F) \cdot (Ltab + Ib \cdot Es \cdot \cos(\theta b) \cdot (1 - \varepsilon b))) \cdot (1 - \varepsilon)$$

$$dL1_{dLu} := 1$$

These derivatives are used to form the components of the Beers error calculation:

$s\varepsilon := 0.025$	$sLt := 0.09$	$sIt := 0$	$sLu := 0.02$
$sEs := 0$	$sLd := 0.25$	$s\theta b := 0.05236$	$\rho_{\tau 2Lu} := -0.8381$
$s\theta s := 0.05236$	$sLtab := 0.09$	$s\varepsilon b := 0.025$	
$sF := 0.10$	$sIb := 0$	$s\tau 2 := 0.03$	

$$sL1_{\varepsilon} := \left(dL1_{d\varepsilon}{}^{2} \cdot s\varepsilon^{2}\right)^{\frac{1}{2}}$$

$$sL1_{\varepsilon} = 0.699$$

$$sL1_{Lt} := \left(dL1_{dLt}{}^{2} \cdot sLt^{2}\right)^{\frac{1}{2}}$$

$$sL1_{Lt} = 0.076$$

$$sL1_{It} := \left(dL1_{dIt}{}^{2} \cdot sIt^{2}\right)^{\frac{1}{2}}$$

$$sL1_{It} = 0$$

$$sL1_{Es} := \left(dL1_{dEs}{}^{2} \cdot sEs^{2}\right)^{\frac{1}{2}}$$

$$sL1_{Es} = 0$$

$$sL1_{\theta s} := \left(dL1_{d\theta s}{}^{2} \cdot s\theta s^{2}\right)^{\frac{1}{2}}$$

$$sL1_{\theta s} = 0$$

$$sL1_{F} := \left(dL1_{dF}{}^{2} \cdot sF^{2}\right)^{\frac{1}{2}}$$

$$sL1_{F} = 0.376$$

$$sL1_{Ld} := \left(dL1_{dLd}{}^{2} \cdot sLd^{2}\right)^{\frac{1}{2}}$$

$$sL1_{Ld} = 0.031$$

$$sL1_{Ltab} := \left(dL1_{dLtab}{}^{2} \cdot sLtab^{2}\right)^{\frac{1}{2}}$$

$$sL1_{Ltab} = 0$$

$$sL1_{Ib} := \left(dL1_{dIb}{}^{2} \cdot sIb^{2}\right)^{\frac{1}{2}}$$

$$sL1_{Ib} = 0$$

$$sL1_{\theta b} := \left(dL1_{d\theta b}{}^{2} \cdot s\theta b^{2}\right)^{\frac{1}{2}}$$

$$sL1_{\theta b} = 0$$

$$sL1_{\varepsilon b} := \left(dL1_{d\varepsilon b}{}^{2} \cdot s\varepsilon b^{2}\right)^{\frac{1}{2}}$$

$$sL1_{\varepsilon b} = 0$$

$$sL1_{\tau 2} := \left(dL1_{d\tau 2}{}^{2} \cdot s\tau 2^{2}\right)^{\frac{1}{2}}$$

$$sL1_{\tau 2} = 1.01$$

$$sL1_{Lu} := \left(dL1_{dLu}{}^{2} \cdot sLu^{2}\right)^{\frac{1}{2}}$$

$$sL1_{Lu} = 0.02$$

The cross term for the correlated variables Tau2 and Lu is:

$$xterm := \left[\rho_{\tau 2Lu} \cdot \left(dL1_{d\tau 2}\right) \cdot \left(dL1_{dLu}\right) \cdot s\tau 2 \cdot sLu\right]$$

$$xterm = -0.017$$

The total Beers error is expressed as:

$$sL1_{part1} := sL1_{\varepsilon}^{2} + sL1_{It}^{2} + sL1_{Is}^{2} + sL1_{\theta s}^{2} + sL1_{F}^{2} + sL1_{Ld}^{2} + sL1_{Ltab}^{2}$$

$$sL1_{part2} := sL1_{Ib}^{2} + sL1_{\theta b}^{2} + sL1_{\varepsilon b}^{2} + sL1_{\tau 2}^{2} + sL1_{Lu}^{2} + xterm$$

$$sL1_{total} := \left(sL1_{part1} + sL1_{part2}\right)^{\frac{1}{2}}$$

$$sL1_{total} = 1.281$$

The starting values for the equation are as follows:

$\varepsilon := .873$	$\varepsilon b := .900$	$Ld := 8.50$	$Lu := 0.90$
$Lt := 37.34$	$Ltab := 39.00$	$\tau 2 := 0.97$	
$\theta s := .523599$	$\theta b := .523599$	$Es := 0.00$	
$It := 1$	$Ib := 1$	$F := 1$	

Case 1: Diffuse target hit

$$L1 := (\varepsilon \cdot Lt + (It \cdot Es \cdot \cos(\theta s) + F \cdot (Ld) + (1 - F) \cdot (Ltab + Ib \cdot Es \cdot \cos(\theta b) \cdot (1 - \varepsilon b))) \cdot (1 - \varepsilon)) \cdot \tau 2 + Lu$$

$$L1 = 33.567$$

The MAPLE symbolic processor in MathCad was used to calculate the following derivatives:

$$dL1_{d\varepsilon} := (Lt - It \cdot Es \cdot \cos(\theta s) - F \cdot Ld - (1 - F) \cdot (Ltab + Ib \cdot Es \cdot \cos(\theta b) \cdot (1 - \varepsilon b))) \cdot \tau 2$$

$$dL1_{dLt} := \varepsilon \cdot \tau 2$$

$$dL1_{dIt} := Es \cdot \cos(\theta s) \cdot (1 - \varepsilon) \cdot \tau 2$$

$$dL1_{dEs} := (It \cdot \cos(\theta s) + (1 - F) \cdot Ib \cdot \cos(\theta b) \cdot (1 - \varepsilon b)) \cdot (1 - \varepsilon) \cdot \tau 2$$

$$dL1_{d\theta s} := -It \cdot Es \cdot \sin(\theta s) \cdot (1 - \varepsilon) \cdot \tau 2$$

$$dL1_{dF} := (Ld - Ltab - Ib \cdot Es \cdot \cos(\theta b) \cdot (1 - \varepsilon b)) \cdot (1 - \varepsilon) \cdot \tau 2$$

$$dL1_{dLd} := F \cdot (1 - \varepsilon) \cdot \tau 2$$

$$dL1_{dLtab} := (1 - F) \cdot (1 - \varepsilon) \cdot \tau 2$$

$$dL1_{dIb} := (1 - F) \cdot Es \cdot \cos(\theta b) \cdot (1 - \varepsilon b) \cdot (1 - \varepsilon) \cdot \tau 2$$

$$dL1_{d\theta b} := -(1 - F) \cdot Ib \cdot Es \cdot \sin(\theta b) \cdot (1 - \varepsilon b) \cdot (1 - \varepsilon) \cdot \tau 2$$

$$dL1_{d\varepsilon b} := -(1 - F) \cdot Ib \cdot Es \cdot \cos(\theta b) \cdot (1 - \varepsilon) \cdot \tau 2$$

$$dL1_{d\tau 2} := \varepsilon \cdot Lt + (It \cdot Es \cdot \cos(\theta s) + F \cdot Ld + (1 - F) \cdot (Ltab + Ib \cdot Es \cdot \cos(\theta b) \cdot (1 - \varepsilon b))) \cdot (1 - \varepsilon)$$

$$dL1_{dLu} := 1$$

These derivatives are used to form the components of the Beers error calculation:

$s\varepsilon := 0.05$	$sLt := 0.63$	$sIt := 0$	$sLu := .16$
$sEs := 0$	$sLd := 2.26$	$s\theta b := 0.1309$	$\rho_{\tau 2Lu} := -0.8381$
$s\theta s := 0.1309$	$sLtab := 0.63$	$s\varepsilon b := 0.05$	
$sF := 0.20$	$sIb := 0$	$s\tau 2 := 0.03$	

$$sL1_{\varepsilon} := \left(dL1_{d\varepsilon}{}^{2} \cdot s\varepsilon^{2}\right)^{\frac{1}{2}}$$

$$sL1_{\varepsilon} = 1.399$$

$$sL1_{Lt} := \left(dL1_{dLt}{}^{2} \cdot sLt^{2}\right)^{\frac{1}{2}}$$

$$sL1_{Lt} = 0.533$$

$$sL1_{It} := \left(dL1_{dIt}{}^{2} \cdot sIt^{2}\right)^{\frac{1}{2}}$$

$$sL1_{It} = 0$$

$$sL1_{Es} := \left(dL1_{dEs}{}^{2} \cdot sEs^{2}\right)^{\frac{1}{2}}$$

$$sL1_{Es} = 0$$

$$sL1_{\theta s} := \left(dL1_{d\theta s}{}^{2} \cdot s\theta s^{2}\right)^{\frac{1}{2}}$$

$$sL1_{\theta s} = 0$$

$$sL1_{F} := \left(dL1_{dF}{}^{2} \cdot sF^{2}\right)^{\frac{1}{2}}$$

$$sL1_{F} = 0.751$$

$$sL1_{Ld} := \left(dL1_{dLd}{}^{2} \cdot sLd^{2}\right)^{\frac{1}{2}}$$

$$sL1_{Ld} = 0.278$$

$$sL1_{Ltab} := \left(dL1_{dLtab}{}^{2} \cdot sLtab^{2}\right)^{\frac{1}{2}}$$

$$sL1_{Ltab} = 0$$

$$sL1_{Ib} := \left(dL1_{dIb}{}^{2} \cdot sIb^{2}\right)^{\frac{1}{2}}$$

$$sL1_{Ib} = 0$$

$$sL1_{\theta b} := \left(dL1_{d\theta b}{}^{2} \cdot s\theta b^{2}\right)^{\frac{1}{2}}$$

$$sL1_{\theta b} = 0$$

$$sL1_{\varepsilon b} := \left(dL1_{d\varepsilon b}{}^{2} \cdot s\varepsilon b^{2}\right)^{\frac{1}{2}}$$

$$sL1_{\varepsilon b} = 0$$

$$sL1_{\tau 2} := \left(dL1_{d\tau 2}{}^{2} \cdot s\tau 2^{2}\right)^{\frac{1}{2}}$$

$$sL1_{\tau 2} = 1.01$$

$$sL1_{Lu} := \left(dL1_{dLu}{}^{2} \cdot sLu^{2}\right)^{\frac{1}{2}}$$

$$sL1_{Lu} = 0.16$$

The cross term for the correlated variables Tau2 and Lu is:

$$xterm := \left[\rho_{\tau 2Lu} \cdot \left(dL1_{d\tau 2}\right) \cdot \left(dL1_{dLu}\right) \cdot s\tau 2 \cdot sLu\right]$$

$$xterm = -0.135$$

The total Beers error is expressed as:

$$sL1_{part1} := sL1_{\varepsilon}^{2} + sL1_{Lt}^{2} + sL1_{It}^{2} + sL1_{Es}^{2} + sL1_{\theta s}^{2} + sL1_{F}^{2} + sL1_{Ld}^{2} + sL1_{Ltab}^{2}$$

$$sL1_{part2} := sL1_{Ib}^{2} + sL1_{\theta b}^{2} + sL1_{\varepsilon b}^{2} + sL1_{\tau 2}^{2} + sL1_{Lu}^{2} + xterm$$

$$sL1_{total} := \left(sL1_{part1} + sL1_{part2}\right)^{\frac{1}{2}}$$

$$sL1_{total} = 1.948$$

The starting values for the equation are as follows:

$\varepsilon := .873$ $\quad \varepsilon b := .900$ $\quad Ld := 8.50$ $\quad Lu := 0.90$

$Lt := 37.34$ $\quad Ltab := 39.00$ $\quad \tau 2 := 0.97$

$\theta s := .523599$ $\quad \theta b := .523599$ $\quad Es := 0.00$

$It := 1$ $\quad Ib := 1$ $\quad F := 1$

Case 1: Diffuse target hit

$$L1 := (\varepsilon \cdot Lt + (It \cdot Es \cdot \cos(\theta s) + F \cdot (Ld) + (1 - F) \cdot (Ltab + Ib \cdot Es \cdot \cos(\theta b) \cdot (1 - \varepsilon b))) \cdot (1 - \varepsilon)) \cdot \tau 2 + Lu$$

$$L1 = 33.567$$

The MAPLE symbolic processor in MathCad was used to calculate the following derivatives:

$$dL1_{d\varepsilon} := (Lt - It \cdot Es \cdot \cos(\theta s) - F \cdot Ld - (1 - F) \cdot (Ltab + Ib \cdot Es \cdot \cos(\theta b) \cdot (1 - \varepsilon b))) \cdot \tau 2$$

$$dL1_{dLt} := \varepsilon \cdot \tau 2$$

$$dL1_{dIt} := Es \cdot \cos(\theta s) \cdot (1 - \varepsilon) \cdot \tau 2$$

$$dL1_{dEs} := (It \cdot \cos(\theta s) + (1 - F) \cdot Ib \cdot \cos(\theta b) \cdot (1 - \varepsilon b)) \cdot (1 - \varepsilon) \cdot \tau 2$$

$$dL1_{d\theta s} := -It \cdot Es \cdot \sin(\theta s) \cdot (1 - \varepsilon) \cdot \tau 2$$

$$dL1_{dF} := (Ld - Ltab - Ib \cdot Es \cdot \cos(\theta b) \cdot (1 - \varepsilon b)) \cdot (1 - \varepsilon) \cdot \tau 2$$

$$dL1_{dLd} := F \cdot (1 - \varepsilon) \cdot \tau 2$$

$$dL1_{dLtab} := (1 - F) \cdot (1 - \varepsilon) \cdot \tau 2$$

$$dL1_{dIb} := (1 - F) \cdot Es \cdot \cos(\theta b) \cdot (1 - \varepsilon b) \cdot (1 - \varepsilon) \cdot \tau 2$$

$$dL1_{d\theta b} := -(1 - F) \cdot Ib \cdot Es \cdot \sin(\theta b) \cdot (1 - \varepsilon b) \cdot (1 - \varepsilon) \cdot \tau 2$$

$$dL1_{d\varepsilon b} := -(1 - F) \cdot Ib \cdot Es \cdot \cos(\theta b) \cdot (1 - \varepsilon) \cdot \tau 2$$

$$dL1_{d\tau 2} := \varepsilon \cdot Lt + (It \cdot Es \cdot \cos(\theta s) + F \cdot Ld + (1 - F) \cdot (Ltab + Ib \cdot Es \cdot \cos(\theta b) \cdot (1 - \varepsilon b))) \cdot (1 - \varepsilon)$$

$$dL1_{dLu} := 1$$

These derivatives are used to form the components of the Beers error calculation:

$s\varepsilon := 0.05$	$sLt := 1.73$	$sIt := 0$	$sLu := 0.16$
$sEs := 0$	$sLd := 2.26$	$s\theta b := 0.1309$	$\rho_{\tau 2Lu} := -0.8381$
$s\theta s := 0.1309$	$sLtab := 1.73$	$s\varepsilon b := 0.05$	
$sF := 0.20$	$sIb := 0$	$s\tau 2 := 0.03$	

$$sL1_{\varepsilon} := \left(dL1_{d\varepsilon}^{2} \cdot s\varepsilon^{2}\right)^{\frac{1}{2}}$$

$$sL1_{\varepsilon} = 1.399$$

$$sL1_{Lt} := \left(dL1_{dLt}^{2} \cdot sLt^{2}\right)^{\frac{1}{2}}$$

$$sL1_{Lt} = 1.465$$

$$sL1_{It} := \left(dL1_{dIt}^{2} \cdot sIt^{2}\right)^{\frac{1}{2}}$$

$$sL1_{It} = 0$$

$$sL1_{Es} := \left(dL1_{dEs}^{2} \cdot sEs^{2}\right)^{\frac{1}{2}}$$

$$sL1_{Es} = 0$$

$$sL1_{\theta s} := \left(dL1_{d\theta s}^{2} \cdot s\theta s^{2}\right)^{\frac{1}{2}}$$

$$sL1_{\theta s} = 0$$

$$sL1_{F} := \left(dL1_{dF}^{2} \cdot sF^{2}\right)^{\frac{1}{2}}$$

$$sL1_{F} = 0.751$$

$$sL1_{Ld} := \left(dL1_{dLd}^{2} \cdot sLd^{2}\right)^{\frac{1}{2}}$$

$$sL1_{Ld} = 0.278$$

$$sL1_{Ltab} := \left(dL1_{dLtab}^{2} \cdot sLtab^{2}\right)^{\frac{1}{2}}$$

$$sL1_{Ltab} = 0$$

$$sL1_{Ib} := \left(dL1_{dIb}^{2} \cdot sIb^{2}\right)^{\frac{1}{2}}$$

$$sL1_{Ib} = 0$$

$$sL1_{\theta b} := \left(dL1_{d\theta b}^{2} \cdot s\theta b^{2}\right)^{\frac{1}{2}}$$

$$sL1_{\theta b} = 0$$

$$sL1_{\varepsilon b} := \left(dL1_{d\varepsilon b}^{2} \cdot s\varepsilon b^{2}\right)^{\frac{1}{2}}$$

$$sL1_{\varepsilon b} = 0$$

$$sL1_{\tau 2} := \left(dL1_{d\tau 2}^{2} \cdot s\tau 2^{2}\right)^{\frac{1}{2}}$$

$$sL1_{\tau 2} = 1.01$$

$$sL1_{Lu} := \left(dL1_{dLu}^{2} \cdot sLu^{2}\right)^{\frac{1}{2}}$$

$$sL1_{Lu} = 0.16$$

The cross term for the correlated variables Tau2 and Lu is:

$$xterm := \left[\rho_{\tau 2Lu} \cdot \left(dL1_{d\tau 2}\right) \cdot \left(dL1_{dLu}\right) \cdot s\tau 2 \cdot sLu\right]$$

$$xterm = -0.135$$

The total Beers error is expressed as:

$$sL1_{part1} := sL1_{\varepsilon}^{2} + sL1_{Lt}^{2} + sL1_{It}^{2} + sL1_{Es}^{2} + sL1_{\theta s}^{2} + sL1_{F}^{2} + sL1_{Ld}^{2} + sL1_{Ltab}^{2}$$

$$sL1_{part2} := sL1_{Ib}^{2} + sL1_{\theta b}^{2} + sL1_{\varepsilon b}^{2} + sL1_{\tau 2}^{2} + sL1_{Lu}^{2} + xterm$$

$$sL1_{total} := \left(sL1_{part1} + sL1_{part2}\right)^{\frac{1}{2}}$$

$$sL1_{total} = 2.378$$

The starting values for the equation are as follows:

$\varepsilon := .873$	$\varepsilon b := .900$	$Ld := 8.50$	$Lu := 0.90$
$Lt := 37.34$	$Ltab := 39.00$	$\tau 2 := 0.97$	
$\theta s := .523599$	$\theta b := .523599$	$Es := 0.00$	
$It := 1$	$Ib := 1$	$F := 1$	

Case 1: Diffuse target hit

$$L1 := (\varepsilon \cdot Lt + (It \cdot Es \cdot \cos(\theta s) + F \cdot (Ld) + (1 - F) \cdot (Ltab + Ib \cdot Es \cdot \cos(\theta b) \cdot (1 - \varepsilon b))) \cdot (1 - \varepsilon)) \cdot \tau 2 + Lu$$

$$L1 = 33.567$$

The MAPLE symbolic processor in MathCad was used to calculate the following derivatives:

$$dL1_{d\varepsilon} := (Lt - It \cdot Es \cdot \cos(\theta s) - F \cdot Ld - (1 - F) \cdot (Ltab + Ib \cdot Es \cdot \cos(\theta b) \cdot (1 - \varepsilon b))) \cdot \tau 2$$

$$dL1_{dLt} := \varepsilon \cdot \tau 2$$

$$dL1_{dIt} := Es \cdot \cos(\theta s) \cdot (1 - \varepsilon) \cdot \tau 2$$

$$dL1_{dEs} := (It \cdot \cos(\theta s) + (1 - F) \cdot Ib \cdot \cos(\theta b) \cdot (1 - \varepsilon b)) \cdot (1 - \varepsilon) \cdot \tau 2$$

$$dL1_{d\theta s} := -It \cdot Es \cdot \sin(\theta s) \cdot (1 - \varepsilon) \cdot \tau 2$$

$$dL1_{dF} := (Ld - Ltab - Ib \cdot Es \cdot \cos(\theta b) \cdot (1 - \varepsilon b)) \cdot (1 - \varepsilon) \cdot \tau 2$$

$$dL1_{dLd} := F \cdot (1 - \varepsilon) \cdot \tau 2$$

$$dL1_{dLtab} := (1 - F) \cdot (1 - \varepsilon) \cdot \tau 2$$

$$dL1_{dIb} := (1 - F) \cdot Es \cdot \cos(\theta b) \cdot (1 - \varepsilon b) \cdot (1 - \varepsilon) \cdot \tau 2$$

$$dL1_{d\theta b} := -(1 - F) \cdot Ib \cdot Es \cdot \sin(\theta b) \cdot (1 - \varepsilon b) \cdot (1 - \varepsilon) \cdot \tau 2$$

$$dL1_{d\varepsilon b} := -(1 - F) \cdot Ib \cdot Es \cdot \cos(\theta b) \cdot (1 - \varepsilon) \cdot \tau 2$$

$$dL1_{d\tau 2} := \varepsilon \cdot Lt + (It \cdot Es \cdot \cos(\theta s) + F \cdot Ld + (1 - F) \cdot (Ltab + Ib \cdot Es \cdot \cos(\theta b) \cdot (1 - \varepsilon b))) \cdot (1 - \varepsilon)$$

$$dL1_{dLu} := 1$$

These derivatives are used to form the components of the Beers error calculation:

$s\varepsilon := 0.05$ $\quad sLt := 1.73$ $\quad sIt := 0$ $\quad sLu := 0.54$

$sEs := 0$ $\quad sLd := 5.10$ $\quad s\theta b := 0.1309$ $\quad \rho_{\tau 2Lu} := -0.8381$

$s\theta s := 0.1309$ $\quad sLtab := 1.73$ $\quad s\varepsilon b := 0.05$

$sF := 0.20$ $\quad sIb := 0$ $\quad s\tau 2 := 0.03$

$$sL1_{\varepsilon} := \left(dL1_{d\varepsilon}^{2} \cdot s\varepsilon^{2}\right)^{\frac{1}{2}}$$

$$sL1_{\varepsilon} = 1.399$$

$$sL1_{Lt} := \left(dL1_{dLt}^{2} \cdot sLt^{2}\right)^{\frac{1}{2}}$$

$$sL1_{Lt} = 1.465$$

$$sL1_{It} := \left(dL1_{dIt}^{2} \cdot sIt^{2}\right)^{\frac{1}{2}}$$

$$sL1_{It} = 0$$

$$sL1_{Es} := \left(dL1_{dEs}^{2} \cdot sEs^{2}\right)^{\frac{1}{2}}$$

$$sL1_{Es} = 0$$

$$sL1_{\theta s} := \left(dL1_{d\theta s}^{2} \cdot s\theta s^{2}\right)^{\frac{1}{2}}$$

$$sL1_{\theta s} = 0$$

$$sL1_{F} := \left(dL1_{dF}^{2} \cdot sF^{2}\right)^{\frac{1}{2}}$$

$$sL1_{F} = 0.751$$

$$sL1_{Ld} := \left(dL1_{dLd}^{2} \cdot sLd^{2}\right)^{\frac{1}{2}}$$

$$sL1_{Ld} = 0.628$$

$$sL1_{Ltab} := \left(dL1_{dLtab}^{2} \cdot sLtab^{2}\right)^{\frac{1}{2}}$$

$$sL1_{Ltab} = 0$$

$$sL1_{Ib} := \left(dL1_{dIb}^{2} \cdot sIb^{2}\right)^{\frac{1}{2}}$$

$$sL1_{Ib} = 0$$

$$sL1_{\theta b} := \left(dL1_{d\theta b}^{2} \cdot s\theta b^{2}\right)^{\frac{1}{2}}$$

$$sL1_{\theta b} = 0$$

$$sL1_{\varepsilon b} := \left(dL1_{d\varepsilon b}^{2} \cdot s\varepsilon b^{2}\right)^{\frac{1}{2}}$$

$$sL1_{\varepsilon b} = 0$$

$$sL1_{\tau 2} := \left(dL1_{d\tau 2}^{2} \cdot s\tau 2^{2}\right)^{\frac{1}{2}}$$

$$sL1_{\tau 2} = 1.01$$

$$sL1_{Lu} := \left(dL1_{dLu}^{2} \cdot sLu^{2}\right)^{\frac{1}{2}}$$

$$sL1_{Lu} = 0.54$$

The cross term of the correlated variables Tau2 and Lu is:

$$xterm := \left[\rho_{\tau 2Lu} \cdot \left(dL1_{d\tau 2}\right) \cdot \left(dL1_{dLu}\right) \cdot s\tau 2 \cdot sLu\right]$$

$$xterm = -0.457$$

The total Beers error is expressed as:

$$sL1_{part1} := sL1_{\varepsilon}^{2} + sL1_{Lt}^{2} + sL1_{It}^{2} + sL1_{Es}^{2} + sL1_{\theta s}^{2} + sL1_{F}^{2} + sL1_{Ld}^{2} + sL1_{Ltab}^{2}$$

$$sL1_{part2} := sL1_{Ib}^{2} + sL1_{\theta b}^{2} + sL1_{\varepsilon b}^{2} + sL1_{\tau 2}^{2} + sL1_{Lu}^{2} + xterm$$

$$sL1_{total} := \left(sL1_{part1} + sL1_{part2}\right)^{\frac{1}{2}}$$

$$sL1_{total} = 2.433$$

The starting values for the equation are as follows:

$\varepsilon := .873$	$\varepsilon b := .900$	$Ld := 8.50$	$Lu := 3.533$
$Lt := 37.34$	$Ltab := 39.00$	$\tau 2 := 0.873$	
$\theta s := .523599$	$\theta b := .523599$	$Es := 0.00$	
$It := 1$	$Ib := 1$	$F := 1$	

Case 1: Diffuse target hit

$$L1 := (\varepsilon \cdot Lt + (It \cdot Es \cdot \cos(\theta s) + F \cdot (Ld) + (1 - F) \cdot (Ltab + Ib \cdot Es \cdot \cos(\theta b) \cdot (1 - \varepsilon b))) \cdot (1 - \varepsilon)) \cdot \tau 2 + Lu$$

$$L1 = 32.933$$

The MAPLE symbolic processor in MathCad was used to calculate the following derivatives:

$$dL1_{d\varepsilon} := (Lt - It \cdot Es \cdot \cos(\theta s) - F \cdot Ld - (1 - F) \cdot (Ltab + Ib \cdot Es \cdot \cos(\theta b) \cdot (1 - \varepsilon b))) \cdot \tau 2$$

$$dL1_{dLt} := \varepsilon \cdot \tau 2$$

$$dL1_{dIt} := Es \cdot \cos(\theta s) \cdot (1 - \varepsilon) \cdot \tau 2$$

$$dL1_{dEs} := (It \cdot \cos(\theta s) + (1 - F) \cdot Ib \cdot \cos(\theta b) \cdot (1 - \varepsilon b)) \cdot (1 - \varepsilon) \cdot \tau 2$$

$$dL1_{d\theta s} := -It \cdot Es \cdot \sin(\theta s) \cdot (1 - \varepsilon) \cdot \tau 2$$

$$dL1_{dF} := (Ld - Ltab - Ib \cdot Es \cdot \cos(\theta b) \cdot (1 - \varepsilon b)) \cdot (1 - \varepsilon) \cdot \tau 2$$

$$dL1_{dLd} := F \cdot (1 - \varepsilon) \cdot \tau 2$$

$$dL1_{dLtab} := (1 - F) \cdot (1 - \varepsilon) \cdot \tau 2$$

$$dL1_{dIb} := (1 - F) \cdot Es \cdot \cos(\theta b) \cdot (1 - \varepsilon b) \cdot (1 - \varepsilon) \cdot \tau 2$$

$$dL1_{d\theta b} := -(1 - F) \cdot Ib \cdot Es \cdot \sin(\theta b) \cdot (1 - \varepsilon b) \cdot (1 - \varepsilon) \cdot \tau 2$$

$$dL1_{d\varepsilon b} := -(1 - F) \cdot Ib \cdot Es \cdot \cos(\theta b) \cdot (1 - \varepsilon) \cdot \tau 2$$

$$dL1_{d\tau 2} := \varepsilon \cdot Lt + (It \cdot Es \cdot \cos(\theta s) + F \cdot Ld + (1 - F) \cdot (Ltab + Ib \cdot Es \cdot \cos(\theta b) \cdot (1 - \varepsilon b))) \cdot (1 - \varepsilon)$$

$$dL1_{dLu} := 1$$

These derivatives are used to form the components of the Beers error calculation:

$s\varepsilon := 0.025$	$sLt := 0.09$	$sIt := 0$	$sLu := 0.071$
$sEs := 0$	$sLd := 0.25$	$s\theta b := 0.05236$	$\rho_{\tau 2Lu} := -0.8381$
$s\theta s := 0.05236$	$sLtab := 0.09$	$s\varepsilon b := 0.025$	
$sF := 0.10$	$sIb := 0$	$s\tau 2 := 0.03$	

$$sL1_{\varepsilon} := \left(dL1_{d\varepsilon}^{2} \cdot s\varepsilon^{2}\right)^{\frac{1}{2}}$$

$$sL1_{\varepsilon} = 0.629$$

$$sL1_{Lt} := \left(dL1_{dLt}^{2} \cdot sLt^{2}\right)^{\frac{1}{2}}$$

$$sL1_{Lt} = 0.069$$

$$sL1_{It} := \left(dL1_{dIt}^{2} \cdot sIt^{2}\right)^{\frac{1}{2}}$$

$$sL1_{It} = 0$$

$$sL1_{Es} := \left(dL1_{dEs}^{2} \cdot sEs^{2}\right)^{\frac{1}{2}}$$

$$sL1_{Es} = 0$$

$$sL1_{\theta s} := \left(dL1_{d\theta s}^{2} \cdot s\theta s^{2}\right)^{\frac{1}{2}}$$

$$sL1_{\theta s} = 0$$

$$sL1_{F} := \left(dL1_{dF}^{2} \cdot sF^{2}\right)^{\frac{1}{2}}$$

$$sL1_{F} = 0.338$$

$$sL1_{Ld} := \left(dL1_{dLd}^{2} \cdot sLd^{2}\right)^{\frac{1}{2}}$$

$$sL1_{Ld} = 0.028$$

$$sL1_{Ltab} := \left(dL1_{dLtab}^{2} \cdot sLtab^{2}\right)^{\frac{1}{2}}$$

$$sL1_{Ltab} = 0$$

$$sL1_{Ib} := \left(dL1_{dIb}^{2} \cdot sIb^{2}\right)^{\frac{1}{2}}$$

$$sL1_{Ib} = 0$$

$$sL1_{\theta b} := \left(dL1_{d\theta b}^{2} \cdot s\theta b^{2}\right)^{\frac{1}{2}}$$

$$sL1_{\theta b} = 0$$

$$sL1_{\varepsilon b} := \left(dL1_{d\varepsilon b}^{2} \cdot s\varepsilon b^{2}\right)^{\frac{1}{2}}$$

$$sL1_{\varepsilon b} = 0$$

$$sL1_{\tau 2} := \left(dL1_{d\tau 2}^{2} \cdot s\tau 2^{2}\right)^{\frac{1}{2}}$$

$$sL1_{\tau 2} = 1.01$$

$$sL1_{Lu} := \left(dL1_{dLu}^{2} \cdot sLu^{2}\right)^{\frac{1}{2}}$$

$$sL1_{Lu} = 0.071$$

The cross term of the correlated variables Tau2 and Lu is:

$$xterm := \left[\rho_{\tau 2Lu} \cdot \left(dL1_{d\tau 2}\right) \cdot \left(dL1_{dLu}\right) \cdot s\tau 2 \cdot sLu\right] \qquad xterm = -0.06$$

The total Beers error is expressed as:

$$sL1_{part1} := sL1_{\varepsilon}^{2} + sL1_{Lt}^{2} + sL1_{It}^{2} + sL1_{Es}^{2} + sL1_{\theta s}^{2} + sL1_{F}^{2} + sL1_{Ld}^{2} + sL1_{Ltab}^{2}$$

$$sL1_{part2} := sL1_{Ib}^{2} + sL1_{\theta b}^{2} + sL1_{\varepsilon b}^{2} + sL1_{\tau 2}^{2} + sL1_{Lu}^{2} + xterm$$

$$sL1_{total} := \left(sL1_{part1} + sL1_{part2}\right)^{\frac{1}{2}}$$

$$sL1_{total} = 1.217$$

The starting values for the equation are as follows:

$\varepsilon := .873$	$\varepsilon b := .900$	$Ld := 8.50$	$Lu := 3.533$
$Lt := 37.34$	$Ltab := 39.00$	$\tau 2 := 0.873$	
$\theta s := .523599$	$\theta b := .523599$	$Es := 0.00$	
$It := 1$	$Ib := 1$	$F := 1$	

Case 1: Diffuse target hit

$$L1 := (\varepsilon \cdot Lt + (It \cdot Es \cdot \cos(\theta s) + F \cdot (Ld) + (1 - F) \cdot (Ltab + Ib \cdot Es \cdot \cos(\theta b) \cdot (1 - \varepsilon b))) \cdot (1 - \varepsilon)) \cdot \tau 2 + Lu$$

$$L1 = 32.933$$

The MAPLE symbolic processor in MathCad was used to calculate the following derivatives:

$$dL1_{d\varepsilon} := (Lt - It \cdot Es \cdot \cos(\theta s) - F \cdot Ld - (1 - F) \cdot (Ltab + Ib \cdot Es \cdot \cos(\theta b) \cdot (1 - \varepsilon b))) \cdot \tau 2$$

$$dL1_{dLt} := \varepsilon \cdot \tau 2$$

$$dL1_{dIt} := Es \cdot \cos(\theta s) \cdot (1 - \varepsilon) \cdot \tau 2$$

$$dL1_{dEs} := (It \cdot \cos(\theta s) + (1 - F) \cdot Ib \cdot \cos(\theta b) \cdot (1 - \varepsilon b)) \cdot (1 - \varepsilon) \cdot \tau 2$$

$$dL1_{d\theta s} := -It \cdot Es \cdot \sin(\theta s) \cdot (1 - \varepsilon) \cdot \tau 2$$

$$dL1_{dF} := (Ld - Ltab - Ib \cdot Es \cdot \cos(\theta b) \cdot (1 - \varepsilon b)) \cdot (1 - \varepsilon) \cdot \tau 2$$

$$dL1_{dLd} := F \cdot (1 - \varepsilon) \cdot \tau 2$$

$$dL1_{dLtab} := (1 - F) \cdot (1 - \varepsilon) \cdot \tau 2$$

$$dL1_{dIb} := (1 - F) \cdot Es \cdot \cos(\theta b) \cdot (1 - \varepsilon b) \cdot (1 - \varepsilon) \cdot \tau 2$$

$$dL1_{d\theta b} := -(1 - F) \cdot Ib \cdot Es \cdot \sin(\theta b) \cdot (1 - \varepsilon b) \cdot (1 - \varepsilon) \cdot \tau 2$$

$$dL1_{d\varepsilon b} := -(1 - F) \cdot Ib \cdot Es \cdot \cos(\theta b) \cdot (1 - \varepsilon) \cdot \tau 2$$

$$dL1_{d\tau 2} := \varepsilon \cdot Lt + (It \cdot Es \cdot \cos(\theta s) + F \cdot Ld + (1 - F) \cdot (Ltab + Ib \cdot Es \cdot \cos(\theta b) \cdot (1 - \varepsilon b))) \cdot (1 - \varepsilon)$$

$$dL1_{dLu} := 1$$

These derivatives are used to form the components of the Beers error calculation:

$s\varepsilon := 0.05$	$sLt := 0.63$	$sIt := 0$	$sLu := 0.636$
$sEs := 0$	$sLd := 2.26$	$s\theta b := 0.1309$	$\rho_{\tau 2Lu} := -0.8381$
$s\theta s := 0.1309$	$sLtab := 0.63$	$s\varepsilon b := 0.05$	
$sF := 0.20$	$sIb := 0$	$s\tau 2 := .03$	

$$sL1_{\varepsilon} := \left(dL1_{d\varepsilon}{}^{2} \cdot s\varepsilon^{2}\right)^{\frac{1}{2}}$$

$$sL1_{\varepsilon} = 1.259$$

$$sL1_{Lt} := \left(dL1_{dLt}{}^{2} \cdot sLt^{2}\right)^{\frac{1}{2}}$$

$$sL1_{Lt} = 0.48$$

$$sL1_{It} := \left(dL1_{dIt}{}^{2} \cdot sIt^{2}\right)^{\frac{1}{2}}$$

$$sL1_{It} = 0$$

$$sL1_{Es} := \left(dL1_{dEs}{}^{2} \cdot sEs^{2}\right)^{\frac{1}{2}}$$

$$sL1_{Es} = 0$$

$$sL1_{\theta s} := \left(dL1_{d\theta s}{}^{2} \cdot s\theta s^{2}\right)^{\frac{1}{2}}$$

$$sL1_{\theta s} = 0$$

$$sL1_{F} := \left(dL1_{dF}{}^{2} \cdot sF^{2}\right)^{\frac{1}{2}}$$

$$sL1_{F} = 0.676$$

$$sL1_{Ld} := \left(dL1_{dLd}{}^{2} \cdot sLd^{2}\right)^{\frac{1}{2}}$$

$$sL1_{Ld} = 0.251$$

$$sL1_{Ltab} := \left(dL1_{dLtab}{}^{2} \cdot sLtab^{2}\right)^{\frac{1}{2}}$$

$$sL1_{Ltab} = 0$$

$$sL1_{Ib} := \left(dL1_{dIb}{}^{2} \cdot sIb^{2}\right)^{\frac{1}{2}}$$

$$sL1_{Ib} = 0$$

$$sL1_{\theta b} := \left(dL1_{d\theta b}{}^{2} \cdot s\theta b^{2}\right)^{\frac{1}{2}}$$

$$sL1_{\theta b} = 0$$

$$sL1_{\varepsilon b} := \left(dL1_{d\varepsilon b}{}^{2} \cdot s\varepsilon b^{2}\right)^{\frac{1}{2}}$$

$$sL1_{\varepsilon b} = 0$$

$$sL1_{\tau 2} := \left(dL1_{d\tau 2}{}^{2} \cdot s\tau 2^{2}\right)^{\frac{1}{2}}$$

$$sL1_{\tau 2} = 1.01$$

$$sL1_{Lu} := \left(dL1_{dLu}{}^{2} \cdot sLu^{2}\right)^{\frac{1}{2}}$$

$$sL1_{Lu} = 0.636$$

The cross term of the correlated variables Tau2 and Lu is:

$$xterm := \left[\rho_{\tau 2Lu} \cdot \left(dL1_{d\tau 2}\right) \cdot \left(dL1_{dLu}\right) \cdot s\tau 2 \cdot sLu\right] \qquad xterm = -0.539$$

The total Beers error is expressed as:

$$sL1_{part1} := sL1_{\varepsilon}^{2} + sL1_{Lt}^{2} + sL1_{It}^{2} + sL1_{Es}^{2} + sL1_{\theta s}^{2} + sL1_{F}^{2} + sL1_{Ld}^{2} + sL1_{Ltab}^{2}$$

$$sL1_{part2} := sL1_{Ib}^{2} + sL1_{\theta b}^{2} + sL1_{\varepsilon b}^{2} + sL1_{\tau 2}^{2} + sL1_{Lu}^{2} + xterm$$

$$sL1_{total} := \left(sL1_{part1} + sL1_{part2}\right)^{\frac{1}{2}}$$

$$sL1_{total} = 1.795$$

Error Type: P

The starting values for the equation are as follows:

$\varepsilon := .873$	$\varepsilon b := .900$	$Ld := 8.50$	$Lu := 3.533$
$Lt := 37.34$	$Ltab := 39.00$	$\tau 2 := 0.873$	
$\theta s := .523599$	$\theta b := .523599$	$Es := 0.00$	
$It := 1$	$Ib := 1$	$F := 1$	

Case 1: Diffuse target hit

$$L1 := (\varepsilon \cdot Lt + (It \cdot Es \cdot \cos(\theta s) + F \cdot (Ld) + (1 - F) \cdot (Ltab + Ib \cdot Es \cdot \cos(\theta b) \cdot (1 - \varepsilon b))) \cdot (1 - \varepsilon)) \cdot \tau 2 + Lu$$

$$L1 = 32.933$$

The MAPLE symbolic processor in MathCad was used to calculate the following derivatives:

$$dL1_{d\varepsilon} := (Lt - It \cdot Es \cdot \cos(\theta s) - F \cdot Ld - (1 - F) \cdot (Ltab + Ib \cdot Es \cdot \cos(\theta b) \cdot (1 - \varepsilon b))) \cdot \tau 2$$

$$dL1_{dLt} := \varepsilon \cdot \tau 2$$

$$dL1_{dIt} := Es \cdot \cos(\theta s) \cdot (1 - \varepsilon) \cdot \tau 2$$

$$dL1_{dEs} := (It \cdot \cos(\theta s) + (1 - F) \cdot Ib \cdot \cos(\theta b) \cdot (1 - \varepsilon b)) \cdot (1 - \varepsilon) \cdot \tau 2$$

$$dL1_{d\theta s} := -It \cdot Es \cdot \sin(\theta s) \cdot (1 - \varepsilon) \cdot \tau 2$$

$$dL1_{dF} := (Ld - Ltab - Ib \cdot Es \cdot \cos(\theta b) \cdot (1 - \varepsilon b)) \cdot (1 - \varepsilon) \cdot \tau 2$$

$$dL1_{dLd} := F \cdot (1 - \varepsilon) \cdot \tau 2$$

$$dL1_{dLtab} := (1 - F) \cdot (1 - \varepsilon) \cdot \tau 2$$

$$dL1_{dIb} := (1 - F) \cdot Es \cdot \cos(\theta b) \cdot (1 - \varepsilon b) \cdot (1 - \varepsilon) \cdot \tau 2$$

$$dL1_{d\theta b} := -(1 - F) \cdot Ib \cdot Es \cdot \sin(\theta b) \cdot (1 - \varepsilon b) \cdot (1 - \varepsilon) \cdot \tau 2$$

$$dL1_{d\varepsilon b} := -(1 - F) \cdot Ib \cdot Es \cdot \cos(\theta b) \cdot (1 - \varepsilon) \cdot \tau 2$$

$$dL1_{d\tau 2} := \varepsilon \cdot Lt + (It \cdot Es \cdot \cos(\theta s) + F \cdot Ld + (1 - F) \cdot (Ltab + Ib \cdot Es \cdot \cos(\theta b) \cdot (1 - \varepsilon b))) \cdot (1 - \varepsilon)$$

$$dL1_{dLu} := 1$$

These derivatives are used to form the components of the Beers error calculation:

$s\varepsilon := 0.05$	$sLt := 1.73$	$sIt := 0$	$sLu := 0.636$
$sEs := 0$	$sLd := 2.26$	$s\theta b := 0.1309$	$\rho_{\tau 2Lu} := -0.8381$
$s\theta s := 0.1309$	$sLtab := 1.73$	$s\varepsilon b := 0.05$	
$sF := 0.20$	$sIb := 0$	$s\tau 2 := 0.03$	

$$sL1_{\varepsilon} := \left(dL1_{d\varepsilon}{}^{2} \cdot s\varepsilon^{2}\right)^{\frac{1}{2}}$$

$$sL1_{\varepsilon} = 1.259$$

$$sL1_{Lt} := \left(dL1_{dLt}{}^{2} \cdot sLt^{2}\right)^{\frac{1}{2}}$$

$$sL1_{Lt} = 1.318$$

$$sL1_{It} := \left(dL1_{dIt}{}^{2} \cdot sIt^{2}\right)^{\frac{1}{2}}$$

$$sL1_{It} = 0$$

$$sL1_{Es} := \left(dL1_{dEs}{}^{2} \cdot sEs^{2}\right)^{\frac{1}{2}}$$

$$sL1_{Es} = 0$$

$$sL1_{\theta s} := \left(dL1_{d\theta s}{}^{2} \cdot s\theta s^{2}\right)^{\frac{1}{2}}$$

$$sL1_{\theta s} = 0$$

$$sL1_{F} := \left(dL1_{dF}{}^{2} \cdot sF^{2}\right)^{\frac{1}{2}}$$

$$sL1_{F} = 0.676$$

$$sL1_{Ld} := \left(dL1_{dLd}{}^{2} \cdot sLd^{2}\right)^{\frac{1}{2}}$$

$$sL1_{Ld} = 0.251$$

$$sL1_{Ltab} := \left(dL1_{dLtab}{}^{2} \cdot sLtab^{2}\right)^{\frac{1}{2}}$$

$$sL1_{Ltab} = 0$$

$$sL1_{Ib} := \left(dL1_{dIb}{}^{2} \cdot sIb^{2}\right)^{\frac{1}{2}}$$

$$sL1_{Ib} = 0$$

$$sL1_{\theta b} := \left(dL1_{d\theta b}{}^{2} \cdot s\theta b^{2}\right)^{\frac{1}{2}}$$

$$sL1_{\theta b} = 0$$

$$sL1_{\varepsilon b} := \left(dL1_{d\varepsilon b}{}^{2} \cdot s\varepsilon b^{2}\right)^{\frac{1}{2}}$$

$$sL1_{\varepsilon b} = 0$$

$$sL1_{\tau 2} := \left(dL1_{d\tau 2}{}^{2} \cdot s\tau 2^{2}\right)^{\frac{1}{2}}$$

$$sL1_{\tau 2} = 1.01$$

$$sL1_{Lu} := \left(dL1_{dLu}{}^{2} \cdot sLu^{2}\right)^{\frac{1}{2}}$$

$$sL1_{Lu} = 0.636$$

The cross term of the correlated variables Tau2 and Lu is:

$$xterm := \left[\rho_{\tau 2Lu} \cdot \left(dL1_{d\tau 2}\right) \cdot \left(dL1_{dLu}\right) \cdot s\tau 2 \cdot sLu\right]$$

$$xterm = -0.539$$

The total Beers error is expressed as:

$$sL1_{part1} := sL1_{\varepsilon}^{2} + sL1_{Lt}^{2} + sL1_{It}^{2} + sL1_{Es}^{2} + sL1_{\theta s}^{2} + sL1_{F}^{2} + sL1_{Ld}^{2} + sL1_{Ltab}^{2}$$

$$sL1_{part2} := sL1_{Ib}^{2} + sL1_{\theta b}^{2} + sL1_{\varepsilon b}^{2} + sL1_{\tau 2}^{2} + sL1_{Lu}^{2} + xterm$$

$$sL1_{total} := \left(sL1_{part1} + sL1_{part2}\right)^{\frac{1}{2}}$$

$$sL1_{total} = 2.175$$

The starting values for the equation are as follows:

$\varepsilon := .873$	$\varepsilon b := .900$	$Ld := 8.50$	$Lu := 3.533$
$Lt := 37.34$	$Ltab := 39.00$	$\tau 2 := 0.873$	
$\theta s := .523599$	$\theta b := .523599$	$Es := 0.00$	
$It := 1$	$Ib := 1$	$F := 1$	

Case 1: Diffuse target hit

$$L1 := (\varepsilon \cdot Lt + (It \cdot Es \cdot \cos(\theta s) + F \cdot (Ld) + (1 - F) \cdot (Ltab + Ib \cdot Es \cdot \cos(\theta b) \cdot (1 - \varepsilon b))) \cdot (1 - \varepsilon)) \cdot \tau 2 + Lu$$

$$L1 = 32.933$$

The MAPLE symbolic processor in MathCad was used to calculate the following derivatives:

$$dL1_{d\varepsilon} := (Lt - It \cdot Es \cdot \cos(\theta s) - F \cdot Ld - (1 - F) \cdot (Ltab + Ib \cdot Es \cdot \cos(\theta b) \cdot (1 - \varepsilon b))) \cdot \tau 2$$

$$dL1_{dLt} := \varepsilon \cdot \tau 2$$

$$dL1_{dIt} := Es \cdot \cos(\theta s) \cdot (1 - \varepsilon) \cdot \tau 2$$

$$dL1_{dEs} := (It \cdot \cos(\theta s) + (1 - F) \cdot Ib \cdot \cos(\theta b) \cdot (1 - \varepsilon b)) \cdot (1 - \varepsilon) \cdot \tau 2$$

$$dL1_{d\theta s} := -It \cdot Es \cdot \sin(\theta s) \cdot (1 - \varepsilon) \cdot \tau 2$$

$$dL1_{dF} := (Ld - Ltab - Ib \cdot Es \cdot \cos(\theta b) \cdot (1 - \varepsilon b)) \cdot (1 - \varepsilon) \cdot \tau 2$$

$$dL1_{dLd} := F \cdot (1 - \varepsilon) \cdot \tau 2$$

$$dL1_{dLtab} := (1 - F) \cdot (1 - \varepsilon) \cdot \tau 2$$

$$dL1_{dIb} := (1 - F) \cdot Es \cdot \cos(\theta b) \cdot (1 - \varepsilon b) \cdot (1 - \varepsilon) \cdot \tau 2$$

$$dL1_{d\theta b} := -(1 - F) \cdot Ib \cdot Es \cdot \sin(\theta b) \cdot (1 - \varepsilon b) \cdot (1 - \varepsilon) \cdot \tau 2$$

$$dL1_{d\varepsilon b} := -(1 - F) \cdot Ib \cdot Es \cdot \cos(\theta b) \cdot (1 - \varepsilon) \cdot \tau 2$$

$$dL1_{d\tau 2} := \varepsilon \cdot Lt + (It \cdot Es \cdot \cos(\theta s) + F \cdot Ld + (1 - F) \cdot (Ltab + Ib \cdot Es \cdot \cos(\theta b) \cdot (1 - \varepsilon b))) \cdot (1 - \varepsilon)$$

$$dL1_{dLu} := 1$$

These derivatives are used to form the components of the Beers error calculation:

$s\varepsilon := 0.05$	$sLt := 1.73$	$sIt := 0$	$sLu := 2.120$
$sEs := 0$	$sLd := 5.10$	$s\theta b := 0.1309$	$\rho_{\tau 2Lu} := -0.8381$
$s\theta s := 0.1309$	$sLtab := 1.73$	$s\varepsilon b := 0.05$	
$sF := 0.20$	$sIb := 0$	$s\tau 2 := 0.03$	

$$sL1_{\varepsilon} := \left(dL1_{d\varepsilon}{}^{2} \cdot s\varepsilon^{2}\right)^{\frac{1}{2}}$$

$$sL1_{\varepsilon} = 1.259$$

$$sL1_{Lt} := \left(dL1_{dLt}{}^{2} \cdot sLt^{2}\right)^{\frac{1}{2}}$$

$$sL1_{Lt} = 1.318$$

$$sL1_{It} := \left(dL1_{dIt}{}^{2} \cdot sIt^{2}\right)^{\frac{1}{2}}$$

$$sL1_{It} = 0$$

$$sL1_{Es} := \left(dL1_{dEs}{}^{2} \cdot sEs^{2}\right)^{\frac{1}{2}}$$

$$sL1_{Es} = 0$$

$$sL1_{\theta s} := \left(dL1_{d\theta s}{}^{2} \cdot s\theta s^{2}\right)^{\frac{1}{2}}$$

$$sL1_{\theta s} = 0$$

$$sL1_{F} := \left(dL1_{dF}{}^{2} \cdot sF^{2}\right)^{\frac{1}{2}}$$

$$sL1_{F} = 0.676$$

$$sL1_{Ld} := \left(dL1_{dLd}{}^{2} \cdot sLd^{2}\right)^{\frac{1}{2}}$$

$$sL1_{Ld} = 0.565$$

$$sL1_{Ltab} := \left(dL1_{dLtab}{}^{2} \cdot sLtab^{2}\right)^{\frac{1}{2}}$$

$$sL1_{Ltab} = 0$$

$$sL1_{Ib} := \left(dL1_{dIb}{}^{2} \cdot sIb^{2}\right)^{\frac{1}{2}}$$

$$sL1_{Ib} = 0$$

$$sL1_{\theta b} := \left(dL1_{d\theta b}{}^{2} \cdot s\theta b^{2}\right)^{\frac{1}{2}}$$

$$sL1_{\theta b} = 0$$

$$sL1_{\varepsilon b} := \left(dL1_{d\varepsilon b}{}^{2} \cdot s\varepsilon b^{2}\right)^{\frac{1}{2}}$$

$$sL1_{\varepsilon b} = 0$$

$$sL1_{\tau 2} := \left(dL1_{d\tau 2}{}^{2} \cdot s\tau 2^{2}\right)^{\frac{1}{2}}$$

$$sL1_{\tau 2} = 1.01$$

$$sL1_{Lu} := \left(dL1_{dLu}{}^{2} \cdot sLu^{2}\right)^{\frac{1}{2}}$$

$$sL1_{Lu} = 2.12$$

The cross term of the correlated variables Tau2 and Lu is:

$$xterm := \left[\rho_{\tau 2Lu} \cdot \left(dL1_{d\tau 2}\right) \cdot \left(dL1_{dLu}\right) \cdot s\tau 2 \cdot sLu\right] \qquad xterm = -1.795$$

The total Beers error is expressed as:

$$sL1_{part1} := sL1_{\varepsilon}^{2} + sL1_{Lt}^{2} + sL1_{It}^{2} + sL1_{Es}^{2} + sL1_{\theta s}^{2} + sL1_{F}^{2} + sL1_{Ld}^{2} + sL1_{Ltab}^{2}$$

$$sL1_{part2} := sL1_{Ib}^{2} + sL1_{\theta b}^{2} + sL1_{\varepsilon b}^{2} + sL1_{\tau 2}^{2} + sL1_{Lu}^{2} + xterm$$

$$sL1_{total} := \left(sL1_{part1} + sL1_{part2}\right)^{\frac{1}{2}}$$

$$sL1_{total} = 2.796$$

The cross term of the correlated variables Tau2 and Lu is:

$$xterm := \left[\rho_{\tau 2Lu} \cdot \left(dL1_{d\tau 2}\right) \cdot \left(dL1_{dLu}\right) \cdot s\tau 2 \cdot sLu\right] \qquad xterm = -1.795$$

The total Beers error is expressed as:

$$sL1_{part1} := sL1_{\varepsilon}^{2} + sL1_{Lt}^{2} + sL1_{It}^{2} + sL1_{Es}^{2} + sL1_{\theta s}^{2} + sL1_{F}^{2} + sL1_{Ld}^{2} + sL1_{Ltab}^{2}$$

$$sL1_{part2} := sL1_{Ib}^{2} + sL1_{\theta b}^{2} + sL1_{\varepsilon b}^{2} + sL1_{\tau 2}^{2} + sL1_{Lu}^{2} + xterm$$

$$sL1_{total} := \left(sL1_{part1} + sL1_{part2}\right)^{\frac{1}{2}}$$

$$sL1_{total} = 2.796$$

Ray_Interaction Type 2
Specular Bounce to Sky (Water)

Rooftop Simulation
Error Type: I

The starting values for the equation are as follows:

$\varepsilon := 0.702$ $\quad Lt := 32.15$ $\quad It := 1$ $\quad Es := 0.0$

$\theta s := .349066$ $\quad Ldhat := 8.5$ $\quad \tau 2 := 0.97$ $\quad Luhat := 0.90$

Case 2: Specular bounce to sky

$$L2 := (\varepsilon \cdot Lt + (It \cdot Es \cdot \cos(\theta s) + Ldhat) \cdot (1 - \varepsilon)) \cdot \tau 2 + Luhat$$

$$L2 = 25.249$$

The MAPLE symbolic processor in MathCad was used to calculate the following derivatives:

$$dL2_{d\varepsilon} := (Lt - It \cdot Es \cdot \cos(\theta s) - Ldhat) \cdot \tau 2$$

$$dL2_{dLt} := \varepsilon \cdot \tau 2$$

$$dL2_{dIt} := Es \cdot \cos(\theta s) \cdot (1 - \varepsilon) \cdot \tau 2$$

$$dL2_{dEs} := It \cdot \cos(\theta s) \cdot (1 - \varepsilon) \cdot \tau 2$$

$$dL2_{d\theta s} := -It \cdot Es \cdot \sin(\theta s) \cdot (1 - \varepsilon) \cdot \tau 2$$

$$dL2_{dLdhat} := (1 - \varepsilon) \cdot \tau 2$$

$$dL2_{d\tau 2} := \varepsilon \cdot Lt + (It \cdot Es \cdot \cos(\theta s) + Ldhat) \cdot (1 - \varepsilon)$$

$$dL2_{dLuhat} := 1$$

These derivatives are used to form the components of the Beers error calculation:

$s\varepsilon := 0.025$ $\quad sLt := 0.09$ $\quad sIt := 0$ $\quad sEs := 0$

$s\theta s := 0.05236$ $\quad sLdhat := 0.25$ $\quad s\tau 2 := 0.03$ $\quad sLuhat := 0.02$

$\rho_{\tau 2Lu} := -0.8381$

$$sL2_{\varepsilon} := \left(dL2_{d\varepsilon}^{2} \cdot s\varepsilon^{2}\right)^{\frac{1}{2}} \qquad sL2_{\varepsilon} = 0.574$$

$$sL2_{\ldots} := \left(dL2_{\ldots}^{2} \cdot s\ldots^{2}\right)^{\frac{1}{2}}$$

$$sL2_{It} := \left(dL2_{dIt}^{2} \cdot sIt^{2}\right)^{\frac{1}{2}}$$

$$sL2_{It} = 0$$

$$sL2_{Es} := \left(dL2_{dEs}^{2} \cdot sEs^{2}\right)^{\frac{1}{2}}$$

$$sL2_{Es} = 0$$

$$sL2_{\theta s} := \left(dL2_{d\theta s}^{2} \cdot s\theta s^{2}\right)^{\frac{1}{2}}$$

$$sL2_{\theta s} = 0$$

$$sL2_{Ldhat} := \left(dL2_{dLdhat}^{2} \cdot sLdhat^{2}\right)^{\frac{1}{2}}$$

$$sL2_{Ldhat} = 0.653$$

$$sL2_{\tau 2} := \left(dL2_{d\tau 2}^{2} \cdot s\tau 2^{2}\right)^{\frac{1}{2}}$$

$$sL2_{\tau 2} = 0.753$$

$$sL2_{Luhat} := \left(dL2_{dLuhat}^{2} \cdot sLuhat^{2}\right)^{\frac{1}{2}}$$

$$sL2_{Luhat} = 0.16$$

The cross term for the correlated variables Tau2 and Lu is:

$$xterm := \left[\rho_{\tau 2Lu} \cdot \left(dL2_{d\tau 2}\right) \cdot \left(dL2_{dLuhat}\right) \cdot s\tau 2 \cdot sLuhat\right]$$

$$xterm = -0.101$$

The total Beers error is expressed as:

$$sL2_{total} := \left(sL2_{\varepsilon}^{2} + sL2_{Lt}^{2} + sL2_{It}^{2} + sL2_{Es}^{2} + sL2_{\theta s}^{2} + sL2_{Ldhat}^{2} + sL2_{\tau 2}^{2} + sL2_{Luhat}^{2} + xterm\right)^{\frac{1}{2}}$$

$$sL2_{total} = 1.555$$

The starting values for the equation are as follows:

$\varepsilon := 0.702$ $\quad Lt := 32.15$ $\quad It := 1$ $\quad Es := 0.0$

$\theta s := .349066$ $\quad Ldhat := 8.5$ $\quad \tau 2 := 0.97$ $\quad Luhat := 0.90$

Case 2: Specular bounce to sky

$$L2 := (\varepsilon \cdot Lt + (It \cdot Es \cdot \cos(\theta s) + Ldhat) \cdot (1 - \varepsilon)) \cdot \tau 2 + Luhat$$

$$L2 = 25.249$$

The MAPLE symbolic processor in MathCad was used to calculate the following derivatives:

$$dL2_{d\varepsilon} := (Lt - It \cdot Es \cdot \cos(\theta s) - Ldhat) \cdot \tau 2$$

$$dL2_{dLt} := \varepsilon \cdot \tau 2$$

$$dL2_{dIt} := Es \cdot \cos(\theta s) \cdot (1 - \varepsilon) \cdot \tau 2$$

$$dL2_{dEs} := It \cdot \cos(\theta s) \cdot (1 - \varepsilon) \cdot \tau 2$$

$$dL2_{d\theta s} := -It \cdot Es \cdot \sin(\theta s) \cdot (1 - \varepsilon) \cdot \tau 2$$

$$dL2_{dLdhat} := (1 - \varepsilon) \cdot \tau 2$$

$$dL2_{d\tau 2} := \varepsilon \cdot Lt + (It \cdot Es \cdot \cos(\theta s) + Ldhat) \cdot (1 - \varepsilon)$$

$$dL2_{dLuhat} := 1$$

These derivatives are used to form the components of the Beers error calculation:

$s\varepsilon := 0.05$ $\quad sLt := 1.73$ $\quad sIt := 0$ $\quad sEs := 0$

$s\theta s := 0.1309$ $\quad sLdhat := 2.26$ $\quad s\tau 2 := 0.03$ $\quad sLuhat := 0.16$

$\rho_{\tau 2Lu} := -0.8381$

$$sL2_{\varepsilon} := \left(dL2_{d\varepsilon}^{2} \cdot s\varepsilon^{2}\right)^{\frac{1}{2}} \qquad sL2_{\varepsilon} = 1.147$$

$$sL2_{Lt} := \left(dL2_{dLt}^{2} \cdot sLt^{2}\right)^{\frac{1}{2}} \qquad sL2_{Lt} = 1.178$$

$$sL2_{It} := \left(dL2_{dIt}^{2} \cdot sIt^{2}\right)^{\frac{1}{2}}$$

$$sL2_{It} = 0$$

$$sL2_{Es} := \left(dL2_{dEs}^{2} \cdot sEs^{2}\right)^{\frac{1}{2}}$$

$$sL2_{Es} = 0$$

$$sL2_{\theta s} := \left(dL2_{d\theta s}^{2} \cdot s\theta s^{2}\right)^{\frac{1}{2}}$$

$$sL2_{\theta s} = 0$$

$$sL2_{Ldhat} := \left(dL2_{dLdhat}^{2} \cdot sLdhat^{2}\right)^{\frac{1}{2}}$$

$$sL2_{Ldhat} = 0.653$$

$$sL2_{\tau 2} := \left(dL2_{d\tau 2}^{2} \cdot s\tau 2^{2}\right)^{\frac{1}{2}}$$

$$sL2_{\tau 2} = 0.753$$

$$sL2_{Luhat} := \left(dL2_{dLuhat}^{2} \cdot sLuhat^{2}\right)^{\frac{1}{2}}$$

$$sL2_{Luhat} = 0.16$$

The cross term for the correlated variables Tau2 and Lu is:

$$xterm := \left[\rho_{\tau 2Lu} \cdot \left(dL2_{d\tau 2}\right) \cdot \left(dL2_{dLuhat}\right) \cdot s\tau 2 \cdot sLuhat\right]$$

$$xterm = -0.101$$

The total Beers error is expressed as:

$$sL2_{total} := \left(sL2_{\varepsilon}^{2} + sL2_{Lt}^{2} + sL2_{It}^{2} + sL2_{Es}^{2} + sL2_{\theta s}^{2} + sL2_{Ldhat}^{2} + sL2_{\tau 2}^{2} + sL2_{Luhat}^{2} + xterm\right)^{\frac{1}{2}}$$

$$sL2_{total} = 1.903$$

The starting values for the equation are as follows:

$\varepsilon := 0.702$ $\quad Lt := 32.15$ $\quad It := 1$ $\quad Es := 0.0$

$\theta s := .349066$ $\quad Ldhat := 8.5$ $\quad \tau 2 := 0.97$ $\quad Luhat := 0.90$

Case 2: Specular bounce to sky

$$L2 := (\varepsilon \cdot Lt + (It \cdot Es \cdot \cos(\theta s) + Ldhat) \cdot (1 - \varepsilon)) \cdot \tau 2 + Luhat$$

$$L2 = 25.249$$

The MAPLE symbolic processor in MathCad was used to calculate the following derivatives:

$$dL2_{d\varepsilon} := (Lt - It \cdot Es \cdot \cos(\theta s) - Ldhat) \cdot \tau 2$$

$$dL2_{dLt} := \varepsilon \cdot \tau 2$$

$$dL2_{dIt} := Es \cdot \cos(\theta s) \cdot (1 - \varepsilon) \cdot \tau 2$$

$$dL2_{dEs} := It \cdot \cos(\theta s) \cdot (1 - \varepsilon) \cdot \tau 2$$

$$dL2_{d\theta s} := -It \cdot Es \cdot \sin(\theta s) \cdot (1 - \varepsilon) \cdot \tau 2$$

$$dL2_{dLdhat} := (1 - \varepsilon) \cdot \tau 2$$

$$dL2_{d\tau 2} := \varepsilon \cdot Lt + (It \cdot Es \cdot \cos(\theta s) + Ldhat) \cdot (1 - \varepsilon)$$

$$dL2_{dLuhat} := 1$$

These derivatives are used to form the components of the Beers error calculation:

$s\varepsilon := 0.05$ $\quad sLt := 1.73$ $\quad sIt := 0$ $\quad sEs := 0$

$s\theta s := 0.1309$ $\quad sLdhat := 5.10$ $\quad s\tau 2 := 0.03$ $\quad sLuhat := 0.54$

$\rho_{\tau 2Lu} := -0.8381$

$$sL2_{\varepsilon} := \left(dL2_{d\varepsilon}^{\,2} \cdot s\varepsilon^{2}\right)^{\frac{1}{2}} \qquad sL2_{\varepsilon} = 1.147$$

$$sL2_{Lt} := \left(dL2_{dLt}^{\,2} \cdot sLt^{2}\right)^{\frac{1}{2}} \qquad sL2_{Lt} = 1.178$$

$$sL2_{It} := \left(dL2_{dIt}^{2} \cdot sIt^{2}\right)^{\frac{1}{2}}$$

$$sL2_{It} = 0$$

$$sL2_{Es} := \left(dL2_{dEs}^{2} \cdot sEs^{2}\right)^{\frac{1}{2}}$$

$$sL2_{Es} = 0$$

$$sL2_{\theta s} := \left(dL2_{d\theta s}^{2} \cdot s\theta s^{2}\right)^{\frac{1}{2}}$$

$$sL2_{\theta s} = 0$$

$$sL2_{Ldhat} := \left(dL2_{dLdhat}^{2} \cdot sLdhat^{2}\right)^{\frac{1}{2}}$$

$$sL2_{Ldhat} = 1.474$$

$$sL2_{\tau 2} := \left(dL2_{d\tau 2}^{2} \cdot s\tau 2^{2}\right)^{\frac{1}{2}}$$

$$sL2_{\tau 2} = 0.753$$

$$sL2_{Luhat} := \left(dL2_{dLuhat}^{2} \cdot sLuhat^{2}\right)^{\frac{1}{2}}$$

$$sL2_{Luhat} = 0.54$$

The cross term for the correlated variables Tau2 and Lu is:

$$xterm := \left[\rho_{\tau 2Lu} \cdot \left(dL2_{d\tau 2}\right) \cdot \left(dL2_{dLuhat}\right) \cdot s\tau 2 \cdot sLuhat\right]$$

$$xterm = -0.341$$

The total Beers error is expressed as:

$$sL2_{total} := \left(sL2_{\varepsilon}^{2} + sL2_{Lt}^{2} + sL2_{It}^{2} + sL2_{Es}^{2} + sL2_{\theta s}^{2} + sL2_{Ldhat}^{2} + sL2_{\tau 2}^{2} + sL2_{Luhat}^{2} + xterm\right)^{\frac{1}{2}}$$

$$sL2_{total} = 2.323$$

The starting values for the equation are as follows:

$\varepsilon := 0.702$ $\quad Lt := 32.15$ $\quad It := 1$ $\quad Es := 0.0$

$\theta s := .349066$ $\quad Ldhat := 8.5$ $\quad \tau 2 := 0.873$ $\quad Luhat := 3.533$

Case 2: Specular bounce to sky

$$L2 := (\varepsilon \cdot Lt + (It \cdot Es \cdot \cos(\theta s) + Ldhat) \cdot (1 - \varepsilon)) \cdot \tau 2 + Luhat$$

$$L2 = 25.447$$

The MAPLE symbolic processor in MathCad was used to calculate the following derivatives:

$$dL2_{d\varepsilon} := (Lt - It \cdot Es \cdot \cos(\theta s) - Ldhat) \cdot \tau 2$$

$$dL2_{dLt} := \varepsilon \cdot \tau 2$$

$$dL2_{dIt} := Es \cdot \cos(\theta s) \cdot (1 - \varepsilon) \cdot \tau 2$$

$$dL2_{dEs} := It \cdot \cos(\theta s) \cdot (1 - \varepsilon) \cdot \tau 2$$

$$dL2_{d\theta s} := -It \cdot Es \cdot \sin(\theta s) \cdot (1 - \varepsilon) \cdot \tau 2$$

$$dL2_{dLdhat} := (1 - \varepsilon) \cdot \tau 2$$

$$dL2_{d\tau 2} := \varepsilon \cdot Lt + (It \cdot Es \cdot \cos(\theta s) + Ldhat) \cdot (1 - \varepsilon)$$

$$dL2_{dLuhat} := 1$$

These derivatives are used to form the components of the Beers error calculation:

$s\varepsilon := 0.025$ $\quad sLt := 0.09$ $\quad sIt := 0$ $\quad sEs := 0$

$s\theta s := 0.05236$ $\quad sLdhat := 0.25$ $\quad s\tau 2 := 0.03$ $\quad sLuhat := 0.07$

$\rho_{\tau 2Lu} := -0.8381$

$$sL2_{\varepsilon} := \left(dL2_{d\varepsilon}^{2} \cdot s\varepsilon^{2}\right)^{\frac{1}{2}} \qquad sL2_{\varepsilon} = 0.516$$

$$sL2_{Lt} := \left(dL2_{dLt}^{2} \cdot sLt^{2}\right)^{\frac{1}{2}} \qquad sL2_{Lt} = 0.055$$

$$sL2_{It} := \left(dL2_{dIt}^{2} \cdot sIt^{2}\right)^{\frac{1}{2}}$$

$$sL2_{It} = 0$$

$$sL2_{Es} := \left(dL2_{dEs}^{2} \cdot sEs^{2}\right)^{\frac{1}{2}}$$

$$sL2_{Es} = 0$$

$$sL2_{\theta s} := \left(dL2_{d\theta s}^{2} \cdot s\theta s^{2}\right)^{\frac{1}{2}}$$

$$sL2_{\theta s} = 0$$

$$sL2_{Ldhat} := \left(dL2_{dLdhat}^{2} \cdot sLdhat^{2}\right)^{\frac{1}{2}}$$

$$sL2_{Ldhat} = 0.065$$

$$sL2_{\tau 2} := \left(dL2_{d\tau 2}^{2} \cdot s\tau 2^{2}\right)^{\frac{1}{2}}$$

$$sL2_{\tau 2} = 0.753$$

$$sL2_{Luhat} := \left(dL2_{dLuhat}^{2} \cdot sLuhat^{2}\right)^{\frac{1}{2}}$$

$$sL2_{Luhat} = 0.07$$

The cross term for the correlated variables Tau2 and Lu is:

$$xterm := \left[\rho_{\tau 2Lu} \cdot \left(dL2_{d\tau 2}\right) \cdot \left(dL2_{dLuhat}\right) \cdot s\tau 2 \cdot sLuhat\right]$$

$$xterm = -0.044$$

The total Beers error is expressed as:

$$sL1_{part1} := sL2_{\varepsilon}^{2} + sL2_{Lt}^{2} + sL2_{It}^{2} + sL2_{Es}^{2} + sL2_{\theta s}^{2}$$

$$sL1_{part2} := sL2_{Ldhat}^{2} + sL2_{\tau 2}^{2} + sL2_{Luhat}^{2} + xterm$$

$$sL1_{total} := \left(sL1_{part1} + sL1_{part2}\right)^{\frac{1}{2}}$$

$$sL1_{total} = 0.895$$

The starting values for the equation are as follows:

$\varepsilon := 0.702$ $\quad Lt := 32.15$ $\quad It := 1$ $\quad Es := 0.0$

$\theta s := .349066$ $\quad Ldhat := 8.5$ $\quad \tau 2 := 0.873$ $\quad Luhat := 3.533$

Case 2: Specular bounce to sky

$$L2 := (\varepsilon \cdot Lt + (It \cdot Es \cdot \cos(\theta s) + Ldhat) \cdot (1 - \varepsilon)) \cdot \tau 2 + Luhat$$

$$L2 = 25.447$$

The MAPLE symbolic processor in MathCad was used to calculate the following derivatives:

$$dL2_{d\varepsilon} := (Lt - It \cdot Es \cdot \cos(\theta s) - Ldhat) \cdot \tau 2$$

$$dL2_{dLt} := \varepsilon \cdot \tau 2$$

$$dL2_{dIt} := Es \cdot \cos(\theta s) \cdot (1 - \varepsilon) \cdot \tau 2$$

$$dL2_{dEs} := It \cdot \cos(\theta s) \cdot (1 - \varepsilon) \cdot \tau 2$$

$$dL2_{d\theta s} := -It \cdot Es \cdot \sin(\theta s) \cdot (1 - \varepsilon) \cdot \tau 2$$

$$dL2_{dLdhat} := (1 - \varepsilon) \cdot \tau 2$$

$$dL2_{d\tau 2} := \varepsilon \cdot Lt + (It \cdot Es \cdot \cos(\theta s) + Ldhat) \cdot (1 - \varepsilon)$$

$$dL2_{dLuhat} := 1$$

These derivatives are used to form the components of the Beers error calculation:

$s\varepsilon := 0.05$ $\quad sLt := 0.63$ $\quad sIt := 0$ $\quad sEs := 0$

$s\theta s := 0.1309$ $\quad sLdhat := 2.26$ $\quad s\tau 2 := 0.03$ $\quad sLuhat := 0.636$

$\rho_{\tau 2Lu} := -0.8381$

$$sL2_{\varepsilon} := \left(dL2_{d\varepsilon}^{\,2} \cdot s\varepsilon^{2}\right)^{\frac{1}{2}} \qquad sL2_{\varepsilon} = 1.032$$

$$sL2_{Lt} := \left(dL2_{dLt}^{\,2} \cdot sLt^{2}\right)^{\frac{1}{2}} \qquad sL2_{Lt} = 0.386$$

$$sL2_{It} := \left(dL2_{dIt}^{2} \cdot sIt^{2}\right)^{\frac{1}{2}}$$

$$sL2_{It} = 0$$

$$sL2_{Es} := \left(dL2_{dEs}^{2} \cdot sEs^{2}\right)^{\frac{1}{2}}$$

$$sL2_{Es} = 0$$

$$sL2_{\theta s} := \left(dL2_{d\theta s}^{2} \cdot s\theta s^{2}\right)^{\frac{1}{2}}$$

$$sL2_{\theta s} = 0$$

$$sL2_{Ldhat} := \left(dL2_{dLdhat}^{2} \cdot sLdhat^{2}\right)^{\frac{1}{2}}$$

$$sL2_{Ldhat} = 0.588$$

$$sL2_{\tau 2} := \left(dL2_{d\tau 2}^{2} \cdot s\tau 2^{2}\right)^{\frac{1}{2}}$$

$$sL2_{\tau 2} = 0.753$$

$$sL2_{Luhat} := \left(dL2_{dLuhat}^{2} \cdot sLuhat^{2}\right)^{\frac{1}{2}}$$

$$sL2_{Luhat} = 0.636$$

The cross term for the correlated variables Tau2 and Lu is:

$$xterm := \left[\rho_{\tau 2Lu} \cdot \left(dL2_{d\tau 2}\right) \cdot \left(dL2_{dLuhat}\right) \cdot s\tau 2 \cdot sLuhat\right] \qquad xterm = -0.401$$

The total Beers error is expressed as:

$$sL1_{part1} := sL2_{\varepsilon}^{2} + sL2_{Lt}^{2} + sL2_{It}^{2} + sL2_{Es}^{2} + sL2_{\theta s}^{2}$$

$$sL1_{part2} := sL2_{Ldhat}^{2} + sL2_{\tau 2}^{2} + sL2_{Luhat}^{2} + xterm$$

$$sL1_{total} := \left(sL1_{part1} + sL1_{part2}\right)^{\frac{1}{2}}$$

$$sL1_{total} = 1.46$$

The starting values for the equation are as follows:

$\varepsilon := 0.702$ $\quad Lt := 32.15$ $\quad It := 1$ $\quad Es := 0.0$

$\theta s := .349066$ $\quad Ldhat := 8.5$ $\quad \tau 2 := 0.873$ $\quad Luhat := 3.533$

Case 2: Specular bounce to sky

$$L2 := (\varepsilon \cdot Lt + (It \cdot Es \cdot \cos(\theta s) + Ldhat) \cdot (1 - \varepsilon)) \cdot \tau 2 + Luhat$$

$$L2 = 25.447$$

The MAPLE symbolic processor in MathCad was used to calculate the following derivatives:

$$dL2_{d\varepsilon} := (Lt - It \cdot Es \cdot \cos(\theta s) - Ldhat) \cdot \tau 2$$

$$dL2_{dLt} := \varepsilon \cdot \tau 2$$

$$dL2_{dIt} := Es \cdot \cos(\theta s) \cdot (1 - \varepsilon) \cdot \tau 2$$

$$dL2_{dEs} := It \cdot \cos(\theta s) \cdot (1 - \varepsilon) \cdot \tau 2$$

$$dL2_{d\theta s} := -It \cdot Es \cdot \sin(\theta s) \cdot (1 - \varepsilon) \cdot \tau 2$$

$$dL2_{dLdhat} := (1 - \varepsilon) \cdot \tau 2$$

$$dL2_{d\tau 2} := \varepsilon \cdot Lt + (It \cdot Es \cdot \cos(\theta s) + Ldhat) \cdot (1 - \varepsilon)$$

$$dL2_{dLuhat} := 1$$

These derivatives are used to form the components of the Beers error calculation:

$s\varepsilon := 0.05$ $\quad sLt := 1.73$ $\quad sIt := 0$ $\quad sEs := 0$

$s\theta s := 0.1309$ $\quad sLdhat := 2.26$ $\quad s\tau 2 := 0.03$ $\quad sLuhat := 0.636$

$\rho_{\tau 2Lu} := -0.8381$

$$sL2_{\varepsilon} := \left(dL2_{d\varepsilon}^{2} \cdot s\varepsilon^{2}\right)^{\frac{1}{2}} \qquad sL2_{\varepsilon} = 1.032$$

$$sL2_{Lt} := \left(dL2_{dLt}^{2} \cdot sLt^{2}\right)^{\frac{1}{2}} \qquad sL2_{Lt} = 1.06$$

$sL2_{It} := \left(dL2_{dIt}^{2} \cdot sIt^{2}\right)^{\frac{1}{2}}$

$sL2_{It} = 0$

$sL2_{Es} := \left(dL2_{dEs}^{2} \cdot sEs^{2}\right)^{\frac{1}{2}}$

$sL2_{Es} = 0$

$sL2_{\theta s} := \left(dL2_{d\theta s}^{2} \cdot s\theta s^{2}\right)^{\frac{1}{2}}$

$sL2_{\theta s} = 0$

$sL2_{Ldhat} := \left(dL2_{dLdhat}^{2} \cdot sLdhat^{2}\right)^{\frac{1}{2}}$

$sL2_{Ldhat} = 0.588$

$sL2_{\tau 2} := \left(dL2_{d\tau 2}^{2} \cdot s\tau 2^{2}\right)^{\frac{1}{2}}$

$sL2_{\tau 2} = 0.753$

$sL2_{Luhat} := \left(dL2_{dLuhat}^{2} \cdot sLuhat^{2}\right)^{\frac{1}{2}}$

$sL2_{Luhat} = 0.636$

The cross term for the correlated variables Tau2 and Lu is:

$xterm := \left[\rho_{\tau 2Lu} \cdot \left(dL2_{d\tau 2}\right) \cdot \left(dL2_{dLuhat}\right) \cdot s\tau 2 \cdot sLuhat\right]$ $\quad xterm = -0.401$

The total Beers error is expressed as:

$sL1_{part1} := sL2_{\varepsilon}^{2} + sL2_{Lt}^{2} + sL2_{It}^{2} + sL2_{Es}^{2} + sL2_{\theta s}^{2}$

$sL1_{part2} := sL2_{Ldhat}^{2} + sL2_{\tau 2}^{2} + sL2_{Luhat}^{2} + xterm$

$sL1_{total} := \left(sL1_{part1} + sL1_{part2}\right)^{\frac{1}{2}}$

$sL1_{total} = 1.762$

The starting values for the equation are as follows:

$\varepsilon := 0.702$ $\quad Lt := 32.15$ $\quad It := 1$ $\quad Es := 0.0$

$\theta s := .349066$ $\quad Ldhat := 8.5$ $\quad \tau 2 := 0.873$ $\quad Luhat := 3.533$

Case 2: Specular bounce to sky

$$L2 := (\varepsilon \cdot Lt + (It \cdot Es \cdot \cos(\theta s) + Ldhat) \cdot (1 - \varepsilon)) \cdot \tau 2 + Luhat$$

$$L2 = 25.447$$

The MAPLE symbolic processor in MathCad was used to calculate the following derivatives:

$$dL2_{d\varepsilon} := (Lt - It \cdot Es \cdot \cos(\theta s) - Ldhat) \cdot \tau 2$$

$$dL2_{dLt} := \varepsilon \cdot \tau 2$$

$$dL2_{dIt} := Es \cdot \cos(\theta s) \cdot (1 - \varepsilon) \cdot \tau 2$$

$$dL2_{dEs} := It \cdot \cos(\theta s) \cdot (1 - \varepsilon) \cdot \tau 2$$

$$dL2_{d\theta s} := -It \cdot Es \cdot \sin(\theta s) \cdot (1 - \varepsilon) \cdot \tau 2$$

$$dL2_{dLdhat} := (1 - \varepsilon) \cdot \tau 2$$

$$dL2_{d\tau 2} := \varepsilon \cdot Lt + (It \cdot Es \cdot \cos(\theta s) + Ldhat) \cdot (1 - \varepsilon)$$

$$dL2_{dLuhat} := 1$$

These derivatives are used to form the components of the Beers error calculation:

$s\varepsilon := 0.05$ $\quad sLt := 1.73$ $\quad sIt := 0$ $\quad sEs := 0$

$s\theta s := 0.1309$ $\quad sLdhat := 5.10$ $\quad s\tau 2 := 0.03$ $\quad sLuhat := 2.120$

$\rho_{\tau 2Lu} := -0.8381$

$$sL2_{\varepsilon} := \left(dL2_{d\varepsilon}^{2} \cdot s\varepsilon^{2}\right)^{\frac{1}{2}} \qquad sL2_{\varepsilon} = 1.032$$

$$sL2_{Lt} := \left(dL2_{dLt}^{2} \cdot sLt^{2}\right)^{\frac{1}{2}} \qquad sL2_{Lt} = 1.060$$

$sL2_{It} := \left(dL2_{dIt}^{2} \cdot sIt^{2}\right)^{\frac{1}{2}}$

$sL2_{It} = 0$

$sL2_{Es} := \left(dL2_{dEs}^{2} \cdot sEs^{2}\right)^{\frac{1}{2}}$

$sL2_{Es} = 0$

$sL2_{\theta s} := \left(dL2_{d\theta s}^{2} \cdot s\theta s^{2}\right)^{\frac{1}{2}}$

$sL2_{\theta s} = 0$

$sL2_{Ldhat} := \left(dL2_{dLdhat}^{2} \cdot sLdhat^{2}\right)^{\frac{1}{2}}$

$sL2_{Ldhat} = 1.327$

$sL2_{\tau 2} := \left(dL2_{d\tau 2}^{2} \cdot s\tau 2^{2}\right)^{\frac{1}{2}}$

$sL2_{\tau 2} = 0.753$

$sL2_{Luhat} := \left(dL2_{dLuhat}^{2} \cdot sLuhat^{2}\right)^{\frac{1}{2}}$

$sL2_{Luhat} = 2.12$

The cross term for the correlated variables Tau2 and Lu is:

$xterm := \left[\rho_{\tau 2Lu} \cdot \left(dL2_{d\tau 2}\right) \cdot \left(dL2_{dLuhat}\right) \cdot s\tau 2 \cdot sLuhat\right]$

$xterm = -1.338$

The total Beers error is expressed as:

$sL1_{part1} := sL2_{\varepsilon}^{2} + sL2_{Lt}^{2} + sL2_{It}^{2} + sL2_{Es}^{2} + sL2_{\theta s}^{2}$

$sL1_{part2} := sL2_{Ldhat}^{2} + sL2_{\tau 2}^{2} + sL2_{Luhat}^{2} + xterm$

$sL1_{total} := \left(sL1_{part1} + sL1_{part2}\right)^{\frac{1}{2}}$

$sL1_{total} = 2.77$

Ray_Interaction Type 3
Specular Bounce to Background (Asphalt to Car)

Rooftop Simulation
Error Type: I

The starting values for the equation are as follows:

$\varepsilon := 0.916$	$Lt := 39.47$	$\theta s := 0.785398$	$It := 1$
$\varepsilon b := 0.939$	$Ltb := 55.69$	$\theta b := 0.785398$	$Ib := 1$
$Es := 0.0$	$\tau 2 := 0.97$	$Lu := 0.90$	

Case 3: Specular bounce to background

$$L3 := (\varepsilon \cdot Lt + (It \cdot Es \cdot \cos(\theta s) + \varepsilon b \cdot Ltb + Ib \cdot Es \cdot \cos(\theta b) \cdot (1 - \varepsilon b)) \cdot (1 - \varepsilon)) \cdot \tau 2 + Lu$$

$$L3 = 40.231$$

The MAPLE symbolic processor in MathCad was used to calculate the following derivatives:

$$dL3_{d\varepsilon} := (Lt - It \cdot Es \cdot \cos(\theta s) - \varepsilon b \cdot Ltb - Ib \cdot Es \cdot \cos(\theta b) \cdot (1 - \varepsilon b)) \cdot \tau 2$$

$$dL3_{dLt} := \varepsilon \cdot \tau 2$$

$$dL3_{dIt} := Es \cdot \cos(\theta s) \cdot (1 - \varepsilon) \cdot \tau 2$$

$$dL3_{dEs} := (It \cdot \cos(\theta s) + Ib \cdot \cos(\theta b) \cdot (1 - \varepsilon b)) \cdot (1 - \varepsilon) \cdot \tau 2$$

$$dL3_{d\theta s} := -It \cdot Es \cdot \sin(\theta s) \cdot (1 - \varepsilon) \cdot \tau 2$$

$$dL3_{d\varepsilon b} := (Ltb - Ib \cdot Es \cdot \cos(\theta b)) \cdot (1 - \varepsilon) \cdot \tau 2$$

$$dL3_{dLtb} := \varepsilon b \cdot (1 - \varepsilon) \cdot \tau 2$$

$$dL3_{dIb} := Es \cdot \cos(\theta b) \cdot (1 - \varepsilon b) \cdot (1 - \varepsilon) \cdot \tau 2$$

$$dL3_{d\theta b} := -Ib \cdot Es \cdot \sin(\theta b) \cdot (1 - \varepsilon b) \cdot (1 - \varepsilon) \cdot \tau 2$$

$$dL3_{d\tau 2} := \varepsilon \cdot Lt + (It \cdot Es \cdot \cos(\theta s) + \varepsilon b \cdot Ltb + Ib \cdot Es \cdot \cos(\theta b) \cdot (1 - \varepsilon b)) \cdot (1 - \varepsilon)$$

$$dL3_{dLu} := 1$$

These derivatives are used to form the components of the Beers error calculation:

$s\varepsilon := 0.025$	$sLt := 0.09$	$sIt := 0$	$s\theta s := 0.05236$
$s\varepsilon b := 0.025$	$sLtb := 0.09$	$sIb := 0$	$s\theta b := 0.05236$
$sEs := 0.0$	$s\tau 2 := 0.03$	$sLu := 0.02$	$\rho_{\tau 2Lu} := -0.8381$

$sL3_{\varepsilon} := \left(dL3_{d\varepsilon}{}^{2} \cdot s\varepsilon^{2}\right)^{\frac{1}{2}}$ $\qquad sL3_{\varepsilon} = 0.311$

$sL3_{Lt} := \left(dL3_{dLt}{}^{2} \cdot sLt^{2}\right)^{\frac{1}{2}}$ $\qquad sL3_{Lt} = 0.08$

$sL3_{It} := \left(dL3_{dIt}{}^{2} \cdot sIt^{2}\right)^{\frac{1}{2}}$ $\qquad sL3_{It} = 0$

$sL3_{Es} := \left(dL3_{dEs}{}^{2} \cdot sEs^{2}\right)^{\frac{1}{2}}$ $\qquad sL3_{Es} = 0$

$sL3_{\theta s} := \left(dL3_{d\theta s}{}^{2} \cdot s\theta s^{2}\right)^{\frac{1}{2}}$ $\qquad sL3_{\theta s} = 0$

$sL3_{\varepsilon b} := \left(dL3_{d\varepsilon b}{}^{2} \cdot s\varepsilon b^{2}\right)^{\frac{1}{2}}$ $\qquad sL3_{\varepsilon b} = 0.113$

$sL3_{Ltb} := \left(dL3_{dLtb}{}^{2} \cdot sLtb^{2}\right)^{\frac{1}{2}}$ $\qquad sL3_{Ltb} = 0.007$

$sL3_{Ib} := \left(dL3_{dIb}{}^{2} \cdot sIb^{2}\right)^{\frac{1}{2}}$ $\qquad sL3_{Ib} = 0$

$sL3_{\theta b} := \left(dL3_{d\theta b}{}^{2} \cdot s\theta b^{2}\right)^{\frac{1}{2}}$ $\qquad sL3_{\theta b} = 0$

$sL3_{\tau 2} := \left(dL3_{d\tau 2}{}^{2} \cdot s\tau 2^{2}\right)^{\frac{1}{2}}$ $\qquad sL3_{\tau 2} = 1.216$

$sL3_{Lu} := \left(dL3_{dLu}{}^{2} \cdot sLu^{2}\right)^{\frac{1}{2}}$ $\qquad sL3_{Lu} = 0.02$

The cross term of the correlated variables Tau2 and Lu is:

$xterm := \left[\rho_{\tau 2Lu} \cdot \left(dL3_{d\tau 2}\right) \cdot \left(dL3_{dLu}\right) \cdot s\tau 2 \cdot sLu\right]$ $\qquad xterm = -0.02$

The total Beers error is expressed as:

$sL3_{part1} := sL3_{\varepsilon}{}^{2} + sL3_{Lt}{}^{2} + sL3_{It}{}^{2} + sL3_{Es}{}^{2} + sL3_{\theta s}{}^{2} + sL3_{\varepsilon b}{}^{2}$

$sL3_{part2} := sL3_{Ltb}{}^{2} + sL3_{Ib}{}^{2} + sL3_{\theta b}{}^{2} + sL3_{\tau 2}{}^{2} + sL3_{Lu}{}^{2} + xterm$

$sL3_{total} := \left(sL3_{part1} + sL3_{part2}\right)^{\frac{1}{2}}$

$sL3_{total} = 1.255$

The starting values for the equation are as follows:

$\varepsilon := 0.916$	$Lt := 39.47$	$\theta s := 0.785398$	$It := 1$
$\varepsilon b := 0.939$	$Ltb := 55.69$	$\theta b := 0.785398$	$Ib := 1$
$Es := 0.0$	$\tau 2 := 0.97$	$Lu := 0.90$	

Case 3: Specular bounce to background

$$L3 := (\varepsilon \cdot Lt + (It \cdot Es \cdot \cos(\theta s) + \varepsilon b \cdot Ltb + Ib \cdot Es \cdot \cos(\theta b) \cdot (1 - \varepsilon b)) \cdot (1 - \varepsilon)) \cdot \tau 2 + Lu$$

$$L3 = 40.231$$

The MAPLE symbolic processor in MathCad was used to calculate the following derivatives:

$$dL3_{d\varepsilon} := (Lt - It \cdot Es \cdot \cos(\theta s) - \varepsilon b \cdot Ltb - Ib \cdot Es \cdot \cos(\theta b) \cdot (1 - \varepsilon b)) \cdot \tau 2$$

$$dL3_{dLt} := \varepsilon \cdot \tau 2$$

$$dL3_{dIt} := Es \cdot \cos(\theta s) \cdot (1 - \varepsilon) \cdot \tau 2$$

$$dL3_{dEs} := (It \cdot \cos(\theta s) + Ib \cdot \cos(\theta b) \cdot (1 - \varepsilon b)) \cdot (1 - \varepsilon) \cdot \tau 2$$

$$dL3_{d\theta s} := -It \cdot Es \cdot \sin(\theta s) \cdot (1 - \varepsilon) \cdot \tau 2$$

$$dL3_{d\varepsilon b} := (Ltb - Ib \cdot Es \cdot \cos(\theta b)) \cdot (1 - \varepsilon) \cdot \tau 2$$

$$dL3_{dLtb} := \varepsilon b \cdot (1 - \varepsilon) \cdot \tau 2$$

$$dL3_{dIb} := Es \cdot \cos(\theta b) \cdot (1 - \varepsilon b) \cdot (1 - \varepsilon) \cdot \tau 2$$

$$dL3_{d\theta b} := -Ib \cdot Es \cdot \sin(\theta b) \cdot (1 - \varepsilon b) \cdot (1 - \varepsilon) \cdot \tau 2$$

$$dL3_{d\tau 2} := \varepsilon \cdot Lt + (It \cdot Es \cdot \cos(\theta s) + \varepsilon b \cdot Ltb + Ib \cdot Es \cdot \cos(\theta b) \cdot (1 - \varepsilon b)) \cdot (1 - \varepsilon)$$

$$dL3_{dLu} := 1$$

These derivatives are used to form the components of the Beers error calculation:

$s\varepsilon := 0.05$	$sLt := 0.63$	$sIt := 0$	$s\theta s := 0.1309$
$s\varepsilon b := 0.05$	$sLtb := 0.63$	$sIb := 0$	$s\theta b := 0.1309$
$sEs := 0.0$	$s\tau 2 := 0.03$	$sLu := 0.16$	$\rho_{\tau 2Lu} := -0.8381$

$$sL3_{\varepsilon} := \left(dL3_{d\varepsilon}^{2} \cdot s\varepsilon^{2}\right)^{\frac{1}{2}}$$

$$sL3_{\varepsilon} = 0.622$$

$$sL3_{Lt} := \left(dL3_{dLt}^{2} \cdot sLt^{2}\right)^{\frac{1}{2}}$$

$$sL3_{Lt} = 0.56$$

$$sL3_{It} := \left(dL3_{dIt}^{2} \cdot sIt^{2}\right)^{\frac{1}{2}}$$

$$sL3_{It} = 0$$

$$sL3_{Es} := \left(dL3_{dEs}^{2} \cdot sEs^{2}\right)^{\frac{1}{2}}$$

$$sL3_{Es} = 0$$

$$sL3_{\theta s} := \left(dL3_{d\theta s}^{2} \cdot s\theta s^{2}\right)^{\frac{1}{2}}$$

$$sL3_{\theta s} = 0$$

$$sL3_{\varepsilon b} := \left(dL3_{d\varepsilon b}^{2} \cdot s\varepsilon b^{2}\right)^{\frac{1}{2}}$$

$$sL3_{\varepsilon b} = 0.227$$

$$sL3_{Ltb} := \left(dL3_{dLtb}^{2} \cdot sLtb^{2}\right)^{\frac{1}{2}}$$

$$sL3_{Ltb} = 0.048$$

$$sL3_{Ib} := \left(dL3_{dIb}^{2} \cdot sIb^{2}\right)^{\frac{1}{2}}$$

$$sL3_{Ib} = 0$$

$$sL3_{\theta b} := \left(dL3_{d\theta b}^{2} \cdot s\theta b^{2}\right)^{\frac{1}{2}}$$

$$sL3_{\theta b} = 0$$

$$sL3_{\tau 2} := \left(dL3_{d\tau 2}^{2} \cdot s\tau 2^{2}\right)^{\frac{1}{2}}$$

$$sL3_{\tau 2} = 1.216$$

$$sL3_{Lu} := \left(dL3_{dLu}^{2} \cdot sLu^{2}\right)^{\frac{1}{2}}$$

$$sL3_{Lu} = 0.16$$

The cross term of the correlated variables Tau2 and Lu is:

$$xterm := \left[\rho_{\tau 2Lu} \cdot \left(dL3_{d\tau 2}\right) \cdot \left(dL3_{dLu}\right) \cdot s\tau 2 \cdot sLu\right]$$

$$xterm = -0.163$$

The total Beers error is expressed as:

$$sL3_{part1} := sL3_{\varepsilon}^{2} + sL3_{Lt}^{2} + sL3_{It}^{2} + sL3_{Es}^{2} + sL3_{\theta s}^{2} + sL3_{\varepsilon b}^{2}$$

$$sL3_{part2} := sL3_{Ltb}^{2} + sL3_{Ib}^{2} + sL3_{\theta b}^{2} + sL3_{\tau 2}^{2} + sL3_{Lu}^{2} + xterm$$

$$sL3_{total} := \left(sL3_{part1} + sL3_{part2}\right)^{\frac{1}{2}}$$

$$sL3_{total} = 1.448$$

The starting values for the equation are as follows:

$\varepsilon := 0.916$	$Lt := 39.47$	$\theta s := 0.785398$	$It := 1$
$\varepsilon b := 0.939$	$Ltb := 55.69$	$\theta b := 0.785398$	$Ib := 1$
$Es := 0.0$	$\tau 2 := 0.97$	$Lu := 0.90$	

Case 3: Specular bounce to background

$$L3 := (\varepsilon \cdot Lt + (It \cdot Es \cdot \cos(\theta s) + \varepsilon b \cdot Ltb + Ib \cdot Es \cdot \cos(\theta b) \cdot (1 - \varepsilon b)) \cdot (1 - \varepsilon)) \cdot \tau 2 + Lu$$

$$L3 = 40.231$$

The MAPLE symbolic processor in MathCad was used to calculate the following derivatives:

$$dL3_{d\varepsilon} := (Lt - It \cdot Es \cdot \cos(\theta s) - \varepsilon b \cdot Ltb - Ib \cdot Es \cdot \cos(\theta b) \cdot (1 - \varepsilon b)) \cdot \tau 2$$

$$dL3_{dLt} := \varepsilon \cdot \tau 2$$

$$dL3_{dIt} := Es \cdot \cos(\theta s) \cdot (1 - \varepsilon) \cdot \tau 2$$

$$dL3_{dEs} := (It \cdot \cos(\theta s) + Ib \cdot \cos(\theta b) \cdot (1 - \varepsilon b)) \cdot (1 - \varepsilon) \cdot \tau 2$$

$$dL3_{d\theta s} := -It \cdot Es \cdot \sin(\theta s) \cdot (1 - \varepsilon) \cdot \tau 2$$

$$dL3_{d\varepsilon b} := (Ltb - Ib \cdot Es \cdot \cos(\theta b)) \cdot (1 - \varepsilon) \cdot \tau 2$$

$$dL3_{dLtb} := \varepsilon b \cdot (1 - \varepsilon) \cdot \tau 2$$

$$dL3_{dIb} := Es \cdot \cos(\theta b) \cdot (1 - \varepsilon b) \cdot (1 - \varepsilon) \cdot \tau 2$$

$$dL3_{d\theta b} := -Ib \cdot Es \cdot \sin(\theta b) \cdot (1 - \varepsilon b) \cdot (1 - \varepsilon) \cdot \tau 2$$

$$dL3_{d\tau 2} := \varepsilon \cdot Lt + (It \cdot Es \cdot \cos(\theta s) + \varepsilon b \cdot Ltb + Ib \cdot Es \cdot \cos(\theta b) \cdot (1 - \varepsilon b)) \cdot (1 - \varepsilon)$$

$$dL3_{dLu} := 1$$

These derivatives are used to form the components of the Beers error calculation:

$s\varepsilon := 0.05$	$sLt := 1.73$	$sIt := 0$	$s\theta s := 0.1309$
$s\varepsilon b := 0.05$	$sLtb := 1.73$	$sIb := 0$	$s\theta b := 0.1309$
$sEs := 0.0$	$s\tau 2 := 0.03$	$sLu := 0.16$	$\rho_{\tau 2Lu} := -0.8381$

$$sL3_{\varepsilon} := \left(dL3_{d\varepsilon}^{2} \cdot s\varepsilon^{2}\right)^{\frac{1}{2}} \qquad sL3_{\varepsilon} = 0.622$$

$$sL3_{Lt} := \left(dL3_{dLt}^{2} \cdot sLt^{2}\right)^{\frac{1}{2}} \qquad sL3_{Lt} = 1.537$$

$$sL3_{It} := \left(dL3_{dIt}^{2} \cdot sIt^{2}\right)^{\frac{1}{2}} \qquad sL3_{It} = 0$$

$$sL3_{Es} := \left(dL3_{dEs}^{2} \cdot sEs^{2}\right)^{\frac{1}{2}} \qquad sL3_{Es} = 0$$

$$sL3_{\theta s} := \left(dL3_{d\theta s}^{2} \cdot s\theta s^{2}\right)^{\frac{1}{2}} \qquad sL3_{\theta s} = 0$$

$$sL3_{\varepsilon b} := \left(dL3_{d\varepsilon b}^{2} \cdot s\varepsilon b^{2}\right)^{\frac{1}{2}} \qquad sL3_{\varepsilon b} = 0.227$$

$$sL3_{Ltb} := \left(dL3_{dLtb}^{2} \cdot sLtb^{2}\right)^{\frac{1}{2}} \qquad sL3_{Ltb} = 0.132$$

$$sL3_{Ib} := \left(dL3_{dIb}^{2} \cdot sIb^{2}\right)^{\frac{1}{2}} \qquad sL3_{Ib} = 0$$

$$sL3_{\theta b} := \left(dL3_{d\theta b}^{2} \cdot s\theta b^{2}\right)^{\frac{1}{2}} \qquad sL3_{\theta b} = 0$$

$$sL3_{\tau 2} := \left(dL3_{d\tau 2}^{2} \cdot s\tau 2^{2}\right)^{\frac{1}{2}} \qquad sL3_{\tau 2} = 1.216$$

$$sL3_{Lu} := \left(dL3_{dLu}^{2} \cdot sLu^{2}\right)^{\frac{1}{2}} \qquad sL3_{Lu} = 0.16$$

The cross term of the correlated variables Tau2 and Lu is:

$$xterm := \left[\rho_{\tau 2Lu} \cdot \left(dL3_{d\tau 2}\right) \cdot \left(dL3_{dLu}\right) \cdot s\tau 2 \cdot sLu\right] \qquad xterm = -0.163$$

The total Beers error is expressed as:

$$sL3_{part1} := sL3_{\varepsilon}^{2} + sL3_{Lt}^{2} + sL3_{It}^{2} + sL3_{Es}^{2} + sL3_{\theta s}^{2} + sL3_{\varepsilon b}^{2}$$

$$sL3_{part2} := sL3_{Ltb}^{2} + sL3_{Ib}^{2} + sL3_{\theta b}^{2} + sL3_{\tau 2}^{2} + sL3_{Lu}^{2} + xterm$$

$$sL3_{total} := \left(sL3_{part1} + sL3_{part2}\right)^{\frac{1}{2}}$$

$$sL3_{total} = 2.04$$

The starting values for the equation are as follows:

$\varepsilon := 0.916$	$Lt := 39.47$	$\theta s := 0.785398$	$It := 1$
$\varepsilon b := 0.939$	$Ltb := 55.69$	$\theta b := 0.785398$	$Ib := 1$
$Es := 0.0$	$\tau 2 := 0.97$	$Lu := 0.90$	

Case 3: Specular bounce to background

$$L3 := (\varepsilon \cdot Lt + (It \cdot Es \cdot \cos(\theta s) + \varepsilon b \cdot Ltb + Ib \cdot Es \cdot \cos(\theta b) \cdot (1 - \varepsilon b)) \cdot (1 - \varepsilon)) \cdot \tau 2 + Lu$$

$$L3 = 40.231$$

The MAPLE symbolic processor in MathCad was used to calculate the following derivatives:

$$dL3_{d\varepsilon} := (Lt - It \cdot Es \cdot \cos(\theta s) - \varepsilon b \cdot Ltb - Ib \cdot Es \cdot \cos(\theta b) \cdot (1 - \varepsilon b)) \cdot \tau 2$$

$$dL3_{dLt} := \varepsilon \cdot \tau 2$$

$$dL3_{dIt} := Es \cdot \cos(\theta s) \cdot (1 - \varepsilon) \cdot \tau 2$$

$$dL3_{dEs} := (It \cdot \cos(\theta s) + Ib \cdot \cos(\theta b) \cdot (1 - \varepsilon b)) \cdot (1 - \varepsilon) \cdot \tau 2$$

$$dL3_{d\theta s} := -It \cdot Es \cdot \sin(\theta s) \cdot (1 - \varepsilon) \cdot \tau 2$$

$$dL3_{d\varepsilon b} := (Ltb - Ib \cdot Es \cdot \cos(\theta b)) \cdot (1 - \varepsilon) \cdot \tau 2$$

$$dL3_{dLtb} := \varepsilon b \cdot (1 - \varepsilon) \cdot \tau 2$$

$$dL3_{dIb} := Es \cdot \cos(\theta b) \cdot (1 - \varepsilon b) \cdot (1 - \varepsilon) \cdot \tau 2$$

$$dL3_{d\theta b} := -Ib \cdot Es \cdot \sin(\theta b) \cdot (1 - \varepsilon b) \cdot (1 - \varepsilon) \cdot \tau 2$$

$$dL3_{d\tau 2} := \varepsilon \cdot Lt + (It \cdot Es \cdot \cos(\theta s) + \varepsilon b \cdot Ltb + Ib \cdot Es \cdot \cos(\theta b) \cdot (1 - \varepsilon b)) \cdot (1 - \varepsilon)$$

$$dL3_{dLu} := 1$$

These derivatives are used to form the components of the Beers error calculation:

$s\varepsilon := 0.05$	$sLt := 1.73$	$sIt := 0$	$s\theta s := 0.1309$
$s\varepsilon b := 0.05$	$sLtb := 1.73$	$sIb := 0$	$s\theta b := 0.1309$
$sEs := 0.0$	$s\tau 2 := 0.03$	$sLu := 0.54$	$\rho_{\tau 2Lu} := -0.8381$

$$sL3_{\varepsilon} := \left(dL3_{d\varepsilon}{}^{2} \cdot s\varepsilon^{2}\right)^{\frac{1}{2}}$$

$$sL3_{\varepsilon} = 0.622$$

$$sL3_{Lt} := \left(dL3_{dLt}{}^{2} \cdot sLt^{2}\right)^{\frac{1}{2}}$$

$$sL3_{Lt} = 1.537$$

$$sL3_{It} := \left(dL3_{dIt}{}^{2} \cdot sIt^{2}\right)^{\frac{1}{2}}$$

$$sL3_{It} = 0$$

$$sL3_{Es} := \left(dL3_{dEs}{}^{2} \cdot sEs^{2}\right)^{\frac{1}{2}}$$

$$sL3_{Es} = 0$$

$$sL3_{\theta s} := \left(dL3_{d\theta s}{}^{2} \cdot s\theta s^{2}\right)^{\frac{1}{2}}$$

$$sL3_{\theta s} = 0$$

$$sL3_{\varepsilon b} := \left(dL3_{d\varepsilon b}{}^{2} \cdot s\varepsilon b^{2}\right)^{\frac{1}{2}}$$

$$sL3_{\varepsilon b} = 0.227$$

$$sL3_{Ltb} := \left(dL3_{dLtb}{}^{2} \cdot sLtb^{2}\right)^{\frac{1}{2}}$$

$$sL3_{Ltb} = 0.132$$

$$sL3_{Ib} := \left(dL3_{dIb}{}^{2} \cdot sIb^{2}\right)^{\frac{1}{2}}$$

$$sL3_{Ib} = 0$$

$$sL3_{\theta b} := \left(dL3_{d\theta b}{}^{2} \cdot s\theta b^{2}\right)^{\frac{1}{2}}$$

$$sL3_{\theta b} = 0$$

$$sL3_{\tau 2} := \left(dL3_{d\tau 2}{}^{2} \cdot s\tau 2^{2}\right)^{\frac{1}{2}}$$

$$sL3_{\tau 2} = 1.216$$

$$sL3_{Lu} := \left(dL3_{dLu}{}^{2} \cdot sLu^{2}\right)^{\frac{1}{2}}$$

$$sL3_{Lu} = 0.54$$

The cross term of the correlated variables Tau2 and Lu is:

$$xterm := \left[\rho_{\tau 2Lu} \cdot \left(dL3_{d\tau 2}\right) \cdot \left(dL3_{dLu}\right) \cdot s\tau 2 \cdot sLu\right]$$

$$xterm = -0.551$$

The total Beers error is expressed as:

$$sL3_{part1} := sL3_{\varepsilon}{}^{2} + sL3_{Lt}{}^{2} + sL3_{It}{}^{2} + sL3_{Es}{}^{2} + sL3_{\theta s}{}^{2} + sL3_{\varepsilon b}{}^{2}$$

$$sL3_{part2} := sL3_{Ltb}{}^{2} + sL3_{Ib}{}^{2} + sL3_{\theta b}{}^{2} + sL3_{\tau 2}{}^{2} + sL3_{Lu}{}^{2} + xterm$$

$$sL3_{total} := \left(sL3_{part1} + sL3_{part2}\right)^{\frac{1}{2}}$$

$$sL3_{total} = 2.01$$

The starting values for the equation are as follows:

$\varepsilon := 0.916$	$Lt := 39.47$	$\theta s := 0.785398$	$It := 1$
$\varepsilon b := 0.939$	$Ltb := 55.69$	$\theta b := 0.785398$	$Ib := 1$
$Es := 0.0$	$\tau 2 := 0.873$	$Lu := 3.533$	

Case 3: Specular bounce to background

$$L3 := (\varepsilon \cdot Lt + (It \cdot Es \cdot \cos(\theta s) + \varepsilon b \cdot Ltb + Ib \cdot Es \cdot \cos(\theta b) \cdot (1 - \varepsilon b)) \cdot (1 - \varepsilon)) \cdot \tau 2 + Lu$$

$$L3 = 38.931$$

The MAPLE symbolic processor in MathCad was used to calculate the following derivatives:

$$dL3_{d\varepsilon} := (Lt - It \cdot Es \cdot \cos(\theta s) - \varepsilon b \cdot Ltb - Ib \cdot Es \cdot \cos(\theta b) \cdot (1 - \varepsilon b)) \cdot \tau 2$$

$$dL3_{dLt} := \varepsilon \cdot \tau 2$$

$$dL3_{dIt} := Es \cdot \cos(\theta s) \cdot (1 - \varepsilon) \cdot \tau 2$$

$$dL3_{dEs} := (It \cdot \cos(\theta s) + Ib \cdot \cos(\theta b) \cdot (1 - \varepsilon b)) \cdot (1 - \varepsilon) \cdot \tau 2$$

$$dL3_{d\theta s} := -It \cdot Es \cdot \sin(\theta s) \cdot (1 - \varepsilon) \cdot \tau 2$$

$$dL3_{d\varepsilon b} := (Ltb - Ib \cdot Es \cdot \cos(\theta b)) \cdot (1 - \varepsilon) \cdot \tau 2$$

$$dL3_{dLtb} := \varepsilon b \cdot (1 - \varepsilon) \cdot \tau 2$$

$$dL3_{dIb} := Es \cdot \cos(\theta b) \cdot (1 - \varepsilon b) \cdot (1 - \varepsilon) \cdot \tau 2$$

$$dL3_{d\theta b} := -Ib \cdot Es \cdot \sin(\theta b) \cdot (1 - \varepsilon b) \cdot (1 - \varepsilon) \cdot \tau 2$$

$$dL3_{d\tau 2} := \varepsilon \cdot Lt + (It \cdot Es \cdot \cos(\theta s) + \varepsilon b \cdot Ltb + Ib \cdot Es \cdot \cos(\theta b) \cdot (1 - \varepsilon b)) \cdot (1 - \varepsilon)$$

$$dL3_{dLu} := 1$$

These derivatives are used to form the components of the Beers error calculation:

$s\varepsilon := 0.025$	$sLt := 0.09$	$sIt := 0$	$s\theta s := 0.05236$
$s\varepsilon b := 0.025$	$sLtb := 0.09$	$sIb := 0$	$s\theta b := 0.05236$
$sEs := 0.0$	$s\tau 2 := 0.03$	$sLu := 0.07$	$\rho_{\tau 2Lu} := -0.8381$

$$sL3_{\varepsilon} := \left(dL3_{d\varepsilon}^{2} \cdot s\varepsilon^{2}\right)^{\frac{1}{2}}$$

$$sL3_{\varepsilon} = 0.28$$

$$sL3_{Lt} := \left(dL3_{dLt}^{2} \cdot sLt^{2}\right)^{\frac{1}{2}}$$

$$sL3_{Lt} = 0.072$$

$$sL3_{It} := \left(dL3_{dIt}^{2} \cdot sIt^{2}\right)^{\frac{1}{2}}$$

$$sL3_{It} = 0$$

$$sL3_{Es} := \left(dL3_{dEs}^{2} \cdot sEs^{2}\right)^{\frac{1}{2}}$$

$$sL3_{Es} = 0$$

$$sL3_{\theta s} := \left(dL3_{d\theta s}^{2} \cdot s\theta s^{2}\right)^{\frac{1}{2}}$$

$$sL3_{\theta s} = 0$$

$$sL3_{\varepsilon b} := \left(dL3_{d\varepsilon b}^{2} \cdot s\varepsilon b^{2}\right)^{\frac{1}{2}}$$

$$sL3_{\varepsilon b} = 0.102$$

$$sL3_{Ltb} := \left(dL3_{dLtb}^{2} \cdot sLtb^{2}\right)^{\frac{1}{2}}$$

$$sL3_{Ltb} = 0.006$$

$$sL3_{Ib} := \left(dL3_{dIb}^{2} \cdot sIb^{2}\right)^{\frac{1}{2}}$$

$$sL3_{Ib} = 0$$

$$sL3_{\theta b} := \left(dL3_{d\theta b}^{2} \cdot s\theta b^{2}\right)^{\frac{1}{2}}$$

$$sL3_{\theta b} = 0$$

$$sL3_{\tau 2} := \left(dL3_{d\tau 2}^{2} \cdot s\tau 2^{2}\right)^{\frac{1}{2}}$$

$$sL3_{\tau 2} = 1.216$$

$$sL3_{Lu} := \left(dL3_{dLu}^{2} \cdot sLu^{2}\right)^{\frac{1}{2}}$$

$$sL3_{Lu} = 0.07$$

The cross term of the correlated variables Tau2 and Lu is:

$$xterm := \left[\rho_{\tau 2Lu} \cdot \left(dL3_{d\tau 2}\right) \cdot \left(dL3_{dLu}\right) \cdot s\tau 2 \cdot sLu\right]$$

$$xterm = -0.071$$

The total Beers error is expressed as:

$$sL3_{part1} := sL3_{\varepsilon}^{2} + sL3_{Lt}^{2} + sL3_{It}^{2} + sL3_{Es}^{2} + sL3_{\theta s}^{2} + sL3_{\varepsilon b}^{2}$$

$$sL3_{part2} := sL3_{Ltb}^{2} + sL3_{Ib}^{2} + sL3_{\theta b}^{2} + sL3_{\tau 2}^{2} + sL3_{Lu}^{2} + xterm$$

$$sL3_{total} := \left(sL3_{part1} + sL3_{part2}\right)^{\frac{1}{2}}$$

$$sL3_{total} = 1.228$$

The starting values for the equation are as follows:

$\varepsilon := 0.916$	$Lt := 39.47$	$\theta s := 0.785398$	$It := 1$
$\varepsilon b := 0.939$	$Ltb := 55.69$	$\theta b := 0.785398$	$Ib := 1$
$Es := 0.0$	$\tau 2 := 0.873$	$Lu := 3.533$	

Case 3: Specular bounce to background

$$L3 := (\varepsilon \cdot Lt + (It \cdot Es \cdot \cos(\theta s) + \varepsilon b \cdot Ltb + Ib \cdot Es \cdot \cos(\theta b) \cdot (1 - \varepsilon b)) \cdot (1 - \varepsilon)) \cdot \tau 2 + Lu$$

$$L3 = 38.931$$

The MAPLE symbolic processor in MathCad was used to calculate the following derivatives:

$$dL3_{d\varepsilon} := (Lt - It \cdot Es \cdot \cos(\theta s) - \varepsilon b \cdot Ltb - Ib \cdot Es \cdot \cos(\theta b) \cdot (1 - \varepsilon b)) \cdot \tau 2$$

$$dL3_{dLt} := \varepsilon \cdot \tau 2$$

$$dL3_{dIt} := Es \cdot \cos(\theta s) \cdot (1 - \varepsilon) \cdot \tau 2$$

$$dL3_{dEs} := (It \cdot \cos(\theta s) + Ib \cdot \cos(\theta b) \cdot (1 - \varepsilon b)) \cdot (1 - \varepsilon) \cdot \tau 2$$

$$dL3_{d\theta s} := -It \cdot Es \cdot \sin(\theta s) \cdot (1 - \varepsilon) \cdot \tau 2$$

$$dL3_{d\varepsilon b} := (Ltb - Ib \cdot Es \cdot \cos(\theta b)) \cdot (1 - \varepsilon) \cdot \tau 2$$

$$dL3_{dLtb} := \varepsilon b \cdot (1 - \varepsilon) \cdot \tau 2$$

$$dL3_{dIb} := Es \cdot \cos(\theta b) \cdot (1 - \varepsilon b) \cdot (1 - \varepsilon) \cdot \tau 2$$

$$dL3_{d\theta b} := -Ib \cdot Es \cdot \sin(\theta b) \cdot (1 - \varepsilon b) \cdot (1 - \varepsilon) \cdot \tau 2$$

$$dL3_{d\tau 2} := \varepsilon \cdot Lt + (It \cdot Es \cdot \cos(\theta s) + \varepsilon b \cdot Ltb + Ib \cdot Es \cdot \cos(\theta b) \cdot (1 - \varepsilon b)) \cdot (1 - \varepsilon)$$

$$dL3_{dLu} := 1$$

These derivatives are used to form the components of the Beers error calculation:

$s\varepsilon := 0.05$	$sLt := 0.63$	$sIt := 0$	$s\theta s := 0.1309$
$s\varepsilon b := 0.05$	$sLtb := 0.63$	$sIb := 0$	$s\theta b := 0.1309$
$sEs := 0.0$	$s\tau 2 := 0.03$	$sLu := 0.636$	$\rho_{\tau 2Lu} := -0.8381$

$sL3_{\varepsilon} := \left(dL3_{d\varepsilon}{}^{2} \cdot s\varepsilon^{2}\right)^{\frac{1}{2}}$ $\qquad sL3_{\varepsilon} = 0.56$

$sL3_{Lt} := \left(dL3_{dLt}{}^{2} \cdot sLt^{2}\right)^{\frac{1}{2}}$ $\qquad sL3_{Lt} = 0.504$

$sL3_{It} := \left(dL3_{dIt}{}^{2} \cdot sIt^{2}\right)^{\frac{1}{2}}$ $\qquad sL3_{It} = 0$

$sL3_{Es} := \left(dL3_{dEs}{}^{2} \cdot sEs^{2}\right)^{\frac{1}{2}}$ $\qquad sL3_{Es} = 0$

$sL3_{\theta s} := \left(dL3_{d\theta s}{}^{2} \cdot s\theta s^{2}\right)^{\frac{1}{2}}$ $\qquad sL3_{\theta s} = 0$

$sL3_{\varepsilon b} := \left(dL3_{d\varepsilon b}{}^{2} \cdot s\varepsilon b^{2}\right)^{\frac{1}{2}}$ $\qquad sL3_{\varepsilon b} = 0.204$

$sL3_{Ltb} := \left(dL3_{dLtb}{}^{2} \cdot sLtb^{2}\right)^{\frac{1}{2}}$ $\qquad sL3_{Ltb} = 0.043$

$sL3_{Ib} := \left(dL3_{dIb}{}^{2} \cdot sIb^{2}\right)^{\frac{1}{2}}$ $\qquad sL3_{Ib} = 0$

$sL3_{\theta b} := \left(dL3_{d\theta b}{}^{2} \cdot s\theta b^{2}\right)^{\frac{1}{2}}$ $\qquad sL3_{\theta b} = 0$

$sL3_{\tau 2} := \left(dL3_{d\tau 2}{}^{2} \cdot s\tau 2^{2}\right)^{\frac{1}{2}}$ $\qquad sL3_{\tau 2} = 1.216$

$sL3_{Lu} := \left(dL3_{dLu}{}^{2} \cdot sLu^{2}\right)^{\frac{1}{2}}$ $\qquad sL3_{Lu} = 0.636$

The cross term of the correlated variables Tau2 and Lu is:

$xterm := \left[\rho_{\tau 2Lu} \cdot \left(dL3_{d\tau 2}\right) \cdot \left(dL3_{dLu}\right) \cdot s\tau 2 \cdot sLu\right]$ $\qquad xterm = -0.648$

The total Beers error is expressed as:

$sL3_{part1} := sL3_{\varepsilon}{}^{2} + sL3_{Lt}{}^{2} + sL3_{It}{}^{2} + sL3_{Es}{}^{2} + sL3_{\theta s}{}^{2} + sL3_{\varepsilon b}{}^{2}$

$sL3_{part2} := sL3_{Ltb}{}^{2} + sL3_{Ib}{}^{2} + sL3_{\theta b}{}^{2} + sL3_{\tau 2}{}^{2} + sL3_{Lu}{}^{2} + xterm$

$sL3_{total} := \left(sL3_{part1} + sL3_{part2}\right)^{\frac{1}{2}}$

$sL3_{total} = 1.359$

The starting values for the equation are as follows:

$\varepsilon := 0.916$	$Lt := 39.47$	$\theta s := 0.785398$	$It := 1$
$\varepsilon b := 0.939$	$Ltb := 55.69$	$\theta b := 0.785398$	$Ib := 1$
$Es := 0.0$	$\tau 2 := 0.873$	$Lu := 3.533$	

Case 3: Specular bounce to background

$$L3 := (\varepsilon \cdot Lt + (It \cdot Es \cdot \cos(\theta s) + \varepsilon b \cdot Ltb + Ib \cdot Es \cdot \cos(\theta b) \cdot (1 - \varepsilon b)) \cdot (1 - \varepsilon)) \cdot \tau 2 + Lu$$

$$L3 = 38.931$$

The MAPLE symbolic processor in MathCad was used to calculate the following derivatives:

$$dL3_{d\varepsilon} := (Lt - It \cdot Es \cdot \cos(\theta s) - \varepsilon b \cdot Ltb - Ib \cdot Es \cdot \cos(\theta b) \cdot (1 - \varepsilon b)) \cdot \tau 2$$

$$dL3_{dLt} := \varepsilon \cdot \tau 2$$

$$dL3_{dIt} := Es \cdot \cos(\theta s) \cdot (1 - \varepsilon) \cdot \tau 2$$

$$dL3_{dEs} := (It \cdot \cos(\theta s) + Ib \cdot \cos(\theta b) \cdot (1 - \varepsilon b)) \cdot (1 - \varepsilon) \cdot \tau 2$$

$$dL3_{d\theta s} := -It \cdot Es \cdot \sin(\theta s) \cdot (1 - \varepsilon) \cdot \tau 2$$

$$dL3_{d\varepsilon b} := (Ltb - Ib \cdot Es \cdot \cos(\theta b)) \cdot (1 - \varepsilon) \cdot \tau 2$$

$$dL3_{dLtb} := \varepsilon b \cdot (1 - \varepsilon) \cdot \tau 2$$

$$dL3_{dIb} := Es \cdot \cos(\theta b) \cdot (1 - \varepsilon b) \cdot (1 - \varepsilon) \cdot \tau 2$$

$$dL3_{d\theta b} := -Ib \cdot Es \cdot \sin(\theta b) \cdot (1 - \varepsilon b) \cdot (1 - \varepsilon) \cdot \tau 2$$

$$dL3_{d\tau 2} := \varepsilon \cdot Lt + (It \cdot Es \cdot \cos(\theta s) + \varepsilon b \cdot Ltb + Ib \cdot Es \cdot \cos(\theta b) \cdot (1 - \varepsilon b)) \cdot (1 - \varepsilon)$$

$$dL3_{dLu} := 1$$

These derivatives are used to form the components of the Beers error calculation:

$s\varepsilon := 0.05$	$sLt := 1.73$	$sIt := 0$	$s\theta s := 0.1309$
$s\varepsilon b := 0.05$	$sLtb := 1.73$	$sIb := 0$	$s\theta b := 0.1309$
$sEs := 0.0$	$s\tau 2 := 0.03$	$sLu := 0.636$	$\rho_{\tau 2 Lu} := -0.8381$

$$sL3_{\varepsilon} := \left(dL3_{d\varepsilon}^{2} \cdot s\varepsilon^{2}\right)^{\frac{1}{2}} \qquad sL3_{\varepsilon} = 0.56$$

$$sL3_{Lt} := \left(dL3_{dLt}^{2} \cdot sLt^{2}\right)^{\frac{1}{2}} \qquad sL3_{Lt} = 1.383$$

$$sL3_{It} := \left(dL3_{dIt}^{2} \cdot sIt^{2}\right)^{\frac{1}{2}} \qquad sL3_{It} = 0$$

$$sL3_{Es} := \left(dL3_{dEs}^{2} \cdot sEs^{2}\right)^{\frac{1}{2}} \qquad sL3_{Es} = 0$$

$$sL3_{\theta s} := \left(dL3_{d\theta s}^{2} \cdot s\theta s^{2}\right)^{\frac{1}{2}} \qquad sL3_{\theta s} = 0$$

$$sL3_{\varepsilon b} := \left(dL3_{d\varepsilon b}^{2} \cdot s\varepsilon b^{2}\right)^{\frac{1}{2}} \qquad sL3_{\varepsilon b} = 0.204$$

$$sL3_{Ltb} := \left(dL3_{dLtb}^{2} \cdot sLtb^{2}\right)^{\frac{1}{2}} \qquad sL3_{Ltb} = 0.119$$

$$sL3_{Ib} := \left(dL3_{dIb}^{2} \cdot sIb^{2}\right)^{\frac{1}{2}} \qquad sL3_{Ib} = 0$$

$$sL3_{\theta b} := \left(dL3_{d\theta b}^{2} \cdot s\theta b^{2}\right)^{\frac{1}{2}} \qquad sL3_{\theta b} = 0$$

$$sL3_{\tau 2} := \left(dL3_{d\tau 2}^{2} \cdot s\tau 2^{2}\right)^{\frac{1}{2}} \qquad sL3_{\tau 2} = 1.216$$

$$sL3_{Lu} := \left(dL3_{dLu}^{2} \cdot sLu^{2}\right)^{\frac{1}{2}} \qquad sL3_{Lu} = 0.636$$

The cross term of the correlated variables Tau2 and Lu is:

$$xterm := \left[\rho_{\tau 2Lu} \cdot \left(dL3_{d\tau 2}\right) \cdot \left(dL3_{dLu}\right) \cdot s\tau 2 \cdot sLu\right] \qquad xterm = -0.648$$

The total Beers error is expressed as:

$$sL3_{part1} := sL3_{\varepsilon}^{2} + sL3_{Lt}^{2} + sL3_{It}^{2} + sL3_{Es}^{2} + sL3_{\theta s}^{2} + sL3_{\varepsilon b}^{2}$$

$$sL3_{part2} := sL3_{Ltb}^{2} + sL3_{Ib}^{2} + sL3_{\theta b}^{2} + sL3_{\tau 2}^{2} + sL3_{Lu}^{2} + xterm$$

$$sL3_{total} := \left(sL3_{part1} + sL3_{part2}\right)^{\frac{1}{2}}$$

$$sL3_{total} = 1.876$$

The starting values for the equation are as follows:

$\varepsilon := 0.916$	$Lt := 39.47$	$\theta s := 0.785398$	$It := 1$
$\varepsilon b := 0.939$	$Ltb := 55.69$	$\theta b := 0.785398$	$Ib := 1$
$Es := 0.0$	$\tau 2 := 0.873$	$Lu := 3.533$	

Case 3: Specular bounce to background

$$L3 := (\varepsilon \cdot Lt + (It \cdot Es \cdot \cos(\theta s) + \varepsilon b \cdot Ltb + Ib \cdot Es \cdot \cos(\theta b) \cdot (1 - \varepsilon b)) \cdot (1 - \varepsilon)) \cdot \tau 2 + Lu$$

$$L3 = 38.931$$

The MAPLE symbolic processor in MathCad was used to calculate the following derivatives:

$$dL3_{d\varepsilon} := (Lt - It \cdot Es \cdot \cos(\theta s) - \varepsilon b \cdot Ltb - Ib \cdot Es \cdot \cos(\theta b) \cdot (1 - \varepsilon b)) \cdot \tau 2$$

$$dL3_{dLt} := \varepsilon \cdot \tau 2$$

$$dL3_{dIt} := Es \cdot \cos(\theta s) \cdot (1 - \varepsilon) \cdot \tau 2$$

$$dL3_{dEs} := (It \cdot \cos(\theta s) + Ib \cdot \cos(\theta b) \cdot (1 - \varepsilon b)) \cdot (1 - \varepsilon) \cdot \tau 2$$

$$dL3_{d\theta s} := -It \cdot Es \cdot \sin(\theta s) \cdot (1 - \varepsilon) \cdot \tau 2$$

$$dL3_{d\varepsilon b} := (Ltb - Ib \cdot Es \cdot \cos(\theta b)) \cdot (1 - \varepsilon) \cdot \tau 2$$

$$dL3_{dLtb} := \varepsilon b \cdot (1 - \varepsilon) \cdot \tau 2$$

$$dL3_{dIb} := Es \cdot \cos(\theta b) \cdot (1 - \varepsilon b) \cdot (1 - \varepsilon) \cdot \tau 2$$

$$dL3_{d\theta b} := -Ib \cdot Es \cdot \sin(\theta b) \cdot (1 - \varepsilon b) \cdot (1 - \varepsilon) \cdot \tau 2$$

$$dL3_{d\tau 2} := \varepsilon \cdot Lt + (It \cdot Es \cdot \cos(\theta s) + \varepsilon b \cdot Ltb + Ib \cdot Es \cdot \cos(\theta b) \cdot (1 - \varepsilon b)) \cdot (1 - \varepsilon)$$

$$dL3_{dLu} := 1$$

These derivatives are used to form the components of the Beers error calculation:

$s\varepsilon := 0.05$	$sLt := 1.73$	$sIt := 0$	$s\theta s := 0.1309$
$s\varepsilon b := 0.05$	$sLtb := 1.73$	$sIb := 0$	$s\theta b := 0.1309$
$sEs := 0.0$	$s\tau 2 := 0.03$	$sLu := 2.120$	$\rho_{\tau 2Lu} := -0.8381$

$$sL3_{\varepsilon} := \left(dL3_{d\varepsilon}{}^{2} \cdot s\varepsilon^{2}\right)^{\frac{1}{2}} \qquad sL3_{\varepsilon} = 0.56$$

$$sL3_{Lt} := \left(dL3_{dLt}{}^{2} \cdot sLt^{2}\right)^{\frac{1}{2}} \qquad sL3_{Lt} = 1.383$$

$$sL3_{It} := \left(dL3_{dIt}{}^{2} \cdot sIt^{2}\right)^{\frac{1}{2}} \qquad sL3_{It} = 0$$

$$sL3_{Es} := \left(dL3_{dEs}{}^{2} \cdot sEs^{2}\right)^{\frac{1}{2}} \qquad sL3_{Es} = 0$$

$$sL3_{\theta s} := \left(dL3_{d\theta s}{}^{2} \cdot s\theta s^{2}\right)^{\frac{1}{2}} \qquad sL3_{\theta s} = 0$$

$$sL3_{\varepsilon b} := \left(dL3_{d\varepsilon b}{}^{2} \cdot s\varepsilon b^{2}\right)^{\frac{1}{2}} \qquad sL3_{\varepsilon b} = 0.204$$

$$sL3_{Ltb} := \left(dL3_{dLtb}{}^{2} \cdot sLtb^{2}\right)^{\frac{1}{2}} \qquad sL3_{Ltb} = 0.119$$

$$sL3_{Ib} := \left(dL3_{dIb}{}^{2} \cdot sIb^{2}\right)^{\frac{1}{2}} \qquad sL3_{Ib} = 0$$

$$sL3_{\theta b} := \left(dL3_{d\theta b}{}^{2} \cdot s\theta b^{2}\right)^{\frac{1}{2}} \qquad sL3_{\theta b} = 0$$

$$sL3_{\tau 2} := \left(dL3_{d\tau 2}{}^{2} \cdot s\tau 2^{2}\right)^{\frac{1}{2}} \qquad sL3_{\tau 2} = 1.216$$

$$sL3_{Lu} := \left(dL3_{dLu}{}^{2} \cdot sLu^{2}\right)^{\frac{1}{2}} \qquad sL3_{Lu} = 2.12$$

The cross term of the correlated variables Tau2 and Lu is:

$$xterm := \left[\rho_{\tau 2Lu} \cdot \left(dL3_{d\tau 2}\right) \cdot \left(dL3_{dLu}\right) \cdot s\tau 2 \cdot sLu\right]$$

$$xterm = -2.161$$

The total Beers error is expressed as:

$$sL3_{part1} := sL3_{\varepsilon}^{2} + sL3_{Lt}^{2} + sL3_{It}^{2} + sL3_{Es}^{2} + sL3_{\theta s}^{2} + sL3_{\varepsilon b}^{2}$$

$$sL3_{part2} := sL3_{Ltb}^{2} + sL3_{Ib}^{2} + sL3_{\theta b}^{2} + sL3_{\tau 2}^{2} + sL3_{Lu}^{2} + xterm$$

$$sL3_{total} := \left(sL3_{part1} + sL3_{part2}\right)^{\frac{1}{2}}$$

$$sL3_{total} = 2.469$$

These derivatives are used to form the components of the Beers error calculation:

$s\varepsilon := 0.05$	$sLt := 1.73$	$sIt := 0$	$s\theta s := 0.1309$
$s\varepsilon b := 0.05$	$sLtb := 1.73$	$sIb := 0$	$s\theta b := 0.1309$
$sEs := 0.0$	$s\tau 2 := 0.03$	$sLu := 2.120$	$\rho_{\tau 2Lu} := -0.8381$

$$sL3_{\varepsilon} := \left(dL3_{d\varepsilon}{}^{2} \cdot s\varepsilon^{2}\right)^{\frac{1}{2}} \qquad sL3_{\varepsilon} = 0.56$$

$$sL3_{Lt} := \left(dL3_{dLt}{}^{2} \cdot sLt^{2}\right)^{\frac{1}{2}} \qquad sL3_{Lt} = 1.383$$

$$sL3_{It} := \left(dL3_{dIt}{}^{2} \cdot sIt^{2}\right)^{\frac{1}{2}} \qquad sL3_{It} = 0$$

$$sL3_{Es} := \left(dL3_{dEs}{}^{2} \cdot sEs^{2}\right)^{\frac{1}{2}} \qquad sL3_{Es} = 0$$

$$sL3_{\theta s} := \left(dL3_{d\theta s}{}^{2} \cdot s\theta s^{2}\right)^{\frac{1}{2}} \qquad sL3_{\theta s} = 0$$

$$sL3_{\varepsilon b} := \left(dL3_{d\varepsilon b}{}^{2} \cdot s\varepsilon b^{2}\right)^{\frac{1}{2}} \qquad sL3_{\varepsilon b} = 0.204$$

$$sL3_{Ltb} := \left(dL3_{dLtb}{}^{2} \cdot sLtb^{2}\right)^{\frac{1}{2}} \qquad sL3_{Ltb} = 0.119$$

$$sL3_{Ib} := \left(dL3_{dIb}{}^{2} \cdot sIb^{2}\right)^{\frac{1}{2}} \qquad sL3_{Ib} = 0$$

$$sL3_{\theta b} := \left(dL3_{d\theta b}{}^{2} \cdot s\theta b^{2}\right)^{\frac{1}{2}} \qquad sL3_{\theta b} = 0$$

$$sL3_{\tau 2} := \left(dL3_{d\tau 2}{}^{2} \cdot s\tau 2^{2}\right)^{\frac{1}{2}} \qquad sL3_{\tau 2} = 1.216$$

$$sL3_{Lu} := \left(dL3_{dLu}{}^{2} \cdot sLu^{2}\right)^{\frac{1}{2}} \qquad sL3_{Lu} = 2.12$$

The cross term of the correlated variables Tau2 and Lu is:

$$xterm := \left[\rho_{\tau 2Lu} \cdot \left(dL3_{d\tau 2}\right) \cdot \left(dL3_{dLu}\right) \cdot s\tau 2 \cdot sLu\right]$$

$$xterm = -2.161$$

The total Beers error is expressed as:

$$sL3_{part1} := sL3_{\varepsilon}^{2} + sL3_{Lt}^{2} + sL3_{It}^{2} + sL3_{Es}^{2} + sL3_{\theta s}^{2} + sL3_{\varepsilon b}^{2}$$

$$sL3_{part2} := sL3_{Ltb}^{2} + sL3_{Ib}^{2} + sL3_{\theta b}^{2} + sL3_{\tau 2}^{2} + sL3_{Lu}^{2} + xterm$$

$$sL3_{total} := \left(sL3_{part1} + sL3_{part2}\right)^{\frac{1}{2}}$$

$$sL3_{total} = 2.469$$

Ray_Interaction Type 4: Missed Scene

$L4 = Ldhat$

The derivative of L4:

$dL4_{dLdhat} := 1$

This derivative is used for the component of the Beers error calculation:

$sLdhat := 2.26$

$sL4_{Ldhat} := \left(dL4_{dLdhat}^{2} \cdot sLdhat^{2}\right)^{\frac{1}{2}}$

The total Beers error is expressed as:

$sL4_{total} := \left(sL4_{Ldhat}^{2}\right)^{\frac{1}{2}}$

$sL4_{total} = 2.26$

APPENDIX E

Weather Data from June 1992 & October 1990 Data Collections

Weather 6/22/92

	Time	Air Temp	Pressure	Humidity	Dew Point	Wind Speed	Direct Ins
1	0.000	7.800	1015.600	0.930	-1.000	1.000	0.000
2	0.250	7.800	1015.600	0.930	-1.000	1.000	0.000
3	0.500	7.800	1015.700	0.930	-1.000	1.000	0.000
4	0.750	7.800	1015.800	0.930	-1.000	1.000	0.000
5	1.000	7.800	1015.800	0.930	-1.000	1.000	0.000
6	1.250	7.800	1015.900	0.930	-1.000	1.000	0.000
7	1.500	7.800	1015.900	0.930	-1.000	1.000	0.000
8	1.750	7.800	1016.000	0.930	-1.000	1.000	0.000
9	2.000	7.800	1016.000	0.930	-1.000	1.000	0.000
10	2.250	7.700	1016.000	0.930	-1.000	1.000	0.000
11	2.500	7.600	1016.000	0.930	-1.000	1.000	0.000
12	2.750	7.600	1016.000	0.930	-1.000	1.000	0.000
13	3.000	7.500	1016.000	0.930	-1.000	1.000	0.000
14	3.250	7.400	1016.000	0.930	-1.000	1.000	0.000
15	3.500	7.300	1016.000	0.930	-1.000	1.000	0.000
16	3.750	7.300	1016.000	0.930	-1.000	1.000	0.000
17	4.000	7.200	1016.000	0.930	-1.000	1.000	0.000
18	4.250	7.200	1016.100	0.930	-1.000	1.000	0.000
19	4.500	7.200	1016.200	0.920	-1.000	1.000	0.000
20	4.750	7.200	1016.300	0.920	-1.000	1.000	0.000
21	5.000	7.200	1016.400	0.910	-1.000	1.000	0.000
22	5.250	7.200	1016.500	0.910	-1.000	1.000	0.000
23	5.500	7.200	1016.500	0.900	-1.000	1.000	0.000
24	5.750	7.200	1016.600	0.900	-1.000	1.000	0.000
25	6.000	7.200	1016.600	0.890	-1.000	1.000	0.000
26	6.250	7.000	1016.800	0.880	-1.000	2.000	0.000
27	6.500	6.900	1016.900	0.870	-1.000	2.000	0.069
28	6.750	6.800	1017.000	0.860	-1.000	2.000	0.080
29	7.000	6.700	1017.200	0.860	-1.000	2.000	0.120
30	7.250	7.200	1017.300	0.850	-1.000	2.000	0.344
31	7.500	7.400	1017.400	0.840	-1.000	2.000	0.500
32	7.750	7.600	1017.500	0.830	-1.000	2.000	0.600
33	8.000	7.800	1017.600	0.830	-1.000	2.000	0.700
34	8.250	7.900	1017.600	0.820	-1.000	2.000	0.800
35	8.500	8.000	1017.600	0.810	-1.000	2.000	0.950
36	8.750	8.100	1017.600	0.800	-1.000	2.000	1.150
37	9.000	8.200	1017.600	0.800	-1.000	2.000	1.376
38	9.250	8.400	1017.600	0.790	-1.000	2.000	1.720
39	9.500	8.600	1017.600	0.790	-1.000	2.000	1.720
40	9.750	8.800	1017.600	0.780	-1.000	2.000	2.408
41	10.000	8.900	1017.600	0.770	-1.000	2.000	3.784
42	10.250	9.500	1017.600	0.740	-1.000	2.000	4.128
43	10.500	10.000	1017.600	0.720	-1.000	2.000	3.440
44	10.750	10.500	1017.600	0.700	-1.000	2.000	13.416
45	11.000	11.000	1017.600	0.680	-1.000	2.000	25.456
46	11.250	11.500	1017.600	0.650	-1.000	2.000	29.584
47	11.500	12.100	1017.600	0.630	-1.000	2.000	24.768
48	11.750	12.500	1017.600	0.590	-1.000	3.000	54.352
49	12.000	12.800	1017.600	0.570	-1.000	3.000	42.656
50	12.250	13.000	1017.500	0.560	-1.000	3.000	42.312
51	12.500	13.200	1017.500	0.550	-1.000	3.000	41.280
52	12.750	13.400	1017.500	0.540	-1.000	2.000	52.976
53	13.000	13.600	1017.400	0.530	-1.000	2.000	37.496
54	13.250	13.800	1017.400	0.520	-1.000	2.000	43.344
55	13.500	14.000	1017.300	0.510	-1.000	3.000	60.200
56	13.750	14.200	1017.300	0.500	-1.000	3.000	66.392

Weather 6/22/92

	Diffuse Ins	Sky Exposure	Cloud Type	Rain Type	Rain Rate	Rain Temp	Time
1	0.000	0.000	5.000	1.000	0.250	7.000	0.000
2	0.000	0.000	5.000	1.000	0.025	7.000	0.250
3	0.000	0.000	5.000	1.000	0.025	7.000	0.500
4	0.000	0.000	5.000	1.000	0.025	7.000	0.750
5	0.000	0.000	5.000	0.000	0.000	0.000	1.000
6	0.000	0.000	5.000	0.000	0.000	0.000	1.250
7	0.000	0.000	5.000	0.000	0.000	0.000	1.500
8	0.000	0.000	5.000	0.000	0.000	0.000	1.750
9	0.000	0.000	5.000	0.000	0.000	0.000	2.000
10	0.000	0.000	5.000	0.000	0.000	0.000	2.250
11	0.000	0.000	5.000	0.000	0.000	0.000	2.500
12	0.000	0.000	5.000	0.000	0.000	0.000	2.750
13	0.000	0.000	5.000	0.000	0.000	0.000	3.000
14	0.000	0.000	5.000	0.000	0.000	0.000	3.250
15	0.000	0.000	5.000	0.000	0.000	0.000	3.500
16	0.000	0.000	5.000	0.000	0.000	0.000	3.750
17	0.000	0.000	5.000	0.000	0.000	0.000	4.000
18	0.000	0.000	5.000	0.000	0.000	0.000	4.250
19	0.000	0.000	5.000	0.000	0.000	0.000	4.500
20	0.000	0.000	5.000	0.000	0.000	0.000	4.750
21	0.000	0.000	5.000	0.000	0.000	0.000	5.000
22	0.000	0.000	5.000	0.000	0.000	0.000	5.250
23	0.000	0.000	5.000	0.000	0.000	0.000	5.500
24	0.344	0.000	5.000	0.000	0.000	0.000	5.750
25	0.344	0.000	5.000	1.000	0.025	6.600	6.000
26	0.500	0.000	5.000	1.000	0.025	6.600	6.250
27	0.600	0.000	5.000	1.000	0.025	6.600	6.500
28	1.000	0.000	5.000	1.000	0.025	6.600	6.750
29	1.500	0.000	5.000	0.000	0.000	0.000	7.000
30	2.000	0.000	5.000	0.000	0.000	0.000	7.250
31	3.000	0.000	5.000	0.000	0.000	0.000	7.500
32	4.000	0.000	5.000	0.000	0.000	0.000	7.750
33	5.000	0.000	5.000	0.000	0.000	0.000	8.000
34	6.000	0.050	5.000	0.000	0.000	0.000	8.250
35	8.000	0.050	5.000	0.000	0.000	0.000	8.500
36	10.000	0.100	5.000	0.000	0.000	0.000	8.750
37	12.384	0.100	5.000	0.000	0.000	0.000	9.000
38	9.907	0.200	5.000	0.000	0.000	0.000	9.250
39	14.448	0.300	5.000	0.000	0.000	0.000	9.500
40	18.163	0.400	5.000	0.000	0.000	0.000	9.750
41	25.594	0.500	5.000	0.000	0.000	0.000	10.000
42	26.006	0.500	5.000	0.000	0.000	0.000	10.250
43	22.291	0.500	5.000	0.000	0.000	0.000	10.500
44	35.088	0.400	5.000	0.000	0.000	0.000	10.750
45	38.803	0.400	5.000	0.000	0.000	0.000	11.000
46	36.326	0.400	5.000	0.000	0.000	0.000	11.250
47	33.024	0.400	5.000	0.000	0.000	0.000	11.500
48	28.483	0.500	5.000	0.000	0.000	0.000	11.750
49	30.960	0.500	5.000	0.000	0.000	0.000	12.000
50	33.850	0.500	3.000	0.000	0.000	0.000	12.250
51	30.134	0.500	3.000	0.000	0.000	0.000	12.500
52	28.483	0.500	3.000	0.000	0.000	0.000	12.750
53	30.960	0.500	3.000	0.000	0.000	0.000	13.000
54	28.070	0.500	3.000	0.000	0.000	0.000	13.250
55	22.291	0.500	3.000	0.000	0.000	0.000	13.500
56	24.768	0.500	3.000	0.000	0.000	0.000	13.750

Weather 6/22/92

	Time	Air Temp	Pressure	Humidity	Dew Point	Wind Speed	Direct Ins
57	14.000	14.400	1017.300	0.490	-1.000	3.000	64.672
58	14.250	14.500	1016.900	0.480	-1.000	3.000	54.008
59	14.500	14.600	1016.700	0.470	-1.000	2.000	69.144
60	14.750	14.700	1016.500	0.460	-1.000	2.000	61.576
61	15.000	14.800	1016.300	0.450	-1.000	2.000	61.576
62	15.250	15.000	1016.300	0.440	-1.000	2.000	63.296
63	15.500	15.100	1016.100	0.431	-1.000	1.600	62.608
64	15.750	14.700	1015.600	0.455	-1.000	1.500	59.168
65	16.000	14.900	1015.600	0.469	-1.000	1.360	55.040
66	16.250	15.000	1015.000	0.470	-1.000	2.010	51.256
67	16.500	15.000	1015.500	0.490	-1.000	1.250	49.880
68	16.750	15.500	1015.000	0.480	-1.000	2.210	47.472
69	17.000	15.500	1015.000	0.465	-1.000	1.600	43.668
70	17.250	15.500	1015.000	0.460	-1.000	3.060	41.624
71	17.500	15.500	1015.000	0.455	-1.000	2.200	37.152
72	17.750	16.000	1015.000	0.450	-1.000	1.960	34.744
73	18.000	16.000	1015.000	0.445	-1.000	2.520	30.272
74	18.250	16.000	1015.000	0.435	-1.000	2.160	27.176
75	18.500	16.000	1015.000	0.430	-1.000	1.930	26.832
76	18.750	16.000	1015.000	0.430	-1.000	1.800	16.512
77	19.000	16.000	1015.000	0.425	-1.000	1.490	12.384
78	19.250	15.000	1015.000	0.430	-1.000	1.680	9.632
79	19.500	15.000	1015.000	0.440	-1.000	1.310	6.192
80	19.750	15.000	1015.000	0.450	-1.000	0.890	2.064
81	20.000	14.500	1015.000	0.460	-1.000	1.170	2.064
82	20.250	14.000	1015.000	0.470	-1.000	0.650	1.032
83	20.500	12.500	1015.000	0.485	-1.000	0.000	0.344
84	20.750	11.000	1015.000	0.525	-1.000	0.020	0.000
85	21.000	11.000	1015.000	0.550	-1.000	0.000	0.000
86	21.250	10.000	1015.000	0.580	-1.000	0.000	0.000
87	21.500	12.100	1014.900	0.569	-1.000	0.010	0.000
88	21.750	11.500	1014.500	0.569	-1.000	0.010	0.000
89	22.000	11.300	1014.800	0.578	-1.000	0.010	0.000
90	22.250	11.100	1014.400	0.591	-1.000	0.000	0.000
91	22.500	10.900	1014.200	0.590	-1.000	0.010	0.000
92	22.750	10.600	1014.100	0.600	-1.000	0.000	0.000
93	23.000	10.500	1014.800	0.621	-1.000	0.320	0.000
94	23.250	10.100	1014.000	0.719	-1.000	1.090	0.000
95	23.500	9.900	1014.000	0.783	-1.000	0.010	0.000
96	23.750	9.100	1013.900	0.830	-1.000	0.010	0.000
97	0.000	9.100	1014.000	0.871	-1.000	0.000	0.000
98	0.250	8.700	1014.000	0.893	-1.000	0.010	0.000
99	0.500	8.300	1014.000	0.905	-1.000	0.010	0.000
100	0.750	8.300	1014.000	0.927	-1.000	0.000	0.000
101	1.000	8.000	1014.000	0.936	-1.000	0.010	0.000
102	1.250	8.400	1014.000	0.947	-1.000	0.010	0.000
103	1.500	8.100	1014.000	0.950	-1.000	0.010	0.000
104	1.750	7.900	1014.000	0.955	-1.000	0.000	0.000
105	2.000	7.400	1013.500	0.953	-1.000	0.000	0.000
106	2.250	7.000	1013.300	0.960	-1.000	0.350	0.000
107	2.500	7.100	1013.400	0.960	-1.000	0.420	0.000
108	2.750	7.400	1013.200	0.963	-1.000	0.000	0.000
109	3.000	7.200	1013.900	0.957	-1.000	0.000	0.000
110	3.250	6.800	1013.500	0.961	-1.000	0.010	0.000
111	3.500	7.000	1013.100	0.961	-1.000	0.010	0.000
112	3.750	6.100	1013.300	0.960	-1.000	0.010	0.000

Weather 6/22/92

	Diffuse Ins	Sky Exposure	Cloud Type	Rain Type	Rain Rate	Rain Temp	Time
57	23.117	0.500	3.000	0.000	0.000	0.000	14.000
58	24.355	0.600	3.000	0.000	0.000	0.000	14.250
59	21.878	7.000	3.000	0.000	0.000	0.000	14.500
60	23.530	0.800	3.000	0.000	0.000	0.000	14.750
61	21.053	0.900	3.000	0.000	0.000	0.000	15.000
62	18.576	0.800	5.000	0.000	0.000	0.000	15.250
63	15.686	0.700	5.000	0.000	0.000	0.000	15.500
64	15.686	0.720	5.000	0.000	0.000	0.000	15.750
65	13.210	0.720	5.000	0.000	0.000	0.000	16.000
66	14.035	0.850	5.000	0.000	0.000	0.000	16.250
67	13.210	0.800	5.000	0.000	0.000	0.000	16.500
68	14.035	0.850	5.000	0.000	0.000	0.000	16.750
69	11.971	0.900	5.000	0.000	0.000	0.000	17.000
70	11.971	0.900	5.000	0.000	0.000	0.000	17.250
71	11.146	0.900	5.000	0.000	0.000	0.000	17.500
72	10.733	0.900	5.000	0.000	0.000	0.000	17.750
73	10.320	0.900	5.000	0.000	0.000	0.000	18.000
74	10.320	0.900	5.000	0.000	0.000	0.000	18.250
75	9.082	0.900	1.000	0.000	0.000	0.000	18.500
76	9.082	0.920	1.000	0.000	0.000	0.000	18.750
77	7.843	0.900	1.000	0.000	0.000	0.000	19.000
78	7.018	0.900	1.000	0.000	0.000	0.000	19.250
79	6.605	0.880	1.000	0.000	0.000	0.000	19.500
80	4.954	0.880	1.000	0.000	0.000	0.000	19.750
81	4.128	0.850	1.000	0.000	0.000	0.000	20.000
82	2.477	0.820	1.000	0.000	0.000	0.000	20.250
83	0.826	0.820	1.000	0.000	0.000	0.000	20.500
84	0.413	0.850	1.000	0.000	0.000	0.000	20.750
85	0.000	0.900	1.000	0.000	0.000	0.000	21.000
86	0.000	0.900	1.000	0.000	0.000	0.000	21.250
87	0.000	0.900	1.000	0.000	0.000	0.000	21.500
88	0.000	0.900	1.000	0.000	0.000	0.000	21.750
89	0.000	0.950	1.000	0.000	0.000	0.000	22.000
90	0.000	1.000	0.000	0.000	0.000	0.000	22.250
91	0.000	1.000	0.000	0.000	0.000	0.000	22.500
92	0.000	1.000	0.000	0.000	0.000	0.000	22.750
93	0.000	1.000	0.000	0.000	0.000	0.000	23.000
94	0.000	1.000	0.000	0.000	0.000	0.000	23.250
95	0.000	1.000	0.000	0.000	0.000	0.000	23.500
96	0.000	1.000	0.000	0.000	0.000	0.000	23.750
97	0.000	1.000	0.000	0.000	0.000	0.000	24.000
98	0.000	1.000	0.000	0.000	0.000	0.000	24.250
99	0.000	1.000	0.000	0.000	0.000	0.000	24.500
100	0.000	1.000	0.000	0.000	0.000	0.000	24.750
101	0.000	1.000	0.000	0.000	0.000	0.000	25.000
102	0.000	1.000	0.000	0.000	0.000	0.000	25.250
103	0.000	1.000	0.000	0.000	0.000	0.000	25.500
104	0.000	1.000	0.000	0.000	0.000	0.000	25.750
105	0.000	1.000	0.000	0.000	0.000	0.000	26.000
106	0.000	1.000	0.000	0.000	0.000	0.000	26.250
107	0.000	1.000	0.000	0.000	0.000	0.000	26.500
108	0.000	1.000	0.000	0.000	0.000	0.000	26.750
109	0.000	1.000	0.000	0.000	0.000	0.000	27.000
110	0.000	1.000	0.000	0.000	0.000	0.000	27.250
111	0.000	1.000	0.000	0.000	0.000	0.000	27.500
112	0.000	1.000	0.000	0.000	0.000	0.000	27.750

Weather 6/22/92

	Time	Air Temp	Pressure	Humidity	Dew Point	Wind Speed	Direct Ins
113	4.000	5.600	1012.800	0.957	-1.000	1.170	0.000
114	4.250	5.900	1012.700	0.961	-1.000	0.010	0.000
115	4.500	5.900	1013.000	0.972	-1.000	0.000	0.000
116	4.750	5.700	1013.200	0.971	-1.000	0.050	0.000
117	5.000	5.800	1013.200	0.970	-1.000	0.010	0.000
118	5.250	5.000	1013.000	0.975	-1.000	0.010	0.000
119	5.500	5.700	1013.000	0.971	-1.000	0.000	0.000
120	5.750	5.900	1013.000	0.973	-1.000	0.000	0.000
121	6.000	5.900	1013.000	0.972	-1.000	0.000	0.344
122	6.250	6.750	1013.100	0.955	-1.000	0.000	0.344
123	6.500	6.750	1013.100	0.933	-1.000	0.010	6.192
124	6.750	7.200	1013.300	0.905	-1.000	0.890	6.880
125	7.000	7.550	1013.300	0.870	-1.000	1.330	10.664
126	7.250	8.450	1013.600	0.830	-1.000	1.230	13.072
127	7.500	9.150	1013.800	0.795	-1.000	0.010	16.200
128	7.750	9.800	1013.900	0.760	-1.000	0.020	17.200
129	8.000	10.600	1014.000	0.720	-1.000	0.000	21.328
130	8.250	11.400	1014.000	0.680	-1.000	0.000	21.328
131	8.500	11.500	1014.000	0.670	-1.000	0.280	22.360
132	8.750	12.500	1014.000	0.623	-1.000	0.720	31.648
133	9.000	12.500	1014.000	0.590	-1.000	0.010	33.712
134	9.250	13.300	1014.000	0.573	-1.000	0.980	35.776
135	9.500	13.500	1014.100	0.551	-1.000	0.590	22.704
136	9.750	13.500	1014.000	0.550	-1.000	0.270	37.840
137	10.000	13.500	1014.000	0.543	-1.000	0.080	41.968
138	10.250	13.500	1014.000	0.541	-1.000	0.000	48.848
139	10.500	14.500	1014.000	0.518	-1.000	0.870	35.776
140	10.750	15.000	1014.000	0.492	-1.000	0.440	42.312
141	11.000	15.800	1014.000	0.463	-1.000	0.010	47.816
142	11.250	15.800	1014.000	0.440	-1.000	0.000	51.256
143	11.500	16.000	1014.000	0.440	-1.000	0.160	45.408
144	11.750	15.800	1014.300	0.428	-1.000	0.550	36.808
145	12.000	15.800	1014.300	0.412	-1.000	0.050	43.344
146	12.250	16.300	1014.300	0.380	-1.000	0.000	59.856
147	12.500	16.800	1014.100	0.375	-1.000	0.590	63.296
148	12.750	16.500	1014.100	0.378	-1.000	1.240	67.080
149	13.000	17.000	1014.000	0.360	-1.000	0.360	64.328
150	13.250	17.100	1013.500	0.333	-1.000	0.900	63.984
151	13.500	18.900	1014.000	0.337	-1.000	0.100	44.376
152	13.750	19.500	1014.000	0.309	-1.000	0.750	50.912
153	14.000	19.300	1014.100	0.310	-1.000	1.670	61.576
154	14.250	18.800	1014.000	0.298	-1.000	1.290	53.320
155	14.500	18.500	1013.800	0.292	-1.000	0.000	61.232
156	14.750	19.100	1013.800	0.297	-1.000	0.130	60.888
157	15.000	19.500	1013.600	0.298	-1.000	0.850	44.376
158	15.250	19.700	1013.300	0.278	-1.000	0.340	55.728
159	15.500	19.900	1012.500	0.281	-1.000	1.210	27.176
160	15.750	19.300	1013.200	0.305	-1.000	1.980	14.448
161	16.000	19.500	1013.200	0.310	-1.000	2.400	29.240
162	16.250	19.600	1012.700	0.310	-1.000	1.900	29.928
163	16.500	19.500	1012.900	0.312	-1.000	2.240	6.880
164	16.750	19.800	1013.000	0.310	-1.000	1.430	6.192
165	17.000	19.500	1012.800	0.303	-1.000	1.860	7.568
166	17.250	19.000	1012.300	0.288	-1.000	1.860	19.264
167	17.500	18.900	1012.100	0.302	-1.000	1.800	8.600
168	17.750	17.500	1012.300	0.320	-1.000	1.330	5.160

Weather 6/22/92

	Diffuse Ins	Sky Exposure	Cloud Type	Rain Type	Rain Rate	Rain Temp	Time
113	0.000	1.000	0.000	0.000	0.000	0.000	28.000
114	0.000	1.000	0.000	0.000	0.000	0.000	28.250
115	0.000	1.000	0.000	0.000	0.000	0.000	28.500
116	0.000	1.000	0.000	0.000	0.000	0.000	28.750
117	0.000	0.900	6.000	0.000	0.000	0.000	29.000
118	0.000	0.900	6.000	0.000	0.000	0.000	29.250
119	0.000	0.900	6.000	0.000	0.000	0.000	29.500
120	0.344	0.920	6.000	0.000	0.000	0.000	29.750
121	1.651	0.920	6.000	0.000	0.000	0.000	30.000
122	2.890	0.950	6.000	0.000	0.000	0.000	30.250
123	9.907	0.950	6.000	0.000	0.000	0.000	30.500
124	7.018	0.950	6.000	0.000	0.000	0.000	30.750
125	8.256	0.950	6.000	0.000	0.000	0.000	31.000
126	8.669	0.940	6.000	0.000	0.000	0.000	31.250
127	9.494	0.940	6.000	0.000	0.000	0.000	31.500
128	9.494	0.900	6.000	0.000	0.000	0.000	31.750
129	10.733	0.900	6.000	0.000	0.000	0.000	32.000
130	12.384	0.900	6.000	0.000	0.000	0.000	32.250
131	11.146	0.900	6.000	0.000	0.000	0.000	32.500
132	12.384	0.800	6.000	0.000	0.000	0.000	32.750
133	13.622	0.800	6.000	0.000	0.000	0.000	33.000
134	14.861	0.750	6.000	0.000	0.000	0.000	33.250
135	20.227	0.750	6.000	0.000	0.000	0.000	33.500
136	14.861	0.800	6.000	0.000	0.000	0.000	33.750
137	14.448	0.800	6.000	0.000	0.000	0.000	34.000
138	16.512	0.800	6.000	0.000	0.000	0.000	34.250
139	21.053	0.750	6.000	0.000	0.000	0.000	34.500
140	21.878	0.700	6.000	0.000	0.000	0.000	34.750
141	20.277	0.700	6.000	0.000	0.000	0.000	35.000
142	19.402	0.750	6.000	0.000	0.000	0.000	35.250
143	18.576	0.750	6.000	0.000	0.000	0.000	35.500
144	16.512	0.450	6.000	0.000	0.000	0.000	35.750
145	21.053	0.500	6.000	0.000	0.000	0.000	36.000
146	15.686	0.650	6.000	0.000	0.000	0.000	36.250
147	13.622	0.700	6.000	0.000	0.000	0.000	36.500
148	14.448	0.600	6.000	0.000	0.000	0.000	36.750
149	16.925	0.700	6.000	0.000	0.000	0.000	37.000
150	17.338	0.250	6.000	0.000	0.000	0.000	37.250
151	32.611	0.400	6.000	0.000	0.000	0.000	37.500
152	32.198	0.600	6.000	0.000	0.000	0.000	37.750
153	26.832	0.550	6.000	0.000	0.000	0.000	38.000
154	32.611	0.600	6.000	0.000	0.000	0.000	38.250
155	23.942	0.700	6.000	0.000	0.000	0.000	38.500
156	19.402	0.700	6.000	0.000	0.000	0.000	38.750
157	20.640	0.650	6.000	0.000	0.000	0.000	39.000
158	25.181	0.550	6.000	0.000	0.000	0.000	39.250
159	33.024	0.400	6.000	0.000	0.000	0.000	39.500
160	35.088	0.400	3.000	0.000	0.000	0.000	39.750
161	34.675	0.400	3.000	0.000	0.000	0.000	40.000
162	34.262	0.250	6.000	0.000	0.000	0.000	40.250
163	28.483	0.200	6.000	0.000	0.000	0.000	40.500
164	28.896	0.100	6.000	0.000	0.000	0.000	40.750
165	30.547	0.050	6.000	0.000	0.000	0.000	41.000
166	26.832	0.050	6.000	0.000	0.000	0.000	41.250
167	21.878	0.050	4.000	0.000	0.000	0.000	41.500
168	23.842	0.050	6.000	0.000	0.000	0.000	41.750

Weather 6/22/92

	Time	Air Temp	Pressure	Humidity	Dew Point	Wind Speed	Direct Ins
169	18.000	18.200	1012.000	0.320	-1.000	1.820	18.232
170	18.250	17.800	1012.000	0.325	-1.000	1.690	24.080
171	18.500	17.800	1011.400	0.340	-1.000	1.410	5.160
172	18.750	18.000	1012.500	0.350	-1.000	1.090	4.816
173	19.000	18.500	1012.000	0.353	-1.000	1.210	1.376
174	19.250	17.200	1012.100	0.370	-1.000	1.320	1.032
175	19.500	17.000	1012.000	0.382	-1.000	0.000	1.032
176	19.750	18.000	1012.000	0.397	-1.000	0.240	0.344
177	20.000	16.800	1012.000	0.403	-1.000	0.870	0.344
178	20.250	16.500	1011.700	0.418	-1.000	0.540	0.000
179	20.500	16.400	1011.700	0.427	-1.000	0.590	0.000
180	20.750	15.300	1011.700	0.450	-1.000	0.010	0.000
181	21.000	16.100	1011.100	0.512	-1.000	0.020	0.000
182	21.250	16.400	1011.100	0.559	-1.000	0.000	0.000
183	21.500	14.900	1011.000	0.675	-1.000	0.000	0.000
184	21.750	13.900	1011.000	0.760	-1.000	0.000	0.000
185	22.000	14.000	1011.000	0.810	-1.000	0.000	0.000
186	22.250	13.900	1011.000	0.822	-1.000	0.000	0.000
187	22.500	13.900	1010.700	0.840	-1.000	0.000	0.000
188	22.750	13.600	1010.500	0.810	-1.000	0.000	0.000
189	23.000	13.800	1010.100	0.763	-1.000	0.010	0.000
190	23.250	13.900	1010.000	0.787	-1.000	0.000	0.000
191	23.500	13.500	1009.800	0.770	-1.000	0.010	0.000
192	23.750	13.700	1009.800	0.710	-1.000	0.020	0.000
193	0.000	13.900	1009.800	0.687	-1.000	0.000	0.000
194	0.250	13.900	1009.800	0.675	-1.000	0.010	0.000
195	0.500	13.900	1009.400	0.668	-1.000	0.000	0.000
196	0.750	13.900	1009.000	0.648	-1.000	0.000	0.000
197	1.000	14.000	1009.000	0.622	-1.000	0.050	0.000
198	1.250	13.900	1008.700	0.611	-1.000	0.000	0.000
199	1.500	13.900	1009.000	0.610	-1.000	0.000	0.000
200	1.750	13.900	1008.500	0.645	-1.000	0.000	0.000
201	2.000	13.800	1008.100	0.649	-1.000	0.000	0.000
202	2.250	13.500	1008.500	0.655	-1.000	0.000	0.000
203	2.500	13.800	1008.100	0.694	-1.000	0.000	0.000
204	2.750	13.800	1008.800	0.729	-1.000	0.000	0.000
205	3.000	12.900	1007.500	0.779	-1.000	0.000	0.000

Weather 6/22/92

	Diffuse Ins	Sky Exposure	Cloud Type	Rain Type	Rain Rate	Rain Temp	Time
169	23.942	0.150	6.000	0.000	0.000	0.000	42.000
170	17.750	0.150	6.000	0.000	0.000	0.000	42.250
171	16.925	0.150	6.000	0.000	0.000	0.000	42.500
172	15.686	0.150	6.000	0.000	0.000	0.000	42.750
173	11.146	0.100	6.000	0.000	0.000	0.000	43.000
174	6.192	0.050	6.000	0.000	0.000	0.000	43.250
175	4.954	0.050	6.000	0.000	0.000	0.000	43.500
176	3.715	0.000	6.000	0.000	0.000	0.000	43.750
177	1.651	0.000	6.000	0.000	0.000	0.000	44.000
178	1.238	0.050	6.000	0.000	0.000	0.000	44.250
179	0.344	0.050	6.000	0.000	0.000	0.000	44.500
180	0.000	0.000	6.000	0.000	0.000	0.000	44.750
181	0.000	0.000	6.000	1.000	0.025	12.000	45.000
182	0.000	0.000	6.000	1.000	0.025	12.000	45.250
183	0.000	0.000	6.000	1.000	0.025	12.000	45.500
184	0.000	0.000	6.000	1.000	0.025	12.000	45.750
185	0.000	0.000	6.000	1.000	0.025	12.000	46.000
186	0.000	0.000	6.000	0.000	0.000	0.000	46.250
187	0.000	0.000	6.000	0.000	0.000	0.000	46.500
188	0.000	0.000	6.000	0.000	0.000	0.000	46.750
189	0.000	0.000	6.000	0.000	0.000	0.000	47.000
190	0.000	0.000	6.000	0.000	0.000	0.000	47.250
191	0.000	0.000	6.000	0.000	0.000	0.000	47.500
192	0.000	0.000	6.000	0.000	0.000	0.000	47.750
193	0.000	0.000	6.000	0.000	0.000	0.000	48.000
194	0.000	0.000	6.000	0.000	0.000	0.000	48.250
195	0.000	0.000	6.000	0.000	0.000	0.000	48.500
196	0.000	0.000	6.000	0.000	0.000	0.000	48.750
197	0.000	0.000	6.000	1.000	0.010	12.000	49.000
198	0.000	0.000	6.000	1.000	0.010	12.000	49.250
199	0.000	0.000	6.000	1.000	0.010	12.000	49.500
200	0.000	0.000	6.000	0.000	0.000	0.000	49.750
201	0.000	0.000	6.000	0.000	0.000	0.000	50.000
202	0.000	0.000	6.000	1.000	0.010	12.000	50.250
203	0.000	0.000	6.000	0.000	0.000	0.000	50.500
204	0.000	0.000	6.000	1.000	0.010	10.000	50.750
205	0.000	0.000	6.000	1.000	0.500	10.000	51.000

Oct Weather Data

	Time	Air Temp	Air Pressure	Rel. Humidity	Dew Point	Wind Speed	Direct
1	5.000	10.560	1008.000	0.800	-1.000	0.833	0.000
2	5.250	9.940	1008.100	0.800	-1.000	0.278	0.000
3	5.500	9.440	1006.500	0.800	-1.000	0.556	0.000
4	5.750	9.720	1006.500	0.800	-1.000	0.278	0.000
5	6.000	9.830	1006.500	0.800	-1.000	0.833	0.000
6	6.250	9.750	1006.500	0.800	-1.000	0.556	0.000
7	6.500	9.800	1006.600	0.800	-1.000	0.278	0.000
8	6.750	9.850	1006.600	0.800	-1.000	0.278	0.000
9	7.000	9.900	1006.600	0.860	-1.000	0.278	0.000
10	7.250	10.100	1007.000	0.860	-1.000	3.330	0.344
11	7.500	11.500	1007.500	0.860	-1.000	0.833	0.688
12	7.750	12.100	1007.800	0.860	-1.000	4.170	2.064
13	8.000	12.900	1009.500	0.770	-1.000	1.940	5.848
14	8.250	13.000	1009.500	0.770	-1.000	1.390	9.632
15	8.500	13.000	1009.500	0.770	-1.000	2.500	13.760
16	8.750	13.000	1009.600	0.770	-1.000	1.940	17.200
17	9.000	13.000	1009.600	0.690	-1.000	1.110	21.672
18	9.250	12.900	1009.600	0.690	-1.000	0.833	25.456
19	9.500	12.900	1009.700	0.690	-1.000	4.170	29.584
20	9.750	13.000	1010.000	0.690	-1.000	3.330	33.024
21	10.000	13.000	1010.200	0.550	-1.000	3.610	36.464
22	10.250	15.000	1011.000	0.550	-1.000	3.330	39.044
23	10.500	14.900	1010.500	0.550	-1.000	3.890	42.312
24	10.750	15.000	1010.800	0.550	-1.000	4.720	45.408
25	11.000	15.000	1010.600	0.480	-1.000	2.220	47.816
26	11.250	15.500	1010.900	0.480	-1.000	3.890	50.224
27	11.500	16.100	1010.900	0.480	-1.000	5.560	52.288
28	11.750	16.800	1011.100	0.480	-1.000	5.000	54.008
29	12.000	17.100	1011.500	0.423	-1.000	1.111	54.696
30	12.250	18.000	1011.100	0.419	-1.000	5.000	56.072
31	12.500	18.100	1011.700	0.404	-1.000	4.167	56.760
32	12.750	18.000	1011.500	0.413	-1.000	3.333	57.792
33	13.000	18.200	1011.400	0.449	-1.000	3.611	50.568
34	13.250	17.700	1011.500	0.475	-1.000	4.167	41.624
35	13.500	18.500	1011.400	0.471	-1.000	5.560	55.728
36	13.750	18.500	1011.100	0.465	-1.000	6.390	56.072
37	14.000	18.800	1011.000	0.481	-1.000	0.560	54.352
38	14.250	19.500	1011.000	0.480	-1.000	5.000	53.320
39	14.500	19.000	1010.500	0.490	-1.000	6.100	51.600
40	14.750	19.000	1010.500	0.461	-1.000	2.920	43.344
41	15.000	19.800	1010.500	0.440	-1.000	5.000	45.408
42	15.250	20.000	1010.500	0.410	-1.000	4.170	49.192
43	15.500	20.000	1010.700	0.396	-1.000	3.330	43.000
44	15.750	20.000	1010.200	0.373	-1.000	4.170	41.968
45	16.000	20.000	1010.500	0.362	-1.000	1.390	38.184
46	16.250	20.000	1010.500	0.360	-1.000	3.890	22.360
47	16.500	20.200	1010.500	0.362	-1.000	3.610	11.696
48	16.750	20.500	1010.000	0.365	-1.000	4.440	23.392
49	17.000	20.000	1010.200	0.395	-1.000	2.770	6.880
50	17.250	20.000	1010.000	0.405	-1.000	2.500	7.224
51	17.500	20.000	1010.200	0.425	-1.000	3.890	5.848
52	17.750	20.000	1010.400	0.445	-1.000	4.440	5.504
53	18.000	19.800	1010.300	0.460	-1.000	2.220	6.192
54	18.250	19.000	1010.000	0.480	-1.000	2.220	4.472
55	18.500	18.400	1010.200	0.520	-1.000	1.390	2.580
56	18.750	17.900	1010.000	0.535	-1.000	2.780	0.344

Oct Weather Data

	Diffuse	sky exposure	cloud type	precip type	precip rate	precip temp	Time
1	0.000	0.400	2.000	0.000	0.000	0.000	5.000
2	0.000	0.700	2.000	0.000	0.000	0.000	5.250
3	0.000	1.000	0.000	0.000	0.000	0.000	5.500
4	0.000	1.000	0.000	0.000	0.000	0.000	5.750
5	0.000	1.000	0.000	0.000	0.000	0.000	6.000
6	0.000	0.950	1.000	0.000	0.000	0.000	6.250
7	0.000	0.970	1.000	0.000	0.000	0.000	6.500
8	0.000	0.980	1.000	0.000	0.000	0.000	6.750
9	0.000	0.980	1.000	0.000	0.000	0.000	7.000
10	0.000	0.980	1.000	0.000	0.000	0.000	7.250
11	0.688	1.000	0.000	0.000	0.000	0.000	7.500
12	1.376	1.000	0.000	0.000	0.000	0.000	7.750
13	2.064	1.000	0.000	0.000	0.000	0.000	8.000
14	2.064	1.000	0.000	0.000	0.000	0.000	8.250
15	2.752	1.000	0.000	0.000	0.000	0.000	8.500
16	2.752	1.000	0.000	0.000	0.000	0.000	8.750
17	3.096	1.000	0.000	0.000	0.000	0.000	9.000
18	3.440	1.000	0.000	0.000	0.000	0.000	9.250
19	3.440	1.000	0.000	0.000	0.000	0.000	9.500
20	3.440	1.000	0.000	0.000	0.000	0.000	9.750
21	3.784	0.980	2.000	0.000	0.000	0.000	10.000
22	3.784	0.980	2.000	0.000	0.000	0.000	10.250
23	3.784	1.000	0.000	0.000	0.000	0.000	10.500
24	4.128	1.000	0.000	0.000	0.000	0.000	10.750
25	3.784	1.000	0.000	0.000	0.000	0.000	11.000
26	4.128	1.000	0.000	0.000	0.000	0.000	11.250
27	4.128	1.000	0.000	0.000	0.000	0.000	11.500
28	4.128	0.990	0.000	0.000	0.000	0.000	11.750
29	4.128	0.990	0.000	0.000	0.000	0.000	12.000
30	4.128	0.970	0.000	0.000	0.000	0.000	12.250
31	4.472	0.970	0.000	0.000	0.000	0.000	12.500
32	8.944	0.900	1.000	0.000	0.000	0.000	12.750
33	6.192	0.800	2.000	0.000	0.000	0.000	13.000
34	7.568	0.850	2.000	0.000	0.000	0.000	13.250
35	9.288	0.850	2.000	0.000	0.000	0.000	13.500
36	5.160	0.900	2.000	0.000	0.000	0.000	13.750
37	4.472	0.950	1.000	0.000	0.000	0.000	14.000
38	4.128	0.950	2.000	0.000	0.000	0.000	14.250
39	4.472	0.950	2.000	0.000	0.000	0.000	14.500
40	6.192	0.950	2.000	0.000	0.000	0.000	14.750
41	6.192	0.950	1.000	0.000	0.000	0.000	15.000
42	8.944	0.900	1.000	0.000	0.000	0.000	15.250
43	4.816	0.930	1.000	0.000	0.000	0.000	15.500
44	6.536	0.700	1.000	0.000	0.000	0.000	15.750
45	5.848	0.700	3.000	0.000	0.000	0.000	16.000
46	11.008	0.300	5.000	0.000	0.000	0.000	16.250
47	9.632	0.300	3.000	0.000	0.000	0.000	16.500
48	12.040	0.300	3.000	0.000	0.000	0.000	16.750
49	6.192	0.200	3.000	0.000	0.000	0.000	17.000
50	6.536	0.150	3.000	0.000	0.000	0.000	17.250
51	5.160	0.100	3.000	0.000	0.000	0.000	17.500
52	4.472	0.200	3.000	0.000	0.000	0.000	17.750
53	3.784	0.300	3.000	0.000	0.000	0.000	18.000
54	3.440	0.500	3.000	0.000	0.000	0.000	18.250
55	1.720	0.600	3.000	0.000	0.000	0.000	18.500
56	0.000	0.700	3.000	0.000	0.000	0.000	18.750

Oct Weather Data

	Time	Air Temp	Air Pressure	Rel. Humidity	Dew Point	Wind Speed	Direct
57	19.000	17.800	1010.100	0.555	-1.000	0.560	0.000
58	19.250	17.500	1010.100	0.575	-1.000	0.560	0.000
59	19.500	17.000	1010.100	0.598	-1.000	0.560	0.000
60	19.750	16.800	1010.100	0.615	-1.000	0.560	0.000
61	20.000	16.800	1010.100	0.630	-1.000	0.280	0.000
62	20.250	15.000	1009.900	0.650	-1.000	0.280	0.000
63	20.500	16.000	1009.900	0.660	-1.000	0.280	0.000
64	20.750	15.500	1009.800	0.675	-1.000	0.280	0.000
65	21.000	15.800	1009.800	0.685	-1.000	0.560	0.000
66	21.250	15.500	1009.800	0.687	-1.000	0.560	0.000
67	21.500	16.000	1009.800	0.700	-1.000	0.280	0.000
68	21.750	15.500	1009.600	0.708	-1.000	0.280	0.000
69	22.000	15.500	1009.500	0.710	-1.000	0.560	0.000
70	22.250	16.500	1009.500	0.701	-1.000	1.400	0.000
71	22.500	16.100	1009.900	0.701	-1.000	0.560	0.000
72	22.750	16.200	1009.100	0.700	-1.000	1.400	0.000
73	23.000	16.200	1009.900	0.675	-1.000	2.240	0.000
74	23.250	16.800	1009.800	0.653	-1.000	2.800	0.000
75	23.500	16.800	1009.900	0.645	-1.000	0.840	0.000
76	23.750	17.000	1009.900	0.649	-1.000	0.560	0.000
77	24.000	17.000	1009.900	0.649	-1.000	1.400	0.000
78	24.250	17.500	1009.900	0.622	-1.000	1.400	0.000
79	24.500	18.000	1009.900	0.592	-1.000	1.120	0.000
80	24.750	18.000	1009.900	0.578	-1.000	3.080	0.000
81	25.000	19.300	1009.900	0.567	-1.000	2.240	0.000
82	25.250	19.000	1010.000	0.552	-1.000	3.360	0.000
83	25.500	19.300	1010.000	0.540	-1.000	2.800	0.000
84	25.750	19.900	1010.100	0.543	-1.000	2.240	0.000
85	26.000	19.900	1010.200	0.540	-1.000	1.400	0.000
86	26.250	19.800	1010.200	0.538	-1.000	2.800	0.000
87	26.500	19.800	1011.000	0.535	-1.000	2.800	0.000
88	26.750	19.700	1011.000	0.532	-1.000	5.600	0.000
89	27.000	19.900	1010.800	0.532	-1.000	3.360	0.000
90	27.250	19.900	1010.900	0.542	-1.000	6.160	0.000
91	27.500	19.800	1011.000	0.542	-1.000	2.800	0.000
92	27.750	19.300	1011.000	0.551	-1.000	2.800	0.000
93	28.000	18.900	1011.200	0.575	-1.000	2.800	0.000
94	28.250	18.500	1011.200	0.600	-1.000	0.560	0.000
95	28.500	18.000	1011.100	0.618	-1.000	1.400	0.000
96	28.750	17.900	1011.100	0.620	-1.000	3.360	0.000
97	29.000	18.000	1011.000	0.622	-1.000	2.800	0.000
98	29.250	18.000	1011.000	0.622	-1.000	2.240	0.000
99	29.500	18.000	1011.000	0.621	-1.000	1.400	0.000
100	29.750	17.800	1011.100	0.640	-1.000	0.560	0.000
101	30.000	17.000	1011.000	0.662	-1.000	0.556	0.000
102	30.250	17.000	1011.100	0.670	-1.000	0.556	0.000
103	30.500	16.900	1011.100	0.680	-1.000	2.222	0.000
104	30.750	17.100	1011.000	0.680	-1.000	0.278	0.000
105	31.000	17.100	1011.100	0.680	-1.000	0.278	0.000
106	31.250	16.800	1011.000	0.680	-1.000	0.278	0.000
107	31.500	16.900	1011.200	0.675	-1.000	0.556	0.344
108	31.750	16.900	1011.400	0.690	-1.000	0.833	1.376
109	32.000	17.000	1011.300	0.689	-1.000	2.778	4.128
110	32.250	16.800	1011.300	0.678	-1.000	1.389	8.256
111	32.500	17.000	1011.500	0.669	-1.000	0.278	11.352
112	32.750	17.200	1011.600	0.651	-1.000	1.944	16.168

Oct Weather Data

	Diffuse	sky exposure	cloud type	precip type	precip rate	precip temp	Time
57	0.000	0.700	3.000	0.000	0.000	0.000	19.000
58	0.000	0.800	6.000	0.000	0.000	0.000	19.250
59	0.000	0.850	6.000	0.000	0.000	0.000	19.500
60	0.000	0.850	6.000	0.000	0.000	0.000	19.750
61	0.000	0.900	6.000	0.000	0.000	0.000	20.000
62	0.000	0.950	6.000	0.000	0.000	0.000	20.250
63	0.000	0.950	6.000	0.000	0.000	0.000	20.500
64	0.000	0.950	6.000	0.000	0.000	0.000	20.750
65	0.000	0.950	6.000	0.000	0.000	0.000	21.000
66	0.000	0.900	6.000	0.000	0.000	0.000	21.250
67	0.000	0.950	6.000	0.000	0.000	0.000	21.500
68	0.000	0.950	6.000	0.000	0.000	0.000	21.750
69	0.000	0.950	6.000	0.000	0.000	0.000	22.000
70	0.000	0.950	6.000	0.000	0.000	0.000	22.250
71	0.000	0.900	6.000	0.000	0.000	0.000	22.500
72	0.000	0.900	6.000	0.000	0.000	0.000	22.750
73	0.000	0.900	6.000	0.000	0.000	0.000	23.000
74	0.000	0.900	6.000	0.000	0.000	0.000	23.250
75	0.000	0.900	6.000	0.000	0.000	0.000	23.500
76	0.000	0.900	6.000	0.000	0.000	0.000	23.750
77	0.000	0.500	6.000	0.000	0.000	0.000	24.000
78	0.000	0.250	6.000	0.000	0.000	0.000	24.250
79	0.000	0.600	6.000	0.000	0.000	0.000	24.500
80	0.000	0.900	6.000	0.000	0.000	0.000	24.750
81	0.000	0.950	6.000	0.000	0.000	0.000	25.000
82	0.000	1.000	0.000	0.000	0.000	0.000	25.250
83	0.000	1.000	0.000	0.000	0.000	0.000	25.500
84	0.000	1.000	0.000	0.000	0.000	0.000	25.750
85	0.000	1.000	0.000	0.000	0.000	0.000	26.000
86	0.000	1.000	0.000	0.000	0.000	0.000	26.250
87	0.000	1.000	0.000	0.000	0.000	0.000	26.500
88	0.000	1.000	0.000	0.000	0.000	0.000	26.750
89	0.000	1.000	0.000	0.000	0.000	0.000	27.000
90	0.000	1.000	0.000	0.000	0.000	0.000	27.250
91	0.000	1.000	0.000	0.000	0.000	0.000	27.500
92	0.000	1.000	0.000	0.000	0.000	0.000	27.750
93	0.000	1.000	0.000	0.000	0.000	0.000	28.000
94	0.000	1.000	0.000	0.000	0.000	0.000	28.250
95	0.000	1.000	0.000	0.000	0.000	0.000	28.500
96	0.000	1.000	0.000	0.000	0.000	0.000	28.750
97	0.000	1.000	0.000	0.000	0.000	0.000	29.000
98	0.000	1.000	0.000	0.000	0.000	0.000	29.250
99	0.000	1.000	0.000	0.000	0.000	0.000	29.500
100	0.000	1.000	0.000	0.000	0.000	0.000	29.750
101	0.000	1.000	1.000	0.000	0.000	0.000	30.000
102	0.000	0.900	1.000	0.000	0.000	0.000	30.250
103	0.000	0.950	1.000	0.000	0.000	0.000	30.500
104	0.000	0.900	1.000	0.000	0.000	0.000	30.750
105	0.000	0.950	1.000	0.000	0.000	0.000	31.000
106	0.000	0.950	1.000	0.000	0.000	0.000	31.250
107	0.344	0.900	1.000	0.000	0.000	0.000	31.500
108	1.376	0.950	1.000	0.000	0.000	0.000	31.750
109	1.720	0.900	1.000	0.000	0.000	0.000	32.000
110	2.752	0.900	1.000	0.000	0.000	0.000	32.250
111	2.752	0.950	1.000	0.000	0.000	0.000	32.500
112	3.440	0.950	1.000	0.000	0.000	0.000	32.750

Oct Weather Data

	Time	Air Temp	Air Pressure	Rel. Humidity	Dew Point	Wind Speed	Direct
113	33.000	18.400	1011.800	0.632	-1.000	0.556	19.952
114	33.250	19.100	1011.800	0.622	-1.000	2.222	23.048
115	33.500	19.700	1011.900	0.610	-1.000	2.778	27.520
116	33.750	20.000	1011.900	0.600	-1.000	5.000	31.648
117	34.000	20.200	1011.800	0.589	-1.000	2.778	8.342
118	34.250	21.000	1011.800	0.580	-1.000	3.333	37.496
119	34.500	21.800	1011.800	0.570	-1.000	3.333	40.592
120	34.750	21.900	1011.900	0.551	-1.000	1.389	43.344
121	35.000	21.800	1011.900	0.543	-1.000	1.111	45.752
122	35.250	22.500	1011.900	0.529	-1.000	0.833	48.160
123	35.500	22.300	1011.900	0.528	-1.000	1.111	50.568
124	35.750	23.200	1011.800	0.494	-1.000	1.389	51.944
125	36.000	23.900	1011.900	0.473	-1.000	0.833	53.320
126	36.250	24.200	1011.400	0.430	-1.000	4.444	54.696
127	36.500	24.900	1011.800	0.401	-1.000	2.778	55.384
128	36.750	25.200	1011.300	0.377	-1.000	3.333	55.728
129	37.000	26.200	1011.500	0.379	-1.000	2.778	54.696
130	37.250	26.500	1011.100	0.352	-1.000	5.556	55.728
131	37.500	26.700	1011.000	0.344	-1.000	2.778	56.072
132	37.750	26.800	1010.500	0.328	-1.000	4.167	56.416
133	38.000	26.500	1010.500	0.320	-1.000	6.944	54.696
134	38.250	26.800	1010.300	0.320	-1.000	5.556	55.040
135	38.500	26.500	1010.500	0.322	-1.000	5.556	51.944
136	38.750	26.600	1010.700	0.323	-1.000	5.556	49.880
137	39.000	26.500	1010.200	0.325	-1.000	6.944	46.096
138	39.250	26.600	1010.100	0.330	-1.000	5.556	43.688
139	39.500	26.600	1010.200	0.338	-1.000	5.000	41.280
140	39.750	26.800	1010.100	0.345	-1.000	2.222	38.528
141	40.000	26.700	1009.800	0.350	-1.000	5.556	35.432
142	40.250	26.600	1009.800	0.353	-1.000	3.056	32.336
143	40.500	26.500	1010.000	0.358	-1.000	3.333	28.208
144	40.750	26.500	1010.000	0.360	-1.000	2.778	25.112
145	41.000	26.500	1010.000	0.362	-1.000	4.167	20.984
146	41.250	26.300	1009.900	0.364	-1.000	4.167	17.544
147	41.500	26.300	1009.900	0.368	-1.000	4.167	13.760
148	41.750	26.000	1010.000	0.371	-1.000	2.778	10.320
149	42.000	25.500	1010.100	0.383	-1.000	2.222	6.880
150	42.250	25.200	1010.200	0.390	-1.000	1.389	3.784
151	42.500	24.500	1010.500	0.413	-1.000	2.222	1.376
152	42.750	24.000	1010.500	0.420	-1.000	1.111	0.000
153	43.000	23.500	1010.600	0.430	-1.000	1.389	0.000
154	43.250	23.000	1010.800	0.445	-1.000	1.389	0.000
155	43.500	22.500	1011.000	0.453	-1.000	0.278	0.000
156	43.750	22.000	1011.200	0.440	-1.000	0.556	0.000
157	44.000	21.600	1011.200	0.472	-1.000	0.556	0.000
158	44.250	21.800	1011.200	0.475	-1.000	0.556	0.000
159	44.500	21.700	1011.200	0.476	-1.000	2.222	0.000
160	44.750	21.700	1011.200	0.480	-1.000	0.833	0.000
161	45.000	21.300	1011.500	0.490	-1.000	0.556	0.000
162	45.250	21.000	1011.700	0.503	-1.000	0.278	0.000
163	45.500	20.500	1011.700	0.524	-1.000	0.556	0.000
164	45.750	20.200	1012.000	0.540	-1.000	0.278	0.000
165	46.000	19.800	1012.200	0.560	-1.000	0.556	0.000
166	46.250	19.300	1012.800	0.579	-1.000	0.278	0.000
167	46.500	19.300	1012.900	0.599	-1.000	1.389	0.000
168	46.750	19.200	1012.900	0.600	-1.000	1.111	0.000

Oct Weather Data

	Diffuse	sky exposure	cloud type	precip type	precip rate	precip temp	Time
113	4.128	0.970	1.000	0.000	0.000	0.000	33.000
114	4.128	0.970	1.000	0.000	0.000	0.000	33.250
115	3.784	0.970	1.000	0.000	0.000	0.000	33.500
116	4.472	0.970	1.000	0.000	0.000	0.000	33.750
117	4.472	1.000	0.000	0.000	0.000	0.000	34.000
118	4.472	1.000	0.000	0.000	0.000	0.000	34.250
119	4.128	1.000	0.000	0.000	0.000	0.000	34.500
120	4.472	1.000	0.000	0.000	0.000	0.000	34.750
121	4.128	1.000	0.000	0.000	0.000	0.000	35.000
122	4.472	1.000	0.000	0.000	0.000	0.000	35.250
123	4.472	1.000	0.000	0.000	0.000	0.000	35.500
124	4.472	1.000	0.000	0.000	0.000	0.000	35.750
125	4.816	1.000	0.000	0.000	0.000	0.000	36.000
126	4.472	0.990	1.000	0.000	0.000	0.000	36.250
127	5.504	0.970	1.000	0.000	0.000	0.000	36.500
128	5.848	0.950	6.000	0.000	0.000	0.000	36.750
129	6.192	0.900	6.000	0.000	0.000	0.000	37.000
130	5.848	0.850	6.000	0.000	0.000	0.000	37.250
131	5.848	0.850	6.000	0.000	0.000	0.000	37.500
132	5.848	0.900	6.000	0.000	0.000	0.000	37.750
133	5.848	0.850	6.000	0.000	0.000	0.000	38.000
134	7.568	0.800	6.000	0.000	0.000	0.000	38.250
135	6.536	0.850	1.000	0.000	0.000	0.000	38.500
136	5.848	0.800	1.000	0.000	0.000	0.000	38.750
137	6.880	0.850	1.000	0.000	0.000	0.000	39.000
138	5.504	0.850	1.000	0.000	0.000	0.000	39.250
139	4.816	0.900	1.000	0.000	0.000	0.000	39.500
140	5.160	0.900	1.000	0.000	0.000	0.000	39.750
141	4.472	0.900	1.000	0.000	0.000	0.000	40.000
142	4.472	0.900	1.000	0.000	0.000	0.000	40.250
143	4.128	0.950	1.000	0.000	0.000	0.000	40.500
144	3.784	0.950	1.000	0.000	0.000	0.000	40.750
145	3.784	0.950	1.000	0.000	0.000	0.000	41.000
146	3.440	0.950	1.000	0.000	0.000	0.000	41.250
147	2.752	0.950	1.000	0.000	0.000	0.000	41.500
148	2.752	0.950	1.000	0.000	0.000	0.000	41.750
149	2.064	0.950	3.000	0.000	0.000	0.000	42.000
150	1.720	0.950	3.000	0.000	0.000	0.000	42.250
151	0.688	0.950	3.000	0.000	0.000	0.000	42.500
152	0.000	0.950	3.000	0.000	0.000	0.000	42.750
153	0.000	0.950	3.000	0.000	0.000	0.000	43.000
154	0.000	0.950	3.000	0.000	0.000	0.000	43.250
155	0.000	1.000	0.000	0.000	0.000	0.000	43.500
156	0.000	1.000	0.000	0.000	0.000	0.000	43.750
157	0.000	1.000	0.000	0.000	0.000	0.000	44.000
158	0.000	1.000	0.000	0.000	0.000	0.000	44.250
159	0.000	0.800	1.000	0.000	0.000	0.000	44.500
160	0.000	0.800	1.000	0.000	0.000	0.000	44.750
161	0.000	0.950	1.000	0.000	0.000	0.000	45.000
162	0.000	0.950	1.000	0.000	0.000	0.000	45.250
163	0.000	0.970	1.000	0.000	0.000	0.000	45.500
164	0.000	1.000	0.000	0.000	0.000	0.000	45.750
165	0.000	1.000	0.000	0.000	0.000	0.000	46.000
166	0.000	1.000	0.000	0.000	0.000	0.000	46.250
167	0.000	1.000	0.000	0.000	0.000	0.000	46.500
168	0.000	1.000	0.000	0.000	0.000	0.000	46.750

Oct Weather Data

	Time	Air Temp	Air Pressure	Rel. Humidity	Dew Point	Wind Speed	Direct
169	47.000	19.200	1013.100	0.602	-1.000	1.389	0.000
170	47.250	19.200	1013.100	0.601	-1.000	0.278	0.000
171	47.500	18.900	1013.100	0.615	-1.000	1.389	0.000
172	47.750	18.400	1013.000	0.612	-1.000	1.389	0.000
173	48.000	18.900	1013.800	0.626	-1.000	0.833	0.000
174	48.250	18.700	1013.900	0.630	-1.000	2.778	0.000
175	48.500	18.600	1013.700	0.640	-1.000	0.278	0.000
176	48.750	18.500	1013.900	0.645	-1.000	0.278	0.000
177	49.000	18.400	1013.900	0.644	-1.000	1.111	0.000
178	49.250	18.200	1013.500	0.632	-1.000	1.667	0.000
179	49.500	18.300	1014.000	0.649	-1.000	1.389	0.000
180	49.750	18.200	1014.000	0.652	-1.000	0.278	0.000
181	50.000	18.200	1014.100	0.661	-1.000	0.278	0.000
182	50.250	18.100	1014.500	0.668	-1.000	0.833	0.000
183	50.500	18.100	1014.800	0.680	-1.000	0.278	0.000
184	50.750	17.500	1014.000	0.693	-1.000	1.389	0.000
185	51.000	17.800	1014.500	0.700	-1.000	0.556	0.000
186	51.250	17.000	1014.800	0.720	-1.000	0.278	0.000
187	51.500	16.800	1014.800	0.740	-1.000	0.278	0.000
188	51.750	16.500	1014.200	0.749	-1.000	0.278	0.000
189	52.000	16.400	1014.200	0.761	-1.000	0.000	0.000
190	52.250	16.100	1014.000	0.770	-1.000	0.278	0.000
191	52.500	16.500	1014.500	0.781	-1.000	0.278	0.000
192	52.750	16.000	1014.400	0.788	-1.000	0.278	0.000
193	53.000	16.200	1014.700	0.788	-1.000	0.556	0.000

Oct Weather Data

	Diffuse	sky exposure	cloud type	precip type	precip rate	precip temp	Time
169	0.000	0.900	6.000	0.000	0.000	0.000	47.000
170	0.000	0.850	6.000	0.000	0.000	0.000	47.250
171	0.000	0.900	6.000	0.000	0.000	0.000	47.500
172	0.000	0.900	6.000	0.000	0.000	0.000	47.750
173	0.000	0.950	6.000	0.000	0.000	0.000	48.000
174	0.000	1.000	0.000	0.000	0.000	0.000	48.250
175	0.000	0.950	6.000	0.000	0.000	0.000	48.500
176	0.000	1.000	0.000	0.000	0.000	0.000	48.750
177	0.000	1.000	0.000	0.000	0.000	0.000	49.000
178	0.000	0.950	6.000	0.000	0.000	0.000	49.250
179	0.000	1.000	0.000	0.000	0.000	0.000	49.500
180	0.000	1.000	0.000	0.000	0.000	0.000	49.750
181	0.000	1.000	0.000	0.000	0.000	0.000	50.000
182	0.000	1.000	0.000	0.000	0.000	0.000	50.250
183	0.000	1.000	0.000	0.000	0.000	0.000	50.500
184	0.000	1.000	0.000	0.000	0.000	0.000	50.750
185	0.000	0.900	6.000	0.000	0.000	0.000	51.000
186	0.000	0.800	6.000	0.000	0.000	0.000	51.250
187	0.000	0.950	6.000	0.000	0.000	0.000	51.500
188	0.000	0.950	6.000	0.000	0.000	0.000	51.750
189	0.000	0.900	6.000	0.000	0.000	0.000	52.000
190	0.000	0.900	6.000	0.000	0.000	0.000	52.250
191	0.000	0.900	6.000	0.000	0.000	0.000	52.500
192	0.000	0.800	6.000	0.000	0.000	0.000	52.750
193	0.000	0.800	6.000	0.000	0.000	0.000	53.000

APPENDIX F

Radiosonde Data for June 1992 & October 1990 Data Collections

June 1992
Buffalo Airport Decoded Radiosonde Data

June 22, 1992 00Z

Altitude	Temperature	Dew Point	Pressure
2.18e+2	8.2e+0	7e+0	9.89e+2
7.87e+2	3.8e+0	3e+0	9.25e+2
1.454e+3	2e-1	-8e-1	8.5e+2
2.409e+3	-4.5e+0	-5.6e+0	7.57e+2
2.995e+3	-4.1e+0	-5.2e+0	7e+2
3.059e+3	-3.7e+0	-4.8e+0	6.95e+2
3.509e+3	-5.9e+0	-7.1e+0	6.6e+2
3.753e+3	-6.7e+0	-1.27e+1	6.41e+2
4.138e+3	-9.1e+0	-1.71e+1	6.11e+2
4.524e+3	-1.17e+1	-1.66e+1	5.81e+2
4.755e+3	-1.31e+1	-1.91e+1	5.63e+2
4.909e+3	-1.27e+1	-2.27e+1	5.51e+2
5.32e+3	-1.59e+1	-2.09e+1	5.19e+2
5.5e+3	-1.71e+1	-4.71e+1	5.05e+2
7.401e+3	-3.59e+1	-6.59e+1	3.57e+2
7.697e+3	-3.99e+1	-4.79e+1	3.34e+2
9.071e+3	-4.83e+1		2.27e+2
9.251e+3	-4.51e+1		2.13e+2
1.0125e+4	-4.63e+1		1.45e+2

June 22, 1992 12Z

Altitude	Temperature	Dew Point	Pressure
2.18e+2	7e+0	4.3e+0	9.92e+2
2.44e+2	7.6e+0	4.5e+0	9.89e+2
1.054e+3	6e-1	-3e-1	8.97e+2
1.467e+3	-5e-1	-3.3e+0	8.5e+2
1.868e+3	-3.3e+0	-4.2e+0	8.11e+2
2.002e+3	-1.9e+0	-3.2e+0	7.98e+2
2.023e+3	-1.5e+0	-4.7e+0	7.96e+2
2.074e+3	-9e-1	-3.09e+1	7.91e+2
2.372e+3	-1.7e+0	-3.17e+1	7.62e+2
2.424e+3	-1.9e+0	-1.49e+1	7.57e+2
2.507e+3	-1.9e+0	-3.19e+1	7.49e+2
2.579e+3	-2.3e+0	-1.73e+1	7.42e+2
2.836e+3	-3.3e+0	-3.33e+1	7.17e+2
2.949e+3	-3.1e+0	-1.51e+1	7.06e+2
3.011e+3	-3.7e+0	-1.47e+1	7e+2

3.151e+3	-4.1e+0	-1.41e+1	6.89e+2
3.253e+3	-4.5e+0	-1.95e+1	6.81e+2
3.381e+3	-5.3e+0	-1.53e+1	6.71e+2
3.572e+3	-6.5e+0	-3.65e+1	6.56e+2
4.834e+3	-1.35e+1	-4.35e+1	5.57e+2
5.56e+3	-1.87e+1	-4.87e+1	5e+2
6.381e+3	-2.25e+1	-5.25e+1	4.62e+2
7.72e+3	-3.17e+1	-6.17e+1	4e+2
9.084e+3	-4.01e+1	-7.01e+1	3.38e+2
9.92e+3	-4.49e+1		3e+2
1.004e+4	-4.93e+1		2.5e+2
1.2187e+4	-4.79e+1		2e+2
1.2713e+4	-4.69e+1		1.88e+2
1.4377e+4	-4.95e+1		1.5e+2
1.5011e+4	-5.03e+1		1.36e+2
1.5283e+4	-4.81e+1		1.3e+2
1.6641e+4	-5.27e+1		1e+2

June 23, 1992 00Z

Altitude	Temperature	Dew Point	Pressure
2.18e+2	9.91e+2	1.58e+1	7.8e+0
6.79e+2	9.4e+2	1.08e+1	6.7e+0
8.14e+2	9.25e+2	1.06e+1	3.6e+0
1.492e+3	8.5e+2	4.8e+0	0e+0
2.096e+3	7.92e+2	0e+0	-3.3e+0
2.262e+3	7.74e+2	4e-1	-2.2e+0
2.449e+3	7.58e+2	1.2e+0	-3.12e+1
3.053e+3	7e+2	-1.5e+0	-3.15e+1
3.832e+3	6.38e+2	-6.1e+0	-3.61e+1
4.209e+3	6.08e+2	-5.7e+0	-3.57e+1
5.566e+3	5e+2	-1.65e+1	-4.65e+1
6.302e+3	4.66e+2	-1.91e+1	-4.91e+1
7.32e+3	4.19e+2	-2.49e+1	-5.49e+1
7.731e+3	4e+2	-2.77e+1	-3.57e+1
8.215e+3	3.78e+2	-3.11e+1	-3.61e+1
9.513e+3	3.19e+2	-3.99e+1	-4.89e+1
9.931e+3	3e+2	-4.33e+1	
1.0051e+4	2.5e+2	-5.35e+1	
1.155e+4	2.15e+2	-6.01e+1	
1.2064e+4	2.03e+2	-5.31e+1	
1.2193e+4	2e+2	-5.29e+1	
1.368e+4	1.66e+2	-4.99e+1	
1.438e+4	1.5e+2	-5.05e+1	
1.6642e+4	1e+2	-5.23e+1	

June 23, 1992 12Z

Altitude	Temperature	Dew Point	Pressure
2.18e+2	9.9e+2	7.6e+0	5.4e+0
2.63e+2	9.85e+2	7.4e+0	6e+0
3.17e+2	9.79e+2	9.6e+0	7.8e+0
3.44e+2	9.76e+2	1.02e+1	2.2e+0
4.25e+2	9.67e+2	1.1e+1	-2e+0
1.271e+3	8.73e+2	4.8e+0	-3.2e+0
1.352e+3	8.64e+2	4.8e+0	-2.52e+1
1.478e+3	8.5e+2	4.4e+0	-2.56e+1
1.812e+3	8.18e+2	4.2e+0	-2.58e+1
2.731e+3	7.3e+2	0e+0	-3e+1
3.044e+3	7e+2	-2.5e+0	-2.15e+1
4.654e+3	5.76e+2	-1.13e+1	-2.93e+1
4.9e+3	5.57e+2	-1.33e+1	-2.13e+1
4.939e+3	5.54e+2	-1.37e+1	-3.07e+1
4.965e+3	5.52e+2	-1.37e+1	-2.67e+1
5.017e+3	5.48e+2	-1.41e+1	-4.41e+1
5.316e+3	5.25e+2	-1.65e+1	-2.15e+1
5.445e+3	5.15e+2	-1.67e+1	-1.86e+1
5.64e+3	5e+2	-1.75e+1	-1.93e+1
6.911e+3	4.22e+2	-2.63e+1	-2.89e+1
7.27e+3	4e+2	-2.93e+1	-3.34e+1
9.26e+3	3e+2	-4.47e+1	
1.0046e+4	2.5e+2	-5.53e+1	
1.187e+4	2e+2	-5.35e+1	
1.374e+4	1.5e+2	-5.13e+1	
1.636e+4	1e+2	-5.37e+1	

June 24, 1992 00Z

Altitude	Temperature	Dew Point	Pressure
2.18e+2	9.85e+2	1.74e+1	7.4e+0
5.02e+2	9.54e+2	1.58e+1	1.38e+1
1.456e+3	8.5e+2	6.8e+0	2.9e+0
1.685e+3	8.28e+2	4.8e+0	2.9e+0
2.299e+3	7.69e+2	0e+0	-1e+0
2.913e+3	7.1e+2	-4.3e+0	-5.3e+0
3.017e+3	7e+2	-4.1e+0	-5.1e+0
3.335e+3	6.75e+2	-3.1e+0	-4.1e+0
4.315e+3	5.98e+2	-7.5e+0	-8.7e+0
5.563e+3	5e+2	-1.63e+1	-1.78e+1
7.727e+3	4e+2	-2.87e+1	-3.21e+1
8.073e+3	3.84e+2	-3.09e+1	-3.51e+1

June 24, 1992 12Z

Altitude	Temperature	Dew Point	Pressure
2.18e+2	9.79e+2	1.2e+1	1.02e+1
3.55e+2	9.64e+2	1.28e+1	1.14e+1
9.76e+2	8.96e+2	9.6e+0	8.9e+0
1.396e+3	8.5e+2	8e+0	7.2e+0
2.973e+3	7e+2	-1.9e+0	-4.5e+0
3.749e+3	6.4e+2	6.5e+0	-9.2e+0
3.8e+3	6.36e+2	-6.7e+0	-9.9e+0
3.942e+3	6.25e+2	-6.9e+0	-2.09e+1
4.188e+3	6.06e+2	-8.3e+0	-1.53e+1
4.382e+3	5.91e+2	-8.9e+0	-3.89e+1
5.558e+3	5e+2	-6.9e+0	-4.69e+1
7.721e+3	4e+2	-3.11e+1	-6.11e+1
8.973e+3	3.43e+2	-3.99e+1	-6.99e+1
9.918e+3	3e+2	-4.43e+1	
1.0038e+4	2.5e+2	-5.11e+1	
1.0553e+4	2.38e+2	-5.21e+1	
1.2184e+4	2e+2	-4.81e+1	
1.4373e+4	1.5e+2	-4.97e+1	
1.469e+4	1.43e+2	-4.87e+1	
1.6275e+4	1.08e+2	-5.41e+1	
1.6637e+4	1e+2	-5.23e+1	

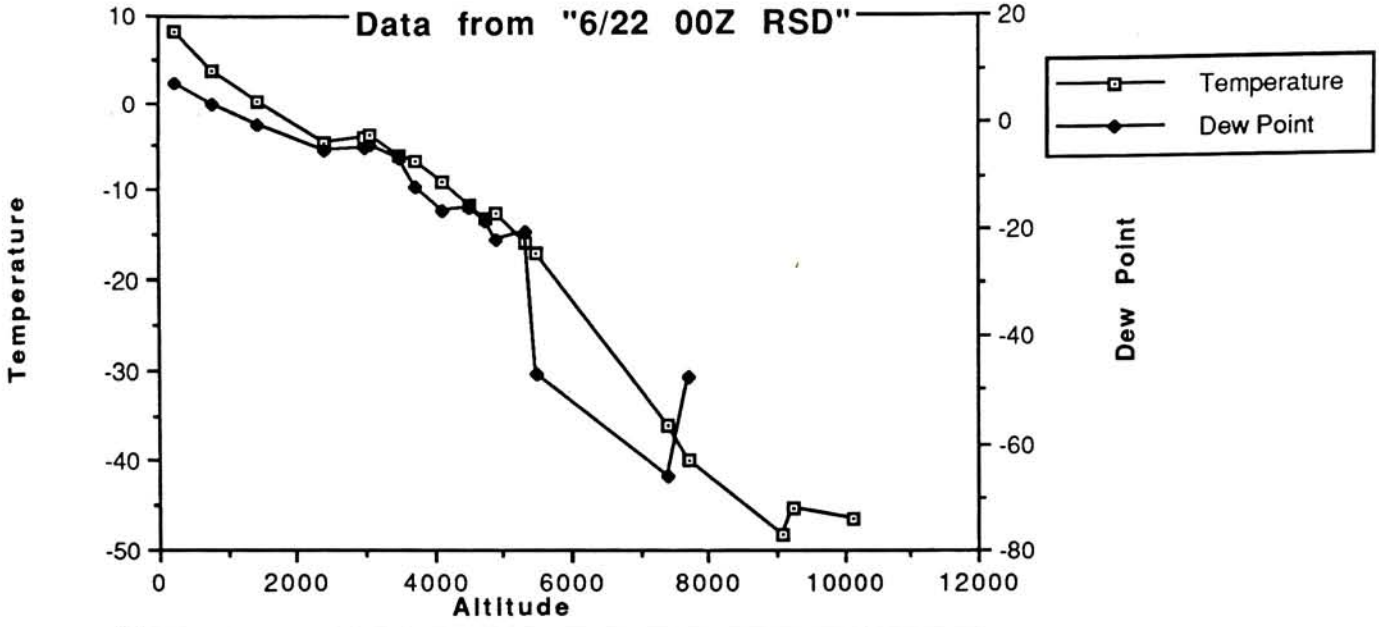
Data from "6/22 00Z RSD"
Temperature
Dew Point
Temperature
Dew Point
Altitude
10
0
-10
-20
-30
-40
-50
20
0
-20
-40
-60
-80
0
2000
4000
6000
8000
10000
12000

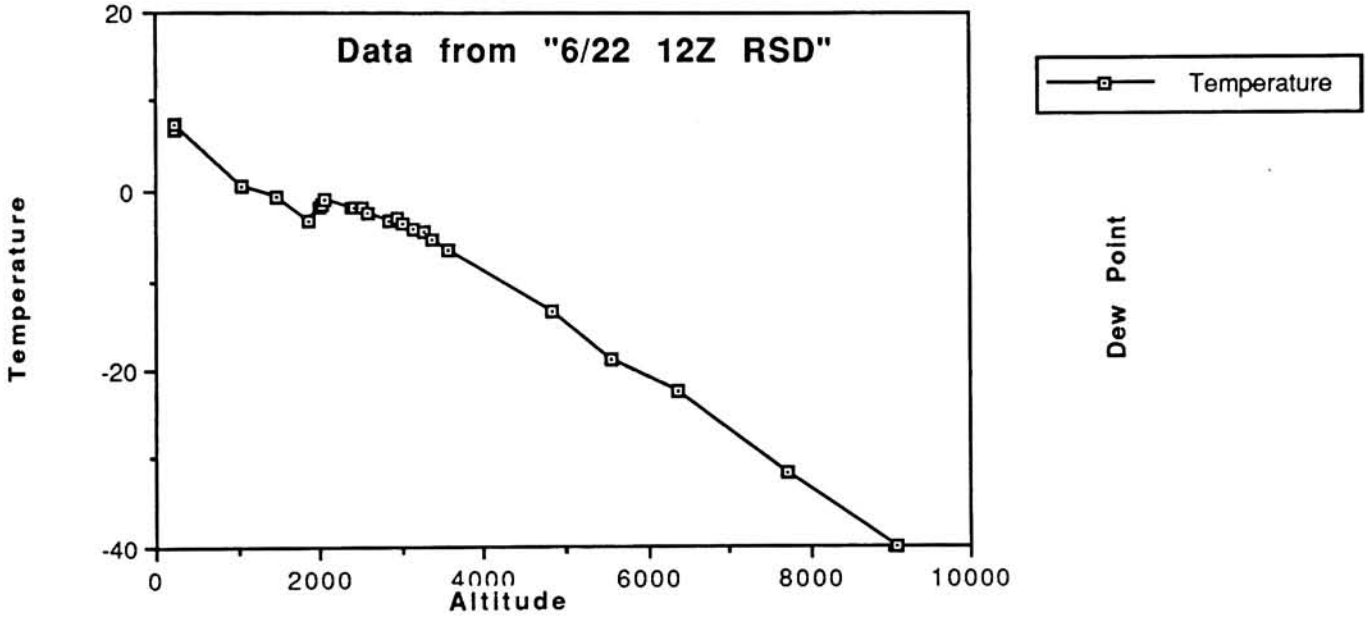
Data from "6/22 12Z RSD"
Temperature
Temperature
Dew Point
Altitude
20
0
-20
-40
0
2000
4000
6000
8000
10000

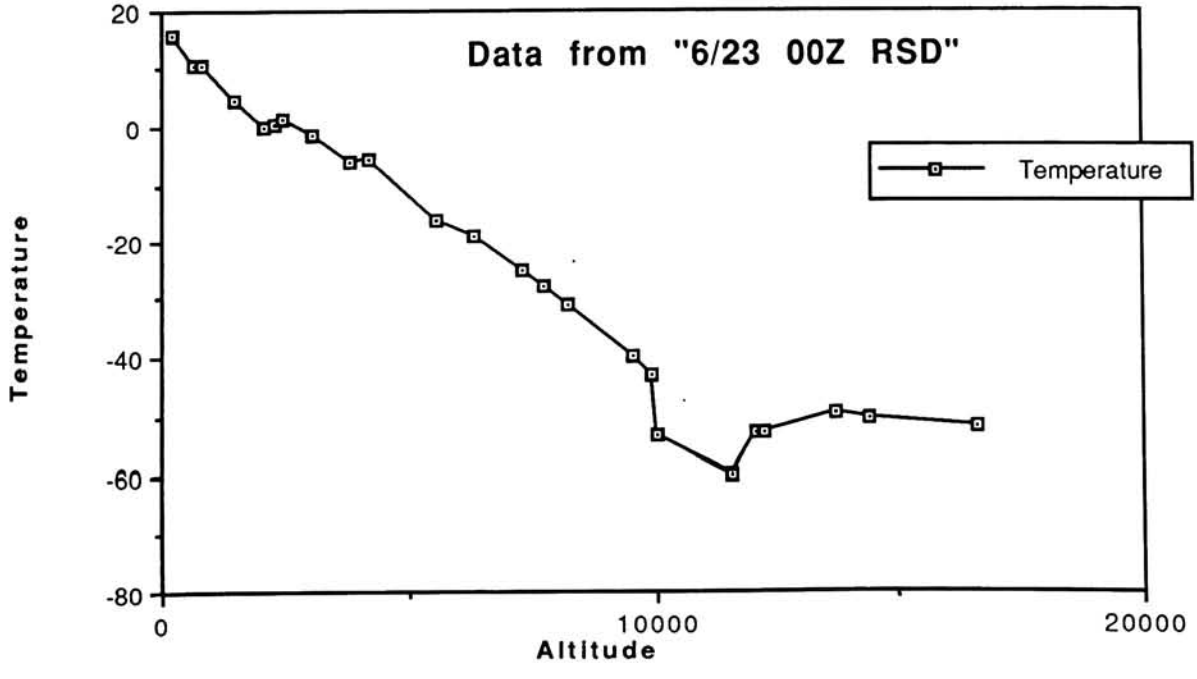
Data from "6/23 00Z RSD"
Temperature
Temperature
Altitude
20
0
-20
-40
-60
-80
0
10000
20000

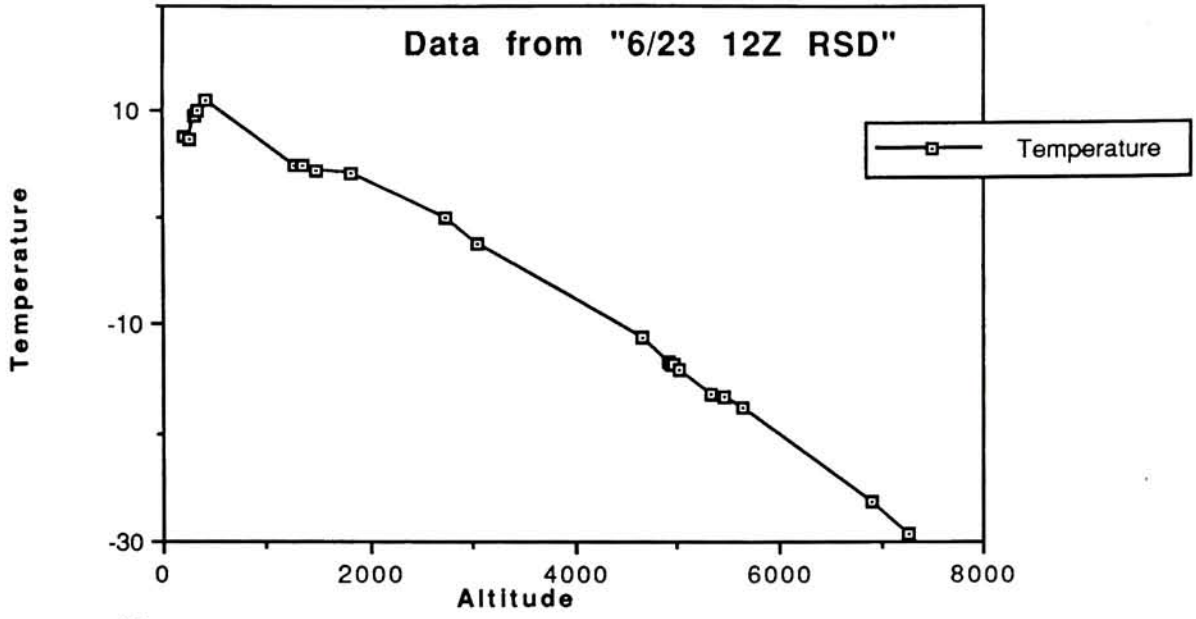
Data from "6/23 12Z RSD"
Temperature
Temperature
Altitude
10
-10
-30
0
2000
4000
6000
8000

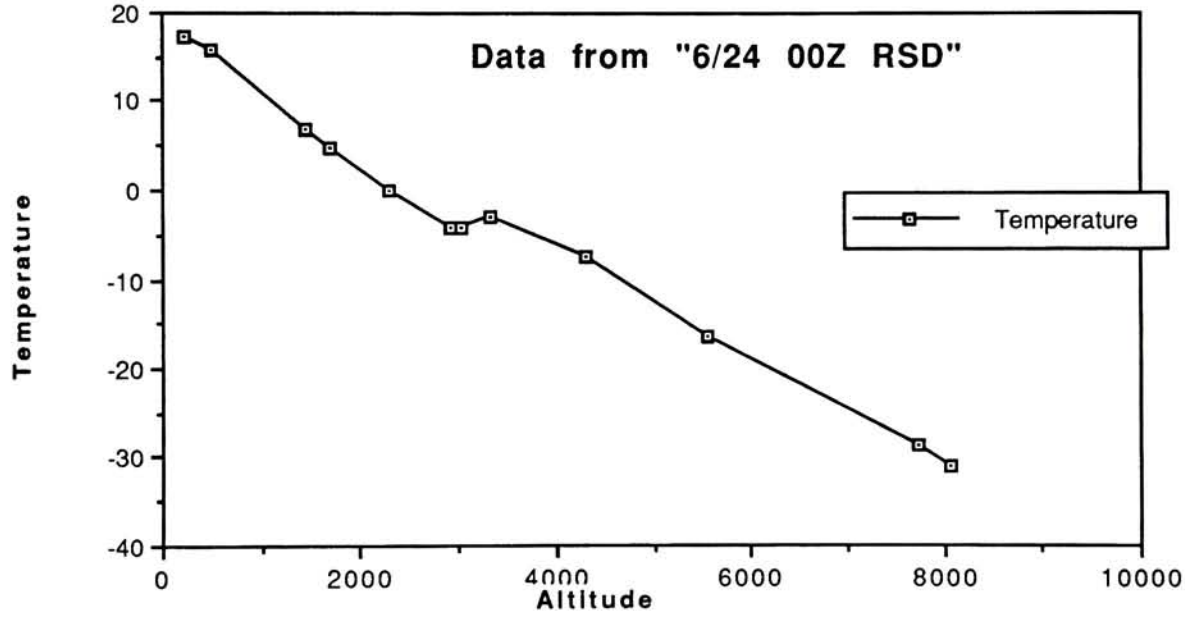
Data from "6/24 00Z RSD"
Temperature
Temperature
Altitude
20
10
0
-10
-20
-30
-40
0
2000
4000
6000
8000
10000

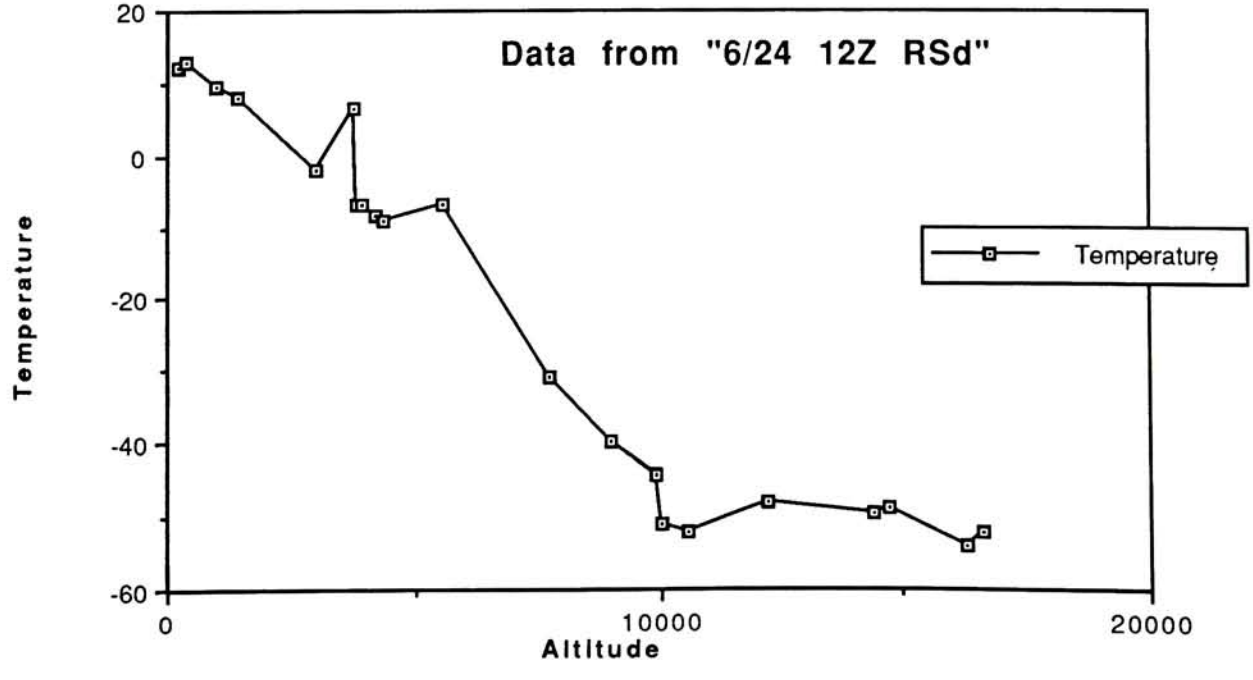
Data from "6/24 12Z RSd"
Temperature
Temperature
Altitude
20
0
-20
-40
-60
0
10000
20000

BUFFALO, NEW YORK 10- 6-1990 PRELIMINARY

RADIOSONDE/RAWINSONDE OBSERVATION WBAN NO. 14733 TIME (GMT) 00 Z

ELAP TIME (MIN/SEC)	PRESSURE (MBS)	HEIGHT (M-MSL)	TEMP (DEG C)	DP DEPR (DEG C)	RH %	WIND DIR(DEG)	WIN SPD(M
.00	985.60	218	18.4	6.8	64.0	220	7
.12	979.10	275	18.3	7.3	62.2	223	9
.48	959.40	449	17.3	7.0	63.0	230	18
1.00	.00	509	.0	.0	.0	233	21
1.06	949.30	539	17.6	7.7	60.2	233	21
1.30	937.80	644	19.1	10.9	49.1	232	22
2.00	.00	793	.0	.0	.0	231	23
3.00	.00	1092	.0	.0	.0	235	25
4.00	.00	1391	.0	.0	.0	246	25
4.18	850.00	1481	13.4	8.9	54.6	249	26
5.00	.00	1681	.0	.0	.0	255	27
5.06	827.10	1710	11.1	7.3	60.5	256	27
6.00	.00	1976	.0	.0	.0	265	31
6.06	798.20	2006	9.7	7.4	59.6	266	31
6.48	780.00	2198	8.8	5.0	70.5	274	33
7.00	.00	2251	.0	.0	.0	276	34
7.06	772.60	2277	8.5	4.8	71.6	277	34
7.36	760.00	2413	9.2	7.5	59.3	280	34
8.00	.00	2515	.0	.0	.0	282	34
8.24	741.50	2617	8.3	9.4	51.6	282	33
9.00	.00	2784	.0	.0	.0	283	32
10.00	.00	3062	.0	.0	.0	283	30
10.06	700.00	3090	4.5	7.6	57.5	283	30
11.00	.00	3333	.0	.0	.0	284	29
12.00	656.90	3604	.1	6.3	62.3	286	30
13.00	.00	3893	.0	.0	.0	286	31
13.24	624.40	4008	-3.4	4.2	72.5	286	31
14.00	.00	4181	.0	.0	.0	287	30
14.18	604.20	4268	-5.3	5.4	65.7	287	30
15.00	.00	4460	.0	.0	.0	286	30
16.00	.00	4733	.0	.0	.0	285	29
16.12	565.20	4788	-9.6	2.1	84.7	286	29
16.30	558.80	4876	-9.9	4.0	72.5	287	29
17.00	.00	5007	.0	.0	.0	289	29
17.54	532.70	5244	-11.7	3.5	75.2	293	28
18.00	.00	5271	.0	.0	.0	293	28
18.12	527.20	5324	-11.9	5.0	66.0	294	28
19.00	.00	5526	.0	.0	.0	296	28
19.48	500.00	5727	-14.4	6.9	55.8	296	30
20.00	.00	5781	.0	.0	.0	296	31
21.00	.00	6048	.0	.0	.0	297	32
21.54	464.00	6289	-18.7	5.3	62.9	296	32
22.00	.00	6317	.0	.0	.0	296	32
22.42	450.10	6516	-19.5	7.3	52.4	293	30
23.00	.00	6597	.0	.0	.0	292	30
24.00	.00	6866	.0	.0	.0	289	30
24.30	421.50	7001	-22.9	9.8	40.7	290	30
25.00	.00	7128	.0	.0	.0	290	31
26.00	400.00	7382	-26.5	8.1	46.2	292	32
27.00	.00	7675	.0	.0	.0	291	34
28.00	.00	7969	.0	.0	.0	294	33
28.18	364.00	8057	-31.3	10.9	33.4	295	32
29.00	.00	8256	.0	.0	.0	296	30
29.42	344.00	8454	-34.8	12.2	27.4	295	28

BUFFALO, NEW YORK 10- 6-1990 PRELIMINARY

RADIOSONDE/RAWINSONDE OBSERVATION WBAN NO. 14733 TIME (GMT) 00 Z

ELAP TIME (MIN/SEC)	PRESSURE (MBS)	HEIGHT (M-MSL)	TEMP (DEG C)	DP DEPR (DEG C)	RH %	WIND DIR(DEG)	WIND SPD(M/
30.00	.00	8542	.0	.0	.0	295	27.
31.00	.00	8834	.0	.0	.0	291	28.
31.42	316.10	9038	-39.9	11.2	28.7	290	30.
32.00	.00	9127	.0	.0	.0	289	31.
32.54	300.00	9393	-43.2	99.9	999.9	289	34.
33.00	.00	9423	.0	.0	.0	289	34.
34.00	.00	9723	.0	.0	.0	289	37.
35.00	.00	10022	.0	.0	.0	290	35.
35.12	270.50	10082	-48.8	99.9	999.9	290	35.
36.00	.00	10308	.0	.0	.0	289	32.
36.06	260.20	10336	-50.5	99.9	999.9	289	32.
37.00	250.00	10596	-51.4	99.9	999.9	289	37.
38.00	.00	10901	.0	.0	.0	290	48.
39.00	.00	11206	.0	.0	.0	291	43.
40.00	.00	11511	.0	.0	.0	294	28.
40.48	208.60	11755	-57.9	99.9	999.9	288	28.
41.00	.00	11816	.0	.0	.0	287	28.
41.12	204.60	11877	-58.0	99.9	999.9	288	30.
41.42	200.00	12021	-56.8	99.9	999.9	289	36.
42.00	.00	12117	.0	.0	.0	290	39.
42.12	195.00	12181	-57.3	99.9	999.9	291	41.
42.42	190.50	12329	-56.6	99.9	999.9	292	47.
43.00	.00	12427	.0	.0	.0	293	50.
43.54	179.10	12719	-58.1	99.9	999.9	285	48.
44.00	.00	12753	.0	.0	.0	284	47.
44.30	173.40	12923	-56.6	99.9	999.9	282	49.
45.00	.00	13077	.0	.0	.0	280	51.
45.42	163.60	13292	-56.5	99.9	999.9	281	52.
46.00	.00	13389	.0	.0	.0	282	52.
47.00	.00	13712	.0	.0	.0	280	39.
47.24	150.00	13841	-58.3	99.9	999.9	281	37.
48.00	.00	14038	.0	.0	.0	282	34.
49.00	.00	14365	.0	.0	.0	284	29.
50.00	.00	14693	.0	.0	.0	288	24.
50.24	128.20	14824	-60.5	99.9	999.9	288	23.
51.00	.00	15019	.0	.0	.0	289	21.
51.06	123.60	15052	-60.5	99.9	999.9	289	21.
51.48	119.40	15268	-58.8	99.9	999.9	290	20.
52.00	.00	15335	.0	.0	.0	290	20.
52.48	113.20	15602	-59.6	99.9	999.9	289	19.
53.00	.00	15670	.0	.0	.0	289	19.
53.30	109.00	15839	-57.9	99.9	999.9	291	20.
54.00	.00	16020	.0	.0	.0	293	22.
54.30	102.90	16201	-60.3	99.9	999.9	290	24.
55.00	100.00	16379	-59.9	99.9	999.9	288	27.
55.24	98.00	16505	-60.1	99.9	999.9	292	25.
56.00	.00	16720	.0	.0	.0	300	23.
56.24	92.50	16863	-62.6	99.9	999.9	302	22.
57.00	.00	17093	.0	.0	.0	305	21.
57.12	88.00	17170	-63.6	99.9	999.9	304	18.
57.36	86.30	17290	-62.9	99.9	999.9	303	13.
58.00	84.20	17443	-60.8	99.9	999.9	302	8.
58.24	82.40	17577	-60.7	99.9	999.9	311	6.
59.00	.00	17807	.0	.0	.0	327	3.

BUFFALO, NEW YORK 10- 6-1990 PRELIMINARY

RADIOSONDE/RAWINSONDE OBSERVATION WBAN NO. 14733 TIME (GMT) 00 Z

ELAP TIME (MIN/SEC)	PRESSURE (MBS)	HEIGHT (M-MSL)	TEMP (DEG C)	DP DEPR (DEG C)	RH %	WIND DIR(DEG)	WIND SPD(M/S)
59.24	77.50	17960	-58.7	99.9	999.9	293	5.1
60.00	.00	18169	.0	.0	.0	246	6.7
60.48	71.70	18448	-59.4	99.9	999.9	253	10.8
61.00	.00	18523	.0	.0	.0	255	11.8
61.12	70.00	18598	-60.4	99.9	999.9	258	13.9
62.00	.00	18893	.0	.0	.0	271	22.1
63.00	.00	19261	.0	.0	.0	273	20.1
64.00	.00	19629	.0	.0	.0	289	19.5
64.36	57.30	19850	-58.8	99.9	999.9	294	17.0
65.00	.00	20004	.0	.0	.0	297	14.9
65.54	52.90	20351	-59.8	99.9	999.9	307	12.3
66.00	.00	20386	.0	.0	.0	308	11.8
66.54	50.00	20704	-58.3	99.9	999.9	299	10.3
67.00	.00	20743	.0	.0	.0	298	10.3
67.24	48.50	20897	-56.2	99.9	999.9	293	9.3
68.00	.00	21121	.0	.0	.0	286	8.2
68.54	44.40	21456	-58.0	99.9	999.9	277	6.7
69.00	.00	21495	.0	.0	.0	276	6.7
70.00	.00	21886	.0	.0	.0	268	6.7
71.00	.00	22277	.0	.0	.0	260	5.1
71.36	37.60	22511	-55.1	99.9	999.9	252	6.2
72.00	.00	22669	.0	.0	.0	246	6.7
73.00	.00	23065	.0	.0	.0	238	7.7
74.00	.00	23461	.0	.0	.0	236	8.2
74.24	31.60	23619	-56.0	99.9	999.9	246	9.3
75.00	.00	23840	.0	.0	.0	260	10.8
75.18	30.00	23950	-54.8	99.9	999.9	263	11.3
76.00	.00	24275	.0	.0	.0	270	11.8
77.00	.00	24739	.0	.0	.0	283	14.9
77.30	25.60	24971	-52.1	99.9	999.9	285	15.9
78.00	.00	25207	.0	.0	.0	288	17.5
78.30	23.80	25444	-51.8	99.9	999.9	287	18.0
79.00	.00	25643	.0	.0	.0	286	18.0
79.42	22.10	25921	-54.2	99.9	999.9	290	18.5
80.00	.00	26050	.0	.0	.0	292	18.5
81.00	.00	26478	.0	.0	.0	284	15.9
81.12	20.00	26564	-52.9	99.9	999.9	283	15.4
82.00	.00	26928	.0	.0	.0	280	12.3
83.00	.00	27383	.0	.0	.0	272	10.8
83.42	16.80	27701	-48.0	99.9	999.9	262	9.3
84.00	.00	27833	.0	.0	.0	258	8.7
85.00	.00	28274	.0	.0	.0	262	7.7
86.00	.00	28716	.0	.0	.0	259	8.2
86.24	14.00	28892	-52.6	99.9	999.9	263	7.2
87.00	.00	29183	.0	.0	.0	270	5.1
87.48	12.60	29572	-53.3	99.9	999.9	999	999.9

END OF AVAILABLE PRELIMINARY DATA

BUFFALO, NEW YORK 10- 6-1990 PRELIMINARY

RADIOSONDE/RAWINSONDE OBSERVATION WBAN NO. 14733 TIME (GMT) 12 Z

ELAP TIME (MIN/SEC)	PRESSURE (MBS)	HEIGHT (M-MSL)	TEMP (DEG C)	DP DEPR (DEG C)	RH %	WIND DIR(DEG)	WIND SPD(M/S)
.00	987.30	218	19.3	8.9	56.0	200	7.7
.06	983.60	250	19.1	8.4	57.8	203	9.8
1.00	.00	524	.0	.0	.0	225	25.7
2.00	.00	829	.0	.0	.0	239	26.2
2.36	899.70	1012	15.3	5.9	67.7	249	25.7
2.54	891.20	1093	15.2	5.3	70.3	254	25.7
3.00	.00	1116	.0	.0	.0	255	25.7
3.06	886.40	1139	16.9	8.3	57.9	256	25.2
3.18	881.60	1185	17.3	7.9	59.4	257	24.7
3.36	873.50	1264	17.0	8.7	56.5	260	23.7
4.00	.00	1367	.0	.0	.0	263	22.1
4.30	850.00	1496	15.0	4.3	75.0	261	20.6
5.00	.00	1624	.0	.0	.0	259	19.0
5.06	834.70	1650	14.3	4.5	73.9	258	19.0
5.24	826.50	1734	14.9	10.4	49.7	256	20.1
6.00	.00	1902	.0	.0	.0	252	21.6
6.42	791.70	2097	13.5	16.6	31.7	250	24.2
7.00	.00	2187	.0	.0	.0	249	25.7
8.00	.00	2488	.0	.0	.0	249	24.7
9.00	.00	2788	.0	.0	.0	250	23.1
10.00	.00	3089	.0	.0	.0	252	24.2
10.06	700.00	3119	5.5	11.7	42.8	252	24.2
11.00	.00	3389	.0	.0	.0	253	24.2
12.00	.00	3688	.0	.0	.0	257	24.2
12.12	647.60	3748	-.1	8.4	53.1	258	24.2
13.00	.00	3975	.0	.0	.0	260	23.7
13.36	616.10	4145	-4.0	5.4	65.9	263	23.7
13.54	609.00	4237	-4.2	10.9	42.8	265	23.7
14.00	.00	4260	.0	.0	.0	265	23.7
14.30	598.30	4376	-4.3	16.1	27.6	268	23.7
15.00	.00	4506	.0	.0	.0	272	23.7
16.00	.00	4765	.0	.0	.0	275	24.7
16.24	561.90	4869	-6.6	30.0	20.0	275	24.7
17.00	.00	5033	.0	.0	.0	274	24.7
18.00	.00	5305	.0	.0	.0	276	24.7
19.00	.00	5578	.0	.0	.0	278	24.7
19.42	500.00	5769	-13.6	30.0	20.0	280	25.2
20.00	.00	5850	.0	.0	.0	281	25.2
20.06	492.90	5877	-14.4	12.5	34.0	281	25.2
21.00	.00	6134	.0	.0	.0	281	25.7
22.00	.00	6420	.0	.0	.0	280	27.3
22.48	444.70	6648	-20.6	7.6	50.8	999	999.9
23.00	.00	6705	.0	.0	.0	999	999.9
23.06	439.60	6733	-21.2	7.6	50.4	999	999.9
23.30	432.60	6852	-21.5	12.0	33.3	999	999.9
24.00	423.70	7005	-22.5	14.5	25.5	282	28.3
24.48	409.70	7251	-22.6	30.0	20.0	999	999.9
25.00	.00	7310	.0	.0	.0	999	999.9
25.24	400.00	7427	-23.8	15.0	23.6	999	999.9
26.00	.00	7608	.0	.0	.0	284	26.2
26.30	382.20	7758	-26.6	9.8	39.2	283	26.8
27.00	.00	7909	.0	.0	.0	282	27.8
28.00	.00	8212	.0	.0	.0	281	28.8
28.12	355.70	8273	-30.2	4.9	62.1	280	29.3

BUFFALO, NEW YORK 10- 6-1990 PRELIMINARY
RADIOSONDE/RAWINSONDE OBSERVATION WBAN NO. 14733 TIME (GMT) 12 Z

ELAP TIME (MIN/SEC)	PRESSURE (MBS)	HEIGHT (M-MSL)	TEMP (DEG C)	DP DEPR (DEG C)	RH %	WIND DIR(DEG)	WIND SPD(M/S)
29.00	.00	8501	.0	.0	.0	278	31.4
29.06	343.10	8529	-32.0	6.9	49.9	278	31.4
29.54	331.60	8769	-33.8	7.1	48.6	277	31.9
30.00	.00	8800	.0	.0	.0	277	31.9
30.36	321.60	8983	-34.8	10.7	32.5	277	32.9
31.00	.00	9105	.0	.0	.0	277	33.4
31.18	311.90	9196	-36.6	14.2	20.9	278	33.4
32.00	.00	9431	.0	.0	.0	279	34.0
32.06	300.00	9464	-39.0	13.4	22.2	280	34.0
32.30	295.20	9574	-40.0	12.2	25.2	281	34.5
33.00	.00	9729	.0	.0	.0	284	35.0
34.00	.00	10038	.0	.0	.0	999	999.9
35.00	.00	10347	.0	.0	.0	290	29.8
36.00	.00	10656	.0	.0	.0	293	30.4
36.06	250.00	10687	-49.2	99.9	999.9	293	30.9
37.00	.00	10972	.0	.0	.0	292	33.4
37.42	231.30	11193	-53.2	99.9	999.9	293	37.6
38.00	.00	11282	.0	.0	.0	294	39.1
39.00	.00	11580	.0	.0	.0	290	40.6
40.00	.00	11877	.0	.0	.0	292	36.0
40.48	200.00	12115	-59.7	99.9	999.9	297	33.4
41.00	.00	12171	.0	.0	.0	298	32.9
41.54	190.40	12422	-61.2	99.9	999.9	295	32.9
42.00	.00	12454	.0	.0	.0	295	32.9
42.30	184.70	12611	-60.6	99.9	999.9	293	35.5
43.00	.00	12767	.0	.0	.0	292	37.6
44.00	.00	13079	.0	.0	.0	999	999.9
44.06	170.40	13110	-63.0	99.9	999.9	999	999.9
44.36	166.20	13264	-62.4	99.9	999.9	999	999.9
45.00	.00	13384	.0	.0	.0	293	33.4
45.36	158.30	13563	-63.8	99.9	999.9	288	34.0
46.00	.00	13695	.0	.0	.0	285	34.0
46.36	150.00	13894	-63.1	99.9	999.9	286	35.5
47.00	.00	14032	.0	.0	.0	287	36.5
48.00	.00	14377	.0	.0	.0	287	37.0
48.06	137.90	14412	-62.9	99.9	999.9	288	37.0
48.30	135.10	14539	-60.6	99.9	999.9	290	36.5
48.48	132.90	14641	-60.5	99.9	999.9	292	36.0
49.00	.00	14710	.0	.0	.0	293	35.5
49.18	129.30	14813	-59.0	99.9	999.9	294	34.0
50.00	.00	15038	.0	.0	.0	295	30.9
51.00	.00	15360	.0	.0	.0	300	25.7
51.18	116.60	15456	-62.5	99.9	999.9	301	23.7
52.00	112.30	15688	-62.7	99.9	999.9	304	19.0
52.42	107.60	15952	-60.9	99.9	999.9	296	18.0
53.00	.00	16063	.0	.0	.0	293	17.5
53.24	103.20	16211	-62.0	99.9	999.9	290	16.5
54.00	100.00	16406	-62.0	99.9	999.9	287	14.9
55.00	94.50	16755	-63.3	99.9	999.9	279	15.4
55.12	93.50	16820	-63.2	99.9	999.9	278	15.4
55.36	91.60	16947	-61.5	99.9	999.9	275	14.9
56.00	.00	17073	.0	.0	.0	272	14.4
56.06	89.30	17104	-62.0	99.9	999.9	271	14.4
56.18	88.30	17174	-61.3	99.9	999.9	269	13.9

BUFFALO, NEW YORK 10- 6-1990 PRELIMINARY

RADIOSONDE/RAWINSONDE OBSERVATION WBAN NO. 14733 TIME (GMT) 12 Z

ELAP TIME (MIN/SEC)	PRESSURE (MBS)	HEIGHT (M-MSL)	TEMP (DEG C)	DP DEPR (DEG C)	RH %	WIND DIR(DEG)	WIND SPD(M/
56.36	86.80	17281	-59.1	99.9	999.9	266	13.
57.00	.00	17435	.0	.0	.0	261	12.
57.06	84.20	17473	-57.2	99.9	999.9	260	12.
58.00	.00	17819	.0	.0	.0	255	12.
59.00	74.90	18204	-62.3	99.9	999.9	259	11.
59.42	71.70	18473	-63.4	99.9	999.9	272	11.
60.00	.00	18584	.0	.0	.0	278	11.
60.06	70.00	18621	-63.1	99.9	999.9	279	11.
61.00	.00	18963	.0	.0	.0	293	10.
61.12	65.40	19039	-63.2	99.9	999.9	296	10.
61.42	63.40	19231	-61.3	99.9	999.9	305	10.
62.00	.00	19345	.0	.0	.0	310	10.
63.00	.00	19727	.0	.0	.0	304	8.
64.00	.00	20108	.0	.0	.0	268	7.
64.12	54.40	20184	-59.7	99.9	999.9	257	7.
64.42	52.80	20372	-58.1	99.9	999.9	229	5.
65.00	.00	20486	.0	.0	.0	212	4.
65.36	50.00	20714	-59.4	99.9	999.9	224	6.
66.00	.00	20897	.0	.0	.0	233	8.
66.18	47.50	21034	-61.1	99.9	999.9	223	7.
67.00	.00	21329	.0	.0	.0	203	4.
67.06	45.00	21371	-59.6	99.9	999.9	210	5.
67.42	43.20	21625	-60.6	99.9	999.9	250	7.
68.00	.00	21742	.0	.0	.0	268	8.
68.30	41.10	21937	-58.6	99.9	999.9	275	9.
69.00	.00	22149	.0	.0	.0	282	11.
70.00	.00	22574	.0	.0	.0	290	11.
70.06	36.90	22616	-57.5	99.9	999.9	290	11.
70.48	35.10	22934	-55.3	99.9	999.9	293	12.
71.00	.00	23021	.0	.0	.0	294	13.
72.00	.00	23459	.0	.0	.0	36	3.
73.00	.00	23896	.0	.0	.0	305	10.
73.06	30.00	23940	-53.4	99.9	999.9	304	10.
74.00	.00	24408	.0	.0	.0	289	7.
75.00	.00	24928	.0	.0	.0	262	9.
76.00	.00	25448	.0	.0	.0	261	19.
77.00	.00	25968	.0	.0	.0	231	11.
78.00	.00	26488	.0	.0	.0	222	7.
78.06	20.00	26540	-55.2	99.9	999.9	227	8.
79.00	.00	26957	.0	.0	.0	264	19.
79.24	18.20	27142	-55.2	99.9	999.9	269	16.
80.00	.00	27453	.0	.0	.0	277	11.
80.06	17.20	27505	-52.9	99.9	999.9	278	13.
81.00	.00	28077	.0	.0	.0	283	27.
82.00	.00	28712	.0	.0	.0	285	32.
82.30	13.60	29030	-49.9	99.9	999.9	285	28.
83.00	.00	29344	.0	.0	.0	285	24.
84.00	.00	29972	.0	.0	.0	281	36.
85.00	.00	30599	.0	.0	.0	279	22.
85.06	10.60	30662	-49.5	99.9	999.9	999	999.

END OF AVAILABLE PRELIMINARY DATA

BUFFALO, NEW YORK 10- 7-1990 PRELIMINARY

RADIOSONDE/RAWINSONDE OBSERVATION WBAN NO. 14733 TIME (GMT) 00 Z

ELAP TIME (MIN/SEC)	PRESSURE (MBS)	HEIGHT (M-MSL)	TEMP (DEG C)	DP DEPR (DEG C)	RH %	WIND DIR(DEG)	WIND SPD(M/
.00	987.00	218	25.5	15.4	38.0	210	7.
.06	983.30	251	25.1	14.1	41.4	212	8.
1.00	.00	528	.0	.0	.0	225	18.
2.00	.00	835	.0	.0	.0	234	22.
3.00	.00	1143	.0	.0	.0	243	27.
4.00	.00	1450	.0	.0	.0	254	28.
4.12	850.00	1512	16.8	9.5	53.3	256	28.
4.48	833.80	1676	16.3	12.5	43.5	260	28.
5.00	.00	1732	.0	.0	.0	261	28.
5.30	814.70	1873	14.8	7.4	61.0	264	27.
6.00	.00	2007	.0	.0	.0	266	27.
7.00	776.70	2276	12.2	6.8	63.1	275	25.
7.42	759.80	2460	11.5	7.8	58.4	277	23.
8.00	.00	2540	.0	.0	.0	278	23.
8.30	740.70	2673	11.4	16.3	31.9	275	21.
8.42	736.00	2726	11.2	16.2	32.1	274	21.
9.00	.00	2804	.0	.0	.0	273	20.
10.00	.00	3065	.0	.0	.0	269	18.
10.18	700.00	3143	8.8	18.5	26.1	269	18.
11.00	.00	3342	.0	.0	.0	269	18.
12.00	.00	3626	.0	.0	.0	266	18.
13.00	.00	3910	.0	.0	.0	269	16.
13.54	617.40	4165	-.1	11.0	43.5	275	15.
14.00	.00	4195	.0	.0	.0	276	15.
15.00	.00	4492	.0	.0	.0	278	15.
16.00	.00	4790	.0	.0	.0	280	15.
16.48	553.50	5028	-7.7	5.6	64.0	277	17.
17.00	.00	5091	.0	.0	.0	276	17.
17.54	529.20	5376	-9.8	9.5	46.2	276	18.
18.00	.00	5408	.0	.0	.0	276	18.
18.54	507.50	5698	-12.2	10.0	43.5	281	19.
19.00	.00	5727	.0	.0	.0	281	19.
19.06	503.70	5755	-12.4	10.8	40.5	281	20.
19.18	500.00	5812	-12.4	15.0	27.5	281	20.
19.42	491.70	5940	-12.6	15.5	26.3	280	21.
20.00	.00	6028	.0	.0	.0	280	22.
21.00	467.70	6320	-15.3	15.8	24.6	281	26.
21.42	456.30	6506	-16.1	11.6	36.3	284	26.
22.00	.00	6580	.0	.0	.0	285	26.
22.54	438.70	6801	-18.5	13.9	28.5	285	26.
23.00	.00	6825	.0	.0	.0	285	26.
23.42	427.50	6993	-19.2	30.0	20.0	282	26.
24.00	.00	7071	.0	.0	.0	280	26.
25.00	.00	7330	.0	.0	.0	275	24.
25.36	400.00	7486	-21.5	30.0	20.0	275	24.
26.00	.00	7605	.0	.0	.0	275	24.
27.00	.00	7903	.0	.0	.0	275	25.
28.00	.00	8202	.0	.0	.0	278	26.
28.18	358.10	8291	-28.1	15.6	20.6	278	26.
29.00	.00	8514	.0	.0	.0	279	27.
30.00	.00	8833	.0	.0	.0	275	26.
31.00	.00	9152	.0	.0	.0	272	28.
32.00	.00	9470	.0	.0	.0	273	32.
32.12	300.00	9534	-38.8	12.7	24.2	273	32.

BUFFALO, NEW YORK 10- 7-1990 PRELIMINARY

RADIOSONDE/RAWINSONDE OBSERVATION WBAN NO. 14733 TIME (GMT) 00 Z

ELAP TIME (MIN/SEC)	PRESSURE (MBS)	HEIGHT (M-MSL)	TEMP (DEG C)	DP DEPR (DEG C)	RH %	WIND DIR(DEG)	WIND SPD(M/S)
32.42	293.10	9693	-40.0	12.6	24.1	274	30.4
33.00	.00	9775	.0	.0	.0	274	29.3
34.00	.00	10049	.0	.0	.0	269	27.3
35.00	.00	10322	.0	.0	.0	269	27.8
36.00	.00	10596	.0	.0	.0	274	29.8
36.36	250.00	10760	-48.3	99.9	999.9	274	31.4
37.00	.00	10878	.0	.0	.0	274	32.4
38.00	.00	11174	.0	.0	.0	274	32.4
39.00	.00	11469	.0	.0	.0	276	30.9
40.00	.00	11764	.0	.0	.0	273	27.8
40.06	213.10	11794	-56.0	99.9	999.9	273	27.8
41.00	.00	12052	.0	.0	.0	270	28.3
41.30	200.00	12196	-57.7	99.9	999.9	273	30.4
42.00	.00	12323	.0	.0	.0	275	32.4
43.00	.00	12578	.0	.0	.0	275	36.0
43.54	181.50	12807	-58.6	99.9	999.9	274	36.0
44.00	.00	12837	.0	.0	.0	274	36.0
45.00	.00	13138	.0	.0	.0	277	35.0
46.00	.00	13439	.0	.0	.0	279	30.4
46.36	159.30	13620	-62.2	99.9	999.9	280	26.2
47.00	.00	13744	.0	.0	.0	281	23.1
47.48	150.00	13991	-63.1	99.9	999.9	286	22.1
48.00	.00	14059	.0	.0	.0	287	21.6
49.00	.00	14397	.0	.0	.0	289	21.1
49.48	134.30	14667	-65.7	99.9	999.9	286	20.6
50.00	.00	14737	.0	.0	.0	285	20.6
51.00	.00	15086	.0	.0	.0	274	20.6
51.36	121.20	15295	-62.9	99.9	999.9	269	20.1
52.00	.00	15431	.0	.0	.0	266	20.1
52.18	116.60	15533	-64.0	99.9	999.9	264	19.5
53.00	.00	15769	.0	.0	.0	258	19.0
53.06	111.60	15803	-61.8	99.9	999.9	259	19.0
54.00	.00	16123	.0	.0	.0	266	17.5
55.00	100.00	16479	-63.6	99.9	999.9	275	16.5
56.00	.00	16841	.0	.0	.0	286	15.4
56.18	92.60	16950	-64.7	99.9	999.9	287	14.9
57.00	88.80	17205	-66.2	99.9	999.9	288	13.4
57.24	86.90	17336	-65.1	99.9	999.9	280	12.3
57.42	85.50	17436	-62.9	99.9	999.9	274	11.3
57.54	84.60	17501	-62.6	99.9	999.9	270	10.8
58.00	.00	17532	.0	.0	.0	268	10.8
58.30	82.10	17687	-59.1	99.9	999.9	264	9.8
58.54	80.20	17835	-58.2	99.9	999.9	259	9.3
59.00	.00	17881	.0	.0	.0	258	8.7
60.00	.00	18338	.0	.0	.0	244	7.2
60.12	72.90	18430	-61.8	99.9	999.9	248	8.2
60.48	70.00	18682	-62.1	99.9	999.9	259	11.3
61.00	.00	18747	.0	.0	.0	262	11.8
62.00	.00	19071	.0	.0	.0	274	15.9
62.48	63.00	19330	-63.7	99.9	999.9	278	10.3
63.00	.00	19415	.0	.0	.0	279	8.2
64.00	.00	19838	.0	.0	.0	272	9.3
65.00	.00	20262	.0	.0	.0	249	5.7
65.06	53.80	20304	-61.7	99.9	999.9	236	5.7

BUFFALO, NEW YORK 10- 7-1990 PRELIMINARY
RADIOSONDE/RAWINSONDE OBSERVATION WBAN NO. 14733 TIME (GMT) 00 Z

ELAP TIME (MIN/SEC)	PRESSURE (MBS)	HEIGHT (M-MSL)	TEMP (DEG C)	DP DEPR (DEG C)	RH %	WIND DIR(DEG)	WIND SPD(M/
65.42	52.00	20516	-59.2	99.9	999.9	168	4.
66.00	.00	20621	.0	.0	.0	135	3.
66.24	50.00	20761	-58.9	99.9	999.9	170	4.
67.00	.00	20997	.0	.0	.0	229	6.
68.00	.00	21390	.0	.0	.0	239	7.
69.00	.00	21783	.0	.0	.0	232	3.
69.06	42.20	21822	-60.5	99.9	999.9	234	3.
70.00	.00	22176	.0	.0	.0	249	8.
71.00	.00	22570	.0	.0	.0	250	8.
71.12	37.00	22649	-56.6	99.9	999.9	252	8.
72.00	.00	22954	.0	.0	.0	258	7.
73.00	.00	23335	.0	.0	.0	266	12.
74.00	.00	23716	.0	.0	.0	289	9.
74.42	30.00	23983	-55.2	99.9	999.9	291	11.
75.00	.00	24113	.0	.0	.0	292	11.
76.00	.00	24547	.0	.0	.0	292	9.
76.42	26.20	24851	-53.4	99.9	999.9	286	5.
77.00	.00	24982	.0	.0	.0	284	3.
78.00	.00	25420	.0	.0	.0	134	2.
78.18	23.50	25551	-53.5	99.9	999.9	165	3.
79.00	.00	25832	.0	.0	.0	231	5.
79.30	21.80	26032	-55.5	99.9	999.9	233	6.
80.00	.00	26228	.0	.0	.0	234	6.
80.54	20.00	26582	-55.1	99.9	999.9	255	10.
81.00	.00	26625	.0	.0	.0	257	11.
82.00	.00	27050	.0	.0	.0	262	17.
83.00	.00	27475	.0	.0	.0	267	14.
83.42	16.60	27772	-55.3	99.9	999.9	270	16.
84.00	.00	27899	.0	.0	.0	271	17.
85.00	.00	28321	.0	.0	.0	279	20.
86.00	.00	28744	.0	.0	.0	280	21.
86.24	13.90	28913	-52.3	99.9	999.9	281	23.
87.00	.00	29182	.0	.0	.0	282	26.
87.36	12.80	29451	-48.1	99.9	999.9	284	27.
88.00	.00	29662	.0	.0	.0	285	28.
89.00	.00	30189	.0	.0	.0	282	28.
89.30	11.00	30453	-47.2	99.9	999.9	999	999.

END OF AVAILABLE PRELIMINARY DATA

BUFFALO, NEW YORK 10- 7-1990 PRELIMINARY

RADIOSONDE/RAWINSONDE OBSERVATION WBAN NO. 14733 TIME (GMT) 12 Z

ELAP TIME (MIN/SEC)	PRESSURE (MBS)	HEIGHT (M-MSL)	TEMP (DEG C)	DP DEPR (DEG C)	RH %	WIND DIR(DEG)	WIND SPD(M/S)
.00	991.70	218	18.7	6.4	66.0	200	4.6
.12	985.30	274	18.1	5.9	68.1	207	6.7
.48	966.00	443	18.5	6.7	64.6	227	13.4
1.00	.00	498	.0	.0	.0	234	15.4
2.00	.00	774	.0	.0	.0	254	12.9
2.06	926.30	802	16.2	5.9	67.8	255	12.9
2.48	904.70	1004	17.3	9.3	54.1	264	11.8
3.00	.00	1063	.0	.0	.0	267	11.3
3.42	876.90	1270	16.0	10.9	48.3	266	10.8
3.54	870.80	1329	15.5	8.4	57.0	265	10.8
4.00	.00	1358	.0	.0	.0	265	10.8
4.36	850.00	1534	13.6	6.8	63.2	260	10.3
5.00	.00	1650	.0	.0	.0	257	10.3
6.00	.00	1941	.0	.0	.0	245	11.8
6.18	801.30	2028	9.3	1.4	90.9	242	13.4
6.30	796.20	2081	9.1	99.9	80.4	240	13.9
6.54	786.00	2188	9.5	14.7	35.4	237	15.4
7.00	.00	2216	.0	.0	.0	236	15.9
7.24	772.70	2329	9.6	16.9	30.0	235	17.0
8.00	.00	2504	.0	.0	.0	233	19.0
8.24	746.00	2621	8.4	17.5	28.2	235	19.5
8.42	738.30	2706	9.1	19.3	24.6	237	20.1
9.00	.00	2794	.0	.0	.0	239	20.6
10.00	.00	3087	.0	.0	.0	248	21.1
10.12	700.00	3146	7.2	19.6	23.5	249	21.1
11.00	.00	3370	.0	.0	.0	255	20.1
12.00	658.10	3651	4.6	20.7	20.7	255	20.6
13.00	.00	3941	.0	.0	.0	253	21.6
14.00	.00	4231	.0	.0	.0	252	22.1
14.12	608.10	4289	.1	18.8	23.0	252	21.6
15.00	.00	4541	.0	.0	.0	253	20.1
16.00	.00	4857	.0	.0	.0	255	18.0
17.00	.00	5172	.0	.0	.0	254	18.5
17.48	526.70	5424	-7.6	17.8	22.6	254	18.5
18.00	.00	5491	.0	.0	.0	254	18.5
19.00	500.00	5826	-11.0	14.4	29.6	254	18.0
20.00	.00	6121	.0	.0	.0	254	19.5
21.00	.00	6417	.0	.0	.0	255	21.6
21.24	455.40	6535	-17.7	10.2	40.8	257	21.6
21.54	446.20	6687	-18.9	6.0	58.9	259	21.6
22.00	.00	6718	.0	.0	.0	259	21.6
22.24	437.10	6841	-20.3	4.7	66.1	260	22.6
23.00	.00	7036	.0	.0	.0	261	24.2
24.00	.00	7361	.0	.0	.0	260	26.2
24.24	400.00	7491	-25.6	2.8	77.5	260	25.2
25.00	.00	7698	.0	.0	.0	260	24.2
25.06	386.90	7732	-27.7	1.8	84.3	260	24.2
26.00	.00	8034	.0	.0	.0	264	23.1
27.00	.00	8370	.0	.0	.0	265	23.7
27.54	338.90	8672	-34.1	2.9	74.9	261	23.1
28.00	.00	8706	.0	.0	.0	261	23.1
29.00	.00	9045	.0	.0	.0	259	23.1
29.30	313.40	9214	-38.9	3.6	67.9	261	25.2
29.42	310.40	9280	-39.1	4.0	65.3	262	25.7

Therm Object Parameters

October 1992
Optimum and Generic Object Parameters

Name	Density	Specific Heat	Thermal Conduct.	Thick-ness	Visible Emiss.	Thermal Emiss.	Exposed Area	Self. Power	Slope	Azi-muth
Aluminum	2.700	.2198	2064	0.0	.15	.10	-1.0	0	45	60
Asphalt	2.114	.2200	5.93	2.4	.93	.93	.40	2.2	0	0
Brick	0.768	.2098	8.17	5.0	.79	.93	-.34	0	45	60
Car Side	7.833	.1111	464.4	.21	.74	.44	1.0	1.45	90	90
Car Roof	7.833	.1111	464.4	.13	.74	.44	.53	0	0	0
Concrete	1.600	.1600	15.48	1.13	.90	.99	-.44	0	42.5	60
Grass	0.160	1.000	0.0	0.0	1.0	.98	.08	1.1	85	180
Gravel	1.000	.3400	17.2	.60	.90	.90	-.375	0	32	60
Sand	1.520	.1911	2.84	1.3	.76	.90	.39	0	0	0
Tire	1.198	.2986	1.3	.15	.93	.90	-.82	0	90	90
Water	1.000	1.000	11.0	14.0	.07	1.0	-.46	0	0	0
Window	1.000	.5200	12.04	.31	.61	.61	.95	.80	67	90
Windshield	1.000	.5200	12.04	.11	.61	.61	.52	0	17	180
Wood	0.400	.6689	1.1	2.15	.78	.90	.27	0	32	60

Field Optimized Values

Name	Density	Specific Heat	Thermal Conduct.	Thick-ness	Visible Emiss.	Thermal Emiss.	Exposed Area	Self. Power	Slope	Azi-muth
Aluminum	2.700	.2198	2064	0.50	.74	.90	-.40	0	45	60
Asphalt	2.114	.2200	5.93	3.0	.93	.93	-.50	0	0	0
Brick	0.768	.2098	8.17	5.0	.75	.93	-.40	0	45	60
Car Side	7.833	.1111	464.4	0.5	.74	.44	.30	0	90	90
Car Roof	7.833	.1111	464.4	0.5	.74	.44	.50	0	0	0
Concrete	1.600	.1600	15.48	3.0	.90	.99	-.40	0	42.5	60
Grass	1.000	1.000	0.0	0.2	.91	.88	.16	-3.5	85	180
Gravel	1.700	.2000	17.20	3.0	.90	.90	-.40	0	32	60
Sand	1.510	.1900	2.67	5.0	.60	.90	-.40	0	0	0
Tire	1.198	.2986	1.30	2.0	.95	.99	-.30	0	90	90
Water	1.000	1.000	5.13	30.0	.50	.96	-.40	0	0	0
Window	2.600	.2000	12.04	2.0	.18	.79	.25	0	70	90
Windshield	2.600	.2000	12.04	2.0	.18	.79	.40	0	32	180
Wood	0.400	.6689	1.10	2.0	.78	.90	-.40	0	32	60

Generic ("Textbook") Values

June 1992
Optimum and Generic Object Parameters

Name	Density	Specific Heat	Thermal Conduct.	Thick-ness	Visible Emiss.	Thermal Emiss.	Exposed Area	Self. Power	Slope	Azi-muth
Asphalt	2.114	.22	5.93	2.4	.93	.93	.40	2.2	0	0
Blue Wood	.60	.67	.86	2.4	.60	.78	-.77	0	69	90
Bumper	7.833	.1111	464.4	.12	.88	.44	.69	0	90	90
Car Roof	7.833	.1111	464.4	.09	.88	.44	.53	0	0	0
Car Side	7.833	.1111	464.4	.01	.88	.44	1.0	1.8	90	90
Concrete	2.28	.1601	15.48	4.5	.73	.94	.39	0	0	0
Front Black	.60	.67	.86	2.4	.90	.78	-.77	0	90	90
Front White	.60	.67	.86	2.4	.20	.78	-.77	0	90	90
Green Wood	.60	.67	.86	2.4	.55	.78	-.77	0	69	90
Grey 1	.60	.67	.86	2.4	.50	.78	-.77	0	69	90
Grey 2	.60	.67	.86	2.4	.60	.78	-.77	0	69	90
Grey 3	.60	.67	.86	2.4	.70	.78	-.77	0	69	90
Grey 4	.60	.67	.86	2.4	.80	.78	-.77	0	69	90
Grey 5	.60	.67	.86	6.0	.72	.87	-.55	0	69	90
Red	.60	.67	.86	2.4	.65	.78	-.77	0	69	90
Sand	1.52	.1911	2.84	1.3	.76	.90	.39	0	0	0
Windshield	1.0	.52	12.04	.11	.61	.61	.52	0	17	180
Shingles	1.3	.35	6.36	.05	.74	.91	-.66	0	29	90
Specular	.60	.67	.86	3.0	.72	.87	-.45	0	0	0
Tire	1.198	.2986	1.3	.15	.93	.90	-.82	0	90	90
Water	1.0	1.0	11.0	47.0	.09	000	-.57	0	0	0
Window	1.0	.52	12.04	.31	.61	.61	.95	.80	67	90

Field Optimized Values

Name	Density	Specific Heat	Thermal Conduct.	Thick-ness	Visible Emiss.	Thermal Emiss.	Exposed Area	Self. Power	Slope	Azi-muth
Asphalt	2.114	.22	5.93	3.0	.93	.93	-.50	0	0	0
Blue Wood	.40	.6689	1.10	1.0	.60	.90	-.40	0	69	90
Bumper	7.833	.1111	464.4	2.0	.94	.90	.40	0	90	90
Car Roof	7.833	.1111	464.4	.25	.60	.90	.50	0	0	0
Car Side	7.833	.1111	464.4	.25	.60	.90	.30	0	90	90
Concrete	1.600	.1600	15.48	5.0	.60	.88	-.40	0	0	0
Front Black	.40	.6689	1.10	1.0	.94	.90	-.30	0	90	90
Front White	.40	.6689	1.10	1.0	.16	.90	-.30	0	90	90
GreenWood	.40	.6689	1.10	1.0	.5	.90	-.40	0	69	90
Grey 1	.40	.6689	1.10	1.0	.30	.90	-.40	0	69	90
Grey 2	.40	.6689	1.10	1.0	.50	.90	-.40	0	69	90
Grey 3	.40	.6689	1.10	1.0	.75	.90	-.40	0	69	90
Grey 4	.40	.6689	1.10	1.0	.90	.90	-.40	0	69	90
Grey 5	.40	.6689	1.10	1.0	.70	.90	-.40	0	69	90
Red	.40	.6689	1.10	1.0	.65	.90	-.40	0	69	90
Sand	1.51	.19	2.67	2.5	.60	.90	-.40	0	0	0
Windshield	2.6	.20	12.04	2.0	.18	.79	.40	0	27	180
Shingles	1.3	.35	6.36	.30	.86	.91	-.40	0	29	90
Specular	.40	.6689	1.10	1.0	.50	.90	-.30	0	0	0
Tire	1.198	.2986	1.3	2.0	.95	.99	-.30	0	90	90
Water	1.0	1.0	5.13	30.0	.50	.96	-.40	0	0	0
Window	2.6	.20	12.04	2.0	.18	.79	.25	0	67	90

Textbook ("Generic") Values

June 1992 Object Parameters

Generic Object Parameters
Provided by DCS Corporation

Density	SpHt	ThmCond	Thick	EmV	EmTh	XpA	dPw	Slop	Azmh	Name
1.600	.1600	0.0	12.0	.60	.88	.55	-3.5	0.	0.	'Concrete - Smooth'
1.600	.1600	0.0	12.0	.90	.99	.70	-0.3	0.	0.	'Concrete - Roadway'
1.300	.2000	0.0	12.0	.93	.97	.70	-0.8	0.	0.	'Asphalt - Dry'
2.000	.2000	0.0	12.0	.86	.93	.80	-2.0	0.	0.	'Macadam - Roadway'
.130	.5000	0.0	12.0	.25	.82	.38	-5.2	0.	0.	'Snow - Fresh'
.160	.5000	0.0	12.0	.95	.89	.72	-10.0	0.	0.	'Snow - Dry, w/Crust'
.900	.4900	0.0	12.0	.80	.99	.65	-10.0	0.	0.	'Ice - Thick'
1.030	.9400	0.0	12.0	.79	.96	.65	-10.0	0.	0.	'Marsh - Salty'
1.000	1.000	0.0	12.0	.96	.96	.73	-10.0	0.	0.	'Stream - w/Weeds, Sedge'
1.000	1.000	0.0	12.0	.90	.96	.70	-10.0	0.	0.	'River - Muddy'
1.000	1.000	0.0	12.0	.89	.96	.70	-10.0	0.	0.	'Pond - Clear'
2.700	.2200	0.0	.16	.20	.88	.15	-3.5	0.	0.	'Aluminum Siding, White'
.600	.6700	0.0	5.0	.16	.95	.15	-1.4	0.	0.	'Wall - Wood, Wht Paint'
.600	.6700	0.0	5.0	.72	.78	.20	-6.4	0.	0.	'Wall - Wood, Unpainted'
1.600	.1600	0.0	10.0	.16	.94	.15	-1.7	0.	0.	'Wall - Concrete, Wht Pt'
1.750	.2300	0.0	10.0	.83	.93	.25	-2.0	0.	0.	'Wall - Red Brick'
1.800	.2300	0.0	10.0	.70	.84	.20	-4.5	0.	0.	'Wall - Masonry'
2.300	.2200	0.0	10.0	.80	.93	.25	-2.0	0.	0.	'Wall - Stonework'
7.350	.1000	0.0	.15	.26	.49	.38	-14.2	0.	0.	'Roof - Galv. Metal, New'
1.300	.2000	0.0	.65	.89	.88	.70	-3.5	0.	0.	'Roof - Heavy Felt w/Tar'
1.300	.2000	0.0	.65	.86	.91	.68	-2.6	0.	0.	'Roof - Asphalt Shingles'
.320	.2000	0.0	2.5	.81	.98	.66	-0.6	0.	0.	'Roof - Old Straw'
.750	.6000	0.0	1.27	.72	.82	.61	-5.2	0.	0.	'Roof - Oak Shingles'
1.000	.2300	0.0	4.35	.75	.82	.63	-5.2	0.	0.	'Roof - Red Clay'
.600	.6700	0.0	5.0	.20	.88	.15	-3.5	0.	0.	'Door - Wht Alum on Wood'
.600	.6700	0.0	5.0	.16	.95	.15	-1.4	0.	0.	'Door - Wood, Wht Paint'
.600	.6700	0.0	5.0	.72	.78	.20	-6.4	0.	0.	'Door - Wood, Unpainted'
2.600	.2000	0.0	.65	.18	.79	.15	-6.1	0.	0.	'Window'
7.500	.1100	0.0	.12	.91	.25	.25	-24.5	0.	0.	'Fence - Chain Link, New'
.600	.6700	0.0	3.5	.85	.90	.25	-2.9	0.	0.	'Fence - Wooden'
.600	.6700	0.0	7.7	.85	.90	.25	-2.9	0.	0.	'Telephone Pole - Pine'
2.000	.1600	0.0	12.0	.90	.99	.70	-0.3	0.	0.	'Bridge Base - Concrete'
1.300	.2000	0.0	12.0	.93	.97	.72	-0.8	0.	0.	'Bridge Base - Asphalt'
7.500	.1100	0.0	.3	.91	.25	.25	-24.5	0.	0.	'Bridge Side - Steel,New'
7.350	.1100	0.0	1.36	.26	.49	.20	-14.2	0.	0.	'Bridge Side - Glv Metal'
.800	.5700	0.0	7.7	.75	.90	.20	-2.9	0.	0.	'Bridge Side - Dark Oak'
7.350	.1100	0.0	.15	.26	.49	.38	-14.2	0.	0.	'Silo Top - Galv. Metal'
2.700	.2200	0.0	.17	.20	.88	.35	-3.5	0.	0.	'Silo Top - Alum., White'
7.350	.1100	0.0	.15	.26	.49	.20	-14.2	0.	0.	'Silo Side - Galv. Metal'
2.700	.2200	0.0	.17	.20	.88	.15	-3.5	0.	0.	'Silo Side - Alum, White'
7.500	.1100	0.0	.6	.91	.25	.25	-24.5	0.	0.	'Firetwr - Steel Lattice'
.600	.6700	0.0	3.5	.72	.85	.20	-4.4	0.	0.	'Firetwr - Rough Pine Lt'
.800	.5700	0.0	3.5	.75	.90	.20	-2.9	0.	0.	'Firetwr - Dark Oak Latt'
7.350	.1100	0.0	1.36	.26	.49	.38	-14.2	0.	0.	'Trns Base Top - Glv Mtl'
2.700	.2200	0.0	.34	.96	.88	.73	-3.5	0.	0.	'Trns Base Top - Alm,Blk'
7.350	.1100	0.0	1.36	.26	.49	.20	-14.2	0.	0.	'Trns Base Side - Gl Mtl'
2.700	.2200	0.0	.34	.96	.88	.25	-3.5	0.	0.	'Trns Base Side - Al,Blk'
7.500	.1100	0.0	.42	.91	.25	.25	-24.5	0.	0.	'Trns Base Latt - Steel'
7.350	.1100	0.0	1.86	.26	.49	.20	-14.2	0.	0.	'Trns Base Latt - Gl Mtl'
.600	.6700	0.0	3.5	.72	.85	.20	-4.4	0.	0.	'Trns Suprt - Rough Pine'
.800	.5700	0.0	3.5	.75	.90	.20	-2.9	0.	0.	'Trns Suprt - Dark Oak'

Column #	Variable
1	Density
2	Specific Heat
3	Thermal Conductivity
4	Thickness
5	Visible Emissivity
6	Thermal Emissivity
7	Exposed Area
8	Self-Generated Power
9	Slope
10	Azimuth
11	Name

1.700	.2000	4.32	16.7	.89	.94	.5	0.	0.	0.	'Soil - Sandy, Wet'
2.032	.2198	4.30	1.0	.75	.94	.5	0.	0.	0.	'Soil - Black, Plowed'
2.032	.2198	4.30	1.0	.39	.94	.5	0.	0.	0.	'Soil - Clay'
1.000	.2000	2.88	16.7	.69	.95	.5	0.	0.	0.	'Soil - Clay, Dry'
1.750	.2000	4.32	16.7	.86	.98	.5	0.	0.	0.	'Soil - Clay, Wet'
.770	.2000	61.06	16.7	.38	.93	.5	0.	0.	0.	'Salt Pan'
1.000	1.000	5.13	1.0	.50	.96	.5	0.	0.	0.	'Water - Deep, Norm Inc'
1.000	1.000	5.00	16.6	.50	.96	.5	0.	0.	0.	'Fresh Water'
1.030	.9600	4.90	16.6	.50	.96	.5	0.	0.	0.	'Salt Water'
1.030	.9400	4.90	16.7	.79	.96	.5	0.	0.	0.	'Marsh / Swamp / Paddy'
.920	.4900	19.35	16.7	.80	.99	.5	0.	0.	0.	'Ice'
.918	.5017	19.44	1.0	.50	.98	.5	0.	0.	0.	'Ice - Rough'
.130	.5000	1.38	16.7	.25	.82	.5	0.	0.	0.	'Snow - Fluffy'
.160	.5017	.60	1.0	.28	.82	.5	0.	0.	0.	'Snow - Fine Particles'
.160	.5000	1.55	16.7	.95	.89	.5	0.	0.	0.	'Snow - Packed'
.600	.6700	.86	13.6	.99	.97	.5	0.	0.	0.	'Tree Trunks - Evergreen'
.800	.5700	.86	13.6	.95	.96	.5	0.	0.	0.	'Tree Trunks - Deciduous'
.600	.6700	.86	9.6	.85	.90	.5	0.	0.	0.	'Telephone Pole - Wood'
1.000	1.000	0.0	1.6	.99	.96	.13	-1.2	0.	0.	'Forest - Coniferous,Sum'
1.000	1.000	0.0	1.7	.88	.90	.15	-2.9	0.	0.	'Forest - Deciduous, Sum'
1.000	1.000	0.0	1.6	.82	.90	.12	-2.9	0.	0.	'Tree - Birch, Summer'
1.000	1.000	0.0	1.6	.97	.90	.14	-2.9	0.	0.	'Tree - Elm, Summer'
1.000	1.000	0.0	1.9	.90	.92	.17	-2.3	0.	0.	'Tree - Oak, Summer'
1.000	1.000	0.0	1.6	.90	.92	.13	-2.3	0.	0.	'Tree - Silver Maple,Avg'
1.000	1.000	0.0	1.6	.99	.96	.13	-1.2	0.	0.	'Tree - Pine, Summer'
1.000	1.000	0.0	1.6	.90	.96	.17	-1.2	0.	0.	'Bush, Summer'
1.000	1.000	0.0	1.6	.91	.88	.17	-3.5	0.	0.	'Dry Grass, Summer'
1.000	1.000	0.0	1.8	.67	.98	.17	-0.6	0.	0.	'Grass after Rain,Summer'
1.000	1.000	0.0	1.0	.85	.94	.17	-1.7	0.	0.	'Corn'
1.000	1.000	0.0	0.8	.85	.96	.25	-1.2	0.	0.	'Cotton'
1.000	1.000	0.0	0.2	.85	.97	.40	-0.8	0.	0.	'Tobacco'
1.000	1.000	0.0	0.5	.85	.96	.11	-1.2	0.	0.	'Wheat'
1.000	1.000	0.0	0.6	.80	.95	.15	-1.4	0.	0.	'Tree Trunk - Birch, Avg'
1.000	1.000	0.0	0.6	.88	.94	.15	-1.7	0.	0.	'Tree Trunk - Elm, Avg'
1.000	1.000	0.0	1.0	.95	.96	.15	-1.2	0.	0.	'Tree Trunk - Oak, Avg'
1.000	1.000	0.0	0.3	.99	.97	.15	-0.8	0.	0.	'Tree Trunk - Pine, Avg'
1.000	1.000	0.0	0.2	.99	.96	.13	-1.2	0.	0.	'Forest - Coniferous,Win'
1.000	1.000	0.0	0.4	.88	.95	.15	-1.4	0.	0.	'Forest - Deciduous, Win'
1.000	1.000	0.0	0.4	.80	.95	.12	-1.4	0.	0.	'Tree - Birch, Winter'
1.000	1.000	0.0	0.4	.88	.94	.14	-1.7	0.	0.	'Tree - Elm, Winter'
1.000	1.000	0.0	0.5	.95	.96	.17	-1.2	0.	0.	'Tree - Oak, Winter'
1.000	1.000	0.0	0.2	.99	.96	.13	-1.2	0.	0.	'Tree - Pine, Winter'
1.000	1.000	0.0	0.2	.90	.96	.16	-1.2	0.	0.	'Bush, Winter'
1.000	1.000	0.0	0.2	.91	.88	.16	-3.5	0.	0.	'Dry Grass, Winter'
1.000	1.000	0.0	0.3	.67	.98	.14	-0.6	0.	0.	'Grass after Rain,Winter'
2.600	.2000	0.0	11.2	.55	.89	.53	-3.2	0.	0.	'Rough Granite (1m dia.)'
2.600	.2000	0.0	5.6	.55	.89	.53	-3.2	0.	0.	'Rough Granite (.5m dia)'
2.500	.2200	0.0	11.2	.45	.95	.48	-1.4	0.	0.	'Limestone (1m dia.)'
2.500	.2200	0.0	5.6	.45	.95	.48	-1.4	0.	0.	'Limestone (.5m dia.)'
1.500	.2000	0.0	12.0	.60	.90	.55	-2.9	0.	0.	'Sand - Dry, Flat'
2.000	.2000	0.0	12.0	.70	.95	.60	-1.4	0.	0.	'Sand - Wet, Flat'
1.500	.2000	0.0	12.0	.60	.90	.45	-2.9	0.	0.	'Sand - White, Powdered'
1.400	.2000	0.0	12.0	.73	.95	.58	-1.4	0.	0.	'Dirt - Light'
1.400	.2000	0.0	12.0	.92	.93	.71	-2.0	0.	0.	'Dirt - Dark'
1.350	.2000	0.0	12.0	.73	.90	.58	-2.9	0.	0.	'Dirt - Dry'
1.400	.2000	0.0	12.0	.91	.95	.70	-1.4	0.	0.	'Dirt - Wet'
1.500	.2000	0.0	12.0	.80	.94	.65	-1.7	0.	0.	'Loam - Sandy, Fine, Dry'
1.700	.2000	0.0	12.0	.89	.94	.70	-1.7	0.	0.	'Loam - Sandy, Fine, Wet'
1.000	.2000	0.0	12.0	.96	.97	.73	-0.8	0.	0.	'Loam - Dark, Clayey'
1.000	.2000	0.0	12.0	.69	.95	.60	-1.4	0.	0.	'Clay - Dry'
1.750	.2000	0.0	12.0	.86	.98	.68	-0.6	0.	0.	'Clay - Wet'
1.500	.2000	0.0	12.0	.80	.90	.64	-2.9	0.	0.	'Gravel - Dry'
2.000	.2000	0.0	12.0	.90	.90	.70	-2.9	0.	0.	'Gravel - Wet'
1.600	.1600	0.0	12.0	.70	.95	.60	-1.4	0.	0.	'Concrete - Rough, Dry'

7.500	.1100	559.00	.3	.74	.44	.5	0.	0.	0.	'Steel - Dull'
7.833	.1111	464.40	.3	.74	.12	.5	0.	0.	0.	'Carbon Steel - Nominal'
7.833	.1111	464.40	.3	.54	.10	.5	0.	0.	0.	'Carbon Steel - Cleaned'
7.833	.1111	464.40	.3	.41	.07	.5	0.	0.	0.	'Carbon Steel - Polished'
7.833	.1111	464.40	.3	.74	.80	.5	0.	0.	0.	'Carbon Steel - Oxidized'
7.833	.1111	464.40	.3	.74	.90	.5	0.	0.	0.	'Carbon Steel - ForstGrn'
7.833	.1111	464.40	.3	.54	.90	.5	0.	0.	0.	'Carbon Steel - Sand'
7.833	.1111	464.40	.3	.64	.90	.5	0.	0.	0.	'Carbon Steel - OlivDrab'
7.833	.1111	464.40	.3	.94	.90	.5	0.	0.	0.	'Carbon Steel - Black'
7.833	.1111	464.40	.3	.95	.95	.5	0.	0.	0.	'Steel Grills - CavtyEff'
2.390	.2200	1754.40	1.0	.63	.19	.5	0.	0.	0.	'Aluminum - Dull'
2.700	.2198	2064.00	1.0	.49	.216	.5	0.	0.	0.	'Aluminum - Galvanized'
2.390	.2198	1754.40	1.0	.10	.04	.5	0.	0.	0.	'Aluminum - Polished'
2.700	.2198	2064.00	1.0	.74	.90	.5	0.	0.	0.	'Aluminum - Green'
7.960	.0900	3448.60	1.0	.60	.73	.5	0.	0.	0.	'Copper - Dull'
8.960	.0910	3440.00	1.0	.64	.60	.5	0.	0.	0.	'Copper - Tarnished'
7.960	.0900	3448.60	1.0	.27	.05	.5	0.	0.	0.	'Copper - Polished'
7.300	.0526	576.20	1.0	.39	.08	.5	0.	0.	0.	'Tin - Commercial'
8.858	.0898	684.60	1.0	.34	.09	.5	0.	0.	0.	'Bronze - Oxidized'
8.409	.0898	1008.80	1.0	.50	.61	.5	0.	0.	0.	'Brass - Oxidized'
.600	.6700	.86	2.4	.72	.85	.5	0.	0.	0.	'Wood - Thick, Rough'
.600	.6700	.86	2.4	.72	.78	.5	0.	0.	0.	'Wood - Thick, Smooth'
.400	.6689	1.10	1.0	.78	.90	.5	0.	0.	0.	'Wood - Unpainted'
.400	.6689	1.10	1.0	.74	.90	.5	0.	0.	0.	'Wood - Green Paint'
.030	.3106	.51	.3	.80	.90	.5	0.	0.	0.	'Canvas - Dark'
.030	.3106	.51	.1	.80	.90	.5	0.	0.	0.	'Camo Nets - Average'
1.160	.3799	2.15	.1	.13	.77	.5	0.	0.	0.	'Nylon Cloth'
1.190	.4491	1.38	.3	.73	.92	.5	0.	0.	0.	'Rubber - Hard'
1.198	.2986	1.30	.3	.95	.99	.5	0.	0.	0.	'Rubber - Tire'
2.600	.2000	12.04	.5	.18	.79	.5	0.	0.	0.	'Glass - Thick'
2.707	.1911	6.54	.3	.05	.95	.5	0.	0.	0.	'Glass Window'
1.400	.0400	64.50	1.0	.07	.72	.5	0.	0.	0.	'Plastic - Thick Sheet'
1.400	.0400	64.50	.005	.28	.72	.5	0.	0.	0.	'Plastic Film'
1.400	.2389	1.29	.3	.25	.95	.5	0.	0.	0.	'Plastic - White PVC'
1.400	.2389	1.29	.3	.90	.95	.5	0.	0.	0.	'Plastic - Dark PVC'
2.600	.1887	29.24	1.0	.55	.45	.5	0.	0.	0.	'Granite'
2.600	.2000	17.20	.5	.55	.89	.5	0.	0.	0.	'Granite - Thin'
2.600	.2000	17.20	16.7	.55	.89	.5	0.	0.	0.	'Stone - Rough,Weathered'
2.590	.2100	22.27	16.7	.80	.90	.5	0.	0.	0.	'Stone - Smooth'
2.500	.2102	15.48	1.0	.46	.95	.5	0.	0.	0.	'Marble - White'
2.700	.3100	12.81	.4	.70	.90	.5	0.	0.	0.	'Slate (1)'
2.800	.1801	16.06	.3	.88	.75	.5	0.	0.	0.	'Slate (2)'
.768	.2098	8.17	.5	.75	.93	.5	0.	0.	0.	'Brick - Red, Rough'
.800	.2501	3.44	.3	.50	.93	.5	0.	0.	0.	'Masonry'
.800	.2602	6.02	.3	.78	.85	.5	0.	0.	0.	'Gypsum Board'
1.400	.0400	64.50	.05	.10	.72	.5	0.	0.	0.	'Vinyl Siding'
1.000	.2300	9.46	.4	.75	.82	.5	0.	0.	0.	'Clay Tile'
.750	.6000	.86	.4	.72	.82	.5	0.	0.	0.	'Shingles - Wood'
1.300	.3500	6.36	.2	.86	.91	.5	0.	0.	0.	'Shingles - Asphalt'
2.400	.2500	1.46	16.7	.50	.10	.5	0.	0.	0.	'Asbestos'
2.280	.1601	15.48	1.0	.73	.94	.5	0.	0.	0.	'Concrete - Rough'
2.280	.1601	15.48	.3	.25	.92	.5	0.	0.	0.	'Concrete - White Paint'
2.110	.2200	6.36	16.7	.86	.98	.5	0.	0.	0.	'Asphalt (1)
2.114	.2200	5.93	1.0	.93	.93	.5	0.	0.	0.	'Asphalt (2)
2.800	.2000	7.22	16.7	.96	.90	.5	0.	0.	0.	'Lava'
2.800	.2000	2.58	16.7	.96	.90	.5	0.	0.	0.	'Basalt'
1.500	.2000	17.20	16.7	.80	.90	.5	0.	0.	0.	'Gravel (1)'
1.650	.1887	7.00	1.0	.29	.28	.5	0.	0.	0.	'Gravel (2)'
1.700	.2000	17.20	16.7	.90	.90	.5	0.	0.	0.	'Pebbles'
2.600	.2000	17.20	1.7	.55	.89	.5	0.	0.	0.	'Rocks'
2.500	.2200	15.48	83.3	.45	.95	.5	0.	0.	0.	'Boulders'
1.520	.1911	2.84	1.0	.76	.90	.5	0.	0.	0.	'Sand - Dry'
1.510	.1900	2.67	16.7	.60	.90	.5	0.	0.	0.	'Desert Sand'
1.500	.2000	2.88	16.7	.80	.94	.5	0.	0.	0.	'Soil - Sandy, Dry'

2.114	.2200	5.93	3.0	.93	.93	.70	0.	0.	0.	'Paved Road'
2.110	.2200	6.36	3.0	.86	.98	.70	0.	0.	0.	'Road 2'
2.110	.2200	6.36	3.0	.86	.98	.70	0.	0.	0.	'Asphalt (1)'
2.114	.2200	5.93	3.0	.93	.93	.70	0.	0.	0.	'Asphalt (2)'
1.300	.2000	5.93	3.0	.93	.97	.70	0.	0.	0.	'Asphalt - Dry'
2.000	.2000	6.36	3.0	.86	.93	.70	0.	0.	0.	'Macadam - Roadway'
1.500	.2000	4.62	3.0	.80	.94	.80	0.	0.	0.	'Dirt Road'
1.500	.2000	17.20	3.0	.80	.90	.70	0.	0.	0.	'Gravel (1)'
1.500	.2000	2.88	3.0	.80	.94	.70	0.	0.	0.	'Soil - Sandy, Dry'
1.700	.2000	4.32	3.0	.89	.94	.70	0.	0.	0.	'Soil - Sandy, Wet'
2.032	.2198	4.30	3.0	.75	.94	.70	0.	0.	0.	'Soil - Black, Plowed'
1.000	.2000	2.88	3.0	.69	.95	.70	0.	0.	0.	'Soil - Clay, Dry'
1.750	.2000	4.32	3.0	.86	.98	.70	0.	0.	0.	'Soil - Clay, Wet'
1.000	1.000	0.0	0.0	.99	.96	.50	-4.5	0.	180.	'Forest - Coniferous,Sum'
1.000	1.000	0.0	0.0	.88	.90	.50	-4.5	0.	180.	'Forest - Deciduous, Sum'
1.000	1.000	0.0	0.0	.91	.88	.50	-4.5	85.	180.	'Grass'
1.000	1.000	0.0	0.0	.91	.88	.50	-4.5	85.	180.	'Dry Grass, Summer'
1.000	1.000	0.0	0.0	.67	.98	.50	-1.6	85.	180.	'Grass after Rain,Summer'

Table 3. Suggested Object Parameters for Metals

Density	SpHt	ThmCond	Thick	EmV	EmTh	XpA	dPw	Slop	Azmh	Name
2.390	.2200	1754.40	-	.63	.19	.5	0.	-	-	'Aluminum - Dull'
2.700	.2198	2064.00	-	.49	.216	.5	0.	-	-	'Aluminum - Galvanized'
2.390	.2198	1754.40	-	.10	.04	.5	0.	-	-	'Aluminum - Polished'
2.700	.2200	2064.00	-	.96	.88	.5	0.	-	-	'Aluminum - Black'
2.700	.2198	2064.00	-	.74	.90	.5	0.	-	-	'Aluminum - Green'
2.700	.2200	2064.00	-	.20	.88	.5	0.	-	-	'Aluminum - White'
7.960	.0900	3448.60	-	.60	.73	.5	0.	-	-	'Copper - Dull'
7.960	.0900	3448.60	-	.27	.05	.5	0.	-	-	'Copper - Polished'
8.960	.0910	3440.00	-	.64	.60	.5	0.	-	-	'Copper - Tarnished'
8.409	.0898	1008.80	-	.50	.61	.5	0.	-	-	'Brass - Oxidized'
8.858	.0898	684.60	-	.34	.09	.5	0.	-	-	'Bronze - Oxidized'
7.350	.1100	559.00	-	.26	.49	.5	0.	-	-	'Galvanized Metal - New'
7.500	.1100	559.00	-	.74	.44	.5	0.	-	-	'Steel - Dull'
7.500	.1100	559.00	-	.91	.25	.5	0.	-	-	'Steel - New'
7.833	.1111	464.40	-	.74	.12	.5	0.	-	-	'Carbon Steel - Nominal'
7.833	.1111	464.40	-	.54	.10	.5	0.	-	-	'Carbon Steel - Cleaned'
7.833	.1111	464.40	-	.74	.80	.5	0.	-	-	'Carbon Steel - Oxidized'
7.833	.1111	464.40	-	.41	.07	.5	0.	-	-	'Carbon Steel - Polished'
7.833	.1111	464.40	-	.54	.90	.5	0.	-	-	'Carbon Steel - Sand'
7.833	.1111	464.40	-	.64	.90	.5	0.	-	-	'Carbon Steel - OlivDrab'
7.833	.1111	464.40	-	.74	.90	.5	0.	-	-	'Carbon Steel - ForstGrn'
7.833	.1111	464.40	-	.94	.90	.5	0.	-	-	'Carbon Steel - Black'
7.833	.1111	464.40	-	.95	.95	.5	0.	-	-	'Steel Grills - CavtyEff'
7.300	.0526	576.20	-	.39	.08	.5	0.	-	-	'Tin - Commercial'

Table 4. Suggested Object Parameters for Building Materials

Density	SpHt	ThmCond	Thick	EmV	EmTh	XpA	dPw	Slop	Azmh	Name
2.400	.2500	1.46	-	.50	.10	-.5	0.	-	-	'Asbestos'
.768	.2098	8.17	-	.75	.93	-.5	0.	-	-	'Brick - Red, Rough'
.030	.3106	.51	-	.80	.90	.35	0.	-	-	'Camo Net - Average'
1.400	.0400	64.50	.005	.80	.72	.35	0.	-	-	'Camo Net - Radar'
.030	.3106	.51	-	.80	.90	.5	0.	-	-	'Canvas - Dark'
1.000	.2300	9.46	.5	.75	.82	-.5	0.	-	-	'Clay Tile'
.600	.6700	-	-	.20	.88	-.5	0.	90.	-	'Door - Wht Alum on Wood'
.600	.6700	.86	-	.16	.95	-.5	0.	90.	-	'Door - Wood, Wht Paint'
.600	.6700	.86	-	.72	.78	-.5	0.	90.	-	'Door - Wood, Unpainted'
7.500	.1100	559.00	-	.91	.25	.5	0.	-	-	'Fence - Chain Link, New'
.600	.6700	.86	-	.85	.90	-.5	0.	90.	-	'Fence - Wooden'
2.600	.2000	12.04	-	.18	.79	.5	0.	-	-	'Glass'
2.600	.2000	12.04	.15	.18	.79	.5	0.	90.	-	'Glass Window (1)'
2.707	.1911	6.54	.15	.05	.95	.5	0.	90.	-	'Glass Window (2)'
2.600	.1887	29.24	-	.55	.45	-.5	0.	-	-	'Granite'
2.600	.2000	17.20	-	.55	.89	-.5	0.	-	-	'Granite - Thin'
.800	.2602	6.02	-	.78	.85	-.5	0.	-	-	'Gypsum Board'
2.500	.2102	15.48	-	.46	.95	-.5	0.	-	-	'Marble - White'
.800	.2501	3.44	-	.50	.93	-.5	0.	-	-	'Masonry'
1.160	.3799	2.15	-	.13	.77	.5	0.	-	-	'Nylon Cloth'
1.400	.0400	64.50	-	.07	.72	.5	0.	-	-	'Plastic Sheet'
1.400	.0400	64.50	.005	.28	.72	.5	0.	-	-	'Plastic Film'
1.400	.2389	1.29	-	.25	.95	.5	0.	-	-	'Plastic - White PVC'
1.400	.2389	1.29	-	.90	.95	.5	0.	-	-	'Plastic - Dark PVC'
1.300	.3500	6.36	-	.86	.91	-.5	0.	-	-	'Roof - Asphalt Shingles'
1.000	.2300	9.46	.5	.75	.82	-.5	0.	-	-	'Roof - Red Clay'
1.300	.2000	-	-	.89	.88	-.5	0.	-	-	'Roof - Heavy Felt w/Tar'
7.350	.1000	559.00	-	.26	.49	-.5	0.	-	-	'Roof - Galv. Metal, New'
.750	.6000	.86	-	.72	.82	-.5	0.	-	-	'Roof - Oak Shingles'
.320	.2000	-	-	.81	.98	-.5	0.	-	-	'Roof - Old Straw'
1.190	.4491	1.38	-	.73	.92	-.5	0.	-	-	'Rubber - Hard'
1.198	.2986	1.30	-	.95	.99	-.5	0.	-	-	'Rubber - Tire'
2.700	.2200	2064.00	.05	.20	.88	.5	0.	90.	-	'Siding - Aluminum, Wht'
1.400	.0400	64.50	.05	.10	.72	.5	0.	90.	-	'Siding - Vinyl'
2.700	.3100	12.81	-	.70	.90	-.5	0.	-	-	'Slate (1)'
2.800	.1801	16.06	-	.88	.75	-.5	0.	-	-	'Slate (2)'
2.600	.2000	17.20	-	.55	.89	-.5	0.	-	-	'Stone - Rough,Weathered'
2.590	.2100	22.27	-	.80	.90	-.5	0.	-	-	'Stone - Smooth'
1.750	.2300	3.87	-	.83	.93	-.5	0.	90.	-	'Wall - Brick, Red'
1.600	.1600	15.48	-	.16	.94	-.5	0.	90.	-	'Wall - Concrete, Wht Pt'
1.800	.2300	5.66	-	.70	.84	-.5	0.	90.	-	'Wall - Masonry'
2.300	.2200	15.48	-	.80	.93	-.5	0.	90.	-	'Wall - Stonework'
.600	.6700	.86	-	.16	.95	-.5	0.	90.	-	'Wall - Wood, Wht Paint'
.600	.6700	.86	-	.72	.78	-.5	0.	90.	-	'Wall - Wood, Unpainted'
.800	.5700	.86	-	.75	.90	-.5	0.	-	-	'Wood - Dark Oak'
.600	.6700	.86	-	.72	.85	-.5	0.	-	-	'Wood - Rough Pine'
.600	.6700	.86	-	.72	.78	-.5	0.	-	-	'Wood - Smooth'

Table 4. Suggested Object Parameters for Building Materials (Continued)

Density	SpHt	ThmCond	Thick	EmV	EmTh	XpA	dPw	Slop	Azmh	Name
.400	.6689	1.10	-	.78	.90	-.5	0.	-	-	'Wood - Unpainted'
.400	.6689	1.10	-	.74	.90	-.5	0.	-	-	'Wood - Green Paint'

Table 5. Suggested Object Parameters for Surface Materials

Density	SpHt	ThmCond	Thick	EmV	EmTh	XpA	dPw	Slop	Azmh	Name
2.110	.2200	6.36	-	.86	.98	-.5	0.	0.	0.	'Asphalt (1)'
2.114	.2200	5.93	-	.93	.93	-.5	0.	0.	0.	'Asphalt (2)'
1.300	.2000	6.36	-	.93	.97	-.5	0.	0.	0.	'Asphalt - Dry'
2.800	.2000	2.58	-	.96	.90	-.5	0.	0.	0.	'Basalt'
2.500	.2200	15.48	-	.45	.95	-.5	0.	0.	0.	'Boulders'
1.000	.2000	2.88	-	.69	.95	-.5	0.	0.	0.	'Clay - Dry'
1.750	.2000	4.32	-	.86	.98	-.5	0.	0.	0.	'Clay - Wet'
2.000	.1600	15.48	-	.90	.99	-.5	0.	0.	0.	'Concrete - Bridge Base'
2.280	.1601	15.48	-	.73	.94	-.5	0.	0.	0.	'Concrete - Rough'
2.280	.1601	15.48	-	.25	.92	-.5	0.	0.	0.	'Concrete - White Paint'
1.600	.1600	15.48	-	.70	.95	-.5	0.	0.	0.	'Concrete - Rough, Dry'
1.600	.1600	15.48	-	.60	.88	-.5	0.	0.	0.	'Concrete - Smooth'
1.600	.1600	15.48	-	.90	.99	-.5	0.	0.	0.	'Concrete - Roadway'
1.400	.2000	2.88	-	.73	.95	-.5	0.	0.	0.	'Dirt - Light'
1.400	.2000	4.32	-	.92	.93	-.5	0.	0.	0.	'Dirt - Dark'
1.350	.2000	2.88	-	.73	.90	-.5	0.	0.	0.	'Dirt - Dry'
1.400	.2000	4.32	-	.91	.95	-.5	0.	0.	0.	'Dirt - Wet'
2.600	.2000	17.20	-	.55	.89	-.5	0.	0.	0.	'Granite - Rough'
1.650	.1887	7.00	-	.29	.28	-.5	0.	0.	0.	'Gravel'
1.500	.2000	17.20	-	.80	.90	-.5	0.	0.	0.	'Gravel - Dry'
2.000	.2000	-	-	.90	.90	-.5	0.	0.	0.	'Gravel - Wet'
2.800	.2000	7.22	-	.96	.90	-.5	0.	0.	0.	'Lava'
2.500	.2200	15.48	-	.45	.95	-.5	0.	0.	0.	'Limestone'
1.500	.2000	2.88	-	.80	.94	-.5	0.	0.	0.	'Loam - Sandy, Fine, Dry'
1.700	.2000	4.32	-	.89	.94	-.5	0.	0.	0.	'Loam - Sandy, Fine, Wet'
1.000	.2000	2.88	-	.96	.97	-.5	0.	0.	0.	'Loam - Dark, Clayey'
2.000	.2000	-	-	.86	.93	-.5	0.	0.	0.	'Macadam - Roadway'
1.700	.2000	17.20	-	.90	.90	-.5	0.	0.	0.	'Pebbles'
2.600	.2000	17.20	-	.55	.89	-.5	0.	0.	0.	'Rocks'
.770	.2000	61.06	-	.38	.93	-.5	0.	0.	0.	'Salt Pan'
1.510	.1900	2.67	-	.60	.90	-.5	0.	0.	0.	'Sand - Desert'
1.520	.1911	2.84	-	.76	.90	-.5	0.	0.	0.	'Sand - Dry'
1.500	.2000	2.67	-	.60	.90	-.5	0.	0.	0.	'Sand - Dry, Flat'
2.000	.2000	4.32	-	.70	.95	-.5	0.	0.	0.	'Sand - Wet, Flat'
1.500	.2000	2.67	-	.60	.90	-.5	0.	0.	0.	'Sand - White, Powdered'
1.500	.2000	2.88	-	.80	.94	-.5	0.	0.	0.	'Soil - Sandy, Dry'
1.700	.2000	4.32	-	.89	.94	-.5	0.	0.	0.	'Soil - Sandy, Wet'
2.032	.2198	4.30	-	.75	.94	-.5	0.	0.	0.	'Soil - Black, Plowed'
1.000	.2000	2.88	-	.69	.95	-.5	0.	0.	0.	'Soil - Clay, Dry'
1.750	.2000	4.32	-	.86	.98	-.5	0.	0.	0.	'Soil - Clay, Wet'

Table 6. Suggested Object Parameters for Vegetation

Density	SpHt	ThmCond	Thick	EmV	EmTh	XpA	dPw	Slop	Azmh	Name
1.000	1.000	5.00	.05	.90	.96	.17	-1.2	0.	0.	'Bush, Summer'
1.000	1.000	5.00	-	.90	.96	.16	-1.2	0.	0.	'Bush, Winter'
1.000	1.000	5.00	.05	.89	.90	.11	-1.2	0.	0.	'Crop - Alfalfa'
1.000	1.000	5.00	.05	.85	.94	.17	-1.7	0.	0.	'Crop - Corn'
1.000	1.000	5.00	.05	.85	.96	.25	-1.2	0.	0.	'Crop - Cotton'
1.000	1.000	5.00	.05	.85	.97	.40	-0.8	0.	0.	'Crop - Tobacco'
1.000	1.000	5.00	.05	.85	.96	.11	-1.2	0.	0.	'Crop - Wheat'
1.000	1.000	5.00	.05	.99	.96	.13	-1.2	0.	0.	'Forest - Coniferous,Sum'
1.000	1.000	5.00	.05	.99	.96	.13	-1.2	0.	0.	'Forest - Coniferous,Win'
1.000	1.000	5.00	.05	.88	.90	.15	-2.9	0.	0.	'Forest - Deciduous, Sum'
1.000	1.000	5.00	-	.88	.95	.15	-1.4	0.	0.	'Forest - Deciduous, Win'
1.000	1.000	5.00	.05	.91	.88	.17	-3.5	0.	0.	'Grass - Dry, Summer'
1.000	1.000	5.00	.05	.91	.88	.16	-3.5	0.	0.	'Grass - Dry, Winter'
1.000	1.000	5.00	.05	.67	.98	.17	-0.6	0.	0.	'Grass after Rain,Summer'
1.000	1.000	5.00	.05	.67	.98	.14	-0.6	0.	0.	'Grass after Rain,Winter'
1.000	1.000	5.00	.05	.78	.98	.11	-1.2	0.	0.	'Pasture'
.600	.6700	.86	.5	.85	.90	-.5	0.	90.	-	'Telephone Pole - Wood'
1.000	1.000	5.00	.05	.82	.90	.12	-2.9	0.	0.	'Tree - Birch, Summer'
1.000	1.000	5.00	-	.80	.95	.12	-1.4	0.	0.	'Tree - Birch, Winter'
1.000	1.000	5.00	.05	.97	.90	.14	-2.9	0.	0.	'Tree - Elm, Summer'
1.000	1.000	5.00	-	.88	.94	.14	-1.7	0.	0.	'Tree - Elm, Winter'
1.000	1.000	5.00	.05	.90	.92	.17	-2.3	0.	0.	'Tree - Oak, Summer'
1.000	1.000	5.00	-	.95	.96	.17	-1.2	0.	0.	'Tree - Oak, Winter'
1.000	1.000	5.00	.05	.99	.96	.13	-1.2	0.	0.	'Tree - Pine, Summer'
1.000	1.000	5.00	.05	.99	.96	.13	-1.2	0.	0.	'Tree - Pine, Winter'
1.000	1.000	5.00	.05	.90	.92	.13	-2.3	0.	0.	'Tree - Silver Maple,Avg'
.600	.6700	.86	.5	.99	.97	-.15	0.	90.	-	'Tree Trunk - Evergreen'
.800	.5700	.86	.5	.95	.96	-.15	0.	90.	-	'Tree Trunk - Deciduous'
.800	.5700	.86	.5	.80	.95	-.15	0.	90.	-	'Tree Trunk - Birch, Avg'
.800	.5700	.86	.5	.88	.94	-.15	0.	90.	-	'Tree Trunk - Elm, Avg'
.800	.5700	.86	.5	.95	.96	-.15	0.	90.	-	'Tree Trunk - Oak, Avg'
.600	.6700	.86	.5	.99	.97	-.15	0.	90.	-	'Tree Trunk - Pine, Avg'

Table 7. Suggested Object Parameters for Water

Density	SpHt	ThmCond	Thick	EmV	EmTh	XpA	dPw	Slop	Azmh	Name
.920	.4900	19.35	-	.80	.99	-.5	0.	0.	0.	'Ice'
.918	.5017	19.44	-	.50	.98	-.5	0.	0.	0.	'Ice - Rough'
1.030	.9400	4.90	-	.79	.96	-.5	0.	0.	0.	'Marsh / Swamp / Paddy'
1.000	1.000	5.00	-	.89	.96	-.5	0.	0.	0.	'Pond - Clear'
1.000	1.000	5.00	-	.90	.96	-.5	0.	0.	0.	'River - Muddy'
.160	.5017	.60	-	.28	.82	-.5	0.	0.	0.	'Snow - Fine Particles'
.130	.5000	1.38	-	.25	.82	-.5	0.	0.	0.	'Snow - Fluffy, Fresh'
.160	.5000	1.55	-	.95	.89	-.5	0.	0.	0.	'Snow - Packed, Crusty'
1.000	1.000	5.00	-	.96	.96	-.5	0.	0.	0.	'Stream - w/Weeds, Sedge'
1.000	1.000	5.13	-	.50	.96	-.5	0.	0.	0.	'Deep Water - Normal Inc'
1.000	1.000	5.00	-	.50	.96	-.5	0.	0.	0.	'Fresh Water'
1.030	.9600	4.90	-	.50	.96	-.5	0.	0.	0.	'Salt Water'

APPENDIX H

Radiance and Temperature Plots and Data June 1992 & October 1990 Data Collections

I.) June 1992 Radiance and Temperature Data

II.) June 1992 Radiance and Temperature Plots

III.) October 1990 Radiance and Temperature Data

IV.) October 1990 Radiance and Temperature Plots

Dirsig Radiance (JUNE)

	Time	Water	Grass	Asphalt	Halo	Car Door	Car Window	Car Roof	Car Tire
1	0.000	28.920	29.407	28.432	30.057	30.382	27.457	23.555	28.107
2	1.000	28.498	28.990	28.007	29.481	29.809	27.024	23.255	27.679
3	2.000	28.251	28.568	27.618	29.201	29.518	26.826	23.025	27.459
4	3.000	27.804	28.502	27.386	28.920	29.478	26.688	22.921	27.246
5	4.000	27.490	27.651	27.006	28.457	28.618	26.200	22.493	27.006
6	5.000	27.077	27.722	26.594	28.205	28.688	25.950	22.405	26.433
7	6.000	26.853	27.824	26.529	28.148	29.444	26.205	22.642	27.015
8	7.000	26.662	29.164	28.449	30.057	35.239	30.593	25.411	33.452
9	8.000	26.837	31.146	31.434	33.158	48.816	37.898	29.422	43.788
10	9.000	27.352	32.974	35.558	37.229	57.439	43.611	34.190	50.753
11	10.000	27.962	33.994	39.700	41.493	57.796	46.384	38.396	51.927
12	11.000	28.811	36.033	44.841	46.602	58.052	48.364	44.312	51.887
13	12.000	29.691	36.100	47.360	49.092	48.572	44.068	43.722	44.242
14	13.000	30.644	37.433	51.184	41.436	40.044	40.914	48.747	37.433
15	14.000	31.710	39.156	53.338	41.106	42.169	38.624	48.019	40.928
16	15.000	32.720	38.046	53.164	41.138	41.997	37.359	45.433	39.764
17	16.000	33.148	37.934	48.019	42.720	42.891	38.618	38.789	41.524
18	17.000	33.065	37.176	43.857	43.171	43.343	39.060	35.977	42.144
19	18.000	32.948	36.141	41.182	41.518	41.014	36.981	34.125	39.838
20	19.000	32.513	35.494	38.476	39.703	39.002	35.670	30.935	37.774
21	20.000	32.126	33.999	35.684	37.370	36.059	33.624	28.192	35.122
22	21.000	31.682	33.754	33.566	35.638	35.638	32.435	27.160	33.943
23	22.000	31.380	32.451	32.808	34.593	34.415	31.737	26.382	32.987
24	23.000	30.918	32.432	32.432	34.137	34.326	31.486	26.373	32.811

Dirsig Radiance (JUNE)

	House Roof	Black Side	White Side	Time
1	26.319	28.107	28.107	0.000
2	25.713	27.679	27.679	1.000
3	25.559	27.301	27.301	2.000
4	25.433	27.246	27.246	3.000
5	25.394	26.845	26.845	4.000
6	24.661	26.433	26.433	5.000
7	25.233	26.691	26.529	6.000
8	30.414	32.916	31.129	7.000
9	38.042	43.932	38.473	8.000
10	45.890	51.968	44.067	9.000
11	50.623	54.372	45.732	10.000
12	57.171	54.881	46.602	11.000
13	54.288	47.879	42.336	12.000
14	56.406	38.999	36.911	13.000
15	52.097	41.637	39.156	14.000
16	46.635	40.966	38.561	15.000
17	43.404	42.037	39.643	16.000
18	42.144	42.315	40.088	17.000
19	39.166	40.006	38.326	18.000
20	36.547	38.300	37.073	19.000
21	33.437	35.497	34.935	20.000
22	32.624	33.754	33.754	21.000
23	31.737	32.808	32.808	22.000
24	31.675	32.622	32.622	23.000

Truth Radiance II (JUNE)

	Time	Water	Asphalt	Halo	Car Side	Window	Car Roof	House Roof	Left Side
1	0.000	27.618	27.618	14.614	25.342	23.229	22.254	23.067	24.529
2	1.000	27.188	26.860	12.441	25.221	23.419	21.780	23.583	24.894
3	2.000	27.616	26.982	14.946	25.557	24.765	23.340	24.607	25.398
4	3.000	27.000	26.600	14.500	25.300	24.370	22.589	24.000	25.000
5	4.000	26.300	25.800	13.900	25.000	24.300	22.100	23.900	24.750
6	5.000	25.500	25.400	13.730	25.040	24.400	22.460	24.270	24.800
7	6.000	24.750	25.500	10.510	28.590	25.900	22.750	24.960	26.570
8	7.000	24.698	27.557	-2.824	41.497	28.987	25.413	30.417	33.812
9	8.000	26.836	30.571	9.023	46.230	33.875	29.853	38.472	38.760
10	9.000	28.264	33.734	6.079	51.968	38.597	39.052	51.664	53.032
11	10.000	29.268	36.768	10.519	51.767	39.213	42.474	55.354	53.723
12	11.000	29.338	40.787	16.128	50.299	40.083	44.838	58.577	51.179
13	12.000	29.691	43.028	18.431	44.760	39.391	44.760	56.539	45.107
14	13.000	31.000	46.000	22.000	41.000	38.000	44.900	54.000	40.500
15	14.000	32.000	50.510	20.860	41.420	37.450	50.330	56.330	40.630
16	15.000	31.820	48.462	20.094	39.754	36.651	41.998	47.177	38.546
17	16.000	32.000	45.016	21.844	37.117	33.821	36.790	39.561	36.336
18	17.000	32.230	41.247	22.793	36.012	33.094	34.038	36.270	35.068
19	18.000	31.637	40.525	22.017	36.111	33.076	33.244	35.079	34.875
20	19.000	32.100	37.500	34.000	34.000	32.400	31.400	32.000	32.500
21	20.000	31.834	35.327	25.480	32.016	31.094	29.898	30.541	31.187
22	21.000	31.721	33.300	26.502	30.691	30.134	29.200	29.121	29.863
23	22.000	31.625	32.263	26.972	30.065	29.520	28.972	28.972	29.703
24	23.000	31.426	31.426	26.522	30.106	29.257	28.879	28.879	29.352

Truth Radiance II (JUNE)

	Right Side	Tire	Grass	Time
1	24.529	25.505	23.717	0.000
2	24.894	25.385	23.910	1.000
3	25.557	26.349	24.923	2.000
4	25.000	25.750	24.550	3.000
5	24.800	25.100	24.800	4.000
6	24.960	25.360	25.200	5.000
7	26.330	27.790	24.800	6.000
8	32.561	40.067	26.306	7.000
9	36.174	44.649	29.135	8.000
10	45.890	53.640	33.430	9.000
11	46.224	53.071	33.996	10.000
12	44.838	53.469	35.327	11.000
13	41.123	42.682	34.194	12.000
14	39.000	39.500	34.800	13.000
15	38.422	37.360	37.452	14.000
16	36.994	36.737	35.354	15.000
17	34.945	34.251	33.917	16.000
18	33.780	33.351	35.235	17.000
19	33.772	33.304	32.608	18.000
20	32.200	32.200	31.093	19.000
21	31.187	31.094	30.175	20.000
22	29.863	30.319	29.577	21.000
23	29.703	29.978	29.426	22.000
24	29.352	30.012	29.352	23.000

Dirsig Temp's (JUNE)

	Time	Water	Grass	Grey 1	Grey 2	Grey 3	Grey 4	Car Door	Window
1	0.000	14.382	8.469	2.998	2.998	2.998	2.998	9.408	6.590
2	1.000	13.609	7.379	1.984	1.984	1.984	1.984	8.325	5.711
3	2.000	12.881	6.781	1.505	1.505	1.505	1.505	7.770	5.242
4	3.000	12.038	6.594	1.203	1.203	1.203	1.203	7.545	4.797
5	4.000	11.236	5.011	0.782	0.782	0.782	0.782	5.819	3.823
6	5.000	10.439	5.179	-0.450	-0.450	-0.450	-0.450	6.125	3.285
7	6.000	9.829	5.418	-0.130	0.045	0.089	0.132	7.645	3.801
8	7.000	9.579	7.866	10.778	12.777	13.462	14.147	18.372	12.662
9	8.000	9.834	11.633	25.337	30.598	32.259	33.920	39.595	25.614
10	9.000	10.764	14.674	36.835	43.912	46.333	48.568	50.989	34.787
11	10.000	12.284	16.579	42.147	50.125	52.784	55.238	51.352	38.875
12	11.000	14.156	20.042	46.796	55.358	58.033	60.709	51.345	41.713
13	12.000	15.797	19.974	41.640	48.688	51.037	53.386	38.507	35.375
14	13.000	17.878	22.527	35.311	41.122	42.865	44.899	25.723	30.662
15	14.000	19.983	24.997	27.504	30.549	31.623	32.518	28.579	26.788
16	15.000	21.921	23.444	24.629	27.506	28.353	29.368	28.353	24.798
17	16.000	22.748	23.043	26.978	29.635	30.520	31.406	29.536	26.782
18	17.000	22.816	21.866	27.961	30.414	31.285	32.076	30.256	27.486
19	18.000	22.405	20.210	24.525	26.568	27.325	28.007	26.720	24.222
20	19.000	21.812	19.084	21.617	22.981	23.448	23.916	23.760	21.929
21	20.000	21.125	16.824	17.461	17.939	18.098	18.257	18.872	18.349
22	21.000	20.150	16.239	14.611	14.634	14.656	14.656	18.432	16.261
23	22.000	19.360	13.840	13.498	13.498	13.498	13.498	16.258	14.646
24	23.000	18.644	13.821	13.119	13.119	13.119	13.119	16.199	14.432

Dirsig Temp's (JUNE)

	Car Roof	Car Tire	House Roof	Black Side	White Side	Asphalt	Time
1	6.645	4.711	2.722	4.656	4.656	8.358	0.000
2	5.711	3.820	1.762	3.653	3.653	7.435	1.000
3	5.187	3.263	1.120	3.208	3.208	6.891	2.000
4	4.850	2.947	0.886	2.788	2.788	6.224	3.000
5	3.728	2.445	0.877	2.207	2.207	5.391	4.000
6	3.337	1.444	-0.608	1.233	1.233	4.758	5.000
7	4.238	2.578	0.700	1.705	1.486	4.719	6.000
8	11.007	15.060	10.949	14.375	10.892	8.494	7.000
9	20.354	32.259	23.815	32.674	23.815	14.125	8.000
10	30.504	42.422	35.718	44.471	32.738	21.379	9.000
11	38.670	43.988	42.352	47.466	35.397	28.443	10.000
12	49.204	43.586	50.810	48.134	36.362	36.095	11.000
13	48.165	32.242	47.382	38.246	29.632	39.812	12.000
14	56.230	21.074	50.129	24.270	20.493	45.189	13.000
15	55.441	26.609	44.338	28.400	24.281	48.099	14.000
16	51.202	24.798	36.985	27.337	23.106	47.986	15.000
17	39.671	27.470	32.193	28.946	25.010	40.851	16.000
18	34.134	28.356	30.493	29.464	25.745	34.926	17.000
19	30.656	24.676	25.736	25.887	22.860	30.883	18.000
20	24.033	21.617	21.695	22.747	20.721	26.566	19.000
21	17.939	17.028	16.346	18.121	17.415	21.785	20.000
22	15.628	15.357	15.018	15.063	15.041	18.251	21.000
23	13.693	13.522	13.351	13.718	13.693	16.722	22.000
24	13.549	13.368	13.187	13.323	13.323	16.040	23.000

June92 Temp's (JUNE)

	Time	Asphalt-Sun	Halo	Car Side	Car Roof	Water	Car Window	House Roof	Left Side
1	0.000	12.150	11.870	4.530	-0.450	15.400	5.020	1.240	3.610
2	1.000	10.780	11.260	4.230	1.250	14.560	4.820	2.410	4.220
3	2.000	9.780	10.980	3.490	0.460	13.960	3.930	1.480	3.320
4	3.000	9.030	10.510	3.630	0.560	13.320	4.010	2.000	3.690
5	4.000	8.000	10.100	3.320	1.160	12.590	3.720	2.370	3.440
6	5.000	7.380	9.690	2.930	0.880	11.800	3.010	1.060	2.410
7	6.000	7.360	9.690	6.240	0.340	11.350	4.790	1.600	5.240
8	7.000	9.980	11.740	28.110	6.980	10.990	15.060	9.320	15.610
9	8.000	15.740	16.660	44.870	16.900	11.120	28.310	27.200	38.580
10	9.000	22.430	22.580	51.320	35.880	12.270	37.340	39.710	41.000
11	10.000	28.380	27.410	51.160	43.340	13.580	40.310	47.250	45.590
12	11.000	34.950	31.370	47.620	49.810	15.220	40.950	50.690	43.380
13	12.000	37.730	24.680	39.320	50.910	16.580	37.540	49.220	36.150
14	13.000	45.100	22.190	32.590	56.770	18.350	37.820	50.570	30.980
15	14.000	47.020	21.940	31.560	57.640	20.000	34.520	46.580	30.110
16	15.000	46.690	21.280	31.320	49.250	21.630	33.260	39.850	27.980
17	16.000	43.950	21.200	27.460	47.350	21.980	27.600	33.320	25.430
18	17.000	36.660	20.790	25.410	32.440	22.100	25.230	26.100	23.200
19	18.000	35.500	20.420	24.880	33.970	21.870	24.740	23.730	22.930
20	19.000	30.370	19.660	21.280	20.910	21.170	21.950	20.310	19.550
21	20.000	25.900	18.730	17.870	16.130	20.510	18.250	16.410	16.370
22	21.000	22.050	17.940	14.580	11.110	20.020	14.700	12.210	13.860
23	22.000	19.440	16.390	12.880	10.810	19.410	13.130	10.870	12.610
24	23.000	17.950	15.630	12.750	10.850	19.010	12.630	11.160	12.730

June92 Temp's (JUNE)

	Right Side	Tire	Time
1	3.770	5.190	0.000
2	4.040	4.700	1.000
3	3.310	4.030	2.000
4	3.610	3.950	3.000
5	3.530	3.760	4.000
6	2.660	3.100	5.000
7	4.140	4.410	6.000
8	15.430	24.970	7.000
9	33.000	37.490	8.000
10	42.540	43.580	9.000
11	43.020	45.200	10.000
12	40.390	42.060	11.000
13	34.170	36.360	12.000
14	30.720	32.520	13.000
15	29.040	28.200	14.000
16	27.280	26.530	15.000
17	23.900	22.700	16.000
18	22.070	21.310	17.000
19	21.800	21.010	18.000
20	18.940	18.930	19.000
21	16.150	16.770	20.000
22	14.040	14.670	21.000
23	12.560	13.220	22.000
24	12.770	12.940	23.000

Thermistors 6/22/92

	Time	Car Side	White Front	Roof Shingles	Asphalt Shade	Windshield	Tire
1	15.500	22.690	21.880	30.170	16.000	30.140	20.910
2	15.750	21.790	21.110	28.440	15.920	29.240	20.230
3	16.000	21.570	21.070	29.370	15.930	30.450	19.950
4	16.250	20.940	20.350	25.370	16.020	28.520	19.400
5	16.500	21.830	20.780	25.770	16.160	29.400	19.740
6	16.750	21.390	21.140	24.910	16.260	29.590	19.750
7	17.000	21.540	21.090	23.060	16.350	28.890	19.500
8	17.250	21.050	19.740	21.530	16.230	27.240	18.900
9	17.500	21.510	19.590	20.830	16.390	27.920	19.100
10	17.750	21.450	19.200	19.580	16.310	27.110	18.680
11	18.000	21.640	19.150	18.840	16.420	27.480	18.780
12	18.250	20.790	18.630	16.900	16.410	25.050	18.250
13	18.500	20.910	18.130	15.970	16.330	25.140	18.010
14	18.750	20.800	17.850	15.660	16.280	24.910	17.740
15	19.000	19.930	17.460	15.270	16.130	24.660	17.430
16	19.250	19.320	16.950	14.900	16.050	23.920	17.090
17	19.500	18.370	16.510	14.450	16.000	23.140	16.710
18	19.750	17.550	15.680	13.680	15.820	21.790	16.110
19	20.000	16.480	14.620	12.960	15.570	19.950	15.320
20	20.250	15.470	13.560	11.910	15.410	18.350	14.590
21	20.500	14.040	11.760	9.630	15.200	16.400	13.250
22	20.750	12.520	10.090	8.220	14.900	13.660	11.820
23	21.000	10.780	8.380	6.510	14.590	11.380	10.320
24	21.250	9.400	7.250	5.850	14.110	9.720	9.270
25	21.500	8.650	6.500	5.060	13.850	8.600	8.400
26	21.750	8.030	5.900	4.440	13.630	7.770	7.800
27	22.000	7.310	5.400	3.590	13.480	6.940	7.350
28	22.250	6.740	4.920	3.260	13.090	6.440	6.810
29	22.500	6.390	4.660	2.920	12.930	5.970	6.610
30	22.750	6.110	4.610	2.330	12.670	5.290	6.470
31	23.000	6.270	5.420	4.240	12.480	5.260	6.500
32	23.250	6.300	5.710	4.340	12.430	5.300	6.540
33	23.500	5.620	5.290	2.820	12.450	4.840	6.070
34	23.750	4.950	4.360	1.580	12.310	4.040	5.670
35	24.000	4.530	3.770	1.240	11.870	3.320	5.190
36	0.250	4.420	3.600	0.980	11.890	3.090	5.080
37	0.500	4.200	3.350	1.380	11.810	2.720	4.660
38	0.750	4.270	3.760	2.010	11.370	3.010	4.640
39	1.000	4.230	4.040	2.410	11.260	3.210	4.700
40	1.250	3.610	3.180	0.340	11.380	2.260	4.280
41	1.500	3.720	3.350	1.080	11.180	2.150	4.280
42	1.750	3.540	3.210	1.100	11.070	2.420	4.370
43	2.000	3.490	3.310	1.480	10.980	2.400	4.030
44	2.250	3.690	3.640	2.220	10.820	2.560	4.100
45	2.500	3.960	3.990	2.760	10.740	2.740	4.310
46	2.750						
47	3.000						
48	3.250	3.430	3.390	2.030	10.520	2.060	3.840
49	3.500	2.800	2.850	0.950	10.500	1.720	3.400
50	3.750	2.280	2.140	0.360	10.310	1.110	2.820
51	4.000	3.320	3.530	2.370	10.100	2.130	3.760
52	4.250	3.030	3.380	2.120	9.990	1.980	3.550
53	4.500	2.980	3.320	1.930	9.970	1.710	3.390
54	4.750	2.900	2.760	1.280	9.740	1.810	3.150
55	5.000	2.930	2.660	1.060	9.690	1.920	3.100
56	5.250	2.330	2.370	0.440	9.770	1.220	2.790

Thermistors 6/22/92

	Car Roof	Side Window	Black Front	Middle Asphalt	Specular Board	Water	Sand
1	43.300	24.090	22.730	33.960	39.550	18.750	37.400
2	40.470	23.900	21.960	28.690	36.900	19.150	36.250
3	41.410	23.360	22.130	26.510	21.430	19.360	35.490
4	37.050	22.790	20.970	23.900	17.700	19.490	31.690
5	38.450	24.140	21.480	22.890	16.600	19.580	29.480
6	37.110	23.410	21.700	22.020	16.080	19.610	25.270
7	35.230	23.790	21.430	21.230	15.460	20.010	22.580
8	32.460	23.020	20.040	20.150	14.600	19.790	20.230
9	33.040	23.760	20.220	20.090	14.600	20.150	19.210
10	31.010	23.250	19.580	19.390	14.050	19.880	18.040
11	30.700	23.560	19.470	19.080	14.080	19.410	17.400
12	27.060	21.650	18.870	18.600	13.770	19.680	16.790
13	26.010	22.280	18.300	18.050	13.230	19.800	16.120
14	24.770	22.050	18.040	17.750	13.010	19.570	15.690
15	23.550	20.950	17.700	17.390	12.740	19.470	15.220
16	21.540	20.830	17.160	17.090	12.590	19.180	14.780
17	19.670	19.900	16.780	16.880	12.090	19.010	14.530
18	17.650	20.060	15.810	16.410	11.490	19.040	14.070
19	15.410	19.240	14.820	15.850	10.640	18.530	13.450
20	13.250	18.380	13.750	15.500	9.620	18.140	12.830
21	10.060	17.000	11.760	14.970	7.230	18.250	12.180
22	8.030	14.640	10.060	14.520	5.120	18.020	11.210
23	5.130	12.580	8.250	13.900	2.780	17.890	10.220
24	4.270	11.160	7.330	13.300	1.570	17.690	9.300
25	3.510	10.060	6.600	12.790	0.880	17.290	8.500
26	2.980	9.220	5.730	12.330	0.170	17.170	7.840
27	1.690	8.540	5.590	12.050	0.020	17.270	7.360
28	2.280	7.830	4.970	11.640	-0.300	16.960	6.850
29	1.820	7.360	4.890	11.380	-0.410	16.570	6.490
30	0.610	6.940	4.680	11.040	-0.390	16.360	6.170
31	2.330	6.880	5.520	10.830	2.170	15.980	6.140
32	3.050	6.960	5.820	10.720	2.710	15.820	6.270
33	1.110	6.500	5.300	10.640	1.690	15.840	6.310
34	-0.090	5.710	4.470	10.550	-0.010	15.620	6.020
35	-0.450	5.020	3.610	10.040	-0.420	15.400	5.780
36	-0.220	4.960	3.690	10.000	-0.540	15.290	5.540
37	-0.120	4.640	3.240	9.740	-0.700	15.120	5.230
38	1.120	4.770	3.840	9.330	0.380	14.490	4.960
39	1.250	4.820	4.220	9.220	1.130	14.560	5.000
40	-1.130	4.040	3.190	9.270	-1.030	14.410	4.760
41	-0.020	4.050	3.390	9.040	-0.820	14.396	4.450
42	0.050	4.040	3.350	8.860	-0.730	14.160	4.400
43	0.460	3.930	3.320	8.620	0.000	13.960	4.320
44	1.020	4.030	3.500	8.440	0.850	13.950	4.200
45	1.390	4.250	3.900	8.390	1.850	13.590	4.500
46							
47							
48	0.390	3.780	3.240	8.030	0.760	13.170	4.360
49	-0.200	3.240	2.750	7.950	-0.030	13.250	4.350
50	-1.480	2.690	1.990	7.680	-1.530	12.750	3.850
51	1.160	3.720	3.440	7.540	1.580	12.590	4.120
52	0.520	3.410	3.260	7.360	1.620	12.320	4.180
53	0.220	3.260	3.260	7.330	1.380	12.380	4.140
54	0.750	2.990	2.660	7.200	0.500	12.130	4.060
55	0.880	3.010	2.410	7.120	0.290	11.800	4.040
56	-0.800	2.660	2.250	7.110	-0.360	11.880	3.840

Thermistors 6/22/92

Grey Patch	Car Bumper	Rear Asphalt	Sun Asphalt	Concrete	Time 2
21.070	25.310	31.130	38.910	32.940	15.500
20.460	23.460	27.980	38.360	33.040	15.750
21.010	24.260	26.400	38.770	32.900	16.000
20.650	21.630	24.730	37.150	32.080	16.250
21.480	23.040	23.820	37.510	31.990	16.500
21.940	22.420	23.000	36.980	31.480	16.750
21.010	21.850	22.220	35.830	30.890	17.000
20.460	20.710	21.150	34.570	29.790	17.250
21.550	20.660	20.730	34.230	29.290	17.500
21.070	19.830	20.020	33.090	28.330	17.750
21.790	19.790	19.610	32.290	27.420	18.000
20.870	18.890	19.060	31.440	24.390	18.250
20.720	18.370	18.550	30.170	22.490	18.500
20.590	18.130	18.150	29.310	21.230	18.750
20.170	17.850	17.750	28.020	20.140	19.000
19.490	17.320	17.380	27.260	19.100	19.250
18.400	16.820	17.070	25.820	18.140	19.500
15.220	16.180	16.590	24.900	17.260	19.750
13.590	15.440	16.160	23.650	16.340	20.000
12.350	14.490	15.680	22.570	15.640	20.250
9.530	12.520	15.210	21.130	14.670	20.500
7.520	10.870	14.590	20.010	13.790	20.750
5.880	9.160	13.870	18.920	12.910	21.000
5.220	8.090	13.150	17.820	12.100	21.250
4.390	7.730	12.590	16.940	11.310	21.500
4.100	7.540	12.180	16.270	10.650	21.750
3.680	6.510	11.720	15.550	10.070	22.000
3.660	6.620	11.300	14.880	9.490	22.250
3.720	6.440	11.010	14.540	8.990	22.500
3.200	5.980	10.690	14.000	8.470	22.750
4.680	6.600	10.380	13.350	8.040	23.000
5.320	6.950	10.230	12.980	7.800	23.250
4.360	6.060	10.080	12.830	7.500	23.500
2.960	4.970	9.920	12.530	7.220	23.750
2.450	4.410	9.550	12.150	6.760	24.000
2.320	4.330	9.440	12.100	6.410	24.250
2.190	4.190	9.110	11.450	6.150	24.500
2.700	4.490	8.780	11.050	5.790	24.750
3.110	4.570	8.630	10.780	5.590	25.000
1.720	3.670	8.560	10.610	5.340	25.250
2.030	4.000	8.370	10.300	5.050	25.500
2.540	4.130	8.160	10.120	4.860	25.750
2.920	4.150	7.970	9.780	4.670	26.000
3.080	4.390	7.770	9.530	4.530	26.250
3.930	4.640	7.680	9.600	4.520	26.500
					26.750
					27.000
2.800	4.070	7.320	8.740	3.960	27.250
2.530	3.480	7.170	8.730	3.790	27.500
1.260	2.970	6.940	8.380	3.450	27.750
3.450	4.100	6.780	8.000	3.560	28.000
2.940	3.880	6.640	7.780	3.280	28.250
3.170	3.660	6.530	7.710	3.300	28.500
2.890	3.700	6.450	7.660	3.110	28.750
2.800	3.690	6.390	7.380	2.970	29.000
1.990	3.030	6.260	7.290	2.830	29.250

Thermistors 6/22/92

	Time	Car Side	White Front	Roof Shingles	Asphalt Shade	Windshield	Tire
57	5.500	2.440	2.370	0.470	9.610	1.290	2.800
58	5.750	3.480	2.390	0.370	9.530	1.300	3.090
59	6.000	6.240	4.140	1.600	9.690	2.240	4.410
60	6.250	8.840	6.050	2.740	10.080	2.760	6.940
61	6.500	15.690	11.400	6.540	10.610	5.050	13.100
62	6.750	22.300	15.400	9.050	11.010	7.160	18.530
63	7.000	28.110	15.430	9.320	11.740	8.680	24.970
64	7.250	33.880	23.810	13.560	12.750	10.630	30.110
65	7.500	36.160	26.430	16.070	13.800	12.140	31.330
66	7.750	42.040	29.590	19.300	15.480	14.390	34.500
67	8.000	44.870	33.000	27.200	16.660	17.470	37.490
68	8.250	35.930	29.610	25.550	16.450	18.090	33.890
69	8.500	46.160	35.680	33.290	18.710	19.480	38.920
70	8.750	50.750	40.090	38.330	20.680	23.560	44.180
71	9.000	51.320	42.540	39.710	22.580	26.070	43.580
72	9.250	49.920	40.990	38.270	23.250	28.120	44.450
73	9.500	45.330	37.510	37.180	23.580	26.150	39.780
74	9.750	48.990	39.770	36.610	25.770	29.270	41.790
75	10.000	51.160	43.020	47.250	27.410	29.900	45.200
76	10.250	52.350	42.750	48.730	29.680	33.600	43.990
77	10.500	48.320	39.500	48.100	29.090	34.320	42.150
78	10.750	49.820	40.770	50.800	29.990	34.670	44.140
79	11.000	47.620	40.390	50.690	31.370	36.170	42.060
80	11.250	46.700	39.920	51.450	31.360	37.220	42.730
81	11.500	44.700	38.650	49.290	27.890	36.370	40.640
82	11.750	35.840	32.010	43.190	25.960	33.630	30.180
83	12.000	39.320	34.170	49.220	24.680	34.840	36.360
84	12.250	39.460	33.760	52.120	24.420	37.260	35.870
85	12.500	36.110	33.050	52.480	23.550	38.370	33.910
86	12.750	35.980	31.880	50.430	22.540	37.130	34.280
87	13.000	32.590	30.720	50.570	22.190	38.400	32.520
88	13.250	32.700	29.220	48.420	22.110	38.800	29.420
89	13.500	34.520	29.840	50.500	22.110	39.140	29.960
90	13.750	32.350	28.980	46.460	22.210	38.390	27.890
91	14.000	31.560	29.040	46.580	21.940	39.990	28.200
92	14.250	31.920	29.290	45.270	21.910	39.350	28.360
93	14.500	31.280	28.860	47.700	21.750	41.600	27.410
94	14.750	31.150	28.130	43.520	21.360	39.080	27.330
95	15.000	31.320	27.280	39.850	21.280	37.130	26.530
96	15.250	32.040	28.420	44.060	21.320	40.700	27.380
97	15.500	28.320	25.710	34.710	21.340	36.130	24.620
98	15.750	26.150	23.150	28.830	21.060	30.760	22.130
99	16.000	27.460	23.900	33.320	21.200	33.920	22.700
100	16.250	26.280	23.920	30.730	21.070	33.130	22.900
101	16.500	25.190	22.560	26.480	20.790	28.070	21.970
102	16.750	25.500	22.290	26.810	20.820	28.160	22.030
103	17.000	25.410	22.070	26.100	20.790	27.970	21.310
104	17.250	25.170	22.330	26.110	20.590	29.630	21.530
105	17.500	24.050	21.070	23.670	20.460	26.020	20.650
106	17.750	24.600	21.530	25.090	20.500	26.640	21.030
107	18.000	24.880	21.800	23.730	20.420	29.850	21.010
108	18.250	24.630	21.310	21.370	20.110	30.500	20.430
109	18.500	23.170	20.290	21.510	19.870	26.040	19.720
110	18.750	22.490	19.850	21.610	19.770	24.750	19.640
111	19.000	21.280	18.940	20.310	19.660	22.350	18.930
112	19.250	20.010	17.870	18.790	19.330	20.570	18.150

Thermistors 6/22/92

	Car Roof	Side Window	Black Front	Middle Asphalt	Specular Board	Water	Sand
57	-0.160	2.630	2.250	6.910	-0.140	11.990	3.710
58	-0.520	2.930	2.530	6.920	-0.580	11.490	3.490
59	0.340	4.790	5.240	7.110	-0.530	11.350	3.540
60	0.450	5.690	7.380	7.480	-0.470	11.340	3.630
61	2.600	9.770	13.340	8.120	1.630	11.160	3.880
62	5.060	11.920	20.640	8.910	4.390	11.210	4.630
63	6.980	15.060	15.610	9.990	5.050	10.990	5.530
64	9.270	20.510	28.240	11.310	8.380	10.950	7.040
65	11.280	22.950	31.680	12.380	10.580	10.700	8.400
66	14.590	26.930	35.070	14.260	12.740	11.130	10.090
67	16.900	28.310	38.580	15.790	15.420	11.120	11.360
68	13.780	27.330	31.710	15.800	16.800	11.190	12.790
69	22.380	30.540	41.260	18.250	22.910	11.570	14.070
70	31.400	34.900	44.360	20.610	27.600	11.790	16.580
71	35.880	37.340	31.840	22.430	31.390	12.270	19.210
72	37.090	38.270	31.240	24.120	33.810	12.530	21.590
73	31.550	35.220	30.080	24.070	31.690	12.890	22.300
74	38.580	37.590	32.830	26.670	35.280	12.930	24.090
75	43.340	40.310	45.590	28.550	38.850	13.580	25.810
76	48.920	41.230	47.570	31.040	41.960	14.170	28.460
77	46.840	39.980	43.870	31.540	41.630	14.460	29.470
78	50.330	41.250	44.610	33.070	43.720	14.880	30.710
79	49.810	40.950	43.380	34.590	45.380	15.220	32.660
80	51.630	42.280	42.710	36.090	46.660	15.840	34.160
81	50.700	41.490	40.330	37.160	46.960	16.200	35.050
82	39.810	33.880	33.850	35.280	40.900	16.320	33.840
83	50.910	37.540	36.150	37.300	45.430	16.580	35.280
84	55.230	39.220	35.730	39.880	48.630	16.920	37.090
85	54.800	37.750	34.220	41.080	50.450	17.480	38.660
86	52.120	39.740	32.730	42.130	50.050	17.840	40.100
87	56.770	37.820	30.980	43.240	51.030	18.350	40.930
88	54.140	37.170	30.050	42.830	49.340	18.730	41.960
89	57.730	37.290	30.980	44.320	50.330	19.240	41.340
90	51.950	34.590	30.670	44.270	48.610	19.790	41.910
91	57.640	34.520	30.110	45.430	51.280	20.000	42.910
92	53.370	34.710	29.930	44.900	49.640	20.590	43.140
93	57.120	33.210	30.460	46.030	51.490	20.950	43.210
94	52.760	33.660	29.100	45.370	47.760	21.260	42.910
95	49.250	33.260	27.980	44.090	44.620	21.630	41.510
96	58.580	33.770	30.040	45.510	49.110	22.020	41.970
97	40.270	29.490	26.670	41.090	39.040	21.430	39.440
98	33.880	26.390	23.840	37.470	31.030	21.960	35.240
99	47.350	27.600	25.430	37.400	30.030	21.980	34.590
100	37.590	26.710	25.100	35.550	28.570	22.410	34.430
101	29.490	25.230	23.190	34.030	26.470	22.140	31.330
102	31.800	25.200	23.480	33.750	26.460	22.180	29.320
103	32.440	25.230	23.200	32.990	26.060	22.100	28.000
104	35.200	25.140	23.560	31.530	24.300	22.110	26.710
105	26.020	24.350	22.130	31.000	22.950	22.070	25.480
106	30.510	24.380	22.760	30.960	24.630	21.930	25.160
107	33.970	24.740	22.930	29.690	22.560	21.870	24.630
108	33.350	24.350	22.280	28.220	20.010	21.960	23.050
109	26.060	23.350	21.020	27.870	20.390	21.740	22.410
110	25.120	22.850	20.630	27.690	20.790	21.390	22.240
111	20.910	21.950	19.550	26.940	19.830	21.170	21.640
112	18.940	20.450	18.330	26.140	18.250	21.190	20.900

Thermistors 6/22/92

	Grey Patch	Car Bumper	Rear Asphalt	Sun Asphalt	Concrete	Time 2
57	2.540	3.110	6.090	7.100	2.730	29.500
58	2.690	3.410	6.180	7.120	2.620	29.750
59	2.040	3.910	6.380	7.360	2.600	30.000
60	3.730	4.430	6.730	7.520	2.610	30.250
61	9.210	9.140	7.560	8.520	2.910	30.500
62	11.740	11.490	8.480	8.940	3.410	30.750
63	7.520	15.520	9.650	9.980	4.180	31.000
64	14.800	19.780	11.130	10.720	4.870	31.250
65	20.180	21.300	12.380	12.430	5.790	31.500
66	27.810	25.720	14.140	13.920	7.050	31.750
67	31.170	28.620	16.010	15.740	8.260	32.000
68	27.950	24.000	16.190	15.550	8.610	32.250
69	35.670	31.760	18.830	18.060	10.630	32.500
70	41.150	35.680	21.300	20.510	12.410	32.750
71	41.640	37.740	23.530	22.430	14.030	33.000
72	40.760	35.620	25.190	23.720	15.320	33.250
73	36.110	32.470	25.440	24.120	16.000	33.500
74	39.850	34.820	28.000	26.910	17.920	33.750
75	43.520	39.720	30.360	28.380	20.160	34.000
76	44.840	39.930	32.640	31.490	21.810	34.250
77	42.200	37.050	33.200	31.890	22.670	34.500
78	43.790	39.890	35.070	33.960	24.480	34.750
79	43.830	37.980	36.690	34.950	25.830	35.000
80	43.600	39.310	38.300	36.930	27.320	35.250
81	41.250	37.940	39.080	37.470	28.530	35.500
82	34.090	27.480	37.600	36.250	27.860	35.750
83	37.770	35.670	39.820	37.730	29.340	36.000
84	38.950	36.040	41.900	40.340	30.930	36.250
85	39.480	33.970	43.580	42.250	32.570	36.500
86	37.100	34.910	44.410	42.890	33.350	36.750
87	34.980	33.880	45.730	45.100	34.840	37.000
88	33.860	35.270	45.480	43.980	34.740	37.250
89	33.650	34.730	46.660	45.810	36.160	37.500
90	32.510	31.550	46.300	45.590	36.160	37.750
91	31.560	33.640	47.390	47.020	37.550	38.000
92	30.350	32.700	46.950	45.600	37.580	38.250
93	29.490	32.030	48.670	48.350	38.680	38.500
94	26.560	32.300	47.440	47.180	38.650	38.750
95	25.230	31.070	45.620	46.690	37.770	39.000
96	27.870	33.710	47.150	48.560	39.220	39.250
97	26.230	25.540	41.100	43.630	35.870	39.500
98	24.340	22.280	37.710	41.150	34.140	39.750
99	27.330	25.060	36.740	43.950	36.460	40.000
100	25.520	23.940	35.130	41.950	34.520	40.250
101	23.570	22.100	33.750	38.190	31.580	40.500
102	23.700	22.270	33.350	38.120	30.850	40.750
103	24.120	21.450	32.480	36.660	30.460	41.000
104	25.300	22.000	31.030	37.470	30.440	41.250
105	21.850	20.410	30.400	34.730	28.160	41.500
106	23.940	21.050	30.410	34.950	28.330	41.750
107	25.510	20.840	29.000	35.500	28.240	42.000
108	24.500	20.480	27.600	35.290	26.410	42.250
109	22.050	19.770	27.300	32.880	25.410	42.500
110	21.530	19.370	26.990	32.040	24.850	42.750
111	18.890	18.480	26.340	30.370	23.670	43.000
112	17.750	17.520	25.460	28.860	22.720	43.250

Thermistors 6/22/92

	Time	Car Side	White Front	Roof Shingles	Asphalt Shade	Windshield	Tire
113	19.500	19.480	17.140	18.040	19.140	19.440	17.710
114	19.750	18.800	16.710	17.240	19.060	18.800	17.270
115	20.000	17.870	16.150	16.410	18.730	17.680	16.770
116	20.250	17.290	15.630	15.610	18.540	17.080	16.330
117	20.500	16.840	15.250	15.030	18.370	16.520	15.950
118	20.750	16.270	14.760	14.320	18.050	15.710	15.500
119	21.000	14.580	14.040	12.210	17.940	13.850	14.670
120	21.250	13.350	13.130	11.130	17.370	12.450	13.790
121	21.500	13.210	12.940	11.160	16.870	12.470	13.680
122	21.750	12.960	12.720	10.870	16.430	12.330	13.500
123	22.000	12.880	12.560	10.870	16.390	12.410	13.220
124	22.250	13.020	12.490	11.090	16.130	12.370	13.140
125	22.500	12.810	12.670	11.210	16.170	12.240	12.930
126	22.750	12.650	12.890	11.300	15.840	12.160	12.980
127	23.000	12.750	12.770	11.160	15.630	11.900	12.940
128	23.250	12.500	12.480	10.910	15.460	11.720	12.720
129	23.500	12.630	12.600	10.940	15.480	11.680	12.860
130	23.750	12.810	12.740	10.800	15.320	11.680	13.140
131	24.000	12.570	12.600	10.640	15.090	11.540	13.030
132	0.250	12.740	12.610	10.650	15.030	11.590	13.050
133	0.500	12.750	12.530	10.610	14.860	11.620	13.090
134	0.750	12.800	12.590	10.510	14.660	11.710	13.050
135	1.000	12.850	12.640	10.660	14.530	11.870	13.020
136	1.250	12.870	12.610	10.540	14.310	11.870	13.000
137	1.500	12.640	12.440	10.420	14.270	11.790	12.960
138	1.750	11.450	11.780	10.280	14.150	11.010	12.400
139	2.000	11.890	12.120	10.450	14.120	11.020	12.670
140	2.250	11.890	12.130	10.430	14.040	10.990	12.560
141	2.500	11.960	11.990	10.550	14.060	11.140	12.440
142	2.750	11.700	12.010	10.480	13.980	11.000	12.250
143	3.000	11.500	11.860	10.310	13.880	10.790	12.180
144	3.250	10.930	11.180	10.220	13.460	10.580	11.310
145							
146							
147							
148							
149							
150							
151							

Thermistors 6/22/92

	Car Roof	Side Window	Black Front	Middle Asphalt	Specular Board	Water	Sand
113	17.850	19.740	17.640	25.340	17.210	21.180	20.090
114	17.120	19.210	17.090	25.050	16.380	20.840	19.610
115	16.130	18.250	16.370	24.170	15.830	20.510	18.920
116	15.330	17.780	15.850	23.660	15.080	20.630	18.350
117	14.730	17.250	15.360	23.090	14.410	20.120	17.840
118	13.920	16.460	14.890	22.500	13.880	20.600	17.370
119	11.110	14.700	13.860	20.800	12.200	20.020	16.550
120	10.500	13.210	13.210	19.840	11.170	19.930	15.410
121	11.060	13.280	12.870	19.380	11.210	19.500	14.850
122	10.690	13.120	12.650	18.920	11.170	19.450	14.540
123	10.810	13.130	12.610	18.750	11.170	19.410	14.260
124	11.250	13.280	12.500	18.370	11.360	19.330	14.200
125	11.080	13.030	12.670	18.170	11.350	19.570	14.050
126	11.090	12.740	13.030	17.880	11.760	18.910	14.150
127	10.850	12.630	12.730	17.420	11.290	19.010	13.850
128	10.590	12.550	12.490	17.370	11.160	18.830	13.760
129	10.640	12.550	12.610	17.200	11.070	18.770	13.640
130	10.640	12.780	12.860	17.000	11.050	18.480	13.510
131	10.660	12.700	12.740	16.660	10.640	18.600	13.170
132	10.660	12.840	12.670	16.610	10.640	18.060	13.090
133	10.750	12.970	12.610	16.370	10.540	18.020	12.910
134	10.770	13.120	12.730	16.010	10.560	18.070	12.760
135	10.730	13.200	12.800	15.760	10.570	17.900	12.620
136	10.800	13.130	12.650	15.520	10.650	17.740	12.400
137	10.480	12.920	12.550	15.510	10.680	17.670	12.400
138	9.980	11.580	11.840	15.230	10.480	16.990	12.340
139	10.190	11.610	12.280	15.100	10.550	17.350	12.380
140	10.120	11.680	12.020	15.110	10.660	17.220	12.420
141	10.410	12.000	11.910	15.030	10.880	17.180	12.590
142	10.220	11.630	11.940	14.970	10.940	17.470	12.710
143	10.060	11.400	11.800	14.680	10.710	17.070	12.630
144	9.990	11.200	11.070	14.550	10.550	16.860	12.430
145							
146							
147							
148							
149							
150							
151							

Thermistors 6/22/92

	Grey Patch	Car Bumper	Rear Asphalt	Sun Asphalt	Concrete	Time 2
113	16.820	17.250	24.800	28.200	22.010	43.500
114	16.210	16.830	24.310	27.240	21.280	43.750
115	15.680	16.360	23.480	25.900	20.440	44.000
116	14.990	15.850	22.900	25.340	19.910	44.250
117	14.610	15.610	22.330	24.640	19.210	44.500
118	14.220	15.260	21.850	23.990	18.710	44.750
119	12.450	13.800	19.920	22.050	17.540	45.000
120	11.480	12.190	19.010	20.770	16.580	45.250
121	12.060	12.480	18.630	20.350	16.170	45.500
122	11.740	11.900	18.140	19.700	15.830	45.750
123	11.690	11.830	17.850	19.440	15.440	46.000
124	11.850	12.120	17.560	19.120	15.120	46.250
125	12.050	11.970	17.130	18.590	14.660	46.500
126	12.280	12.340	16.960	18.220	14.590	46.750
127	11.860	12.430	16.710	17.950	14.210	47.000
128	11.430	12.090	16.520	17.790	14.100	47.250
129	11.630	12.370	16.320	17.600	13.830	47.500
130	11.500	12.480	15.990	17.330	13.670	47.750
131	11.310	12.290	15.610	17.050	13.300	48.000
132	11.510	12.480	15.660	16.780	13.190	48.250
133	11.570	12.560	15.390	16.560	13.050	48.500
134	11.730	12.510	15.090	16.460	12.820	48.750
135	11.610	12.590	14.880	16.050	12.610	49.000
136	11.850	12.680	14.660	15.790	12.490	49.250
137	11.540	12.440	14.560	15.610	12.370	49.500
138	10.770	11.910	14.420	15.450	12.220	49.750
139	11.020	12.250	14.350	15.250	12.150	50.000
140	11.240	12.060	14.350	15.410	12.190	50.250
141	11.480	11.960	14.270	15.360	12.250	50.500
142	11.370	11.780	14.180	15.240	12.290	50.750
143	11.000	11.560	14.020	14.970	12.290	51.000
144	10.750	10.910	13.890	14.420	12.020	51.250
145						51.500
146						51.750
147						52.000
148						52.250
149						52.500
150						52.750
151						53.000

JUNE

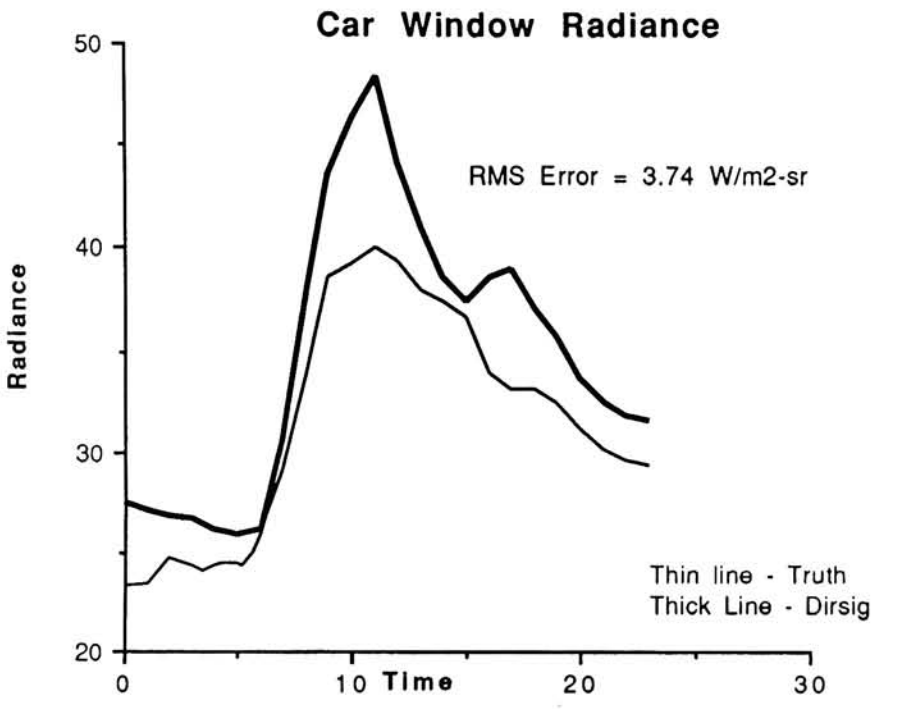
Car Window Radiance
RMS Error = 3.74 W/m2-sr
Thin line - Truth
Thick Line - Dirsig
Radiance
Time
50
40
30
20
0
10
20
30

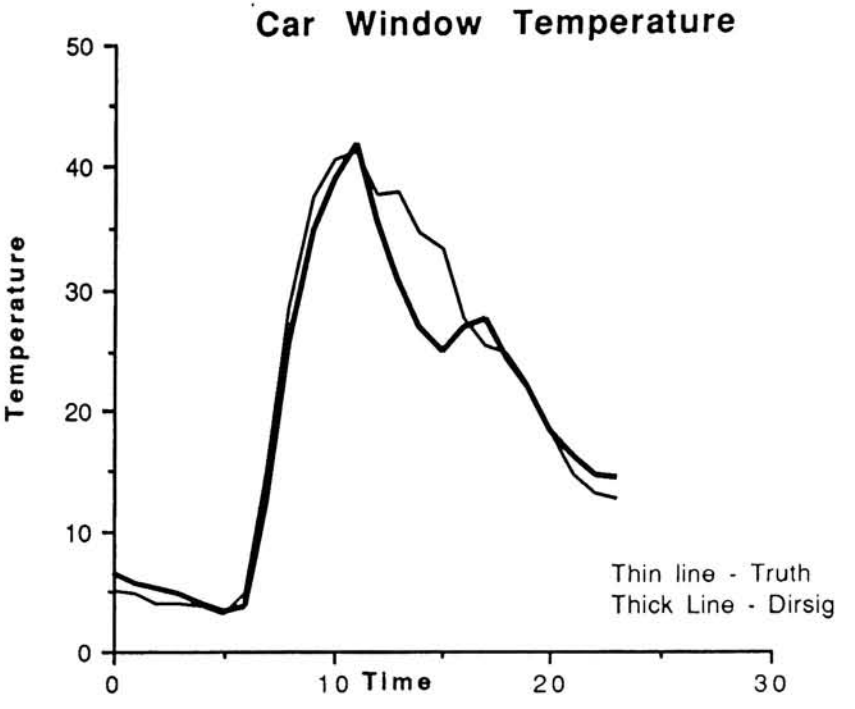
Car Window Temperature
Thin line - Truth
Thick Line - Dirsig
Temperature
Time
50
40
30
20
10
0
0
10
20
30

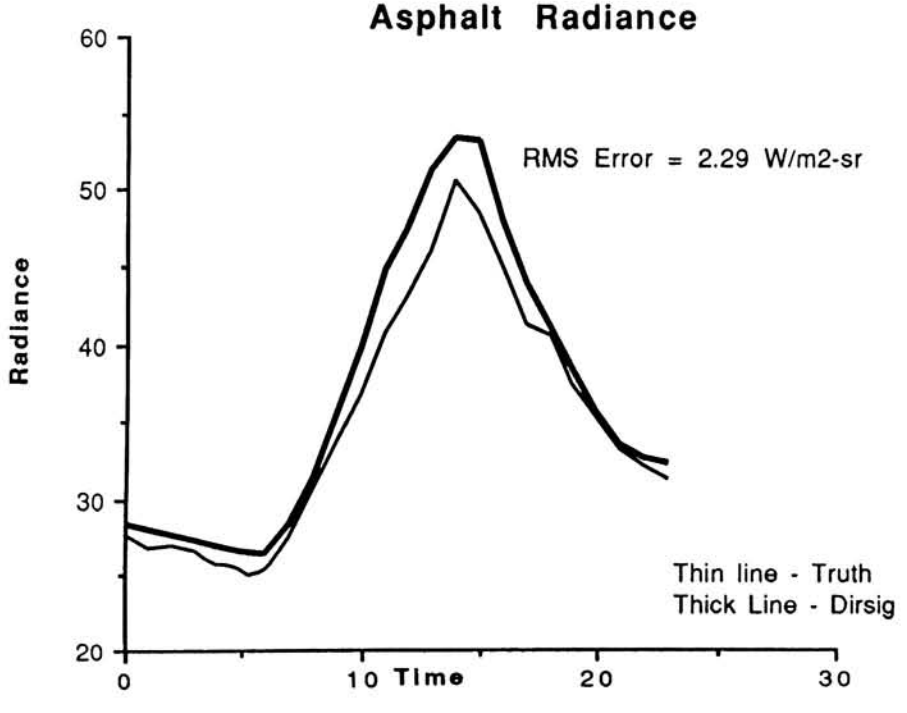
Asphalt Radiance
RMS Error = 2.29 W/m2-sr
Thin line - Truth
Thick Line - Dirsig
Radiance
Time
60
50
40
30
20
0
10
20
30

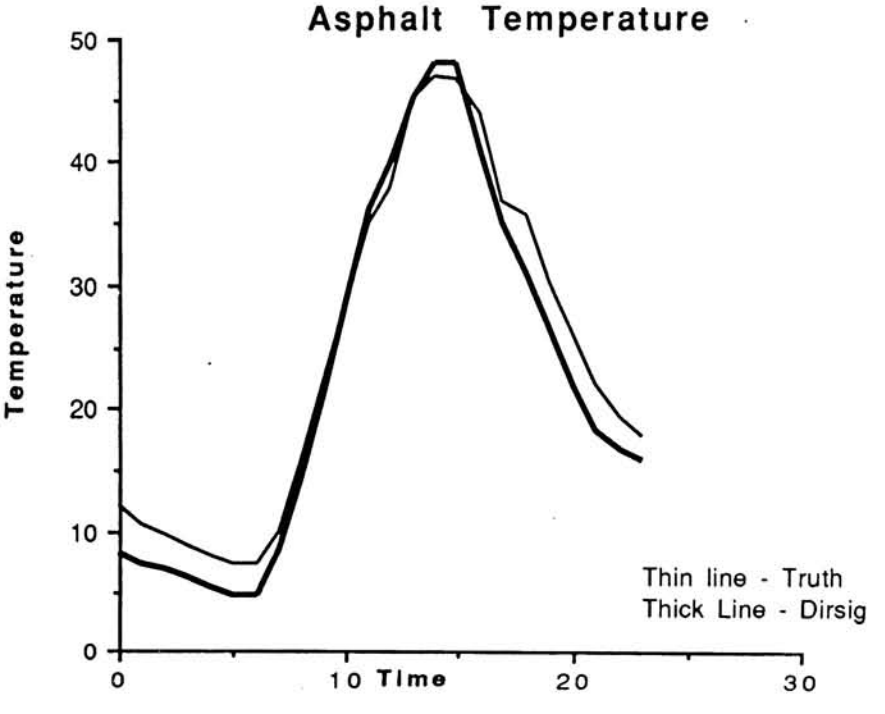
Asphalt Temperature
Thin line - Truth
Thick Line - Dirsig
Temperature
Time
50
40
30
20
10
0
0
10
20
30

JUNE

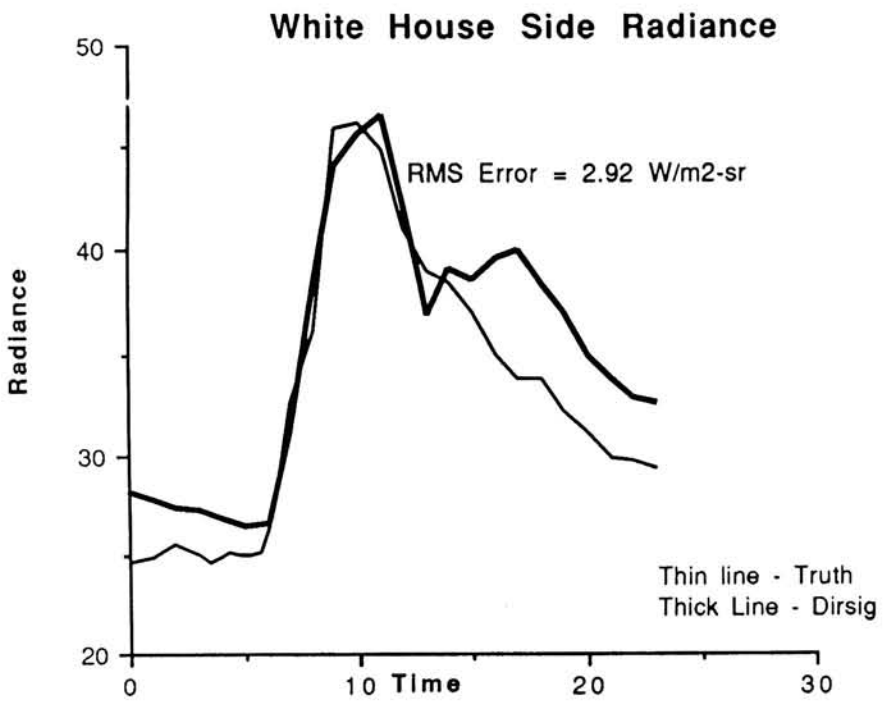
White House Side Radiance
RMS Error = 2.92 W/m2-sr
Radiance
Time
Thin line - Truth
Thick Line - Dirsig
50
40
30
20
0
10
20
30

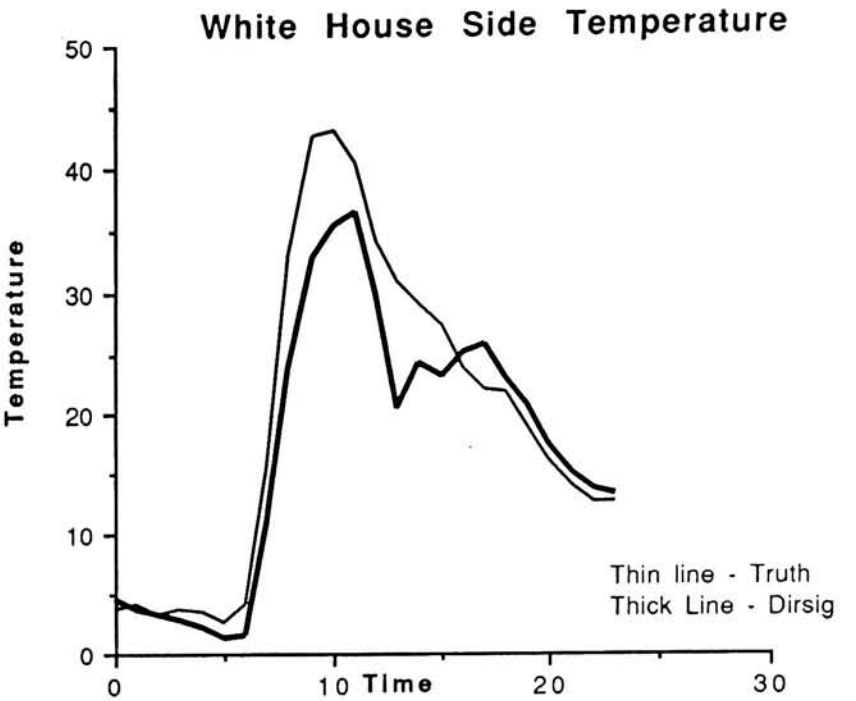
White House Side Temperature
Temperature
Time
Thin line - Truth
Thick Line - Dirsig
50
40
30
20
10
0
0
10
20
30

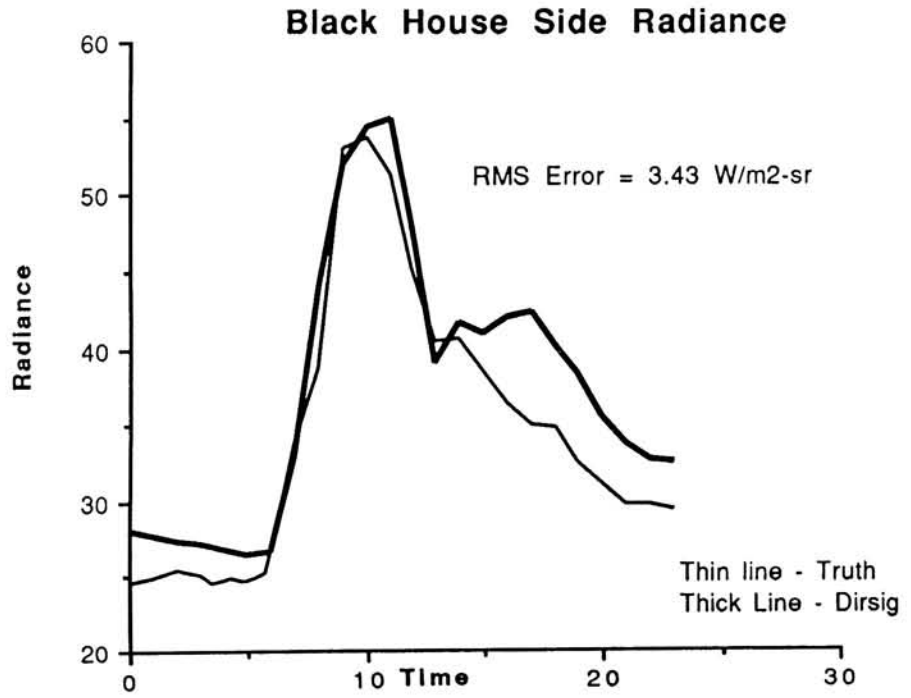
Black House Side Radiance
RMS Error = 3.43 W/m2-sr
Radiance
Time
Thin line - Truth
Thick Line - Dirsig
60
50
40
30
20
0
10
20
30

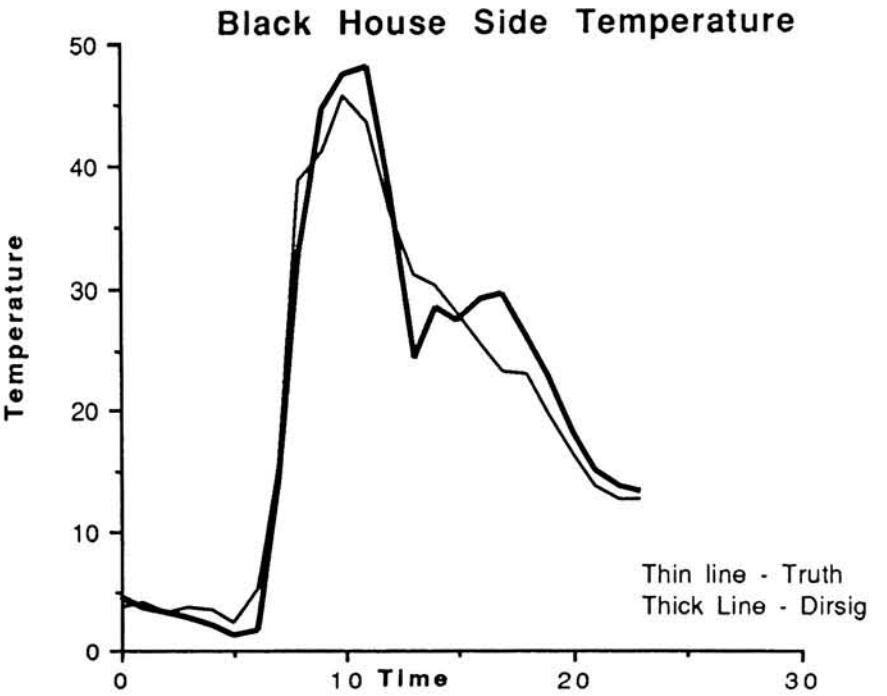
Black House Side Temperature
Temperature
Time
Thin line - Truth
Thick Line - Dirsig
50
40
30
20
10
0
0
10
20
30

JUNE

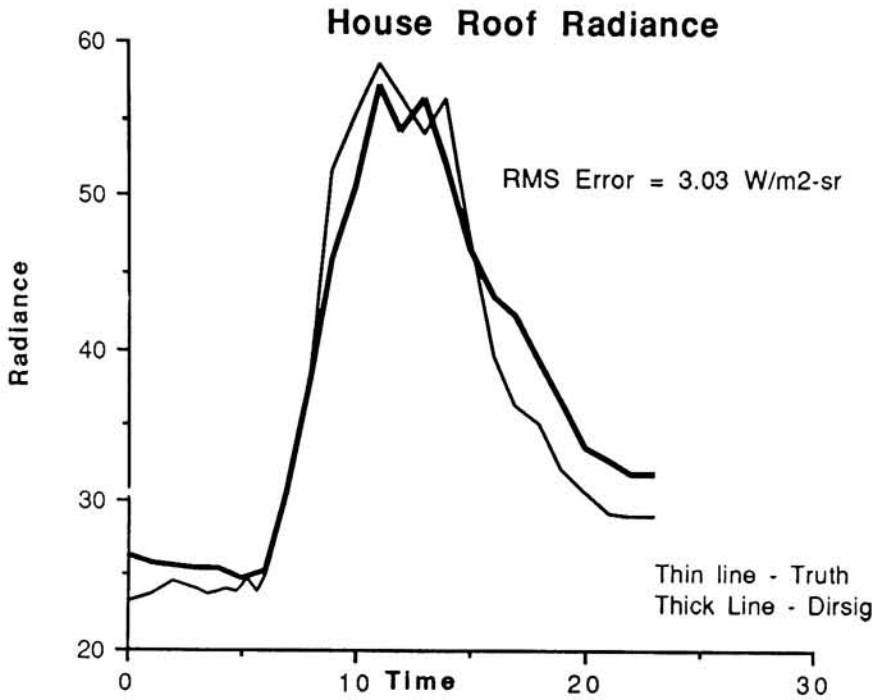
House Roof Radiance
RMS Error = 3.03 W/m2-sr
Thin line - Truth
Thick Line - Dirsig
Radiance
Time
60
50
40
30
20
0
10
20
30

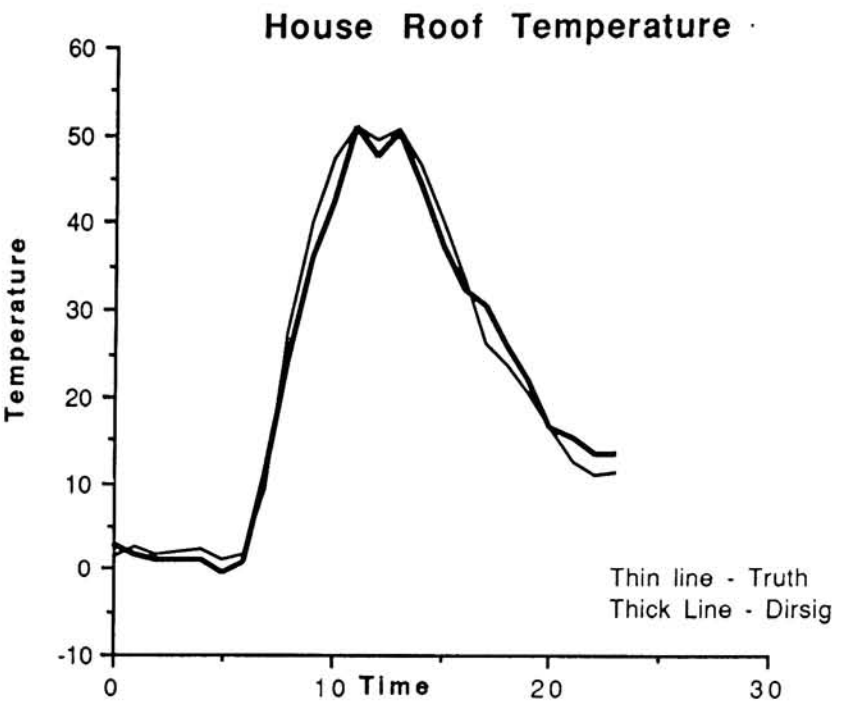
House Roof Temperature
Thin line - Truth
Thick Line - Dirsig
Temperature
Time
60
50
40
30
20
10
0
-10
0
10
20
30

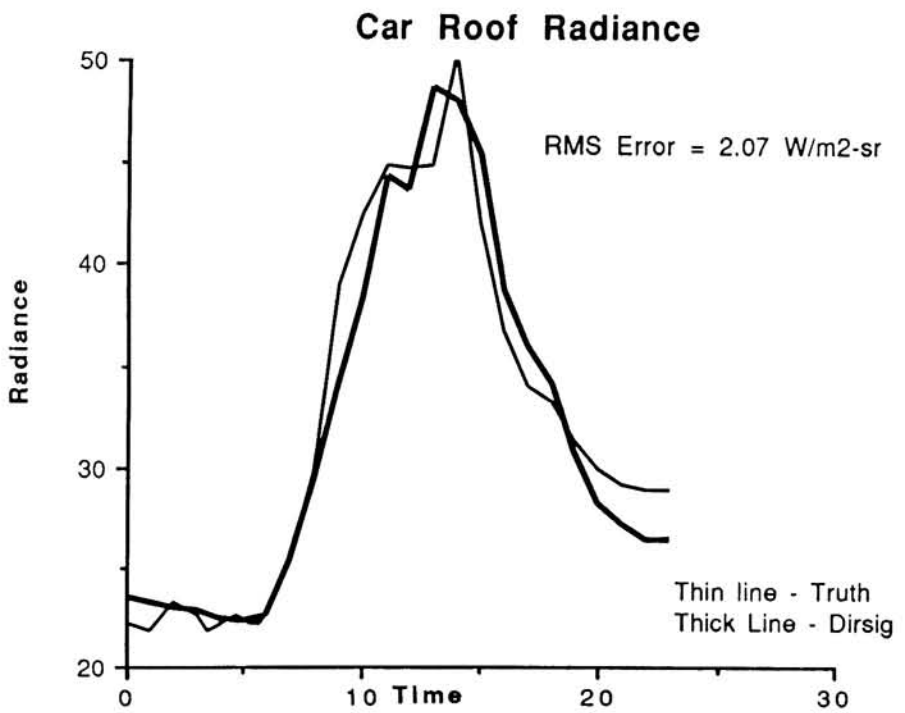
Car Roof Radiance
RMS Error = 2.07 W/m2-sr
Thin line - Truth
Thick Line - Dirsig
Radiance
Time
50
40
30
20
0
10
20
30

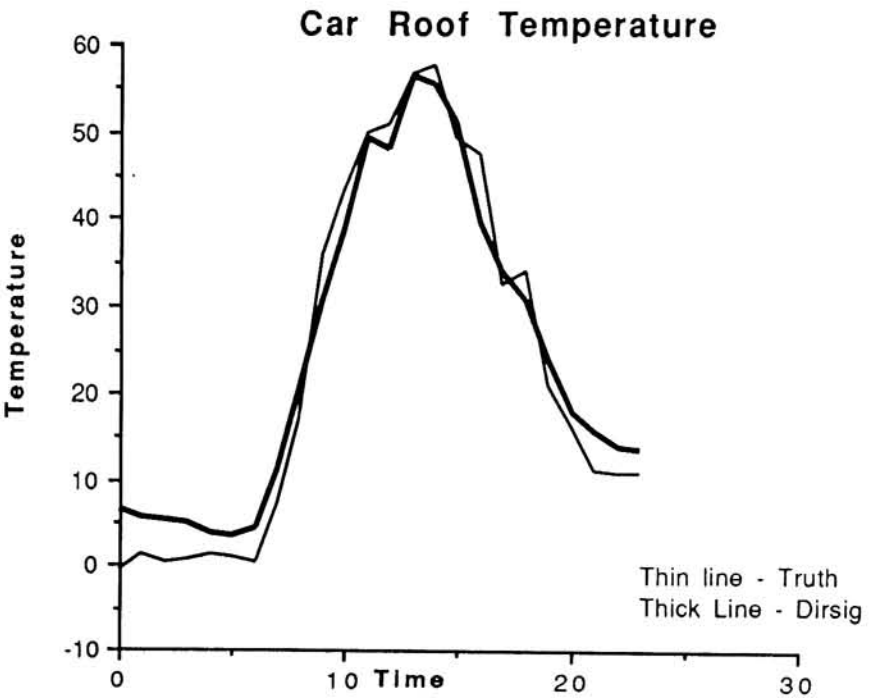
Car Roof Temperature
Thin line - Truth
Thick Line - Dirsig
Temperature
Time
60
50
40
30
20
10
0
-10
0
10
20
30

JUNE

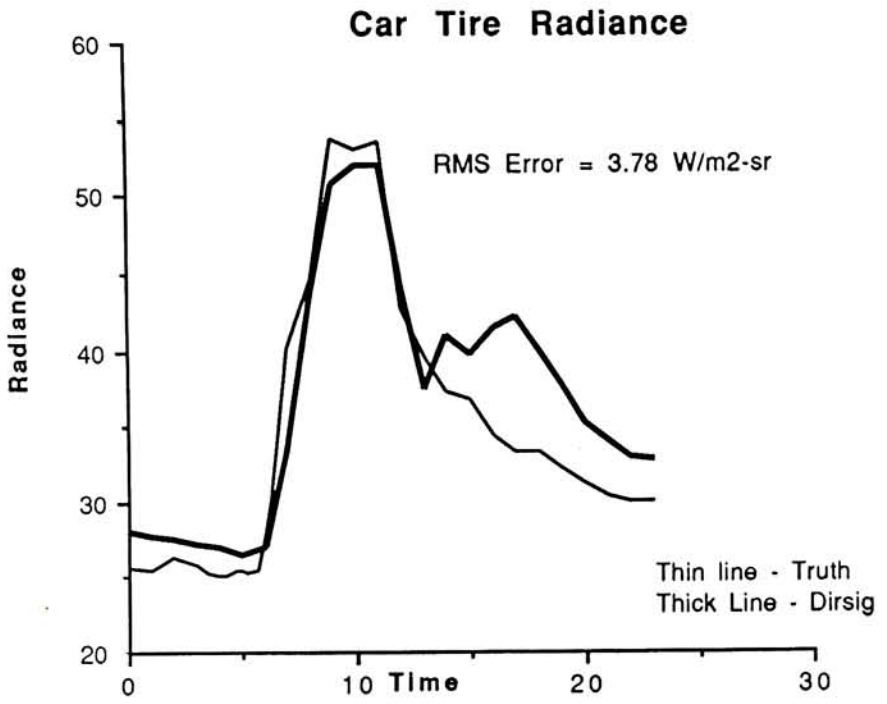
Car Tire Radiance
RMS Error = 3.78 W/m2-sr
Radiance
Time
Thin line - Truth
Thick Line - Dirsig
60
50
40
30
20
0
10
20
30

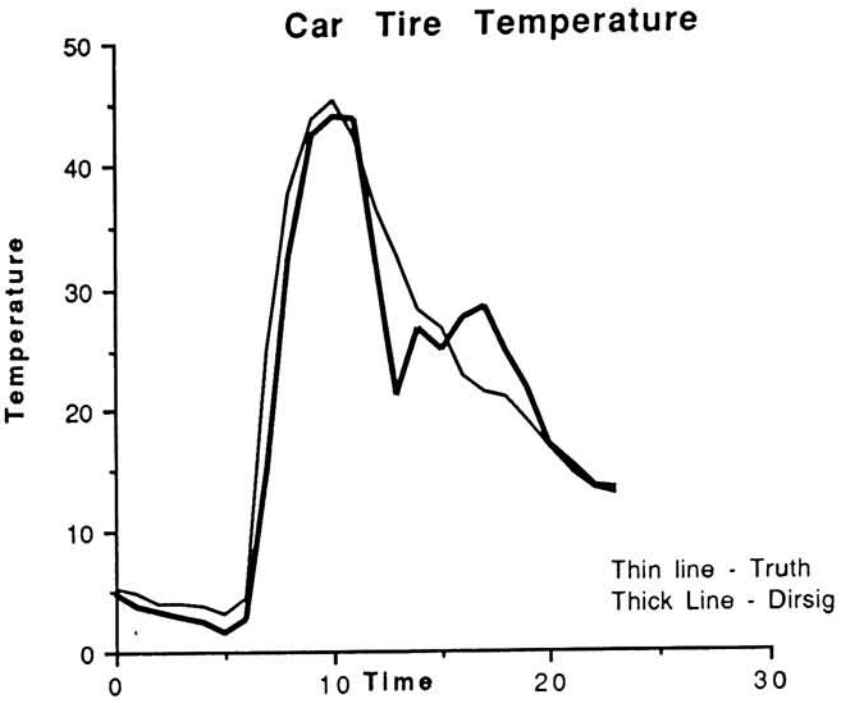
Car Tire Temperature
Temperature
Time
Thin line - Truth
Thick Line - Dirsig
50
40
30
20
10
0
0
10
20
30

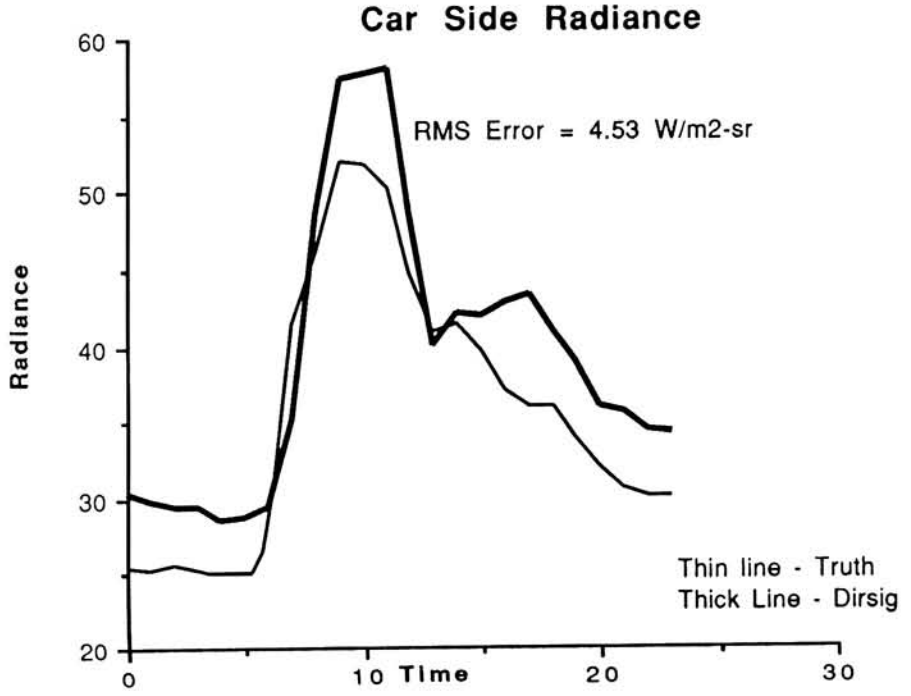
Car Side Radiance
RMS Error = 4.53 W/m2-sr
Radiance
Time
Thin line - Truth
Thick Line - Dirsig
60
50
40
30
20
0
10
20
30

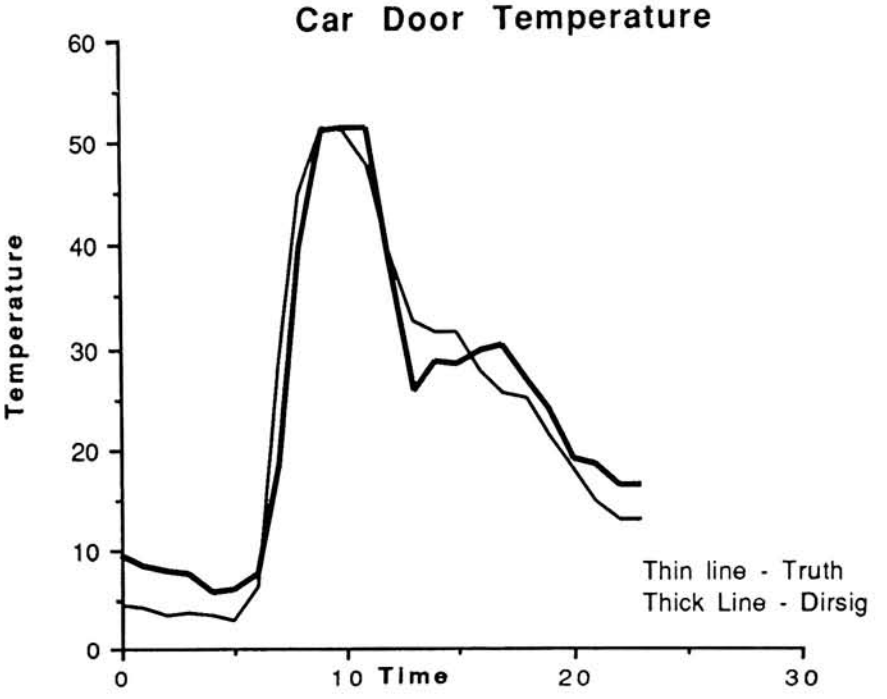
Car Door Temperature
Temperature
Time
Thin line - Truth
Thick Line - Dirsig
60
50
40
30
20
10
0
0
10
20
30

JUNE

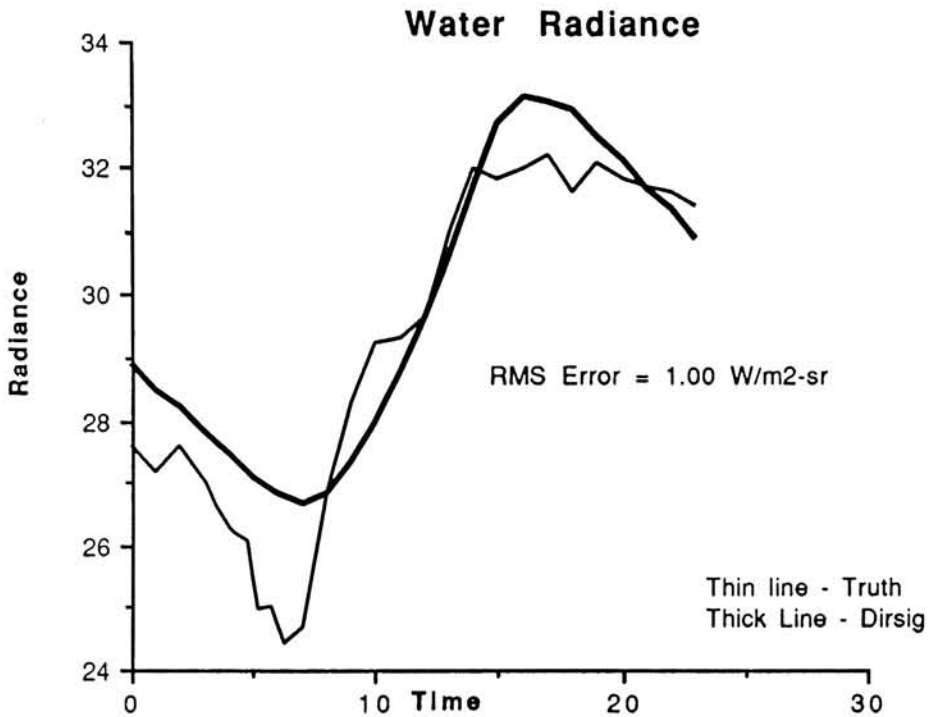

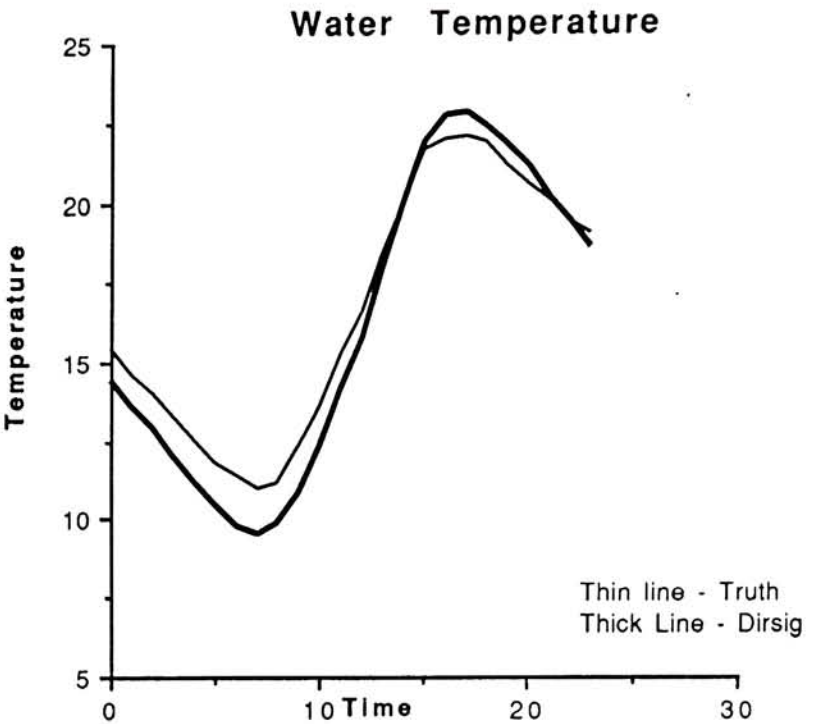

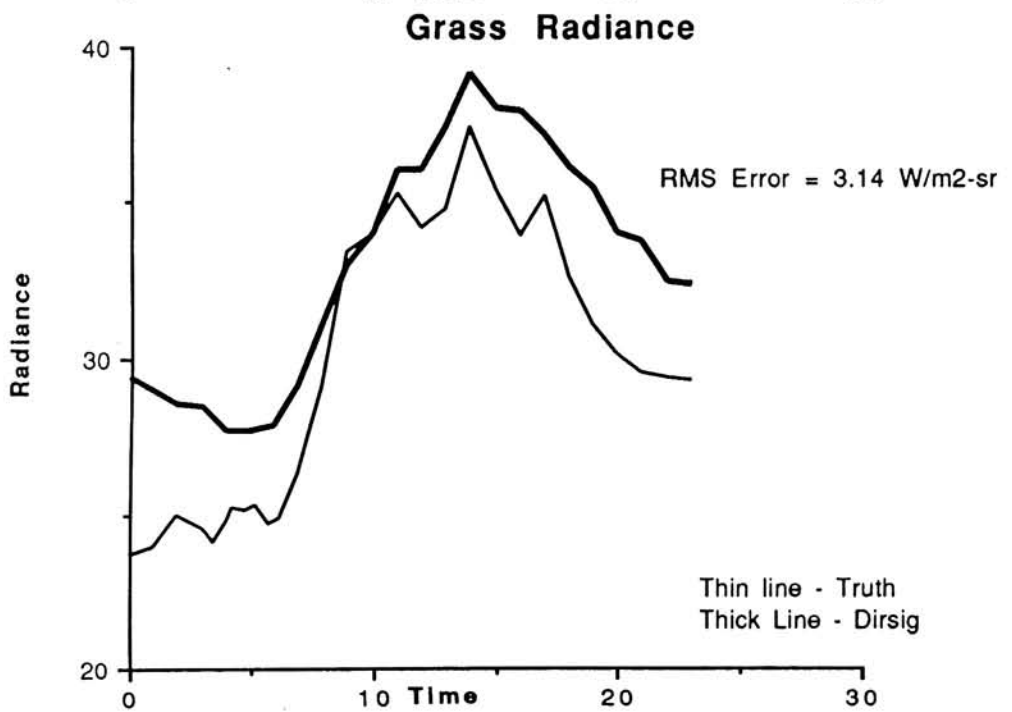

NO TRUTH AVAILABLE
FOR GRASS TEMPERATURE

Oct Truth & Cloud Radiances

	Time	Water Truth	Grass Truth	Asphalt Truth	Car Side Truth	Car Roof Truth	D Water
1	0.000	42.655	43.862	42.655	47.784	42.957	49.292
2	1.000	41.546	43.050	40.042	45.457	40.644	48.766
3	2.000	41.096	42.921	40.184	44.137	41.096	49.003
4	3.000	41.106	43.559	41.413	44.479	42.333	49.386
5	4.000	41.897	42.204	40.977	44.044	41.284	50.176
6	5.000	42.111	43.997	40.854	43.997	41.168	50.912
7	6.000	41.438	41.741	40.530	43.557	40.833	50.518
8	7.000	41.914	42.223	41.604	44.080	40.367	51.197
9	8.000	44.514	44.514	43.606	46.632	43.001	52.382
10	9.000	41.345	43.542	41.973	58.291	45.111	48.563
11	10.000	39.002	40.554	41.795	56.066	44.276	45.207
12	11.000	39.965	40.846	45.834	52.583	45.834	43.487
13	12.000	39.187	38.874	47.636	49.514	46.072	39.500
14	13.000	41.824	44.324	51.825	49.325	47.762	47.762
15	14.000	43.364	44.953	53.852	50.356	47.813	42.728
16	15.000	43.180	43.502	54.781	50.914	46.403	44.147
17	16.000	42.698	42.698	52.437	49.609	45.525	43.640
18	17.000	41.954	40.376	47.319	47.004	42.270	42.585
19	18.000	40.213	39.892	43.746	45.995	40.213	43.746
20	19.000	41.164	40.528	44.340	45.293	40.211	48.469
21	20.000	42.650	42.021	44.536	44.850	40.450	49.250
22	21.000	42.190	42.190	43.775	45.678	40.922	50.117
23	22.000	42.846	42.531	44.103	45.046	41.588	50.705
24	23.000	43.229	43.551	44.194	45.481	41.942	51.271

LOWTRAN 7 PREDICTIONS WITH CLOUDS

Oct Truth & Cloud Radiances

	D Grass	D Asphalt	D Car Side	D Car Roof	Time
1	56.533	54.421	56.533	50.499	0.000
2	57.190	54.181	56.588	50.270	1.000
3	56.911	54.478	56.911	50.220	2.000
4	57.052	54.905	57.052	50.306	3.000
5	56.922	55.082	56.922	50.483	4.000
6	57.512	55.626	57.826	51.226	5.000
7	56.874	55.361	57.177	50.821	6.000
8	58.005	56.148	58.005	51.506	7.000
9	59.342	57.526	59.644	53.592	8.000
10	57.663	55.780	65.509	52.015	9.000
11	53.894	53.894	56.997	48.310	10.000
12	53.463	55.811	62.266	51.116	11.000
13	51.705	57.025	56.086	50.453	12.000
14	54.013	59.327	52.451	50.263	13.000
15	53.852	58.937	52.899	48.449	14.000
16	54.459	57.682	53.815	47.692	15.000
17	53.379	55.264	53.379	46.782	16.000
18	52.369	53.631	52.369	44.479	17.000
19	52.418	51.455	53.061	44.067	18.000
20	56.092	54.822	56.728	48.151	19.000
21	56.793	54.907	56.793	48.936	20.000
22	58.044	55.824	58.044	50.434	21.000
23	58.250	56.364	58.565	51.020	22.000
24	58.669	56.739	58.990	51.592	23.000

LOWTRAN7 PREDICTIONS WITH CLOUDS

Oct No Cloud Radiances

DIRSIG PREDICTIONS

	Time	Grass	Asphalt	Car Door
1	0.000	34.995	33.224	34.995
2	1.000	36.249	33.991	35.955
3	2.000	36.609	34.617	36.609
4	3.000	36.593	34.801	36.593
5	4.000	36.015	34.653	36.209
6	5.000	35.491	34.064	35.491
7	6.000			
8	7.000	34.995	33.410	34.902
9	8.000	35.005	33.514	35.192
10	9.000	36.220	34.749	42.103
11	10.000	37.161	37.161	39.684
12	11.000	39.198	41.292	46.376
13	12.000	40.968	44.983	44.285
14	13.000	42.428	46.403	41.151
15	14.000	42.207	45.855	41.365
16	15.000	41.924	44.194	41.391
17	16.000	41.474	42.889	41.474
18	17.000	40.952	41.196	41.317
19	18.000			
20	19.000	38.706	37.720	39.035
21	20.000	37.624	36.360	37.834
22	21.000	37.455	35.807	37.558
23	22.000	35.580	34.317	35.774
24	23.000	36.210	34.642	36.210

LOWTRAN PREDICTIONS WITHOUT CLOUDS

Oct Thermistor Data

	Time	Car Side	Asphalt-Back	Side Window	Front Window	Asphalt-Front	Asphalt-Sun
1	5.000	8.920	9.410	8.470	7.510	7.600	7.660
2	5.250	8.280	8.760	7.710	7.170	7.960	8.090
3	5.500	8.150	8.570	7.620	6.940	7.350	7.640
4	5.750	7.910	8.360	7.570	7.000	7.830	7.780
5	6.000	7.720	8.490	7.720	7.140	7.840	7.820
6	6.250	7.750	8.420	7.790	7.330	8.250	7.800
7	6.500	7.640	7.980	6.860	6.600	7.460	7.650
8	6.750	6.540	8.310	7.710	7.380	8.390	8.100
9	7.000	7.790	8.260	7.320	6.440	7.600	7.570
10	7.250	8.210	8.620	8.000	8.000	8.810	8.290
11	7.500	10.180	9.320	9.030	9.570	9.180	9.010
12	7.750	10.660	9.770	10.330	10.560	9.920	9.410
13	8.000	10.770	9.400	9.570	9.720	9.650	9.390
14	8.250	11.120	9.780	10.610	11.180	11.110	10.370
15	8.500	14.200	9.690	11.200	11.130	10.300	9.820
16	8.750	30.150	11.810	16.350	13.920	13.020	11.480
17	9.000	33.420	13.160	19.280	15.750	14.990	12.860
18	9.250	35.210	14.350	21.250	17.040	16.150	13.790
19	9.500	35.310	14.480	21.780	18.630	17.630	15.360
20	9.750	35.310	15.670	21.780	17.790	17.490	15.950
21	10.000	35.220	17.090	24.200	21.260	20.660	18.620
22	10.250	35.780	18.170	23.830	20.820	21.560	19.370
23	10.500	33.430	18.910	21.840	19.710	21.260	20.250
24	10.750	31.860	20.790	20.870	19.020	22.750	21.400
25	11.000	33.090	23.030	22.720	21.120	24.110	22.730
26	11.250	30.400	23.220	21.650	20.600	24.590	23.690
27	11.500	29.130	24.400	21.370	20.370	24.660	23.980
28	11.750	28.170	26.020	22.290	21.340	25.730	25.200
29	12.000	28.700	28.000	24.670	24.230	28.770	27.530
30	12.250	25.750	27.090	22.860	22.880	29.860	27.410
31	12.500	24.770	27.620	22.260	22.750	29.110	28.260
32	12.750	23.830	27.690	22.480	22.750	28.600	28.770
33	13.000	23.660	27.080	21.920	23.010	29.270	28.920
34	13.250	22.560	26.360	20.620	21.100	26.340	27.000
35	13.500	23.840	28.120	23.250	23.960	29.900	30.310
36	13.750	23.190	27.960	21.750	23.540	28.800	29.560
37	14.000	24.220	30.520	22.800	24.830	26.130	30.620
38	14.250	24.240	29.130	22.440	24.520	23.470	30.330
39	14.500	25.400	31.020	23.390	25.200	23.670	31.420
40	14.750	23.880	23.890	21.330	23.060	22.280	29.410
41	15.000	24.360	23.190	22.490	24.300	21.790	29.650
42	15.250	25.280	22.950	22.850	24.440	22.090	29.890
43	15.500	25.380	22.460	23.160	24.620	21.230	29.730
44	15.750	25.880	22.380	23.710	25.520	22.060	30.820
45	16.000	25.480	22.230	23.950	25.010	21.810	29.650
46	16.250	23.780	21.680	21.240	21.200	20.750	25.800
47	16.500	23.730	22.090	21.560	21.930	22.050	27.080
48	16.750	22.140	20.550	20.630	20.660	20.410	24.410
49	17.000	21.620	20.810	20.030	20.080	20.260	23.640
50	17.250	21.400	20.700	20.150	20.010	20.200	23.130
51	17.500	21.110	20.550	19.590	19.470	19.630	20.070
52	17.750	21.030	20.840	20.240	20.180	20.300	22.260
53	18.000	19.940	18.760	18.420	18.540	18.310	20.910
54	18.250	19.580	19.270	19.070	18.560	19.020	20.710
55	18.500	18.330	18.250	17.300	16.630	17.590	19.110
56	18.750	17.150	16.620	15.600	15.520	16.700	17.900

Oct Thermistor Data

	Car Tire	Car Roof	Roof Gravel	Polycarbonate	Sand	Brick	Wood
1	8.280	7.400	7.690	7.780	8.210	7.700	6.740
2	8.810	7.560	7.990	7.930	8.570	7.900	7.030
3	8.320	7.030	7.730	7.580	8.340	7.740	6.470
4	8.260	6.800	7.660	7.310	8.150	7.660	6.250
5	8.210	6.540	7.600	7.350	7.960	7.580	6.270
6	8.170	6.720	7.460	7.360	8.100	7.530	6.210
7	8.220	7.300	7.650	7.420	8.290	7.580	6.450
8	8.510	7.400	7.830	7.570	8.470	7.740	6.750
9	8.100	6.600	7.520	7.520	8.070	7.480	6.580
10	9.180	8.850	8.090	8.280	8.540	7.700	7.340
11	10.790	10.700	9.710	10.350	9.540	8.600	9.070
12	11.400	10.180	9.820	10.060	9.500	8.710	8.960
13	11.660	10.040	10.170	10.190	9.790	9.310	9.220
14	12.550	11.170	11.120	11.000	10.650	10.430	10.550
15	13.590	11.890	10.820	10.670	10.250	10.120	9.770
16	33.240	13.040	16.270	13.860	12.000	14.880	13.160
17	39.850	14.990	20.250	12.930	13.440	18.240	15.320
18	41.240	16.240	21.870	12.780	13.560	20.410	15.930
19	45.530	17.890	24.160	13.440	14.570	22.750	18.100
20	41.780	17.660	23.960	13.470	14.640	22.890	17.690
21	46.130	20.960	26.030	14.750	16.890	25.260	19.600
22	43.640	21.140	26.680	14.650	18.180	26.090	19.650
23	40.440	22.650	25.810	14.670	18.500	25.280	19.150
24	38.980	23.030	26.510	17.210	20.220	25.890	19.660
25	40.320	26.190	27.640	20.030	21.820	26.950	21.000
26	34.400	25.350	27.370	20.230	22.750	26.260	20.520
27	27.350	24.800	26.650	26.300	23.050	25.780	16.580
28	24.320	25.520	27.210	28.830	23.930	25.910	16.660
29	23.900	30.330	28.540	27.890	26.000	27.380	18.870
30	22.460	26.760	27.470	22.290	25.980	26.140	20.750
31	21.870	27.120	26.880	20.800	26.780	26.670	21.660
32	21.570	27.940	26.580	20.760	27.100	25.900	21.240
33	21.670	27.620	25.730	20.860	26.450	25.470	21.590
34	20.790	24.620	23.870	19.350	24.590	24.000	19.810
35	22.230	29.520	26.320	21.780	28.530	24.520	22.030
36	21.700	27.360	25.110	20.980	27.720	23.730	21.150
37	22.200	30.000	25.290	21.540	28.220	23.530	21.490
38	22.130	29.460	25.180	21.430	28.270	23.210	21.430
39	22.770	29.460	25.010	21.950	28.150	22.620	21.560
40	21.830	26.930	23.200	20.720	26.410	21.550	20.230
41	22.330	27.230	22.890	20.600	26.750	21.800	20.120
42	22.490	27.140	22.440	20.530	26.730	22.040	20.000
43	22.480	27.520	21.920	20.710	26.510	21.940	19.290
44	23.070	28.930	22.060	21.490	27.180	22.600	20.100
45	22.850	26.020	21.700	21.090	26.270	22.710	19.670
46	21.170	21.870	20.750	19.350	22.450	22.300	19.080
47	22.230	23.520	21.350	20.390	22.130	22.830	20.110
48	20.940	20.450	20.510	18.650	21.650	18.500	18.090
49	20.050	20.170	19.980	18.570	20.070	21.120	17.970
50	20.400	20.280	20.100	19.040	20.310	20.970	18.860
51	19.650	19.500	19.300	18.530	19.340	17.320	18.210
52	20.150	19.940	19.780	18.990	19.590	18.140	18.590
53	19.050	19.020	18.800	18.350	18.810	18.140	17.370
54	19.500	16.970	18.750	16.890	18.100	19.390	16.500
55	17.780	15.260	17.120	15.210	16.410	18.240	14.800
56	16.670	14.450	16.380	15.000	15.690	17.430	14.180

Oct Thermistor Data

	Cement	Aluminum	Water
1	7.070	9.480	10.000
2	7.310	8.600	10.110
3	6.760	8.000	9.350
4	6.790	8.160	9.370
5	6.890	8.310	9.500
6	6.520	8.310	9.630
7	6.800	7.830	9.200
8	7.200	8.060	9.460
9	6.480	8.010	9.470
10	7.600	10.110	11.030
11	8.360	11.430	10.690
12	9.020	11.900	11.230
13	9.080	11.330	11.220
14	10.540	12.110	10.610
15	9.640	12.110	11.110
16	11.100	17.070	11.010
17	15.270	18.490	10.860
18	18.010	19.280	11.230
19	20.460	20.370	11.470
20	20.740	20.100	11.700
21	23.680	20.920	12.060
22	22.910	21.990	12.310
23	22.720	19.540	12.810
24	23.970	22.270	13.480
25	24.680	25.270	13.980
26	23.930	21.560	14.370
27	23.680	21.650	15.020
28	25.150	23.150	15.920
29	27.380	26.360	16.220
30	25.530	22.220	16.600
31	26.000	22.590	16.670
32	24.990	21.710	17.070
33	25.110	22.460	17.370
34	23.330	20.780	17.430
35	24.540	22.110	18.510
36	23.620	21.710	18.840
37	23.780	21.510	19.620
38	23.350	21.450	19.690
39	23.290	22.240	20.200
40	21.570	21.860	19.070
41	21.360	21.380	19.730
42	21.220	21.940	19.770
43	21.130	22.250	19.980
44	21.620	23.710	20.480
45	21.720	22.370	20.840
46	20.660	19.210	19.350
47	21.390	22.750	19.810
48	20.200	18.260	18.750
49	19.790	18.780	18.560
50	20.030	19.440	18.910
51	18.990	18.540	17.560
52	19.290	19.510	18.350
53	18.210	18.500	16.640
54	18.300	18.100	17.510
55	16.720	16.270	16.660
56	15.830	15.640	15.830

Oct Thermistor Data

	Time	Car Side	Asphalt-Back	Side Window	Front Window	Asphalt-Front	Asphalt-Sun
57	19.000	17.060	17.770	16.760	16.530	17.530	18.300
58	19.250	16.330	16.710	15.960	15.780	16.620	17.180
59	19.500	15.740	16.600	15.780	15.160	16.260	16.920
60	19.750	15.670	16.240	15.450	14.960	16.220	16.460
61	20.000	15.620	16.640	16.190	15.510	16.630	16.750
62	20.250	15.300	15.820	14.140	13.440	14.850	15.120
63	20.500	15.020	15.810	14.540	13.830	15.500	15.340
64	20.750	14.880	15.770	14.650	13.910	15.520	15.140
65	21.000	14.300	14.280	13.900	13.380	14.590	14.620
66	21.250	14.550	15.110	14.140	13.580	14.780	14.420
67	21.500	14.730	14.240	13.850	13.490	14.160	14.110
68	21.750	14.900	14.460	14.580	14.320	14.740	14.460
69	22.000	15.120	14.620	14.550	14.260	14.640	14.570
70	22.250	15.870	15.080	14.710	14.400	14.650	14.500
71	22.500	19.500	16.340	18.300	16.700	17.230	15.230
72	22.750	21.780	16.460	19.880	17.590	18.320	15.200
73	23.000	23.220	15.280	21.060	18.750	18.610	14.980
74	23.250	23.830	15.290	21.180	19.010	18.320	14.680
75	23.500	24.090	14.930	21.660	19.510	17.710	14.390
76	23.750	21.690	15.220	20.230	19.920	16.670	14.370
77	24.000	20.070	15.150	19.170	19.900	16.430	14.860
78	24.250	20.570	15.710	19.730	20.050	16.780	15.200
79	24.500	20.120	15.660	19.680	19.980	16.990	15.660
80	24.750	19.250	15.410	18.160	18.310	16.130	15.140
81	25.000	19.280	15.770	18.510	19.090	16.800	15.650
82	25.250	19.800	16.660	19.500	19.690	17.150	16.070
83	25.500	19.510	16.460	18.820	19.050	16.960	15.800
84	25.750	19.340	16.560	18.930	19.090	17.160	16.140
85	26.000	19.240	16.760	19.600	19.910	18.050	16.810
86	26.250	19.030	15.490	17.180	18.220	16.480	15.720
87	26.500	19.560	16.580	18.630	19.250	17.370	16.170
88	26.750	18.780	15.610	17.700	18.560	16.460	15.880
89	27.000	19.540	16.790	18.870	19.560	17.870	16.500
90	27.250	19.220	16.470	18.710	19.300	17.470	16.660
91	27.500	18.980	16.510	18.470	18.790	17.200	16.320
92	27.750	18.950	16.650	18.590	18.900	17.230	16.410
93	28.000	18.480	16.450	17.650	18.130	17.160	16.150
94	28.250	17.520	15.700	16.960	16.980	16.220	15.400
95	28.500	17.630	16.710	17.940	17.390	16.710	16.000
96	28.750	16.620	15.040	15.810	16.080	15.500	14.710
97	29.000	17.040	15.800	16.170	17.060	15.960	15.290
98	29.250	16.740	15.260	16.480	16.960	16.210	15.500
99	29.500	16.580	15.150	16.170	16.810	15.800	15.090
100	29.750	16.680	15.690	16.540	16.360	15.710	14.940
101	30.000	16.570	16.020	16.420	16.290	15.820	14.900
102	30.250	15.160	14.140	14.570	14.610	14.500	13.900
103	30.500	15.970	15.000	15.890	15.760	15.390	14.660
104	30.750	16.090	15.290	15.750	15.810	15.420	14.560
105	31.000	15.360	14.500	14.870	14.910	14.670	14.070
106	31.250	15.920	14.390	15.080	14.630	14.500	13.890
107	31.500	15.340	14.380	15.190	14.830	14.660	13.910
108	31.750	15.770	14.300	15.080	15.000	14.830	14.040
109	32.000	16.550	15.330	16.380	15.900	15.640	14.920
110	32.250	17.820	16.170	17.200	16.810	16.420	15.520
111	32.500	17.920	14.820	16.950	16.540	15.490	14.870
112	32.750	33.490	17.710	22.120	19.910	18.320	16.650

Oct Thermistor Data

	Car Tire	Car Roof	Roof Gravel	Polycarbonate	Sand	Brick	Wood
57	17.080	14.630	16.510	15.270	15.930	17.300	14.210
58	16.500	13.730	15.940	14.820	15.340	16.430	14.070
59	16.150	12.630	15.890	14.970	15.110	16.130	13.900
60	16.080	12.760	15.740	15.080	15.260	16.190	14.310
61	16.430	12.960	15.690	14.470	15.210	15.850	14.000
62	14.790	11.600	14.310	13.300	14.000	14.600	12.360
63	14.980	11.650	14.300	12.950	14.230	14.780	12.360
64	14.770	11.480	14.040	13.110	14.020	14.250	12.260
65	14.470	11.650	13.600	12.990	13.740	13.840	12.530
66	14.470	11.560	13.640	13.390	13.750	13.820	12.740
67	14.580	12.440	13.780	14.270	13.630	13.660	13.410
68	15.420	13.050	14.650	14.640	14.260	14.300	14.230
69	15.570	13.040	14.900	14.900	14.260	14.370	14.140
70	15.690	13.340	15.110	15.310	14.430	14.550	14.310
71	20.750	14.440	15.960	15.670	14.850	15.220	14.870
72	24.620	14.760	16.010	15.800	14.920	15.500	14.910
73	27.240	15.740	16.170	16.030	14.870	15.440	15.290
74	27.530	15.580	16.020	16.080	14.410	15.120	15.140
75	28.460	15.470	16.050	15.670	14.380	15.220	14.620
76	24.610	14.890	15.680	15.370	14.340	15.040	14.330
77	21.720	16.320	16.240	16.430	14.910	15.560	15.520
78	20.150	17.390	16.670	17.280	15.210	15.790	16.340
79	19.900	17.370	17.390	17.620	15.690	16.270	16.800
80	18.940	16.640	17.270	16.780	15.190	16.110	15.920
81	19.390	17.320	18.130	17.860	15.710	16.830	16.720
82	19.700	18.050	18.750	18.400	15.970	17.370	17.230
83	19.440	17.570	18.340	17.980	15.630	16.730	16.610
84	19.570	17.890	18.780	18.270	15.890	17.430	17.210
85	20.440	18.650	19.390	19.050	16.610	18.240	18.230
86	19.370	17.820	18.570	18.420	15.840	17.390	17.280
87	19.490	18.520	18.650	18.480	15.910	17.400	17.520
88	19.300	18.070	18.810	18.450	16.030	17.570	17.500
89	19.760	18.510	19.080	18.610	16.220	18.040	17.920
90	19.810	18.730	19.370	19.030	16.490	18.360	18.110
91	19.420	17.980	18.730	18.230	16.190	17.800	17.290
92	19.530	17.760	18.990	18.210	16.200	18.030	17.390
93	18.850	17.170	18.530	17.790	16.100	18.040	17.180
94	17.900	15.730	17.670	16.520	15.470	17.220	15.880
95	18.380	15.980	17.670	16.580	15.490	17.360	15.910
96	16.800	15.130	16.460	15.680	14.620	16.200	14.950
97	17.440	16.020	16.860	16.340	15.080	16.550	15.710
98	17.800	16.320	17.410	16.920	15.480	16.690	16.050
99	17.620	15.510	16.900	16.610	15.060	16.300	15.480
100	17.090	14.650	16.520	15.660	14.730	16.060	14.930
101	16.790	14.300	16.280	15.440	14.700	15.950	14.510
102	15.660	13.470	15.420	14.630	13.940	15.150	13.820
103	16.220	13.910	15.900	15.340	14.630	15.680	14.760
104	16.620	14.240	15.880	15.500	14.570	15.470	14.530
105	15.880	13.700	15.290	14.830	14.140	15.030	13.910
106	16.060	13.460	15.330	15.260	14.100	15.060	14.440
107	16.000	13.400	15.190	14.250	14.000	15.200	14.010
108	16.100	14.020	15.290	14.610	14.150	15.190	14.440
109	17.110	14.940	16.210	15.760	14.830	15.810	15.270
110	18.170	15.820	16.970	16.400	15.520	16.450	16.110
111	17.900	16.760	16.410	16.020	14.900	15.950	15.590
112	32.650	20.590	20.580	19.910	16.890	20.380	19.680

	Cement	Aluminum	Water
57	16.070	15.790	16.720
58	15.470	15.250	16.080
59	15.140	15.550	15.950
60	15.110	15.770	16.070
61	15.040	15.210	16.330
62	13.790	13.710	14.570
63	13.680	14.110	15.520
64	13.390	13.970	14.770
65	12.980	13.980	14.210
66	13.070	14.570	14.460
67	13.040	14.580	13.590
68	13.950	15.440	14.220
69	14.010	15.010	13.630
70	14.230	15.390	14.040
71	14.870	16.360	14.680
72	14.860	16.130	14.410
73	15.120	16.960	14.110
74	14.770	16.170	13.330
75	14.750	16.250	13.420
76	14.480	15.370	13.010
77	15.010	16.220	13.040
78	15.760	17.560	13.240
79	16.230	17.740	13.270
80	15.790	17.220	13.070
81	16.660	18.560	13.510
82	17.160	19.000	13.830
83	16.670	18.310	13.270
84	17.210	18.790	13.700
85	18.160	19.730	14.180
86	17.180	18.560	13.280
87	17.400	18.780	13.270
88	17.320	18.560	13.040
89	17.760	19.370	13.830
90	18.070	19.430	13.680
91	17.430	18.370	13.320
92	17.880	18.530	13.740
93	17.690	18.150	13.880
94	16.760	16.790	13.640
95	16.650	16.970	13.840
96	15.660	15.980	13.230
97	15.990	17.000	13.580
98	16.410	17.140	13.770
99	15.620	16.550	13.450
100	15.750	16.040	13.660
101	15.440	15.820	14.030
102	14.600	14.790	12.890
103	14.890	16.390	13.730
104	14.920	15.820	13.590
105	14.470	15.050	12.940
106	14.660	15.920	13.130
107	14.530	15.130	13.070
108	14.390	15.160	13.010
109	15.330	16.700	13.440
110	16.070	17.630	14.090
111	15.460	17.910	12.910
112	16.850	22.200	13.540

Oct Thermistor Data

	Time	Car Side	Asphalt-Back	Side Window	Front Window	Asphalt-Front	Asphalt-Sun
113	33.000	33.800	18.050	22.140	20.540	19.520	17.780
114	33.250	34.160	20.130	23.910	22.160	20.740	19.230
115	33.500	36.820	20.880	24.560	22.730	21.400	20.150
116	33.750	37.340	21.510	24.990	23.850	22.480	21.350
117	34.000	33.900	20.570	23.260	22.700	21.850	21.360
118	34.250	37.260	23.470	26.260	24.520	23.830	23.010
119	34.500	35.200	23.820	25.220	25.210	24.990	23.850
120	34.750	32.050	26.610	27.930	27.510	26.780	25.640
121	35.000	30.940	28.030	28.490	29.260	28.610	27.370
122	35.250	33.760	27.890	26.510	27.480	28.000	26.780
123	35.500	34.840	30.000	28.720	29.910	29.620	29.070
124	35.750	34.360	31.520	31.060	31.410	31.720	30.910
125	36.000	33.610	32.810	31.550	31.830	33.240	32.260
126	36.250	32.030	31.870	30.380	30.280	31.760	31.500
127	36.500	30.990	32.580	29.820	30.450	32.230	32.190
128	36.750	29.760	31.050	27.190	28.710	29.840	31.070
129	37.000	30.530	33.140	30.000	30.710	32.660	33.220
130	37.250	32.160	35.950	31.410	32.210	32.410	35.200
131	37.500	30.960	33.800	28.920	29.990	31.860	33.330
132	37.750	31.130	34.360	29.200	31.590	32.150	34.630
133	38.000	31.280	33.880	28.670	30.320	29.150	32.800
134	38.250	31.290	34.320	29.010	30.550	28.240	34.080
135	38.500	31.450	34.660	29.830	31.250	27.640	34.500
136	38.750	31.680	30.500	29.400	29.940	26.030	33.270
137	39.000	30.850	28.590	29.260	30.150	26.340	33.070
138	39.250	31.200	27.580	29.210	30.440	25.660	33.240
139	39.500	31.160	27.120	29.490	30.490	25.430	32.530
140	39.750	31.260	26.430	29.310	30.510	25.130	32.860
141	40.000	31.030	26.020	28.680	29.940	24.810	31.380
142	40.250	31.440	26.560	29.970	30.880	25.920	33.090
143	40.500	30.750	25.280	28.580	29.920	25.310	
144	40.750						
145	41.000						
146	41.250						
147	41.500						
148	41.750	28.270	23.950	26.900	26.780	23.270	26.560
149	42.000	28.480	23.440	24.870	25.620	22.570	25.800
150	42.250	27.460	23.350	25.320	24.630	22.870	24.370
151	42.500	25.620	23.110	25.160	23.980	22.720	23.940
152	42.750	24.160	22.090	22.780	22.780	21.510	22.410
153	43.000	22.990	20.780	22.000	21.340	20.590	21.450
154	43.250	22.760	21.560	21.760	21.420	20.740	21.570
155	43.500	23.160	22.260	22.960	22.500	21.830	22.060
156	43.750	22.540	21.740	22.330	21.770	21.080	21.410
157	44.000	21.920	21.570	21.770	21.380	20.800	21.230
158	44.250	20.740	20.130	20.440	20.160	19.480	19.830
159	44.500	20.770	19.970	20.320	20.220	19.850	20.040
160	44.750	20.510	18.990	19.320	19.520	19.030	19.040
161	45.000	20.380	19.710	19.660	20.000	19.680	19.640
162	45.250	19.580	19.370	19.590	19.560	19.480	19.550
163	45.500	19.500	19.140	19.040	18.370	18.430	18.310
164	45.750	18.720	18.400	17.790	17.650	17.710	17.670
165	46.000	18.680	18.440	18.180	17.920	18.310	18.210
166	46.250	18.060	16.990	16.640	16.310	16.450	16.660
167	46.500	18.320	18.510	18.180	17.960	18.200	18.130
168	46.750	18.260	17.830	17.440	17.440	17.200	17.150

Oct Thermistor Data

	Car Tire	Car Roof	Roof Gravel	Polycarbonate	Sand	Brick	Wood
113	35.170	21.950	22.520	19.800	18.450	21.600	21.350
114	35.450	22.740	23.520	20.570	19.250	23.600	21.930
115	37.500	24.220	24.360	19.140	20.390	25.090	22.760
116	38.510	25.970	25.180	19.460	21.440	27.050	23.370
117	35.420	25.480	25.150	18.990	21.430	26.130	23.110
118	37.270	27.380	26.420	19.440	22.680	27.630	23.960
119	36.260	29.210	27.510	20.240	23.290	27.350	24.560
120	37.160	30.810	28.180	20.870	24.580	29.230	25.210
121	37.500	32.730	29.540	22.240	26.790	30.470	26.900
122	31.340	31.930	28.480	21.720	26.020	29.140	25.720
123	29.790	34.720	30.310	23.990	27.780	30.350	27.340
124	29.340	35.790	31.800	26.380	29.690	31.450	28.580
125	28.510	36.090	32.300	26.910	30.350	31.820	28.700
126	27.300	35.500	31.500	26.780	30.460	30.790	28.020
127	26.940	34.570	31.190	26.850	30.260	31.150	27.760
128	26.080	32.640	29.710	25.490	29.710	29.900	26.310
129	27.540	34.380	30.900	26.880	31.430	31.080	27.280
130	28.790	35.340	32.720	28.320	33.100	31.610	28.610
131	27.290	34.750	30.450	26.880	31.480	29.950	27.170
132	28.170	34.630	30.630	27.290	32.200	30.370	28.040
133	27.100	33.460	29.240	26.890	31.820	28.980	26.970
134	27.490	33.820	29.260	26.800	31.640	28.450	27.190
135	27.650	33.580	29.200	26.970	32.230	28.530	27.450
136	27.030	32.640	28.350	26.830	31.500	27.920	27.150
137	27.800	31.690	28.130	25.920	30.720	27.360	25.920
138	27.380	32.700	27.230	25.920	30.830	27.100	26.090
139	27.220	32.640	26.880	26.290	30.530	26.970	25.940
140	27.460	32.330	26.690	26.230	30.230	26.840	25.080
141	26.720	31.020	26.030	26.290	29.770	26.860	24.990
142	28.100	31.290	26.600	26.810	29.320	27.270	25.480
143							
144							
145							
146							
147							
148	25.680	25.510	24.990	24.480	23.940	25.750	23.660
149	25.630	24.140	24.490	24.200	23.330	25.850	23.160
150	26.190	22.570	24.120	22.870	21.870	25.380	22.390
151	24.530	21.740	23.580	22.140	21.380	24.980	21.590
152	23.070	20.470	22.240	21.500	20.370	23.580	20.490
153	21.650	19.350	21.100	20.400	19.490	22.230	19.220
154	21.640	18.720	21.270	20.260	19.170	22.070	18.910
155	22.930	20.070	22.330	21.600	20.160	22.840	20.580
156	22.300	19.390	21.590	21.130	19.780	21.930	20.030
157	21.840	19.080	21.230	20.310	19.470	21.450	19.160
158	20.660	17.890	20.320	19.500	18.690	20.610	17.870
159	20.940	18.190	20.050	19.420	18.480	20.140	17.890
160	20.120	17.800	19.470	18.620	17.840	19.570	17.530
161	20.730	17.990	19.730	18.760	17.910	19.340	17.070
162	20.520	17.050	19.700	19.010	18.240	19.710	17.460
163	19.160	16.280	18.580	17.610	17.370	18.720	16.130
164	18.480	15.630	17.680	16.820	16.570	17.760	15.430
165	18.900	15.390	18.290	17.740	17.120	18.370	16.430
166	17.720	14.870	17.290	16.700	16.150	17.020	15.310
167	18.760	15.740	18.300	17.580	17.000	18.120	16.370
168	17.860	15.490	17.210	16.640	16.120	17.050	15.430

	Cement	Aluminum	Water
113	20.840	22.400	13.480
114	22.910	23.090	13.830
115	24.280	23.750	13.540
116	25.700	24.890	13.780
117	25.570	23.790	14.040
118	26.420	24.030	14.700
119	26.930	24.590	14.970
120	28.030	26.030	15.970
121	30.250	26.980	17.340
122	28.930	25.610	17.740
123	30.110	28.000	18.550
124	31.550	28.860	19.780
125	31.820	29.250	20.360
126	30.360	28.020	20.430
127	30.310	27.990	20.700
128	29.150	26.160	20.480
129	29.530	26.960	21.720
130	30.700	28.280	23.090
131	29.180	26.450	21.900
132	29.740	27.510	22.930
133	28.660	27.830	22.500
134	28.120	28.140	22.900
135	28.750	28.760	23.450
136	27.750	28.490	23.300
137	26.400	26.360	22.870
138	26.120	26.850	22.680
139	26.150	27.360	22.890
140	25.990	26.880	22.590
141	25.900	26.920	22.580
142	26.550	28.830	23.260
143			
144			
145			
146			
147			
148	25.430	26.180	21.380
149	25.160	25.970	21.610
150	24.010	23.830	20.510
151	24.030	23.170	20.930
152	22.310	20.910	20.070
153	20.840	19.640	18.860
154	20.940	20.820	18.890
155	21.740	22.170	19.960
156	21.110	22.130	19.420
157	20.470	20.850	19.110
158	19.340	19.360	17.840
159	18.970	19.470	17.970
160	18.510	19.680	17.450
161	18.160	19.080	17.010
162	18.590	18.990	17.540
163	17.760	18.000	17.030
164	16.600	16.830	15.970
165	17.470	18.260	16.790
166	15.850	15.990	15.160
167	17.030	18.070	16.290
168	15.960	16.430	15.380

Oct Thermistor Data

	Time	Car Side	Asphalt-Back	Side Window	Front Window	Asphalt-Front	Asphalt-Sun
169	47.000	17.910	16.180	15.400	15.630	15.850	15.940
170	47.250	17.340	16.080	15.810	16.370	16.110	16.320
171	47.500	18.200	18.230	18.250	18.260	18.090	17.770
172	47.750	17.410	16.040	15.050	15.850	16.410	16.110
173	48.000	17.390	16.340	16.740	16.770	16.680	16.620
174	48.250	17.550	16.810	16.560	16.650	16.380	16.540
175	48.500	17.840	16.650	16.330	16.290	16.010	15.870
176	48.750	17.270	16.530	16.460	16.550	16.200	16.190
177	49.000	17.680	16.470	16.210	16.790	16.680	16.410
178	49.250	17.660	16.780	16.600	16.760	16.370	16.120
179	49.500	17.180	16.050	15.600	15.940	15.730	15.400
180	49.750	16.990	15.660	15.650	15.620	15.450	15.160
181	50.000	17.260	15.890	15.810	16.500	16.400	16.160
182	50.250	17.060	16.270	16.480	16.450	16.220	16.050
183	50.500	16.770	15.680	16.190	15.860	15.540	15.590
184	50.750	16.710	16.530	17.410	16.720	16.880	16.350
185	51.000	16.960	16.460	16.430	15.870	15.720	15.260
186	51.250	16.670	16.310	16.410	15.690	15.990	15.370
187	51.500	15.890	14.160	13.960	13.800	14.280	13.740
188	51.750	15.660	14.980	14.700	14.350	14.880	14.360
189	52.000	15.160	14.960	14.510	14.040	14.570	14.150
190	52.250	15.160	15.170	14.760	14.090	14.480	14.120
191	52.500	14.890	14.640	14.400	13.910	14.420	14.110
192	52.750	15.120	15.330	14.570	14.620	15.160	14.680
193	53.000	15.350	14.860	14.760	14.740	15.080	14.610

Oct Thermistor Data

	Car Tire	Car Roof	Roof Gravel	Polycarbonate	Sand	Brick	Wood
169	17.040	15.250	16.480	16.110	15.740	16.370	15.210
170	17.520	15.290	17.050	16.840	15.640	16.500	15.400
171	18.850	16.210	18.300	17.800	17.050	17.650	16.510
172	17.560	15.450	16.940	16.750	16.170	16.780	15.750
173	17.800	15.680	17.060	16.740	16.180	16.340	15.800
174	17.740	15.800	17.280	17.010	16.280	16.900	16.060
175	17.060	14.840	16.480	16.310	15.800	16.240	15.230
176	17.340	15.190	16.700	16.510	15.960	16.450	15.270
177	17.850	15.890	17.280	16.920	16.160	16.690	16.040
178	17.430	15.280	16.850	16.620	15.800	16.380	15.510
179	16.940	14.700	16.670	16.410	15.550	16.460	15.540
180	16.600	14.650	16.360	15.950	15.320	15.910	14.910
181	17.570	15.120	17.090	16.610	15.950	16.670	15.760
182	17.130	14.590	16.550	16.360	15.480	16.250	15.110
183	16.900	14.060	16.480	16.140	15.470	16.180	15.390
184	17.900	14.610	17.390	16.670	16.260	17.060	15.760
185	16.730	13.840	16.340	15.820	15.310	16.160	14.970
186	16.740	13.630	16.110	15.280	15.180	15.850	14.740
187	15.280	12.610	14.720	14.440	14.140	14.940	13.640
188	15.530	12.650	14.810	13.910	14.270	14.960	13.320
189	15.350	12.270	14.320	13.500	14.170	14.760	13.160
190	15.120	11.980	14.090	12.850	13.910	14.440	12.380
191	15.170	12.310	14.150	13.400	13.980	14.600	12.860
192	15.980	12.750	14.770	13.990	14.540	14.900	13.420
193	15.850	13.510	14.990	15.030	14.590	14.740	14.330

Oct Thermistor Data

	Cement	Aluminum	Water
169	15.340	16.430	14.600
170	15.520	16.570	14.780
171	16.800	17.980	15.870
172	16.090	17.110	15.040
173	15.960	17.080	15.010
174	16.290	17.710	15.280
175	15.310	16.500	14.350
176	15.650	16.690	14.580
177	16.160	17.430	14.840
178	15.640	16.480	14.100
179	15.720	16.830	13.900
180	15.190	17.790	13.650
181	16.000	17.030	14.650
182	15.340	16.360	13.700
183	15.590	16.640	13.830
184	15.990	16.650	14.580
185	15.500	16.390	14.320
186	15.280	16.030	14.210
187	14.060	14.790	13.170
188	14.280	14.310	13.510
189	14.250	14.480	13.420
190	13.620	13.820	13.540
191	13.770	14.530	13.640
192	14.110	15.200	14.390
193	14.210	15.870	13.800

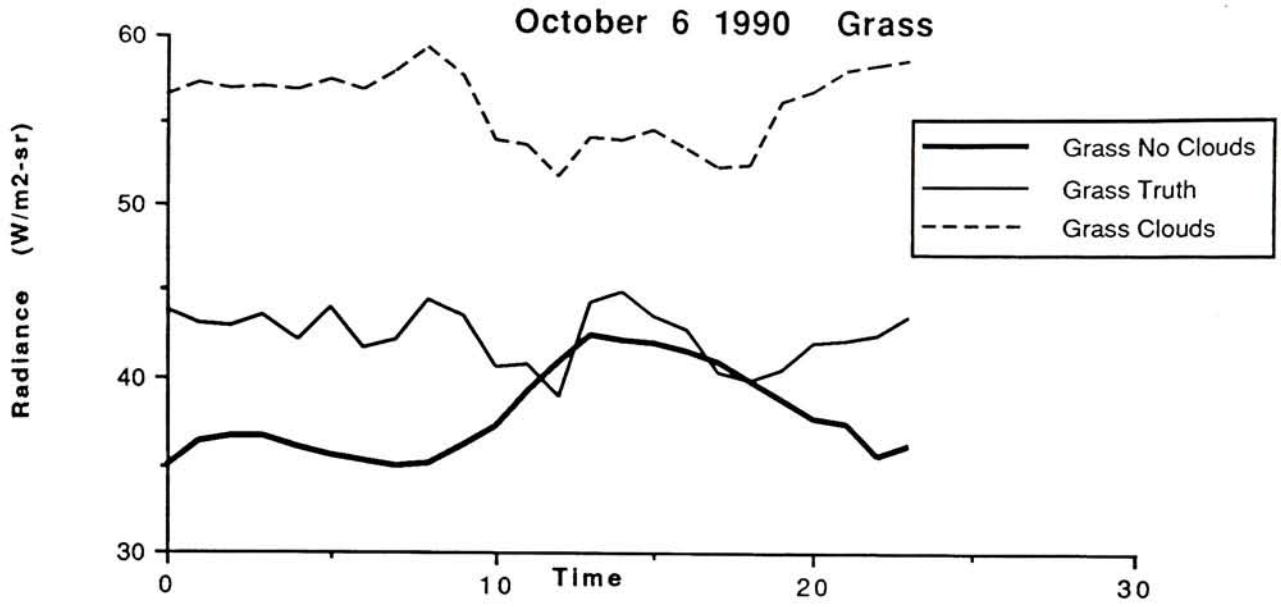
October 6 1990 Grass
Radiance (W/m2-sr)
60
50
40
30
0
10
20
30
Time
Grass No Clouds
Grass Truth
Grass Clouds

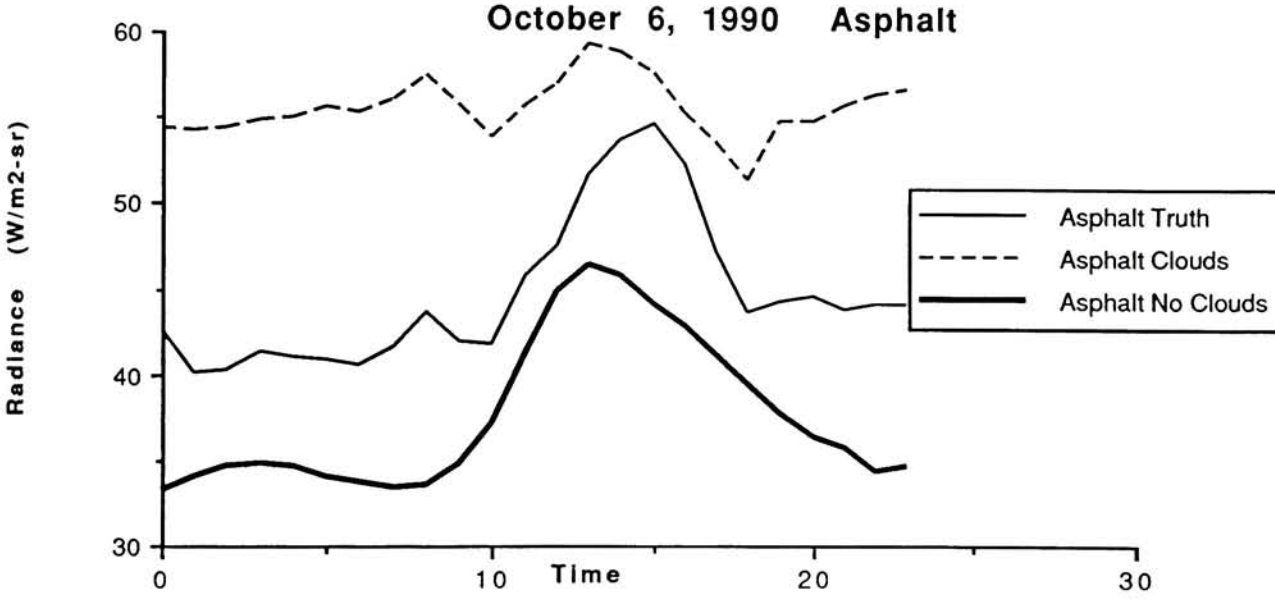
October 6, 1990 Asphalt
Radiance (W/m2-sr)
60
50
40
30
0
10
20
30
Time
Asphalt Truth
Asphalt Clouds
Asphalt No Clouds

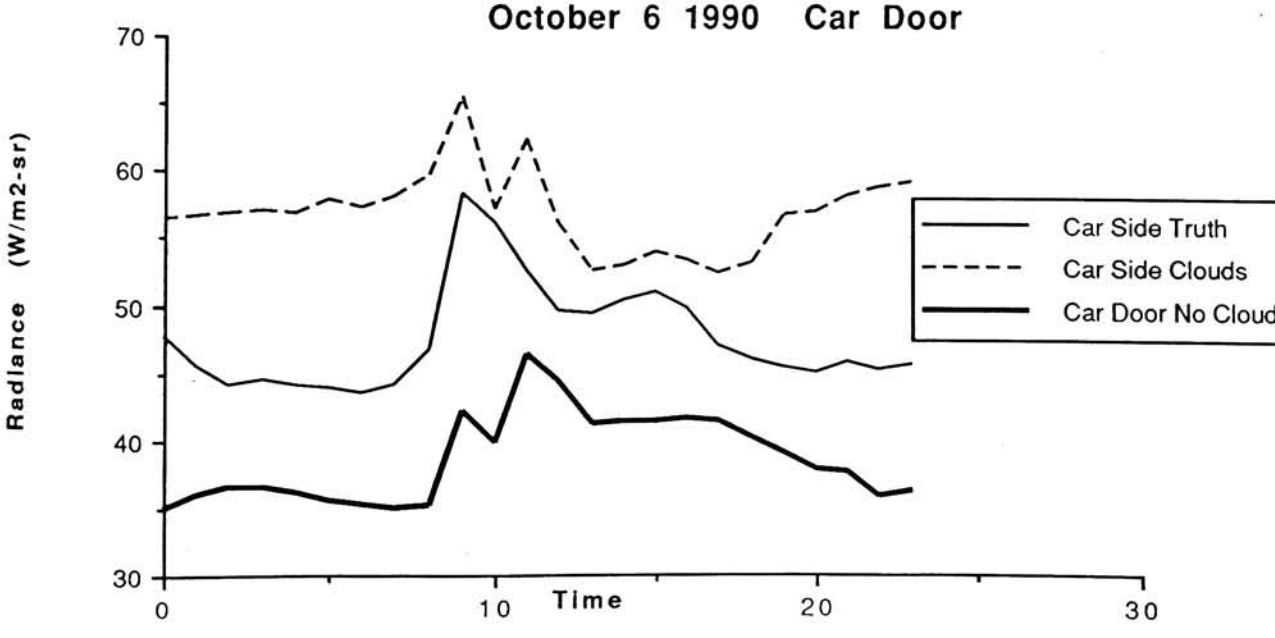
October 6 1990 Car Door
Radiance (W/m2-sr)
70
60
50
40
30
0
10
20
30
Time
Car Side Truth
Car Side Clouds
Car Door No Clouds

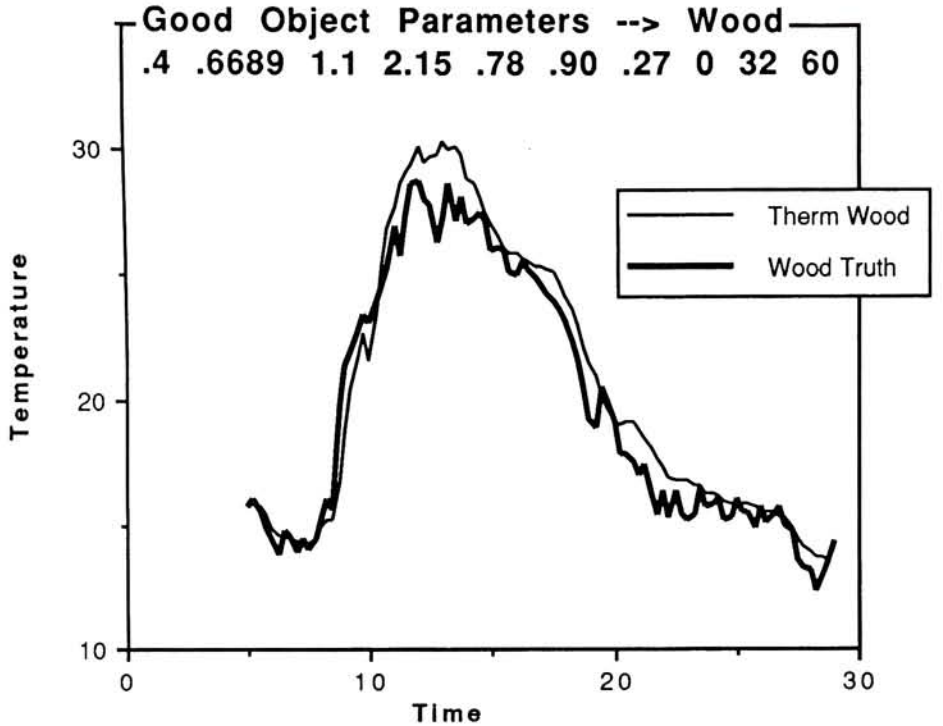
Good Object Parameters --> Wood
.4 .6689 1.1 2.15 .78 .90 .27 0 32 60
Therm Wood
Wood Truth
Temperature
Time
10
20
30
0
10
20
30

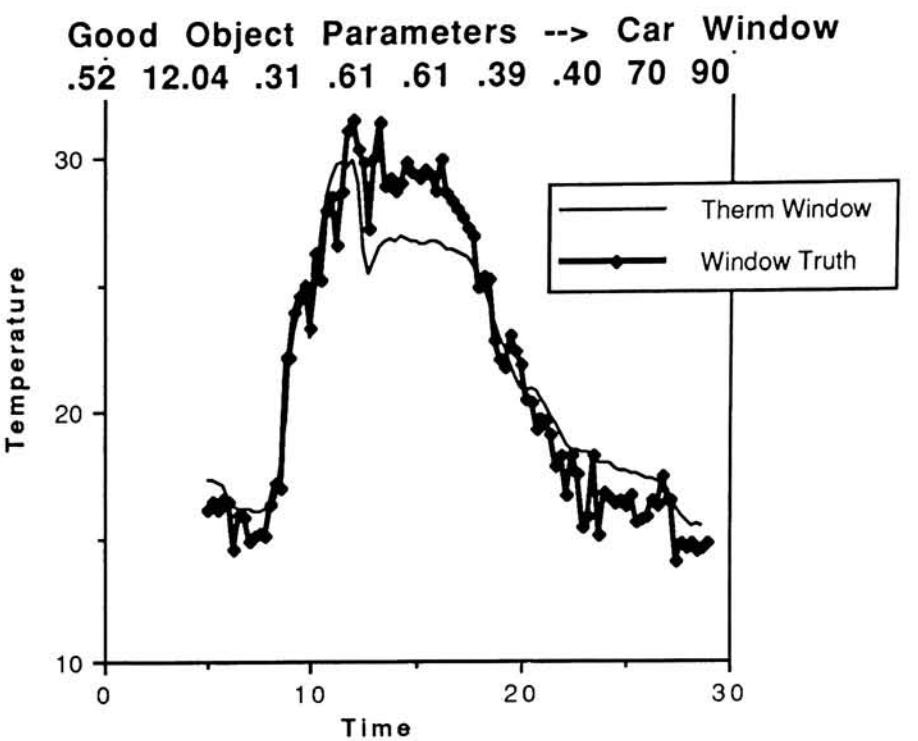
Good Object Parameters --> Car Window
.52 12.04 .31 .61 .61 .39 .40 70 90
Therm Window
Window Truth
Temperature
Time
10
20
30
0
10
20
30

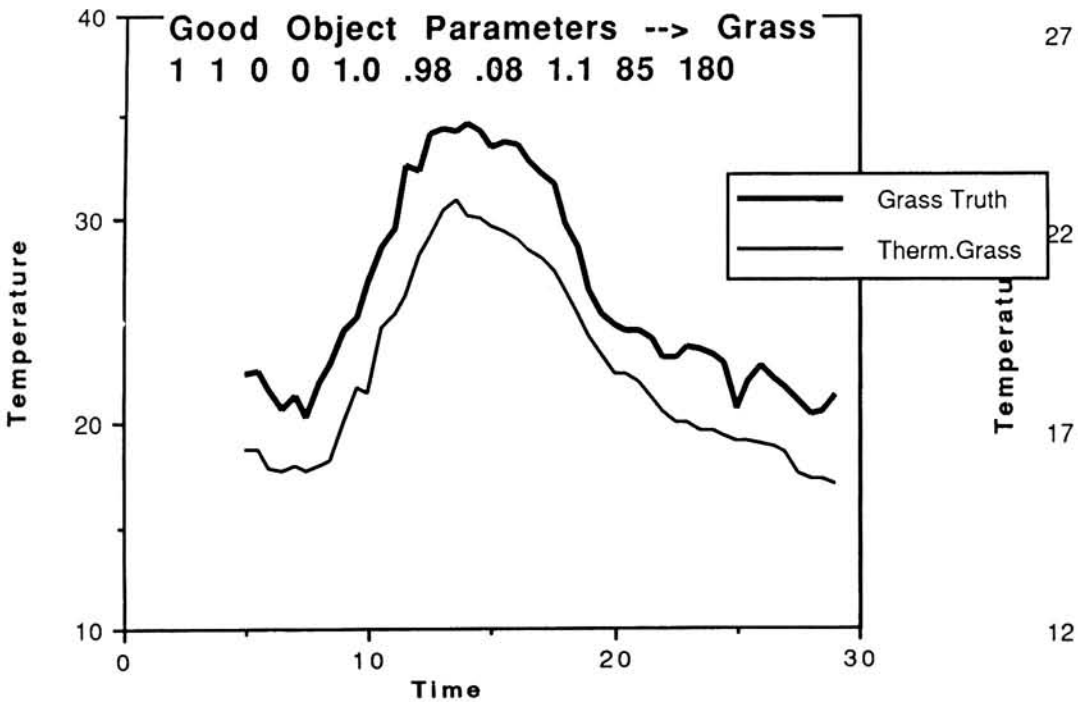
Good Object Parameters --> Grass
1 1 0 0 1.0 .98 .08 1.1 85 180
Grass Truth
Therm.Grass
Temperature
Time
10
20
30
40
0
10
20
30

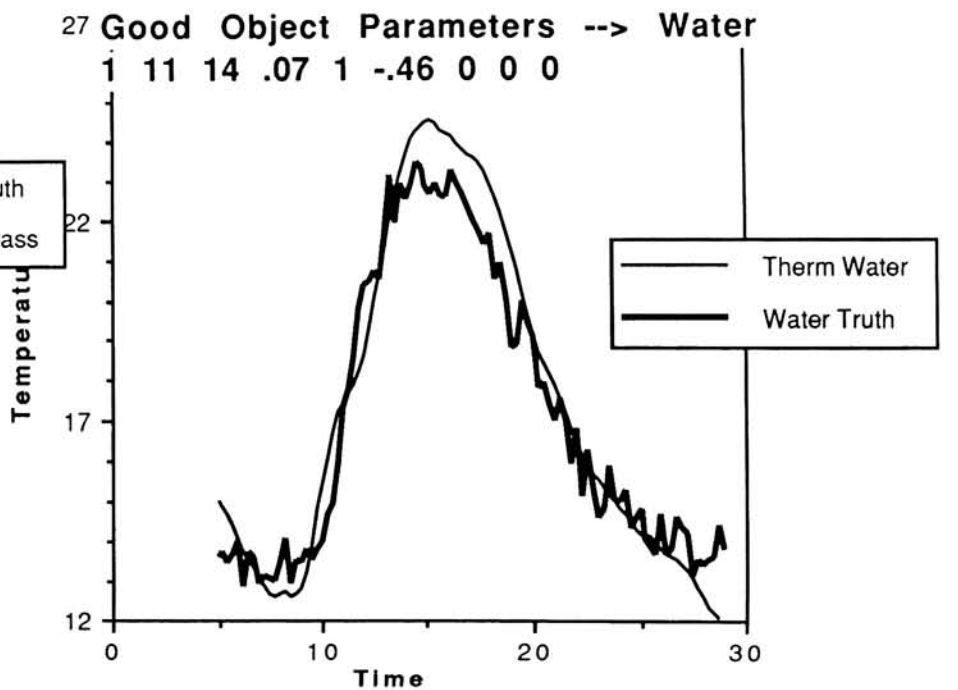
Good Object Parameters --> Water
1 11 14 .07 1 -.46 0 0 0
Therm Water
Water Truth
Temperatu
Time
12
17
22
27
0
10
20
30

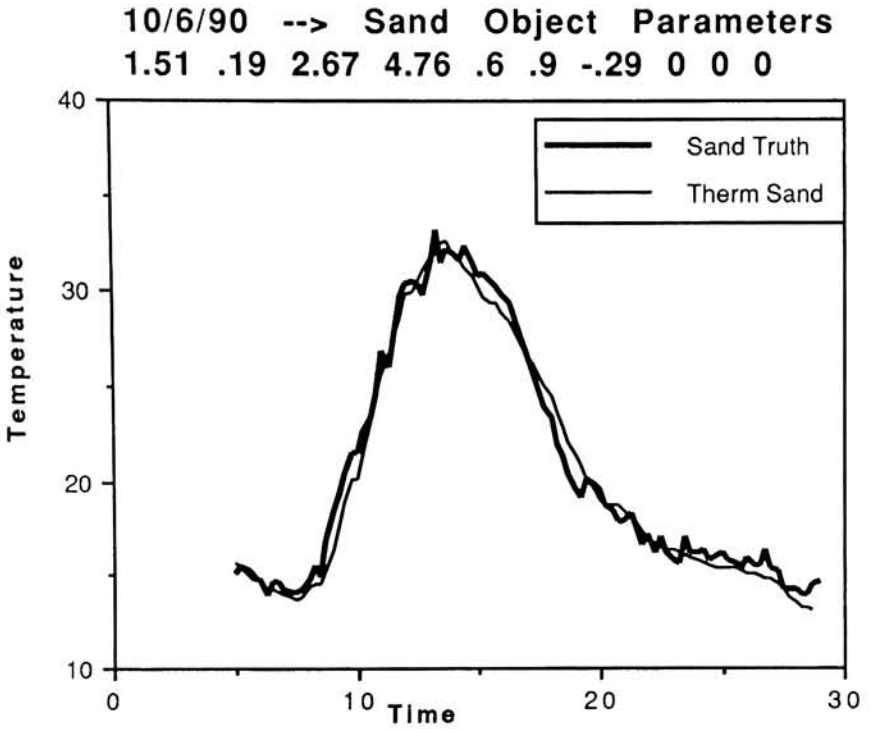
10/6/90 --> Sand Object Parameters
1.51 .19 2.67 4.76 .6 .9 -.29 0 0 0
Sand Truth
Therm Sand
Temperature
Time
40
30
20
10
0
10
20
30

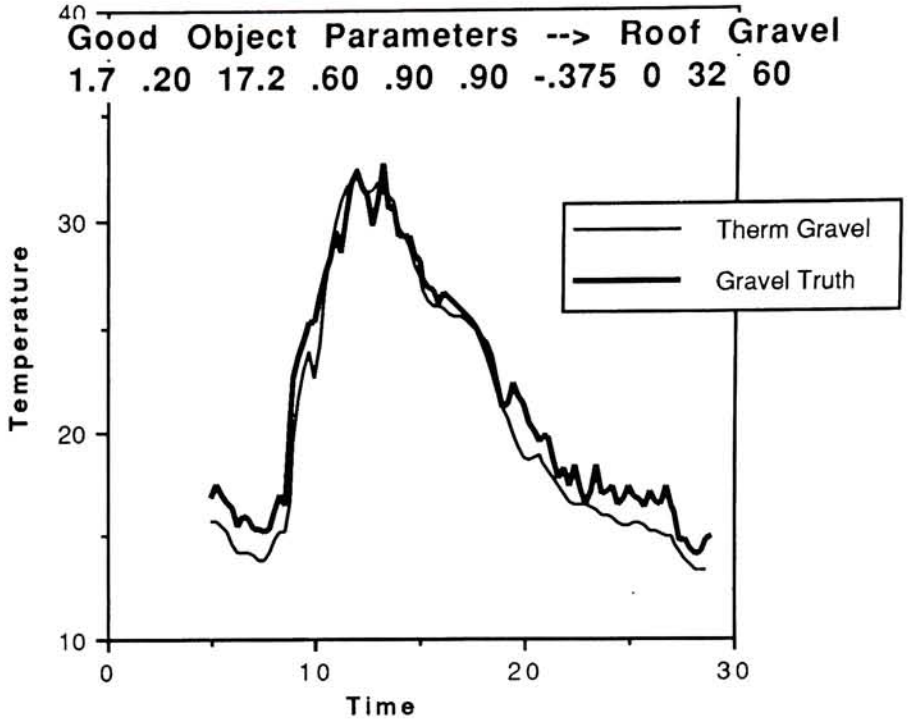
Good Object Parameters --> Roof Gravel
1.7 .20 17.2 .60 .90 .90 -.375 0 32 60
Therm Gravel
Gravel Truth
Temperature
Time
40
30
20
10
0
10
20
30

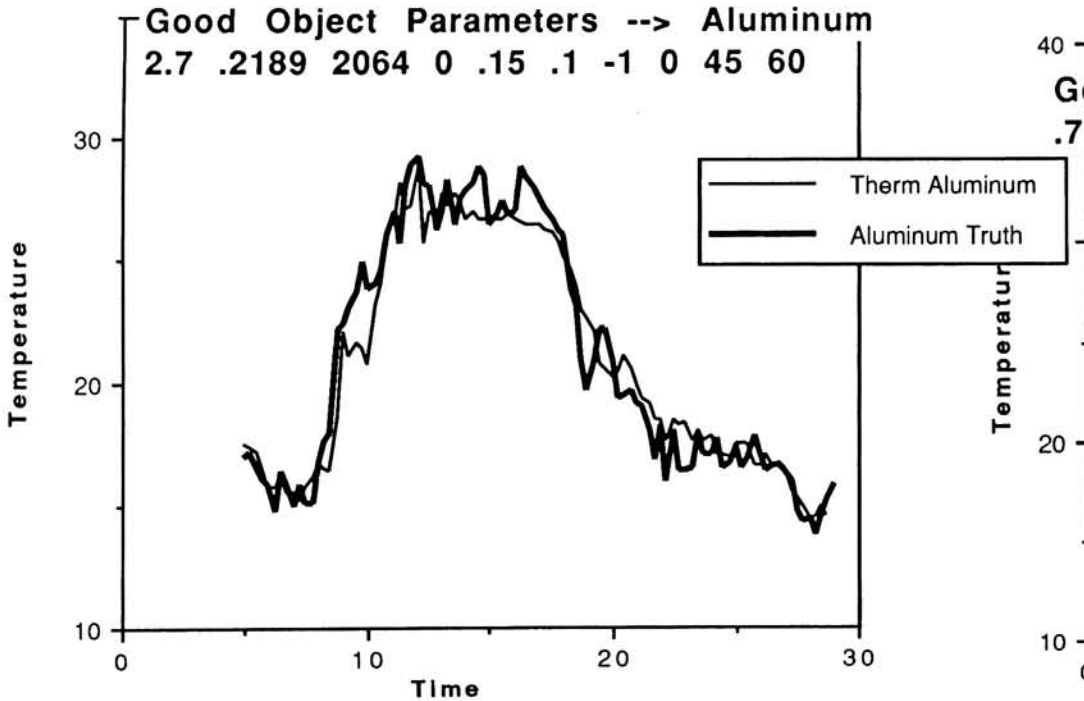
Good Object Parameters --> Aluminum
2.7 .2189 2064 0 .15 .1 -1 0 45 60
Therm Aluminum
Aluminum Truth
Temperature
Time
30
20
10
0
10
20
30

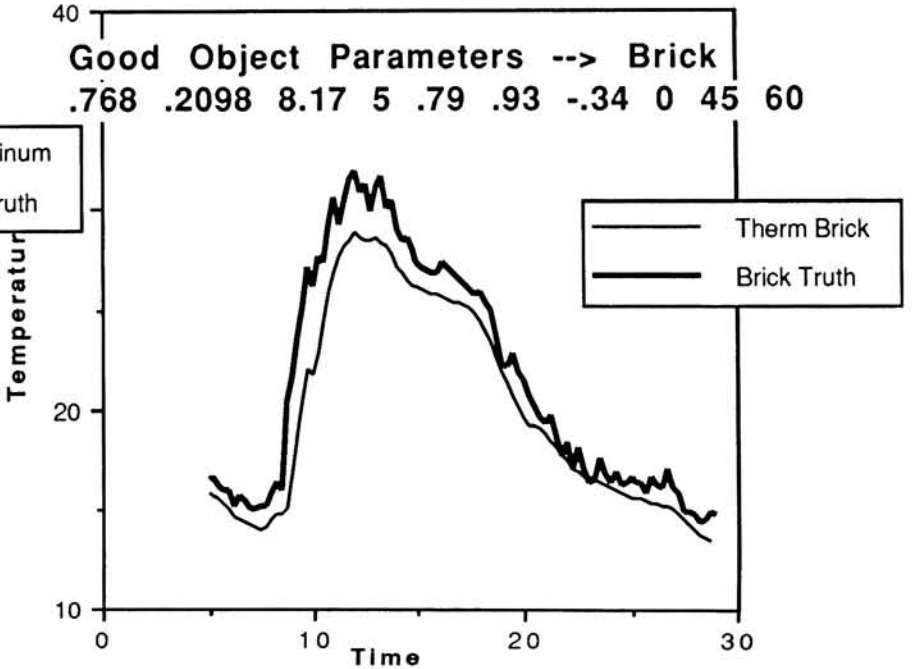
Good Object Parameters --> Brick
.768 .2098 8.17 5 .79 .93 -.34 0 45 60
Therm Brick
Brick Truth
Time
40
20
10
0
10
20
30

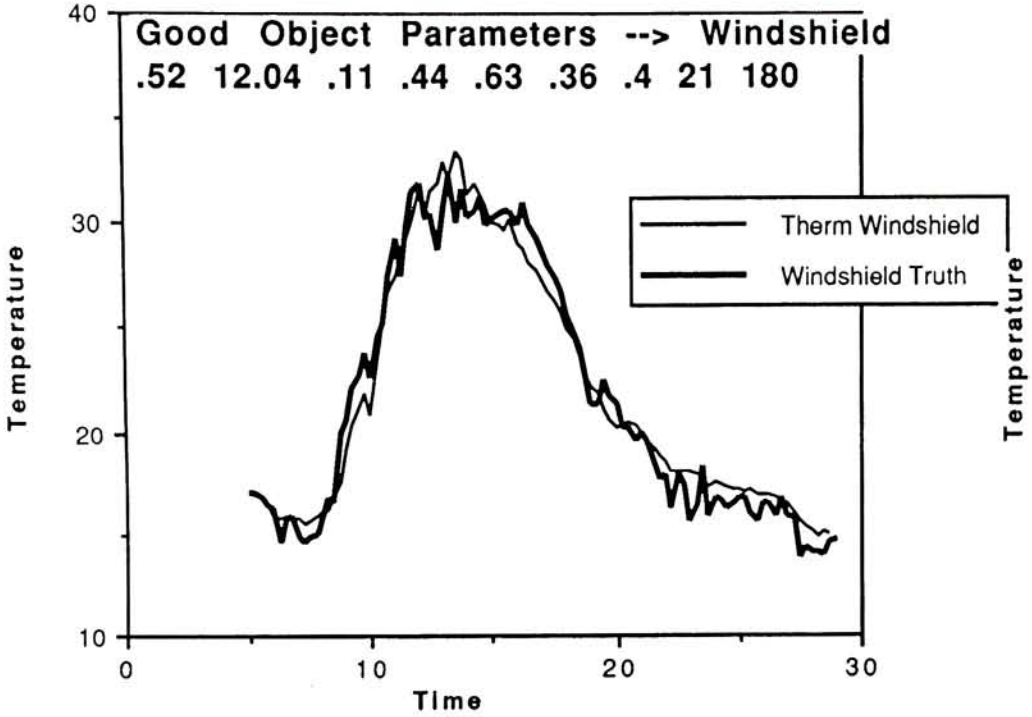
Good Object Parameters --> Windshield
.52 12.04 .11 .44 .63 .36 .4 21 180
Therm Windshield
Windshield Truth
Temperature
Time
40
30
20
10
0
10
20
30

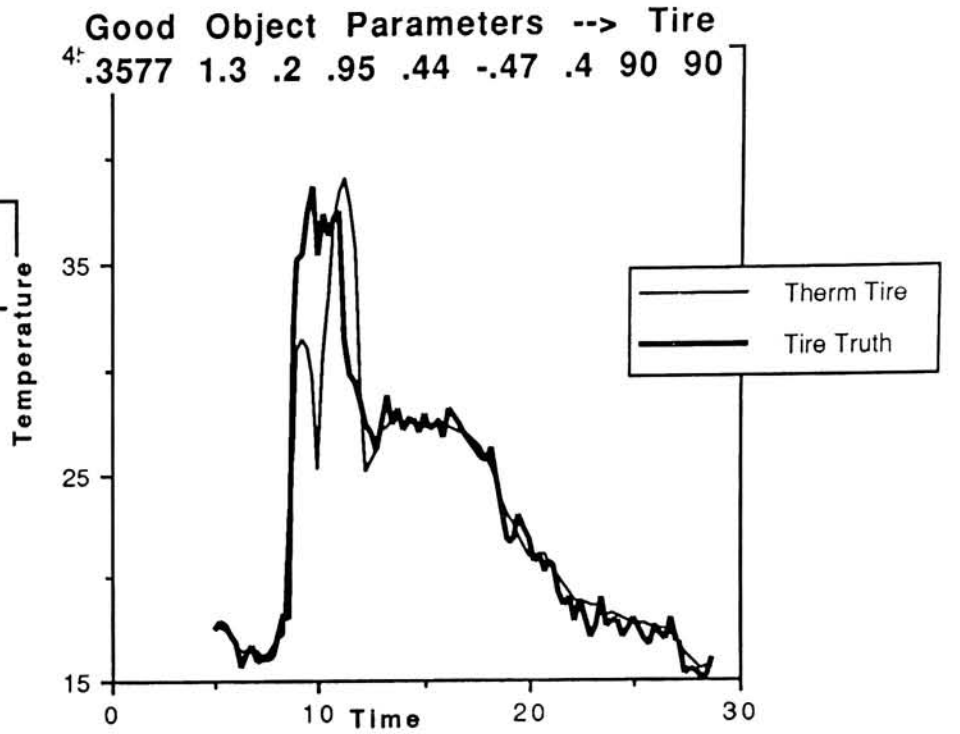
Good Object Parameters --> Tire
.3577 1.3 .2 .95 .44 -.47 .4 90 90
Therm Tire
Tire Truth
Temperature
Time
35
25
15
0
10
20
30

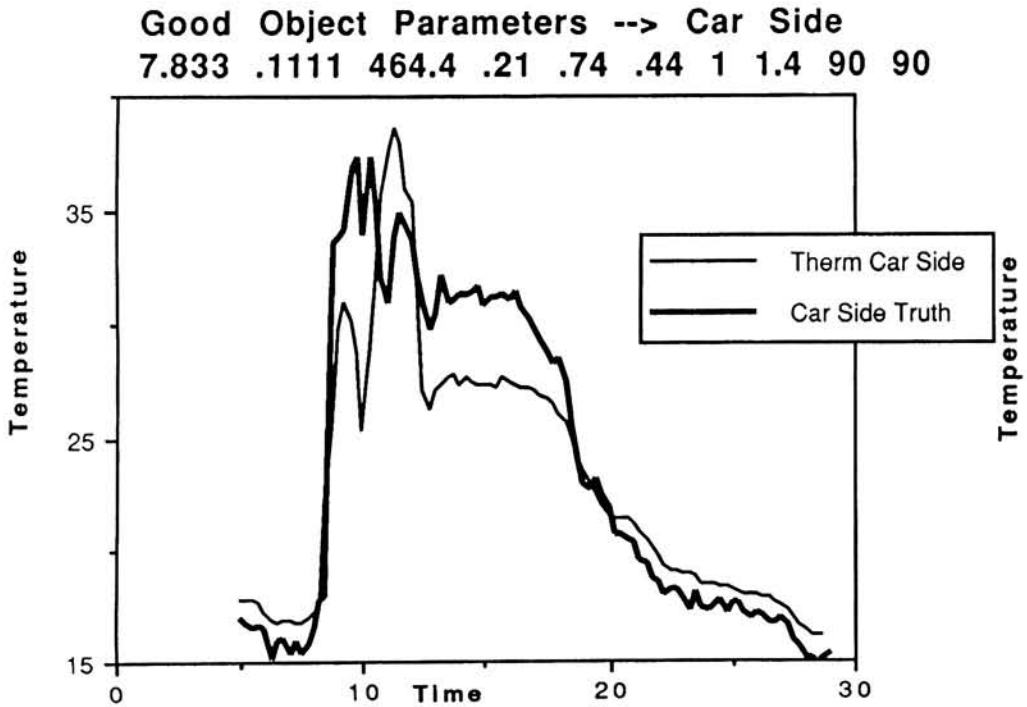
Good Object Parameters --> Car Side
7.833 .1111 464.4 .21 .74 .44 1 1.4 90 90
Therm Car Side
Car Side Truth
Temperature
Time
35
25
15
0
10
20
30

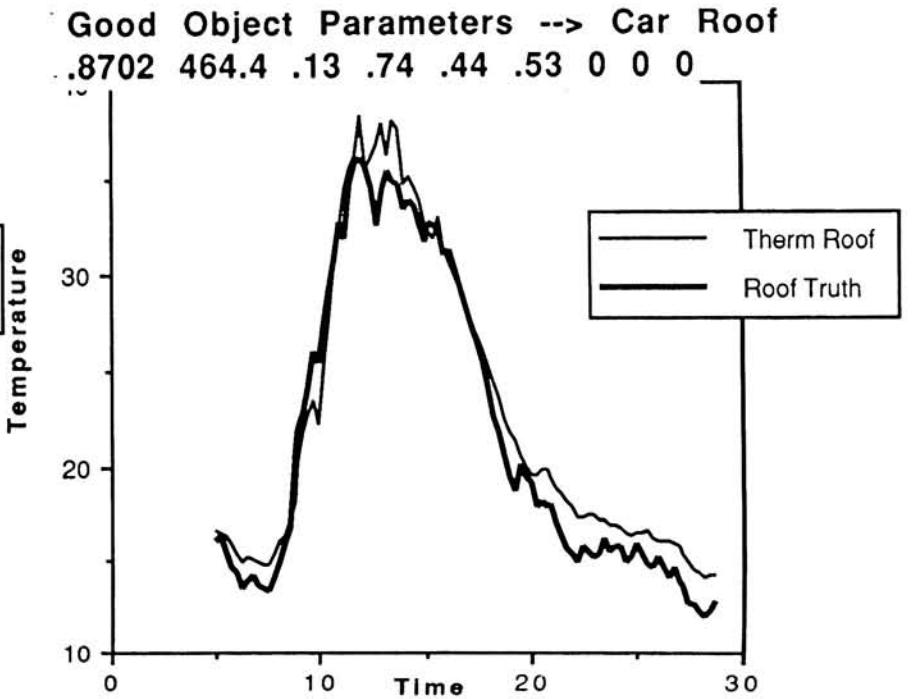
Good Object Parameters --> Car Roof
.8702 464.4 .13 .74 .44 .53 0 0 0
Therm Roof
Roof Truth
Temperature
Time
30
20
10
0
10
20
30

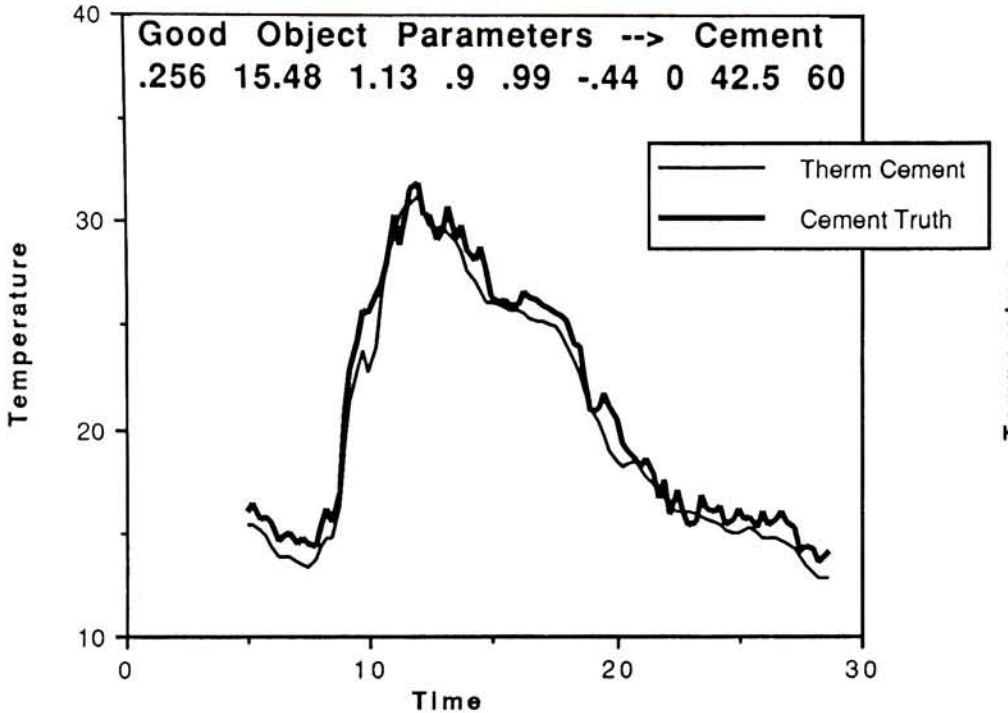
Good Object Parameters --> Cement
.256 15.48 1.13 .9 .99 -.44 0 42.5 60
Therm Cement
Cement Truth
Temperature
Time
40
30
20
10
0
10
20
30

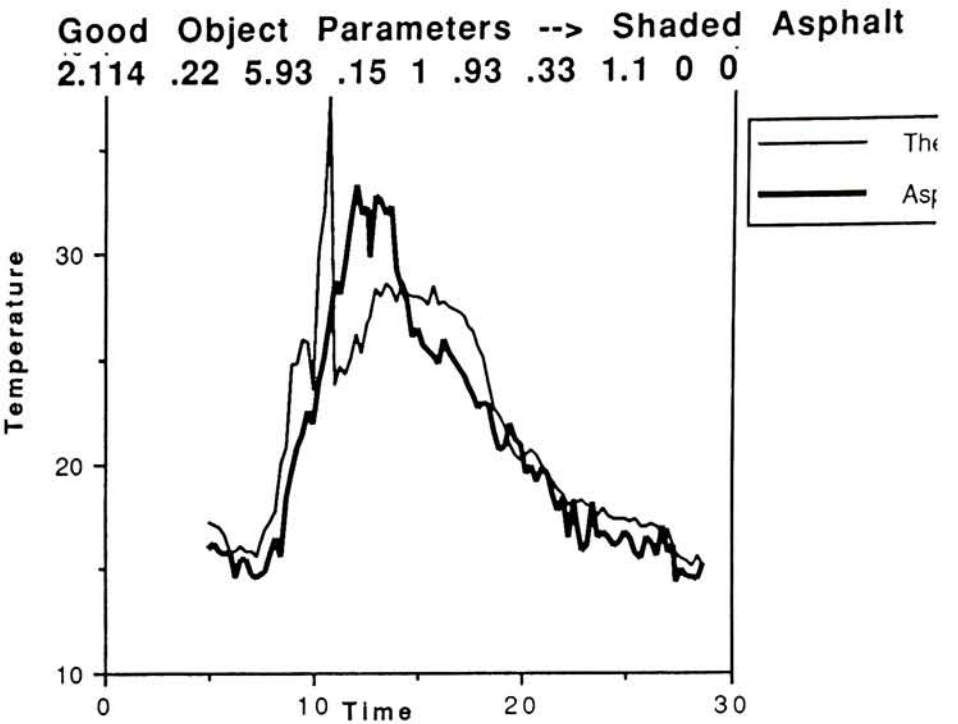
Good Object Parameters --> Shaded Asphalt
2.114 .22 5.93 .15 1 .93 .33 1.1 0 0
Temperature
Time
30
20
10
0
10
20
30

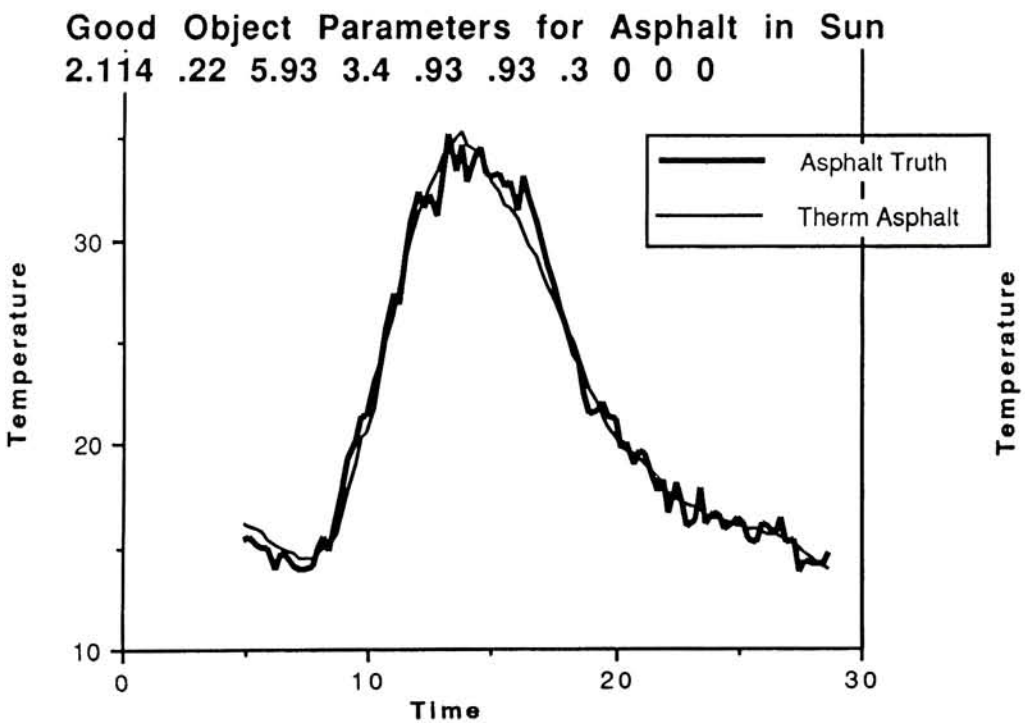
Good Object Parameters for Asphalt in Sun
2.114 .22 5.93 3.4 .93 .93 .3 0 0 0
Asphalt Truth
Therm Asphalt
Temperature
Time
30
20
10
0
10
20
30

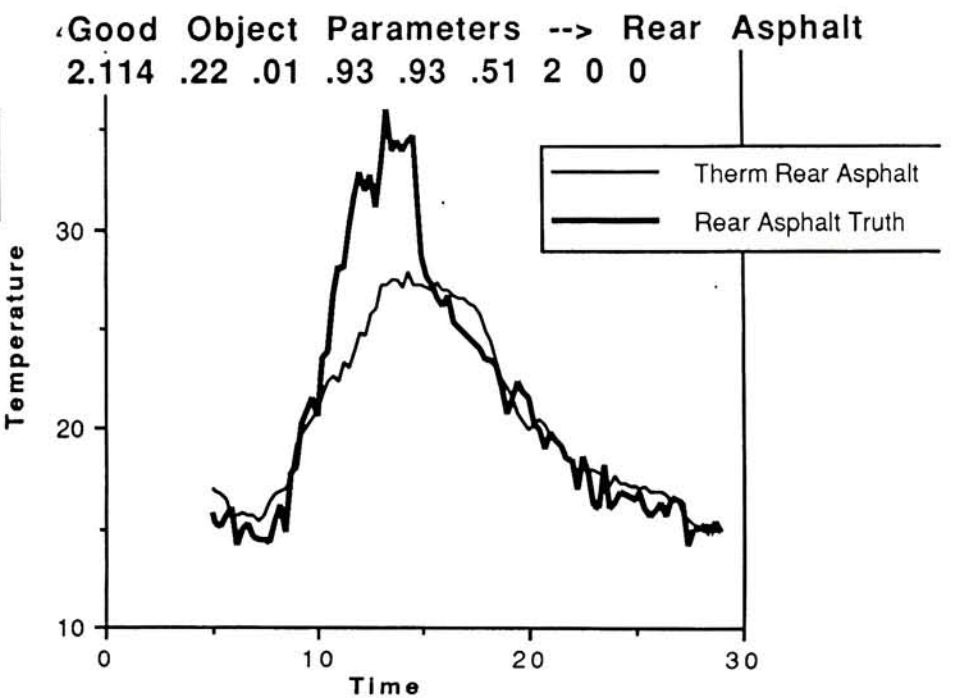
Good Object Parameters --> Rear Asphalt
2.114 .22 .01 .93 .93 .51 2 0 0
Therm Rear Asphalt
Rear Asphalt Truth
Temperature
Time
30
20
10
0
10
20
30

APPENDIX I

DIRSIG Input Files

Example Scene Node File (October or June)

```
0.236
60.0000
90.0000
0.5000
850.0
1250.0
100.0
6
23
92
24
43.08333
77.66667
1
```

Sensor File (October or June)

```
5
1
0
1.000000
1.000000
1.000000
1.000000
1.000000
```

October Autocad_Dview File

```
-22.96  -52.62  0.00
600.0  -2406.0  696.0
15.96  283.83  0.0
300.0
512  512
```

June Autocad_Dview File

```
-70.00  0.00  0.00
-70.00  -5242.0  1844.04
19.38  270.00  0.0
250.0
512  512
```

June Generic Material Parameters File

```
41
painted_steel_roof
1
.1111
464.4
```

-0.40
concrete.ems
rubber
7
0.2986
1.3
1.198
1.0
0.95
0.99
-0.30
tire.ems
fiberglass
8
0.193
35.5
2.5879
1.0
0.5
0.95
0.5
radome_paint6.ems
plexiglas
9
0.35
5.939
1.19
1.0
0.83
0.95
0.5
plexiglas.ems
sand
10
0.19
2.67
1.51
1.0
0.60
0.90
-0.40
sand.ems
coniferous
11
1.0
0.0
1.0
0.0
0.99
0.96
0.13
plant_leaf.ems
roof_gravel
12

0.86
0.91
-0.40
shingles.ems
tree_trunk
18
0.67
0.86
0.6
0.0
0.99
0.97
-0.15
bare_wood.ems
bush
19
1.0
0.0
1.30
0.0
0.9
0.96
0.17
plant_leaf.ems
glass1
20
0.2
12.04
2.6
1.0
0.18
0.79
0.25
glass.ems
pvc
21
0.2389
1.29
1.4
1.0
0.25
0.95
0.5
pvc.ems
road_concrete
22
0.16
0.0
1.6
1.0
0.9
0.94
-0.5
concrete.ems

1.0
1.0
0.18
0.79
0.40
glass.ems
bare_wood
29
0.6689
1.1
0.4
0.0
0.78
0.90
-0.40
bare_wood.ems
painted_steel_bumper
30
.1111
464.4
7.833
1.0
0.94
0.90
0.40
radome_paint6.ems
specular_wood
31
0.6689
1.1
0.4
1.0
0.50
0.90
-0.30
gloss_paint_on_steel.ems
grey1_wood
32
0.6689
1.1
0.4
0.0
0.30
0.90
-0.40
grey1_panel.ems
grey2_wood
33
0.6689
1.1
0.4
0.0
0.30
0.90

```
0.6689
1.1
0.4
0.0
0.74
0.90
-0.40
green_panel.ems
red_wood
40
0.6689
1.1
0.4
0.0
0.54
0.90
-0.40
red_panel.ems
blue_wood
41
0.6689
1.1
0.4
0.0
0.84
0.90
-0.40
blue_panel.ems
```

June Optimum Materials Parameter File

```
41
painted_steel_roof
1
.1111
464.4
7.833
1.0
0.88
0.44
0.53
radome_paint6.ems
water
2
1.0
11.0
1.0
1.0
0.09
0.00
-0.57
water.ems
painted_wood
3
```

0.5
0.95
0.5
radome_paint6.ems
plexiglas
9
0.35
5.939
1.19
1.0
0.83
0.95
0.5
plexiglas.ems
sand
10
0.1911
2.84
1.51
1.0
0.76
0.90
0.39
sand.ems
coniferous
11
1.0
0.0
1.0
0.0
0.99
0.96
0.13
plant_leaf.ems
roof_gravel
12
0.34
17.2
1.0
0.0
0.90
0.90
-0.375
gravel.ems
dirt
13
0.2
0.0
1.35
1.0
0.73
0.90
-0.50
soil.ems

1.0
0.0
0.9
0.96
0.17
plant_leaf.ems
glass1
20
0.52
12.04
1.0
1.0
0.61
0.61
0.95
glass.ems
pvc
21
0.2389
1.29
1.4
1.0
0.25
0.95
0.5
pvc.ems
road_concrete
22
0.16
0.0
1.6
1.0
0.9
0.94
-0.5
concrete.ems
muddy_water
23
1.0
0.0
1.0
1.0
0.9
0.8
-0.5
muddy_water.ems
camouflage_nets
24
0.3106
0.51
0.03
0.0
0.8
0.8

.1111
464.4
7.833
1.0
0.88
0.44
0.69
radome_paint6.ems
specular_wood
31
0.67
0.86
0.6
1.0
0.72
0.87
-0.45
gloss_paint_on_steel.ems
grey1_wood
32
0.67
0.86
0.60
1.0
0.60
0.78
-0.77
grey1_panel.ems
grey2_wood
33
0.67
0.86
0.60
1.0
0.75
0.78
-0.77
grey2_panel.ems
grey3_wood
34
0.67
0.86
0.60
1.0
0.80
0.78
-0.77
grey3_panel.ems
grey4_wood
35
0.67
0.86
0.60
1.0

41
0.67
0.86
0.60
1.0
0.60
0.78
-0.77
blue_panel.ems

October Generic Material Parameters File

30
painted_steel_roof
1
.1111
464.4
7.833
1.0
0.74
0.44
0.50
water
2
1.0
5.13
1.0
1.0
0.50
0.96
-0.40
water.ems
painted_wood
3
0.6689
1.1
0.4
1.0
.74
0.90
-0.5
gloss_paint_on_steel.ems
grass
4
1.0
0.0
1.0
0.0
0.91
0.88
0.16
spring_grass.ems
asphalt
5

0.60
0.90
-0.40
sand.ems
coniferous
11
1.0
0.0
1.0
0.0
0.99
0.96
0.13
plant_leaf.ems
roof_gravel
12
0.20
17.2
1.7
0.0
0.90
0.90
-0.40
gravel.ems
dirt
13
0.2
0.0
1.35
1.0
0.73
0.90
-0.50
soil.ems
plastic
14
0.04
64.50
1.4
1.0
0.07
0.72
0.5
polycarbonate.ems
brick
15
0.2098
8.17
0.768
1.0
0.75
0.93
-0.40
brick.ems

1.4
1.0
0.25
0.95
0.5
pvc.ems
road_concrete
22
0.16
0.0
1.6
1.0
0.9
0.94
-0.5
concrete.ems
muddy_water
23
1.0
0.0
1.0
1.0
0.9
0.8
-0.5
muddy_water.ems
camouflage_nets
24
0.3106
0.51
0.03
0.0
0.8
0.8
0.35
camouflage_nets.ems
decidous
25
1.0
0.0
1.0
0.0
0.88
0.96
0.15
plant_leaf.ems
earth_albedo
26
1.0
0.0
1.0
0.0
0.88
0.96

0.53
water
2
1.0
11.0
1.0
1.0
0.07
1.00
-0.46
water.ems
painted_wood
3
0.6689
1.1
0.4
1.0
.74
0.90
-0.5
gloss_paint_on_steel.ems
grass
4
1.0
0.0
0.16
0.0
1.00
0.98
0.08
spring_grass.ems
asphalt
5
0.22
5.93
2.114
1.0
0.93
0.93
0.40
asphalt_new.ems
concrete
6
0.16
15.48
1.6
1.0
0.90
0.99
-0.44
concrete.ems
rubber
7
0.2986

0.90
-0.375
gravel.ems
dirt
13
0.2
0.0
1.35
1.0
0.73
0.90
-0.50
soil.ems
plastic
14
0.04
64.50
1.4
1.0
0.07
0.72
0.5
polycarbonate.ems
brick
15
0.2098
8.17
0.768
1.0
0.79
0.93
-0.34
brick.ems
aluminum
16
.2198
2064.0
2.7
1.0
0.15
0.10
-1.0
alum_polished.ems
shingles
17
0.35
6.36
1.3
1.0
0.86
0.91
-0.50
shingles.ems
tree_trunk

1.0
0.9
0.8
-0.5
muddy_water.ems
camouflage_nets
24
0.3106
0.51
0.03
0.0
0.8
0.8
0.35
camouflage_nets.ems
decidous
25
1.0
0.0
1.0
0.0
0.88
0.96
0.15
plant_leaf.ems
earth_albedo
26
1.0
0.0
1.0
0.0
0.88
0.96
0.15
albedo_80.ems
painted_steel_side
27
.1111
464.4
7.833
1.0
0.74
0.44
1.0
radome_paint6.ems
glass2
28
0.52
12.04
1.0
1.0
0.61
0.61
0.52

Example Radiance File

```
0.236000
8.000000
11.764706
850.000000
1250.000000
100.000000
5
60.000000
90.000000
0.500000
89.500000
60
8.000000 1250.000000 5.665590e-05 0.177748
8.695652 1150.000000 4.074227e-05 0.515285
9.523810 1050.000000 2.836668e-05 0.524502
10.526316 950.000000 1.903113e-05 0.547495
11.764706 850.000000 1.225699e-05 0.487878
60.000000 0.036000
0.939622 3.626759e-05 6.013345e-11
0.984194 1.032084e-05 6.498824e-10
0.990570 6.513643e-06 4.093048e-10
0.991000 6.325278e-06 2.595901e-10
0.984540 1.053611e-05 1.286477e-10
60.500000 0.036554
0.940103 3.597876e-05 6.095278e-11
0.984331 1.022923e-05 6.557455e-10
0.990661 6.448905e-06 4.130969e-10
0.991089 6.260828e-06 2.625609e-10
0.984684 1.043682e-05 1.300856e-10
61.000000 0.037128
0.938474 3.695718e-05 6.568922e-11
0.983866 1.053077e-05 7.034985e-10
0.990351 6.661248e-06 4.434930e-10
0.990785 6.472777e-06 2.824607e-10
0.984196 1.076789e-05 1.399115e-10
61.500000 0.037723
0.938424 3.698677e-05 6.759728e-11
0.983852 1.053782e-05 7.208114e-10
0.990342 6.665927e-06 4.544365e-10
0.990776 6.477582e-06 2.901322e-10
0.984181 1.077663e-05 1.436798e-10
62.000000 0.038341
0.938115 3.717262e-05 7.004814e-11
0.983764 1.059345e-05 7.440328e-10
0.990283 6.705012e-06 4.692097e-10
0.990718 6.516768e-06 3.001731e-10
0.984088 1.083862e-05 1.486201e-10
62.500000 0.038982
0.936774 3.797772e-05 7.479495e-11
0.983379 1.084214e-05 7.907085e-10
0.990025 6.880738e-06 4.988949e-10
0.990465 6.692487e-06 3.198772e-10
0.983683 1.111278e-05 1.583577e-10
63.000000 0.039648
0.936725 3.800726e-05 7.698166e-11
0.983365 1.084904e-05 8.098633e-10
0.990016 6.885362e-06 5.111248e-10
0.990456 6.697328e-06 3.284295e-10
0.983668 1.112153e-05 1.625104e-10
63.500000 0.040341
0.935656 3.864916e-05 8.145593e-11
0.983057 1.104729e-05 8.534346e-10
0.989809 7.025827e-06 5.387938e-10
0.990253 6.837934e-06 3.469565e-10
0.983344 1.134099e-05 1.716442e-10
64.000000 0.041061
```

0.926834 4.394704e-05 1.420345e-10
0.980488 1.269051e-05 1.408733e-09
0.988065 8.201258e-06 8.934885e-10
0.988533 8.020129e-06 5.908615e-10
0.980610 1.318208e-05 2.911367e-10
70.000000 0.052628
0.926324 4.425336e-05 1.477706e-10
0.980338 1.278552e-05 1.458635e-09
0.987962 8.269758e-06 9.254721e-10
0.988431 8.089292e-06 6.133135e-10
0.980449 1.329003e-05 3.021317e-10
70.500000 0.053923
0.924217 4.551872e-05 1.597437e-10
0.979715 1.318742e-05 1.568652e-09
0.987534 8.561262e-06 9.957283e-10
0.988007 8.383413e-06 6.613440e-10
0.979780 1.374299e-05 3.256186e-10
71.000000 0.055288
0.923044 4.622306e-05 1.686426e-10
0.979368 1.341059e-05 1.648564e-09
0.987294 8.723574e-06 1.046879e-09
0.987770 8.547502e-06 6.968550e-10
0.979405 1.399598e-05 3.430089e-10
71.500000 0.056728
0.923223 4.611559e-05 1.724210e-10
0.979421 1.337339e-05 1.678170e-09
0.987331 8.695986e-06 1.066010e-09
0.987806 8.519873e-06 7.110936e-10
0.979463 1.395532e-05 3.498740e-10
72.000000 0.058249
0.920845 4.754335e-05 1.873060e-10
0.978713 1.383019e-05 1.813193e-09
0.986841 9.029440e-06 1.152180e-09
0.987320 8.857026e-06 7.703714e-10
0.978698 1.447290e-05 3.788722e-10
72.500000 0.059859
0.920143 4.796497e-05 1.956474e-10
0.978503 1.396408e-05 1.884193e-09
0.986696 9.126727e-06 1.197758e-09
0.987176 8.955696e-06 8.025995e-10
0.978471 1.462529e-05 3.947308e-10
73.000000 0.061565
0.919121 4.857854e-05 2.055910e-10
0.978197 1.415874e-05 1.971021e-09
0.986483 9.268902e-06 1.253785e-09
0.986965 9.099664e-06 8.418951e-10
0.978139 1.484780e-05 4.138110e-10
73.500000 0.063377
0.916513 5.014474e-05 2.235367e-10
0.977413 1.466336e-05 2.132682e-09
0.985936 9.639762e-06 1.357016e-09
0.986421 9.475558e-06 9.132766e-10
0.977287 1.542348e-05 4.487037e-10
74.000000 0.065303
0.914377 5.142713e-05 2.402821e-10
0.976768 1.507774e-05 2.281171e-09
0.985485 9.945342e-06 1.452203e-09
0.985970 9.785880e-06 9.793928e-10
0.976583 1.589838e-05 4.809371e-10
74.500000 0.067356
0.914853 5.114124e-05 2.443060e-10
0.976912 1.497994e-05 2.308419e-09
0.985586 9.872178e-06 1.469992e-09
0.986071 9.711717e-06 9.935522e-10
0.976740 1.578833e-05 4.877501e-10
75.000000 0.069547

0.888169 6.716110e-05 5.373129e-10
0.968602 2.029476e-05 4.812028e-09
0.979632 1.387661e-05 3.079888e-09
0.980090 1.381058e-05 2.132031e-09
0.967491 2.200663e-05 1.041041e-09
81.000000 0.115064
0.883068 7.022418e-05 5.957375e-10
0.966960 2.134888e-05 5.312171e-09
0.978429 1.468956e-05 3.401494e-09
0.978871 1.464912e-05 2.358702e-09
0.965627 2.326271e-05 1.151183e-09
81.500000 0.121778
0.880444 7.179932e-05 6.339684e-10
0.966109 2.189140e-05 5.631082e-09
0.977802 1.510924e-05 3.606844e-09
0.978235 1.508309e-05 2.505812e-09
0.964656 2.391356e-05 1.222191e-09
82.000000 0.129335
0.876569 7.412566e-05 6.864374e-10
0.964843 2.270085e-05 6.073130e-09
0.976866 1.573863e-05 3.891620e-09
0.977284 1.573444e-05 2.708410e-09
0.963208 2.488693e-05 1.320495e-09
82.500000 0.137903
0.872636 7.648704e-05 7.416820e-10
0.963549 2.352844e-05 6.538679e-09
0.975904 1.638519e-05 4.191867e-09
0.976305 1.640480e-05 2.922102e-09
0.961721 2.588641e-05 1.423890e-09
83.000000 0.147699
0.865442 8.080684e-05 8.355991e-10
0.961156 2.506442e-05 7.341484e-09
0.974114 1.759397e-05 4.708453e-09
0.974479 1.766079e-05 3.287872e-09
0.958955 2.774994e-05 1.601011e-09
83.500000 0.159006
0.861371 8.325037e-05 8.995675e-10
0.959788 2.593864e-05 7.876688e-09
0.973083 1.828546e-05 5.054261e-09
0.973425 1.838114e-05 3.534538e-09
0.957364 2.881813e-05 1.720088e-09
84.000000 0.172202
0.855352 8.686427e-05 9.909366e-10
0.957744 2.724728e-05 8.645382e-09
0.971536 1.932690e-05 5.549214e-09
0.971840 1.946804e-05 3.887168e-09
0.954978 3.042340e-05 1.890888e-09
84.500000 0.187802
0.846619 9.210742e-05 1.121111e-09
0.954738 2.917570e-05 9.756798e-09
0.969243 2.087400e-05 6.266118e-09
0.969484 2.108668e-05 4.395724e-09
0.951443 3.280355e-05 2.136524e-09
85.000000 0.206527
0.840455 9.580638e-05 1.225974e-09
0.952587 3.055181e-05 1.063862e-08
0.967590 2.198527e-05 6.835005e-09
0.967782 2.225255e-05 4.801890e-09
0.948898 3.451416e-05 2.332415e-09
85.500000 0.229419
0.828155 1.031899e-04 1.426745e-09
0.948223 3.335277e-05 1.235002e-08
0.964208 2.426842e-05 7.938816e-09
0.964287 2.465492e-05 5.584908e-09
0.943693 3.801961e-05 2.710256e-09
86.000000 0.258041

7.568320e-05 1.170066e-08
7.057924e-05 6.808841e-09
6.540189e-05 4.634101e-09
8.062773e-05 2.263835e-09
0.000000 90.000000
2.073157e-04 9.579439e-10
7.568320e-05 1.170066e-08
7.057924e-05 6.808841e-09
6.540189e-05 4.634101e-09
8.062773e-05 2.263835e-09
0.000000 120.000000
2.073157e-04 9.579439e-10
7.568320e-05 1.170066e-08
7.057924e-05 6.808841e-09
6.540189e-05 4.634101e-09
8.062773e-05 2.263835e-09
0.000000 150.000000
2.073157e-04 9.579439e-10
7.568320e-05 1.170066e-08
7.057924e-05 6.808841e-09
6.540189e-05 4.634101e-09
8.062773e-05 2.263835e-09
0.000000 180.000000
2.073157e-04 9.579439e-10
7.568320e-05 1.170066e-08
7.057924e-05 6.808841e-09
6.540189e-05 4.634101e-09
8.062773e-05 2.263835e-09
0.000000 210.000000
2.073157e-04 9.579439e-10
7.568320e-05 1.170066e-08
7.057924e-05 6.808841e-09
6.540189e-05 4.634101e-09
8.062773e-05 2.263835e-09
0.000000 240.000000
2.073157e-04 9.579439e-10
7.568320e-05 1.170066e-08
7.057924e-05 6.808841e-09
6.540189e-05 4.634101e-09
8.062773e-05 2.263835e-09
0.000000 270.000000
2.073157e-04 9.579439e-10
7.568320e-05 1.170066e-08
7.057924e-05 6.808841e-09
6.540189e-05 4.634101e-09
8.062773e-05 2.263835e-09
0.000000 300.000000
2.073157e-04 9.579439e-10
7.568320e-05 1.170066e-08
7.057924e-05 6.808841e-09
6.540189e-05 4.634101e-09
8.062773e-05 2.263835e-09
0.000000 330.000000
2.073157e-04 9.579439e-10
7.568320e-05 1.170066e-08
7.057924e-05 6.808841e-09
6.540189e-05 4.634101e-09
8.062773e-05 2.263835e-09
0.000000 360.000000
2.073157e-04 9.579439e-10
7.568320e-05 1.170066e-08
7.057924e-05 6.808841e-09
6.540189e-05 4.634101e-09
8.062773e-05 2.263835e-09
15.000000 0.000000
2.110753e-04 1.184309e-09

7.755047e-05 1.704031e-08
7.245568e-05 1.000768e-08
6.718397e-05 6.834386e-09
8.272067e-05 3.360912e-09
15.000000 360.000000
2.110753e-04 1.184309e-09
7.755047e-05 1.424522e-08
7.245568e-05 8.325306e-09
6.718397e-05 5.675741e-09
8.272067e-05 2.779113e-09
30.000000 0.000000
2.231445e-04 1.549508e-09
8.366743e-05 1.839934e-08
7.862965e-05 1.080675e-08
7.304931e-05 7.378578e-09
8.958207e-05 3.619617e-09
30.000000 30.000000
2.231445e-04 9.889438e-10
8.366743e-05 1.230307e-08
7.862965e-05 7.154354e-09
7.304931e-05 4.864973e-09
8.958207e-05 2.369273e-09
30.000000 60.000000
2.231445e-04 7.569730e-10
8.366743e-05 9.401479e-09
7.862965e-05 5.445910e-09
7.304931e-05 3.688930e-09
8.958207e-05 1.801107e-09
30.000000 90.000000
2.231445e-04 6.928736e-10
8.366743e-05 8.392821e-09
7.862965e-05 4.862108e-09
7.304931e-05 3.283755e-09
8.958207e-05 1.614813e-09
30.000000 120.000000
2.231445e-04 6.861156e-10
8.366743e-05 8.227430e-09
7.862965e-05 4.768943e-09
7.304931e-05 3.218168e-09
8.958207e-05 1.586873e-09
30.000000 150.000000
2.231445e-04 7.086232e-10
8.366743e-05 8.645426e-09
7.862965e-05 5.008178e-09
7.304931e-05 3.385147e-09
8.958207e-05 1.661169e-09
30.000000 180.000000
2.231445e-04 8.138042e-10
8.366743e-05 1.014666e-08
7.862965e-05 5.882320e-09
7.304931e-05 3.989504e-09
8.958207e-05 1.944756e-09
30.000000 210.000000
2.231445e-04 1.124514e-09
8.366743e-05 1.387175e-08
7.862965e-05 8.087129e-09
7.304931e-05 5.506697e-09
8.958207e-05 2.684655e-09
30.000000 240.000000
2.231445e-04 1.858466e-09
8.366743e-05 2.143803e-08
7.862965e-05 1.264981e-08
7.304931e-05 8.649350e-09
8.958207e-05 4.262987e-09
30.000000 270.000000
2.231445e-04 3.006251e-09

9.646621e-05 1.666954e-08
9.161988e-05 9.733248e-09
8.545370e-05 6.627886e-09
1.040148e-04 3.218217e-09
45.000000 240.000000
2.471138e-04 2.848612e-09
9.646621e-05 3.202338e-08
9.161988e-05 1.905573e-08
8.545370e-05 1.305492e-08
1.040148e-04 6.455859e-09
45.000000 270.000000
2.471138e-04 7.054817e-09
9.646621e-05 6.299466e-08
9.161988e-05 3.847633e-08
8.545370e-05 2.654510e-08
1.040148e-04 1.354444e-08
45.000000 300.000000
2.471138e-04 1.000837e-08
9.646621e-05 8.009556e-08
9.161988e-05 4.943930e-08
8.545370e-05 3.420408e-08
1.040148e-04 1.768062e-08
45.000000 330.000000
2.471138e-04 5.272869e-09
9.646621e-05 5.120417e-08
9.161988e-05 3.100542e-08
8.545370e-05 2.134187e-08
1.040148e-04 1.077432e-08
45.000000 360.000000
2.471138e-04 2.143101e-09
9.646621e-05 2.534805e-08
9.161988e-05 1.497156e-08
8.545370e-05 1.023502e-08
1.040148e-04 5.020932e-09
60.000000 0.000000
2.921465e-04 3.112204e-09
1.229397e-04 3.780760e-08
1.187530e-04 2.246496e-08
1.115465e-04 1.536914e-08
1.340776e-04 7.494614e-09
60.000000 30.000000
2.921465e-04 1.362982e-09
1.229397e-04 1.826303e-08
1.187530e-04 1.065086e-08
1.115465e-04 7.236336e-09
1.340776e-04 3.477648e-09
60.000000 60.000000
2.921465e-04 1.043284e-09
1.229397e-04 1.328470e-08
1.187530e-04 7.745211e-09
1.115465e-04 5.225804e-09
1.340776e-04 2.551903e-09
60.000000 90.000000
2.921465e-04 1.078753e-09
1.229397e-04 1.256792e-08
1.187530e-04 7.374613e-09
1.115465e-04 4.948221e-09
1.340776e-04 2.476134e-09
60.000000 120.000000
2.921465e-04 1.117336e-09
1.229397e-04 1.262165e-08
1.187530e-04 7.419816e-09
1.115465e-04 4.971504e-09
1.340776e-04 2.506831e-09
60.000000 150.000000
2.921465e-04 1.052652e-09

1.939122e-04 2.208939e-08
1.925265e-04 1.311413e-08
1.836146e-04 8.793961e-09
2.153930e-04 4.327753e-09
75.000000 120.000000
3.894378e-04 1.802059e-09
1.939122e-04 2.256826e-08
1.925265e-04 1.338556e-08
1.836146e-04 8.966421e-09
2.153930e-04 4.434544e-09
75.000000 150.000000
3.894378e-04 1.640216e-09
1.939122e-04 2.191743e-08
1.925265e-04 1.299244e-08
1.836146e-04 8.723798e-09
2.153930e-04 4.259277e-09
75.000000 180.000000
3.894378e-04 1.589653e-09
1.939122e-04 2.377335e-08
1.925265e-04 1.397119e-08
1.836146e-04 9.442553e-09
2.153930e-04 4.466721e-09
75.000000 210.000000
3.894378e-04 2.510640e-09
1.939122e-04 3.819245e-08
1.925265e-04 2.255371e-08
1.836146e-04 1.534933e-08
2.153930e-04 7.184621e-09
75.000000 240.000000
3.894378e-04 7.853370e-09
1.939122e-04 9.776798e-08
1.925265e-04 5.941463e-08
1.836146e-04 4.075480e-08
2.153930e-04 1.963980e-08
75.000000 270.000000
3.894378e-04 5.274497e-08
1.939122e-04 3.486255e-07
1.925265e-04 2.243235e-07
1.836146e-04 1.561876e-07
2.153930e-04 8.072883e-08
75.000000 300.000000
3.894378e-04 2.560705e-07
1.939122e-04 8.876786e-07
1.925265e-04 6.032881e-07
1.836146e-04 4.264000e-07
2.153930e-04 2.347428e-07
75.000000 330.000000
3.894378e-04 2.491669e-08
1.939122e-04 2.195620e-07
1.925265e-04 1.380410e-07
1.836146e-04 9.549709e-08
2.153930e-04 4.798590e-08
75.000000 360.000000
3.894378e-04 4.962478e-09
1.939122e-04 6.827933e-08
1.925265e-04 4.098042e-08
1.836146e-04 2.802345e-08
2.153930e-04 1.331280e-08
90.000000 0.000000
6.002081e-04 6.531941e-09
6.433128e-04 1.086867e-07
6.762490e-04 7.245509e-08
6.880971e-04 3.854583e-08
6.738533e-04 1.601579e-08
90.000000 30.000000
6.002081e-04 2.072133e-09

APPENDIX J

Blackbody Data and Sensor Gain & Bias
June 1992 and October 1990 Data Collections

June 1992 Blackbody Data

Time	LWIR 40°C	MWIR 40°C	LWIR 10°C	MWIR 10°C
1.5e+1	1.83164e+2	8.2462e+1	4.7284e+1	0e+0
1.55e+1	1.82229e+2	8.68e+1	4.5635e+1	9.24e-1
1.625e+1	1.83746e+2	9.2793e+1	4.6446e+1	8.871e+0
1.675e+1	1.83756e+2	1.09507e+2	4.9903e+1	2.6563e+1
1.725e+1	1.86023e+2	1.13562e+2	5.0534e+1	2.7418e+1
1.775e+1	1.86421e+2	1.13615e+2	5.1429e+1	2.8111e+1
1.825e+1	1.83931e+2	1.12211e+2	8.2307e+1	2.6261e+1
1.9e+1	1.81848e+2	1.12502e+2	4.8116e+1	2.6377e+1
1.95e+1	1.82841e+2	1.09338e+2	4.7162e+1	1.813e+1
2e+1	1.82023e+2	1.20041e+2	4.7322e+1	3.0619e+1
2.05e+1	1.82581e+2	1.1631e+2	4.6524e+1	2.2378e+1
2.1e+1	1.81495e+2	1.00549e+2	4.5589e+1	7.48e+0
2.15e+1	1.81178e+2	9.3911e+1	4.4893e+1	2.106e+0
2.2e+1	1.77474e+2	9.8088e+1	5.177e+0	4.6789e+1
2.3e+1	2.29296e+2	1.44782e+2	1.13284e+2	5.3962e+1
2.35e+1	2.29737e+2	1.42251e+2	2.29873e+2	5.1914e+1
2.4e+1	2.17241e+2	1.5442e+2	1.03106e+2	6.4678e+1
2.45e+1	2.26245e+2	1.51279e+2	1.09269e+2	6.1147e+1
2.5e+1	2.25893e+2	1.47728e+2	1.12674e+2	5.7689e+1
2.55e+1	2.273e+2	1.46925e+2	1.10152e+2	5.4729e+1
2.6e+1	2.25448e+2	1.43285e+2	1.08306e+2	5.0385e+1
2.65e+1	2.22886e+2	1.35577e+2	1.07082e+2	4.8869e+1
2.7e+1	2.25924e+2	1.40149e+2	9.2945e+1	4.5311e+1
2.75e+1	2.26453e+2	1.39853e+2	1.10393e+2	4.9575e+1
2.825e+1	2.2506e+2	1.37757e+2	1.09966e+2	5.5611e+1
2.875e+1	2.21963e+2	1.43501e+2	1.07605e+2	5.3773e+1
2.925e+1	2.23685e+2	1.43253e+2	1.08531e+2	5.4515e+1
2.975e+1	2.24881e+2	1.44673e+2	1.09463e+2	5.475e+1
3.025e+1	2.25411e+2	1.48339e+2	1.10856e+2	6.1215e+1
3.1e+1	2.15606e+2	1.50384e+2	1.11832e+2	6.3773e+1
3.15e+1	2.24944e+2	1.57216e+2	1.13207e+2	7.473e+1
3.2e+1	1.68619e+2	1.71963e+2	3.948e+1	8.8884e+1
3.25e+1	1.80671e+2	1.65866e+2	3.9183e+1	9.516e+1
3.3e+1	1.63436e+2	1.87032e+2	4.1349e+1	1.06878e+2
3.35e+1	1.39033e+2	1.8807e+2	2.4468e+1	1.0255e+2
3.4e+1	1.3975e+2	1.91415e+2	2.5962e+1	1.0961e+2
3.45e+1	1.25037e+2	2.04572e+2	1.8891e+1	1.21892e+2
3.5e+1	1.25112e+2	2.09776e+2	1.979e+1	1.33367e+2
3.55e+1	1.28482e+2	2.12899e+2	1.9353e+1	1.26725e+2
3.6e+1	1.26801e+2	2.17519e+2	1.9701e+1	1.33445e+2
3.65e+1	2.1175e+1	1.44642e+2	2.095e+1	1.41938e+2
3.725e+1	1.27825e+2	2.27687e+2	2.1247e+1	1.49209e+2

3.775e+1	1.27849e+2	2.36099e+2	2.2179e+1	1.58231e+2
3.825e+1	1.28069e+2	2.31486e+2	2.3424e+1	1.51786e+2
3.875e+1	1.28808e+2	2.28561e+2	2.165e+1	1.45327e+2
3.925e+1	1.29988e+2	2.28217e+2	2.2008e+1	1.52935e+2
3.975e+1	1.28874e+2	2.30782e+2	2.3426e+1	1.49052e+2
4.025e+1	1.29924e+2	2.32462e+2	2.1401e+1	1.50277e+2
4.075e+1	1.28557e+2	2.24895e+2	2.0711e+1	1.40813e+2
4.125e+1	1.30265e+2	2.29536e+2	2.1953e+1	1.42566e+2
4.175e+1	1.18363e+2	2.20024e+2	2.165e+1	1.43626e+2
4.225e+1	1.3354e+2	2.36151e+2	2.3144e+1	1.54441e+2
4.275e+1	1.2646e+2	2.21945e+2	2.0677e+1	1.31992e+2
4.325e+1	4.3185e+1	2.07092e+2	2.0569e+1	1.21214e+2
4.375e+1	1.20966e+2	2.02654e+2	1.8652e+1	1.1796e+2
4.425e+1	1.18154e+2	1.99582e+2	1.9104e+1	1.15843e+2
4.475e+1	1.18344e+2	1.97026e+2	1.7833e+1	1.1632e+2
4.525e+1	1.16014e+2	2.03393e+2	1.7549e+1	1.16851e+2
4.575e+1	1.16799e+2	1.97758e+2	1.7403e+1	1.14948e+2
4.625e+1	1.21314e+2	1.99902e+2	1.739e+1	1.15456e+2
4.675e+1	1.14936e+2	1.92525e+2	1.6176e+1	1.06052e+2
4.725e+1	1.14662e+2	1.89921e+2	1.6684e+1	1.06899e+2
4.775e+1	1.64312e+2	1.91586e+2	4.7898e+1	1.07358e+2
4.825e+1	1.65689e+2	1.92179e+2	4.8613e+1	1.07437e+2
4.875e+1	1.64521e+2	1.90866e+2	4.9626e+1	1.06111e+2
4.925e+1	1.65801e+2	1.89448e+2	4.8617e+1	1.04369e+2
5e+1	1.98121e+2	1.88083e+2	1.03125e+2	8.0498e+1
5.05e+1	1.9866e+2	1.91363e+2	1.04606e+2	7.9563e+1

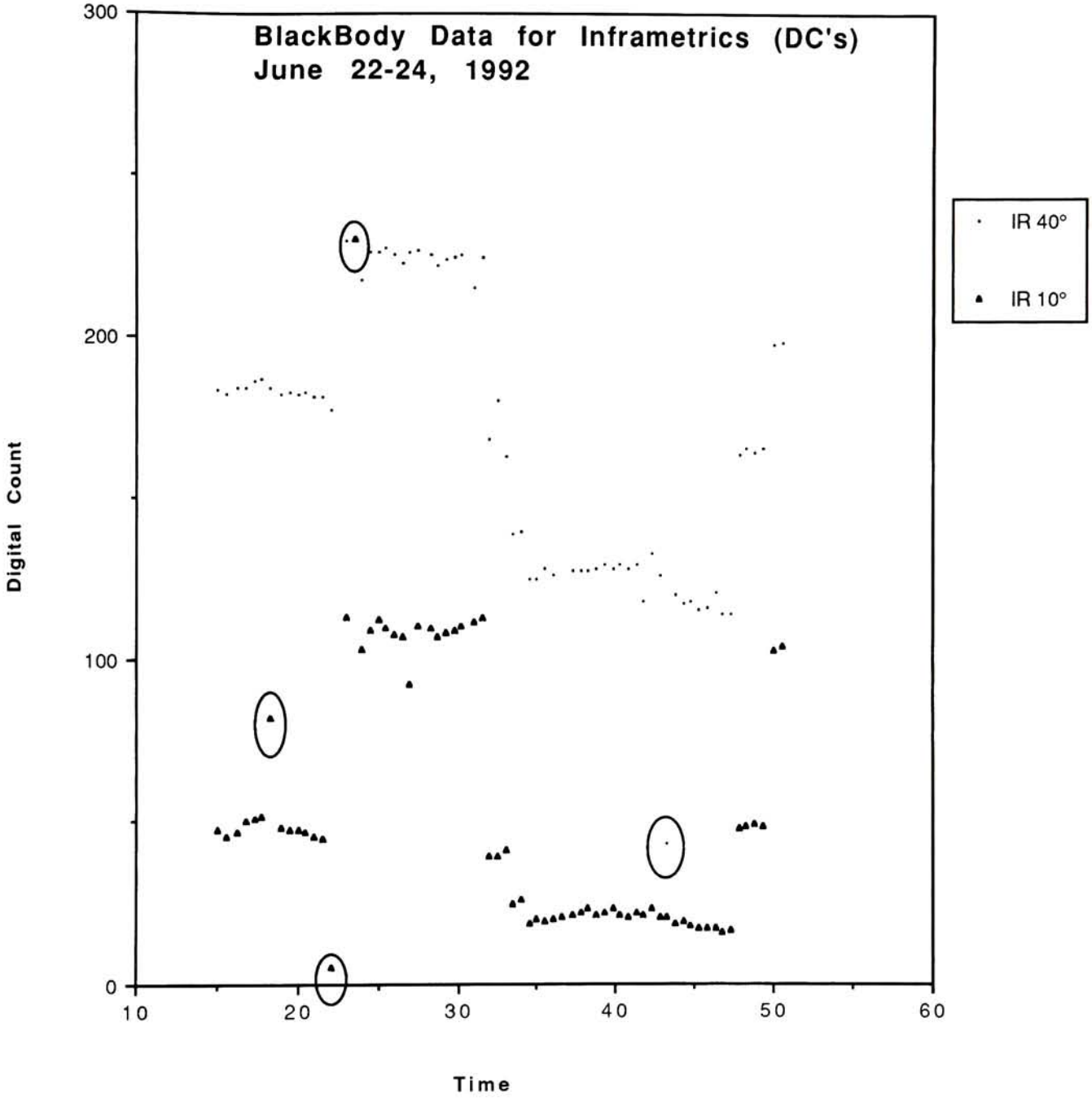
BlackBody Data for Inframetrics (DC's)
June 22-24, 1992
IR 40°
IR 10°
Digital Count
Time
300
200
100
0
10
20
30
40
50
60

	Time	Gain	Bias
1	0.000	4.857	-12.590
2	0.500	4.978	-9.309
3	1.000	4.818	-2.093
4	1.500	4.985	-8.593
5	2.000	4.985	-10.439
6	2.500	4.928	-10.305
7	3.000	5.659	-41.855
8	3.500	4.939	-7.256
9	4.250	4.898	-6.706
10	4.750	4.866	-8.305
11	5.250	4.900	-8.189
12	5.750	4.911	-7.519
13	6.250	4.875	-5.268
14	7.000	4.417	6.585
15	7.500	4.755	-0.059
16	8.000	5.495	-91.413
17	8.500	5.391	-89.233
18	9.000	5.195	-82.398
19	9.500	4.875	-91.656
20	10.000	4.842	-89.376
21	10.500	4.517	-88.706
22	11.000	4.482	-86.973
23	11.500	4.644	-91.269
24	12.000	4.557	-88.849
25	13.250	4.535	-84.779
26	13.750	4.497	84.941
27	14.250	4.453	-82.648
28	14.750	4.560	-86.971
29	15.250	4.595	-87.447
30	15.750	4.486	-83.398
31	16.250	4.618	-88.602
32	16.750	4.589	-88.601
33	17.250	4.609	-87.835
34	17.750	4.115	-76.371
35	18.250	4.698	-88.764
36	18.750	4.501	-86.539
37	19.250	0.962	-2.346
38	19.750	4.354	-85.062
39	20.250	4.215	-81.299
40	20.750	4.277	-84.047
41	21.250	4.190	-82.258
42	21.750	4.230	-83.357
43	22.250	4.422	-87.944
44	22.750	4.203	-83.941
45	23.250	4.169	-82.623
46	23.750	4.954	-70.108
47	24.000	4.982	-70.060

	Time	Gain	Bias
1	0.00	3.315	-39.383
2	1.00	3.324	-36.102
3	2.00	3.288	-32.124
4	3.00	3.261	-31.052
5	4.00	3.261	-32.638
6	5.00	3.182	-32.983
7	6.00	3.304	-39.913
8	7.00	3.232	-39.452
9	8.00	3.305	-48.098
10	9.00	3.187	-29.750
11	10.00	3.223	-15.715
12	11.00	3.408	-15.199
13	12.00	3.196	8.778
14	13.00	3.199	7.188
15	14.00	3.146	9.562
16	15.00	3.103	9.010
17	16.00	3.183	6.091
18	17.00	3.169	9.064
19	18.00	3.113	6.800
20	19.00	3.148	-12.594
21	20.00	3.182	-20.707
22	21.00	3.154	-24.058
23	22.00	3.181	-30.285
24	23.00	3.109	-29.391
25	24.00	3.145	-31.322
26	25.00	2.783	-29.893
27	26.00	3.097	-32.953
28	27.00	3.105	-33.574
29	28.00	3.091	-48.308
30	29.00	3.006	-36.259

APPENDIX K

Data Collection Instrumentation Specs

Inframetrics Infrared Camera: Model 600-L

CI Systems SR80-4D Blackbody

Eppley Precision Pyranometer: Model PSP

Infrared Systems Compurad Spectroradiometer

Barnes PRT-5 Radiometer

YSI Series 400 Thermistors: Model 409B

4. SPECIFICATIONS

The following specifications are defined for the SR 80-4D model in differential control mode. The same specifications apply to absolute control mode in reference to the ambient temperature unless otherwise specified.

Note:

Differential Temperatures are referred to as dT.

Differential Temperature Range:	-20C to +75C (optional -35C to +100C)
Absolute Temperature Range:	+5C to +100C (optional -10C to +125C)
Set-Point Resolution:	0.01C
Read-Out Resolution:	0.01C
|dT| < 20C	(optional - 0.001C)
Short Term Temperature Stability:	
|dT| < 10C	±0.003C
|dT| ≥ 10C	±0.01C
|dT| > 50C	±0.05C
Long Term Temperature Stability:	
Per 1C Ambient Change (<2C/hr)	0.002C
Per Year:	±0.04C
Line Voltage Sensitivity (for 10% voltage changes):	±0.01C
Calibration Accuracy: |dT| < 5C	±0.008C
5C < |dT| < 10C	±0.02C
|dT| > 10C	±0.03C
Absolute, full range:	±0.04C

PRICE INCLUDING HANDLING $1.00

INSTRUCTIONS FOR YSI SERIES 400 TEMPERATURE PROBES

GENERAL DESCRIPTION

YSI Series 400 probes are recommended for direct temperature measurement and control with YSI Tele-Thermometers, temperature controllers, or with other instruments specifically designed for use with these probes. Three classes of probes are offered: Standard, Disposable, and Super-Stable. All YSI Series 400 probes are electrically interchangeable.

Standard Series 400 probes come in many designs for a wide variety of applications. Probe modifications to suit specific purposes may be specially ordered for many of these probes.

Disposable probes are designed for single-use applications. They are furnished in packages of 25 probes, each in a separate sterile pouch.

Super-Stable probes are usable as secondary or transfer standards and for those applications where long-term stability is essential. See individual descriptions.

Maximum measurement temperatures or measurement temperature ranges are indicated in the individual descriptions for each probe.

Construction

The thermistor, which is the temperature sensing element in each probe, is a small sintered metallic oxide disk that decreases in electrical resistance as the temperature increases. Thermistors are located within the tips of the flexible and tubular probes. In probes with a disk-shaped tip, the thermistors are near the centers of the disks; some of these probes have epoxy on one side of the disk; the other, metal side should be used for making measurements.

Probes have vinyl-jacketed leads, unless otherwise specified. Leads are terminated with a phone plug, except for the disposable models which plug into a 10' reusable instrument cable. Standard probe leads are 10' long. Disposable probe leads are 3', and Super-Stable probe leads are 5' long. The vinyl-covered lead wires and phone plugs should not be exposed to temperatures above 100°C.

Except as otherwise indicated in the individual descriptions, probes are constructed with the thermistor electrically isolated from the outer probe surfaces. However, since this isolation could be lost if the probe is damaged by abuse or mishandling, the instrument with which it is used must provide ground fault isolation. (Consult instrument specifications.) In medical use, the patient should be isolated from accidental electrical grounds.

PROBE CHARACTERISTICS

Interchangeability and Stability

YSI's unique manufacturing process produces thermistors with matching temperature/resistance characteristics. Standard Series 400 probes are interchangeable to within 0.1°C at measurement temperatures between 0 and 70°C, increasing to 0.25°C at -40°C and 0.4°C at +150°C. All probes are warranted to remain within interchangeability tolerances for a year.

Super-Stable probe models are typically stable within 0.015°C, and warranted to an interchangeability within 0.06°C, for three years at use and storage temperatures between 0 and 70°C. At temperatures between 70 and 150°C, their stability is typically within 0.03°C for at least a year.

Disposable probe models are interchangeable within 0.2°C between 34 and 41°C, and within 0.5°C from 20 to 34°C and from 41 to 45°C.

Time Constant

Time constant, the standard measure of probe response time, is the time required for a probe to read 63% of a newly impressed temperature change. YSI time constants are derived from measurements in water moving past the probe at 3 ft/sec, except in the case of air or gas temperature probes which are measured in air at standard conditions flowing past the probe at 3 ft/sec (equivalent to 12 to 15 L/min. through a standard 22 mm respiratory airway.) The time constant in air decreases as humidity increases. Approximately five time constants are required for a probe to reach 99% of the total change. Time constants are representative values and are subject to variation because of small differences in probe construction.

Stem Effect

Stem effect refers to the potential error in measurement caused by heat transfer through the body or leads of a probe. The leads of some probes are relatively more massive for the sake of handling ruggedness; such leads introduce potentially greater stem effects. These effects may be lessened by minimizing the difference between probe tip temperature and lead temperature by means of appropriate insulation, isolation or immersion as each application dictates.

Temperature/Resistance Characteristics

The table below lists the temperature/resistance characteristics for YSI Series 400 probes with standard leads. Probes with leads hundreds of feet long can be provided, but it may then be necessary to consider errors introduced by lead resistance, which is approximately 1.6 ohms per hundred feet. Generally, this is only significant at high temperatures.

YSI probes are calibrated against reference standards traceable to NBS or to accepted values of natural physical constants.

Temperature Versus Resistance: -40 to +150°C

Temp. °C	Res. Ohms	Temp. °C	Res. Ohms	Temp. °C	Res. Ohms	Temp. °C	Res. Ohms
-40	75.80K	+10	4484	+ 60	560.5	+110	115.2
39	70.94K	11	4275	61	540.7	111	112.0
38	66.42K	12	4076	62	521.7	112	109.0
37	62.22K	13	3888	63	503.5	113	106.1
36	58.31K	14	3710	64	486.1	114	103.2
35	54.66K	15	3540	65	469.3	115	100.5
34	51.27K	16	3380	66	453.1	116	97.8
33	48.11K	17	3227	67	437.7	117	95.2
32	45.17K	18	3083	68	422.8	118	92.7
31	42.42K	19	2945	69	408.5	119	90.3
-30	39.86K	+20	2815	+ 70	394.8	+120	87.9
29	37.47K	21	2691	71	381.5	121	85.6
28	35.23K	22	2573	72	368.8	122	83.4
27	33.15K	23	2461	73	356.6	123	81.3
26	31.20K	24	2354	74	344.9	124	79.2
25	29.37K	25	2253	75	333.5	125	75.2
24	27.67K	26	2157	76	322.7	126	75.2
23	26.07K	27	2065	77	312.2	127	73.3
22	24.57K	28	1978	78	302.1	128	71.5
21	23.17K	29	1894	79	292.4	129	69.7
-20	21.86K	+30	1815	+ 80	283.1	+130	68.0
19	20.63K	31	1740	81	274.1	131	66.3
18	19.48K	32	1668	82	265.4	132	64.7
17	18.40K	33	1599	83	257.1	133	63.1
16	17.38K	34	1534	84	249.0	134	61.5
15	16.43K	35	1472	85	241.3	135	60.0
14	15.53K	36	1412	86	233.8	136	58.6
13	14.69K	37	1355	87	226.6	137	57.2
12	13.90K	38	1301	88	219.7	138	55.8
11	13.16K	39	1249	89	213.0	139	54.5
-10	12.46K	+40	1200	+ 90	206.5	+140	53.2
9	11.80K	41	1153	91	200.3	141	51.9
8	11.18K	42	1108	92	194.3	142	50.7
7	10.60K	43	1065	93	188.5	143	49.5
6	10.05K	44	1023	94	182.8	144	48.4
5	9534	45	984.1	95	177.4	145	47.3
4	9045	46	946.5	96	172.2	146	46.2
3	8586	47	910.4	97	167.2	147	45.1
2	8152	48	876.0	98	162.3	148	44.1
1	7742	49	843.0	99	157.6	149	43.1
0	7356	+50	811.5	+100	153.1	+150	42.1
+ 1	6991	51	781.3	101	148.7		
2	6646	52	752.4	102	144.4		
3	6320	53	724.7	103	140.3		
4	6012	54	698.1	104	136.4		
5	5721	55	672.7	105	132.5		
6	5446	56	648.3	106	128.8		
7	5185	57	625.0	107	125.3		
8	4939	58	602.6	108	121.8		
9	4705	59	581.1	109	118.4		

YSI Incorporated
Yellow Springs Instrument Co., Inc., Yellow Springs, Ohio 45387 USA
Phone 513 767-7241 • 800 343 HELP • Fax 513 767-9353 • Telex 205437

CLEANING, STERILIZATION, STORAGE AND HANDLING

Cleaning Cautions

Several precautions must be observed when cleaning and sterilizing probes, as they are easily destroyed by improper handling.

NEVER BOIL OR AUTOCLAVE THE VINYL JACKETED LEAD WIRE. The vinyl may safely be exposed to temperatures up to 100°C, but above 90°C the vinyl softens and can be deformed permanently by mechanical stress. Handle gently while hot.

Avoid contact with strong, aromatic, chlorinated, ketone, ether or ester solvents. Prolonged immersion in alcohols or mild organic solvents, detergent solutions or highly alkaline solutions will cause the vinyl to lose flexibility. In medical applications, the user must determine that a probe is suitable and sufficiently flexible for esophageal or rectal use.

During cleaning or sterilization, probes should be handled gently. When wiping clean, hold the probe in one hand at the sensing tip and wipe the probe and lead wire toward the plug end. Excessive pressure could stretch the covering and break the internal wires, which would destroy the probe.

Continued flexing of lead wires in use and cleaning will also break the internal wires. Failure from this cause is not covered by the warranty.

NOTE: YSI disposable probes are designed for a single use only. The reusable cable used with disposable probes may be disinfected or sterilized the same way as the standard, reusable probes.

Disinfection

Probes may be disinfected and sanitized by washing with 3% hydrogen peroxide or 70% isopropanol. 70% ethanol is nearly as effective, but 100% alocohols are less germicidal. Dakin's solution (sodium hypochlorite in neutral buffer) is also suitable. Brief immersion of the probe in detergent solutions is not harmful. Activated dialdehyde solutions, such as Cidex, are also effective. Probe plugs and connectors should not be immersed.

If the connector on any extension or reusable instrument cable is inadvertently wetted during cleaning or disinfection, flush the connector with distilled or deionized water and dry it in a 40 to 80°C oven for at least an hour.

Sterilization

NEVER BOIL ANY YSI SERIES 400 TEMPERATURE PROBE. The detachable probe portion of the YSI 416 and 421 may be autoclaved. On probes other than the 416 and 421, autoclaving may cause the insulation to fail, and may also cause the probe to give inaccurate readings.

Ethylene oxide sterilization does not damage the probes, but the gas is absorbed by the plastic parts. Before handling or use, probes must be safely and thoroughly ventilated to eliminate the absorbed EtO. Because of variations in EtO sterilization equipment, equipment cycles, and variations in absorption from one probe style to another, adequate outgassing must be determined by appropriate testing.

Storage and Handling

When not in use, probes and leads should be formed into loose loops. If wires are stretched or wrapped tightly around instrument cases, stresses sufficient to cause mechanical failure may occur. Store probes at temperatures below 50°C, preferably at room temperatures. Store Super-Stable probes in cases supplied.

All probes should be handled with care, particularly those with icate leads, and the Super-Stable probes which use glass-apsulated thermistors. Mechanical shock can damage any be.

STOMER INFORMATION

be Modifications

he following probe modifications will be quoted on request.

Contact the YSI Customer Service Department.

YSI 402 — Length to 24"; Teflon® instead of vinyl.
YSI 403, 408, 410, 416, 418 — Lengths to 36"; bends to 90° with 3/8" to 1/2" radius.
YSI 404 — Lengths from 1" to 5".
YSI 405 — Probe without cage; longer probe-stem to 12".
YSI 406 — Same as YSI 403, except 1/8" to 3/8" bend radius.
YSI 408 — Bends to 90°; probe length to 12".
YSI 415 — Lengths from 5" to 24".
YSI 419 — Lengths from 6" to 70".
YSI 409A, 421, 427 — Teflon® covered lead to 60" (consult factory for possible temperature error); epoxy encapsulated thermistor without stainless steel disc.
YSI 423 — Length to 5".
YSI 429 — Stainless steel sheath to 12".

Leads to 250' may be ordered for all but the Super-Stable and disposable probes. Consult factory for leads longer than 250'.

Special probes manufactured to customer specification, including waterproof probes utilizing marine cable for deep water applications.

Accessories

Standard extensions are available as follows: junctions are not water-resistant (not for use with Super-Stable probes):

YSI 4010 — 10' YSI 4025 — 25' YSI 4050 — 50'

YSI 4009 Tempheart™ Heat Shields: Used with any skin temperature probe to deflect heat, to shield probe from ambient temperature fluctuations, and to hold probe securely in place. Boxes of 100.

YSI 4900A and YSI 4910 Reusable Instrument Cables. Used with YSI Disposable probes. They are described at the end of the probe descriptions.

YSI 4084 Manifold Outlet: Used with the YSI 441 Airway Probe to connect it to a standard 22 mm respiratory airway. One is supplied with each 441 probe.

Warranty

All reusable probes and instrument cables carry a one year warranty on workmanship and components. Damage through misuse or tampering is not covered. Probe life will vary from a few months to many years depending mainly on the amount of cable flexing. Normal life exceeds one year.

Super-stable probe specifications are warranted for three years.

YSI Series 400 Disposable Probes are warranted to be functional for one year from date of purchase *for single-use applications only;* sterility is warranted unless package is opened, damaged or wet.

Warning

All wire-lead patient-connected transducer assemblies are subject to reading error, local heating and possible damage from high-intensity sources of RF energy. Inadequately grounded electrosurgical equipment represents one such source in that capacitively-coupled currents may seek alternate paths to ground through probe cables and associated instruments. Patient burns may result.

If at all possible, remove the probe from patient contact before activating the surgical unit or other RF source. If probes must be used simultaneously with electrosurgical apparatus, the instruments to which the probes are connected should be checked for adequate isolation from electrical grounds at radio frequencies. Hazards can be reduced by selecting a temperature monitoring point which is remote from the expected RF current path to the ground return pad, and by using pads having the largest practical contact area.

YSI Series 400 Super-Stable Probe Styles

Probe No.	Description & Applications	Time Constant Temperature Range	Configuration
07	SUPER-STABLE REFERENCE, METAL: Stainless steel. For use as a secondary or transfer standard, and for those applications where long-term stability is essential. Useful for verifying accuracy of control probes in medical and scientific applications. Typically stable within ±0.015°C and warranted to an interchangeability within ±0.06°C for three years at measurement and storage temperatures between 0 and 70°C.	6.0 sec. 0 to 70°C	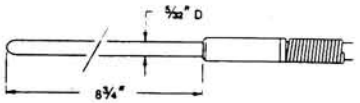
1	SUPER-STABLE REFERENCE, GLASS: Tubular glass. Same specifications as 407.	6.0 sec. 0 to 70°C	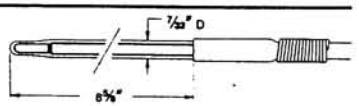

YSI Series 400 Standard Probe Styles

Probe No.	Description & Applications	Time Constant and Maximum Temperature	Configuration
401	GENERAL PURPOSE: Esophageal or rectal temperature. Used for water temperatures (short term), and often buried for sub-soil readings. Used for air where fast response is not required. Most rugged probe. Vinyl tip and lead.	7.0 sec. 100°C (212°F)	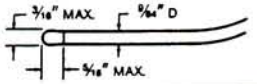
402	SMALL FLEXIBLE VINYL: Esophageal or rectal temperatures of infants, small animals. Cuvette temperatures. Vinyl sheath and tip.	3.2 sec. 100°C (212°F)	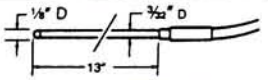
423	SMALL SEMI-FLEXIBLE NYLON: Frozen food package temperatures. Oral and rectal readings. Cuvette temperatures. Nylon with epoxy tip.	1.4 sec. 100°C (212°F)	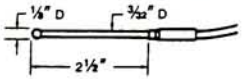
408	"BANJO" SURFACE TEMPERATURE. Skin, oral, axillary, water bath, and flat surface temperatures. Excellent for many air temperature applications. Handle aids in probe use. Stainless steel.	0.6 sec. 150°C (300°F)	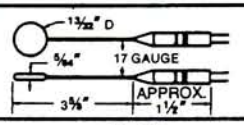
409A	ATTACHABLE SURFACE TEMPERATURE: Stainless steel cup, epoxy backed with Teflon covered flexible wire. Easy to tape on flat surfaces. Good for heat loss or compression efficiency study of piping. CAUTION: This probe is fragile.	1.1 sec. 150°C (300°F)	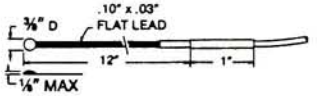
409B	ATTACHABLE SURFACE TEMPERATURE: Tape on skin or flat surfaces. Good for heat loss and compression efficiency study of piping systems. Similar to 409A but less flexible and more rugged. Vinyl covered parallel lead. Stainless steel cup, epoxy backed.	1.1 sec. 100°C (212°F)	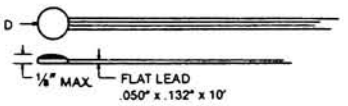
421	SMALL SURFACE TEMPERATURE: 24" Teflon covered flexible wire. Stainless steel disc with epoxy back. Can be autoclaved. Probe head electrically isolated, connector not isolated. Detachable lead. Fastest probe.	0.3 sec. 150°C (300°F)	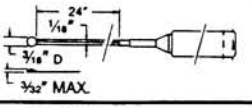
427	SMALL SURFACE TEMPERATURE: Like YSI 421, but with YSI 402 type juncture. Non-detachable lead, non-autoclavable.	0.3 sec. 150°C (300°F)	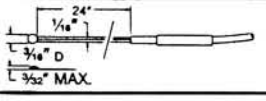
441	AIRWAY TEMPERATURE: For measurements in anesthesia and respiratory airways. Supplied with one YSI 4084 Airway Probe Adapter.	30.0 sec. in dry air 0 to 50°C (32 to 122°F)	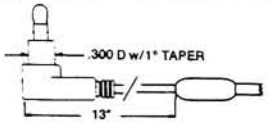
405	AIR TEMPERATURE: Test rooms, incubators, remote air readings, gas streams, etc. Stainless steel cage around epoxy encapsulated thermistor.	10.0 sec. in dry air 150°C (300°F)	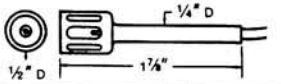
403	TUBULAR: For rugged duty in liquid immersion. Fast response oral or rectal. Stainless steel.	3.4 sec. 150°C (300°F)	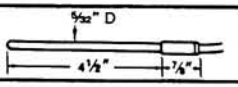
406	THIN TUBULAR: Same as YSI 403, except smaller diameter and is less rugged. Response is faster.	2.5 sec. 150°C (300°F)	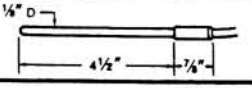
410	TUBULAR WITH FITTING: For readings in pipes or closed vessels. Stainless steel. Fitting withstands 500 psi.	3.4 sec. 150°C (300°F)	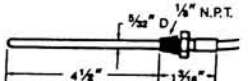

EPPLEY PRECISION PYRANOMETER

Model PSP

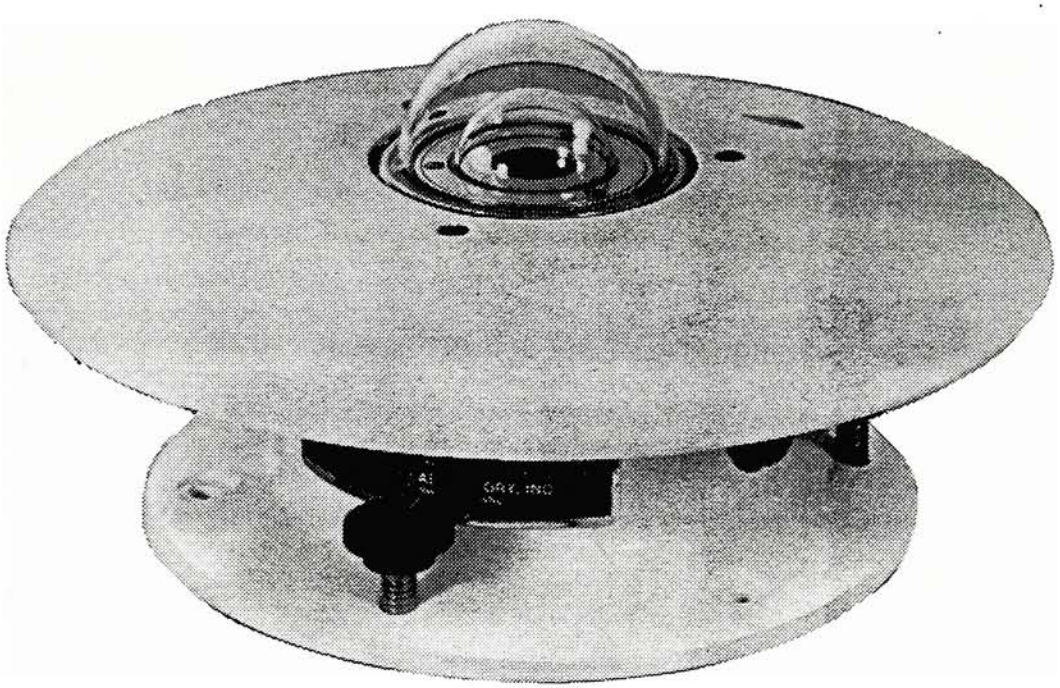

INSTRUMENT CHARACTERISTICS

Sensitivity	9 microvolts per watt meter^{-2} approx.
Impedance	650 ohms approx.
Receiver	circular 1 cm^{-2}, coated with Parsons' black optical lacquer
Temperature dependance	± 1 per cent over ambient temperature range -20 to +40°C (temperature compensation of sensitivity can be supplied over other ranges at additional charge
Linearity	± 0.5 per cent from 0 to 2800 watts m^{-2}
Response time	1 second (i/e signal)
Cosine	± 1 per cent from normalization 0-70° zenith angle ± 3 per cent 70-80° zenith angle
Orientation	no effect on instrument performance
Mechanical vibration	tested up to 20g's without damage
Calibration	integrating hemisphere (approx. 700 watts/meter, ambient temperature +25°C): calibration reference Eppley primary standards
Readout	reproducing the World Radiation Reference

THE EPPLEY LABORATORY, INC.
12 Sheffield Ave., Newport, R. I. 02840, U.S.A. Telephone 401 847-1020

EPLAB

Scientific Instruments
for Precision Measurements
Since 1917

INSTRUCTIONS FOR THE INSTALLATION AND OPERATION OF THE EPPLEY SHADOW BAND STAND FOR THE MEASUREMENT OF DIFFUSE SKY RADIATION

1. General

This shadow band stand has been designed for use with the 180° Eppley Pyranometers for exposure in the latitude range 0-60° N or S. The appropriate method for correcting for the portion of sky screened by the shadow band and for evaluation of measurements of diffuse sky radiation has been published elsewhere [1-3]. However, for convenience, tabular values of the shadow band corrective factor, applicable to average conditions of partly cloudy skies, are given inthis leaflet.

2. Exposure

The shadow band stand should be mounted on a suitable platform in the desired location. The latter is not supplied but can easily be constructed of angle metal. Provision must be made to permit movement of the radiometer vertically (see Fig. 1). The width (i.e. the E-W axis) of the main supporting stand must not exceed 21 inches.

The main supporting stand must be of rigid construction, especially in regions where high winds are experienced.

The supporting stand should be so oriented that the main axis is as nearly N-S as possible. The other exposure requirements of the shadow band sensor are similar to those for the measurement of total sun and sky radiation.

3. Installation

The shadow band stand should first be placed on the specially constructed supporting stand (not supplied) referred to above. Then it should be verified that the N-S orientation

---

1. Drummond, A.J., 1956: "On the measurement of sky radiation", Arch. Met. Geoph. Biokl., Series B, 7, 413-436.

2. IGY Instruction Manual, 1958, Vol. V, Pt. VI, "Radiation Instruments and Measurements". London, Pergamon Press, 426-429.

3. Drummond, A.J., 1964: "Comments on Sky radiation measurement and corrections", J. App. Meteor., 3, 810-811.

is closely correct (see Fig. 1) and that the base plate is level. The latter should be secured rigidly to the supporting platform with four bolts. It is recommended that slots rather than holes be provided in the supporting platform, to enable a small adjustment to be made for the N-S orientation, if necessary (this is most easily accomplished through visual observations of the symmetry of the shadow at or near sunrise, noon and sunset).

Next, the two wing nuts clamping the side bars carrying the shadow band should be loosened and each bar reset so that the 0° mark of the declination scale engraved on the bar is opposite the index engraved on the plate with the latitude scale. Both wing nuts should then be tightened.

The bolts clamping the latitude adjustment (0-60°) should be loosened and the appropriate latitude setting selected. These bolts should then be tightened - no further adjustment in this plane is required unless the shadow band stand is removed to another latitude.

The pyranometer should be placed on the small adjustable platform and secured. The height of this platform should be set (with the aid of the locking screw on the collar) so that the receiver of the radiation sensor is approximately in the center of the shadow band. Then the two bolts securing the horizontal bars of the stand should be loosened and the bars moved until the receiver of the sensor, as viewed through the two small holes drilled in the band, lies in the vertical plane determined by the positions of these holes. In order to obviate skewness in this setting both bars carry similar relative scales graduated from a common reference mark. Such a provision is, also, made for the latitude and declination settings. The exact height adjustment of the sensor should be effected (this is also easily done by viewing the receiver surface through the sighting holes) and the screw on the collar tightened - no further adjustment, in this connection, is necessary unless the instrument location is changed. Finally, it should be verified that the radiation sensor is properly levelled (i.e. check of spirit level on instrument).

4. Operation

The shadow band will require resetting along the polar axis in accordance with the changing solar declination. Generally, the shadow cast on the radiometer should be checked daily when the sun is unobscured by clouds. However, the position of the band can be adjusted in the absense of sunlight by reference to the graduated declination scale.

5. Evaluation of records

In order to evaluate the assembled records of diffuse

radiation it is necessary to correct the measured values for the fraction of the radiation which is screend by the shadow band. In the following table, the theoretically derived values for the 16th of each calendar month are presented. A small correction (4 per cent) is included to relate isotropic to real sky conditions. Multiplication of the basic measurements by the tabulated factors will yield the desired evaluations of diffuse sky radiation with sufficient accuracy for most practical purposes (± 2 per cent).

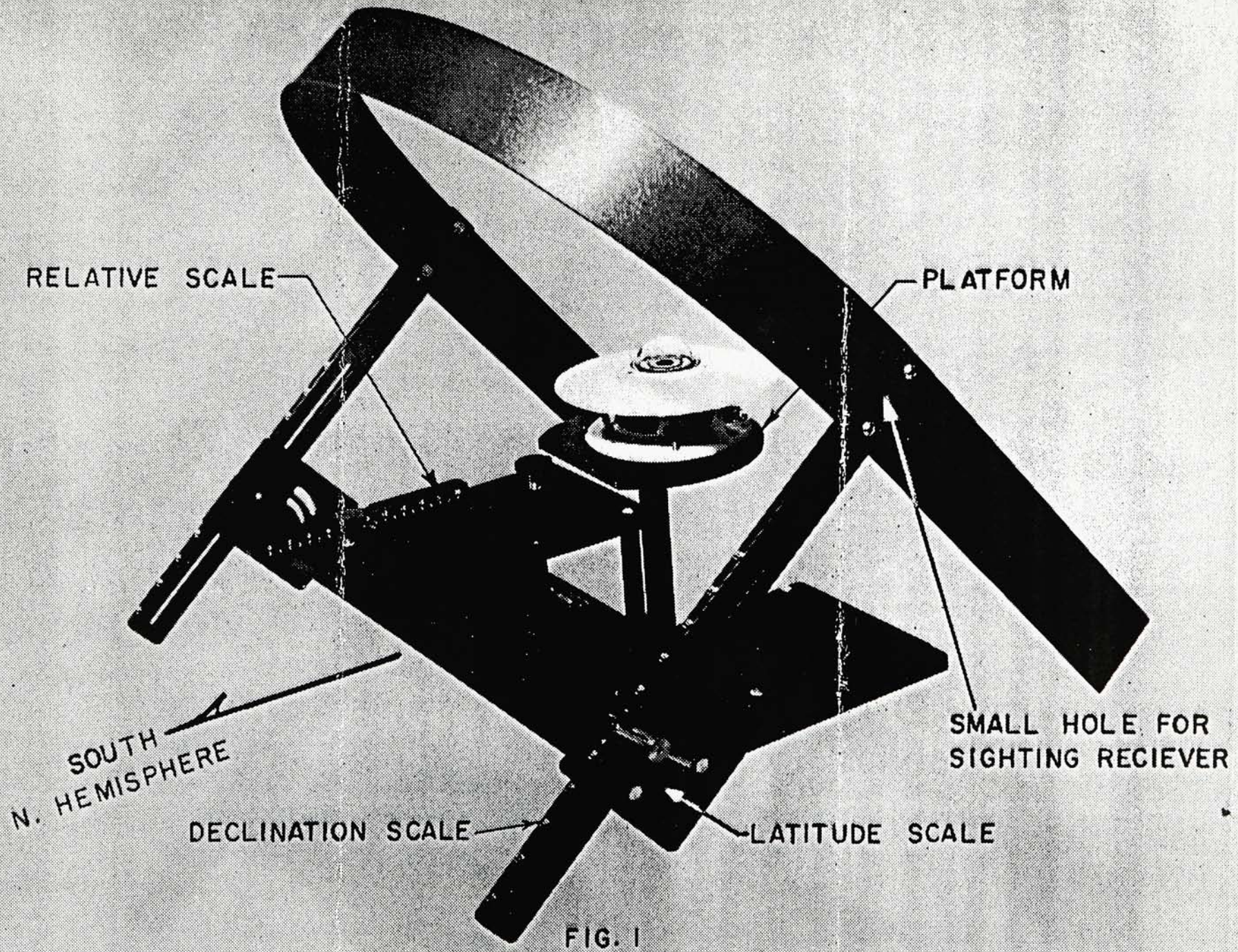
RELATIVE SCALE
PLATFORM
SOUTH
N. HEMISPHERE
SMALL HOLE FOR
SIGHTING RECIEVER
DECLINATION SCALE
LATITUDE SCALE

FIG. 1

Shadow band corrective factors for average partly cloudy skies

Jan. July	Feb. Aug.	Mar. Sept.	Apr. Oct.	May Nov.	June Dec.	July Jan.	Aug. Feb.	Sept. Mar.	Oct. Apr.	Nov. May	Dec. June
1.17	1.21	1.24	1.22	1.19	1.16	1.17	1.20	1.23	1.21	1.19	1.16
1.15	1.19	1.23	1.23	1.20	1.18	1.19	1.21	1.23	1.20	1.16	1.14
1.13	1.16	1.21	1.23	1.21	1.19	1.20	1.21	1.22	1.18	1.14	1.12
1.11	1.14	1.19	1.22	1.21	1.20	1.21	1.21	1.20	1.15	1.12	1.10
1.09	1.12	1.17	1.20	1.21	1.20	1.21	1.21	1.18	1.13	1.10	1.08
1.07	1.10	1.14	1.18	1.20	1.20	1.20	1.19	1.15	1.11	1.08	1.06
1.05	1.07	1.11	1.15	1.19	1.20	1.19	1.17	1.13	1.09	1.06	1.04
-	1.05	1.08	1.13	1.18	1.21	1.19	1.14	1.11	1.06	1.04	-
-	-	1.06	1.11	1.19	1.22	1.20	1.14	1.09	1.04	-	-
-	-	1.05	1.11	1.20	1.23	1.21	1.15	1.07	-	-	-

The Eppley Laboratory, Inc.

Newport, Rhode Island

APPENDIX L

GOES Weather Satellite Cloud Images

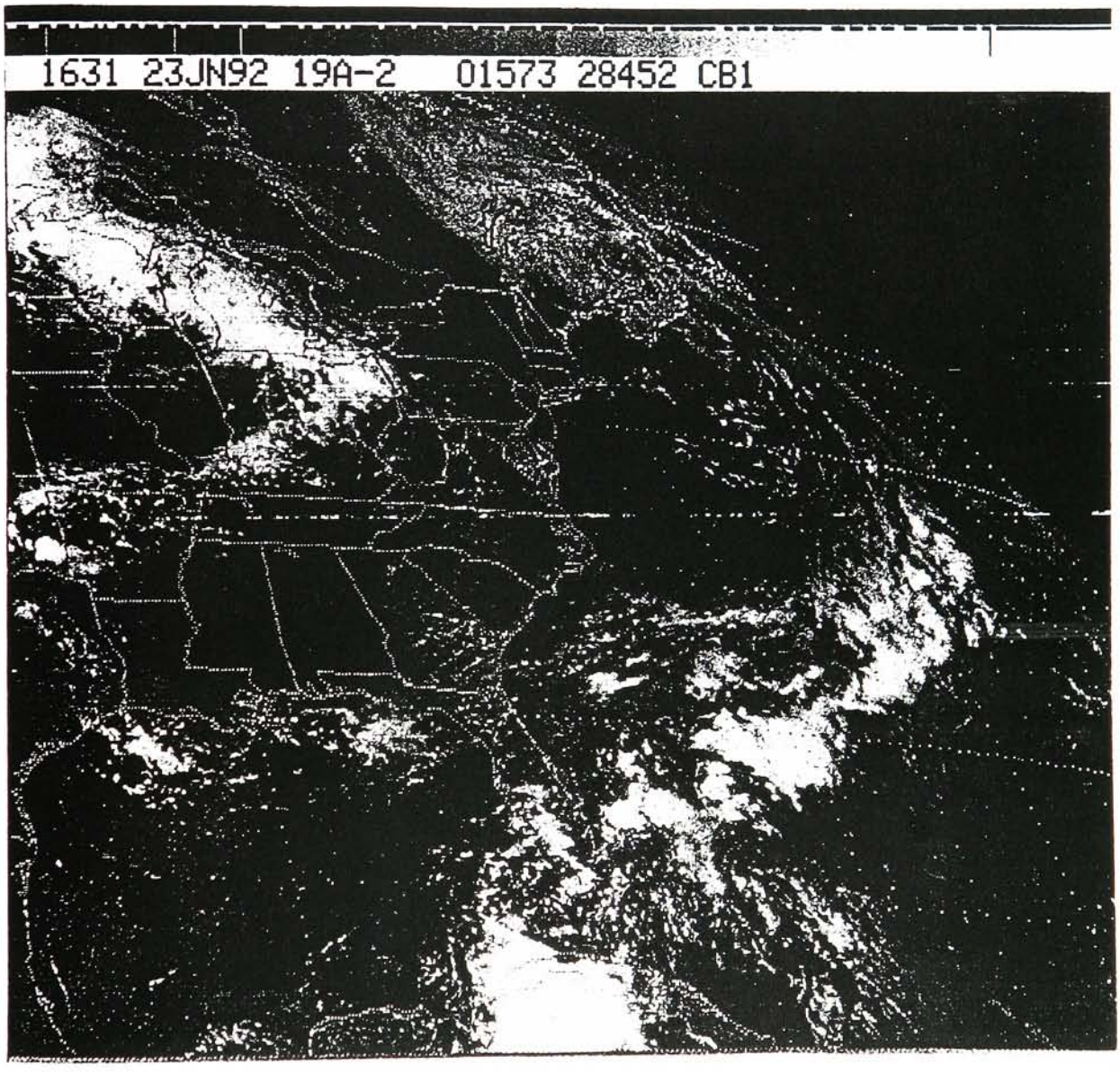

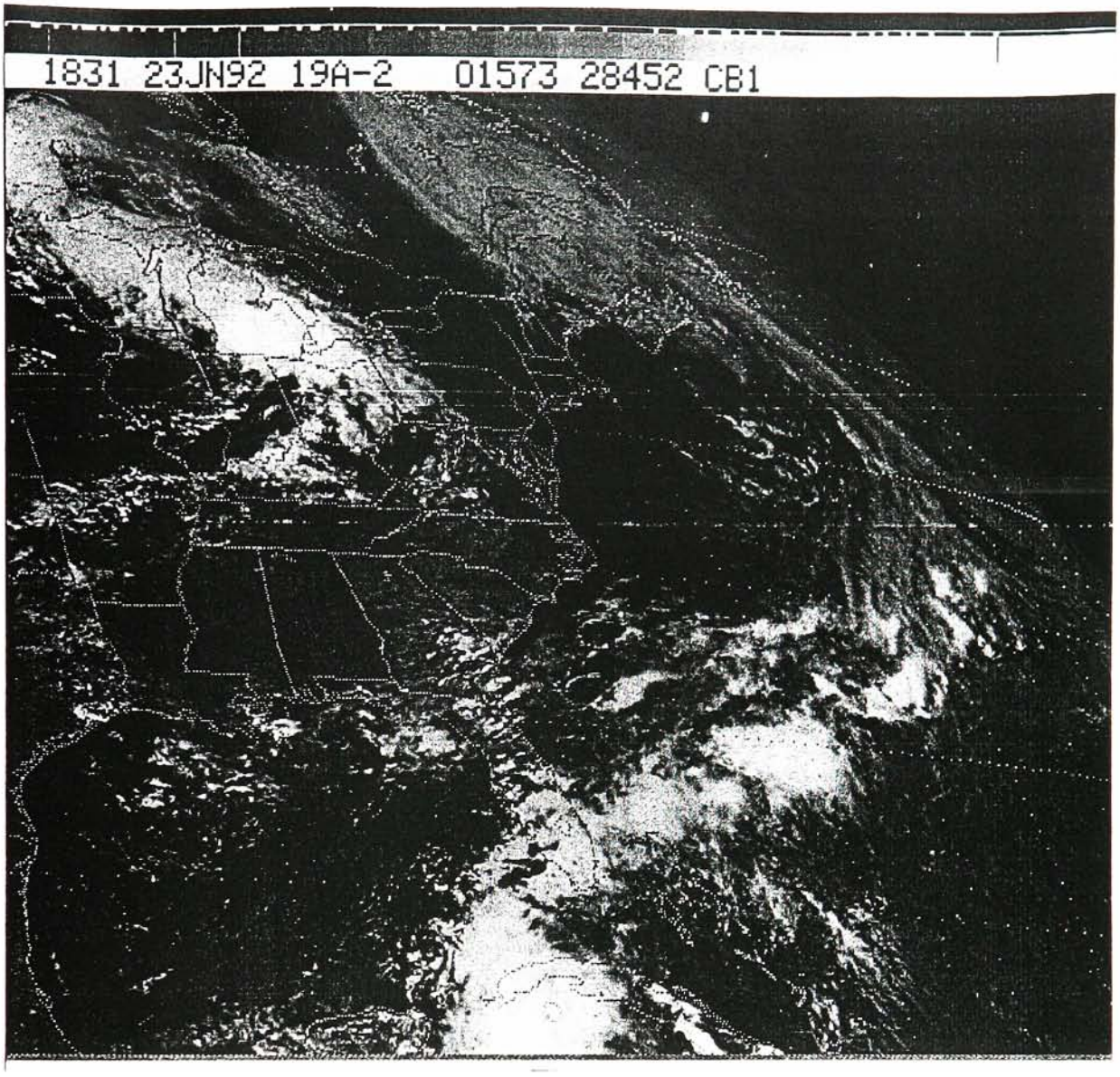
1831 23JN92 19A-2 01573 28452 CB1

2031 23JN92 19A-2 01581 28461 CB1

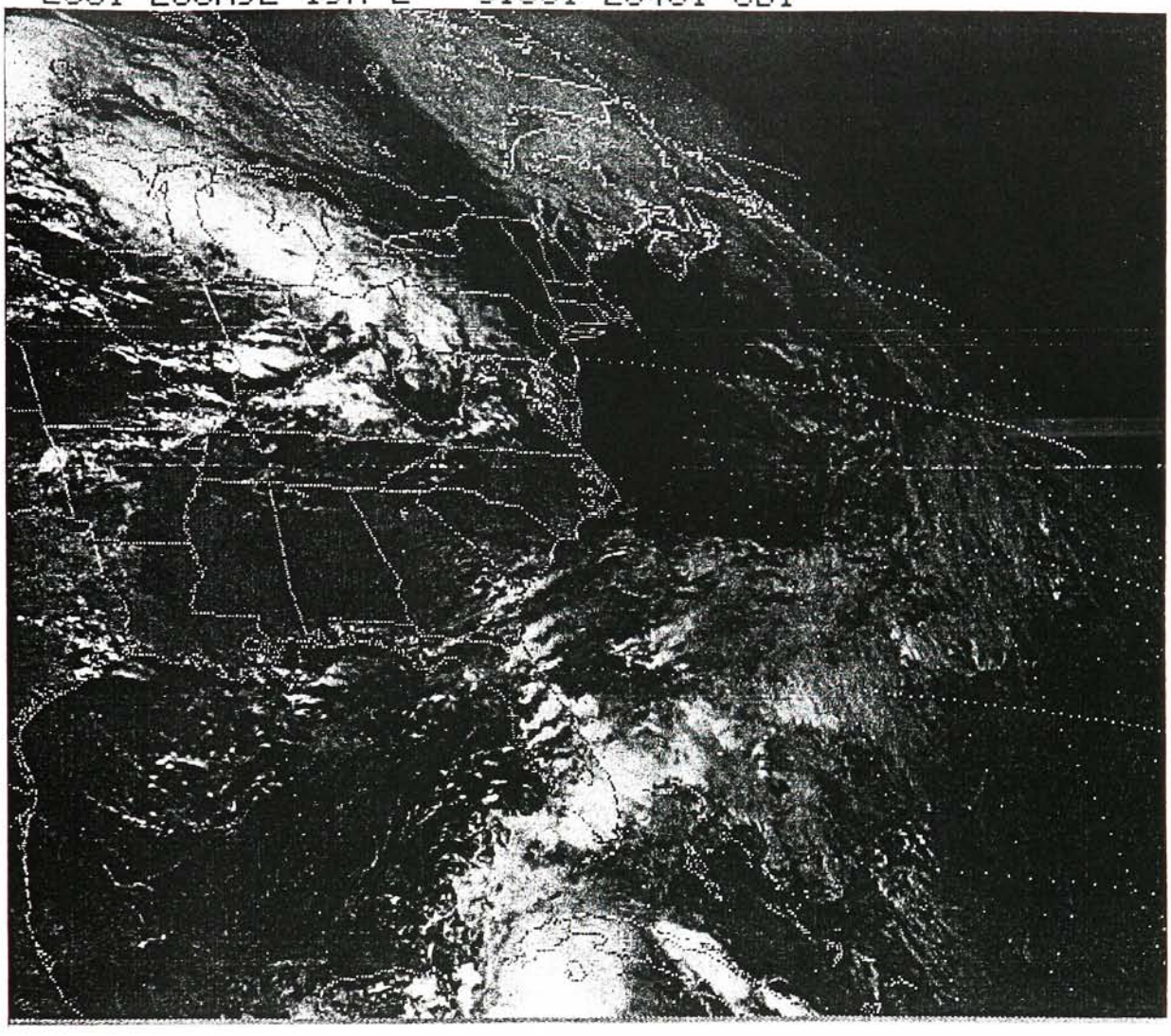

2231 23JN92 19A-2 01581 28462 CB1